ADDITIVE MANUFACTURING

ADDITIVE MANUFACTURING

Edited by
Amit Bandyopadhyay
Susmita Bose


CRC Press
Taylor & Francis Group
Boca Raton London New York

CRC Press is an imprint of the
Taylor & Francis Group, an **informa** business

CRC Press
Taylor & Francis Group
6000 Broken Sound Parkway NW, Suite 300
Boca Raton, FL 33487-2742

Version Date: 20150717

International Standard Book Number-13: 978-1-4822-2360-6 (eBook - PDF)

Contents

Preface

The field of additive manufacturing has seen explosive growth in recent years due to renewed interest in the manufacturing sector in the United States and other developed as well as developing nations. The experience of drawing something in a computer and then seeing that part being printed in a 3D printer that can be touched or felt is still fascinating to many of us. And now we are seeing the same in our children, who are only in their middle school or high school and yet experiencing the revolution of additive manufacturing/3D printing through their own creation. Such transformative change in our society has been made possible only because of a significant reduction in the price of a 3D printer and improvement in part quality. As recently as 10 years back, a good 3D printer cost more than $100,000 in the United States. Due to the high cost of the 3D printers, most people were only able to see a picture or a video of different 3D printers. As the cost of the printer came down significantly along with improvements in 3D printer reliability and part quality, most businesses, universities, and schools are investing in 3D printers to experience, explore, and innovate with these fascinating additive manufacturing technologies. Therefore, we felt that our book will be quite timely as we have tried to capture some of the exciting developments of 3D printing or additive manufacturing technologies in recent years toward advanced materials.

We understand that there are a few other books that deal with additive manufacturing in some form. When we reviewed the literature, we realized that a majority of those books were developed by mechanical engineers, who placed special emphasis on printers rather than on their applications. However, at present, most of the printing technology is quite mature and a majority of the current innovation lies in the areas of their applications. Therefore, our work focuses more on the applications of additive manufacturing than on core 3D printing technologies. Our hope is that readers will be able to see how these technologies are currently being used and then contribute to the field with their own innovation. We have designed the book in a way that can be used in a classroom setting as well. The first few chapters focus on an introduction to various additive manufacturing technologies based on their utilization towards different classes of materials. The next set of chapters discusses important application areas of additive manufacturing. Finally, some discussion on educational aspects and regulatory issues has been added since those factors are becoming important with the emergence of additive manufacturing as a mature technological platform for many industries.

Like any edited book, we recognize all authors, without their help our project would have never been completed. We sincerely thank them for their contributions. We thank many of our students for their support toward developing this book, particularly Tom Gualtieri, Sahar Vahabzadeh, and Dongxu Ke. We would also like to acknowledge support from both our boys, Shohom and Aditya, without which we could not have completed this work.

Even after working in this area for the past 20 years, we still learn new things regularly related to the applications of additive manufacturing. We hope that our book will be useful to many veteran researchers as well as those who are entering this field, helping them understand the subject better to contribute toward making a difference to our future generation.

Amit Bandyopadhyay

and

Susmita Bose
Washington State University

Editors

Amit Bandyopadhyay, a Herman and Brita Lindholm Endowed Chair Professor in the School of Mechanical and Materials Engineering at Washington State University (WSU), received his BS degree in metallurgical engineering from Jadavpur University (Kolkata, India) in 1989, an MS degree in metallurgy from the Indian Institute of Science (Bangalore, India) in 1992, and a PhD in materials science and engineering from the University of Texas at Arlington (Arlington, TX) in 1995. In 1995, he joined the Center for Ceramic Research at Rutgers University for his postdoctoral training. In 1997, he joined WSU as an assistant professor, and was promoted to an associate level in 2001, then to the full professor level in 2006. His research expertise is focused on additive manufacturing of hard materials toward structural and biomedical applications. He has communicated over 250 technical articles. He holds 11 US patents, edited 8 books, and has supervised over 35 graduate students for their degrees in physics, mechanical engineering, and materials science and engineering.

Among others, Professor Bandyopadhyay received the CAREER award from the US National Science Foundation and the Young Investigator Program award from the US Office of Naval Research. Professor Bandyopadhyay is a fellow of the US National Academy of Inventors, the American Ceramic Society, the American Society for Materials, the American Institute for Medical and Biological Engineering, and the American Association for the Advancement of Science. He has been working in the areas of additive manufacturing of advanced materials since 1995.

Susmita Bose, a Herman and Brita Lindholm Endowed Chair Professor in the School of Mechanical and Materials Engineering (MME) at Washington State University (WSU), received her BS degree from Kalyani University (India) in 1990, an MS from the Indian Institute of Technology (IIT)—Kanpur in 1992, and a PhD from Rutgers University, New Jersey, in 1998 in Physical Organic Chemistry. In 1998 she joined the MME, WSU, as a research assistant scientist in materials science and engineering, and since then she has been working with rapid prototyping/3D printing of bone tissue engineering scaffolds with controlled chemistry, especially with calcium phosphates, surface modification of metallic implants, and drug delivery. In 2001, she started as an assistant professor in MME, she was promoted to associate professor in 2006, and to full professor in 2010. Her awards include the prestigious Presidential Early Career Award for Scientist and Engineers (PECASE, the highest honor given to a young scientist by the US president at the White House) from the US National Science Foundation in 2004, the Schwartzwalder-Professional Achievement in Ceramic Engineering (PACE) award in 2009, and Richard M. Fulrath award in 2014 from the American Ceramic Society. Dr. Bose was named as a "Kavli Fellow" by the US National Academy of the Sciences. She has supervised over 30 graduate students in materials science and engineering (MSE), mechanical engineering, chemistry, and bioengineering. Dr. Bose has published over 220 technical papers, edited 6 books, and holds 3 US patents. Dr. Bose is a fellow of the American Institute for Medical and Biological Engineering and the American Ceramic Society. Dr. Bose's group research on 3D printed bone tissue engineering scaffolds with controlled chemistry has been featured by the AP, *BBC,* NPR, *CBS News, MSNBC, ABC News*, and many other TV, radio stations, magazines, and news sites all over the world.

Contributors

Gaurav Ameta
School of Mechanical and Materials Engineering
Washington State University
Pullman, Washington

Vamsi Krishna Balla
Bioceramics and Coating Division
CSIR–Central Glass and Ceramic Research Institute
Kolkata, India

Amit Bandyopadhyay
School of Mechanical and Materials Engineering
Washington State University
Pullman, Washington

Susmita Bose
School of Mechanical and Materials Engineering
Washington State University
Pullman, Washington

Christian Carpenter
Apogee Boost, LLC
Monroe, Washington

Denis Cormier
Department of Industrial and Systems Engineering
Rochester Institute of Technology
Rochester, New York

Mitun Das
Bioceramics and Coating Division
CSIR–Central Glass and Ceramic Research Institute
Kolkata, India

Michael D. Dickey
Department of Chemical and Biomolecular Engineering
North Carolina State University
Raleigh, North Carolina

Michael Jan Galba
Application Development Consultant Medical
EOS GmbH—Electro Optical Systems
Krailling, Germany

Thomas PL. Gualtieri
School of Mechanical and Materials Engineering
Washington State University
Pullman, Washington

Forough Hafezi
Department of Manufacturing and Industrial Engineering
Sabanci University
Istanbul, Turkey

Edward D. Herderick
Rapid prototype+manufacturing (RP+M)
Avon Lake, Ohio

Dongxu Ke
School of Mechanical and Materials Engineering
Washington State University
Pullman, Washington

Bahattin Koc
Department of Manufacturing and Industrial Engineering
Sabanci University
Istanbul, Turkey

Can Kucukgul
Department of Manufacturing and Industrial Engineering
Sabanci University
Istanbul, Turkey

Mukesh Kumar
Advanced Process Technology Group
Biomet Inc.
Warsaw, Indiana

Bryan Morrison
One Patient Solutions
Biomet Inc.
Warsaw, Indiana

S. Burce Ozler
Department of Manufacturing and Industrial Engineering
Sabanci University
Istanbul, Turkey

Dishit Paresh Parekh
Department of Chemical and Biomolecular Engineering
North Carolina State University
Raleigh, North Carolina

Clark Patterson
Rapid prototype+manufacturing (RP+M)
Avon Lake, Ohio

Kirk A. Reinkens
Voiland College of Engineering and Architecture
Washington State University
Pullman, Washington

Teresa Reischle
EOS GmbH—Electro Optical Systems
Krailling, Germany

Sahar Vahabzadeh
School of Mechanical and Materials Engineering
Washington State University
Pullman, Washington

Ranji Vaidyanathan
School of Materials Science and Engineering
Oklahoma State University
Tulsa, Oklahoma

1

Global Engineering and Additive Manufacturing

Amit Bandyopadhyay, Thomas PL. Gualtieri, and Susmita Bose

CONTENTS

1.1 Introduction

Additive manufacturing (AM) is a technology that is rapidly developing and being integrated into manufacturing and our day-to-day lives. Many people have heard of its emergence into the commercial world, though it has been labeled by different names, such as three-dimensional (3D) printing, rapid prototyping (RP), layered manufacturing (LM), and solid freeform fabrication (SFF). Conceptually, AM is an approach where 3D designs

can be built directly from a computer-aided design (CAD) file without any part-specific tools or dies. In this freeform layer-wise fabrication, multiple layers are built in the X–Y direction one on top of the other generating the Z or third dimension. Once the part is built, it can be used for touch and feel for concept models, tested for functional prototypes, or used in practice. AM is much more than a process that can be used to make personalized novel items or prototypes. With new developments in AM, we live in an age on the cusp of industrialized rapid manufacturing taking over as a process to produce many products as well and make it feasible to design and create new ones. This will cause the manufacturing process of many things to change as well as cause a new style of customer-to-manufacturer interaction. Integration of 3D printing will make it so people can contribute to the design process from almost any location and will break the barriers of localized engineering and take it to a global scale. Just as the Internet has given us the ability to spread and access information from any location, digital designing and CAD have given people the ability to make, change, and critique designs from essentially anywhere. With AM, those designs can be made and tested from almost any location with very little lead time. The capabilities of AM machines have surpassed the abilities of CAD, making the design and visualization of a part the more difficult process compared to that for building it.[1] As a new generation grows up with CAD technology and the abilities and availability of AM machines grow, the process of designing a product will mature from being just done by a select group of engineers to being created by the consumer and company together; this technique will enable manufacture of products from anywhere in the world in a timely manner.

1.2 History of AM

1.2.1 Start of 3D Printing

AM developed in the 1980s, when a man named Charles "Chuck" Hull invented the first form of 3D printing, called stereolithography (SLA). It was the advancement in laser technology along with Hull's innovation regarding the materials and process he used that first made this conceptual method a reality.[2] SLA is a system where an ultraviolet (UV) light source is focused down into an UV photo-curable liquid polymer bath where upon contact, the polymer hardens. Patterns can be drawn using the UV source to semicure the polymer layer. Uncured polymer stays in the bath and provides support to the part being built. After a layer of printing is done, the hardened polymer layer moves down on a build plate in the liquid medium and the next layer of polymer is available on top for the following layer. This process continues until the part is finished based on the CAD design and is removed from the liquid medium. In most cases, further curing is needed before the part can be touched. It was in 1983 when Chuck Hull invented this new technology; subsequently, in 1986, he formed the very first company to develop and manufacture 3D printers: 3D Systems.[2] This was the first step in the history of making a RP machine outside of science fiction movies or books. Chuck was also the first person to find a way to allow a CAD file to communicate with the RP system in order to build computer-modeled parts. Such an endeavor was not trivial. In his effort, 3D CAD models had to be sliced in a virtual world; each slice can then be used to build a layer using the 3D printer. In the first-generation CAD for 3D printers, only the surface files matter, which are termed *.stl* files from the SLA process. After developing this technology, the patent application was filed in August 1984, and it was approved in 1986 by the United States Patent and Trademark Office, making it the first patent of a RP system.[3]

Though Chuck Hull patented this technology in 1986, it took several years for 3D Systems to launch the first solid-state SLA system.[2]

1.2.2 Development of Other RP Technologies

While 3D Systems was developing and patenting this technology, other innovators started to develop new types of AM machines that used different methods and materials. Down at the University of Texas at Austin, Carl Deckard, an undergraduate student, and Dr. Joe Beaman, an assistant professor, started work on a new technology known as selective laser sintering (SLS). SLS works by having the powdered form of a material spread on a build plate where a laser selectively sinters the powder in certain areas of the plate. Another layer of powder is then distributed over the previous layer and the process is repeated. In the end, the powder will be sintered together producing a 3D part. Deckard and Beaman started work on this technology in 1984 and made the first SLS machine in 1986. They then commercialized the technology creating the first SLS company, called Nova Automation, which later turned into DTM Corp. In 1989, they made the first commercial machines called Mod A and Mod B and continued advancing and making more SLS machines until the company was acquired by 3D Systems in 2001.[4]

Around the same time, two graduates of Washington State University, Scott and his wife Lisa Crump, were developing another AM technology in their garage. Scott wanted to make a toy for his daughter, so he invented the technology referred to as fused deposition modeling.[5] This technology involves heating of a thermoplastic to a semi-liquid state, which is deposited onto a substrate where it builds the part layer by layer.[6] Scott and Lisa went on to start a company, Stratasys, Inc. in 1989, selling this technology as well as patenting it in 1992.[7,8] Stratasys, Inc. has continued to grow and now has many printers that cost from $2,000 to $600,000 and has over 560 patents pending or granted.[5]

At the same time, another man named Roy Sanders was developing a new RP method. His company, formerly known as Sander Prototype, Inc., now named Solidscape®, released their first 3D printer called the ModelMaker™ 6Pro in 1994.[9] This machine used an inkjet approach to build a part.[10] This method essentially acts the same as SLA but instead of a laser being sprayed into a liquid medium, hot thermoplastic wax liquid is sprayed onto a plate to build each layer of a part. This machine could make high-resolution wax models, which were very popular for businesses that did complex investment casting such as the jewelry industry.[11] The company had commercial success and was bought by Stratasys, Inc. in May of 2011.[12]

These are just some of the original RP systems that were being developed at this time. Yet they were not the only people that saw how special these technologies were. Once 3D Systems patented their 3D printing technology, SLA companies in other countries started to develop this technology as well. In Japan, two companies called NTT Data CMET and Sony/D-MEC started to develop SLA systems in 1988 and 1989, respectively.[13] Along with this, companies in Europe such as Electro Optical Systems (EOS) and Quadrax developed SLA systems in 1990.[13] Many companies around the globe were starting to develop their own 3D printing devices and coming up with new ways to do it. It was apparent the technology has sparked interest around the world and was starting to be rapidly developed.

1.2.3 Moving from RP to AM

At this point, most of the technologies were made to make polymeric objects and had not been able to process other materials such as metals or ceramics. Such machines were RP machines and not suitable for AM, where the finished parts were made to be used.

It took some more development in RP technology in order to make parts out of metals and ceramics. As is the trend, many companies were trying to develop a metal AM machine. One of the first was a company mentioned before, called EOS. EOS was started in 1989 by Dr. Hans J. Langer and Dr. Hans Steinbichler.[14] They started work on printing plastic parts using SLA systems and then SLS. In the early 1990s, they started to research using SLS to make metal parts and presented their first prototype of a direct metal laser sintering (DMLS) machine in 1994. Subsequently, they launched the first DMLS system the next year in 1995.[14] This process essentially works the same as SLS but can sinter metal powders. The metals that can be used in this process are many general engineering materials such as aluminum, cobalt, nickel, stainless steel, and titanium alloys.[14] In 1997, EOS sold their SLA product line to 3D Systems and took over the global patent rights for laser sintering technology.[14] Since then they have significantly advanced SLS and DMLS and have made it one of the most popular AM processes in manufacturing. This has made EOS one of the most successful and competitive AM companies in the world.

Around this same time, another AM technology that could produce metal parts was being developed in Albuquerque, New Mexico, called laser engineered net shaping (LENS®). It was developed by Sandia National Laboratories and was commercialized by Optomec.[15] It was developed in 1997 and the first machine was sold in 1998.[16,17] The LENS system works by having powder deposited under a high power laser where it melts and solidifies on a substrate. The base and head are both mobile, which deposits the metal on selected areas of the substrate. The metal is then deposited layer by layer until the desired part is built.[18] Optomec has continued to advance LENS technology and has delivered AM systems to over 150 customers as of 2012.[16]

Another type of AM process that is very popular now and was also being developed around this time was electron beam melting (EBM). A company called Arcam AB was started in 1997 creating EBM technology.[19] EBM works by shooting an electron beam at a powder bed in selective areas. Once a layer of powder has been melted in selected areas, another layer of powder is laid on top of the previous and the process is continued until the part is complete.[20] Working with Chalmers University of Technology, Arcam AB released their first EBM machines and sold them to two clients in 2002.[19] In 2007, a manufacturer of orthopedic implants made a Fixa Ti-Por hip implant that was CE certified using EBM technology.[19] Since then more implants have been made using EBM. EBM is also being used in the aerospace industry and as it continues to develop more so do the number of applications it is found to be useful for.

1.2.4 Impact of AM

Since the emergence of these technologies and companies, the AM industry has been constantly expanding, growing, and advancing with much enthusiasm. With many industries seeing the lucrative value and abilities of AM, the market has been expanding very quickly. Many new types of RP and AM methods have been created since these original pioneers first started developing the technology. Some new technology has been novel and some just variations of the past types. There has also been a lot of development in the materials that can be used as well as research into making their properties optimal for end use. These original technologies all started as RP, LM, or SFF methods, where they were designed to only be able to make quick prototypes or "show and tell parts" using polymeric materials. Over the years, RP has moved into being AM where functional prototypes and parts can be made to perform in a variety of environments. The rise of AM being incorporated into industry has made it so the global market of AM has been on the

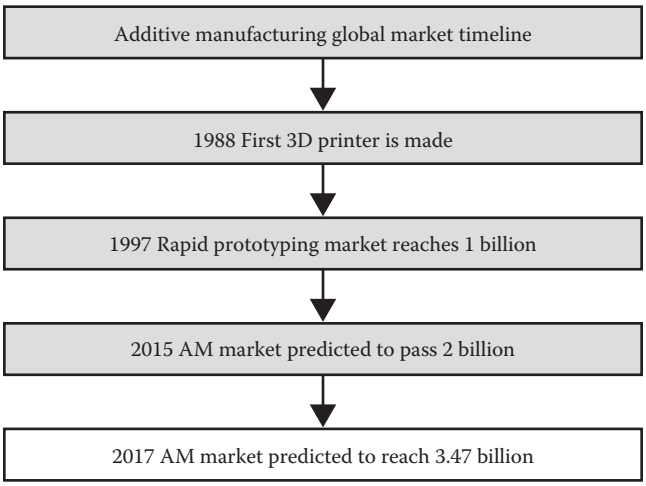

FIGURE 1.1
Growth of additive manufacturing industry.

rise since the first 3D printer was made. Figure 1.1 shows how the AM market has been increasing over the years. In 2012, the market was approximately $1850 million and is projected to almost double and reach $3475 million by 2017.[21] AM will continue to become more integrated into industry and our personal lives as the technology and availability continue to grow.

1.3 Current Manufacturing Challenges

1.3.1 Centralized and Projection-Based Manufacturing Issues

Presently, the standard distribution of goods and products is generally done by large-scale production. This system has many advantages such as low cost of standard goods and high rates of production. Yet, it also has many disadvantages and problems. There can be waste of goods when companies operate on a projection-based manufacturing system and the demand changes due to a variety of reasons. It can result in the waste of many products and sometimes loss of jobs. This would not be an issue if products were made on demand. If mass production is done in other countries, there arises a dependence on foreign markets where the goods are produced. If the foreign market gets cut off by a natural disaster or war, the production does as well.[22] This happened in 2011 when Japan was hit by a tsunami. Many automotive manufacturing plants were damaged, which impacted not only Japanese automotive companies but American companies as well, and significantly disrupted vehicle production.[23] There are also issues like the distributors not allowing all the products to be available on the shelves. The retailers do not always put out the new product because they would rather devote shelf space to an existing one that has a proven record of selling.[24] This could cause a scenario where the newest version of a product could fit the need/want of the consumer but is not available at that time because the store is not

buying the product to preserve shelf space. Of course, these are general issues that tend to arise in large-scale production and could be fixed if the products were made using a small-scale on-demand manufacturing method.

1.3.2 Generalized Designs: Consumer Settling for Only Satisfactory Products

Another issue this method of production often leads to is goods that generally suit most people's needs, but does not cater to the individual consumer's taste. Parts are designed by engineers who make them to fix an issue or fulfill a need of a consumer. Yet for many things, the general item that is made does not fit the needs of the buyer exactly because it is built for the general population, not just for one individual. Likewise, the designers that create the part are sometimes not experiencing the issue first hand. They only make the product to fit within the specifications presented to them from whatever channel it is brought to them by. This trail of information is not always reliable and effective to make an optimal product. Also on a mass-scale production line, it can be hard if not impossible to make custom products based on the tooling and methods that have been established. This can limit the ability of manufacturers to make custom products.[25] Therefore, large-scale production of many goods does not accommodate the individual likes and taste of consumers. As a result, this way of manufacturing ends in the consumer settling for something that is just adequate. Though this is ok for many circumstances, if we have the resources to make things exactly how we want them, then why wouldn't we?

Let's take a scenario where someone wants a table to be used as a desk and desires certain shelves, drawers, and size of the table to fit their office. Possibly they want some custom designs built into the table to make it personal. A manufacturer has built a series of tables with a certain configuration of storage space and has made it so the table can fit through a standard door. Yet maybe none of the available desks are made exactly to what this particular person wishes. The person could try and contact the manufacturer and see if they could custom build a desk for him. Since this would disrupt the production line, it would most likely cost substantially more, if it could even be done at all. Also there usually tends to be an issue with communication from two different locations, and describing exactly what the person wants could be difficult. In the end, this person will most likely buy the desk that fits her or his needs the closest and will settle for something that is not quite exactly what she or he wanted. Now back to the question from before: What if making a perfect desk is possible, could be done easily, and was cost effective?; Do you think the consumer would spend a little more money and effort to buy that? Of course, they would, and with the current state and development of AM, as well as the availability and improvement of CAD, this could soon be a reality.

1.4 AM: Unparalled Manufacturing Paradigm

1.4.1 Current State of AM and How It Generally Works

AM now reached a point where it is ready to be implemented for industrial use. Its advantages over traditional manufacturing methods have caught the interest of most industries. The advantages stem from the machines' ability to create complex geometries using a layer-by-layer build system. Though there are many types of methods and machines, they

all generally work using the same principal process. First, a CAD model of a part or object is made. The CAD file is then converted to an STL file. The STL file is the standard file type for most of all AM machines, which was created by Chuck Hull.[2] The system then cuts the item apart on the computer into layers in the easiest direction to build. Then by various methods, it deposits or binds material layer by layer, stacking each one on the next, until the part is built. This system allows for incredibly complex geometries to be built relatively easily out of a variety of materials. Parts that could not be made using any other manufacturing method now can be made using this technology. Due to its capabilities of making such shapes, the amount of applications it can be used for is unparallel by any other manufacturing method.[1] Industries such as art, aerospace, and medical have applications where AM could be used. This makes it a promising new method that likely will be incorporated into the industrial production of products. It will change the way parts are manufactured, designed, and distributed, as well as the customer–manufacturer relationship.

1.4.2 Advantages of AM: No Restriction on Design

AM will have a profound effect on the manufacturing process of many goods in many different industries. Advantages include its ability to make parts that could not be made before. AM is a start-to-finish process that can make the entire part and does not require multiple machines or processes. It can build complex geometries effectively that are very difficult, costly, or impossible using other methods. This gives the designer a lot more freedom when making a part. Many times the optimal design is not feasible with the types of manufacturing processes available presently. With AM, there is essentially no restriction besides the size of the part has to fit in the machine. Now the designer only has to make it, so the part or item can be installed or be operational for its application. Another benefit to this is the only tooling invol, the one AM machine. No other tooling cost is required. Though some parts must be machined after to have the right surface finish, for the most part much less tooling is required. This eliminates a huge cost of production. The only other cost is maintenance of the machine. AM also saves material because it is an additive technique as opposed to reduction. A reduction manufacturing method is one such as milling where the product starts as a block with dimensions larger than the final product. Then, material is removed until the final dimensions are achieved. The waste material is then either disposed of or recycled, which the manufacturer usually has to pay for. With AM, material is added until the product is made. Therefore, little to no material is lost, so there is up to a 75% reduction in material use and can lower the production time and cost by 50%.[26] These huge savings are one of the reasons AM has sparked so much interest with manufacturers.

1.4.3 Advantages of AM: Versatility in Manufacturing

Another key thing that makes AM so lucrative is its versatility in the parts it builds. If it is found the design that is being produced has a flaw, or there is something that can be changed that would optimize its use, it can be changed instantly. In many traditional manufacturing methods, this can be very difficult. For example, in a casting process, once an expensive die is made, it cannot be changed that day to accommodate an alteration in the design. This is why AM started as RP. It was a process that could be used to make a new part fast and cheap to test and see if it would work. AM still has this capability, which makes it a powerful tool, and now it has moved into being able to produce ready-to-use parts. Therefore, on-demand building is much easier and cost less. If a designer wants

to try something new, or a customer wants a custom part, it can be built easily without disrupting normal production.

1.4.4 Advantages of AM: Altering Materials for Enhanced Performance

AM can now also use many different materials such as various plastics, metals, composites, and ceramics. The type of material depends on the type of AM process. The most popular materials are plastics because they have been studied the most and been around the longest.[1] It has been found that not only can AM use different materials, researchers are finding ways that these processes can be used to alter materials and change their properties. Some of the new freeform fabrication techniques can bond materials like ceramic and metal to create a composite that has increased wear properties.[27] Or AM can be used to deposit a ceramic coating on a metal substrate to increase the materials thermal and wear resistance. Another way AM processes are starting to be used is for repair of broken parts and structures. When a material is broken or has experienced material loss, instead of replacing the part, a machine just adds material back or bonds the two parts together. This process is known as laser cladding and can lower the maintenance cost of many industries that must replace parts or structures frequently.[28] This shows that AM processes do not just provide advantages for making complex geometries, but also optimize material properties to make the final part even more effective, as well as be able to fix damaged parts.

1.4.5 AM Already Incorporated in Modern Manufacturing

Evidence that AM is on the horizon for being a standard part of manufacturing in companies has already created facilities that are dedicated to AM of parts. GE Aviation opened a new facility in December 2013 that can accommodate up to 60 EBM and direct laser sintering machines.[29] The aerospace industry is already moving into using AM machines to build parts that will go into engines. AM makes it, so aerospace manufacturers can optimize parts, lower weight, reduce material loss, and increase the buy-to-fly ratio.[26] Buy-to-fly refers to the time it takes between purchasing the material (generally expensive metals) to the time it is flying and making money. Along with GE, many other aerospace manufacturers are starting to use AM or already are implementing it into their production line. This just shows that AM is already being put into practice in industries. Even though it is only in an industry that can afford expensive processes, it is a precursor to manufacturing other goods. Issues such as surface finish and material properties still pose some issues, but overall it now has the ability to make parts ready for use.[26]

1.4.6 Evolution of CAD to AM and Its Influence on Manufacturing

The immense power of these different machines has made it so the real restraint on making a part is the design.[1] One of the key things that makes AM so groundbreaking is it can build a ready-to-use part from a CAD file. The advancements in CAD have made it, so almost anything can be designed. Any part that can be theorized can now be made in a digital format. The CAD file can then be transferred to an STL file and made on an AM machine. This ability has given engineers and designers the power to design more complex and efficient prototypes and parts than when it was done on paper. Yet even when CAD was developed, designers still had to make parts so they could be made using current manufacturing methods. Now they do not have that restraint and are free to make any geometry to optimize their part. Any geometry made on the computer can become a real part.

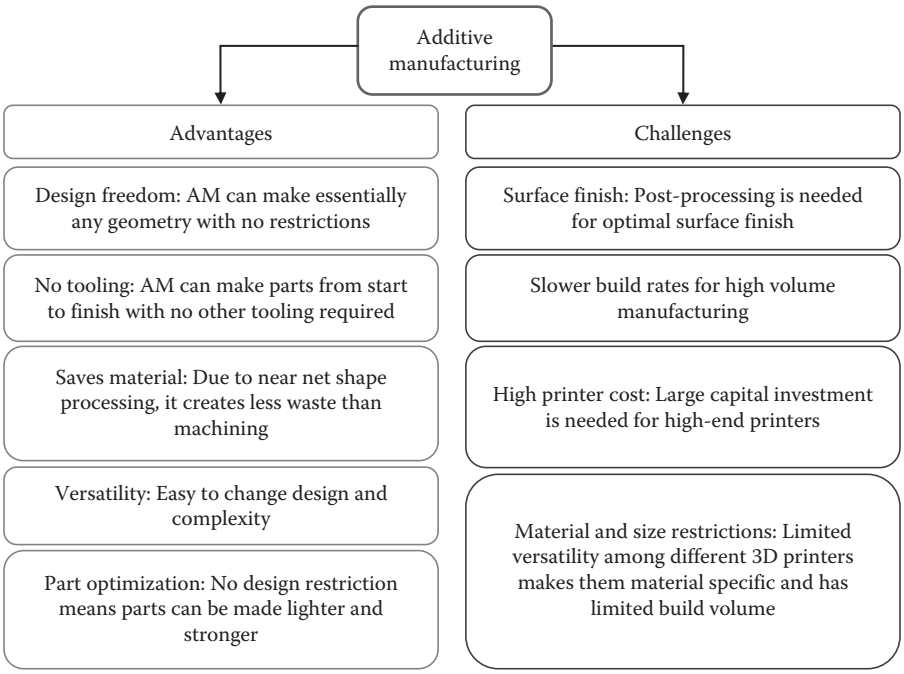

FIGURE 1.2
Summary of advantages and challenges of additive manufacturing.

Figure 1.2 summarizes advantages and challenges of AM as discussed before. Though there are many challenges that need to be overcome, use of AM will significantly increase over the years due to ease of operation, ability to explore creativity, and various other reasons previously mentioned. As it happened with the Internet, it is anticipated that in the next few years, the young generation will lead the development and applications of AM technologies worldwide.

1.5 Global Engineering and AM

1.5.1 Moving from Localized to Globalized Engineering

AM has the ability to build parts from a CAD file; this will make companies and people communicate information with no geopolitical boundaries. Companies will be able to effectively and efficiently communicate designs and concepts anywhere in the world. Anyone who has the ability to operate CAD will have the ability to create a part or alter a design. All designs created will be able to be made into real working parts from a physical distance of 10,000 km or more without any problem. The Internet has provided us with the ability to spread knowledge anywhere; AM and CAD give us that ability as well, except they will not just be able to spread ideas but physical objects as well. Creation of a part can be done from anywhere on Earth, or beyond Earth, so we now have the ability to

FIGURE 1.3
AM and CAD will make it so the transfer and communication of ideas and designs is easy and efficient. (Data from iStock. By Getty Images™ Global Communication—Stock Image. Stock Photo: 20923045. 2014.)

break away from localized engineering and move into global engineering. Figure 1.3 gives a visual of how designs and ideas can be spread across the globe and made physically in almost any location. Anything from simply engineered parts to large architectural designs can be conceptualized and realized from any part of this world. Such openness in design and manufacturing will transform the next generation of products due to inputs from local population who will eventually use them.

1.5.2 Engineer from Anywhere in the World Efficiently and Effectively

AM and CAD will make commercial designing of parts much more efficient and be able to be done from anywhere. The main advantage it gives is it makes communication of ideas and designs much easier and straightforward. Many companies have multiple branches in different countries and locations, and it is imperative that there is clear communication between them. Having key people in the right location to work on a project is not always an option. As well as there is sometimes the problem of having different facilities working on different parts of a project in different locations. These issues can lead to a delay in completing a project because of issues between pairing parts made at different sites or the difficulty in relaying ideas. In the past, schematics or drawings could be sent from other designers to try and interpret what has been done. In current times, CAD files can be sent over the Internet. This has a much greater advantage over trying to interpret 2D images. Yet, still testing and seeing something on the computer is not the same as seeing the real thing and knowing how it will act in real life. This can lead to issues with pairing parts. Boeing experienced this problem with the production of the 787. They had many parts built in many different areas of the globe, and when they were all brought back to Everett Washington to be built, some of the parts did not integrate like they were supposed to.[31] The AM makes it, so these issues are less of a problem. It allows for design teams in different areas to relay information across the globe in the most effective way, by giving them a literal model of the part. Designs can be sent to one location, altered, and sent to another location. As well as they can do it all cost-effectively because they do not need to make new tooling, send people to different sites, or wait very long to have the part built. This capability will have huge effects that will change the way design can be done. Groups of people

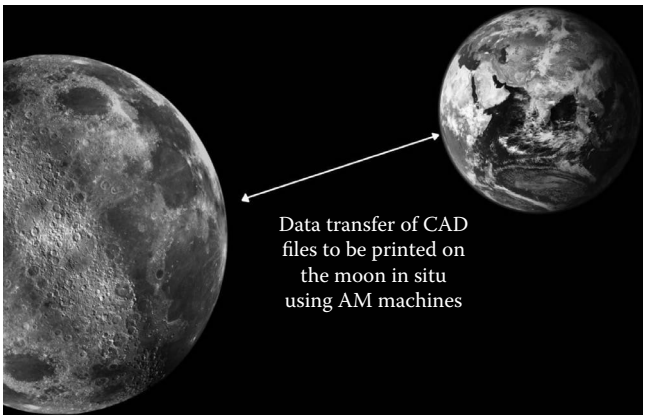

FIGURE 1.4
(See color insert.) Data transfer of CAD between Moon and Earth. (Data from iStock. By Getty Images™ Moon and World—Stock Image. Stock Photo: 3928179. 2014.)

can be anywhere on earth and be a part of a team making designs. AM is already being implemented for these uses in companies like Lockheed Martin. They originally had five different business sectors that worked independent of each other. Qualification of different parts was a slow and difficult process for them. Now they have implemented 3D printers in different areas of production to try and speed this up, so each location is working with the same systems and machines in order to speed up qualification.[26] It is now efficient and feasible to have a design team anywhere in the world.

1.5.3 Manufacturing in Space: No Longer a Dream

This capability can even go beyond Earth. NASA currently is working on trying to develop technology so that settlements can be made on the Moon. They are trying to develop AM machines in order to utilize in situ resources to build structures or parts.[33] If, or more likely when, we make settlements outside of Earth on the Moon or Mars, communication between Earth and astronauts can be very effective and clear using AM machines. If there is a problem and some complex part or device must be made at a satellite location, engineers on Earth will be able to send up CAD files to be printed at the location. Figure 1.4 gives a visual image of this ability AM will provide. Just like a company designing from multiple locations, AM allows the same thing to be done over any space where a signal can transfer data.

1.6 Future Trends

1.6.1 On-Demand Manufacturing of Custom Products

This idea of global engineering does not stop at companies and engineers; it will incorporate the everyday consumer as well. CAD is now a standard tool that almost all people are familiar with. Today kids are learning how to use some sort of 3D modeling software starting from a young age in schools. It is no longer only a drafting tool that is taught in colleges, but has trickled down to being educated as early as middle school.[34] It is almost at the point

where it is like typing; it is assumed that if you were born after a certain age you know how to do it. Therefore, essentially anyone can design something that they want, as long as it is not beyond their CAD abilities. Now with AM, people can build anything they design.

AM will make on-demand manufacturing of custom goods a reality and an easy process. As mentioned earlier, the mass manufacturing method of producing goods has its flaws. In many cases, it would be more economical if the goods could be made closer to the location of sale and made on demand to the customer's exact needs. This system of course would be very costly for most goods and would cause their price to increase dramatically. AM now makes it more economical to manufacture volumes of one.[1] Goods like tables and chairs and other moderately priced home items could now able to be made using the new AM technologies. Many industries that are characterized by increasing demand for individual customization, such as furniture, are incorporating AM.[35] Figure 1.5 shows a very unique intricate chair that has been 3D printed. This shows the complexity and detail that AM can produce. As well as if another customer wanted to change the design or alter it, they could with ease. AM centers could be in many areas and making it so the items would not have to be shipped as far. This makes the customization of those goods very easy as well. In the beginning of this chapter, the example of the person wanting a specific table was brought up. If that person knew how to use CAD, and modeled the exact table he wanted, he could just send it to an AM manufacturer and have it built exactly how he

FIGURE 1.5
3D printed cellular loop chair. (Data from Folkway University of the Arts. Bionic Manufacturing Program. Photo by Nathalie Richter, Design by Anke Bernotat, Partners: Authentics, Plant Biomechanics Group Freiburg, Folkwang University of the Arts, Fraunhofer IWM, Fraunhofer UMSICHT, Fruth, KIT, RPM. Funded by the BIONA funding program of the Federal Ministry of Education and Research.)

wants it. The person could now get the table he needs, as well as add on any custom parts he wants such as having his name engraved on it. Assuming these AM machines were built to make these kinds of structures, it should cost no more than what a standard table would cost when made there. Even if the person did not have CAD experience, in a modern AM company, a consumer ideally would be able to sit down with a designer and make the ideal chair or table for him.[34,35]

1.6.2 Allowing People's Creativity to Become a Reality

This revolution will enable consumers to easily have almost everything custom made to their liking with little to no extra charge. With these capabilities, people will have the aptitude to be creative and come up with new things that were never thought of before. The design team has now moved from the small group of engineers to the collective brains of everybody. Now every person can come up with an idea and have it become a reality with ease. How many times in people's lives have they thought of an invention that could help them in their day-to-day lives or just be something unique they want in their house. Then, they let the idea pass by because they do not have the time, resources, or skills to make this idea come to life. Having readily available AM machines nearby and ready to make parts, all a person has to do is create their idea on a CAD file and it can be made.

1.6.3 Personal AM Machines as a Standard Household Application

There is also a growing industry of personal AM machines or 3D printers. People do not even have to send their CAD file out to be built. This gives the ability to make custom items for people's own home as well as day-to-day items. For instance, if your hose handle breaks, instead of buying a new one you can just design and 3D print one. Figure 1.6 shows an image of a hose valve handle that was 3D printed to replace a broken one. As stated before, the boundaries on what can be made are what the user can imagine. Many companies such as MakerBot® are making printers that are made for home use and are becoming more affordable. Figure 1.7 is an image of the MakerBot Replicator Desktop 3D Printer that is being sold for $2,899 on their website, but they also have printers priced as low as $1,375.[36] As these companies and the technology develop more, the price of household 3D printers should drop and it won't be long before it becomes a standard household item. This just adds to the global engineering by making it easier for people to spread ideas and design new things. Now if somebody wants a custom part such as a unique lamp shade, all they have to do is design it and can print it at home.

1.6.4 AM Advancing Medical Technology and Helping Lives

This globalized engineering does not only help with commercial good, it can be life changing in the medical industry. When it comes to an implant or tissue replacement, nobody wants to settle for something that most closely fits their needs. The patient wants the product to be perfect and is willing to spend any amount of money to make that happen. Currently, in the medical field they have different sizes of implants to fit different patients. Though there is a lot of versatility in different types of implants, it is sometimes necessary to have total custom implants.[37] A custom implant could also better ensure the implant will be successful. Making of a custom implant can be difficult using traditional manufacturing methods and also tends to involve a long demanding adaption phase before an optimum result is achieved.[38] Along with that it also tends to involve high cost to the

FIGURE 1.6
3D printed hose nozzle handle. MakerBot Replicator Desktop 3D Printer was used to build this. (Data from G. Andersen. Valve Handle by Geir. MakerBot. Thingiverse. Published on June 19, 2011. http://www.thingiverse.com/thing:9450; Courtesy of MakerBot, Brooklyn, NY.)

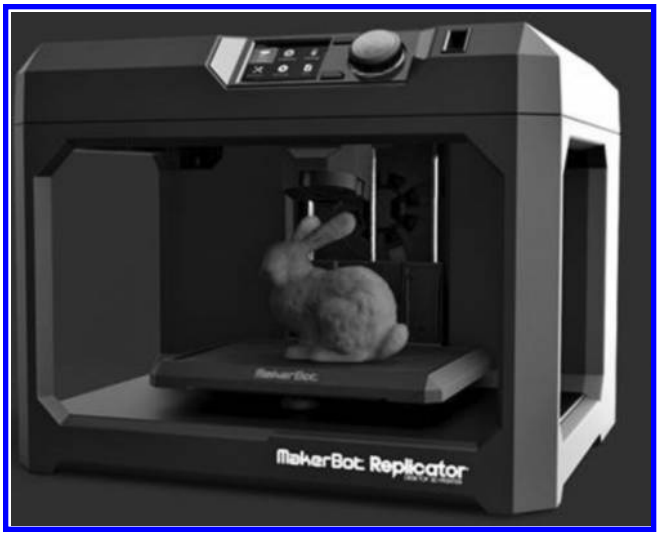

FIGURE 1.7
(See color insert.) MakerBot Replicator Desktop 3D Printer. (Data from MakerBot® Replicator Desktop 3D Printer. Makerbot.com. 2009–2014. http://store.makerbot.com/replicator; Courtesy of MakerBot, Brooklyn, NY.)

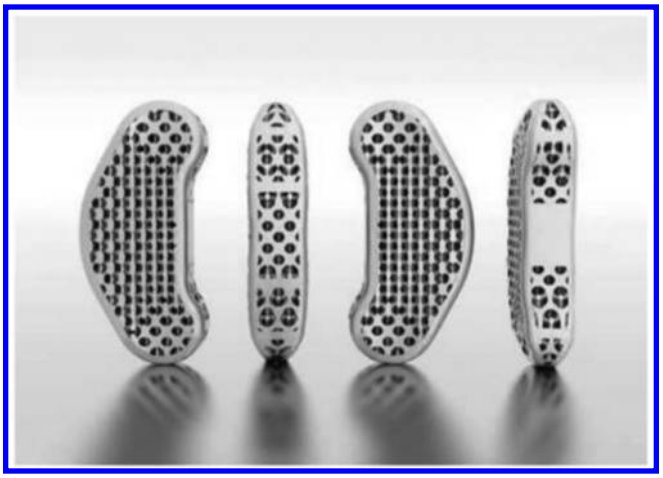

FIGURE 1.8
Spinal implants made of EOS Titanium Ti6Al4V. (Data from EOS. Additive Manufacturing in the Medical Field. EOS. E-Manufacturing Solutions. 2013. http://ip-saas-eos-cms.s3.amazonaws.com/public/b674141e654eb94c/c5240ec3f487106801eb6963b578f75e/medicalbrochure.pdf; Courtesy of EOS, Krailling, Germany.)

patient.[38] Whether the implant is going to replace a bone or act as a scaffold to be placed in a damaged bone or tissue, it will more than likely be a hard or impossible part to machine using traditional methods. AM now has the ability to make implants that fit optimally into a patient as well as create new implants that could not be made before. Figure 1.8 shows an image of some spinal implants made by EOS using AM. The parts are very complex and would not be able to be made using conventional forms of manufacturing. These implants could be made quickly with lower lead and healing time, as well as make it possible to fix problems that we could not before. These implants are more cost effective for the hospital, which can lower the price of the procedure as well as increase patient care.[38] Things such as tissue engineered cranial implants and porous bone scaffolds can now be made using AM.[39] Just like the example of furniture, these implants can be made on demand when the patient comes in. From an X-ray, a CAD model can be made of the injury.[40] That model can then be sent to the AM machine, whether it be down the hall or in another country, and an implant can be printed exactly how the physician thinks is best. This will help to treat patients where there was no treatment before, as well as decrease the time it takes for an injury to heal. This is just another area where AM will make a difference.

1.7 Summary

Overall, AM will have a profound effect on the manufacturing of many goods as well as create a world of global engineering where ideas and designs can be spread in the most effective way. The current state of large-scale manufacturing leaves consumers settling for products that are not quite exactly what they want. Also it does not provide the consumer with customization of products. AM is a method that has the ability to make complex geometries, alter material properties, and allow for versatility in the production of parts.

The applications it can be used for are unparalleled by any other manufacturing method. Incorporating AM into companies will result in our ability to manufacture what was once not possible. One of the most powerful things it will do is make the communication of designs and parts uncomplicated and effective. Therefore, companies, consumers, and anybody with access to CAD can design, critique, or customize a part. As well they can print it on location and test it out physically. AM will make it so companies and design teams in multiple locations can work together in the most effective way possible. In all, AM makes the engineering of a part have no borders or barriers, and changes the world from localized to globalized engineering.

References

1. N. Hopkinson, R.J.M. Hague, P.M. Dickens. *Rapid Manufacturing. An Industrial Revolution for the Digital Age*. John Wiley & Sons, Chichester, 2006.
2. 3D Systems. The Journey of a Lifetime. www.3dsystems.com. 3D Systems, Inc. 2014.
3. C.W. Hull. Apparatus for Production of Three-dimensional Objects by Stereolithography. Uvp, assignee. Patent US 4575330 A. March 11, 1986.
4. Selective Laser Sintering, Birth of an Industry. Department of Mechanical Engineering and Faculty Innovation Center, Cockrell School of Engineering. The University of Texas at Austin, Austin, TX. 2013. http://www.me.utexas.edu/news/2012/0612_selective_laser_sintering.php.
5. Inventor of 3D Printing Scott Crump: "My Dreams Started in a Garage." 3D Printing.com. September 17, 2013. http://on3dprinting.com/2013/09/17/inventor-of-3d-printing-scott-crump-my-dreams-started-in-a-garage/.
6. FDM Technology. Stratasys for a 3D World. Stratasys. 2014. http://www.stratasys.com/3d-printers/technologies/fdm-technology/faqs.
7. S.S. Crump. Apparatus and Method for Creating Three-dimensional Objects. Stratasys, assignee. Patent 5121329. June 9, 1992.
8. *International Directory of Company Histories*, Vol. 67. St. James Press, 2005. Funding Universe.com.
9. Solidscape. About Us. Solidscape: A Stratasys Company. Solid-scape.com. 2013.
10. S. Crawford. How 3-D Printing Works? March 1, 2011. HowStuffWorks.comhttp://computer.howstuffworks.com/3-d-printing.htm.
11. Solidscape. News Release: Sanders Prototype, Inc. Changes Name to Solidscape, Inc. Solid-scape.com. Solidscape, Inc.: A Stratasys Company. 2013
12. Solidscape. News Release: Solidscape Sells to 3D Printer Maker, Stratasys. Solidscape. 2011.
13. T. Wohlers and T. Gornet. History of Additive Manufacturing. State of the Industry. Wohlers Report 2011. Wohlers Associates, Fort Collins, CO. 2011.
14. EOS. History. EOS e-Manufacturing Solutions. http://www.eos.info/about_eos/history.
15. Sandia National Laboratories. News Releases: Creating a Complex Metal Part in a Day Is a Goal of Commercial Consortium. Sandia National Laboratories. December 4, 1997. http://www.sandia.gov/media/lens.htm.
16. Optomec. Company Milestones. Optomec. Production Grade 3D Printers with a Material Difference. 2014. http://www.optomec.com/company/milestones/.
17. Optomec. Company Overview. Optomec. Production Grade 3D Printers with a Material Difference. 2014. http://www.optomec.com/company/.
18. Optomec. LENS Technology. Optomec. Production Grade 3D Printers with a Material Difference. 2014. http://www.optomec.com/printed-metals/lens-technology/.
19. Arcam. Arcam History. Arcam AB® CAD to Metal®. http://www.arcam.com/company/about-arcam/history/.

20. Arcam. EBM® Electron Beam Melting—In the forefront of Additive Manufacturing. Arcam AB® CAD to Metal®. http://www.arcam.com/technology/electron-beam-melting/.
21. L. Wood. Global Additive Manufacturing Market (2012–2017). Globe Newswire. Press Releases. CNBC LLC, Los Angeles, CA. 2014.
22. S. Chand. The Advantages and Disadvantages of Large Scale Production. YourArticleLibrary.com: The Next Generation Library. 2014. http://www.yourarticlelibrary.com/economics/the-advantages-and-disadvantages-of-large-scale-production/10901/.
23. B. Canis. The Motor Vehicle Supply Chain: Effects of the Japanese Earthquake and Tsunami. Congressional Research Service. CRS Report for Congress. 7-5700. R41831. May 23, 2011. www.crs.gov.
24. L. Perner. Distribution: Channels and Logistics. Department of Marketing. Marshall School of Business. USC Marshall. Lars Perner 1999–2008. http://www.consumerpsychologist.com/intro_Distribution.html.
25. G. Hamel. The Definition of High Volume Manufacturing. Small Business by Demand Media. Houston Chronicle: Houston, TX. 2014.
26. G. Warwick. Print to Build. *Aviation Week & Space Technology*. 176(11):40–43, 2014.
27. M. Roy, V.K. Balla, A. Bandyopadhyay, and S. Bose. Compositionally graded hydroxyapatite/tricalcium phosphate coating on Ti by laser and induction plasma. *Acta Biomaterialia* 7:866–873, 2011.
28. Laser Cladding Services. *Services we offer*. www.lasercladding.com. 2014.
29. G. Warwick. Adding Power. *Aviation Week & Space Technology*. 176(11):43–44, 2014.
30. iStock. By Getty Images™ Global Communication—Stock Image. Stock Photo: 20923045. Alberta, Canada. 2014.
31. D. Gates. Boeing 787's problems blamed on outsourcing, lack of oversight. The Seattle Times Company, Seattle, WA. 2014.
32. iStock. By Getty Images™ Moon and World—Stock Image. Stock Photo: 3928179. Alberta, Canada. 2014.
33. M. Green and T. Talbert. Lunar Settlement: Piecing Together a Full Moon Picture. Office of the Chief Technologist. NASA, Washington, DC. October 31, 2012.
34. H. Livingston. Get 'Em While They're Young. *Cadalyst*, Winter 2012, USA. http://www.cadalyst.com/cad/get-039em-while-they039re-young-14242.
35. J. Gausemeier, N. Echterhoff, M. Kokoschka, and M. Wall. Thinking ahead the Future of Additive Manufacturing—Analysis of Promising Industries. Direct Manufacturing Research Center. Heinz Nixdorf Institute. University of Paderborn, Paderborn, Germany, 2011.
36. MakerBot® Replicator Desktop 3D Printer. Makerbot.com. 2009–2014. http://store.makerbot.com/replicator.
37. Specialized and Custom Fitted Hip implant Options. BoneSmart. 2014. http://bonesmart.org/hip/hip-implants-specialized-and-custom-fitted-options/.
38. EOS. Additive Manufacturing in the Medical Field. EOS. E-Manufacturing Solutions. 2013. http://ip-saas-eos-cms.s3.amazonaws.com/public/b674141e654eb94c/c5240ec3f487106801eb6963b578f75e/medicalbrochure.pdf.
39. EnvisionTEC. Tissue Engineering Bone Implants using EnvisionTEC 3D Printer. EnvisionTEC, Dearborn, MI The benchmark in 3D printing. 2014.
40. M. Veselinovic, D. Stevanovic, M. Trajanovic, M. Manic, S. Arsic, M. Trifunovic, and D. Misic. 34th International Conference on Production Engineering. Method for Creating 3D Surface Model of the Human Tibia. September 2011.
41. G. Andersen. Valve Handle by Geir. MakerBot. Thingiverse. Published on June 19, 2011. http://www.thingiverse.com/thing:9450.
42. Folkway University of the Arts. Bionic Manufacturing Program. Photo by Nathalie Richter, Design by Anke Bernotat, Partners: Authentics, Plant Biomechanics Group Freiburg, Folkwang University of the Arts, Fraunhofer IWM, Fraunhofer UMSICHT, Fruth, KIT, RPM. Funded by the BIONA funding program of the Federal Ministry of Education and Research. March 1, 2013.

43. Roland Berger. Additive Manufacturing. A game changer for the manufacturing industry? Roland Berger Strategy Consultants, Munich, Germany. November 2013.
44. Statista. Value of the additive manufacturing (3D printing) market worldwide from 2011 to 2021 (in billion U.S. dollars). Statista. 2014. http://www.statista.com/statistics/261693/3d-printing-market-value-forecast/.

2

Additive Manufacturing Technologies for Polymers and Composites

Ranji Vaidyanathan

CONTENTS

ABSTRACT In this chapter, we describe additive manufacturing (AM) processes for polymers and for composites where polymers are used. These include cases where polymers are the only material used, where they are added as binders in the case of ceramics, and in polymer composites where they are used either as a thermoplastic resin or as a thermoset resin with fiber reinforcement. Examples of AM processes for both chopped fiber and continuous fiber-reinforced composites are described. Some special cases such as nanocomposites and their applications are described. The chapter concludes with current challenges and future trends in the AM field with emphasis on polymers and composites.

2.1 Introduction

Additive manufacturing, or AM processes, initially known as *solid freeform fabrication* and *rapid prototyping* and currently described as *direct digital manufacturing*, or *rapid manufacturing*, *art to part*, *additive layer manufacturing*, or *layer manufacturing*, were originally developed in the late 1980s to early 1990s (Gibson, Rosen, and Stucker 2010). This chapter will discuss some of the historical perspectives on the development of AM technologies as related to polymer-based materials and how that progress has controlled the development of AM process for polymers and composites. Though the industry called these in generic terms as *rapid prototyping*, an ASTM committee defined them more broadly as *additive manufacturing*, under ASTM F2792, which is more descriptive of the current state of the art (ASTM-F2792).

ASTM F2792 has categorized the various AM processes under seven categories (ASTM 2014; Paesano 2014). Among these, the categories that specifically relate to polymers and composites are

- Binder jetting, where a liquid-binding agent is selectively deposited to bind powder materials.
- Material extrusion, where a material is selectively dispensed through a nozzle or orifice.
- Material jetting, where droplets of build material are selectively deposited.
- Powder bed fusion, where particles of a polymer could be bonded together thermally.
- Vat photopolymerization, where a liquid photopolymer is selectively cured by light-activated polymerization.

Table 2.1 describes the various materials and equipment manufacturers who use AM processes for polymers and composites. The earliest materials and equipment almost entirely catered to polymers and for form and fit type of applications. However, as the capabilities of the equipment as well as software have improved, various manufacturers are fabricating functional prototypes that can be directly used in actual applications (direct digital manufacturing; General-Electric).

Among all the AM materials, polymers are perhaps the most advanced materials for AM techniques. A good description of the early beginnings of the technology and the current state of the art in materials is given by Gibson, Rosen, and Stucker (2010), Guo and Leu (2013), and more recently, Paesano (2014). This chapter will however focus on specialized polymers, especially those reinforced with self-reinforcing fibers and chopped fibers as well as continuous fibers. The chapter will also discuss specialized polymers and blends that are required to be added to ceramics to make them suitable to be fabricated into 3D parts. Some additional discussion on polymers and composites that are used for biomedical applications different from traditional materials like polylactic acid-poly(lactic-*co*-glycolic acid) (PLA-PLGA) or hydroxyapatite is also presented here.

Some of the earliest work for AM of polymer composites started in the mid-1990s but is still continuing with new materials and processes, especially for higher strength thermoplastic polymers and composites. A majority of the AM processes developed for polymers

TABLE 2.1

Materials and Manufacturers of AM Technologies Using ASTM F2792 Classification for Polymers and Composites

ASTM F2792 Classification	Materials Used for the AM Technology of Polymers and Composites	Equipment Manufacturer
Binder jetting	Polymers, powders, elastomers	3D Systems, ExOne, Z-Corp (Z-Corporation 2014)
Extrusion	Polymers, short fiber-reinforced polymers, ceramics, continuous fiber-reinforced polymers	Stratasys, MakerBot, Fab at Home, MarkForged (MarkForged 2014) ABB, modified extrusion-based equipments
Material jetting	Polymers, waxes	3D Systems, Solidscape, Objet
Powder bed fusion	Polymers	EOS, 3D Systems
Vat photopolymerization	Photopolymers	3D Systems, Envisiontec

Source: Paesano, A., *SAMPE Journal* 50 (5):34–43, 2014.

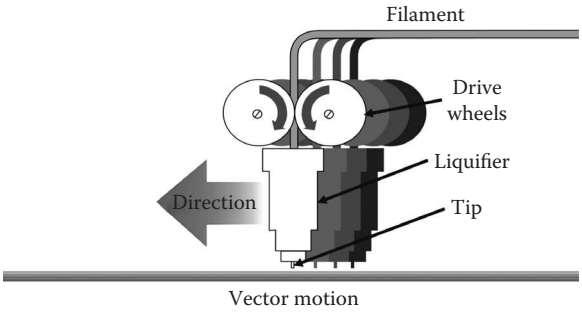

FIGURE 2.1
Schematic of the fused deposition modeling process.

and composites are extrusion-based processes, adapted to the original Stratasys equipment developed by Scott Crump (1992, 1994), shown in the schematic in Figure 2.1.

Even though the original patent by Crump and Stratasys referred to the use of various materials in the fused deposition modeling (FDM) process, such as waxes, thermoplastic resins, and metals, the process is limited to prototypes made using ABS (acrylonitrile butadiene styrene), polycarbonate, and Ultem (based on thermoplastic polyetherimide resins) and a maximum operating temperature of approximately 260°C. This limitation is due to two reasons: (1) temperature limit of the extruder in the FDM equipment limits the polymers that can be used for prototyping and (2) the support material for fabricating the support structures is also temperature limited. Even with the Ultem material, the standard soluble support material cannot be used and only a special thermoplastic support material has to be used. This support material is not water soluble and has to be removed after the fabrication process and could be quite challenging to remove in the case of thin wall sections. This further requires the wall thickness of the parts built to be above a certain value so that the support structure can be removed without damaging the prototype part.

Stereolithography or SLA was the very first AM technology developed by Jacobs and 3D Systems, where a liquid photosensitive resin is converted into a solid by exposing it selectively to an ultraviolet light or an ultraviolet laser (Jacobs 1992, 1995). Figure 2.2 shows a schematic of the SLA process. Variations exist in this process, where suspensions of ceramic or metal particles in a photocurable monomer are used in the SLA process to produce metal or ceramic parts. A typical process for ceramic part manufacturing has been described by Griffith and Halloran (1996).

The selective laser sintering (SLS) technique originally developed at the University of Texas, Austin, by Dr. Joe Beaman and his graduate student at the time Dr. Carl Deckard can make parts out of metal and plastic powders using a high power laser (UT-Austin 2012). Parts can be created from a range of powder materials, including metals, nylon-11 and nylon-12 polyamides, or nylons with fillers such as glass beads or carbon fibers (to enhance physical properties). SLS material properties can be comparable to those found with traditional manufacturing methods. A schematic of the SLS process is shown in Figure 2.3.

Yet another technology using polymers in the process is the three-dimensional printing (3DP™) technology. The 3DP was originally developed at the Massachusetts Institute of Technology in 1993 and is used in the Z Corporation's prototyping process, one among

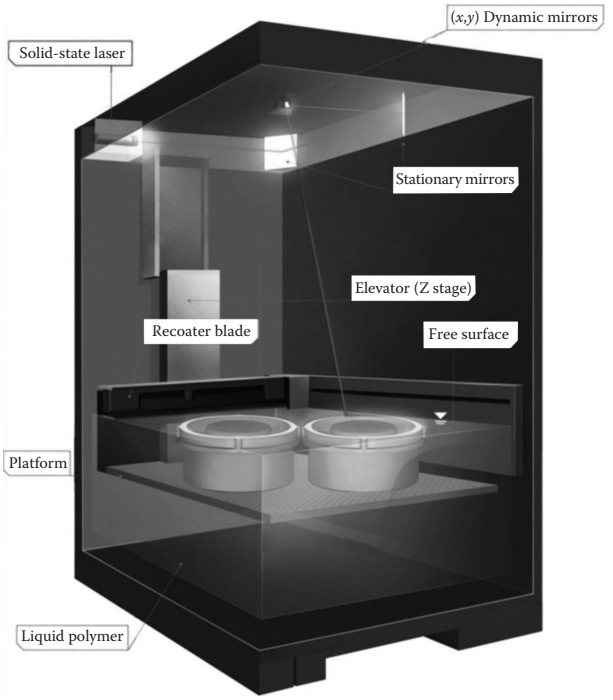

FIGURE 2.2
Schematic of the stereolithography AM process. (Courtesy of www.solidconcepts.com.)

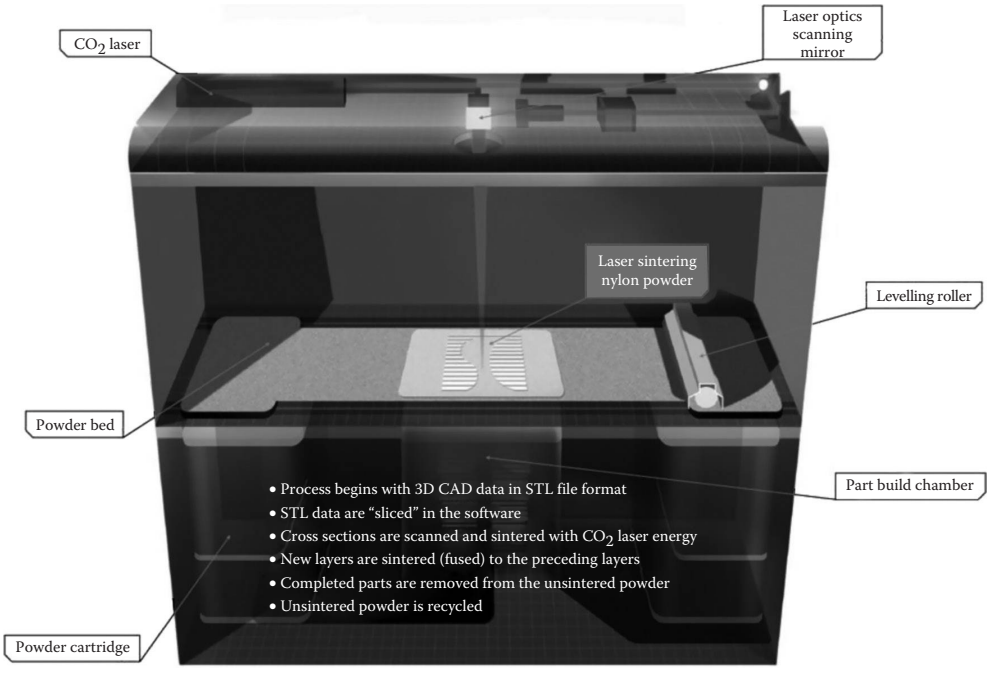

FIGURE 2.3
(See color insert.) Schematic of the selective laser sintering AM process. (Courtesy of www.solidconcepts.com.)

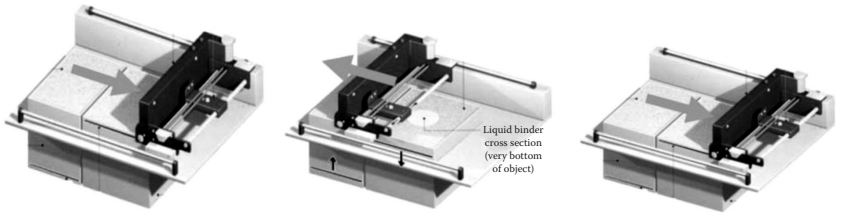

(a) Spread a layer of powder (b) Print cross section (c) Print a layer of powder

FIGURE 2.4
(a–c) Process schematic for the 3DP process used in a typical binder jetting process. (Courtesy of www.3dsystems.com.)

three such AM technologies to be developed from the original Michael Cima patent (Cima et al. 1993). Similar to the process used in other AM technologies, this technology also creates 3D physical prototypes directly from CAD models. A liquid binder is used to bind layers of deposited powders to produce the final prototype.

A schematic of the Z-Corp 3DP process is shown in Figure 2.4. In the 3DP process, the printers use standard ink-jet printing technology. In this case, the parts are created layer by layer by depositing the liquid binder onto thin layers of powder. There is a feed piston and platform that rises incrementally for each layer, while a roller mechanism spreads the powder fed from the feed piston onto the build platform.

A major advantage of this process is that it can utilize standard ink-jet print heads to dispense the binder fluid onto the powder bed. It is a relatively fast process compared to other AM methods because of the multiple ink-jet heads used. The ink-jet print heads print in discrete locations on the powder bed, binding the powder particles together. After each layer is printed, the piston lowers by a set height and a new layer of powder is spread on top of the previous layer. After printing, the new layer is bonded to the previous layer, thus creating the final part.

2.2 AM of High-Strength Thermoplastics and Fiber-Reinforced Thermoplastics

Even though AM processes have been well established for polymers and polymer blends, similar progress in the case of high-strength engineering polymers and fiber-reinforced thermoplastic parts (both short fiber and long fiber reinforced) has been difficult to achieve, primarily due to the following issues:

- The capability to extrude a material is based on its column strength at the extrusion temperature, that is, the amount of material capable of being extruded is dependent on the force exerted at the nozzle tip and is drastically reduced at higher extrusion temperatures. The fused deposition modeler or similar equipment uses a filament type of feeding material, limited to an extrusion temperature of 260°C and a column force of 0.35–0.4 MPa, limiting the choice of engineering polymers that can be extruded (Stuffle et al. 2000).

- The addition of fibers and their preferential alignment during deposition introduces anisotropy in properties in the part (Calvert, Lin, and Martin 1997).
- The choice of fibers and matching polymers is limited.
- The properties of the fibers are anisotropic (thermal expansion coefficient, mechanical properties, etc.), whereas the polymers are isotropic. Since the blend of the fibers and the polymer will need to be heated prior to deposition, they will tend to expand and contract at different rates, potentially leading to cracks during the cooling step.
- This problem is exacerbated in the case of a ceramic composite, which needs to go through a binder debinding and sintering step prior to consolidation. The cracking is typically observed during the cooling step after sintering due to the large difference in thermal expansion coefficient between the carbon or ceramic fibers and the matrix material. Ceramic and carbon fibers typically have a negative expansion coefficient in the thickness direction, while the matrix components can have high, positive expansion coefficients.
- Support structure materials do not always match with the polymer binder or the polymer that is holding the fibers together, leading to difficulties in manufacturing parts with undercuts and overhangs.

To overcome the problems with the choice of thermoplastic polymers for AM technologies, Stuffle et al. developed a high-pressure extrusion head that was attached to an *X*–*Y* table and controlled by CAD software for AM. A schematic of the extrusion head is shown in Figure 2.5 (Stuffle et al. 2000). Figures 2.6 and 2.7 show a fused deposition modeler retrofitted with the high-pressure extrusion head, while Figure 2.8 is a close-up image of an operating high-pressure extrusion head (Vaidyanathan et al. 2000). Table 2.2 shows a list of the different engineering polymers that have been used for AM with this high-pressure extrusion head (Stuffle et al. 2000). Some of the materials were true thermoplastics, while others were melt processed thermoset materials.

The apparatus and process of high-pressure extrusion involve the following:

- Feed rod consolidation—first step
- Extrusion freeforming—second step

Consolidation is the pressing of feed rods that are subsequently used in the extrusion step. The materials from Table 2.2 are typically supplied in pellet form. These pellets are then pressed in a single acting, heated cylindrical die and piston assembly at temperatures near the material's melting point under high pressure to produce a cylindrical feed rod without voids or flaws. The feed rod pressing conditions for each material are shown in Table 2.3 (Stuffle et al. 2000). The optimized temperatures and pressures for fabricating feed rods and the optimized deposition parameters are also included in Table 2.3. The rod pressing cycle is based on 10 min hold at temperature and pressure. The deposition parameters are defined with approximately 0.58 mm (0.023″) diameter extrusion nozzle.

The high-pressure extrusion process works well with materials listed in Table 2.2 as well as acrylic, ABS, silicon nitride, alumina, and zirconia. It is also possible for the high-pressure extrusion head to be stationary while the base is moving or vice versa. Among all the materials from Table 2.2, PEEK 450G, PEEK 450CA30, Lexan (with and without the fiber reinforcement), and Elvacite were good modeling materials and provided consistent results (Stuffle et al. 2000).

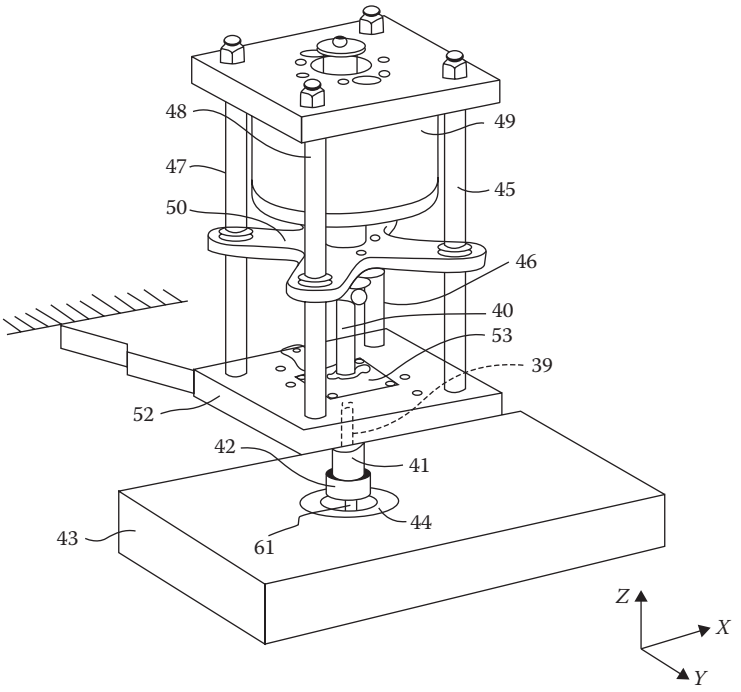

FIGURE 2.5
Schematic of a high-pressure extrusion head for AM of high-strength engineering polymers, ceramics, and metals. (Data from Stuffle, K.L. et al., Method and apparatus for in-situ formation of three-dimensional solid objects by extrusion of polymeric materials, US Patent No. 6,067,480, May 23, 2000.)

FIGURE 2.6
Retrofitted Stratasys FDM modeler. (Data from Vaidyanathan, R. et al., *JOM*, 52, 34–37, 2000.)

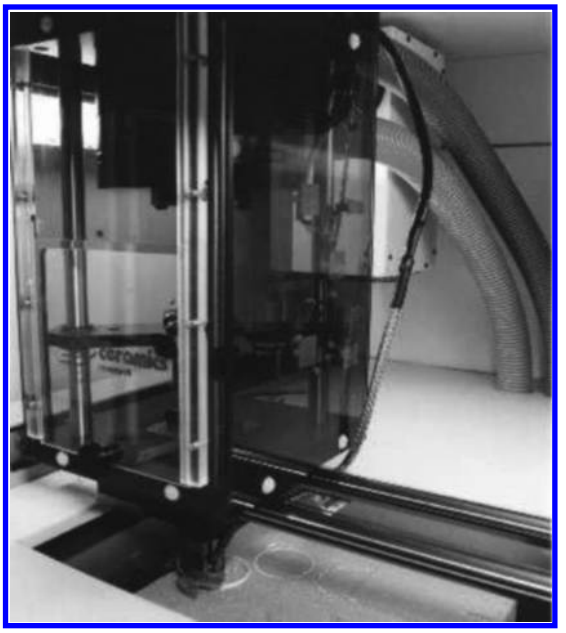

FIGURE 2.7
Operation of FDM modeler with high-pressure extrusion head. (Data from Vaidyanathan, R. et al., *JOM*, 52, 34–37, 2000.)

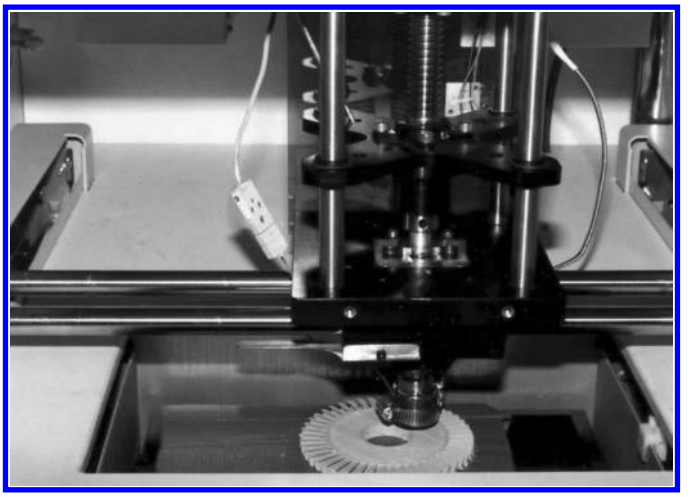

FIGURE 2.8
Close-up view of high-pressure extrusion head in operation inside the FDM modeler. (Data from Vaidyanathan, R. et al., *JOM*, 52, 34–37, 2000.)

Stuffle et al. (2000) also tested the AM materials [polycarbonate, poly(methyl methacrylate) and PEEK, and polycarbonate as well as PEEK with fiber reinforcement] for their tensile, compressive, and fracture toughness properties. Sample densities were also measured using Archimedes' principle. The test specimen geometry was of the typical *dog bone* shape. Two types of specimen orientations were tested. Type V samples were

TABLE 2.2

High-Strength Polymers (Reinforced and Unreinforced) Screened for AM

Polymers Screened			
Trade Name	**Current Manufacturer**	**Polymer**	**Reinforcement**
PEEK 150	Victrex USA Inc.	Polyaryletherketone	None
PEEK 450G	Victrex USA Inc.	Polyaryletherketone	None
PEEK 450CA30	Victrex USA Inc.	Polyaryletherketone	30% carbon fiber
Pellethane 2363	Dow Chemical	Polyurethane	None
Torlon	Sabic Innovative Plastics	Amide-imide	None
Lexan 141	Sabic Innovative Plastics	Polycarbonate	None
Lexan 3413	Sabic Innovative Plastics	Polycarbonate	20% glass fiber
Elvacite 2009	Lucite International Inc.	Poly(methyl methacrylate)	None

Source: Stuffle, K.L. et al., Method and apparatus for in-situ formation of three-dimensional solid objects by extrusion of polymeric materials, US Patent No. 6,067,480, May 23, 2000.

TABLE 2.3

Optimized Rod Pressing and Deposition Parameters for Extrusion-Based AM for Some Typical Engineering Thermoplastics

Optimized Rod Pressing and Deposition Parameters						
Trade Name	**Polymer**	T_R (°C)	P_R (MPa)	T_E (°C)	T_P (°C)	V_E (mm s^{-1})
PEEK 450G	Polyaryletherketone	345	4.1	400	320	0.4
PEEK 450CA30	Polyaryletherketone	345	4.1	390	320	0.4
Pellethane 2363	Polyurethane	190	4.1	210	140	0.4
Lexan 141	Polycarbonate	185	4.1	240	168	0.4
Lexan 3413	Polycarbonate	185	4.1	260	185	0.4
Elvacite 2009	Poly(methyl methacrylate)	120	4.1	185	146	0.4

Source: Stuffle, K.L. et al., Method and apparatus for in-situ formation of three-dimensional solid objects by extrusion of polymeric materials, US Patent No. 6,067,480, May 23, 2000.

T_R, rod pressing temperature; P_R, rod pressing pressure; T_E, extrusion temperature; T_P, deposition tip temperature; V_E, tip velocity.

tested along the writing direction, while type H samples were tested across the writing direction. V and H refer to vertical and horizontal, which denotes the direction of material deposition with respect to the mechanical testing equipment. The equipment used was an Instron model 1011 with a 4448 Newton load cell with vertical specimen loading and wedge-action type grips. The crosshead speed for all specimens was 5 mm min^{-1}. Tensile moduli, strength, 0.2% yield strength, and elongation and strain to fracture were calculated and reported.

Stuffle et al. reported that the measured tensile and compressive strength as well as fracture toughness values were lower than the manufacturer's reported properties. They observed that the densities of the fabricated specimens were only approximately 85% of the values reported in the literature. However, the tensile strength for PEEK with 30% carbon fiber (reported as early as in 1997) (Stuffle et al. 2000) showed approximately 200%

higher tensile strength (71.6 MPa versus 250 MPa) than the strength of the best thermoplastic (Ultem 9085; Stratasys 2014) with approximately 300% improved tensile modulus (2200 MPa vs. 8240 MPa). At the time these properties were reported, the high-pressure extrusion technique was still not a mature technology. With current improvements in materials and AM methods, it can be expected that the properties demonstrated by engineering thermoplastics could possibly show an improvement over the materials supplied by AM equipment manufacturers.

2.3 AM of High-Strength Thermosets and Thermoplastics and Chopped Fiber-Reinforced Composites

For AM of thermoset type of resin systems, there are two possibilities (Calvert 1998). The total shrinkage during curing could be either a combination of minimal shrinkage during deposition followed by large uniform post-cure shrinkage or a shrinkage only during deposition that is as complete as possible before the next layer is deposited (Calvert 1998). Another method to achieve curing of the individual layers would be to internally mineralize the structures by alternating layers of gel containing dissolved salts that will cross-diffuse and precipitate. In an early demonstration of the AM process, Calvert and Liu showed that cross-linked polyacrylamide and polyacrylic acid gels could be freeformed by writing solutions of the monomer, cross-linking agent, and the catalyst onto a hot plate, with the heat inducing the polymerization reaction (Calvert and Zengshe 1998). In the case of polyacrylamide, their recipe was based on 18% aqueous solution of acrylamide, methylene bisacrylamide as a cross-linker at 2%–5% of the monomer, 0.03% potassium persulfate, and 1% tetramethylenediamine as catalyst and activator. 12 wt.% fumed silica was also added to make the mixture thixotropic and control its flow properties. The mixture was freeformed onto a hot plate that was kept at 60°C, with the curing occurring within 3 minutes after deposition (Calvert and Zengshe 1998). Similar shapes were also formed with polyacrylic acid. The major finding in their work was that multilayer stacks of cross-linked hydrogels would swell differently from anticipated behavior if the materials were to be taken separately. This was explained in terms of high per-chain stiffness for one of the components and a negative Poisson's ratio for the other component in a dilute base.

Calvert et al. also showed how freeforming could be used in chopped fiber-reinforced thermoplastic and thermoset composites to obtain improved properties compared to unreinforced composite materials (Calvert, Lin, and Martin 1997). Even though chopped fiber composites are not as stiff as continuous fiber-reinforced composites, they are amenable to scaling up through processes such as injection molding.

Depending upon the particular processing conditions employed, it is well known that the minor phase of a polymer blend has the tendency to become deformed when subjected to shear conditions, especially when applying AM techniques to fiber-reinforced polymers. The amount of deformation experienced by these droplets is a strong function of the shear stress rate imparted to the blend, the viscosity of the individual polymers constituting the blend, and the diameter of the minor phase material. Elmendorp (1986) has proposed a relationship detailing the elongation of a minor phase droplet in a polymer blend when subjected to shear stress.

These factors are strongly dependent upon blend extrusion conditions. The polymer component viscosity and interfacial tensions are influenced by extrusion temperature, while shear stress imparted to the blend increases with extrusion pressure and decreased extruder orifice diameter. Initial (quiescent) droplet diameter of the minor blend component is dependent upon relative concentration of minor phase in the blend. The morphology of these droplets is therefore strongly influenced by the amount of shear imparted to the polymer (Chin and Han 1980; Fayt, Jerome, and Teyssie 1987; Han 1981; Kobayashi, Kaku, and Saegusa et al. 1988; Moore and Kim 1992; Wu 1987). When a blend is initially stressed, the spherical droplets become elongated into an ellipsoidal geometry (Elmendorp 1986). Increased stress causes the ellipsoids to become oriented with their major axes parallel to the polymer extrusion direction. Ultimately, these ellipsoids become elongated into long continuous fibrils, which are oriented parallel to the flow direction. Vanoene (1972) discussed the transition between spherical minor phase to ellipsoids and its subsequent fibrillation while extruding a polymer blend through a nozzle. A schematic of the fibrillation that is usually observed in a nozzle is shown in Figure 2.9. Thus, in this case, it is believed that the rheology of the polymer blend will have the property so that its minor phase will undergo fibrillation when subjected to high shear extrusion through the AM equipment (Vaidyanathan et al. 2000).

The effect of fiber content and fiber orientation in the freeformed mixture controls the mechanical properties of the AM fabricated composites, as seen in the case of thermoset epoxy composites that were freeformed using the extrusion freeform fabrication technique (Calvert, pers. comm.). This is shown in Figure 2.10 for Epon 828 and Araldite MY720 tetrafunctional epoxy resins. The effect of aspect ratio of the fiber size is shown in Figure 2.11,

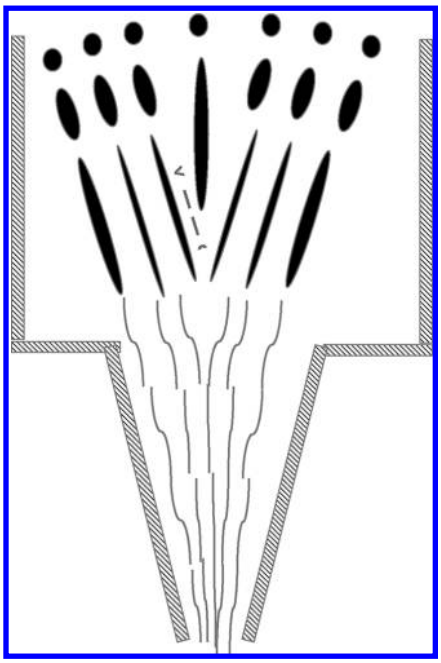

FIGURE 2.9
Schematic describing the fibrillation of a polymer blend through an extrusion orifice. (Adapted from Tsebrenko, M.V. et al., *Polymer*, 17, 831–834, 1976.)

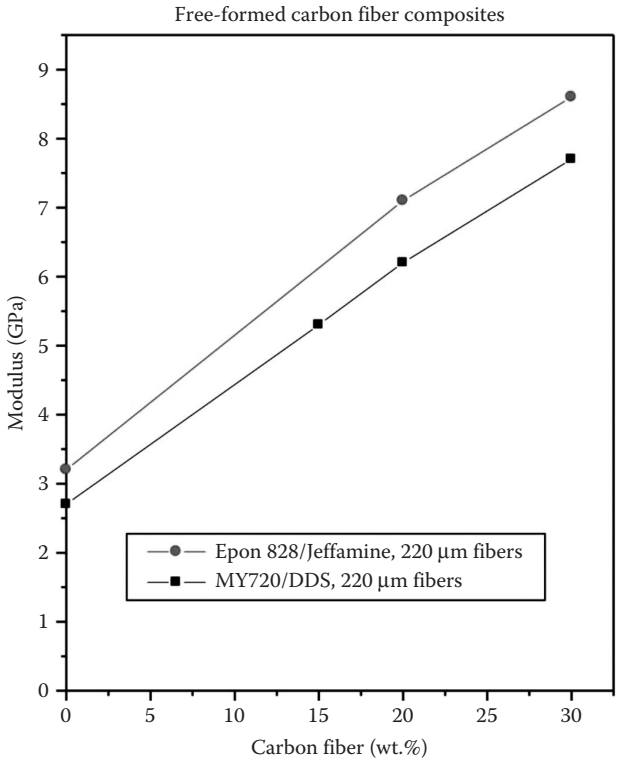

FIGURE 2.10
Correlation of fiber content on the modulus of 220 µm carbon fibers added to Epon 828 and MY720 resins.

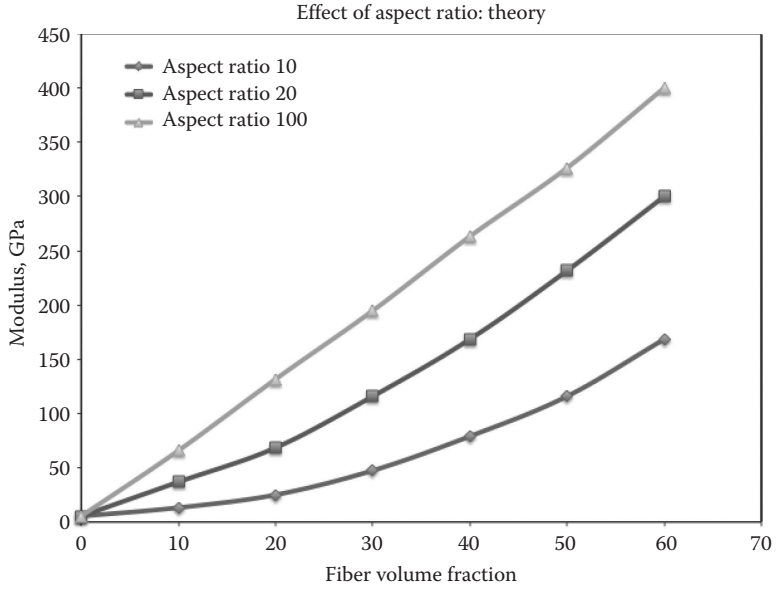

FIGURE 2.11
Predicted modulus versus aspect ratio and fiber volume fraction for Epon 828/glass fiber composites.

TABLE 2.4

Mechanical Properties of Thermoplastic Composite Tensile Bars

Material	Orientation	Modulus (GPa)	Tensile Strength (MPa)	Elongation (%)
PEEK	Parallel	1.7	59	3.3
	Perpendicular	1.8	88	5.3
PEEK + 30 wt.% carbon fiber	Parallel	9.4	257	3.0
Polycarbonate	Parallel	1.1	64	8.7
	Perpendicular	3.6	124	3.6
Polycarbonate + 30 wt.% glass fiber	Parallel	3.0	106	3.8
	Perpendicular	1.0	46	5.6
PMMA	Parallel	1.3	23	1.4
	Perpendicular	1.5	61	5.8

Source: Peng, J. et al., *Compos. A: Appl. Sci. Manufact*., 30, 133–138, 1999.

Note: Instron model 1011; strain rate: 5 mm s^{-1}; load cell: 4448 N; vertical specimen loading; wedge-action type grip.

PEEK, poly(ether ether ketone); PMMA, poly(methyl methacrylate).

based on Halpin-Tsai equations, although the AM process will become complex and difficult beyond a certain fiber aspect ratio and fiber content.

The effects of extrusion are prominent specifically through the addition of second-phase particles that have different properties compared to the polymer (Newtonian vs. viscoelastic). This has been observed both in the case of fiber-reinforced thermoplastic as well as thermoset composites. Calvert et al. (1997) demonstrated the alignment effects due to extrusion of short fiber composites both for thermoplastics and for thermoset composites (Peng, Lin, and Calvert 1999). Table 2.4 is a listing of typical mechanical properties reported by Peng et al. showing the difference in properties when the material is deposited in directions perpendicular and parallel to the length of the bar in a thermoplastic composite material composition. There is a clear anisotropy in the properties in the two directions, which has to be taken into account while designing components to be fabricated using AM techniques. Figure 2.12 shows the fracture surface of a composite, showing alignment of the fibers as a result of extrusion in a thermoset composite material during the AM process (Calvert, Lin, and Martin 1997).

The effect of fiber orientation on the elastic modulus in epoxy/carbon fiber composites is shown in Figure 2.13. These samples were fabricated by writing the composites at varying angles to the axis of the test bars. It was seen that the modulus of the composite when the fiber axis is parallel to the deposition direction is double that of the composite where the material is deposited perpendicular to the testing direction.

Similar property differences have also been observed by a number of other research groups in the case of chopped fiber-reinforced thermoplastic composite materials (Goodridge et al. 2011; Hao et al. 2006; Kumar and Kruth 2010; Nikzad, Masood, and Sbarski 2011; Zhang et al. 2014). Hao et al. suggest that the presence of fibers do not provide a smooth powder bed and lead to issues in obtaining high density and strength. In their case, the best properties were obtained by coating one type of powder with another type so that the composite powder could be fabricated by a standard AM technique such as SLS (Hao et al. 2006). Zhong et al. (2001) added chopped glass fibers to ABS to create filaments that were used as a feedstock in FDM. They observed that the compatibility of

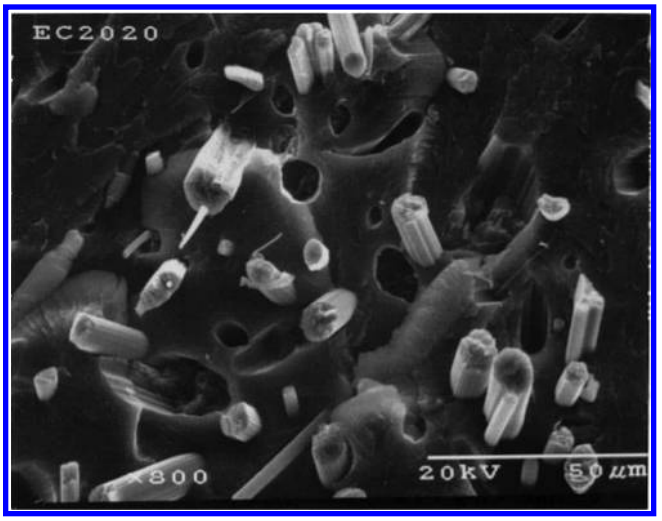

FIGURE 2.12
Fracture surface of a thermoset composite, showing alignment of fibers during extrusion in the AM process. (Data from Calvert, P. et al., *High Perform. Polym.*, 9, 449–456, 1997.)

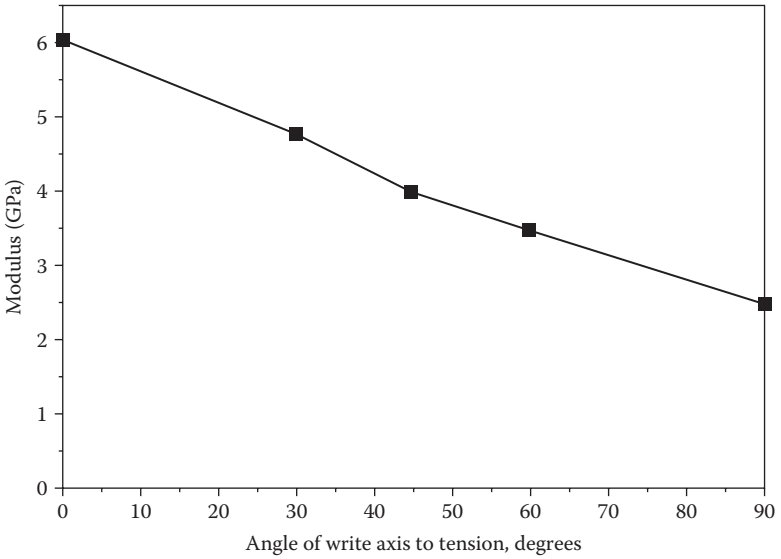

FIGURE 2.13
Measured modulus from three-point bend tests for 18 vol.% glass fibers, aspect ratio 7, formed into bars with the write axis inclined to the long axis of the bar.

glass fibers to the thermoplastic ABS matrix is enhanced through the addition of a compatibilizer like hydrogenated Buna-N that has butadiene and acrylonitrile groups, structurally similar to ABS (Zhong et al. 2001). It was observed that the mechanical properties, toughness, and the appearance of the filament were improved compared to blends with no glass fibers or compatibilizers.

2.4 AM Processes Applicable to Nanocomposites

AM processes are especially suitable for nanocomposites that need very high forces to be extruded into complex shapes, especially since these forces may limit the amount of nanofiller that can be added to the composite beyond a certain level. Additionally, it is well known that the amount of nanofiller that can be added may be limited due to agglomeration and low surface energy of the particles (Njuguna, Pielichowski, and Desai 2008).

Shofner et al. investigated the effect of an AM process (extrusion freeform fabrication) in ABS filled with single-walled nanotubes (SWNTs) and vapor grown carbon fibers (VGCFs). The addition of 5 wt.% SWNT improved tensile modulus by 93% and tensile strength by 31%, respectively. Similarly, 5 wt.% VGCF improved tensile modulus by 44% and tensile strength by approximately 27%, respectively. This is shown in Figures 2.14 (tensile strength) and 2.15 (tensile modulus), respectively (Shofner et al. 2003).

The effect of extrusion in the fiber alignment in a VGCF/ABS composite is shown in Figure 2.16. It can be seen that the AM process would still achieve preferred fiber orientation even when the fibers are nanosized. Compared to an ABS blend with nanofillers that shows uniform dispersion (Figure 2.17), there is clear evidence of fiber alignment after the AM process. The nozzle size that is used for the AM process however would need to be approximately 50–100 times that of the diameter of the fillers, as suggested by Calvert (pers. comm.). Having a nozzle size that is smaller could potentially lead to clogging and rapid increase in the pressure required to extrude the polymer blend. This is one of the reasons why the standard FDM process is not capable of extruding polymer blends with high solids loading (>50% by volume) and high fiber loading (>30% by weight).

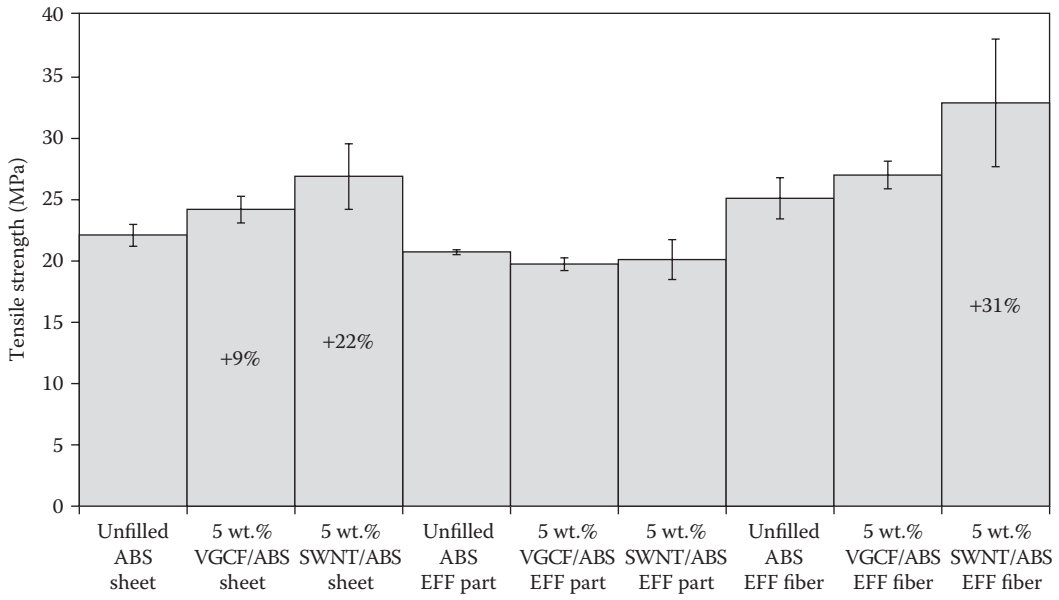

FIGURE 2.14
Tensile strength of filled ABS materials before and after AM processing. Percent changes are given for statistically significant differences.

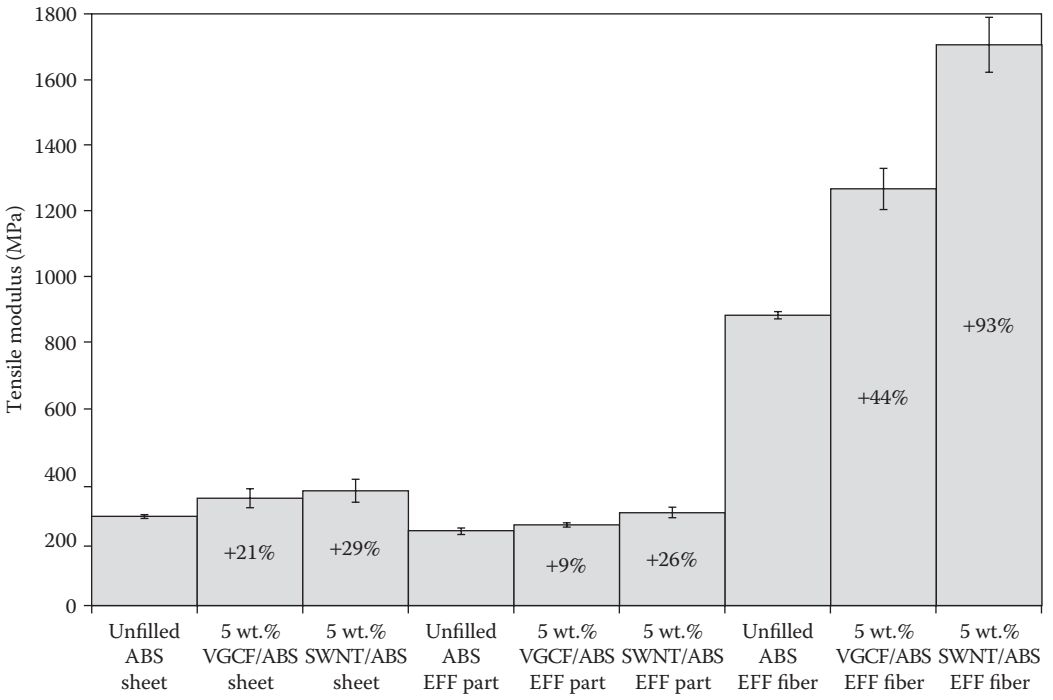

FIGURE 2.15
Tensile modulus of filled ABS materials before and after AM processing. Percent changes are given for statistically significant differences.

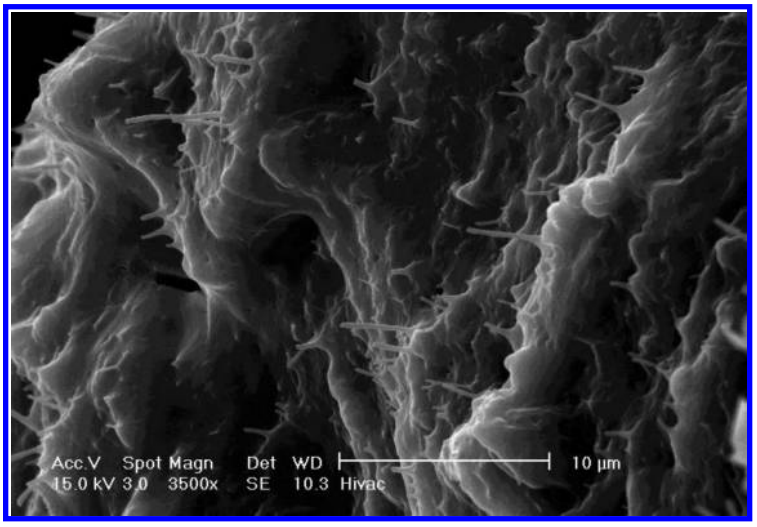

FIGURE 2.16
Scanning electron microscopy (SEM) image of a 5 wt.% VGCF/ABS composite subjected to selective dissolution after AM processing. (Data from Shofner, M.L. et al., *Compos. A: Appl. Sci. Manufact.*, 34, 1207–1217, 2003.)

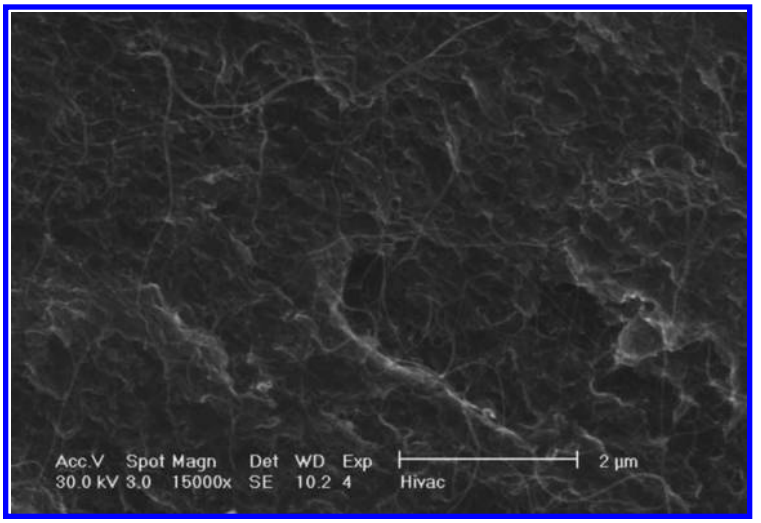

FIGURE 2.17
SEM image of a 5 wt.% SWNT/ABS composite after blending in a high shear mixer, showing good dispersion and distribution. (Data from Shofner, M.L. et al., *Compos. A: Appl. Sci. Manufact.*, 34, 1207–1217, 2003.)

Farmer et al. (2010, 2012) have recently proposed a method for combining the synthesis of aligned carbon nanotube (CNT) *forests* on a substrate, curing a thermoset polymer using a UV curable resin, and building it up layer by layer. Figure 2.18 is a schematic of the proposed AM process. A thin layer of UV curable thermosetting polymer is first spread on the part bed. An array of CNTs are grown in another part of the chamber and transferred onto the part bed. The CNTs are held in place either by interfacial forces or by partially curing the CNT/resin combination. A laser beam is then used to raster the resin surface and cure the resin. The part bed is then dropped such that another thin layer of resin can be introduced on the surface. A second layer of CNTs is introduced on the surface and the process is continued. However, even though the growth of CNT forests is a well-developed

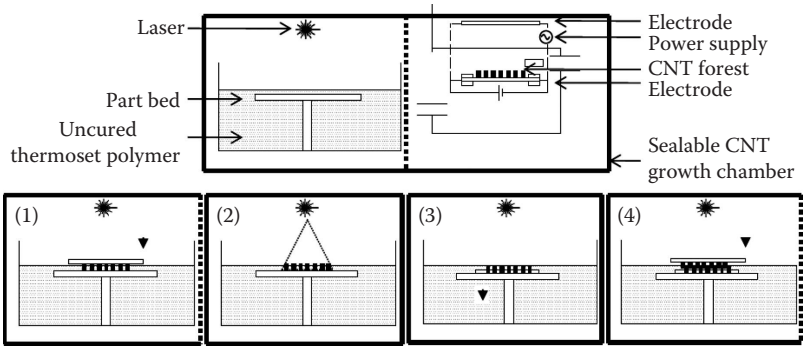

FIGURE 2.18
Schematic of the required apparatus for combined CNT growth and additive manufacturing of nanocomposites. (Data from Farmer, B.L. et al., Strategies to combine nanocomposite and additive layer manufacturing techniques to build materials and structures simultaneously, Paper read at *ECCM15—15th European Conference on Composite Materials*, June 24–28, Venice, Italy, 2012.)

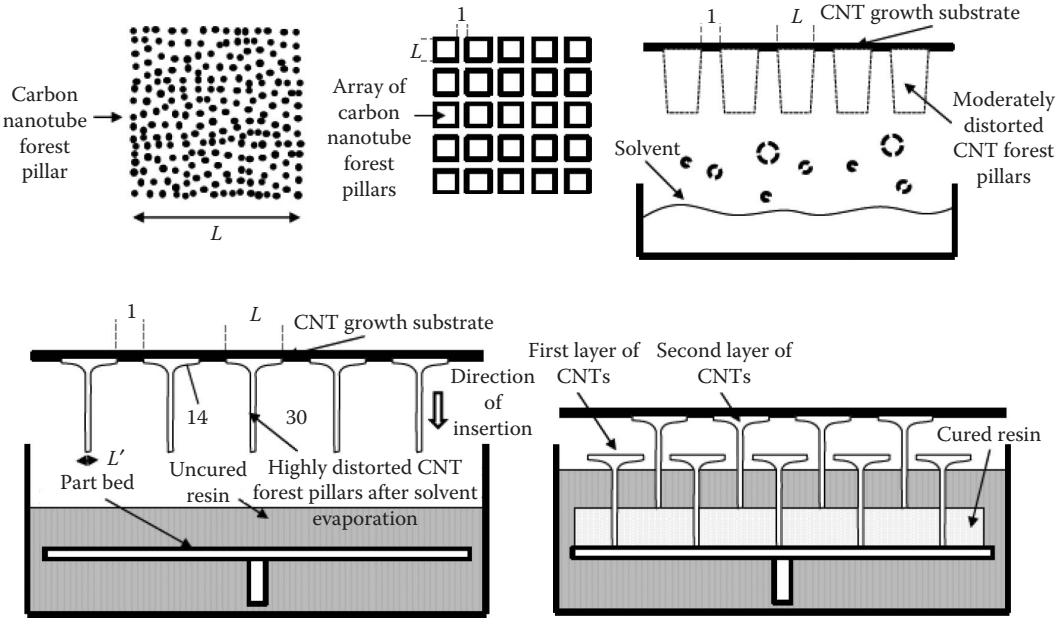

FIGURE 2.19
Process schematic for AM fabrication of polymer composites reinforced with carbon nanotube bundles.

process, the combination of CNT and the AM process is still in development. The technology may become successful after it takes into account the difficulties related to the removal of the resin from areas where it is not needed in the individual layers as well as how support structures could be introduced into the build process.

Farmer et al. also investigated the use of partial wetting of the CNT forest to evaluate interleaving of CNT layers by using a patterned array to ensure through thickness continuity. This was necessary to hold the CNT bundles in place and have the resin wet and cure or bond to the bundles in place. This was done by dipping the CNT bundles in the resin matrix. In the case of thermoset resins, the partial wetting was possible till the curing temperature at which the resin viscosity dropped considerably, leading to wetted areas breaking up into pillars. Partial wetting was possible in the case of thermoplastic resins, but it was a challenge to confirm that partial wetting was obtained (Farmer et al. 2012).

Farmer et al. (2012) also proposed a modification to the procedure described in Figure 2.18 to increase the volume loading of the reinforcements. A schematic strategy for this approach is shown in Figure 2.19. Additional modifications are possible where fiber orientation control would be possible both interlayer and intralayer.

2.5 AM Processes for Continuous Fiber-Reinforced Composites

The AM processes that have been developed so far for continuous fiber-reinforced composites are variations of the automated tow placement (ATP) process originally developed for laying down different composite prepreg layups. One of the earliest processes developed and demonstrated by Don Klosterman and others at University of Dayton

Research Institute (UDRI) was based on an improvement of the laminated object manufacturing (LOM) technique for designing and manufacturing ceramic matrix composites (Klosterman et al. 1998, 1999; Meilunas 2001; Meilunas, Dillon, and Nardiello 2002). This was funded from among the second set of solid freeform fabrication projects funded by DARPA and the Air Force and carried out by a team from Northrop Grumman, Helisys, and UDRI (Meilunas 2001). This team was put together by a set of individuals who had worked on previous DARPA funded projects related to low cost ceramic composites (LC3) and solid freeform fabrication of ceramics from the early to mid-1990s. The AM process that was developed was a follow-up project from the LC3 program (Gonczy and Sikonia 2005) funded by DARPA from 1991 to 1997.

The basic issue with AM of continuous fiber-reinforced composites is that none of the AM processes are really capable of accommodating continuous fiber preforms or prepregs or woven mats, including the use of a laser to accurately machine the ends of the fibers after each layer is laid down over the previous layer. It is difficult or impossible for AM processes to take into account the geometrical issues such as fiber orientation and fiber continuity. For the first time, this group demonstrated that it was possible to modify the LOM process to include fiber-reinforced structures, especially thin, curved shell components. It should be noted that this process was developed when the AM process development was still in its infancy and the software and hardware capabilities were still being resolved. The process needed to take the following issues into account (Meilunas 2001):

- The curved LOM process (previously developed at UDRI under DARPA funding) (Klosterman et al. 1999) had several limitations to generate complex curved structures.
- The curved LOM system as set up originally had several hardware and software inadequacies that impeded further hardware/software upgrades. Additionally, the build envelope of the curved LOM machine after modifications was smaller compared to required part sizes. The curvatures that could be introduced into the component could not be built without introducing wrinkles during the layup process.
- This limited the commercial viability of the LOM process to be adapted for continuous fiber-reinforced composites and components.

In order to account for the possible complex geometries and sizes that could be encountered in a component, it was found necessary to modify the build sequence in the curved LOM so as to avoid the potential to introduce wrinkles in the part during the layup process. The original curved LOM equipment had a scanning galvanometer-based mirror system that had to be changed to a galvo scanner, which provided better laser positioning accuracy and more uniform corner cutting and better edge definition in finished parts (Meilunas 2001). Due to several of these problems, the UDRI-Northrop Grumman team decided to procure a new curved LOM system that was capable of handling all the technical issues raised during the initial stages of the project.

The modification to the original plan combined the commercial 2D LOM build process with a final composites forming step resulting in curved composite components, as shown in Figure 2.20. The final step could be achieved by using either a matched mold or a diaphragm to compact the laminate as the final step. The benefit of this process is that it can decrease manufacturing costs and obtain consistent properties by eliminating any unnecessary or time-consuming hand layup procedures (Meilunas 2001).

In the process schematic shown in Figure 2.20, a series of ply stacks are generated using commercially available CAD/CAM software or other software such as FiberSIM.

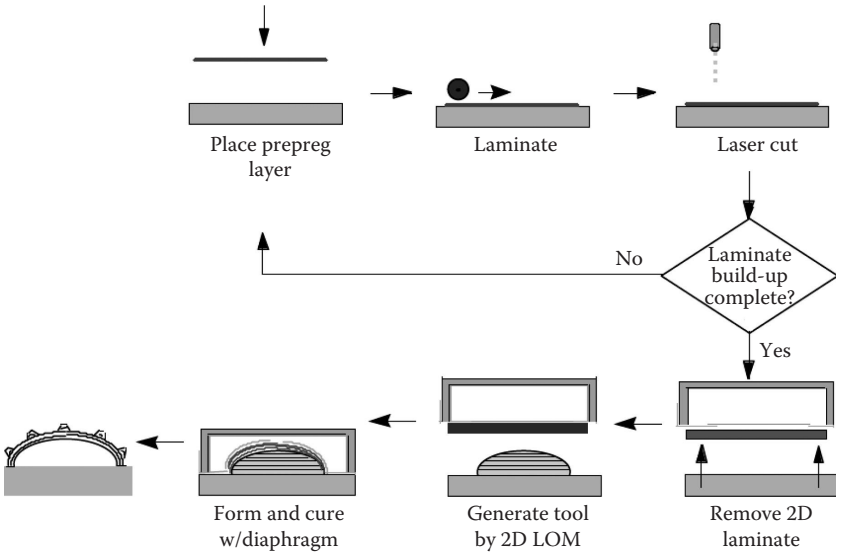

FIGURE 2.20
Schematic of curved LOM/composite forming process developed by UDRI/Northrop Grumman. (Data from Meilunas, R. Laminated object manufacturing-based design ceramic matrix composites. Final Report No. AFRL-ML-WP-TR-2001-4074, DARPA/Wright Patterson AFB, 2001.)

The ply stack data are then utilized by the LOM system to fabricate individual flat 2D laminate preforms incorporating any layup sequence. Utilizing this ply stack data, the LOM system can now fabricate individual (2D) laminate preforms incorporating any cuts or darts in individual ply layers that can be used to drape the laminate over a curved tool. The final step is to place a conformable vacuum diaphragm on top of the tooling and the prepreg layers and to cure it in place. This curing can be done either on the LOM machine itself or in a separate oven. Several other modifications were also made.

The major advantages of this technique are (Meilunas 2001)

- The laser positioning equipment installed in the modified LOM machine allowed increased accuracy and speed.
- The LOM machine allowed the integration of fiber-reinforced composites analysis software to be integrated to the layup selected and built.
- It is possible to modify the geometric shape of the individual plies prior to the final consolidation step, allowing extremely complex geometries to be fabricated using AM processes.

A schematic of the composites forming cell and the actual forming cell built under this project is shown in Figure 2.21, while Figure 2.22 shows the actual setup. It consists of a vacuum box of approximate internal dimensions of 775 mm × 550 mm × 200 mm. There are two 1.9-mm-thick silicone rubber diaphragms that are bonded to individual 76 mm wide aluminum frames and a heat lamp array of six 375-watt IR lamps that are mounted on adjustable sockets. The bottom silicone rubber is opaque while the top silicone rubber is transparent so as to provide efficient heat transfer to the curing process. There is also a

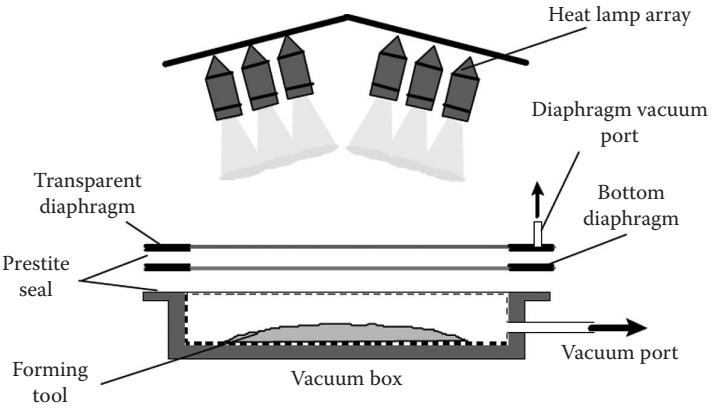

FIGURE 2.21
Schematic of composites forming cell for LOM. (Data from Meilunas, R. Laminated object manufacturing-based design ceramic matrix composites. Final Report No. AFRL-ML-WP-TR-2001-4074, DARPA/Wright Patterson AFB, 2001.)

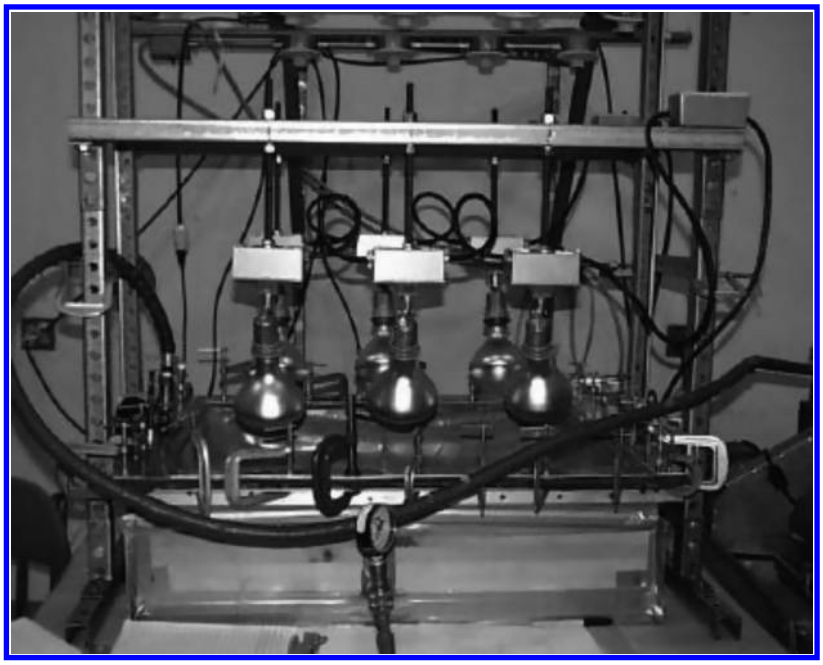

FIGURE 2.22
LOM composites forming system. (Data from Meilunas, R. Laminated object manufacturing-based design ceramic matrix composites. Final Report No. AFRL-ML-WP-TR-2001-4074, DARPA/Wright Patterson AFB, 2001.)

vacuum port on the aluminum frame attached to the top diaphragm for pulling a vacuum during the curing process (Meilunas 2001).

A modified LOM equipment used to fabricate the demonstration component is shown in Figure 2.23, while the demonstration component made using the LOM/composite forming technology is shown in Figure 2.24.

FIGURE 2.23
Modified LOM2030H system with laser scanner subsystem. (Data from Meilunas, R. Laminated object manufacturing-based design ceramic matrix composites. Final Report No. AFRL-ML-WP-TR-2001-4074, DARPA/Wright Patterson AFB, 2001.)

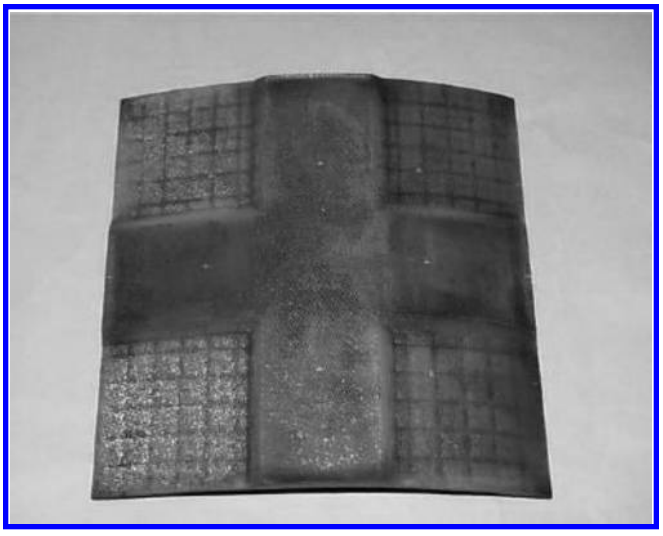

FIGURE 2.24
200 mm × 200 mm Nextel 312/Blackglas resin composite fabricated using LOM/composite forming AM process. (Data from Meilunas, R. Laminated object manufacturing-based design ceramic matrix composites. Final Report No. AFRL-ML-WP-TR-2001-4074, DARPA/Wright Patterson AFB, 2001.)

Yet another method developed in the early 2000s was a technique based on the ATP for polymer composites (Don, Gillespie Jr, and McKnight, 1997) and adapted for ceramic matrix composites such as C/SiC and C/ZrC (Vaidyanathan et al. 2005). The ATP process is an enabling technology, developed originally for thermoset composites and more recently for in situ non-autoclave consolidation of large-scale thermoplastic composite materials for high speed civil transport applications. The knowledge base of the ATP process for thermoplastic prepregs can be utilized to lay down ceramic tows in the desired configuration, thus allowing the use of a proven technology for low cost, rapid fabrication of large complex ceramic parts.

The ATP system employs two hot-gas nitrogen torches to heat the material and two rollers to provide the pressures required for consolidation. The purpose of the first torch and roller is to preheat the composite surface and incoming tow together. The material is thus *tacked* to the surface with this roller. This tacking procedure is useful in that the fed material is carefully bonded to the surface and not pulled with the main consolidation roller. This tacking approach also aids in improving the efficiency of the cut and re-feed mechanism. The second torch (main heater) provides supplemental through thickness heating to facilitate consolidation and bonding of the tow and substrate under the consolidation roller. These rollers provide the necessary forces to achieve complete intimate contact across the tow interface, and as a boundary pressure for preventing any internal void development. The forces applied to both rollers are controlled independently using a series of pneumatic actuators. The composite tows can be placed in a regular repeating pattern or with brick-face symmetry. The brick-face geometry has the advantage that more homogeneity is achieved throughout the composite structure. An image of the ATP equipment used is shown in Figure 2.25, while a schematic of the process is shown in Figure 2.26.

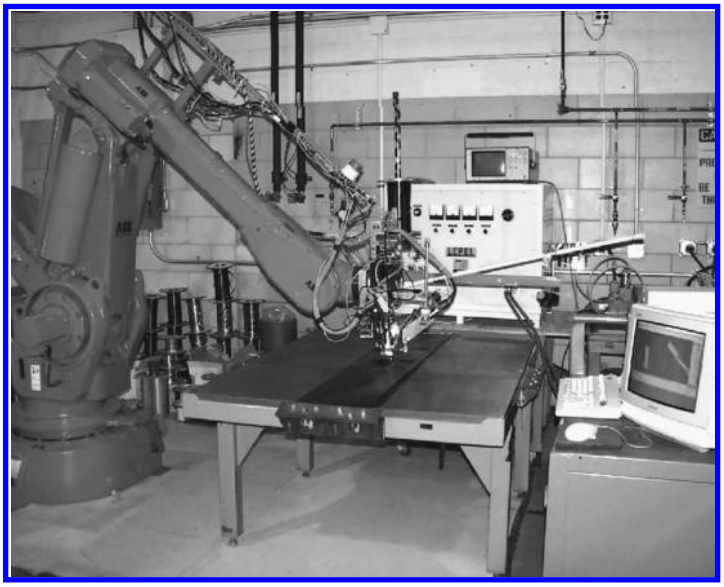

FIGURE 2.25
(See color insert.) A typical ATP setup used. (Data from Yarlagadda, S., Automated Tow Placement of Composites, 2014.)

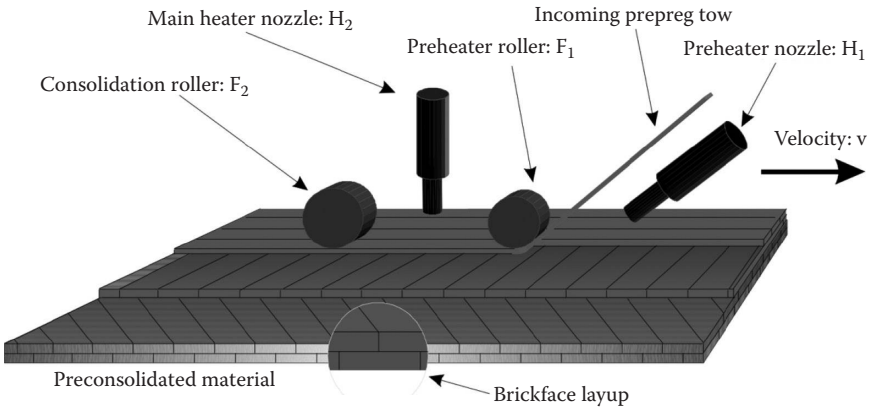

FIGURE 2.26
Schematic of the ATP process. (Data from Yarlagadda, S., Automated Tow Placement of Composites, 2014.)

The ATP process for thermoplastics lays down prepreg tows, typically 0.125–0.2 mm in thickness, with the tow width depending on the hardware. The ATP head can lay down 6.25 mm wide tows, while industrial machines, such as Cincinnati Milacron's Gantry System, can lay down tows as wide as 150 mm. The modified ATP or ceramic composite ATP (CCATP) was primarily developed for a class of materials termed fibrous monoliths (Kovar et al. 1997) reinforced with carbon fiber tows. However, issues such as difference in thermal expansion coefficient between the matrix and the fibers are still outstanding and the technique is not yet fully developed. For example, the large mismatch between the coefficient of thermal expansion (CTE) of ultra high modulus (UHM) carbon fiber (-0.5×10^{-6} ppm K^{-1}) and the SiC matrix (3.6×10^{-6} ppm K^{-1}) will result in residual stresses and cracks within the post-consolidated matrix. Incorporating a suitable interfacial material is crucial in reducing or eliminating matrix cracking in composites caused by the CTE mismatch between matrix and fiber. Composite strength and toughness are improved when the interface material deflects matrix cracks. Accordingly, a boron nitride interface was applied between the fibers and the matrix prior to its introduction into the matrix.

Typical process parameters for tow placement of thermoplastics are listed in Table 2.5. These parameters are optimal for APC/PEEK system, which has a glass transition temperature of 156°C and a melting temperature (PEEK is semi crystalline) of 332°C. In contrast, the thermoplastic binder used in a ceramic matrix system has a processing temperature in the range of 100°C–140°C.

The critical process parameters are torch temperatures, torch heights, head velocity, and consolidation force. Initial estimates on suitable operating ranges for these parameters were based on thermal models developed for the ATP process. Based on these models, process maps relating material temperature, head velocity, and torch temperatures are generated.

Several process modifications were performed to obtain better quality material and are listed as follows:

- The preheater torch is set to operate at 500°C.
- Roller 1 is disabled.
- The main heater torch is positioned to actively cool roller 2.
- Gas flow rate for preheater torch is at 50 L min^{-1} and for main heater torch (now actively cooling) at 25 L min^{-1}.

TABLE 2.5

ATP Process Parameters for Carbon/PEEK Prepreg Tows

Process Parameter	Value
Initial thickness of tow	0.1778 mm
Width of tow	6.35 mm
Radius of roller 1	15.8 mm
Radius of roller 2	19.0 mm
Roller 2 location	80 mm from tacking roller
Initial composite temperature	100°C
Initial roller temperature	25°C
Ambient air temperature	25°C
Gas flow rate in torches	50 L min^{-1}
Location of preheater torch	75 mm from nip point location
Location of main torch	35 mm from nip point
Torch temperatures	850°C
Torch heights	Variable
Head velocity	Variable (up to 100 mm s^{-1})
Consolidation force	300 N
Panel size	150 mm × 150 mm
Fiber orientation	Full range (−90 to +90)

The modified setup is shown in Figure 2.27. Roller 1 has been disabled completely, by positioning it above roller 2. During tow placement of thermoplastic tows, roller 1 was used to tack hot prepreg to the laminate and prevent it from being pulled by the consolidation roller (roller 2). In the present case, the ceramic tows have a much lower processing temperature, so that one heater torch and one roller are sufficient to achieve good tack and consolidation. The main heater torch has been positioned above roller 2 to actively cool it

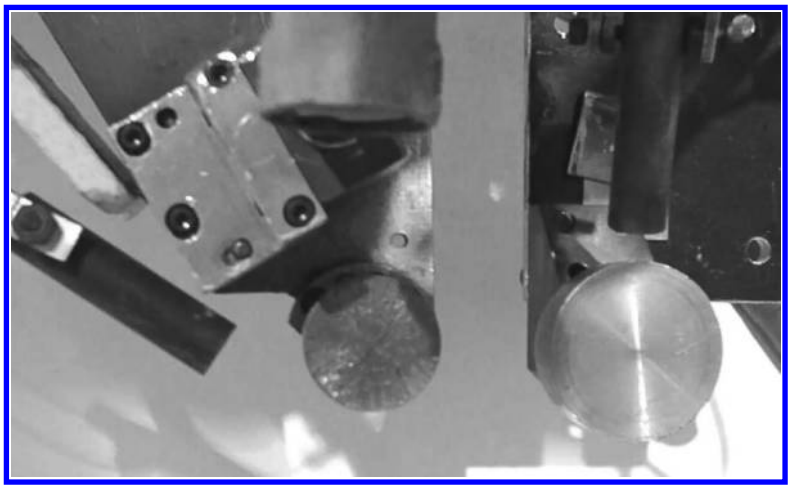

FIGURE 2.27
Modified ATP head configuration for ceramic tow placement, with roller 1 disabled (raised above roller 2). (Data from Vaidyanathan, R. et al., *JOM*, 52, 34–37, 2000.)

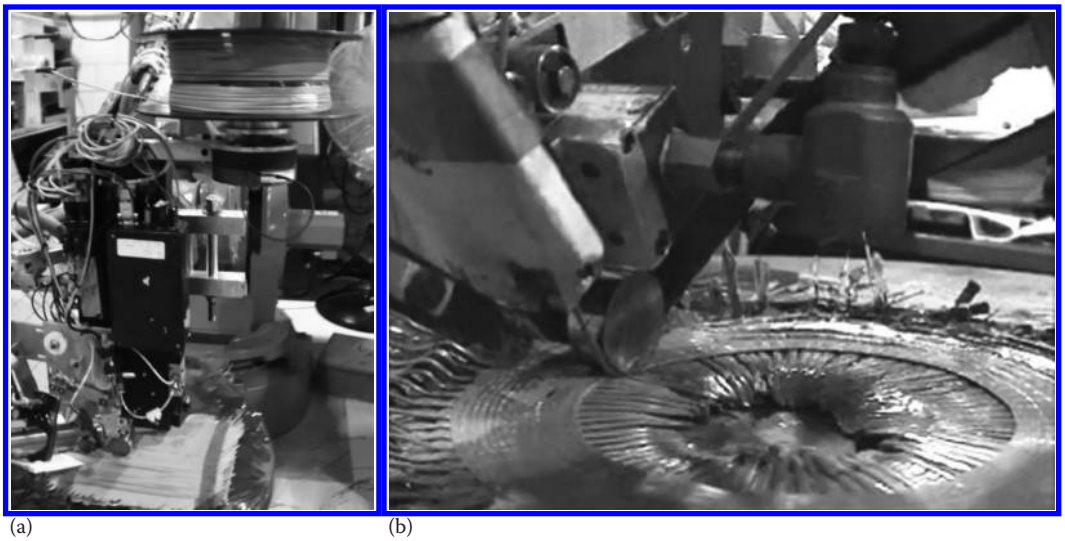

FIGURE 2.28
ATP fabrication of (a) a composite panel and (b) a blisk component using a turntable/winding mandrel consolidating ceramic tows for the laminate. (Data from Vaidyanathan, R. et al., *JOM*, 52, 34–37, 2000.)

and maintain its temperature below the glass transition temperature of the thermoplastic binder. This prevents the matrix of the tows from adhering to the roller and creating bare fiber spots and inconsistent quality.

A turntable/winding mandrel system (Figure 2.28) with an accuracy of ±1° was used. The system can be used in a horizontal mode (for flat components) or vertical mode (for axisymmetric components such as thrusters and cylinders). This device can interface directly with robot programming software to perform the CAD/CAM implementation on the ATP head. This modification can also improve the life of the robot. The Robotstudio software aids in simulating the tow placement process and provides the tool path information to the ABB robot. An image of the simulation from consecutive layers is shown in Figure 2.29.

The process parameters for CCATP are listed in Table 2.6. Some typical components fabricated are shown in Figure 2.30. The entire robot movement sequence is set up by computer programs developed for the ATP thermoplastic tow placement experiments. The torch parameters (temperatures, heights, and gas flow rates), consolidation force, and head velocity can be controlled on the fly as inputs to the computer program. Final panel dimensions and layup sequences are also inputs to the program. Once these inputs are given to the program, it can operate the robot in automatic mode and lays down the tows as specified. Green ceramic matrix laminates of any size (within limits of the robotic workcell), fiber orientation, and material system can be fabricated by this technique. The work in the project was not focused on optimizing process parameters, but on demonstrating the feasibility of rapid, low cost fabrication of fiber-reinforced ceramic composites.

As can be seen from the images of the ATP fabricated panels (Figure 2.30), the tow-placement mechanism experienced some difficulties regarding the nature of the juxtaposed tow placement. Some tows were not placed in a straight, in line fashion, resulting in some gaps between adjacent tows. There are four major issues identified that will need

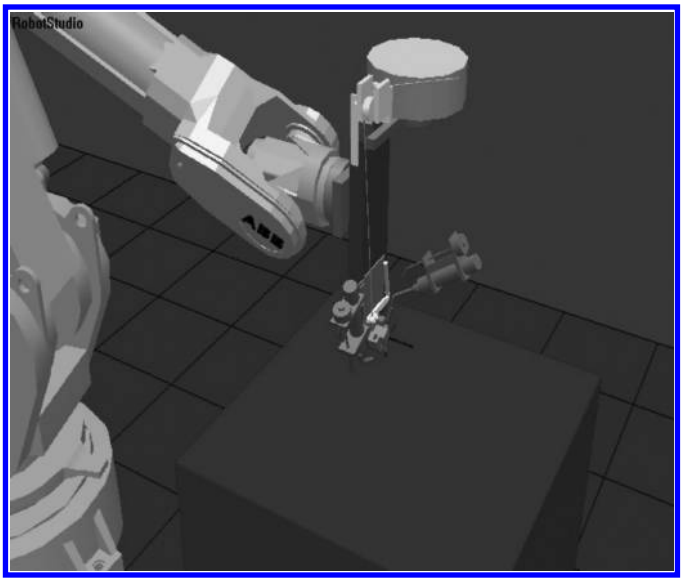

FIGURE 2.29
A simulation of the tool path from Robotstudio software. (Data from Yarlagadda, S., Automated Tow Placement of Composites, 2014.)

TABLE 2.6

Process Parameters for Ceramic Tow Placement of CMC Laminates

Process Parameter	Value
Initial thickness of tow	1.0 mm
Width of tow	2.0 mm
Roller 1	Disabled
Radius of roller 2	19.0 mm
Roller 2 location	80 mm from roller 1
Gas flow rate in preheater torch	50 L min^{-1}
Gas flow rate in main torch	25 L min^{-1}
Location of preheater torch	75 mm from nip point location
Location of main torch	Above roller 2
Preheater torch temperature	500°C
Main torch temperature	25°C
Preheater torch height	Maximum (12 mm)
Head velocity	50 mm s^{-1}
Consolidation force	Minimum (190 N)

to be addressed if the CCATP were to be adopted by the AM enthusiasts. These are as follows:

- Tape width
- Tape overlap requirements in the planar and thickness directions
- Gap between adjacent radial fibers in a polar weave configuration
- Rotation speed

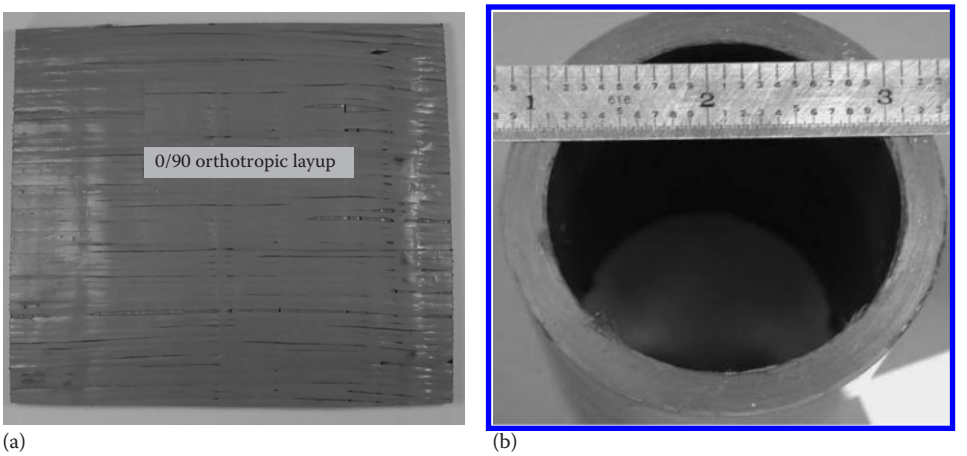

FIGURE 2.30
Some typical components fabricated using the CCATP process. (a) sintered orthotropic 0/90 composite panel and (b) sintered composite tube. (Data from Vaidyanathan, R. et al., *JOM*, 52, 34–37, 2000.)

Jang et al. (1999) also received a patent in 1999 for AM processing of fiber-reinforced composites. However, this is more a description of a process rather than the actual examples of continuous fiber-reinforced composites built by AM processes. Similarly, Ryan Dehoff and Lonnie Love at Oak Ridge National Laboratory run a manufacturing demonstration facility that appears to be more on the lines of the extrusion freeform fabrication of high-strength polymers filled with chopped carbon fibers (Dehoff 2014). MarkForged (2014) is one of the many 3D printing machines that can handle carbon fiber-reinforced composites, although this also seems to be a polymer filled with chopped carbon fibers. What is exciting is that the technology developed at Oak Ridge National Lab is now being used to produce the world's first 3D printed automobile that was test run at the International Manufacturing Technology Show (IMTS) in Chicago in September 2014. Reportedly, the entire car body was built in 44 hours on-site using a huge 3D printing machine. If AM technologies have to truly take off, such acceptance needs to come from the public so that the machine manufacturers as well as users can adopt and adapt to new materials based on fiber-reinforced composites. The challenge of continuous fiber-reinforced composites is still remaining and needs to be resolved for it to be adapted to AM.

2.6 Role and Selection of Appropriate Binders for AM Processes

In an AM freeforming system for ceramics, the feedstock, consisting of ceramic powders plus wax binder, melts during deposition, especially if it is based on extrusion. After extrusion, the binder has to be removed very carefully and the part is then sintered. The feedstock typically comprises a multicomponent blend of waxes and polymers with greater than 50 vol.% ceramic powder (typical volume percentages). The feedstock's melting and flow properties and the binder behavior during removal are crucial to the process and need to be characterized for both process development and QC purposes.

The rheology of particle-filled polymers is very sensitive to particle content, particle surface chemistry, and the binder chemistry at these high volume fractions. Therefore, it is critical that the appropriate binder be chosen based on the type of AM processing methodology chosen.

For example, the quality of the green ceramic feedstock has a strong influence upon the robustness of the process and its ability to reproducibly fabricate high-strength, dimensionally accurate ceramic components using the extrusion-based processes such as fused deposition of ceramics (FDC) (Agarwala et al. 1996) and the extrusion freeforming (EFF) (Vaidyanathan et al. 2000). A high degree of homogeneity is desirable in order to minimize density gradients between the binder and ceramic powders. If density gradients are present in the feedstock, it could lead to non-uniform firing shrinkage and formation of defects within the freeformed ceramic bodies. The feedstock should also possess a reproducible rheology so that it can be accurately freeformed into the desired green ceramic component. Further requirements for the rheology of EFF feedstock are a low melt viscosity (extrudable at low pressures) as well as the ability to undergo rapid solidification upon deposition (enabling more rapid part build rates). The binder should be easily removable from the freeformed green bodies under controlled conditions and leave minimal pyrolysis residue. The ease of binder removal is determined by the binder burnout schedule, which in turn is defined by the part thickness. Finally, the resulting bodies should be readily sinterable into dense ceramic components.

The following is an example of how the rheological properties will affect the AM process and how the polymer binder composition will affect the final component features and properties. Adding a ceramic powder such as Si_3N_4 to the binder increases its viscosity quite considerably, even at very low shear rates (1–10 s^{-1}). There also appears to be a critical solid loading content, beyond which the viscosity of the filled systems would increase dramatically. Figure 2.31 is a representation of the viscosity of the filled systems as a function of solids loading content at a constant shear rate of approximately 1 s^{-1}. The critical

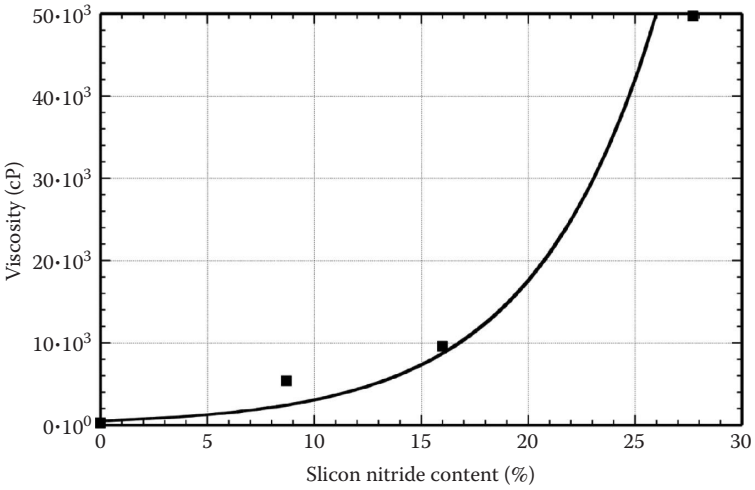

FIGURE 2.31
Variation of viscosity versus silicon nitride content in a typical polyethylene co-ethacrylate (EEA)-based binder system.

viscosity limit for the binder used was obtained at approximately 15% by weight, in the case of Si_3N_4.

Dynamic rheological measurements are another powerful method for predicting the extrusion behavior of a ceramic formulation that is used in an extrusion-based AM process. Dynamic rheological characterizations presented below were made using a Rheometrics model controlled-stress rheometer. Dynamic measurements characterize the flow of materials at near equilibrium states by applying a small strain. There are two types of dynamic measurements. In the first type, external sinusoidal conditions of known frequency and amplitude are imposed on the fluid to induce an oscillatory flow. The frequency, amplitude, and phase of the response of the fluid are measured. The second type is relaxational flow where under external conditions such as force or strain, the fluid undergoes a rapid change from one steady state to a second steady state. The response of the fluid as it approaches a new equilibrium state is then measured.

Dynamic viscosity response as a function of frequency is essentially similar to the steady shear viscosity versus shear rate response for unfilled polymers (Bigg 1982). The basic equations are given below.

$$\gamma = \gamma_o \sin \omega t \tag{2.1}$$

$$\gamma' = \gamma_o \omega \cos \omega t \tag{2.2}$$

$$\tau = \tau_o \sin\left(\omega t + \delta\right) \tag{2.3}$$

where:

τ is the shear stress

t is the time

ω is the frequency of rotation of the viscometer plate

$$G' = \left(\frac{\tau_o}{\gamma_o}\right)\cos\delta \tag{2.4}$$

where:

G' is the storage modulus

$$G'' = \left(\frac{\tau_o}{\gamma_o}\right)\sin\delta \tag{2.5}$$

where:

G'' is the loss modulus

$$\eta^* = \left[\left(\frac{G'}{\omega}\right)^2 + \left(\frac{G''}{\omega}\right)^2\right]^{0.5} \tag{2.6}$$

where:

h^* is the dynamic viscosity

Dynamic measurements are frequently applied at low shear rates approaching zero to characterize polymer structures (Bigg 1983). For uncross-linked polymers, at very low

frequencies, η* approaches to η (steady flow viscosity) but for cross-linked polymers increasing frequency causes η* to fall monotonously. The rheological response of a suspension depends on the degree and strength of particle–particle interactions and particle–matrix interactions. Most suspensions could be classified into three types, based on the concentration. The first type is a dilute concentration, where the individual filler particles do not interact with each other. The response of such a suspension is primarily that of the matrix. At a certain concentration, the individual filler particles begin to interact with neighboring particles. Such interactions are limited to particles in a local neighborhood. This is the second type of suspension. The concentration at which these particle–particle interactions begin depends on the geometry and surface activity of the filler particles. The third type of suspension is where the filler particles form a complete network within the matrix. In such a suspension, the movement of each particle affects the position of all the others, the effect diminishing with distance away from the particle in question. This also depends on the nature of the particles. In an extrusion-based AM process, these forces and interactions are critical and need to be taken into account.

Dynamic measurements should be made at a temperature close to the extrusion temperature. In the case of silicon nitride formulations used in the EFF process (Vaidyanathan et al. 2000), these were made at 150°C, since the extrusion of the standard silicon nitride formulation on the high-pressure extruder head is also performed at 150°C. Figure 2.32 shows the measured viscosity as a function of frequency. It can be seen that the viscosity decreases with increasing frequency. This suggests that the formulation has a very shear dependent behavior over the range of 0.1 to 100 rad s^{-1}. Additionally, the formulations are also non-Newtonian and shear thinning. The non-Newtonian and shear thinning nature is dependent on the particle size of the fillers (Kamal and Mutel 1985).

The free-formable slurry evaluated had 55 vol.% ceramic powder (Starck M-11 silicon nitride). Measurements shown below were done in dynamic oscillatory shear. At 150°C and 2% strain, the viscosity was 36 kPa s (360 kPoise) at 1 rad s^{-1} and dropped by a factor of 6 per decade of frequency increase (Figures 2.33 and 2.34). This compares with 50 Pa s at 25 wt.% silicon nitride loading and 1 rad s^{-1} frequency. The viscosity also drops roughly in proportion to the reciprocal of the strain. Thus, this material is non-ideal and there are strong particle–particle interactions.

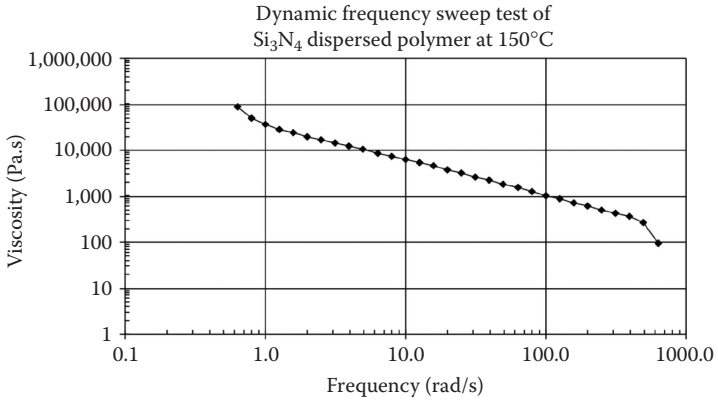

FIGURE 2.32
Viscosity versus frequency response of standard high-pressure extruder-head ceramic feedstock composition.

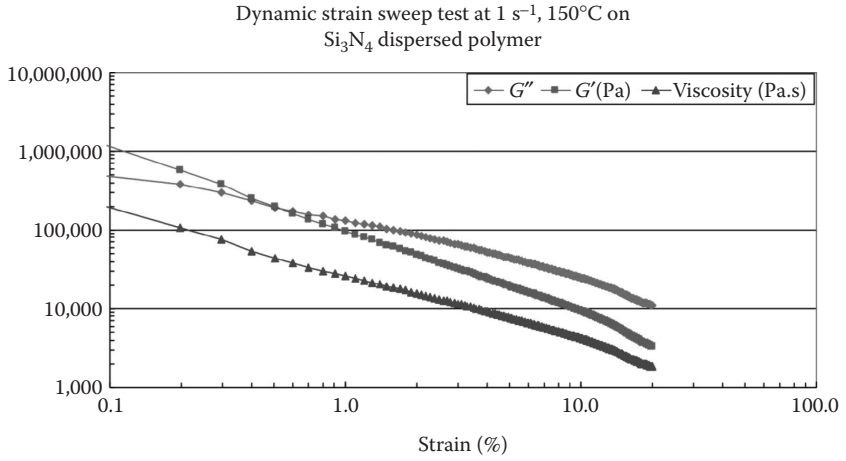

FIGURE 2.33
Storage modulus (G'), loss modulus (G''), and viscosity as a function of strain at a constant frequency of 1 rad s^{-1} and 150°C.

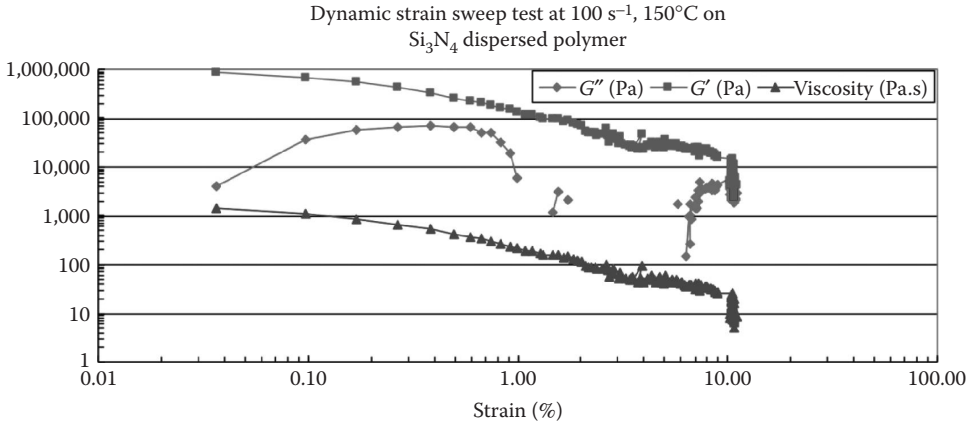

FIGURE 2.34
Storage modulus (G'), loss modulus (G''), and viscosity as a function of strain at a constant frequency of 100 rad s^{-1} and 150°C.

Simple polymer-fluid models predict a viscosity that is roughly constant up to a shear rate equal to the reciprocal of the characteristic relaxation time, after which the viscosity drops. The drop is seen but since there is no plateau at low shear rates, the relaxation time is apparently more than 1 s. The implication is that particle–particle interactions dominate the viscous flow but reform slowly once the melt is sheared.

It is sensible to compare these data with the expected range of operation of this material during freeforming. Taking a capillary of 0.2 mm diameter delivering slurry at 1 cc min^{-1}, a strain rate of about 10^4 s^{-1} could be expected. The viscosity data at 150°C extrapolate to about 30 Pa s at this shear rate. Given a nozzle length of about 3 mm, the drive pressure

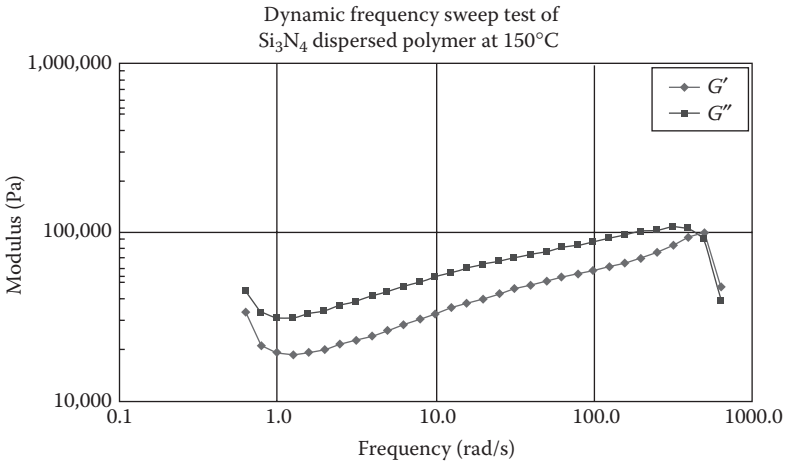

FIGURE 2.35
G′ and *G″* versus ω response of standard silicon nitride feedstock material at 150°C.

needed would be about 3.9 MPa, or 600 psi. However, should the flow stop, the viscosity and pressure would rise by about three orders of magnitude, as there are no shear forces on the material flowing through the capillary. While this may not be the source of any instability that might seen, it is a plausible cause. Another possible reason for the instabilities could be the extensional thickening of the formulation near the capillary opening. The implication is that dispersing agents will need to be added to a ceramic or metal powder formulation that will lead to much lower viscosities at similar particle loadings.

At low frequencies, the response of the polymer dominates the behavior of the system. This accounts for the lower shear modulus at low frequencies. The timescale of the experiment allows for movement of the particles in the molten polymer. From the G′ versus ω and *G″* versus ω plots (Figure 2.35), it can be seen that the loss modulus response as a function of frequency is greater than the storage modulus response. This indicates that the polymer entanglements are not dominating the elastic behavior of the system. If polymer entanglements were to dominate the elastic behavior of the system, the storage modulus response would be greater than the loss modulus response (Dealy 1990). The overall amount of polymer in the binder is lowered or diluted by the addition of a typical plasticizer (Butyl Oleate) and the wax (AL3). This in turn possibly causes the effect of entanglements that are directly attributable to the presence of polymers, to be lowered. At higher frequencies, the particles have less time to move and their motion is further hindered by the close proximity of the neighboring particles. The material behaves more like a solid and *G′* increases with ω. However, we can see a strong dependence of viscosity and *G″* on frequency (Dealy 1982; Ferry 1982; Middleman 1968).

Capillary rheology measurements made using an Instron Model 3211 capillary rheometer are shown here. Viscosity measurements performed at temperatures between 120°C and 150°C. Figure 2.36 shows the viscosity–shear rate response of an EEA-based binder formulation with 55 vol.% Si_3N_4 between 120°C and 150°C. Increasing the temperature from 120°C to 150°C is seen to decrease the viscosity and shear stress by approximately one order of magnitude. These results suggest that the EFF formulations are highly nonstructured and non-Newtonian. Further, the capillary rheometer results generally support the dynamic rheology results.

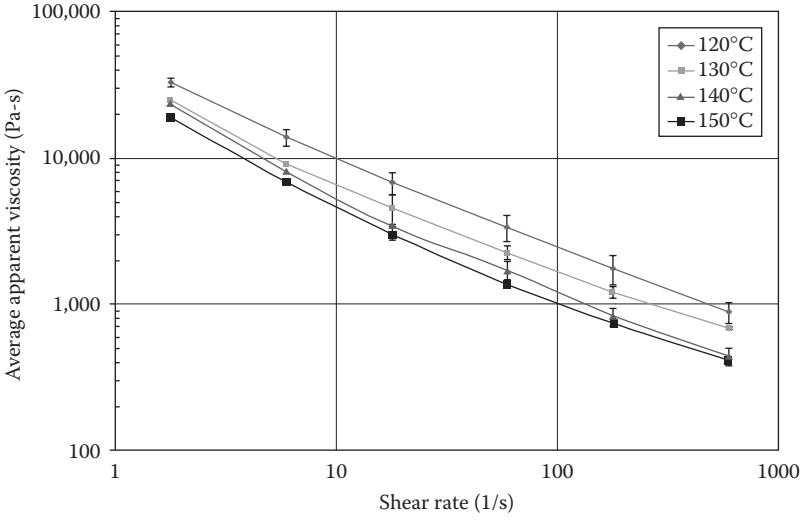

FIGURE 2.36
Shear rate–viscosity relationship for an EEA-based binder system with 55 vol.% Si_3N_4 between 120°C and 150°C.

TABLE 2.7
Typical Green Ceramic Feedstock Composition for EFF

Component	Concentration (vol.%)
Silicon nitride or similar ceramic powder	≈55
Saturated elastomer	≈25
Fatty acid ester plasticizer	≈10
Paraffin wax	≈5
Acryloid additive	≈5

The viscosity of the ceramic feedstock material used in the EFF process is higher than that of the ceramic feedstock material by approximately half order of magnitude in the shear rate ranges investigated. It should be pointed out that 70°C happens to be the FDM temperature of pure binder system used for FDC formulations, due to the reason that the feedstock is in the form of a filament rather than a ceramic powder/polymer binder blend. Therefore, the viscosity of the pure FDC binder system provides a sort of viscosity limit for the FDM process for successful FDC. Since the EFF Si_3N_4 formulation is capable of being freeformed successfully, this suggests that the EFF process can handle the increased viscosity of the ceramic binder systems effectively. This also suggests that increased solids loading in the binder system is possible with the EFF system. A typical feedstock material developed for the EFF process is shown in Table 2.7.

The next step to be taken for a ceramic part to be built with sufficient mechanical properties is to derive an adequate binder burnout cycle to remove the polymer binder. Binder burnout is one of the crucial steps in ceramic processing (Calvert and Cima 1990; Evans and Edirisinghe 1991). The binder is an essential component in ceramic processing, particularly in extrusion freeform fabrication imparting strength to green part (Calvert and Cima 1990). A better understanding and optimization of burnout could allow the processing of

larger ceramic parts by AM processing and prevent defects from being introduced during the decomposition of the binder.

A systematic study of the binder removal process has started only in the last couple of decades (Evans and Edirisinghe 1991). Thus, there is no general basis behind the several nonlinear binder removal temperature–time schedules quoted in the literature, except that the heating rate up to the softening point of the powder-binder formulation is rapid in comparison with that used during the actual pyrolytic degradation of the binder system (Evans and Edirisinghe 1991). It is necessary to modify temperature–time pyrolysis schedules to suit the binder system used, and the powder, which could in some instances assist the thermal decomposition.

A typical process that can be used to optimize the binder burnout cycle, especially those containing a ceramic powder and polymer blend as the binder, is described in the following section. Feed-rods sectioned into pieces with thickness varying from 4 to 20 mm can be used for the optimization of the binder burnout cycle.

The samples are packed in ceramic or graphitic powder bed, placed in high-purity alumina crucibles and heated to 600°C at controlled ramp rates. In most cases, the binder is completely burnt out prior to this temperature. Ramp rates varying from 2, 1, 0.5, 0.2, 0.1, 0.05, 0.03, 0.02 and 0.01°C min^{-1} are chosen. In the experiments conducted, five samples of the same thickness were placed in the crucible and burnt out at each different ramp rate. Samples were taken out of the furnace at regular intervals. The total temperature range from room temperature to 600°C for complete binder burnout was divided into equal temperature zones. All samples were weighed initially before starting the experiment. One sample was drawn during each temperature zone, cooled, and weighed. The weight of the individual samples was normalized to account for the initial weight of the samples. The percentage weight loss was calculated for each temperature zone. The rate of percentage weight loss was calculated by considering the time interval between two temperature set points.

The normalized difference table is shown in Table 2.8 for a sample thickness equal to 5 mm with a ramp rate of 2°C min^{-1}.

The major issues to be concerned with during binder burnout are the prevention of cracks, warpage, delamination, and oxidation. This occurs due to insufficient time for the decomposed products to diffuse out to the component surface and subsequently vaporize.

TABLE 2.8

Normalized Difference Table for a Sample Thickness Equal to 5 mm for a Ramp Rate of 2°C min^{-1}

Temperature (°C)	*%W*	*d(%W)/dt*
35	0	0
85	0	0
135	0	0
185	0.1266	0.005064
235	0.4136	0.001148
285	1.3016	0.03552
335	2.181	0.03517
415	5.2867	0.124288
465	10.6625	0.21503
525	20.5645	0.33
575	20.687	0.0049

TABLE 2.9

Prominent Peak Information from TGA Plot Shown in Figure 2.40

Peak No	Starting Temperature (°C)	End Temperature (°C)	%Wt. Loss Associated
#1	160	250	4.2
#2	350	450	13

Porosity development during this stage can help prevent cracking and warpage. In the EFF process, 3% microcrystalline wax was added as an ingredient. This 3% microcrystalline wax added to the binder may prevent the cracking due to the formation of porous channels. Vaporization at early stages may leave porous channels and help high-temperature degradation products to escape through these channels.

A typical thermogravimetric analysis (TGA) plot showed two prominent peaks at 160°C–250°C and 350°C–450°C, as shown in Table 2.9. These data were obtained by heating the sample in a small platinum pan in flowing nitrogen of 100°C min^{-1} at a ramp rate of 2°C min^{-1}.

The total percentage weight loss in Table 2.9 corresponds to approximately the total initial polymer content in the binder system, suggesting that binder burnout will be complete at 450°C. However, when approximately same weight of the sample (considering same cross-sectional area) was heated at 10°C min^{-1}, the peaks shifted 30°C higher (Figure 2.36). The total area under each peak seemed to be constant. So if the ramp rates are decreased by 5 times (0.4°C min^{-1}), the peaks will shift by 30°C to the left, but this could be compensated with an increase in the thickness of the sample. It was also seen that the individual components are completely burned out by 600°C (Figure 2.37).

Binder evolution events are observed to shift to higher temperatures with increasing ramp rates. Evolution events also should shift to higher temperature with increasing part size (Evans and Edirisinghe 1991). This is mainly because sufficient time is not given to events to reach thermal equilibrium. Due to this thermal excursion, bloating and cracks

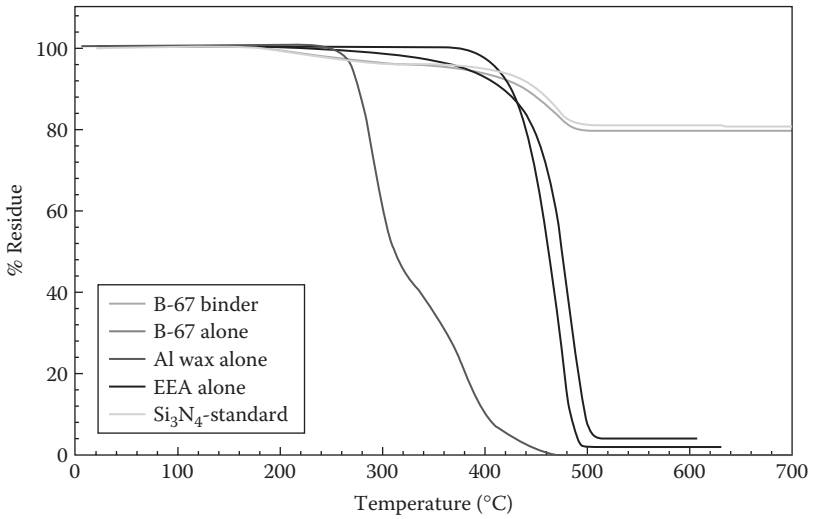

FIGURE 2.37
Thermal decomposition of the binder components and ceramic formulations for AM processes.

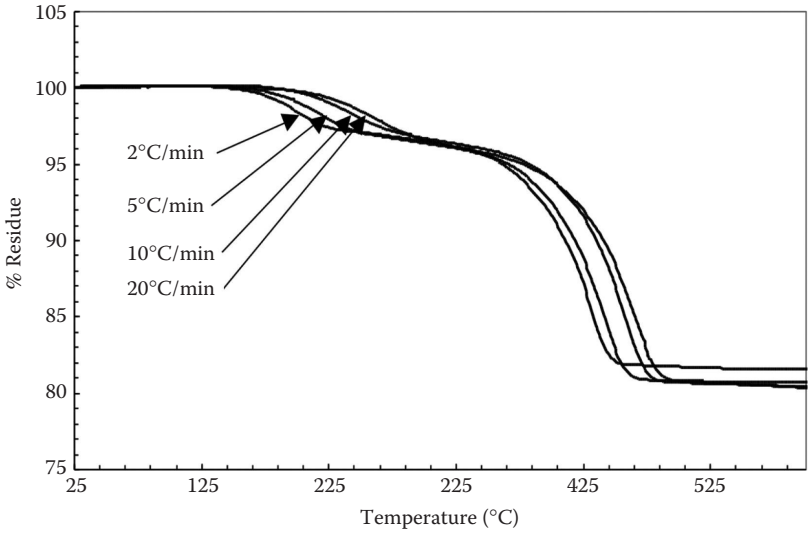

FIGURE 2.38
Effect of ramp rates on the binder burnout of silicon nitride formulations used for extrusion-based AM processes.

are seen in the samples that have undergone higher heating rates, or larger samples where sufficient time is not given for decomposed products to escape to surface (Figure 2.37).

With many factors affecting the binder removal process, the atmosphere surrounding the samples in the furnace is a very important parameter to be considered. The thermogravimetric traces obtained are shown in Figure 2.38. These allow the comparison of thermal decomposition kinetics of the binder system in the different atmospheres used. In the presence of flowing nitrogen, thermal degradation occurs with the major weight loss occurring between 400°C and 500°C. One-third of the binder is lost before 300°C.

In the presence of flowing air and flowing oxygen, oxidative degradation was observed. The major weight loss occurs at a much lower temperature range. It is also clear that compared with static air, the use of flowing air accelerated the binder degradation processes appreciably, due to the efficient removal of decomposition products. In flowing oxygen, at about 240°C, rapid loss of binder is accompanied by a sudden increase in temperature, suggesting that combustion could have occurred. Combustion could lead to the disintegration of the specimen.

In the presence of flowing air, it may be very hard to control a rapid rate of weight loss even with the slowest ramp rates. The next choice is static air, but oxidation can be a problem. Therefore, flowing nitrogen can be chosen as a safe binder burnout atmosphere with reasonable binder burnout schedules (Figure 2.39).

It was already explained how to generate a normalized rate of weight loss table from data collected on actual samples. The process can be repeated with different heating rates on 5-mm thick-section ceramic samples in a nitrogen atmosphere. A binder burnout cycle can be generated by assuming $d(\%W)/dt$ being equal to say 0.003, which may correspond to 0.01 mg min^{-1} weight loss, which is the boundary value between a crack-free and cracked sample. This means that if the rate of weight loss is more than this value, the samples would crack. If this is an acceptable rate of weight loss, which permits to burn out in reasonable amount of time, then a heating rate cycle can be developed as given in Table 2.10.

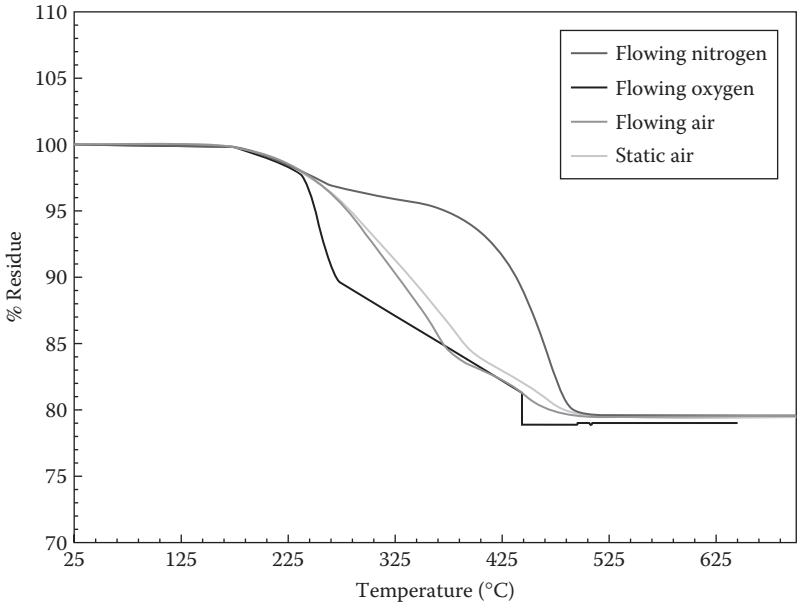

FIGURE 2.39
Effect of binder burnout atmosphere on binder burnout behavior of the silicon nitride formulations used for the AM process.

TABLE 2.10
Binder Burnout Schedule Developed for a 5 mm Ceramic Sample

Temperature (°C)	Ramp Rate (°C min^{-1})	Duration Time (min)
35–135	2	50
135–185	2	50
185–325	0.1	1500
325–375	0.05	1000
375–475	0.03	3332
475–525	0.05	1000
525–575	0.1	500
575–625	1	50

The superimposition of this heating rate diagram on the TGA for the silicon nitride binder is shown in Figure 2.40. It is clear from this that higher the rate of weight loss, slower the optimum ramp rate.

The total burnout cycle time developed in this case was for 5.19 days. This schedule was tested on actual samples. In this case, it was observed that samples with a thickness less than 5 mm did not crack and 10 mm or more cracked. This implied that the boundary line for crack-prone and crack-free zone is in between 5 and 10 mm section thickness for this binder burnout schedule. The above burnout cycle seemed to work successfully for sample thickness less than or equal to 5 mm.

For defining binder burnout variation with respect to the thickness, we could assume a linear dependency or a parabolic rate of weight loss with the section thickness. According to

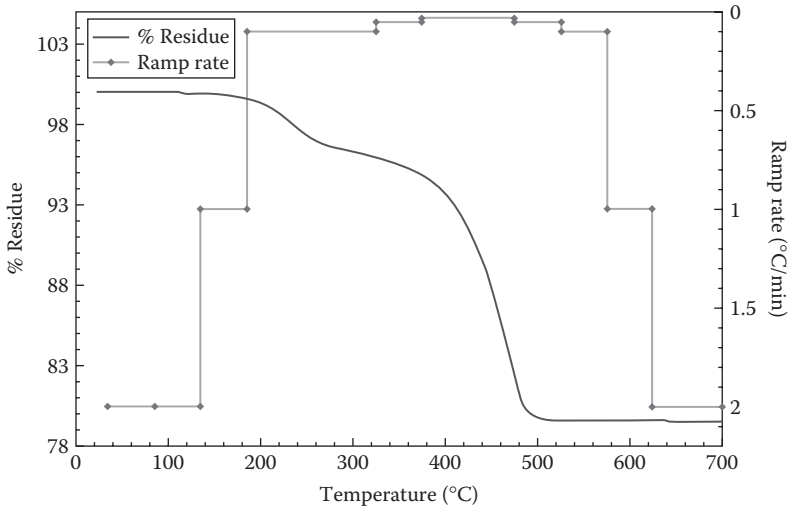

FIGURE 2.40
Superposition of the heating cycle on the TGA curve for a typical AM binder system.

a linear weight loss model, the section thickness is directly proportional to burnout time. By decreasing the time interval at each segment or increasing the ramp rate to four times to its original value in the burnout cycle given in Table 2.10, crack-free samples with section thickness 1.25 mm or less could be burnt out. Similarly, if the section thickness depends on a square law with burnout time, decreasing the cycle time to one-fourth its original value should allow to burn out and produce crack-free samples with section thickness 2.5 mm or less.

A typical graph between log (thickness) versus log (time) for the linear and square law, which has slopes 1 and 2, respectively, are shown in Figure 2.41. The graph can be divided into crack-prone and crack-free zones.

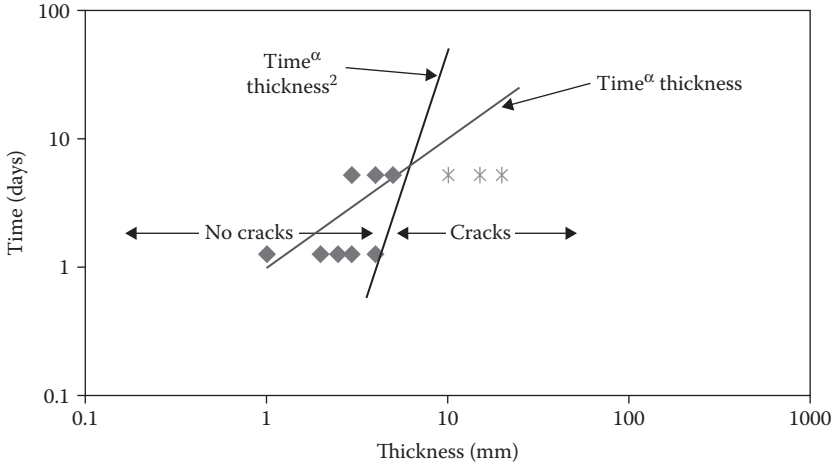

FIGURE 2.41
Crack-free and crack-prone samples for the linear and square law models for a typical formulation used for AM process of ceramics.

A comparison of the linear and parabolic rate loss models is shown in Figure 2.41, which reveals that section thickness dependency follows a square law. This allows to burn out thick samples in less time.

2.7 Special Cases: In Situ Fiber Reinforcement during AM

In some cases, during the AM process, second-phase particles may coalesce due to the action of heat and pressure and combine to create in situ fibers, leading to strengthening during the AM process itself. For example, Lombardi et al. (1998) conducted EFF experiments in polymer blends having controlled microstructures. These blends are composed of at least two immiscible polymer components where its major phase is present in at least twofold excess compared to the minor phase. The major phase is composed of poly-2-ethyl-2-oxazoline (PEOx), a water soluble thermoplastic reinforced with fine talc filler, while the minor phase is composed of a high glass transition temperature styrenic copolymer (Tg ca. 140°C). In this case, the styrenic copolymer was added to the PEOx to increase the heat distortion temperature of the polymer blend as well as reduce its sensitivity to ambient humidity (Lombardi et al. 1998).

As can be seen from the scanning electron microscopy in Figure 2.42 that shows the feedstock microstructure, the styrenic minor phase is present as spherical droplets uniformly dispersed throughout the PEOx major phase. This type of microstructure is typically encountered in blends composed of two immiscible polymer phases where the minor phase adopts a spherical morphology to minimize its surface area and energy (Sperling 1997; Tsebrenko et al. 1976; Utracki 1990; Vanoene 1978, 1972). Coalescence is suppressed within the blend by the presence of a small amount of a third compatibilizing polymer that is miscible in both the styrenic and PEOx polymers by decreasing the compositional

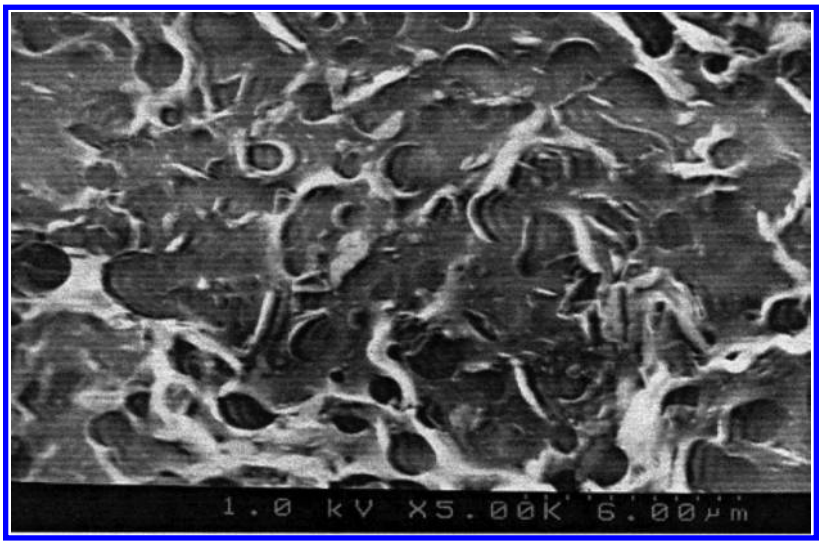

FIGURE 2.42
Microstructure of PEOx/styrenic polymer blend feedstock for extrusion-based AM process.

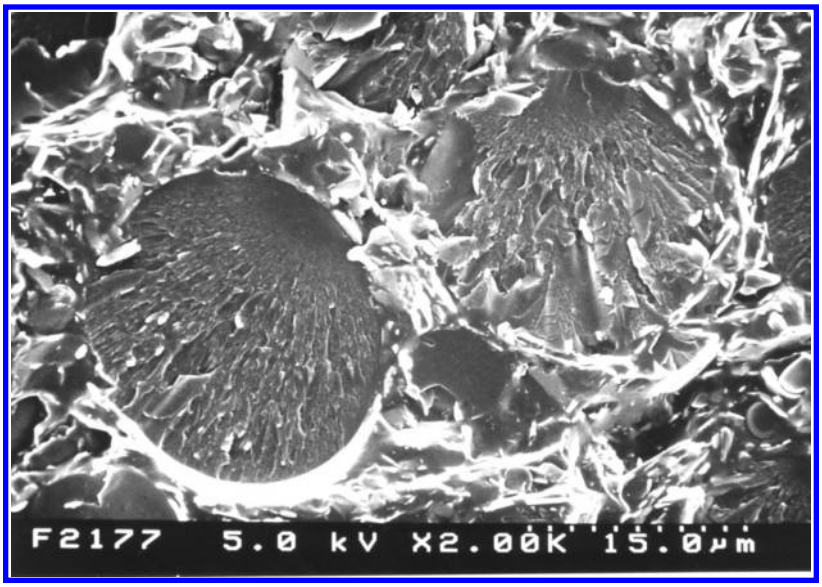

FIGURE 2.43
Microstructure of PEOx/styrenic polymer blend EFF feedstock after heat treatment at 140°C.

gradient and interfacial energy between the minor and major polymer phases (Fayt, Jerome, and Teyssie 1987). Sufficient plasticizer has also been added to modify the rheology of the PEOx phase of these blends such that it can be accurately extrusion freeformed using the extrusion-based AM techniques. Heat treating the feedstock results in a microstructure with perfectly circular second-phase structures, which clearly shows the effect of extrusion on the preferred alignment as shown in Figure 2.43.

The freeformed blend can also function as a water-soluble support structure and was demonstrated for the fabrication of intricate ABS polymer prototype components using extrusion-based AM techniques, as shown in Figure 2.44. This was one of the very first water-soluble support structure materials successfully demonstrated for the FDM process. In this case, the blend was formulated as a filament 1.778 mm in diameter and extruded through a second nozzle, while the ABS filament was extruded in an FDM 1600 modeler (Artz, Lombardi, and Popovich 2000; Lombardi 1998). Figure 2.45 shows the ability to wash out the support material from the AM part. This material could be blended either as a filament or as a feed rod, making it suitable for either the FDM or the EFF AM process.

2.8 Current Challenges and Future Trends

It is an accepted fact that AM processes are well developed for pure polymers or polymer blends and any improvements might be incremental. However, we still have not seen enough enhancements in polymers used in the tissue engineering area. For AM processes to be truly ground breaking, especially for composite materials, it is necessary that new

FIGURE 2.44
(See color insert.) Fabrication of intricate shapes in the FDM process using a water-soluble material as the support material.

FIGURE 2.45
Ability to wash out the support structure from a complex-shaped FDM component using a PEOx/styrenic polymer blend feedstock.

materials, fibers, and interfacial coatings will need to be developed. Since most of the polymer and composite technologies involves the heating and cooling of the ingredients, it is necessary that the thermal expansion and shrinkages need to match or, at the very least, the difference in properties needs to be mitigated with the help of appropriate interfacial coatings. At some point, the ATP technique that is being used to produce components that can be used in real applications will need to be merged with an AM process or the ATP process will have to be modified to become a truly AM process.

The other path-breaking development will be in the chopped fiber composites area, although we have started to see the developments in 3D printed cars and companies like MarkForged. Perhaps these will overlap into the tissue engineering area, leading to new materials, processes, and applications.

The most important requirement that will be needed uniformly by every AM technique would be to obtain the reliability of many parts while only building one or two parts. It is believed that this would be the greatest challenge for any AM technology and parts made by those techniques.

References

Agarwala, M.K., A. Bandyopadhyay, R. van Weeren, A. Safari, S.C. Danforth, N. A. Langrana, V.R. Jamalabad, and P.J. Whalen. 1996. FDC, rapid fabrication of structural components. *American Ceramic Society Bulletin* 75 (11):60–66.

Artz, G.J., J.L. Lombardi, and D. Popovich. 2000. Water soluble rapid prototyping support and mold material. US Patent No. 6,070,107. May 30.

ASTM. 2012. F2792. 2012. Standard terminology for additive manufacturing technologies. ASTM International, West Conshohocken, PA.

Bigg, D.M. 1982. Rheological analysis of highly loaded polymeric composites filled with non-agglomerating spherical filler particles. *Polymer Engineering & Science* 22 (8):512–518.

Bigg, D.M. 1983. Rheological behavior of highly filled polymer melts. *Polymer Engineering & Science* 23 (4):206–210.

Calvert, P. 1998. Freeforming of polymers. *Current Opinion in Solid State and Materials Science* 3 (6):585–588.

Calvert, P., and M. Cima. 1990. Theoretical models for binder burnout. *Journal of the American Ceramic Society* 73 (3):575–579.

Calvert, P., T.L. Lin, and H. Martin. 1997. Extrusion freeform fabrication of chopped-fibre reinforced composites. *High Performance Polymers* 9 (4):449–456.

Calvert, P., and L. Zengshe. 1998. Freeform fabrication of hydrogels. *Acta Materialia* 46 (7):2565–2571.

Chin, H.B., and C. Dae Han. 1980. Studies on droplet deformation and breakup. II. Breakup of a droplet in nonuniform shear flow. *Journal of Rheology (1978-present)* 24 (1):1–37.

Cima, M.J., J.S. Haggerty, E.M. Sachs, and P.A. Williams. 1993. Three-dimensional printing techniques. US Patent No. 5,204,055. April 30.

Crump, S.S. 1992. Apparatus and method for creating three-dimensional objects. US Patent No. 5,121,329. June 9.

Crump, S.S. 1994. Modeling apparatus for three-dimensional objects. US Patent No. 5,340,433. August 23.

Dealy, J.M. 1982. *Rheometers for Modern Plastics*. New York: Van Nostrand Reinhold.

Dealy, J.M. 1990. *K. F. Wissbrun. Melt Rheology and Its Role in Plastics Processing*. New York: Van Nostrand Reinhold.

Dehoff, R. *Made in Chicago: World's First 3D Printed Car.* Available at http://wgntv.com/2014/09/13/made-in-chicago-worlds-first-3d-printed-electric-car/, accessed on September 15, 2014.

Direct-Digital-Manufacturing. 2013. *3D Printing Series #4—Paramount Industries: A 3D Systems Company, an Additive Manufacturing Success Story.* Available at http://www.dvirc.org/3d-printing-series-4-paramount-industries-a-3d-systems-company-an-additive-manufacturing-success-story-2/-sthash.IqiJjOTV.dpuf, accessed on August 13, 2013.

Don, R.C., J.W. Gillespie Jr, and S.H. McKnight. 1997. Bonding techniques for high performance thermoplastic compositions. US Patent No. 5,643,390. July 1.

Elmendorp, J.J. 1986. A study on polymer blending microrheology. *Polymer Engineering & Science* 26 (6):418–426.

Evans, J.R.G., and M.J. Edirisinghe. 1991. Interfacial factors affecting the incidence of defects in ceramic mouldings. *Journal of Materials Science* 26 (8):2081–2088.

Farmer, B.L., R.A. Allen, O. Ghita, M.A. Beard, and K.E. Evans. 2012. Strategies to combine nanocomposite and additive layer manufacturing techniques to build materials and structures simultaneously, Paper read at *ECCM15—15th European Conference on Composite Materials*, June 24–28, Venice, Italy.

Farmer, B.L., M.A. Beard, O. Ghita, R. Allen, and K.E. Evans. 2010. 2010. Assembly strategies for fully aligned and dispersed morphology controlled carbon nanotube reinforced composites grown in net-shape. Paper read at *2010 MRS Fall Meeting—Symposium Z—Hierarchical Materials and Composites—Combining Length Scales from Nano to Macro*, Boston, MA.

Fayt, R., R. Jerome, and Ph. Teyssie. 1987. Characterization and control of interfaces in emulsified incompatible polymer blends. *Polymer Engineering & Science* 27 (5):328–334.

Ferry, J.D. 1982. *Viscoelastic Properties of polymers*. New York: John Wiley & Sons Inc.

General-Electric. 2014. *GE Reports, 2014, This Electron Gun Builds Jet Engines*. Available at http://www.gereports.com/post/94658699280/this-electron-gun-builds-jet-engines, accessed on August 17, 2014.

Gibson, I., D.W. Rosen, and B. Stucker. 2010. *Additive Manufacturing Technologies*. New York: Springer.

Gonczy, S.T., and J.G. Sikonia. 2005. Nextel™ 312/Silicon Oxycarbide Ceramic Composites. In *Handbook of Ceramic Composites*, Narottam P. Bansal, ed. New York: Springer.

Goodridge, R.D., M.L. Shofner, R.J.M. Hague, M. McClelland, M.R. Schlea, R.B. Johnson, and C.J. Tuck. 2011. Processing of a Polyamide-12/carbon nanofibre composite by laser sintering. *Polymer Testing* 30 (1):94–100.

Griffith, M.L., and J.W. Halloran. 1996. Freeform fabrication of ceramics via stereolithography. *Journal of the American Ceramic Society* 79 (10):2601–2608.

Guo, N., and M.C. Leu. 2013. Additive manufacturing: technology, applications and research needs. *Frontiers of Mechanical Engineering* 8 (3):215–243.

Han, C.D. 1981. *Multiphase Flow in Polymer Processing*. New York: Academic.

Hao, L., M.M. Savalani, Y. Zhang, K.E. Tanner, and R.A. Harris. 2006. Effects of material morphology and processing conditions on the characteristics of hydroxyapatite and high-density polyethylene biocomposites by selective laser sintering. *Proceedings of the Institution of Mechanical Engineers, Part L: Journal of Materials Design and Applications* 220 (3):125–137.

Lombardi, J.L., G.J. Artz, D. Popovich, R. Vaidyanathan, and S. Boggavarapu. 1998. Issues associated with the development of a water soluble support material for use in extrusion freeforming & fused deposition modelling. Paper read at *9th Annual Solid Freeform Fabrication Symposium Proceedings*, Austin, TX.

Jacobs, P.F. 1992. *Rapid Prototyping & Manufacturing: Fundamentals of Stereolithography*. Dearborn, MI: Society of Manufacturing Engineers.

Jacobs, P.F. 1995. *Stereolithography and Other RP&M Technologies: From Rapid Prototyping to Rapid Tooling*. New York: Society of Manufacturing Engineers.

Jang, B.Z., E. Ma, and C. Jeff Wang. 1999. Apparatus and process for producing fiber reinforced composite objects. US Patent No. 5,936,861. August 10.

Kamal, M.R., and A. Mutel. 1985. Rheological properties of suspensions in Newtonian and non-Newtonian fluids. *Journal of Polymer Engineering* 5 (4):293–382.

Klosterman, D.A., R.P. Chartoff, G. Graves, N. Osborne, and B. Priore. 1998. Interfacial characteristics of composites fabricated by laminated object manufacturing. *Composites Part A: Applied Science and Manufacturing* 29 (9):1165–1174.

Klosterman, D.A., R.P. Chartoff, N.R. Osborne, G.A. Graves, A. Lightman, G. Han, A. Bezeredi, and S. Rodrigues. 1999. Development of a curved layer LOM process for monolithic ceramics and ceramic matrix composites. *Rapid Prototyping Journal* 5 (2):61–71.

Kobayashi, S., M. Kaku, and T. Saegusa. 1988. Miscibility of poly (2-oxazolines) with commodity polymers. *Macromolecules* 21 (2):334–338.

Kovar, D., B.H. King, R.W. Trice, and J.W. Halloran. 1997. Fibrous monolithic ceramics. *Journal of the American Ceramic Society* 80 (10):2471–2487.

Kumar, S., and J.-P. Kruth. 2010. Composites by rapid prototyping technology. *Materials & Design* 31 (2):850–856.

MarkForged. 2014. World's first carbon fiber 3D printer demonstrated, could change the face of additive manufacturing forever. Available at http://www.extremetech.com/extreme/175518-worlds-first-carbon-fiber-3d-printer-demonstrated-could-change-the-face-of-additive-manufacturing-forever, accessed on June 28, 2014.

Meilunas, R.J. 2001. Laminated object manufacturing-based design ceramic matrix composites. Final Report No. AFRL-ML-WP-TR-2001-4074, DARPA/Wright Patterson AFB, Bethpage, NY: Northrop Grumman Corporation.

Meilunas, R.J., G.P. Dillon, and J.A. Nardiello. 2002. System for constructing a laminate. US Patent No. 6,484,776 B1. November 26.

Middleman, S. 1968. *The Flow Behavior of High Density Polymers*. New York: John Wiley.

Moore, J.A., and J.H. Kim. 1992. Blends of poly (enamino nitrile). *Macromolecules* 25 (5):1427–1432.

Nikzad, M., S.H. Masood, and I. Sbarski. 2011. Thermo-mechanical properties of a highly filled polymeric composites for fused deposition modeling. *Materials & Design* 32 (6):3448–3456.

Njuguna, J., K. Pielichowski, and S. Desai. 2008. Nanofiller reinforced polymer nanocomposites. *Polymers for Advanced Technologies* 19 (8):947–959.

Paesano, A. 2014. Polymers for additive manufacturing: Present and future. *SAMPE Journal* 50 (5):34–43.

Peng, J., T.L. Lin, and P. Calvert. 1999. Orientation effects in freeformed short-fiber composites. *Composites Part A: Applied Science and Manufacturing* 30 (2):133–138.

Shofner, M.L., F.J. Rodríguez-Macías, R. Vaidyanathan, and E.V. Barrera. 2003. Single wall nanotube and vapor grown carbon fiber reinforced polymers processed by extrusion freeform fabrication. *Composites Part A: Applied Science and Manufacturing* 34 (12):1207–1217.

Sperling, L.H. 1997. *Polymeric Multicomponent Materials: An Introduction*. New York: John Wiley.

Stratasys. 2014. Properties for Ultem 9085. Available at http://www.stratasys.com/~/media/Main/Secure/MaterialSpecsMS/Fortus-Material-Specs/Fortus-MS-ULTEM9085-01-13-web.ashx, accessed on August 17, 2014.

Stuffle, K.L., P.J. Creegan, J.L. Lombardi, P.D. Calvert, J.A. O'Kelly, R.A. Hoffman, and G.C. Chambers. 2000. Method and apparatus for in-situ formation of three-dimensional solid objects by extrusion of polymeric materials. US Patent No. 6,067,480. May 23.

Tsebrenko, M.V., A.V. Yudin, T.I. Ablazova, and G.V. Vinogradov. 1976. Mechanism of fibrillation in the flow of molten polymer mixtures. *Polymer* 17 (9):831–834.

UT-Austin. 2012. Selective laser sintering, Birth of an industry 2012. Available at http://www.me.utexas.edu/news/2012/0712_sls_history.php, accessed on August 24, 2014.

Utracki, L.A. 1990. *Polymer Alloys and Blends: Thermodynamics and Rheology*. New York: Hanser Publisher.

Vaidyanathan, R., K. Ranji, J. Walish, M. Fox, J.W. Gillespie Jr, S. Yarlagadda, M.R. Effinger, A.C. Mulligan, and M.J. Rigali. 2005. Continuous fiber reinforced composites and methods, apparatuses, and compositions for making the same. US Patent No. 6,899,777 B2. May 31.

Vaidyanathan, R., J. Walish, J.L. Lombardi, S. Kasichainula, P. Calvert, and K.C. Cooper. 2000. The extrusion freeforming of functional ceramic prototypes. *JOM* 52 (12):34–37.

Vanoene, H. 1972. Modes of dispersion of viscoelastic fluids in flow. *Journal of Colloid and Interface Science* 40 (3):448–467.

Vanoene, H., Ed. 1978. *Polymer Blends*. 2 vols. New York: Academic Press. pp. 295–349.

Wu, S. 1987. Formation of dispersed phase in incompatible polymer blends: Interfacial and rheological effects. *Polymer Engineering & Science* 27 (5):335–343.

Yarlagadda, S. 2014. Automated Tow Placement of Composites. Delaware: Center for Composite Materials, University of Delaware.

Z-Corporation. 2014. *Z Corporation 3D Printing Technology*. Available at http://www.zcorp.com/documents/108_3DPrintingWhitePaperFINAL.pdf, accessed on August 15, 2014.

Zhang, Y., J. Stringer, R. Grainger, P.J. Smith, and A. Hodzic. 2014. Improvements in carbon fibre reinforced composites by inkjet printing of thermoplastic polymer patterns. *Physica Status Solidi (RRL)-Rapid Research Letters* 8 (1):56–60.

Zhong, W., F. Li, Z. Zhang, L. Song, and Z. Li. 2001. Short fiber reinforced composites for fused deposition modeling. *Materials Science and Engineering: A* 301 (2):125–130.

3

Deposition-Based and Solid-State Additive Manufacturing Technologies for Metals

Vamsi Krishna Balla

CONTENTS

3.1 Introduction

Initially technologies to create three-dimensional (3D) components from computer-aided design (CAD) files were termed *rapid prototyping technologies* as these were primarily used to create prototypes of the parts with different materials, primarily plastics. However, there has been a paradigm shift from prototyping to direct manufacturing/production of 3D components, and therefore, these technologies have improved over the last few decades and are now being called additive manufacturing (AM) technologies. Currently, the output of AM technologies includes up to 20% final products and is estimated to increase to 50% by 2020 (The Economist 2011). While the invention of technologies is being argued to be a *Third Industrial Revolution* (The Economist 2012), huge investment and development efforts are required to fully realize their potential (Reeves and Hague 2013). The unique benefits of these agile manufacturing technologies include rapid production of components with efficient utilization of available resources, reverse engineering to develop

functional components, new materials development such as lightweight structures, complex integration of materials including assemblies with moving parts, and functionally graded materials.

Current AM technologies for metals/alloys are aimed at producing complex, unique geometries; tailored materials development and customization; and functionally graded materials development, which find applications in aerospace, defense, automotive, and biomedical industries with demanding requirements. Although several AM techniques have been developed for creating metallic objects, only deposition-based, solid-state and some new AM techniques will be discussed in this chapter. These techniques can be categorized based on energy source, processing state (liquid or solid), and feedstock material as shown in Figure 3.1.

Processes that fuse feedstock material include laser engineered net shaping (LENS™; developed at Sandia National Laboratory, Albuquerque, NM, and marketed by Optomec, Albuquerque, NM), direct metal deposition (DMD; developed at Michigan University, USA, and marketed by Precision Optical Manufacturing, Inc., Plymouth, MI), laser augmented manufacturing (LAM; developed by Aeromet, Eden Prairie, MN), directed light fabrication (DLF), and electron beam freeform fabrication (EBF^3; developed at NASA Langley Research Center, USA). These processes use either lasers or electron beam as energy source to melt the metal during deposition. Other fusion-based processes that use an arc-based energy source are hybrid plasma deposition and milling (HPDM) and shape metal deposition (SMD; developed at Stanford and Carnegie Mellon Universities, USA), where metal wire is used as feedstock. Table 3.1 compares the characteristics of these energy sources. Solid-state deposition processes include ultrasonic consolidation (UC; developed by Solidica, Ann Arbor, MI); electrochemical fabrication (EFAB; marketed by Microfabrica, Inc., Van Nuys, CA, and developed at the University of Southern California, USA); and emerging

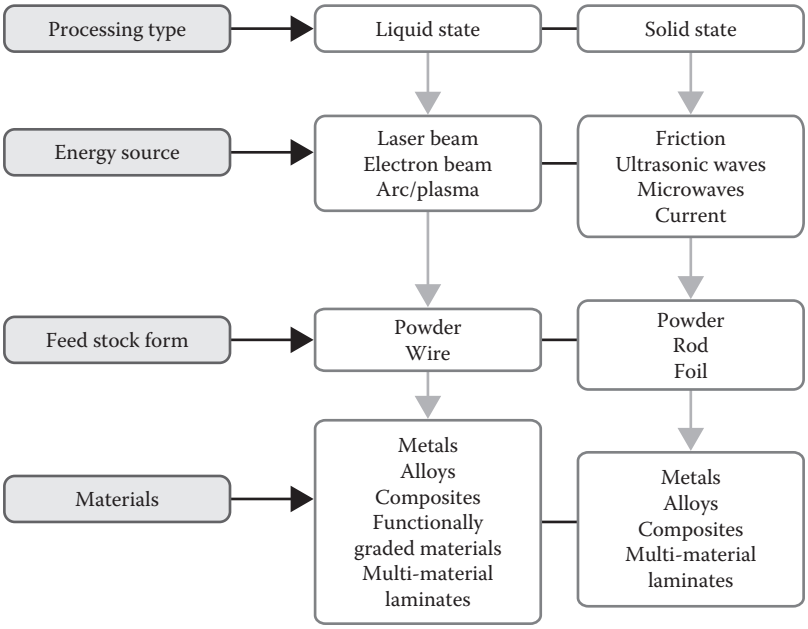

FIGURE 3.1
Classification of AM processes for metallic objects.

TABLE 3.1

Energy Sources Used for Fusion-Based AM Techniques

Characteristic	Laser	Electron Beam	Arc
Atmosphere	Inert	Vacuum	Inert
Energy density (W/mm^2)	10^6	10^8	Very high
Power efficiency (%)	Poor (2–5)	Good (15–20)	Excellent (>80)
Material utilization (%)	10–15 for powder ~100 for wire	~100	~100
Deposition rate	Medium	Medium	High
Unit size and cost	Bulky and expensive	Bulky and expensive	Compact and economical
Deposit quality	Good	Excellent	Good
Geometrical quality	Near net shape	Requires machining	Requires machining

Source: Karunakaran, K.P. et al., *Rapid Prototyping J.*, 18, 264–280, 2012.

technology, namely, friction freeform fabrication (FFF; developed at Indian Institute of Technology Madras, India). Both UC and FFF are considered as hybrid AM technologies as machining is required for each layer to give desired contour, where friction generated heat and plastic deformation are the source of bonding. EFAB is based on electrodeposition and primarily used to fabricate micron-scale devices.

3.2 Current Technologies

3.2.1 Powder Deposition-Based Techniques

The most popular powder deposition-based AM technique uses lasers as an energy source; no other type of energy sources has been reported yet. In this process, the metal powder is delivered to the melt pool using an inert gas such as argon, and therefore, use of electron beam energy sources is precluded as it requires high vacuum. There are four major versions of this process, namely, LENS, DMD, LAM, and DLF that share a common AM principle where high-power laser is used as energy source and metal powder as feedstock material. However, in LENS and DLF the deposition process is carried out in a glove box with controlled atmosphere, and DMD process uses inert gas shroud to prevent oxidation of deposit with process being carried out in a chamber without inert atmosphere. In all techniques, the deposition process begins with creation of small liquid metal pool on the substrate to which predetermined amount of metal powder is delivered using inert gas as carrier. The powder melts in the liquid metal pool and the substrate (fixed to a computer numerical control [CNC] table) moves relative to the deposition head creating solidified metal track. Deposition of overlapping metal tracks completes a layer, and the deposition head along with the powder delivery nozzles moves up by small distance (slice thickness) to deposit the next layer. The process continues for all layers producing near net shape metallic component represented by 3D CAD model. The deposition path, distance between successive metal tracks, and slice thickness are usually created using customized software in each process. Typical processing steps and various components of LENS system are presented in Figure 3.2.

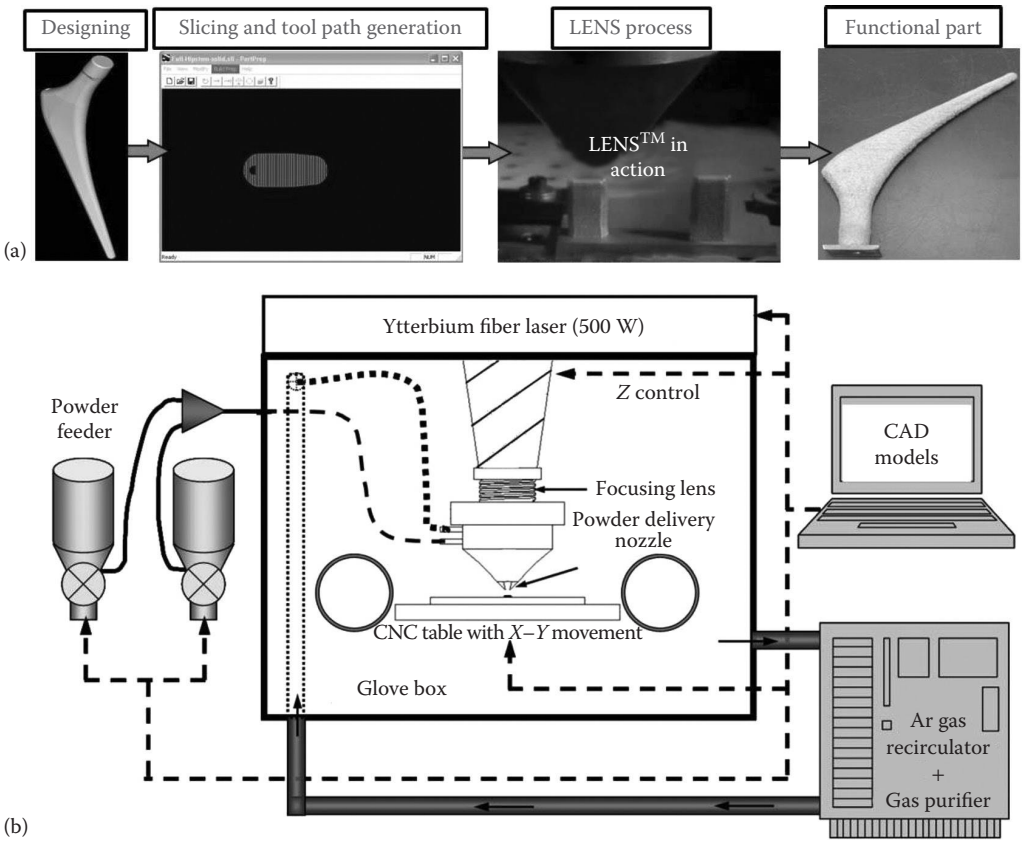

FIGURE 3.2
(a) Typical processing steps involved in laser metal powder deposition (LMPD); (b) schematic of LENS system. (Reprinted with permission from Das, M. et al., *Transac. Indian Ceram. Soc.*, 72, 169–174, 2013.)

Latest laser metal powder deposition (LMPD) systems are equipped with multiple powder feeders, multi-axis deposition, and closed-loop process control systems, which enable fabrication of near net shape metallic components with high surface finish, dimensional accuracy, microstructural uniformity, and compositional and/or structural gradients. These techniques are also being used for repair, remanufacturing, feature addition, cladding, and hardfacing of aerospace and engineering components. However, unique capabilities of laser-based deposition techniques have been effectively exploited to produce new/designed materials such as compositionally graded materials; structurally graded materials; porous structures; and custom implants with tailored mechanical, physical, and chemical properties (Mazumder 2000; Mazumder et al. 2000; Shin et al. 2003).

The stability and hence the quality of deposits prepared by LMPD depends on physical phenomenon of the process, which is dictated by absorbance of laser beam by metals, surface tension, and viscosity of the melt. The laser absorbance of metal powder is very important factor to control heating and melting of the powder—too low absorbance requires high energy input or results in partial melting leading to porous deposits and excessively high could lead to evaporation of material during deposition. For example, net shape bulk alumina ceramic parts have been successfully fabricated at a laser power of 175 W

(Balla, Bose, and Bandyopadhyay 2008) and silica-based lunar regolith parts at 50 W (Balla et al. 2012b), whereas the fabrication of fully dense metallic parts would require much higher laser power. The difference is primarily attributable to more effective laser absorbance of ceramic materials compared to highly conductive metals. The optimal processing window for laser processing of materials also depends on laser light absorptivities of constituent element in the materials. España, Balla, and Bandyopadhyay (2011) processed Al-12Si alloy using LENS where large difference in laser absorptivities of Al and Si posed severe difficulties in achieving sound and stable deposits.

Since LMPD process relies on melting of metals, the surface tension/wettability of liquid metals against substrate and/or previous deposits is very important for deposit stability during processing. Das (2003) reported that formation of oxide layer on the powders due to contamination could lead to defects in the deposits such as balling, and therefore, the protective atmosphere should be carefully controlled using high purity inert gases. Additionally, the viscosity of liquid metal should be optimum to achieve good spreading of freshly deposited metal on previous layers/substrate. It is generally accepted that high total energy input (combined effect of laser power, scan velocity, and powder feed rate) during deposition decreases the melt viscosity and aids spreading in majority of metals and alloys. However, in multi-material deposition, the viscosity may increase with energy input if intermetallic compounds form during deposition. Another important consequence of melt viscosity is the balling effect in the LMPD processing. Very high melt viscosity (at low energy input) generates severe balling effect (Figure 3.3), and high energy input with very low melt viscosity results in melt spreading (España, Balla, and Bandyopadhyay 2011). It appears that precise control of melt pool temperatures and hence the melt viscosity by process parameter optimization is very critical to deposit new materials such as metal matrix composites, where constituent elements/compounds have different laser absorbance capacities.

In general, the surface finish in terms of roughness of the parts produced by LMPD processes is relatively high than the parts fabricated using powder bed-based processes. The surface finish has been reported to be influenced by layer thickness, laser power, deposition speed, and powder feed rate. Gharbi et al. (2013) reported that combination of deep melt pools and thin layers can reduce the surface roughness of Ti6Al4V alloy parts produced using DMD. The surface finish can also be improved with slow deposition speed particularly the speed of wall/contour deposition (Mazumder et al. 2000). However, Kong

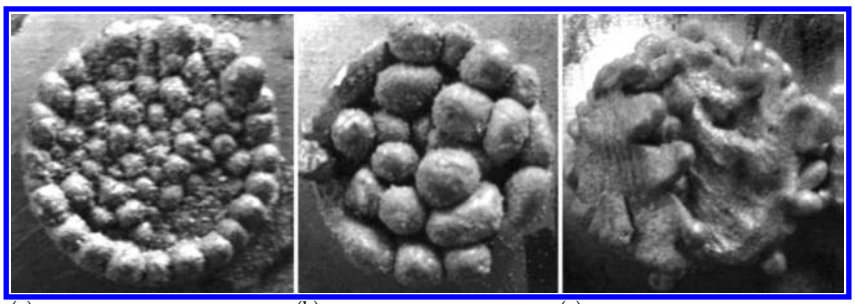

FIGURE 3.3
Laser deposited Al-12Si alloy. (a) Porous deposit at low energy input; (b) severe balling to due high melt viscosity; and (c) melt spreading due to low melt viscosity at excessively high energy input. (Reprinted with permission from España, F.A. et al., *Philos. Mag.*, 91, 574–588, 2011.)

et al. (2007) reported that the Inconel 625 parts produced using finer powder size exhibited superior surface finish and deposition efficiency compared to coarse powder. Further, the surface finish of the DMD processed parts has been shown to improve by changing the position of powder entry into the melt pool (Zhu et al. 2012). Recently, it was found that the use of pulsed lasers, instead of continuous lasers, helps in improving the surface finish (Pinkerton and Li 2003). Deposition of Ni-based super alloy using DMD in pulsed mode resulted in average surface roughness of 2 μm (Xue, Li, and Wang 2011). Reduced thermal gradients and Marangoni flows in the melt pool are thought to be responsible for forming smoother deposits in pulsed mode compared to continuous mode of lasers (Gharbi et al. 2014).

For stable deposition process, continuous and precise control over powder feed rate, laser power, and deposition speed is very essential as these dictate the melt pool size, thermal gradients, and cooling rates (Hofmeister et al. 1995). Therefore, real-time thermal imaging of the melt pool and closed-loop feedback control for melt pool have been developed. The cooling rates during LMPD can vary between 10^3 and 10^8 K/s (Das et al. 2010; Hofmeister et al. 2001; Zheng et al. 2008) and can be controlled via process parameters enabling creation of tailored microstructures and properties. One critical application area of such controlled cooling rates is the processing of metallic glasses. Balla and Bandyopadhyay (2010) fabricated Fe-based bulk glass forming alloy components without losing amorphous structure of feedstock powder via high cooling rates achieved by maintaining low prior deposition temperature using short time delay between successive laser scans. It appears that LMPD techniques present a viable processing route to create amorphous components using existing bulk amorphous alloy powders. However, each deposit experiences several reheating cycles during deposition of fresh layer leading to complex solidification and transformed microstructures (Balla and Bandyopadhyay 2010). In addition, rapid cooling rates are also responsible for locked-in residual stresses leading to warpage, cracking, and deterioration of mechanical properties of final parts. The beneficial effects of rapid cooling rates during LMPD are fine grains, fine precipitates, absence of segregation, and so on. Another inherent characteristic of this process is directional solidification due to preferential heat flow though the substrate, which results in some anisotropic properties. Further, the heat build with deposition of large number of layers could produce large variation in microstructures between the first layer to the last layer of the part (Hofmeister et al. 2001; Wu 2007). A detailed review on laser-based AM of metals can be found in Gu et al. (2012).

Development of materials with gradual change in composition using LMPD is regarded as the best approach to incorporate such variations in net shape components with tailored properties (Banerjee, Collins, and Fraser 2002; Banerjee et al. 2003; Collins et al. 2003; Oruganti and Ghosh 2003; Schwendner et al. 2001). Compositionally graded coatings for biomedical and other applications have been successfully fabricated using LENS (Balla et al. 2007, 2009a; Bandyopadhyay et al. 2007; Dittrick et al. 2011; Krishna et al. 2008a). Balla et al. (2009b) created thin ZrO_2 layer on zirconium via laser-assisted oxidation by controlling the concentration of oxygen in the glove box of LENS. These films have been shown to exhibit good wear resistance and biocompatibility. Similarly, fabrication of unitized acetabular shell structures with porous titanium on one side and compositionally graded TiO_2 on the other side has also been successfully demonstrated (Balla et al. 2009a). Unique capabilities of LENS process in creating novel structures are reported in Bandyopadhyay et al. (2009), Das et al. (2013), DeVasConCellos et al. (2012), and España et al. (2010). Custom implants with desired porosity level in the proximal region of the implant to enable bone ingrowth and the fully dense distal region to support mechanical load fabricated using LENS are shown in Figure 3.4. Another unique possibility of fabricating two separate parts

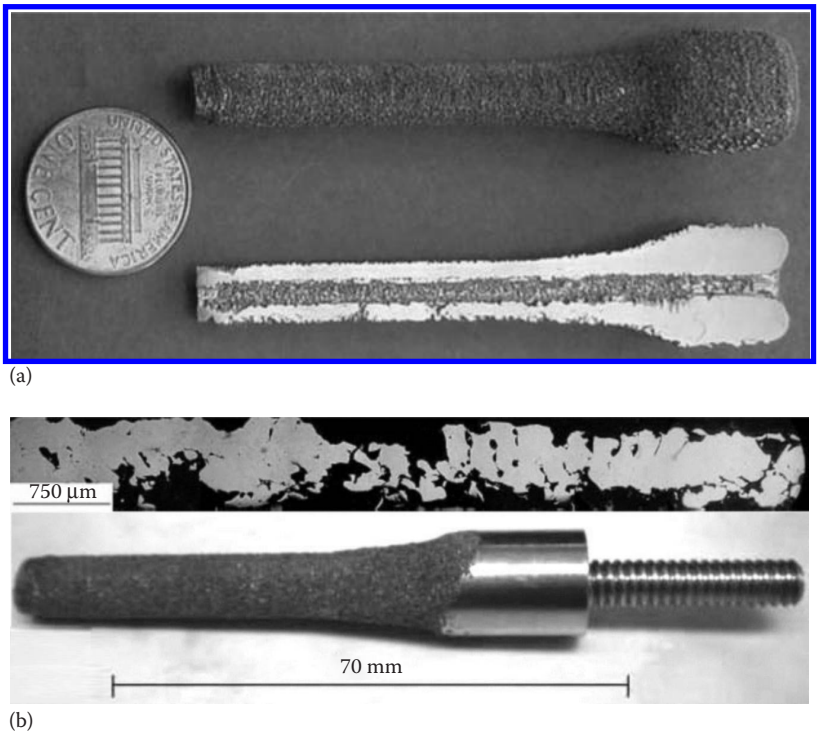

(a)

(b)

FIGURE 3.4
(a) LENS processed custom implants. Lower cross-sectional image shows the porosity in proximal region of the implant; (b) complete assembled implant. (Reprinted with permission from DeVasConCellos, P. et al., *Vet. Comp. Orthop. Traumatol.*, 25, 286–296, 2012.)

in single step using this technique has also been reported by Espana et al. (2010). For example, a part with dense sleeve and porous core requires assembly of these two parts in convention manufacturing and the sharp interface could be a source of failure. However, manufacturing them in single step using AM techniques (Figure 3.5) not only solve this issue but also eliminate time-consuming machining of interface surfaces required for assembly.

Extensive research has also been done in the area of creating porous structures using LMPD process (Balla et al. 2010b; Bandyopadhyay et al. 2010; Krishna, Bose, and Bandyopadhyay 2007, 2009; Krishna et al. 2008b; Xue et al. 2007). Novel design concept has been proposed by Krishna, Bose, and Bandyopadhyay (2007) to create porous structures with desired pore characteristics and distribution as shown in Figure 3.6. It has been demonstrated that by controlling the extent of metal powder melting via appropriate combination of process parameters, the residual porosity in the deposited tracks can be tailored (Figure 3.6a). By utilizing the design flexibility of AM processes, porous structures with designed porosity characteristics (pore size, shape, and distribution) can be fabricated by changing the layer thickness and distance between two successive metal tracks as shown in Figure 3.6b. Three-dimensionally interconnected porosity in the structures can be created by combining the above two approaches (Figure 3.6c). LENS-processed porous titanium samples with and without designed porosity have also been tested for their mechanical properties and deformation behavior (Balla, Bose, and Bandyopadhyay 2010c). It was

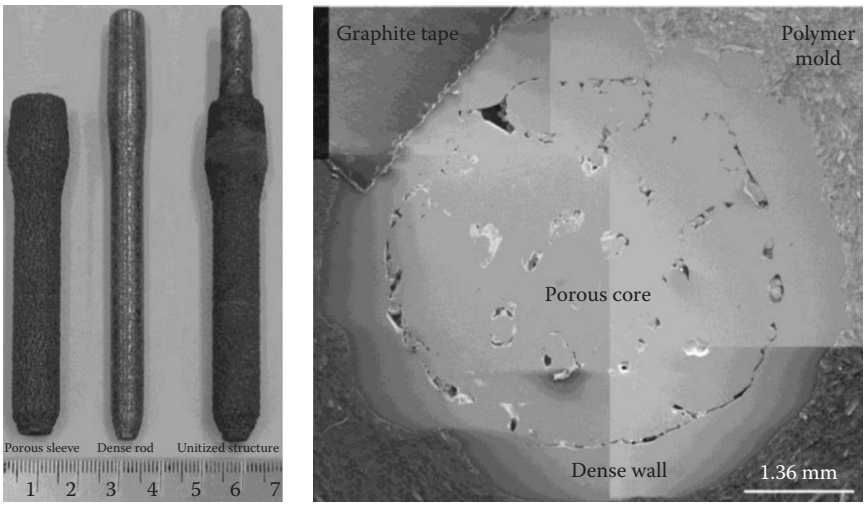

FIGURE 3.5
LENS processed components and materials. (a) Left: porous sleeve; middle: solid core; right: unitized structure fabricated in single step, and (b) CoCrMo alloy structure with solid shell and porous core. (Reprinted with permission from España, F.A. et al., *Mater. Sci. Eng. C*, 30, 50–57, 2010.)

found that regular arrangement of pores (tailored pore distribution) in designed porosity samples improves 0.2% proof strength to 485 MPa from 220 MPa in random porosity samples with comparable total porosity and pore size. This observation clearly demonstrates that drop in mechanical strength of porous metals can be compensated by tailoring pore distribution. Balla et al. (2011) discovered that brittleness associated with porous metals processed using powder metallurgical routes can be eliminated in laser-processed porous metals and is primarily due to differences in particle bonding in these processing routes. However, Bernard et al. (2011) reported that presence of 10% porosity decreases the rotating bending fatigue strength of NiTi alloy by 54%, while compression fatigue testing demonstrated that porous NiTi alloy samples (up to 20% porosity) processed using LENS are able to sustain stresses up to 1.4 times their yield strength without failure (Bernard et al. 2012). Several biocompatible coatings and composite coatings (Balla, Bose, and Bandyopadhyay 2010d; Balla et al. 2010a, 2012a, 2013; Bhat et al. 2011; Das et al. 2011, 2012; Roy et al. 2008, 2012) and bulk ceramics (Balla, Bose, and Bandyopadhyay 2008; Balla et al. 2012b; Bernard et al. 2010) processed using LENS have been reported.

3.2.2 Wire Deposition-Based Processes

Powder deposition-based AM techniques are the most widely used and researched technologies for metals. These technologies demonstrated their capabilities to manufacture complex but small components. However, powder deposition-based techniques suffer from low deposition rate and yield, high surface roughness, and residual gas porosity. For example, the deposition efficiency of powder-based AM techniques depends on melt pool area, and problems associated with powder recycling, contamination, and storage are also high (Kukreja et al. 2012). As a result, fabrication of large area structures using these techniques could become expensive. The majority of these issues can be obviated using alternative feedstock materials, and one such approach is the use of metal wire as feedstock.

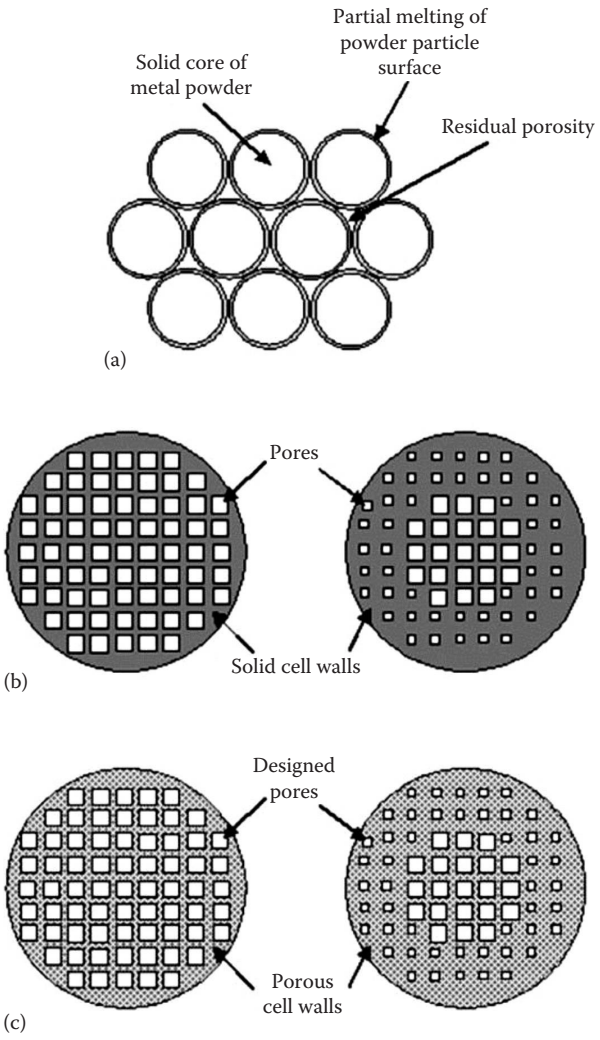

FIGURE 3.6
Design approaches to create functional implants with tailored pore characteristics such as size, shape, and distribution. Approaches: (a) partial melting of metal powders leading to porous structures, (b) porous structure with design porosity, and (c) combinational approach (a + b). (Reprinted with permission from Krishna, B.V. et al., *Acta Biomater.*, 3, 997–1006, 2007.)

Wire-based deposition for AM of components has been found very promising (Heralić 2012; Nurminen 2008) particularly for large components where dimensional accuracy is vital. Figure 3.7 shows the process of wire deposition-based AM of metallic components. The process starts with creating of small melt pool on the substrate using appropriate energy source. Then, the wire is fed to the melt pool at controlled rate and is melted by focused energy source. By moving the wire nozzle and energy source, relative to the substrate, along desired path creates thin metal bead. A complete layer is produced by depositing overlapping beads, and the process is repeated until 3D component is created. Normally, the deposition is carried out in controlled atmosphere. Post-processing such as grinding or machining may be performed depending on the final requirements.

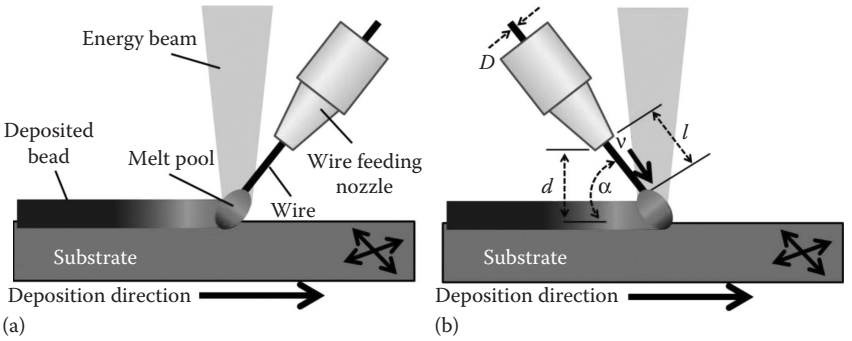

FIGURE 3.7
Schematic showing wire deposition-based additive manufacturing. (a) Front feeding with different components of the processing equipment; (b) rear feeding process and important geometrical process parameters. *D*, wire diameter; *d*, stand-off (too small "*d*" leads to stubbing, and too high results in dripping); α, wire feed angle; ν, wire feed rate; *l*, stick-out length. The wire tip position can be at leading edge, middle edge, or tailing edge of the melt pool.

Compared to powder feeding, the wire feeding for AM of metals offers several benefits. Significantly, high deposition rates up to 1500 cm^3/h have been reported for EBF[3] (Seufzer and Taminger 2007; Taminger and Hafley 2003). Similarly, laser-based wire deposition has been shown to provide high deposition rates (Nurminen 2008; Syed and Li 2005; Syed, Pinkerton and Li 2005). Martina et al. (2012) reported deposition rate of 1.8 kg/h with Ti6Al4V alloy wire using plasma wire deposition. Irrespective of energy source, wire feeding gave better surface finish, material quality (Ader et al. 2003), and usage efficiency (Nurminen 2008; Syed and Li 2005; Syed, Pinkerton and Li 2005). Other benefits include low cost of wire preparation (Kim and Peng 2000), clean work environment due to almost 100% wire utilization, and minimal health hazards. However, wire-based deposition is very sensitive to several process parameters and should be carefully controlled. Therefore, process optimization and control is extremely important to achieve stable deposition. Important process parameters include type of energy source, energy input, wire feed rate and feeding position, wire tip position in the melt pool, and traverse speed (Figure 3.7). Major energy sources used for wire deposition-based AM are laser, electron beam, and electric arc. Among these, laser-based wire deposition has been extensively studied followed by electron beam-based deposition process. Although the electric arc source is not as precise as laser and electron beam, recently 3D net shape components with mesoscale features have been successfully fabricated using miniature deposition process consisting micron-size wire and micron-tungsten inert gas welding system (Horii, Kirihara, and Miyamoto 2009). Combination of wire and powder feeding has also been reported (Syed, Pinkerton and Li 2006; Syed et al. 2007a, 2007b; Wang, Mei and Wu 2006; Wang et al. 2007).

3.2.2.1 Laser-Based Metal Wire Deposition

Laser-based metal wire deposition has been widely used to deposit Ti and Ti6Al4V alloy, and their microstructural and mechanical properties evaluations have also been done (Abioye, Folkes, and Clare 2013; Baufeld, Brandl, and Biest 2011; Brandl, Schoberth, and Leyens 2012; Brandl et al. 2010, 2011a, 2011b, 2011c; Cao et al. 2008; Hussein et al. 2008; Kim and Peng 2000; Medrano et al. 2009; Mok et al. 2008a, 2008b; Miranda et al. 2008).

Detailed microstructural analysis of single bead Ti6Al4V alloy deposited using laser and wire as feedstock material was studied by Brandl et al. (2011a). It appears that the laser power and deposition speed during wire deposition process had similar effect to that of powder deposition processes. The microstructural features such as prior β-grains are found to increase in size with laser power and decrease with deposition speed, while increasing the wire feed factor (deposition speed/wire feed rate) increased the feature size (Brandl et al. 2011a). The influence of these microstructural features on hardness of single beads was studied (Brandl et al. 2011b). In this study, they measured the hardness and bead dimensions and attempted to correlate with thermal history during deposition. The bead dimensions provided good qualitative information of thermal history and hardness mapping failed to provide good correlation. Large columnar grains spanning across many layers were formed (Brandl, Schoberth, and Leyens 2012). Post-deposition heat treatment had stronger influence on hardness compared to process parameters. As-deposited Ti6Al4V alloy exhibited tensile yield strength in the range of 697 to 884 MPa and elongation between 5% and 12% depending on process parameters and post-deposition heat treatment (Brandl et al. 2011c). Importantly the impurity levels of wire-deposited Ti6Al4V alloy were below acceptable levels of aerospace material specifications (AMS 4911L) and mechanical properties meet AMS 4928 specifications (Brandl et al. 2011c). Example of deposits and parts prepared in Brandl et al. (2011b) is shown in Figure 3.8.

Very recently, wire laser deposition has been employed to fabricate Ni-based superalloy, Inconel 625, and process parameters have been optimized to achieve sound beads (Abioye, Folkes, and Clare 2013), wherein energy input and deposition volume per unit track length are identified as key process parameters. As shown in Figure 3.9a, wire dripping occurs when the deposition volume is very low, and when it becomes excessively high, wire stubbing (Figure 3.9c) was observed. Smooth bead deposits with good dimensional stability can only be attained (Figure 3.9b) with parameters that provide smooth wire transfer during deposition (Abioye, Folkes, and Clare 2013). The distance from the wire tip and the substrate (*d* in Figure 3.7) also has been reported to produce similar effect on deposited beads (Heralić 2012). Low dilution was achieved with high wire feed rate, high deposition speed, and low laser power (Abioye, Folkes, and Clare 2013). Wire feeding direction (front feeding or rear feeding, Figure 3.7), feeding angle (α in Figure 3.7b), and the position of wire tip in the melt pool (leading edge, middle or tailing edge) also found to have strong effect on overall quality of the deposit in terms of porosity, surface finish, and geometrical control (Syed and Li 2005). Feeding angle effect on bead roughness depended on wire feeding direction—high angles resulted in rough and smooth beads for front and rear

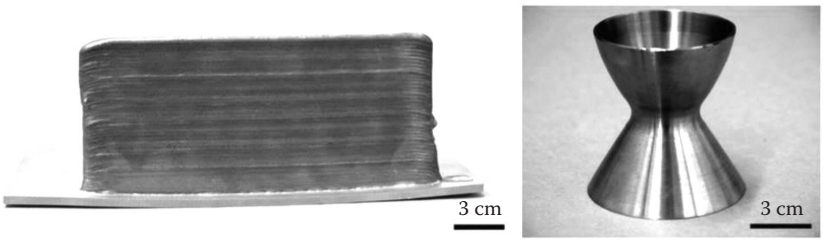

FIGURE 3.8
Archetypal thin wall deposit (a) and machined thruster (b) fabricated using Ti6Al4V wire deposition process. (Reprinted with permission from Brandl et al. 2011b.)

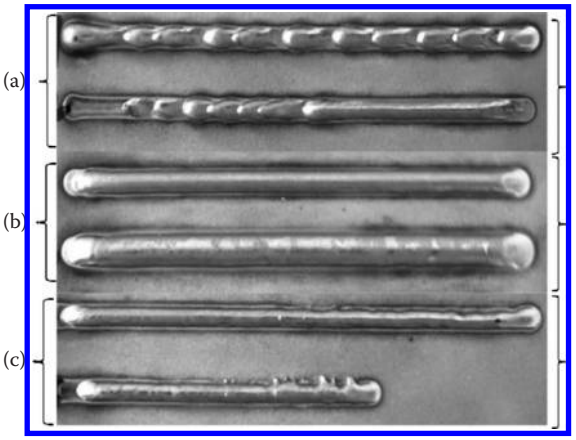

FIGURE 3.9
Laser wire deposited beads of Inconel 625. (a) Wire dripping, (b) smooth wire deposition, and (c) wire stubbing. (Reprinted from Abioye, T.E. et al., *J. Mater. Process. Technol.*, 213, 2145–2151, 2013, Open-access.)

feeding, respectively. For stable bead deposition, the wire tip position in the melt pool should always be away from the solidification start point and good quality deposits can be obtained with either front or rear feeding but with different set of process parameters (Syed and Li 2005).

From the above discussion, it is clear that wire-based deposition process is sensitive to large number of process parameters, and maintaining and controlling stable deposition is of utmost importance to achieve high-quality parts. Therefore, continuous monitoring and control of wire deposition has been attempted by several authors (Hagqvist et al. 2014; Heralic, Christiansson, and Lennartson 2012; Heralic et al. 2008, 2010; Liu et al. 2014). Hagqvist et al. (2014) proposed innovative approach for controlling laser metal wire deposition process via electrical resistance between wire and the melt pool. They demonstrated that this approach effectively control wire dripping and stubbing by automatic adjustment of stand-off distance (d in Figure 3.7b). The result of resistance measurement for online wire deposition control is shown in Figure 3.10. 3D scanning-based system has also been used to control the stand-off distance thus achieving flat deposits (Heralic, Christiansson, and Lennartson 2012). The wire feed rate control based on deposits' 3D scanned data helped to compensate the deviations in deposit heights.

3.2.2.2 Electron Beam Freeform Fabrication

EBF[3] was developed at NASA Langley Research Center, USA, and is cable of producing complex parts using variety of metals and alloys. The process is very similar to laser-based wire deposition process except that it is carried out in high vacuum (typically between

FIGURE 3.10
Wire dipping without online controller (above) and smooth deposit produced using resistance measurement-based online control (below). (Reprinted with permission from Hagqvist, P. et al., *Opt. Laser. Eng.*, 54, 62–67, 2014.)

1×10^{-4} and 1×10^{-5} Torr) with electron beam as energy source. Several advantages of EBF³ over laser-based deposition process have been reported (Stecker et al. 2006) including high power efficiency (≥90%) and high coupling efficiency. Therefore, this process is highly suitable for materials that reflect laser such as aluminum and copper, and is highly flexible in terms of achieving desired surface finish and feature size. High vacuum environment of EBF³ ensures clean deposits, while loss of some elements from the melt pool is also unavoidable. In general, fine diameter wires are used for complex components with fine features and for high deposition rates large diameter wires are preferred. Recent developments enabled deposition of compositionally graded components using dual wire feeders. Further, EBF³ process enables part fabrication in space as well (Taminger 2009). The surface finish of the parts produced using EBF³ is also excellent as shown in Figure 3.11.

EBF³ process is controlled by several parameters, namely, beam power and beam pattern apart from other parameters shown in Figure 3.7 for laser-based deposition process. These parameters strongly influence the deposit quality, residual stresses, final chemical composition, and so on. Matz and Eagar (2002) examined net shape fabrication of alloy 718 using EBF³. It was found that the spherical carbide precipitates size can be significantly reduced using EBF³ process and is attributed to rapid cooling rates. Similarly, detrimental Cr-carbides were suppressed during EBF³ processing of 347 stainless steel leading to tensile properties comparable to that of wrought equivalent (Wanjara, Brochu, and Jahazi 2007). Several authors reported the influence of EBF³ process parameters on microstructures and mechanical properties of aluminum alloys (Taminger and Hafley 2002, 2003;

FIGURE 3.11
Typical part produced using EBF³. Note the macrostructure showing columnar grains oriented along the part axis, which demonstrate EBF³ ability to produce smooth parts. (Data from Taminger, K., *Adv. Mater. Process.*, 11/12, 45, 2009, Open-access.)

Taminger, Hafley, and Domack 2006), which emphasize process optimization and control (Seufzer and Taminger 2007). Other issues that require close attention include loss of certain elements from the deposit (e.g., Al from Ti6Al4V alloy), improvements in repeatability, residual stresses and distortion, gradient deposits, and tailored microstructures.

3.2.2.3 Arc-Based Wire Deposition Processes

Arc-based wire deposition processes are known as SMD and use metal inert gas welding technique to produce dense components (Akula and Karunakaran 2006). The process was originally developed by Rolls-Royce. Typically, the process is controlled by commercial welding robot with dimensional accuracy and surface finish comparable to that of beam-based processes. Advantages of this technique over beam-based processes are relatively high deposition rate, power density at low cost and ability to pulse the arc providing additional microstructural control. Till date, the majority of weldable alloys have been deposited using SMD technique, which include Ti alloys (Baufeld and Van der Biest 2009; Baufeld, Van der Biest, and Gault 2009, 2010; Katou et al. 2007), steels (Skiba, Baufeld, and Van der Biest 2009, 2011), and Ni base alloy (Clark, Bache, and Whittaker 2008). One important challenge in this process is deposition of overhang structures due to lacks of support to liquid metal pool. However, recently electromagnetic confinement of liquid metal pool found to increase the tilt angle by 10° (Bai, Zhang, and Wang 2013). Typical Ti6Al4V alloy components produced using SMD are presented in Figure 3.12.

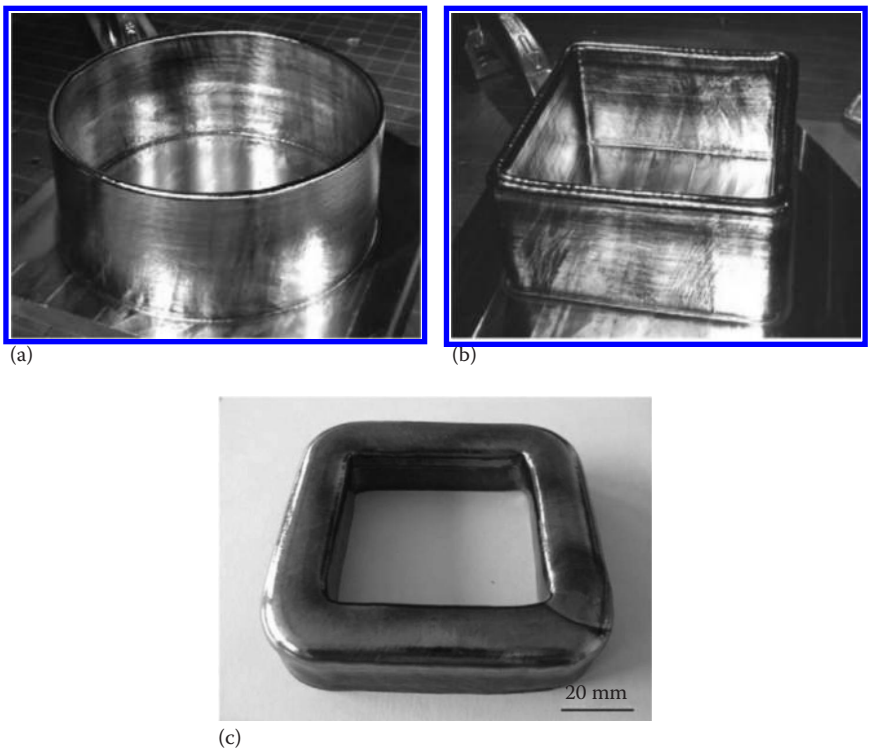

FIGURE 3.12
(See color insert.) Tubular parts fabricated using SMD; (a) and (b) thin wall components and (c) thick wall (20 mm) component. (Reprinted with permission from Baufeld, B. et al., *Mater. Design*, 31, S106–S111, 2010.)

Clark, Bache, and Whittaker (2008) developed combustion outer casing with alloy 718 using SMD based on their initial multi-pass deposits. However, they could not control the formation of laves and delta phases in alloy 718 during solidification. Ti6Al4V alloy samples fabricated by SMD exhibited tensile strength in the range of 929 and 1014 MPa, which are comparable to equivalent cast material (Baufeld, Van der Biest, and Gault 2010). To address feature resolution of SMD, recently micro-arc-based deposition processes have been developed (Horii, Kirihara, and Miyamoto 2009; Jhavar, Jain, and Paul 2014). Net shape manufacturing of mesoscale parts using micro-tungsten inert gas welding was reported by Horii, Kirihara, and Miyamoto (2009). Very recently more energy efficient and cost-effective deposition process based on micro-plasma transferred arc reportedly produced tool steel deposits to repair dies and molds (Jhavar, Jain, and Paul 2014). The process has been demonstrated to achieve wall width of approximately 2 mm with deposition efficiency of 87% and deposition rate of 42 g/h. The deposits were also metallurgically and physically sound without any defects. The properties of Ti6Al4V alloy fabricated using laser and arc beam deposition were found to be comparable (Brandl et al. 2010). Similar observations were also reported by Baufeld, Brandl, and Biest (2011) where properties of same alloy produced via laser beam-based deposition and SMD processes were compared. Other reports include fabrication of Ti6Al4V alloy using wire arc AM process (Wang et al. 2013) and stainless steel powder consolidation using electric arc (Rangesh and O'Neill 2011).

3.2.3 Solid-State AM Processes

Solid-state AM techniques have been developed to create complex 3D structures with metals that are difficult to process using fusion-based techniques such as LENS, DMD, and SMD. Additionally, solid-state processes enable processing of metallurgically incompatible metals and create laminated materials and embedded structures. UC is the only solid-state AM technology based on ultrasonic metal joining that is commercially available since 2000 from Solidica Inc., USA. UC is a hybrid AM technique, and commercial UC machines consist of ultrasonic welding head (sonotrode), thin metal foil feeding system, and a CNC milling station. Like other AM processes, UC also uses custom software to generate layers and processing conditions. However, the layer thickness is decided based on available metal foil thickness. The UC process and bonding mechanism are presented in Figure 3.13.

The process begins with feeding thin metal foil (typically between 100 and 150 μm thick), which will be pressed against base plate using normal load applied through sonotrode. The sonotrode vibrates transversely at 20 kHz under specified normal load and travels across the length of the part creating metallurgical bond. A layer will be created by deposition series of foil strips side-by-side and the final shape/contour of the layer will be achieved using CNC milling. Then compressed air is used to clean the surface off the machining debris and the next layer deposition starts. The CNC milling usually performed after several layers have been deposited and the process of deposition and milling continues until the 3D component is produced. The ultrasonic welding head usually has rough knurl surface, which keeps the foil intact with sonotrode head, while sonotrode oscillates at high frequency. The ultrasonic oscillations of top foil against the bottom foil/base plate create frictional forces and break up oxide layers that bring the atomically clean metal surface together. The preheating and friction-generated heat accelerate the atomic diffusion across the metal interfaces, and strong metallurgical bond forms under the influence of normal force. UC has been extensively

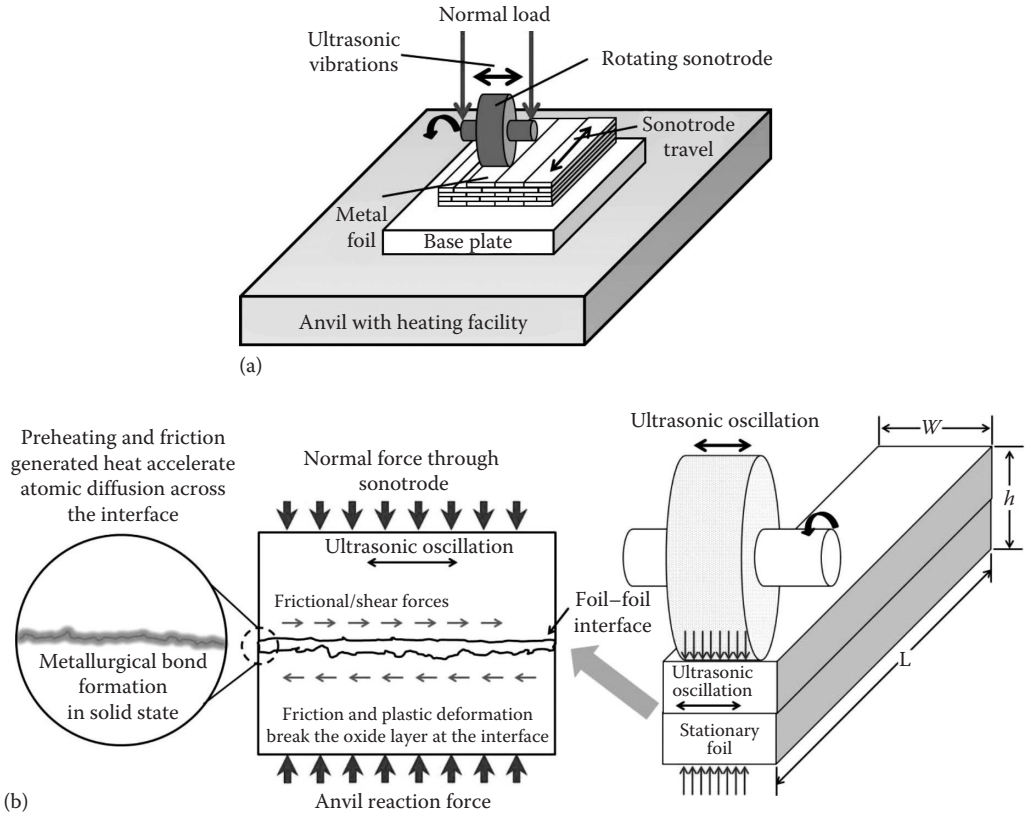

FIGURE 3.13
(See color insert.) (a) Ultrasonic consolidation process and its components; (b) illustration of foil geometrical parameter (right) and formation of metallurgical bond between the foils during ultrasonic consolidation (left).

used to fabricate different multi-material and multi-functional metal structures with embedded sensors and circuits (Friel and Harris 2013; George 2006; Janaki Ram et al. 2007a; Kong 2005; Obielodan et al. 2010; Siggard 2007). It has been demonstrated that metal matrix composites can also be fabricated using UC (Yang, Janaki Ram, and Stucker 2007). Fabrication of novel Al composite with tailored coefficient of thermal expansion has also been attempted by incorporating shape memory alloy in Al 3003 matrix using UC (Hahnlen and Dapino 2014).

Important process parameters include normal force (500 to 2000 N), sonotrode texture (Ra between 4 and 15 μm), sonotrode amplitude (5 to 150 μm) and sonotrode travel speed (10 to 50 mm/s), and preheating temperature (93°C to 150°C). Too low sonotrode amplitude and normal force produce very weak bonds and very high values of these parameters could lead to excessive foil deformation and misalignment of the layers. Therefore, to achieve strong bonding and bulk components, optimal choice of process parameters is very important for each material and part geometry (Kong, Soar, and Dickens 2003, 2004). UC of dissimilar metals has been reported by Obielodan et al. (2011), and the influence of ultrasonic energy on material softening was studied by Langenecker (1966). A study by Gonzalez and Stucker (2012) demonstrated that linear weld density strongly influenced

by process parameters and highest linear weld density of 95.89% was obtained at 1800 N normal load, 27 μm ultrasonic amplitude, 11 mm/s sonotrode travel speed, and a temperature of 204°C. Further, they emphasize the use of high power UC to achieve strong structures using high-strength materials. Recently, the sonotrode surface texture found to influence the bond strength in UC processed Al alloy and surface roughness around 6 μm has been suggested (Li and Soar 2009). Increasing the surface roughness can potentially eliminate foil overlap and crinkling due to high ultrasonic energy transfer to the foil, while improving the peel strength and linear weld density. It is also important to state here that increased surface roughness of sonotrode may transfer this roughness to deposited foils, which may affect bonding of subsequent foils. Excessively high and low roughness of sonotrode was found to result in low linear weld density (Friel et al. 2010). It appears that there exists optimal sonotrode topography that ensures strong and effective bonding during UC due to efficient energy transfer and inter-foil deformation. Similarly, the build geometry strongly influences the stability of UC process (Gibert, Austin, and Fadel 2010).

Understanding the fundamental mechanism of bond formation during UC is still an important but challenging area of research. Plastic deformation is an essential part of UC, which brings the two metals in intimate contact and breaks the surface oxide layer. Earlier studies show that bond formation during ultrasonic welding, after intimate contact is achieved, is due to mechanical interlocking, interfacial melting, and metal diffusion (Joshi 1971). It is extremely important to identify process parameters dependant dominant mechanism and which mechanisms enable formation of strong metallurgical bonding during UC. Experimental investigations on bond formation during UC of similar and dissimilar metals have been reported (Janaki Ram et al. 2007b; Yang, Janaki Ram, and Stucker 2009). The results showed no evidence of above mechanisms, namely, mechanical loading, melting, and diffusion, which suggest that the bonding occurred purely in solid state. It was concluded that removal of oxide layers and formation of intimate contact between the metal surfaces are responsible for bond formation (Yang, Janaki Ram, and Stucker 2009). To understand the influence of process parameters on bonding a term, *total transmitted energy*" (E_t) has been developed, which primarily depends on normal force, sonotrode oscillating amplitude, and sonotrode travel speed (welding speed). Earlier studies show clear dependence of linear weld density on E_t (Janaki Ram, Yang, and Stucker 2007; Kong, Soar, and Dickens 2004), where high E_t improved the bond formation. However, excessively high E_t could damage the previous bonds leading to drop in linear weld density. Interestingly, the deterioration of bonds was found to be influenced by energy input during single cycle of ultrasonic vibration (E_0) and not by E_t (Janaki Ram, Yang, and Stucker 2007; Kong, Soar, and Dickens 2004). These energy terms were defined in Yang, Janaki Ram, and Stucker (2010), where process parameters such as welding speed, sonotrode amplitude, and normal force were correlated with energy terms and linear weld density. In this study, an analytical model also has been developed to estimate the linear weld density from energy input. In line with this study, Kelly et al. (2014) confirmed through experiments that the bonding in UC occurs in solid state and is not due to thermal softening or melting. A model was developed to understand the influence of energy input on weld strength and linear correlation was observed. In another study, acoustic softening was found to reduce the yield strength of Al 1100 foils up to 82% and thermal softening was very minimum (Kelly et al. 2013). Interfacial microstructures of UC processed Al 3003 alloy showed fine-scale microstructural modifications at the foil–foil interface and are due to local plastic deformation as a result of sonotrode texture (Dehoff and Babu 2010).

3.2.4 Electrodeposition-Based Additive Manufacturing

EFAB is one of the AM technologies based on Instant Masking™ and electrodeposition process that can effectively build miniature 3D metal structures with micro-scale resolution. The process is currently being marketed by Microfabrica, Inc. Although originally developed at the University of Southern California in late 1990s (Cohen et al. 1998), later developments (Cohen 1999; Kruglick, Cohen, and Bang 2006; Reid and Webster 2006) enabled the process to fabricate functional components as small as $4 \times 25 \times 25$ μm weighing 0.02 μg can be easily fabricated (Cohen et al. 2010). This flexible process produces highly intricate metallic structures/devices of the order of millimeters to centimeters in size and is cost effective for batches up to 1000 parts. This process can be considered as hybrid AM process where additive and subtractive steps are involved. In general, the process of making each layer consists of electrodeposition of selective pattern followed by blanket deposition and final mechanical planarization. Use of electrodeposition in EFAB enables extremely fine deposits, low residual stresses, no shrinkage, and fine features. Apart from part complexity, the EFAB process can create devices with moving parts that are preassembled during fabrication process. Currently, the process geometrical capabilities include ≥4-μm-thick layers having ± 1.5 μm inter-layer alignment, 10–20 μm in-plane features with tolerances of ± 2 μm and ± 1 μm for *Z*-axis and *X*–*Y* axis, respectively. The surface finish of the devices fabricated using EFAB is typically around 0.15 μm and further improvements are also possible (Cohen et al. 2010).

The EFAB process is a micro AM process and involves three basic steps to generate each layer, and these three steps are repeated until complex 3D component is build (Vaezi, Seitz, and Yang 2013). As with other AM technologies, the EFAB process also relies on deposition of structural material (forming feature of final component/device) and sacrificial material (forming support structures), and both materials should be electrically conductive because these materials are deposited using electrodeposition technique. The three sequential process steps for each layer include (1) electrodeposition of sacrificial material, (2) structural material electrodeposition, and (3) mechanical planarization. The process starts with creation of *instant masks* that include cross-sectional geometry of each layer using custom software (Layerize™) from 3D CAD model of the final device—single part or assembly of multiple parts. Layerize generates (1) 2D cross sections of each layer in a format compatible with commercial photomask pattern generators, and (2) automated EFAB process control file used for electrodeposition of structural and sacrificial materials. The photomask patterns produced using generated 2D cross sections are used to fabricate *instant masks* using micromolding technique (Cohen 2002) and are used in the EFAB machine for selective deposition of materials in each layer. The EFAB process begins with selective electrodeposition of sacrificial material with the use of instant masks. Figure 3.14 shows typical EFAB process.

The first step involves electrodeposition of sacrificial material on a substrate at selected areas predetermined by the *instant mask* of first layer. This is achieved by pressing the substrate (cathode) against *instant mask* (mounted on anode) placed in an electrodeposition cell where the electrolyte occupies the openings in the masks. Then, the electrodeposition process is initiated by passing an electric current through the cell electrodes leading to selective deposition of sacrificial material on the substrate at areas defined by the mask. After this, the *instant mask* along with the anode is removed leaving behind the deposited sacrificial material. In the second step, the structural material is electrodeposited nonselectively (blanket-deposited) covering the entire area including previously deposited materials and other open areas on the substrate. This process takes place in a separate

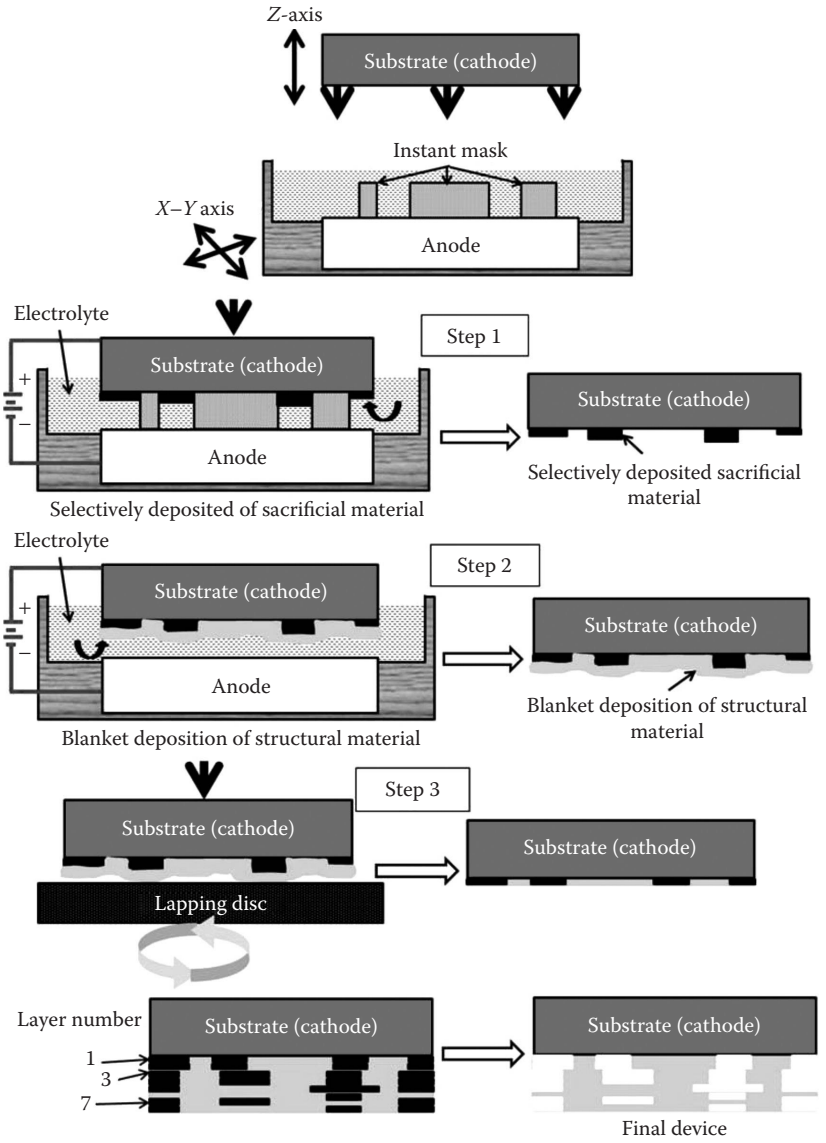

FIGURE 3.14
EFAB process flow.

electrodeposition cell with appropriate electrolyte and anode. As a third step, the entire deposit is mechanically planarized using lapping plate until both materials are visible and desired layer thickness with flatness and smoothness is achieved. Other reasons for planarization can be found in Cohen (2002). Repetition of the above three steps for all layers creates final device embedded in the sacrificial material, which is then chemically etched producing desired structure as represented in 3D CAD model.

In principle, any material that can be deposited using electrolytic/electroless deposition are good candidate materials for EFAB. Therefore, structures with many pure metals and

alloys can be fabricated using EFAB. However, Microfabrica, Inc. developed some limited number of materials such as Ni–Co, rhodium. Ni–Co alloy processed using EFAB has been shown to exhibit good mechanical properties, corrosion resistance, and short-term biocompatibility properties (Cohen et al. 2010). Rhodium also achieved good mechanical properties in as-fabricated condition, and the interlayer adhesion of EFAB structures was also found to be >20% of the bulk strength of the structural material (Cohen 2002). One important material consideration for sacrificial material is that it should be selectively etchable after EFAB process.

EFAB process is an enabling micro AM technology with very strong future potential. However like other processes, EFAB has some liminations, which include throughput, part size, stair-step effect, and maximum number of layers. Compared to other AM technologies, the build rates in Z direction (several hunderd microns/day) is significantly less for EFAB process. The process is limited to maximum 50 number of layers, which is again linked to build rates. Similarly, geometrically large devices (large volume) cannot be easily frabricated using EFAB. The stair-step effect poses some problems in certain devices with moving parts where the clearance between moving parts is smaller than minimum layer thickness. While the effective removal of sacrificial materials requires designed release holes, fabrication of microdevices with moving parts and other elements has been successfully demonstrated by EFAB process (Cohen et al. 2010). Further developments in the area of new metals, alloys, and other sensing devices are also anticipated (Vaezi, Seitz, and Yang 2013).

3.3 Emerging AM Technologies

3.3.1 Friction Freeform Fabrication

Very recently, Dilip et al. (2013) proposed *friction freeform fabrication* that uses friction surfacing, a solid-state surface deposition process, to deposit material layer by layer creating 3D metal structures. In this technique, the process of depositing single track of metal on a substrate is very similar to conventional friction surfacing. A consumable rod is rotated at high speed and is forced against a substrate with desired axial force generating frictional heat sufficient to plastically deform the consumable rod. Then, moving the substrate in a predetermined path creates deposition of consumable rod on to the substrate forming a track. Following this procedure, parallel tracks can be deposited creating a layer, which is then machined using CNC machining to give desired slice/layer contour. The processing of deposition and CNC machining is repeated several times to complete the fabrication of 3D metallic structures. Typically, the track width is of the order of consumable rod diameter but can be varied along with layer thickness depending on the process parameters. Typical FFF process is schematically shown in Figure 3.15.

Different samples with dissimilar metals and structures with enclosed internal cavities have been successfully fabricated using FFF (Dilip et al. 2013). FFF metals exhibited excellent inter-track and inter-layer bonding, fine-grained microstructures, and comparable mechanical properties with that of wrought equivalents (Dilip et al. 2013). FFF processed Inconel 718 alloy also shown to have good room temperature mechanical properties after direct aging (Dilip and Janaki Ram 2014). However, FFF appears to be detrimental to mechanical properties of heat treatable Al alloys due to precipitate

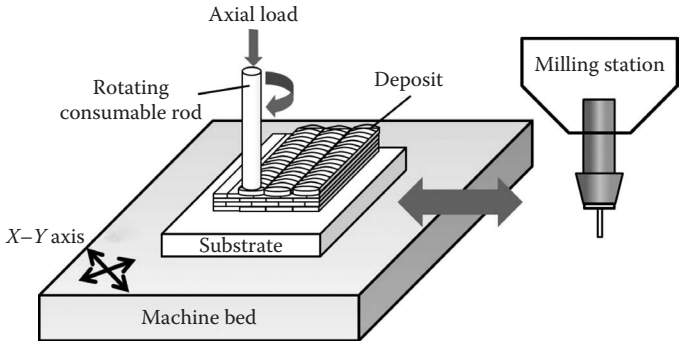

FIGURE 3.15
Friction freeform fabrication process.

coarsening (Dilip and Janaki Ram 2013). The precipitate coarsening is attributable to very high friction generated temperatures and repeated heating and cooling cycles (Puli and Janaki Ram 2012; Rafi et al. 2011). Therefore, like fusion-based AM techniques, evolution of microstructure during FFF of metals is also highly complex.

3.3.2 Hybrid Techniques

A new hybrid AM technique named HPDM has been proposed by Xiong, Haiou, and Guilan (2008). The HPDM unit consists of plasma torch and CNC milling station. In this process, metal is deposited using plasma arc and CNC milling creates layer contour. Important advantages of this process include high deposition rates, near net shape manufacturing, and economical energy source. Good surface finish and dimensional accuracy have been achieved using HPDM (Xiong, Haiou, and Guilan 2008). Another process based on plasma deposition known as electromagnetic compressed plasma deposition manufacturing (PDM) has also been reported (Zhang, Xu, and Wang 2003). The feedstock material is metallic powder that is fed into the molten metal pool created by plasma heating. The powder melts and moving the deposition head relative to the substrate creates thin metal track. Overlapping the tracks creates one layer and the process is repeated to fabricate 3D structure. The major difference compared to HPDM is that the plasma is magnetically confined and this may help in achieving better feature resolution than HPDM. It appears the overall process is similar to laser-based deposition technique, except the energy source. The deposit quality depends on powder feed rate, scan velocity, and arc current (Zou et al. 2009).

Fusion-based AM techniques lack optimal balance of efficiency and accuracy with additional problems such as residual porosity, coarse columnar microstructure, and anisotropic properties (Dinda, Dasgupta, and Mazumder 2009). To address some of these issues, a novel hybrid AM process was introduced by Zhang et al. (2013), which combine all advantages of AM and microstructural benefits of metal deformation. The basic principle of this hybrid AM process is fusion deposition of metal followed by hot deformation the same. To achieve this, a micro roller will be positioned behind the deposition head and the distance between these two is one important process parameter, the other being the rolling deformation. As a result of hot rolling, the deposit top surface is always flat and the microstructure changes from cast to wrought. The flat top surface of the deposit ensures stable and accurate deposition of subsequent layer.

The flatness and quality of deposit after rolling were found to depend on the distance between deposition head and the roller, and the amount of deformation (Zhang et al. 2013). Too short distance between energy source and the roller would lead to deposit surface peel off possibly due to sticking at high temperature, while large distance cannot deform the deposit due to drop in deposit temperature (require high pressure). Good deposit shape and dimensions can be achieved at optimal process parameters. The process refined the deposit microstructure leading to improved mechanical properties (Zhang et al. 2013). Accurate slice thickness control, tailorable deposit width, and economical large-scale part production are some of the other benefits of this process.

3.4 Opportunities and Challenges

Having known the capabilities of various AM technologies available for manufacturing metallic components, it is too early to comment on their readiness to compete conventional manufacturing at least in some important areas (Reeves and Hague 2013). For example, fundamental understanding of the process and precise process control is an essential requirement to reduce or even eliminate variability and uncertainty in product properties. AM standards may be required to qualify their products for use in applications related to aerospace and military. Initially, these materials should meet the performance of materials manufactured via conventional routes. In this context, large number of opportunities and serious challenges exist to realize full potential of these enabling technologies, which are discussed briefly in the following sections.

3.4.1 Materials Related

AM technologies have been used to process several existing metals and alloys but comprehensive correlation and understanding of processing–microstructure–property–performance relationships of these alloys is yet to be established. Such an understanding not only enables development of new materials but also helps designers consider AM-processed existing materials so that full potential of these technologies can be realized (Scott et al. 2012). Other requirements include availability, consistency and quality of feedstock materials (all materials not available in either powder/wire or foil form), complete properties and characteristics of feedstock materials (dictate process stability and quality of final product), creation and access to materials database that includes microstructures and properties of finished product, feedstock, and recycled materials. Further, the influence of post-processing operations on properties and performance also needs to be studied (Roadmap Workshop Summary Report 2013). Important challenges related to AM materials are presented in Table 3.2.

3.4.2 Process Related

Path-dependant attributes such as residual stresses, distortion, microstructure, related properties, and part geometry-dependant temperature fields, thermal gradients/history must be clearly understood for fusion-based technologies to minimize variability and uncertainty. For this purpose, process sensing such as melt pool size, temperature, and temperature variations are required, while these signals are used to control the process online. Similar types of processing monitoring and closed-loop control systems are required

TABLE 3.2

Identified Challenges for AM

Area	Challenges
Materials	• Lack of processing–microstructure–property–performance relationships • Understanding issues related to post-processing of AM parts • Feedstock materials characterization, testing, and availability
Process	• High-speed image process enabling real-time process diagnosis and control • Models and devices for new real-time measurement capabilities composition, dimensions, stresses, distortion • Models that can effectively combine AM design, process, and materials
Machine	• Non-availability of research versions of AM machines with high flexibility • New sensors to monitor and measure process parameters such as temperature, stress, and their effective integration of above for robust feedback control • Real-time measurement and control of microstructures, surface finish, and so on • Ability to produce net shape components (currently near net shape) with improved feature resolution, part size, and isotropic properties • Lack of standards for AM processes, materials properties, defects, geometrical parameters, test procedures, and samples

Source: Roadmap workshop on measurement science for metal-based additive manufacturing, Workshop Summary Report, May 2013. http://events.energetics.com/NIST-AdditiveMfgWorkshop/pdfs/NISTAdd_Mfg_report_FINAL.pdf.

for other solid-state and emerging AM processes as well (Kinsella 2011). Currently, these facilities are partly available in only selected AM processing equipment but they lack desired ability to control and require further improvements. For example, they cannot detect defects and correlate them with processing variations (such as powder, speed, and deposited material thickness variations) in real time and make necessary corrections. Development of non-destructive evaluation systems that can detect defects and provide feedback to control the same in real time is also required to improve the product quality (Bourell, Leu, and Rosen 2009).

Multi-scale and multi-level modeling, simulation, and analysis need to understand the physical phenomenon operating during processing and predict final microstructures, residual stresses, properties, and surface quality (Frazier 2010). It is intuitive to expect that the accuracy of developed models relies on comprehensive and fundamental understanding of AM processes and materials. Moreover, AM machine capabilities in terms of in situ sensing, monitoring, and control process are also essential to develop reliable and accurate models based on information such as temperature fields, dimensions, composition. The modeling efforts provide more options to tailor materials properties to suit desired end use while providing information on essential requirements to achieve these such as sensing, measuring, monitoring, and control systems.

3.4.3 Machine Related

Production type AM machines may be qualified per government qualification procedures thus improving overall repeatability (Kinsella 2011). The most important issue with current AM machines is their flexibility, that is, that they come with restricted ability to create/test custom processing parameters and materials. Therefore, development of new materials and processing routes is hampered. It is opined that AM machine should be grouped into production types and development types, the former types may be customized for

production where new material development is not required. However, AM machines for developmental activities must have greater flexibility to change process parameters, custom materials, and composites. Other immediate requirements appear to be improved overall product quality (dimensional accuracy, surface finish, etc.), production rate, process efficiency, and cost competiveness of AM equipment. Some AM processing require controlled atmosphere and their overall process efficiency is typically less than conventional processing. Standards are another key area, which helps making parts with identical properties and geometrical quality using different AM techniques.

The quality and performance of parts produced by AM depend on inherent physical phenomenon during processing, which rely on manufacturing paths. Therefore, these must be considered at priori and may be right from beginning of designing the components. This approach requires concentrated efforts in the area of design for AM (DAM) (Ponche et al. 2014). DAM enables effective designing of components after considering unique capabilities and limitations of AM processes (Vayrea, Vignata, and Villeneuvea 2012). For example, build orientation has been recognized to strongly affect mechanical properties in different directions of the parts, which must be considered in the process of designing a component. Similarly, rate of acceleration and deceleration during deposition usually leads to variations in deposition height between contour and away from it. Therefore, designing a part without sharp corners may eliminate this problem. Due to the agile nature of AM techniques, designers can consider complex geometries that can improve the performance and efficiency during service.

3.5 Summary and Future Directions

Concentrated efforts over the past two decades made some of the AM technologies matured and are able to produce components that are of high quality and superior properties compared to conventionally processed materials. Some AM technologies offer outstanding benefits in manufacturing components such as micro-scale devices with moving parts. Other demonstrated capabilities of AM technologies for metals include creation of novel compositional variations across the sample, multi-materials such as composites/alloys, structurally graded materials (such as porous metals) with tailored mechanical, physical, chemical, and multifunctional properties. However, fusion-based AM processes are highly complex problems to understand and model primarily due to multi-factorial effects. Solid-state processes also have similar complexities related to material and heat flow, bonding mechanisms, and properties. Several inherent aspects of processes controlling the stability of AM processes, process and microstructural control, process optimization, and machine capabilities still require significant improvements.

The major barriers for widespread utilization and development of AM are relatively immature technology (compared to conventional manufacturing technologies), limited number of available materials, cost-effectiveness, and lack of confidence among various industries as these processes are not robust enough to create components with high repeatability, accuracy, and properties. The future potential of these enabling technologies depends on how effectively we can overcome these barriers. Further, the future research focus will remain on development of novel and unique material with designed properties, feedstock materials providing more flexibility, process modeling, simulation and control, materials and property database and standards.

References

Abioye, T.E., Folkes, J., Clare, A.T. 2013. A parametric study of Inconel 625 wire laser deposition. *Journal of Materials Processing Technology* 213:2145–2151.

Ader, C., Brosemer, M., Freyer, C., Fricke, H., Hennings, D., Klocke, F., Kühne, V., Meiners, W., Over, C., Pleteit, H., Stührmann, S., Wirth, I., Wirtz, T., Wissenbach, K. 2003. In *Solid Freeform Fabrication Symposium Proceedings*, Laboratory for Freeform Fabrication and University of Texas at Austin, Austin, TX, pp. 26–30.

Akula, S., Karunakaran, K.P. 2006. Hybrid adaptive layer manufacturing: An intelligent art of direct metal rapid tooling process. *Robotics and Computer-Integrated Manufacturing* 22:113–123.

Bai, X.W., Zhang, H.O., Wang, G.L. 2013. Electromagnetically confined weld-based additive manufacturing. *Procedia CIRP* 6:515–520.

Balla, V.K., Bandyopadhyay, A. 2010. Laser processing of Fe based bulk amorphous alloy. *Surface and Coatings Technology* 205(7):2661–2667.

Balla, V.K., Bandyopadhyay, P.P., Bose, S., Bandyopadhyay, A. 2007. Compositionally graded yttria stabilized zirconia coating on stainless steel using laser engineered net shaping (LENS™). *Scripta Materialia* 57(9):861–864.

Balla, V.K., Banerjee, S., Bose, S., Bandyopadhyay, A. 2010a. Direct laser processing of tantalum coating on Ti for bone replacement structures. *Acta Biomaterialia* 6(6):2329–2334.

Balla, V.K., Bhat, A., Bose, S., Bandyopadhyay, A. 2012a. Laser processed TiN reinforced Ti6Al4V alloy composite coatings. *Journal of Mechanical Behavior of Biomedical Materials* 6:9–20.

Balla, V.K., Bodhak, S., Bose, S., Bandyopadhyay, A. 2010b. Porous tantalum structures for bone implants: Fabrication, mechanical and in vitro biological properties. *Acta Biomaterialia* 6(8):3349–3359.

Balla, V.K., Bose, S., Bandyopadhyay, A. 2008. Processing of bulk alumina ceramics using laser engineered net shaping. *International Journal of Applied Ceramic Technology* 5(3):234–242.

Balla, V.K., Bose, S., Bandyopadhyay, A. 2010c. Understanding compressive deformation in porous titanium. *Philosophical Magazine* 90(22):3081–3094.

Balla, V.K., Bose, S., Bandyopadhyay, A. 2010d. Microstructure and wear properties of laser deposited WC-12%Co composites. *Materials Science and Engineering A* 527(24/25):6677–6682.

Balla, V.K., Das, M., Bose, D., Ram, G.D.J., Manna, I. 2013. Laser surface modification of 316L stainless steel with bioactive hydroxyapatite. *Materials Science & Engineering C* 33(8):4594–4598.

Balla, V.K., DeVasConCellos, P., Xue, W., Bose, S., Bandyopadhyay, A. 2009a. Fabrication of compositionally and structurally graded Ti-TiO2 structures using laser engineered net shaping (LENS). *Acta Biomaterialia* 5(5):1831–1837.

Balla, V.K., Martinez, S., Rogoza, B.T., Livingston, C., Venkateswaran, D., Bose, S., Bandyopadhyay, A. 2011. Quasi-static torsional deformation behavior of porous Ti–6Al–4V alloy. *Materials Science and Engineering C* 31(5):945–949.

Balla, V.K., Roberson, L.B., O'Connor, G.W., Trigwell, S., Bose, S., Bandyopadhyay, S. 2012b. First demonstration on direct laser fabrication of lunar regolith parts. *Rapid Prototyping Journal* 18(6):451–457.

Balla, V.K., Xue, W., Bose, S., Bandyopadhyay, A. 2009b. Laser assisted Zr/ZrO2 coating on Ti for load-bearing implants. *Acta Biomaterialia* 5(7):2800–2809.

Bandyopadhyay, A., España, F.A., Balla, V.K., Bose, S., Ohgami, Y., Davies, N.M. 2010. Influence of porosity on mechanical properties and in vivo response of Ti6Al4V implants. *Acta Biomaterialia* 6(4):1640–1648.

Bandyopadhyay, A., Krishna, B.V., Xue, W., Bose, S. 2009. Application of laser engineered net shaping (LENS) to manufacture porous and functionally graded structures for load bearing implants. *Journal of Materials Science—Materials in Medicine* 20(S1):S29–S34.

Bandyopadhyay, P.P., Balla, V.K., Bose, S., Bandyopadhyay, A. 2007. Compositionally graded aluminum oxide coatings on stainless steel using laser processing. *Journal of American Ceramic Society* 90(7):1989–1991.

Banerjee, R., Collins, P.C., Bhattacharyya, D., Banerjee, S., Fraser, H.L. 2003. Microstructural evolution in laser deposited compositionally graded α/β titanium-vanadium alloys. *Acta Materialia* 51(11):3277–3292.

Banerjee, R., Collins, P.C., Fraser, H.L. 2002. Phase evolution in laser-deposited titanium-chromium alloys. *Metallurgical and Materials Transactions A* 33A(7):2129–2138.

Baufeld, B., Brandl, E., Biest, O. 2011. Wire based additive layer manufacturing: Comparison of microstructure and mechanical properties of Ti–6Al–4V components fabricated by laser-beam deposition and shaped metal deposition. *Journal of Materials Processing Technology* 211:1146–1158.

Baufeld, B., Van der Biest, O. 2009. Mechanical properties of Ti–6Al–4V specimens produced by shaped metal deposition. *Science and Technology of Advanced Materials* 10(1):015008.

Baufeld, B., Van der Biest, O., Gault, R. 2009. Microstructure of Ti–6Al–4V specimens produced by shaped metal deposition. *International Journal of Materials Research* 100(11):1536–1542.

Baufeld, B., Van der Biest, O., Gault, R. 2010. Additive manufacturing of Ti–6Al–4V components by shaped metal deposition: Microstructure and mechanical properties. *Materials and Design* 31:S106–S111.

Bernard, S., Balla, V.K., Bose, S., Bandyopadhyay, A. 2011. Rotating bending fatigue response of laser processed porous NiTi alloy. *Materials Science and Engineering C* 31(4):815–820.

Bernard, S., Balla, V.K., Bose, S., Bandyopadhyay, A. 2012. Compression fatigue behavior of laser processed porous NiTi alloy. *Journal of Mechanical Behavior of Biomedical Materials* 13:62–68.

Bernard, S.A., Balla, V.K., Bose, S., Bandyopadhyay, A. 2010. Direct laser processing of bulk lead zirconate titanate ceramics. *Materials Science and Engineering B* 172(1):85–88.

Bhat, A., Balla, V.K., Bysakh, S., Basu, D., Bose, S., Bandyopadhyay, A. 2011. Carbon nanotube reinforced Cu-10Sn alloy composites: Mechanical and thermal properties. *Materials Science and Engineering A* 528(22/23):6727–6732.

Bourell, D.L., Leu, M.C., Rosen, D.W. 2009. Roadmap for additive manufacturing: identifying the future of freeform processing, In *SFF Symposium*, Austin, TX.

Brandl, E., Baufeld, B., Leyens, C., Gault, R. 2010. Additive manufactured Ti6Al4V using welding wire: Comparison of laser and arc beam deposition and evaluation with respect to aerospace material specifications. *Physics Procedia* 5:595–606.

Brandl, E., Michailov, V., Viehweger, B., Leyens, C. 2011a. Deposition of Ti–6Al–4V using laser and wire, part I: Microstructural properties of single beads. *Surface & Coatings Technology* 206:1120–1129.

Brandl, E., Michailov, V., Viehweger, B., Leyens, C. 2011b. Deposition of Ti–6Al–4V using laser and wire, part II: Hardness and dimensions of single beads. *Surface & Coatings Technology* 206:1130–1141.

Brandl, E., Palm, F., Michailov, V., Viehweger, B., Leyens, C. 2011c. Mechanical properties of additive manufactured titanium (Ti–6Al–4V) blocks deposited by a solid-state laser and wire. *Materials and Design* 32:4665–4675.

Brandl, E., Schoberth, A., Leyens, C. 2012. Morphology, microstructure, and hardness of titanium (Ti-6Al-4V) blocks deposited by wire-feed additive layer manufacturing (ALM). *Materials Science and Engineering A* 532:295–307.

Cao, X., Jahazi, M., Fournier, J., Alain, M. 2008. Optimization of bead spacing during laser cladding of ZE41A–T5 magnesium alloy castings. *Journal of Materials Processing Technology* 205:322–331.

Clark, D., Bache, M.R., Whittaker, M.T. 2008. Shaped metal deposition of a nickel alloy for aero engine applications. *Journal of Materials Processing Technology* 203:439–448.

Cohen, A. 1999. 3-D micromachining by electrochemical fabrication. *Micromachine Devices* March, 6–7.

Cohen, A., Chen, R., Frodis, U., Wu, M.-T., Folk, C. 2010. Microscale metal additive manufacturing of multi-component medical devices. *Rapid Prototyping Journal* 16(3):209–215.

Cohen, A., Zhang, G., Tseng, F.-G., Mansfield, F., Frodis, U., Will, P. 1998. EFAB: Batch production of functional, fully-dense metal parts with micron-scale features. In *Solid Freeform Fabrication Symposium Proceedings*, Laboratory for Freeform Fabrication and University of Texas, Austin, TX, pp. 161–168.

Cohen, A.L. 2002. Electrochemical fabrication (EFAB™). In *The MEMS Handbook*, Gad-el-Hak, M. (ed). CRC Press, Boca Raton, FL.

Collins, P.C., Banerjee, R., Banerjee, S., Fraser, H.L. 2003. Laser deposition of compositionally graded titanium–vanadium and titanium–molybdenum alloys. *Materials Science and Engineering A* A352(1/2):118–128.

Das, M., Balla, V.K., Basu, D., Bose, S., Bandyopadhyay, A. 2010. Laser processing of SiC-particle-reinforced coating on titanium. *Scripta Materialia* 63(4):438–441.

Das, M., Balla, V.K., Basu, D., Manna, I., Kumar, T.S.S., Bandyopadhyay, A. 2012. Laser processing of in-situ synthesized TiB-TiN reinforced Ti6Al4V alloy composite coatings. *Scripta Materialia* 66(8):578–581.

Das, M., Balla, V.K., Kumar, T.S.S., Manna, I. 2013. Fabrication of biomedical implants using laser engineered net shaping (LENS™). *Transactions of the Indian Ceramic Society* 72(3):169–174.

Das, M., Bysakh, S., Basu, D., Kumar, T.S.S., Balla, V.K., Bose, S., Bandyopadhyay, A. 2011. Microstructure, mechanical and wear properties of laser processed SiC particle reinforced coatings on titanium. *Surface and Coatings Technology* 205(19):4366–4373.

Das, S. 2003. Physical aspects of process control in selective laser sintering of metals. *Advanced Engineering Materials* 5(10):701–711.

Dehoff, R.R., Babu, S.S. 2010. Characterization of interfacial microstructures in 3003 aluminum alloy blocks fabricated by ultrasonic additive manufacturing. *Acta Materialia* 58:4305–4315.

DeVasConCellos, P., Balla, V.K., Bose, S., Bandyopadhyay, A., Fugazzi, R., Dernell, W.S. 2012. Patient specific implants for amputation prostheses: Design, manufacture and analysis. *Veterinary and Comparative Orthopaedics and Traumatology* 25(4):286–296.

Dilip, J.J.S., Babu, S., Rajan, S.V., Rafi, K.H., Janaki Ram, G.D., Stucker, B.E. 2013. Use of friction surfacing for additive manufacturing. *Materials and Manufacturing Processes* 28(2):189–194.

Dilip, J.J.S., Janaki Ram, G.D. 2013. Microstructure evolution in aluminum alloy AA 2014 during multi-layer friction deposition. *Materials Characterization* 86:146–151.

Dilip, J.J.S., Janaki Ram, G.D. 2014. Friction freeform fabrication of superalloy inconel 718: Prospects and problems. *Metallurgical and Materials Transactions B* 45B:182–192.

Dinda, G.P., Dasgupta, A.K., Mazumder, J. 2009. Laser aided direct metal deposition of Inconel 625 superalloy: Microstructural evolution and thermal stability. *Materials Science and Engineering A* 509(1/2):98–104.

Dittrick, S., Balla, V.K., Davies, N.M., Bose, S., Bandyopadhyay, A. 2011. In Vitro wear rate and co ion release of compositionally and structurally graded CoCrMo-Ti6Al4V structures. *Materials Science and Engineering C* 31(4):809–814.

Energetics Incorporated. Roadmap workshop on measurement science for metal-based additive manufacturing, Workshop Summary Report, by Energetics Incorporated, Columbia, Maryland, for the National Institute of Standards and Technology, U.S. Department of Commerce, May 2013. Accessed May 05, 2014. http://events.energetics.com/NIST-AdditiveMfgWorkshop/pdfs/NISTAdd_Mfg_report_FINAL.pdf.

España, F.A., Balla, V.K., Bandyopadhyay, A. 2011. Laser processing of bulk Al-12Si alloy: Influence of microstructure on thermal properties. *Philosophical Magazine* 91(4):574–588.

España, F.A., Balla, V.K., Bose, S., Bandyopadhyay, A. 2010. Design and fabrication of CoCrMo based novel structures for load bearing implants using laser engineered net shaping. *Materials Science and Engineering C* 30(1):50–57.

Frazier, W.E. 2010. Direct digital manufacturing of metallic components: Vision and roadmap. Paper read at *Direct Digital Manufacturing of Metallic Components: Affordable, Durable, and Structurally Efficient Airframes*, Solomons Island, MD.

Friel, R.J., Harris, R.A. 2013. Ultrasonic additive manufacturing A hybrid production process for novel functional products. *Procedia CIRP* 6:35–40.

Friel, R.J., Johnson, K.E., Dickens, P.M., Harris R.A. 2010. The effect of interface topography for Ultrasonic Consolidation of aluminium. *Materials Science and Engineering A* 527:4474–4483.

George, J.L. Utilization of ultrasonic consolidation in fabricating satellite decking. MS dissertation. Utah State University, Logan, UT, 2006.

Gharbi, M., Peyre, P., Gorny, C., Carin, M., Morville, S., Le Masson, P., Carron, D., Fabbro, R. 2013. Influence of various process conditions on surface finishes induced by the direct metal deposition laser technique on a Ti64 alloy. *Journal of Materials Processing Technology* 213:791–800.

Gharbi, M., Peyre, P., Gorny, C., Carin, M., Morville, S., Le Masson, P., Carron, D., Fabbro, R. 2014. Influence of a pulsed laser regime on surface finish induced by the direct metal deposition process on a Ti64 alloy. *Journal of Materials Processing Technology* 214:485–495.

Gibert, J.M., Austin, E.M., Fadel, G. 2010. Effect of height to width ratio on the dynamics of ultrasonic consolidation. *Rapid Prototyping Journal* 16(4):284–294.

Gonzalez, R., Stucker, B. 2012. Experimental determination of optimum parameters for stainless steel 316L annealed ultrasonic consolidation. *Rapid Prototyping Journal* 18(2):172–183.

Gu, D.D., Meiners, W., Wissenbach, K., Poprawe, R. 2012. Laser additive manufacturing of metallic components: Materials, processes and mechanisms. *International Materials Reviews* 57(3):133–164.

Hagqvist, P., Heralić, A., Christiansson, A.-K., Lennartson, B. 2014. Resistance measurements for control of laser metal wire deposition. *Optics and Lasers in Engineering* 54:62–67.

Hahnlen, R., Dapino, M.J. 2014. NiTi-Al interface strength in ultrasonic additive manufacturing composites. *Composites: Part B* 59:101–108.

Heralić, A. Monitoring and control of robotized laser metal-wire deposition. PhD dissertation. Chalmers University of Technology, Gothenburg, Sweden, 2012.

Heralic, A., Christiansson, A.-K., Lennartson, B. 2012. Height control of laser metal-wire deposition based on iterative learning control and 3D scanning. *Optics and Lasers in Engineering* 50:1230–1241.

Heralic, A., Christiansson, A.-K., Ottosson, M., Lennartson, B. 2010. Increased stability in laser metal wire deposition through feedback from optical measurements. *Optics and Lasers in Engineering* 48(4):478–485.

Heralic, A., Ottosson, M., Hurtig, K., Christiansson, A.-K. 2008. Visual feedback for operator interaction in robotized laser metal deposition. In *Proceedings of the 22nd International Conference on Surface Modification Technologies*, University West, Trollhättan, Sweden, pp. 297–304.

Hofmeister, W., Griffith, M., Ensz, M., Smugeresky, J. 2001. Solidification in direct metal deposition by LENS processing. *JOM* 53(9):30–34.

Hofmeister, W., Wert, M., Smugeresky, J., Philliber, J.A., Griffith, M., Ensz, M. 1995. Investigating solidification with the laser-engineered net shaping (LENS™) Process. *JOM* 51(7). Accessed May 5, 2014. http://www.tms.org/pubs/journals/JOM/9907/Hofmeister/Hofmeister-9907.html.

Horii, T., Kirihara, S., Miyamoto, Y. 2009. Freeform fabrication of superalloy objects by 3D micro welding. *Materials & Design* 30:1093–1097.

Hussein, N., Segal, J., Mc Cartney, D., Pashby, I. 2008. Microstructure formation in Waspaloy multilayer builds following direct metal deposition with laser and wire. *Materials Science and Engineering A* 497(1/2):260–269.

Janaki Ram, G.D., Robinson, C., Yang, Y., Stucker, B. 2007a. Use of ultrasonic consolidation for fabrication of multi-material structures. *Rapid Prototyping Journal* 13:226–235.

Janaki Ram, G.D., Yang, Y., Nylander, C., Aydelotte, B., Stucker, B.E., Adams, B.L. 2007b. Interface microstructures and bond formation in ultrasonic consolidation. In *Proceedings of the 18th Solid Freeform Fabrication Symposium*, Austin, TX.

Janaki Ram, G.D., Yang, Y., Stucker, B.E. 2007. Effect of process parameters on bond formation during ultrasonic consolidation of aluminum alloy 3003. *Journal of Manufacturing Systems* 25:221–238.

Jhavar, S., Jain, N.K., Paul, C.P. 2014. Development of micro-plasma transferred arc (-PTA) wire deposition process for additive layer manufacturing applications. *Journal of Materials Processing Technology* 214:1102–1110.

Joshi, K.C. 1971. The formation of ultrasonic bonds between metals. *Welding Journal* 50:840–848.

Karunakaran, K.P., Bernard, A., Suryakumar, S., Dembinski, L., Taillandier, G. 2012. Rapid manufacturing of metallic objects. *Rapid Prototyping Journal* 18(4):264–280.

Katou, M., Oh, J., Miyamoto, Y., Matsuura, K., Kudoh, M. 2007. Freeform fabrication of titanium metal and intermetallic alloys by three-dimensional micro welding. *Materials and Design* 28:2093–2098.

Kelly, G.S., Advania, S.G., Gillespie Jr., J.W., Bogetti, T.A. 2013. A model to characterize acoustic softening during ultrasonic consolidation. *Journal of Materials Processing Technology* 213:1835–1845.

Kelly, G.S., Just Jr., M.S., Advani, S.G., Gillespie Jr., J.W. 2014. Energy and bond strength development during ultrasonic consolidation. *Journal of Materials Processing Technology* 214:1665–1672.

Kim, J.-D., Peng, Y. 2000. Plunging method for Nd:YAG laser cladding with wire feeding. *Optics and Lasers in Engineering* 33:299–309.

Kinsella, M. 2011. *Additive Manufacturing Workshop: Results and Plans*. Washington, DC: Air Force Research Laboratory.

Kong, C., Soar, R., Dickens, P. 2003. Characterization of aluminum alloy 6061 for the ultrasonic consolidation process. *Materials Science and Engineering A* 363:99–106.

Kong, C., Soar, R., Dickens, P. 2004. Optimum process parameters for ultrasonic consolidation of 3003 aluminum. *Journal of Materials Processing Technology* 146:181–187.

Kong, C.Y. Investigation of ultrasonic consolidation for embedding active/passive fibers in aluminum matrices. PhD dissertation. Loughborough University, England, 2005.

Kong, C.Y., Carroll, P.A., Brown, P., Scudamore, R.J. 2007. The effect of average powder particle size on deposition efficiency, deposit height and surface roughness in the direct metal laser deposition process. Paper presented at *14th International Conference on Joining of Materials*, Helsingør, Denmark, April 29–May 2.

Krishna, B.V., Bose, S., Bandyopadhyay, A. 2007. Low stiffness porous Ti structures for load bearing implants. *Acta Biomaterialia* 3(6):997–1006.

Krishna, B.V., Bose, S., Bandyopadhyay, A. 2009. Fabrication of porous NiTi shape memory alloy structures using laser engineered net shaping. *Journal of Biomedical Materials Research Part B—Applied Biomaterials* 89B(2):481–490.

Krishna, B.V., Xue, W., Bose, S., Bandyopadhyay, A. 2008a. Functionally graded Co-Cr-Mo coating on Ti-6Al-4V alloy structures. *Acta Biomaterialia* 4(3): 697–706.

Krishna, B.V., Xue, W., Bose, S., Bandyopadhyay, S. 2008b. Engineered porous metals for implants. *JOM* 60(5):45–48.

Kruglick, E., Cohen, A., Bang, C. 2006. EFAB technology and applications. In *The MEMS Handbook*, Gad-El-Hak, M. (ed.), 2nd edn. CRC Press, Boca Raton, FL, pp. 6-1–6-20.

Kukreja, L.M., Kaul, R., Paul, C.P., Ganesh, P., Rao, B.T. 2012. Emerging laser materials processing techniques for future industrial applications. In *Laser Assisted Fabrication of Materials*, Manna, I., Majumder, J. (eds.), Berlin, Germany: Springer-Verlag, pp. 423–478.

Langenecker, B. 1966. Effects of ultrasound on deformation characteristics of metals. *IEEE Transactions on Sonics and Ultrasonics* 13(1): 1–8.

Li, D., Soar, R. 2009. Influence of sonotrode texture on the performance of an ultrasonic consolidation machine and the interfacial bond strength. *Journal of Materials Processing Technology* 209:1627–1634.

Liu, S., Liu, W., Harooni, M., Ma, J., Kovacevic, R. 2014. Real-time monitoring of laser hot-wire cladding of Inconel 625. *Optics & Laser Technology* 62:124–134.

Martina, F., Mehnen, J., Williams, S.W., Colegrove, P., Wang, F. 2012. Investigation of the benefits of plasma deposition for the additive layer manufacture of Ti–6Al–4V. *Journal of Materials Processing Technology* 212:1377–1386.

Matz, J.E., Eagar, T.W. 2002. Carbide formation in Alloy 718 and electron-beam solid freeform fabrication. *Metallurgical and Materials Transactions* 33A:2559–2567.

Mazumder, J. 2000. Crystal ball view of direct-metal deposition. *JOM* 52(12):28–29.

Mazumder, J., Dutta, D., Kikuchi, N., Ghosh, A. 2000. Closed loop direct metal deposition: Art to part. *Optics and Lasers in Engineering* 34(4–6):397–414.

Medrano, A., Folkes, J., Segal, J., Pashby, I. 2009. Fibre laser metal deposition with wire: Parameters study and temperature monitoring system. *Proceedings of the SPIE* 7131: 713122.

Miranda, R., Lopes, G., Quintino, L., Rodrigues, J., Williams, S. 2008. Rapid prototyping with high power fiber lasers. *Materials & Design* 29:2072–2075.

Mok, S., Bi, G., Folkes, J., Pashby, I. 2008a. Deposition of Ti6Al4V using a high power diode laser and wire, Part I : Investigation on the process characteristics. *Surface and Coatings Technology* 202:3933–3939.

Mok, S., Bi, G., Folkes, J., Pashby, I., Segal, J. 2008b. Deposition of Ti6Al4V using a high power diode laser and wire, Part II: Investigation on the mechanical properties. *Surface and Coatings Technology* 202:4613–4619.

Nurminen, J. Hot-wire laser cladding: Process, materials and their properties. PhD dissertation, Tampere University of Technology, Tampere, Finland, 2008.

Obielodan, J.O., Ceylan, A., Murr, L.E., Stucker, B.E. 2010. Multi-material bonding in ultrasonic consolidation. *Rapid Prototyping Journal* 16(3):180–188.

Obielodan, J.O., Stucker, B.E., Martinez, J.L., Hernandez, D.H., Ramirez, D.A., Murr, L.E. 2011. Optimization of the shear strengths of ultrasonically consolidated Ti/Al 3003 dual-materials structures. *Journal of Materials Processing Technology* 211(6):988–995.

Oruganti, R.K., Ghosh, A.K. 2003. Fabrication and creep properties of superalloy-zirconia composites. *Metallurgical and Materials Transactions A* 34A(11):2643–2653.

Pinkerton, A.J., Li, L. 2003. The effect of laser pulse width on multiple-layer 316L steel clad microstructure and surface finish. *Applied Surface Science* 208–209:405–410.

Ponche, R., Kerbrat, O., Mognol, P., Hascoet, J.-Y. 2014. A novel methodology of design for Additive Manufacturing applied to Additive Laser Manufacturing process. *Robotics and Computer-Integrated Manufacturing* 30:389–398.

Puli, R., Janaki Ram, G.D. 2012. Dynamic recrystallization in friction surfaced austenitic stainless steel coatings. *Materials Characterization* 74:49–54.

Rafi, H.K., Balasubramaniam, K., Phanikumar, G., Prasad Rao, K. 2011. Thermal profiling using infrared thermography in friction surfacing. *Metallurgical and Materials Transactions A* 42:3425–3429.

Rangesh, A., O'Neill, W. 2011. Rapid prototyping by consolidation of stainless steel powder using an electrical arc. *Rapid Prototyping Journal* 17(4) 280–287.

Reeves, P., Hague, R. 2013. Additive manufacturing or 3D printing—You decide! *The Royal Academy of Engineering Magazine* 6:39–45.

Reid, J., Webster, R. 2006. A 55GHz band pass filter realized with integrated TEM transmission lines. In *IEEE MTT-S International Microwave Symposium Digest*, Institute of Electrical and Electronics Engineers (IEEE), San Francisco, CA, pp. 132–135.

Roy, M., Balla, V.K., Bandyopadhyay, A., Bose, S. 2012. MgO doped tantalum coating on Ti: Microstructural study and biocompatibility evaluation. *ACS Applied Materials & Interfaces* 4(2):577–580.

Roy, M., Krishna, B.V., Bandyopadhyay, A., Bose, S. 2008. Laser processing of bioactive tricalcium phosphate coating on titanium for load bearing implant. *Acta Biomaterialia* 4(2):324–333.

Schwendner, K.I., Banerjee, R., Collins, P.C., Brice, C.A., Fraser, H.L. 2001. Direct laser deposition of alloys from elemental powder blends. *Scripta Materialia* 45(10):1123–1129.

Scott, J., Gupta, N., Weber, C., Newsome, S., Wohlers, T., Caffrey, T. 2012. Additive manufacturing: Status and opportunities. *Occasional Papers in Science and Technology Policy*, March. Accessed May 5, 2015. https://cgsr.llnl.gov/content/assets/docs/IDA_AdditiveM3D_33012_Final.pdf.

Seufzer, W.J., Taminger, K.M. 2007. Control methods for the electron beam free form fabrication process. In *Solid Freeform Fabrication Symposium Proceedings*, Laboratory for Freeform Fabrication and University of Texas at Austin, Austin, TX, pp. 13–21.

Shin, K.-H., Natu, H., Dutta, D., Mazumder, J. 2003. A method for the design and fabrication of heterogeneous objects. *Materials and Design* 24(5):339–353.

Siggard, E.J. Investigative research into the structure embedding of electrical and mechanical systems using ultrasonic consolidation (UC). MS dissertation, Utah State University, Logan, UT, 2007.

Skiba, T., Baufeld, B., Van der Biest, O. 2009. Microstructure and mechanical properties of stainless steel component manufactured by shaped metal deposition. *ISIJ International* 49:1588–1591.

Skiba, T., Baufeld, B., Van der Biest, O. 2011. Shaped metal deposition of 300M steel. *Proceedings of the Institution of Mechanical Engineers, Part B: Journal of Engineering Manufacture* 225(6):831–839.

Stecker, S., Lachenberg, K.W., Wang, H., Salo, R.C. 2006. Advanced electron beam free form fabrication methods & technology. In *Professional Program & Poster Session* (Atlanta, GA), Session 2: Electron Beam Welding. American Welding Society, New York, pp. 35–46.

Syed, W.U.H., Li, L. 2005. Effects of wire feeding direction and location in multiple layer diode laser direct metal deposition. *Applied Surface Science* 248:518–524.

Syed, W.U.H., Pinkerton, A.J., Li, L. 2005. A comparative study of wire feeding and powder feeding in direct diode laser deposition for rapid prototyping. *Applied Surface Science* 247:268–276.

Syed, W.U.H., Pinkerton, A.J., Li, L. 2006. Combining wire and coaxial powder feeding in laser direct metal deposition for rapid prototyping. *Applied Surface Science* 252:4803–4808.

Syed, W.U.H., Pinkerton, A.J., Liu, Z., Li, L. 2007a. Coincident wire and powder deposition by laser to form compositionally graded material. *Surface & Coatings Technology* 201:7083–7091.

Syed, W.U.H., Pinkerton, A.J., Liu, Z., Li, L. 2007b. Single-step laser deposition of functionally graded coating by dual "wire–powder" or "powder–powder" feeding—A comparative study. *Applied Surface Science* 253:7926–7931.

Taminger, K. 2009. Electron beam freeform fabrication. *Advanced Materials & Processes* 11/12:45.

Taminger, K.M.B., Hafley, R.A. 2002. Characterization of 2219 aluminum produced by electron beam freeform fabrication. In *Proceedings of 13th SFF symposium*, Laboratory for Freeform Fabrication and University of Texas at Austin, Austin, TX, pp. 482–489.

Taminger, K.M.B., Hafley, R.A. 2003. Electron beam freeform fabrication: A rapid metal deposition process. In *Proceedings of the 3rd* annual automotive composites conference, Troy, MI, September 9–10.

Taminger, K.M.B., Hafley, R.A., Domack, M.S. 2006. Evolution and control of 2219 aluminum microstructural features through electron beam freeform fabrication. *Materials Science Forum* 519/521:1297–1304.

The Economist. The printed world. *The Economist*, February 10, 2011. Accessed May 5, 2014. http://www.economist.com/node/18114221.

The Economist. A third industrial revolution. *The Economist*, April 21, 2012. Accessed May 5, 2014. http://www.economist.com/node/21552901.

Vaezi, M., Seitz, H., Yang, S. 2013. A review on 3D micro-additive manufacturing technologies. *International Journal of Advanced Manufacturing Technology* 67:1721–1754.

Vayrea, B., Vignata, F., Villeneuvea, F. 2012. Designing for additive manufacturing. *Procedia CIRP* 3:632–637.

Wang, F., Mei, J., Jiang, H., Wu, X. 2007. Laser fabrication of Ti6Al4V/TiC composites using simultaneous powder and wire feed. *Materials Science and Engineering A* 445–446:461–466.

Wang, F., Mei, J., Wu, X. 2006. Microstructure study of direct laser fabricated Ti alloys using powder and wire. *Applied Surface Science* 253:1424–1430.

Wang, F., Williams, S., Colegrove, P., Antonysamy, A.A. 2013. Microstructure and mechanical properties of wire and arc additive manufactured Ti-6Al-4V. *Metallurgical and Materials Transactions A* 44A:968–977.

Wanjara, P., Brochu, M., Jahazi, M. 2007. Electron beam freeforming of stainless steel using solid wire feed. *Materials and Design* 28:2278–2286.

Wu, X. 2007. A review of laser fabrication of metallic engineering components and of materials. *Materials Science and Technology* 23(6):631–640.

Xiong, X., Haiou, Z., Guilan, W. 2008. A new method of direct metal prototyping: Hybrid plasma deposition and milling. *Rapid Prototyping Journal* 14(1):53–56.

Xue, L., Li, Y., Wang, S. 2011. Direct manufacturing of net-shape functional components/test pieces for aerospace, automotive and other applications. *Journal of Laser Applications* 23(4):042004.

Xue, W., Krishna, B.V., Bandyopadhyay, A., Bose, S. 2007. Processing and biocompatibility evaluation of laser processed porous titanium. *Acta Biomaterialia* 3(6):1007–1018.

Yang, Y., Janaki Ram, G.D., Stucker, B. 2007. An experimental determination of optimum processing parameters for Al/SiC metal matrix composites made using ultrasonic consolidation. *Journal of Engineering Materials and Technology* 129:538–549.

Yang, Y., Janaki Ram, G.D., Stucker, B.E. 2009. Bond formation and fiber embedment during ultrasonic consolidation. *Journal of Materials Processing Technology* 209:4915–4924.

Yang, Y., Janaki Ram, G.D., Stucker, B.E. 2010. An analytical energy model for metal foil deposition in ultrasonic consolidation. *Rapid Prototyping Journal* 16(1):20–28.

Zhang, H., Wang, X., Wang, G., Zhang, Y. 2013. Hybrid direct manufacturing method of metallic parts using deposition and micro continuous rolling. *Rapid Prototyping Journal* 19(6):387–394.

Zhang, H., Xu, J., Wang, G. 2003. Fundamental study on plasma deposition manufacturing. *Surface and Coatings Technology* 171:112–118.

Zheng, B., Zhou, Y., Smugeresky, J.E., Schoenung, J.M., Lavernia, E.J. 2008. Thermal behavior and microstructural evolution during laser deposition with laser-engineered net shaping: Part I. Numerical calculations. *Metallurgical and Materials Transactions A* 39A(9):2228–2236.

Zhu, G., Li, D., Zhang, A., Pi, G., Tang, Y. 2012. The influence of laser and powder defocusing characteristics on the surface quality in laser direct metal deposition. *Optics & Laser Technology* 44:349–356.

Zou, H., Zhang, H., Wang, G., Li, J. 2009. Rapid manufacturing of FGM components by using electromagnetic compressed plasma deposition. *Progress in Electromagnetics Research Symposium Proceedings*, Moscow, Russia, August 18–21, The Electromagnetics Academy, Cambridge, MA, pp. 1953–1956.

4

Additive Manufacturing of Metals Using Powder-Based Technology

Michael Jan Galba and Teresa Reischle

CONTENTS

ABSTRACT Additive manufacturing (AM) in metal objects can be used in various applications such as aerospace, medical, tooling, automotive, general industry, consumer goods lifestyle, prototyping, and many more. The applications are rapidly growing with the increasing acceptance of the AM capabilities. As a general statement, it is possible to say

that AM will not replace conventional machining in the near future. It is a complementary technology to conventional machining like milling, drilling, welding, turning, and EDM processes that can add value to the product manufactured. This is possible as an example for parts where a near-net shape component is additively manufactured and only final functional features like threads, fittings, and high tolerance areas need to be post machined by conventional machining methods. It can as well aid in the reduction of manufacturing or assembling effort by using functional integration. Very often objects manufactured by AM are more expensive than conventional machining methods but cost benefits could be gained through the lifetime of the component. As an example you could use in aviation components on an aircraft that would save weight. The initial manufacturing and validation costs can be significantly higher than conventional machined components but save the customer in the end a lot of money through reduced fuel consumption over the lifetime of an aircraft. Another example is the medical device sector in which lattice structures on implants can save the manufacturer labor intensive post-processing like plasma spray coatings and bead sintering among others. Lattice structures can also extend the lifetime of implants in two ways. One way is the reduction in stress-shielding caused by stiff implants, which leads to bone resorption. The other is the effect of cell ingrowth that improves the strength of the bone–implant interface for possible better primary fixation and cementless implantation. Selective laser sintering/melting makes it possible to produce complex structures and to create individualized implants with the biocompatible titanium alloy Ti6Al4V. This chapter shall give the reader a brief overview about the selective laser melting/sintering process using a laser as source of energy.

4.1 From Rapid Prototyping to Rapid Manufacturing

Which were the key factors EOS's success story drove? In the end, it is four critical factors that played an essential role: The freedom of *design-driven manufacturing*, the continuous improvement of systems, the development of new materials for new application fields, and consequent strategy on the way to rapid manufacturing.

Dr. Hans Langer, founder and CEO of EOS, recaps the very early days: "We were able to provide our first customers with completely new possibilities for prototype production instead of using slow and costly manual hand work. The creation of complex geometries was possible using stereo-lithography. Our first customer the BMW-group was quickly convinced of a cooperation" (2013, pp. 45–51).

From the very beginning, one of the main drivers for EOS was the idea that design has to drive manufacturing and not the other way around. The industry calls this design-driven manufacturing. What you can design on a computer should be possible to manufacture. A big advantage of AM is the possibility to create complex geometries that are hardly or impossible to manufacture in a conventional way. As a good example, you can think of subsurface cooling channels within a mold for injection molding of plastics, or features inside a part requiring separate manufacturing and assembly. The nice thing about AM can be expressed at its best by the idea that adding features to a design is decreasing the final costs of a component, whereas by conventional machining every bore, thread, taper, chamfer, varying wall thickness, lattice structures for light weight, … is increasing the processing time and therefore increasing the part costs. Thus, every added feature to a design is in the additive world decreasing the amount of material to be solidified and therefore decreasing

the manufacturing costs by decreasing the processing time. The manufacturing costs are decreasing where the possibilities of realization of design ideas are increasing. The part properties have reached meanwhile such good quality that they can be and are already used in very demanding applications like medical or aerospace. High strength, long-term performance under high thermal stresses is no showstopper anymore.

Dr. Langer started developing key components for the laser industry since the early eighties. After founding EOS, it was possible to create prototypes quickly using stereolithography. Until 1994 first commercial systems from the Stereos product line were introduced, using computer-aided design (CAD)-data and light curing resins to produce prototypes. From 1994, laser sintering (2013, pp. 45–51) was introduced into the industry being the first global company to offer stereolithography and laser sintering. Soon disadvantages of the resin-based systems like long building times, low strength, labor intense manual finishing, toxic resins, and cost for the resin appeared. Laser sintering simply allowed more flexibility and functionality. The great potential of laser sintering was clear to Dr. Langer leading to the decision to focus solely on laser sintering in 1997.

What now followed was a remarkable career during the past 20 years of new product launches where only few shall be named. In 1994, the first European polymer-based laser sintering system the EOSINT P350 was introduced. This system has received several upgrades over the past decades and is now available as the EOSINT P396.

In 1995, the world's first direct metal laser sintering system (DMLS) the EOSINT M250 for the production of metallic tools for the injection molding industry was introduced. In 2004, M270 was launched, which is until today the world's most successful in the area of metal laser sintering. The most critical change was the availability of reliable and high power yttrium–aluminium–garnet (YAG)-lasers for affordable prices versus CO_2 lasers having some disadvantages in the additive processing of metals. Today with the EOSINT M290 and M400 the latest developments were made.

In the same year, the EOSINT S700 was introduced as the first technology for AM of cast molds and casting cores using sand in the *direct corning process*. Step by step the company established, so its valid technology leader position until today.

With the introduction of DMLS, a big milestone was set in the area of rapid tooling. With the DCP process, another innovation a twin scan head sand system was released to enable another application-driven market. Today, the sand system is in its version as the S750 available.

In 2000 with the EOSINT P700, the world's first double head polymer sintering system became available. It opened users a whole new world of dimensions. This is not only in terms of productivity, process chamber size, build rate, and part quality but also in economic production of series parts where new standards were set. At the same time, capacities for quick and flexible models for investment and vacuum casting became available; especially, the automotive, medical, and aerospace industries need such systems.

In 2007, the Formiga P100 became a synonym for a high degree of automation, functionality, and quality. Until today, people are requesting from service providers FORMIGA-quality parts. E-manufacturing in the compact class of systems became real. The system in its today's version as the FORMIGA P110 is ideal for economic production of small batch series with complex geometries. Demands are applicable for first-class consumer components or medical devices as well as extremely short cycle times with respect to a low initial investment. At the same time, it offers capacities to manufacture full functional prototypes.

In 2008, the EOSINT P800 another flagship was revealed for totally new dimensions of manufacturing. This is the world's first high-temperature system with process temperatures of up to 385°C for laser sintering of high-performance polymers. This system is based

on the proven and reliable design of the EOSINT P730 and especially designed for the medical device sector as well as the aerospace industry.

With laser sintering, it is not good enough to only release new system innovations on a regularly basis but also to keep the available materials on the same innovative level. They define how systems have to be further developed and serve special customer demands. The beginning of material development at EOS was initiated by polymers.

One of the first customers, Morris Technologies, wanted to make tooling for local healthcare giant Proctor and Gamble. As Dr. Langer (founder of EOS) pointed out:

> In Cincinnati you have not only Proctor and Gamble but also General Electric (GE) who picked up on the technology and started to investigate further. In 2007 Morris and GE visited EOS in Krailling and announced that they were working on a special project together that would come to fruition publicly as the acquisition of Morris by GE Aviation in 2012. (2013, pp. 45–51)

As a turning point to production, GE's involvement in metals AM was a paradigm shift for all involved as for the first time a business model was created that was larger than the companies providing the machinery. This change in the landscape into a true manufacturing technology spurred on a substantial change in the way EOS has organized itself to move forward and points to the direction of the company in future.

> We realised that companies like GE were really serious about series manufacturing using additive manufacturing. If they are being serious, then we also need to be serious, hence the changes to the management structure to ensure that EOS continues to be at the forefront of innovation in the manufacturing applications of AM. (2013, pp. 45–51)

explained Dr. Langer. Moving from prototyping to series production throughout the company's history, the evolution has been easy to chart—from bespoke stereolithography systems to laser sintering systems and eventually sand and metal laser sintering. Until recently however, all of these systems were taken away and used most often in prototyping, but they were being used in some of the most innovative companies in the world, and these companies saw the potential for AM as a serious production tool. And once they had seen it, they wanted it. Where open collaboration with other companies had served EOS well in the early years, it was now time to bring the expertise in-house and make changes to the fundamental structure of the business, as Dr. Adrian Keppler, CMO, went on to explain:

> I started with EOS four years ago as Hans realized that the company needed to move in a different direction. Transforming from a maker of prototyping machines to a solution provider for series production is a big move and we need a different mindset, different tools and different technology. Our technology was developed for mostly rapid prototyping but our customers could see already the value of additive techniques for series parts. Hans asked me to join to help change the direction of the company to the part production focus. I was working for 10 years at Siemens in a number of roles—one of the things I brought with me from there was that a company must sell a solution to a problem. We don't sell a product we sell a solution that includes machine, material services as well as upfront software to design the part, simulate the process, monitor the process and then on to hipping, heat treating, finishing and surface optimisation. Based on our long-term expertise we can help our clients build up this process chain so that they get the best out of the technology. (2013, pp. 45–51)

There have been a host of other changes to the management structure, a QA manager plucked from the medical industry, a software lead from the automotive industry, and a

head of engineering from the laser machining industry. Dr. Tobias Abeln came to EOS just over two years ago with experience that is invaluable for a company looking to break into true production, as he explained:

> Before I came to EOS I worked in the machine tool industry and before that in a company that made special machines for the automotive industry. Both industries share an approach to modularity, reliability and standardisation that is needed when you are making machines that run three shifts per day for 365 days per year. If machines are used in a rapid prototyping environment it is maybe not so much of a problem that the machine doesn't run on Friday afternoons because of maintenance, or that the process of getting the machine running a job is very labour intensive. For a production machine however this is unthinkable, especially when you are competing with other machine tools on the production floor. (2013, pp. 45–51)

The route to production acceptance is no longer about making the most of the freedom of AM; it is about taking the benchmarks set by other manufacturing technologies, meeting them, and then adding the unique benefits of layer-by-layer production to them, as Dr. Keppler explained:

> In the past a user of an additive manufacturing system would look at the parts from their machine and say 'this part looks nice, I can use it.' Now they want the right material, mechanical properties and even microstructure that is available from their existing techniques with the freedom of the AM process as well. We now have to combine something known, such casting, forging, milling with the characteristics only available to AM. (2013, pp. 45–51)

The development of new solutions is driven by three points of interest: the further optimization of the process, the increase in productivity, and the reduction in cost per part combined with offering new features as well as materials. At the moment, the team believes that the main focus should be on the process in combination with the process-relevant hardware and software. Optimizing the process for production includes the reliability and speed to reduce the final cost per part. After the process, materials will become the area that offers the greatest benefits as Dr. Keppler explained: "Once the process is properly optimized people will start to create new alloys that can exploit the unique features of AM, but this will take until certain industries to accept AM as a true manufacturing technology" (2013, pp. 45–51) Meeting production readiness at the upcoming EuroMold in Frankfurt EOS will unveil the first machine that truly reflects the new thinking at the company, the EOS M 400 system. A 400 mm × 400 mm × 400 mm modular metals laser sintering machine, the EOS M 400, is the first step on the road to production machines capable of high-throughput series production and the large-scale production platforms that EOS predict will be the future of AM for series production. Featuring semi-automated process to aid throughput and reduce cycle times, the modular principle will launch first with a single field 1 kW laser before being adapted for a multi-field set up with four 200/400 W lasers in a second step, the EOS M 400-4.

4.2 Functional Description of Powder Bed-Based Additive Manufacturing Systems

Beside EOS, there are a few major providers that manufacture systems using a powder bed-based technology. The phrases selective laser melting (SLM Solutions®), laser cusing (Concept Laser®), laser sintering (PhenixSystems®/3D-Systems®), direct metal laser sintering

(EOS GmbH®), and laser melting (Renishaw®) among others are literally describing the same or similar processes. They all use lasers as source of energy to weld or better said re-melt areas of the applied layer of powder to create a specific component. Of course, all of them have machine-dependant proprietary features, exposure parameters, and an own expertise about ideal building strategies to manufacture components. Since the variety between machine features is very wide, I will describe the EOS process in detail and mention differences, if known.

EOS GmbH, Krailling, Germany is a private-owned machine manufacturer that sees itself as a solution provider with a strong background in AM. The current EOS metal printing machine M280/290/400 is a laser sintering machine, with which it is possible to process different metal powders. In addition to various steels, titanium alloys, nickel-based super alloys, and aluminum alloys are used for production of components [1]. Theoretically, every weld-able material can be processed by these systems; however, the availability of exotic materials as defined metal powders in constant qualities is limited at the moment.

This type of machine (Figure 4.1) is equipped with a 200/400 W Nd:YAG-fiber laser. It combines the advantages of high beam quality, high beam intensity, and high dynamics.

The laser sintering machine is composed of a laser, optical unit, scanner, process computer, process chamber, and inert gas recirculating filter system. The building process is operated under inert gas atmosphere (in general nitrogen or argon but other atmospheres are possible). For controlling the building process, several sensors are available. The systems are controlled by standard industry computers.

It is responsible for the control of machine components, surveillance, calculating of the scanning patterns, and scanner/laser communications.

The central point of the process chamber is the elevator system. These components are the building-, dispenser-, and collector platforms. The build platform lowers while the manufacturing process stepwise depending on the layer thickness and is performed after every exposed layer.

FIGURE 4.1
EOSINT M280. (Data from eos.info.)

The building platform carrier is responsible for movements in *z*-height and thus the required layer thickness of the part. Onto the platform carrier, a replaceable metallic platform is fixed. This metal platform (generally made from the same material as the currently used powder, or materials with similar thermal expansion coefficients) acts as a substrate and has two major functions. It first acts as a heat-sink to absorb the high energy concentrations from the melt pool and second as a bonding substrate for the metallic components printed on top. It holds the parts on position and compensates internal stresses from the process that could cause warpage or delamination off the platform. After the process is finished, the platform together with the printed components is removed from the machine. In general, a stress-relieving heat treatment is performed, and the parts are then separated from the platform by wire EDM or band saw cutting. This platform can be easily recycled after component removal by just milling/grinding it flat again. It is also possible to build hybrid components, so for instance a preform can be mounted to the platform and only complex features are added on top. Part repair is also possible by this technology on turbine blades, gas turbine injection nozzles, among others.

On the right hand side of the building platform, the dispenser platform is located. (It is also possible to feed fresh powder from above.) It feeds fresh metal powder for the manufacturing process. The powder is deposited from the dispenser over the build platform via a recoater arm.

The recoater applies the required amount of powder onto the building platform in the adjusted layer thickness. On the left hand side, the collector system is positioned. It collects the metal powder overflow and process side-products (condensates/splashes) of the building process. Like the building platform, it is lowered after several recoating steps (Figure 4.2).

The laser beam is funneled from the laser rack through an optical fiber into a collimator and then the beam expander (Figure 4.3).

Two deflection mirrors, inside the scanner system, align the beam and position it dynamically onto the powder bed. This beam is focused through an FΘ lens. (Some systems also use 3D-scan optics instead of FΘ lenses.) Specific characteristics of the lens focus the laser beam over the entire surface of the building area in the same height. Hence, the beam quality over the entire building platform is constant, and paralaxation effects are compensated.

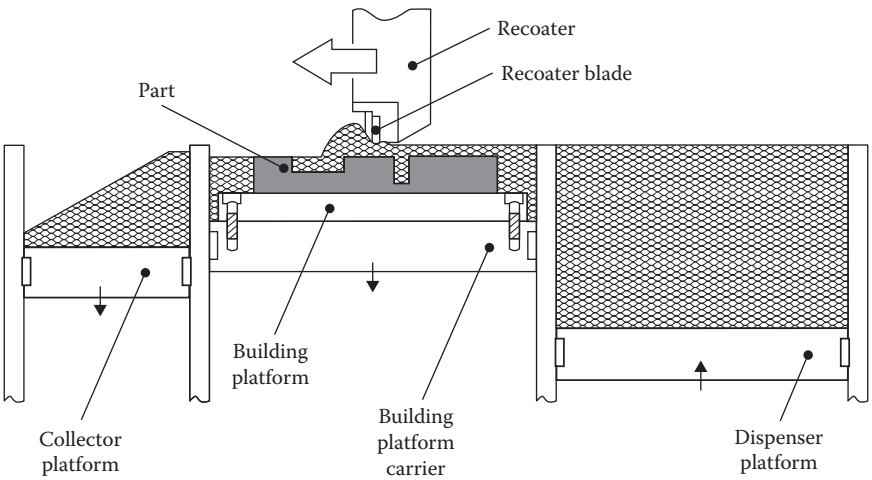

FIGURE 4.2
Functional description of the building process. (Data from EOS Unterlagen.)

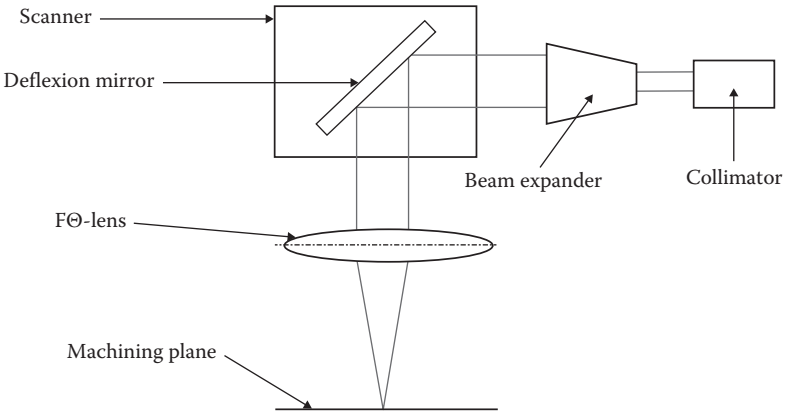

FIGURE 4.3
Simplified optical path of the laser.

The DMLS process is not a conventional sintering process. The energy output of the laser during the DMLS process is so high that the current powder layer is fully melted and welded to the underlying layer. The terminology sintering is misleading from the history. In the very first systems and machine generations (i.e., M250) of the systems were equipped with CO_2 lasers. Nd:YAG fiber lasers were not reliable enough and too expensive at certain high power outputs. For this reason, CO_2 lasers were used to really sinter powder conglomerates of high/low-melting mixtures. Today, each powder particle is already the final alloy or element of the final part material.

During the process, the surface temperature of the melt pool or individual powder beads can exceed the vaporization temperature. Material vaporizes and condenses immediately within the relatively cold protective gas atmosphere of the process chamber and could be deposited inside the process chamber. Since metal condensate emissions or splashes from the melt pool would absorb (in an undefined and non-repetitive way) laser energy in the optical path of the process chamber, it is necessary to remove emerging condensates from the optical path as quickly as possible. EOS solves this problem with the introduction of a laminar flow over the build bed. A constant, material/process-parameter-dependant flow of recirculating protective gas conducts process side products (condensates/splashes/…) away from the melt pool and ensures that a consistent energy deposition into the powder bed is possible. Not taking care of this effect is increasing the variability of material properties (total density/pore size distribution/mechanical properties/surface finish) over different zones in the process chamber as well as consistency from build job to job. In order to ensure the quality of manufacturing, the process chamber needs to be constantly flooded with a small amount of fresh inert gas. This inert gas is filtered and fed back to the process chamber through the recirculating filter system. Depending on the reactivity of the materials, different gas types are used. For instance, a standard for processing highly reactive titanium is argon as protective gas. Aluminum can be processed with either argon or nitrogen. Most nickel-based super alloys are operated under argon atmosphere. Stainless steels or cobalt–chrome superalloys can be processed under nitrogen.

The level to which the build platform is lowered represents the nominal layer thickness. This layer thickness is the powder deposition layer thickness plus *X*. Depending on the material, the powder density is approximately 50% lower compared to solid. Due to the

solidification and increase in density, the *X*-thickness (approximately 1/2 of layer thickness) is added to the nominal layer thickness. After approximately 10 processed layers, a constant real-layer thickness balances between a factor of 1.6 and 2.0. For developing the parameter set, at least 10 layers are required for reliable statements.

EOS uses for reproducibility and high part density a so-called hard recoating technology. For this reason, the recoater blade is made of high-speed steel (HSS) or ceramics ZrO_2 (processing material dependant). The advantage is that the applied layer thickness is constant over the entire building time. This is because there is no significant wear happening since the recoater blade is significantly harder than the material that is processed. Another advantage is that there is no noticeable contamination of the powder happening from recoater residues. Some machine manufacturers use so-called soft recoating technologies like rubber/silicon/carbon–fiber lips, which are prone to wear during build (influence on layer thickness over the jobtime) plus contamination of the powder/parts.

One disadvantage of hard recoating is that the process is not as failure forgiving as soft recoating technologies. For this reason from the very beginning of the process parameter development, recoatability is a significant influencing variable. During the exposure process especially part contours tend to curl creating sharp part edges (wearing down soft recoater technologies quickly). On hard recoating, these are sheared by the recoater blade and deposited into the collector platform. Process-related shear forces can appear between blade and component. Therefore, a strong connection between building platform and part is important.

If, for instance, the process parameters are not very carefully developed, rough recoating appears due to the previously built layer and the part quality can be affected. Due to the relatively cold building process combined with high energy density, extremely high thermal gradients are present. Good heat conduction to the underlying component is necessary to transport the energy away from the melt pool. Heat accumulations cause instability of the building process and can result in job crashes in worst-case/bad surface finishes or increased porosities in best case. As a general statement, thermal conductivity of powder is compared to solidified material very poor. In fact, the powder acts as a thermal isolator because of the embedded atmosphere gasses. There are two possible ways to conduct heat away from the melt pool: a solid bonding to the base plate or the use of support structures.

Internal stresses occur because of the local high temperature differences. This can cause deformations on the parts. In order to eliminate these internal stresses, most materials need to be heat treated in a furnace after the completed building process. It is also possible to decrease the internal part stresses by elevated platform or powder bed heating systems or specific exposure strategies to a certain extent.

The model grows layer by layer out of the powder bed until its final z-height is reached. The building process itself is fully automated and does not need machine operator surveillance. After the building process, unused powder is removed from the process chamber and can directly be recycled by a simple sieving process. The sieved powder is just refilled into the machine and can be reused. The sieving process is important to eliminate sheared particles, splashes, or condensates from the process to having clean powder beads for the next build. It can be distinguished by automatic machine internal powder handling and external powder handling. External powder handling would use in general a conveying module to extract powder out of the machine/a sieving station to sieve the powder amounts and a refilling module. These modules can also be integrated into the system. Most applications see a disadvantage of using internal powder transportation due to possible cross contaminations after material changes or powder batch control issues.

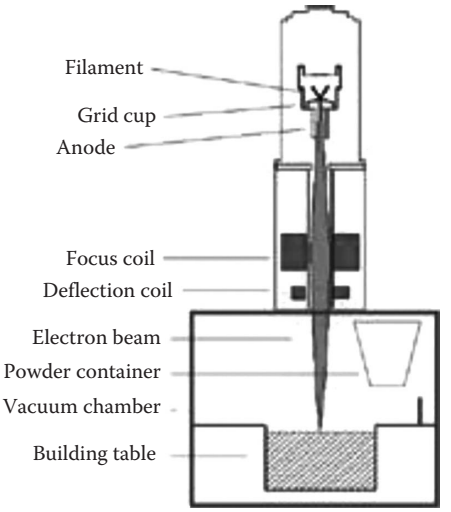

FIGURE 4.4
Principle of EBM. (Data from www.calraminc.com/services.htm.)

However, all of the current available solutions have their very specific advantages and disadvantages. So stating one solution is better than another wouldn't reflect the neutral meaning of this chapter.

A very closely related technology is called electron beam melting (EBM) from Arcam AB (Figure 4.4). It is just another possibility to generate additive components using as a source of energy an electron gun instead of a laser. The basic principles are equal to the laser-based processes with deviations in atmosphere and building temperature. In a direct comparison, the EBM process operates under a high vacuum atmosphere. The EBM process operates in general with an elevated heated powder bed in most cases closer to the melting temperature of the material than on laser-based systems. The electron beam is scanned selectively over the surface and adds the last delta of energy to melt the powder. In a direct comparison today, the EBM process can be seen as a complementary technology. In the past, a big advantage of electron beam processes was higher build rates with the disadvantage of worse surface finishes. However, with new evolutions of machine generations, the EBM process improved significantly on surface finishes. On the other side with the introduction of higher power lasers and more advanced exposure strategies, the laser processes picked up in terms of productivity. One big difference is, however, still present in a direct comparison. Due to the elevated building temperatures, the EBM process is known to have less residual stresses in their components. Some disadvantages to mention in comparison with the laser-based solutions are as follows:

- The powder cake sinters together and the parts need to be blasted free from unmelted powder.
- Time for pulling the vacuum, sensitive vacuum pumping technology.
- Heat-up and cool-down times add on the machine turnaround time.
- Detail resolution worse than on laser-based systems.
- Repeatability tolerances.

Advantages to mention are as follows:

- Less internal stresses.
- Ability to stack components in one job.
- Less support structures necessary than in laser-based systems.

The sintered powder cake together with the embedded parts can be a challenge especially in internal pathways of components as where unmelted powder from laser processes can be just poured out of a component. In the end, the decision which technology to choose depends always on the application and has to be considered very carefully.

4.3 Generic Process

The AM process contains several steps from the virtual CAD file to the manufactured part.

For the generation of a manufactured part, the following steps are necessary:

- Step 1: CAD file
- Step 2: Standard tessellation language (STL) conversion into slice file
- Step 3: File transfer to the machine
- Step 4: Building process
- Step 5: Unpacking
- Step 6: Post-processing

Figure 4.5 shows the general workflow of AM technology. First step is the slicing of the 2D slice data from the 3D STL model. These slice data are uploaded on the corresponding AM machine. Here the part is being processed.

4.3.1 CAD File

It is necessary for all parts to have a CAD model. This model is being converted into an STL file that describes the external surface (Figure 4.6, right side) by triangulation. It is basically needed for the conversion of a slice file.

4.3.2 STL Conversion into Slice File

First, it is necessary for a successful manufacturing process to prepare the build data on a computer. For the preparation, STL files are used. The format is particularly suited to further processing into slice files. At first, the geometry needs to get checked for defects in the surface. That means to fix all potential mistakes in the triangulation like inverted triangles or holes. This is important to prevent problems within the slicing process.

The data preparation is done at EOS via Magics from Materialise, Leuven, Belgium, but other software solutions are available as well. The program also offers the possibility

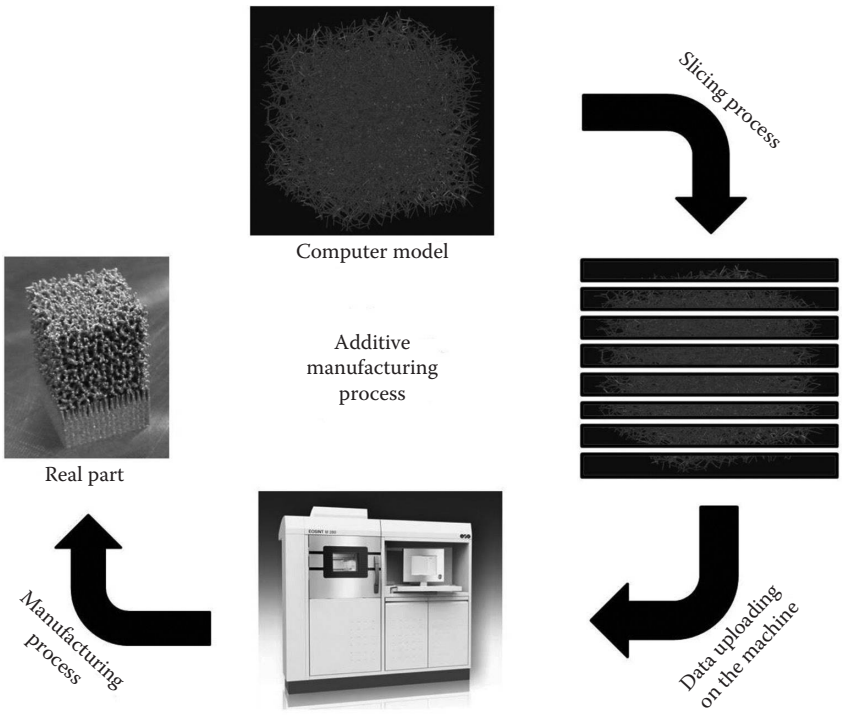

FIGURE 4.5
(See color insert.) Functional sequence of additive manufacturing.

FIGURE 4.6
On the left side a conventional CAD file. On the right side a STL file with triangles. (Data from Gibson, I. et al., *Additive Manufacturing Technologies, Rapid Prototyping to Direct Digital Manufacturing*, Springer-Verlag, 2010.)

of placing parts on a virtual building platform and the processing of simple geometries. A crucial function is the generation of support structures (Figure 4.7).

These support structures are automatically generated by an EOS-specific module within Magics. After creating these, modifications can be made. These structures are a simple rastered hatch (Figure 4.8) made from individual exposure lines. It is possible to adjust several support parameters like raster spacing, fragmentation, and predetermined breaking points among others.

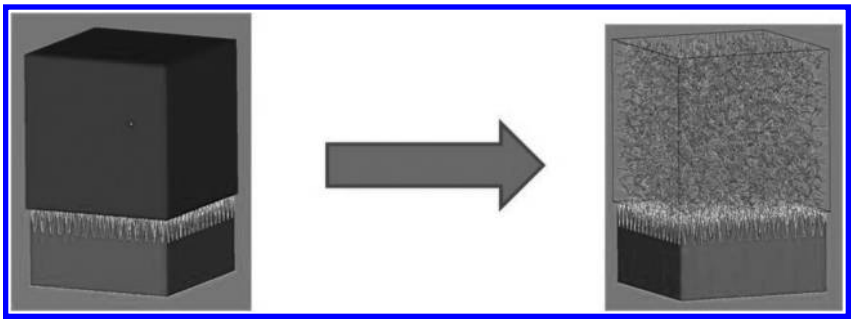

FIGURE 4.7
Sample with a support structure. The left one is a design space with the support structure. The right one is a supported trabecular lattice part.

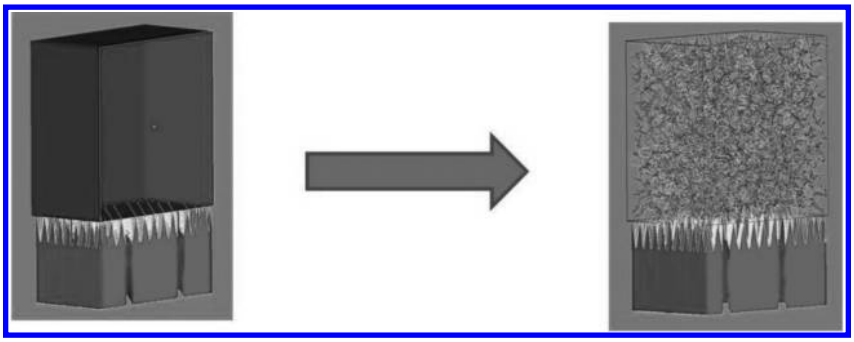

FIGURE 4.8
Rastered spacing of the support structure.

These adaptations are necessary for an individual modification of support within the used lattice structure. While recoating, high forces can be transferred from the recoater arm to the building part. Variations are needed for an adequate connection between support structure and model. Another aspect is the nondestructive removal of the support from the lattice and the building platform.

For generating slice files, EOS *RP tools* are used. After slicing, a check of the exported files should be done to check the correct slicing. For the support structure (Figure 4.9) and

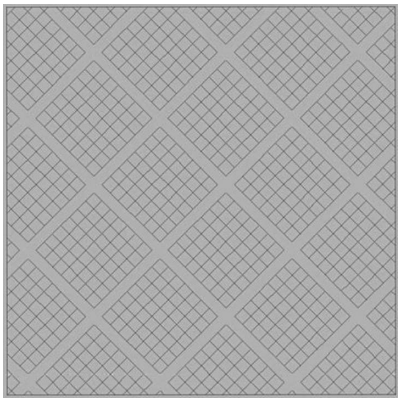

FIGURE 4.9
Slice file support structure of a cube.

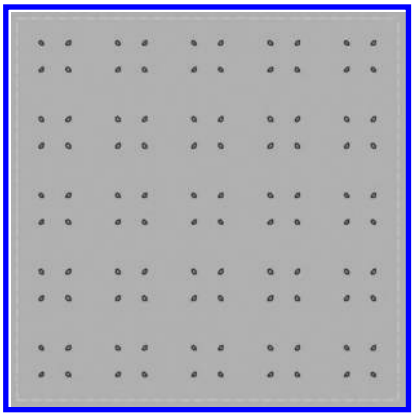

FIGURE 4.10
Slice file of a lattice structure.

the part (Figure 4.10), two different slice files are written to hard disk. This is necessary to allocate different exposure strategies.

4.3.3 File Transfer to the Machine

After finishing the slicing process, all necessary files need to be loaded into the machine computer. The slice files can be uploaded to the process software PSW/EOSPRINT and positioned on the virtual building platform (Figure 4.11). Respectively, the job can be prepared offline and loaded directly into the machine computer.

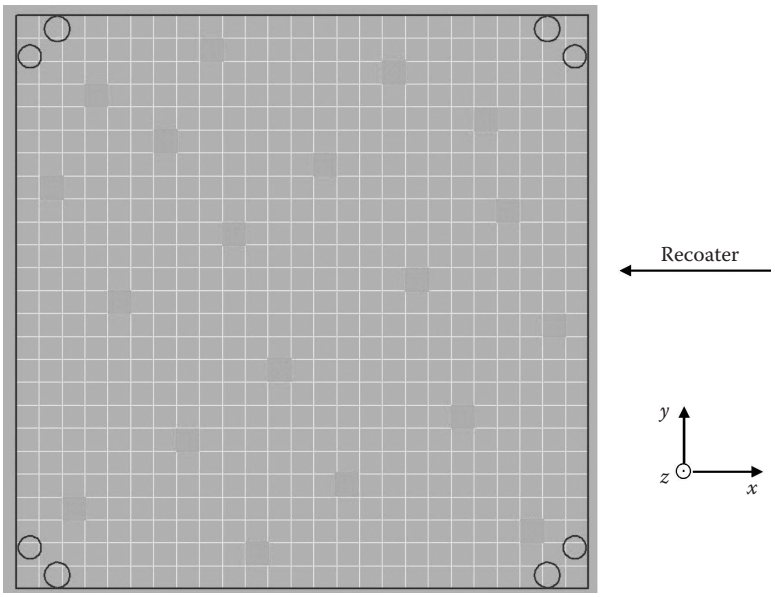

FIGURE 4.11
Virtual building platform.

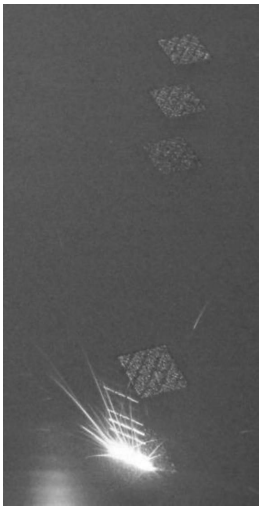

FIGURE 4.12
Example of an exposing process.

4.3.4 Building Process

The manufacturing process of the designed parts is, for the most part, an automated process and laser sintering machine can largely carry on without any supervision.

The operator only needs to assure that an adequate amount of powder for the building process is provided. After starting the manufacturing process, it is advantageous to monitor the exposing of the first few layers. This is necessary to ensure that enough powder is fed and the recoating behavior of the first few layers is correct.

Figure 4.12 is an example for the exposure process of support structures.

4.3.5 Post-Processing

Afterward, the parts are cleaned and the adhesive support structure is removed. Another process is the removal of the embedded powder. For this, several methods exist:

- Use of compressed air
- Shot peening with different media

With respect to shot peening, it is important to consider the size of the blasting media. It needs to be small enough to not clog the lattice structure/internal passages of the parts. Other post-processing steps for lattice cleaning are currently developed like dry-ice blasting and ultrasonic cleaning among others.

4.4 Parameters of the Laser

The radiation of a laser has several properties such as average power, beam diameter, beam divergence, wavelength, and frequency. For this application, the quality of the laser is an important factor as well. Depending on the application output power, wavelength

width, temporal/spatial coherence, and size of beam divergence are important. This is related to the focus ability of the radiation.

The Gaussian beam is best for most applications because of its low divergence. This is the ideal theoretical case for laser beams but in reality deviations often appear. The reason can be oscillation of higher transversal modes. Due to interfering amplitudes or phases of inhomogeneous enhancement of the laser medium, part overlap and radiation can be formed (Figure 4.13).

Real laser beams are having higher divergences. The raw beam is focused by a lens. Afterward, the beam diameter is larger than the diameter of a Gaussian beam. To compensate this effect, power and radiance are reduced.

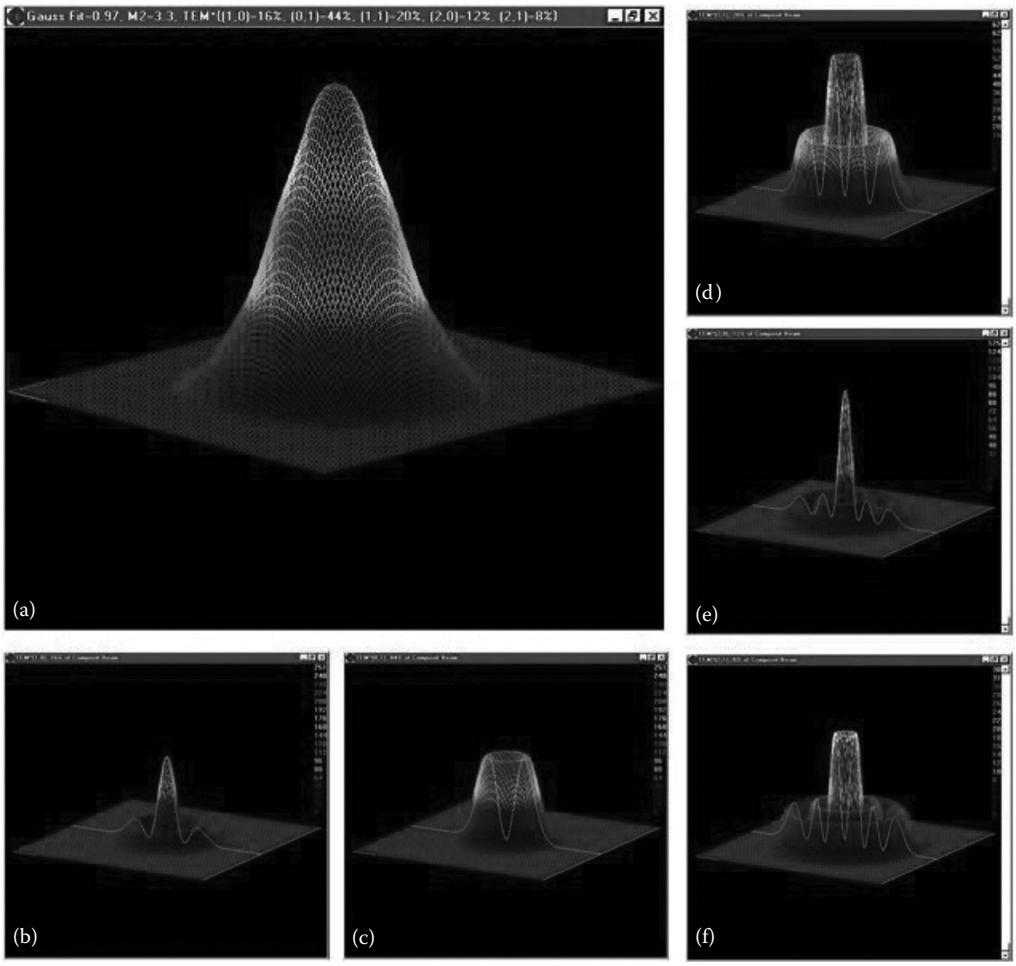

FIGURE 4.13
(See color insert.) Beam characterization: (a) Gaussian fit 0.97, (b) TEM_{10}, (c) TEM_{01}, (d) TEM_{11}, (e) TEM_{20}, and (f) TEM_{21}. (Data from http://www.laserfocusworld.com/articles/2008/04/beam-characterization-camera-based-sensors-characterize-laser-beams.html.)

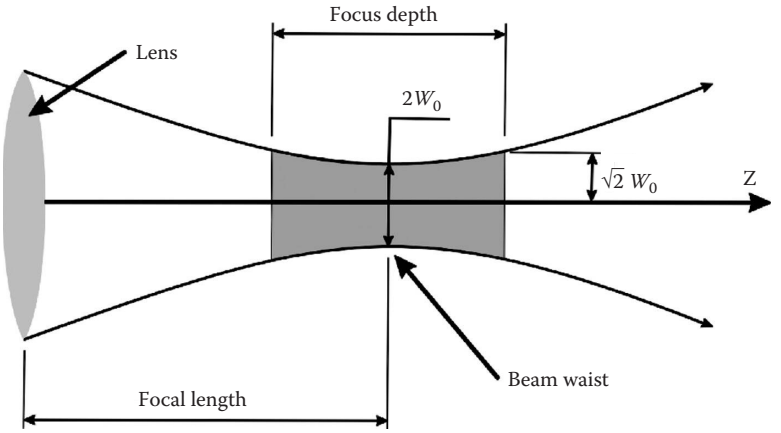

FIGURE 4.14
Parameters of the laser beam. (Data from Boyan, B.D. et al., Titanium—Bone Cell Interface. *Titanium in Medicine*, D. Brunette et al., eds., Berlin, Germany, Springer, 562–579, 2001.)

The Gaussian optical path (Figure 4.14) describes beam course and most of the influencing factors.

1. Optical characteristics
   a. Laser power P [W]

      The power of a laser is not a constant value. It is one of the measurements that varies. This parameter is defined by the user. The current laser has a maximum output power of 400 W. 1 kW lasers are also available on certain machines.

   b. Emission wavelength λ [nm]

      The emission wavelength is the wavelength of the radiation. It is emitted by the stimulated laser medium. The emission wavelength is a fixed parameter with a value of 1070 nm in case of EOS lasers.

   c. Emission line width Δλ [nm]

      The line width of a laser is the width of its optical spectrum.

      It is also one of the parameters defined by the laser itself and not by the user.

      In this case, it has a value of 3.5–5 nm.

2. Optical output (Figure 4.15)
   a. Beam diameter W [mm]

      The beam diameter W (Figure 4.16) is the diameter of the beam's waist. The beam diameter is generally defined as twice the beam's radius. It is the laser beam diameter without focusing [8].

   b. Focal beam diameter, W_f [µm]

      The focal beam diameter W_f of a laser beam in the TEM_{00} grows with the distance z from the beam's waist. Therefore, the beam diameter point $z = 0$ is the

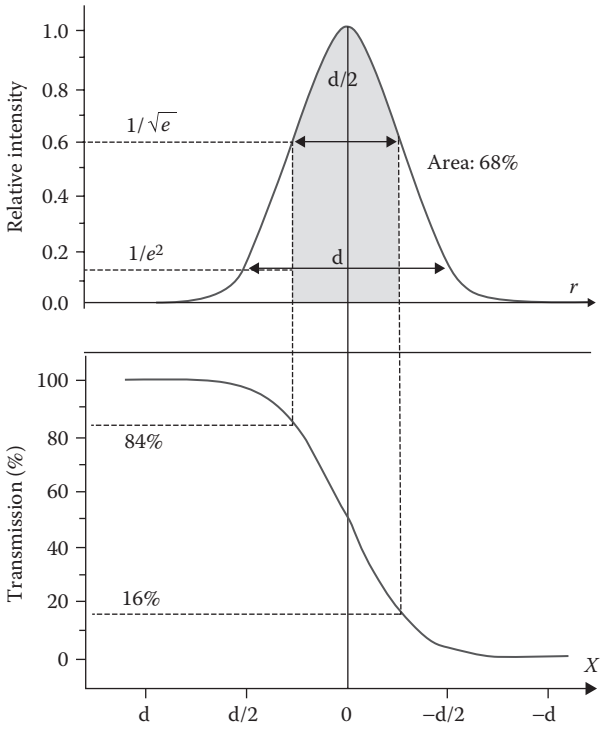

FIGURE 4.15
Diagram of defining the beam diameter. (Data from www.laser-journal.de, Strahlqualität von Lasern.)

smallest possible value and named W_f (Figure 4.16). It can be calculated by the following equation [6]:

$$W_f = \frac{f * \left(\lambda * M^2\right)}{D} * \frac{1}{2\pi} = \frac{\left[\text{mm}^2\right]}{\left[\text{mm}\right]} = \left[\text{mm}\right] \tag{4.1}$$

Focus beam diameter

c. Beam divergence Θ [mrad]

The beam divergence of a laser beam (Figure 4.17) is the value of the expansion rate defined by the divergence angle.
Instead of referring to directions with $1/e^2$ (Figure 4.17) times the maximum intensity, the Gaussian beam radius at full width with half the maximum divergence angle can be used. For this beam, a full beam divergence angle is 1.18 multiplied by half the divergence defined via the Gaussian beam radius ($1/e^2$ radius) (Figure 4.17).
The divergence angle can be calculated with the following equation [6]:

$$\Theta_0 = \frac{\omega_0}{\Theta_0} = \frac{\lambda}{\pi * \omega_0} = \left[\text{mrad}\right] \tag{4.2}$$

Divergence angle

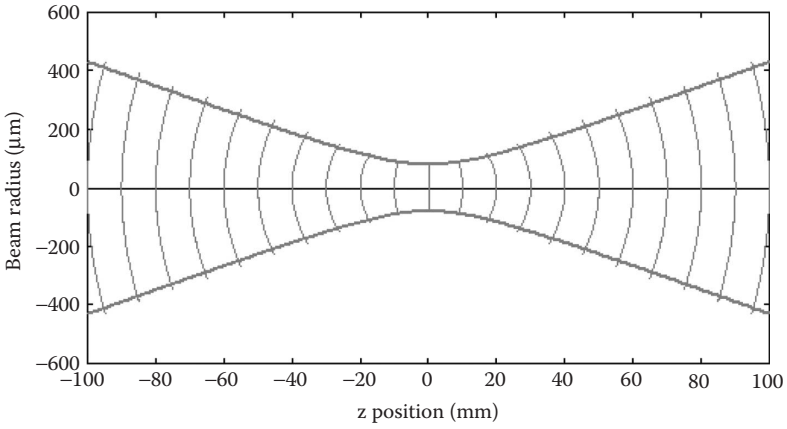

FIGURE 4.16
Beam radius. (Data from http://www.rp-photonics.com/gaussian_beams.html.)

d. Beam quality M^2

The beam quality is defined by the behavior of how tightly a laser beam is focused under certain conditions.

$$M = \frac{1}{K} \tag{4.3}$$

Beam quality

$$1 \leq M \leq \infty \tag{4.4}$$

Area of the beam quality

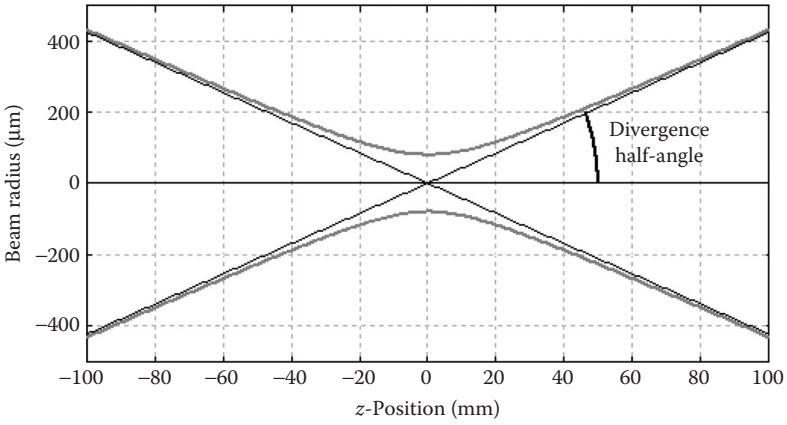

FIGURE 4.17
Definition of the beam divergence. (Data from http://www.rp-photonics.com/gaussian_beams.html.)

A few ways to quantify the beam quality are as follows:

i. The beam parameter product (bpp)
ii. The M^2 factor (ideally 1) [6]
iii. The inverse M^2 factor, named $1/K$ [6]

$$K = \frac{\Theta_0 * w_0}{\Theta * w} = \frac{\lambda}{\pi * \Theta * w} \tag{4.5}$$

Inverse factor of M^2

$$0 \leq K \leq 1 \tag{4.6}$$

Area of the inverse factor of M^2

Equations 4.3 and 4.5 present the area of validity of M^2 and its inverse.

e. Rayleigh length z_R

The Rayleigh length or Rayleigh range of the beam is the distance at which the beam radius increased by a factor of $2^{0,5}$ or the beam diameter doubles, reducing the intensity by half. It can be calculated with the following equation [6]:

$$z_R = \frac{\pi * w_0}{\lambda} = \frac{w_0}{\Theta_0} = [\text{mm}] \tag{4.7}$$

Rayleigh length

f. Beam parameter product q

The bpp is defined as the product of beam radius (measured at the beam's waist) and the beam's half-divergence angle. It is calculated by the following equation [6]:

$$q^* = \Theta_0 * w_0 = \frac{\lambda}{\pi} = [\text{mm} * \text{mrad}] \tag{4.8}$$

Beam parameter product

The bpp is often used to specify the quality of a laser beam. A higher bpp value indicates a lower quality beam (Figure 4.18).

g. Z-shift $Z[\text{mm}]$

Z-shift is defined as an offset of the laser beam's focal position in correlation with the power output of the laser. This is due to thermo-optical effects. The laser focal position moves closer to the lens with increasing power (Figure 4.19).

For a standardized and repeatable flowchart, the z-position of focus location is measured with 10% and 100% power output. The difference of both presents the area of z-shift. A delta z-shift to the value of 1.7 mm is inside tolerances.

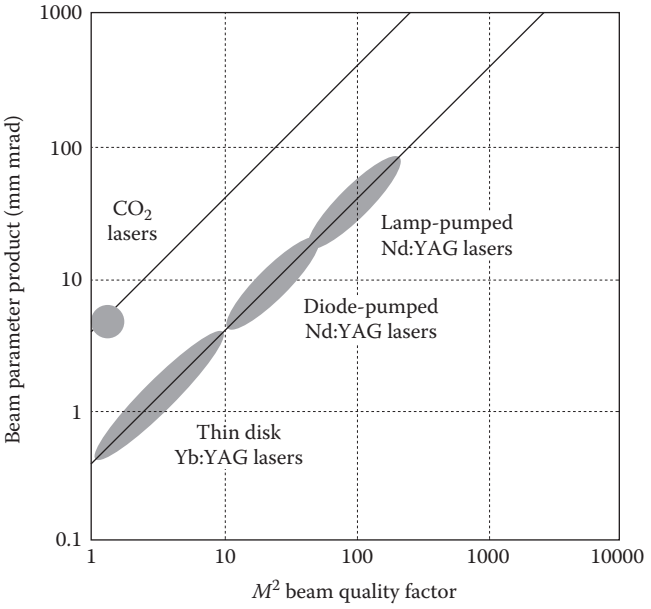

FIGURE 4.18
Beam parameter product and M² values for various laser types. (Data from http://www.rp-photonics.com/gaussian_beams.html.)

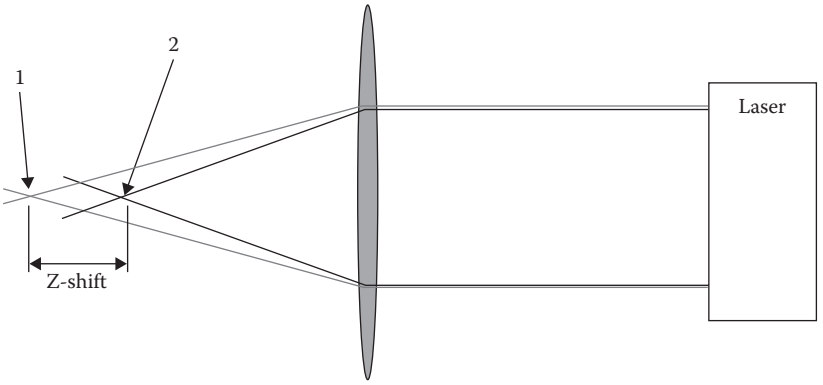

FIGURE 4.19
Simplified optical path of the laser for an explanation of the *z*-shift. (2) Focal position at 20 W (10%) and (1) focal position at 200 W (100%). (Data from eos.datasheet.)

4.5 Specific Requirements for Implants or Biomedical Devices

An implant is any medical device made from one or more materials that is intentionally placed within the body, either totally or partially buried beneath and epithelia surface.

These medical devices are required, if the natural regeneration process due to age, illness, or an accident is not efficient enough or not working any longer. But they do not feature an innate ability of regeneration. These implants, which are inserted into the human body,

need to be manufactured of a biocompatible material. For these medical devices, it is necessary to use a non-viable material. These materials need conventionally to interact with the biological system.

Implants in general need to manifest a high biofunctionality. That means, it is necessary to conform an interchangeability of one or more functions in the biological system by a technical one. For best results, the physical and chemical properties of the implant's material and the replacing tissue should cooperate widely. A significant restriction is the fact that the natural tissue is a living system. Regarding this, it has the ability to regenerate self-contained.

For load-bearing medical devices, the application of force should occur in a physiological way. So the bones integrity needs to be respected especially on the cutting edge between implant and bone. The majority of defects are located on this transition because of the change in physiological stiffness of substrates. Simulations of mechanical stress at cutting edges confirm the effect of stress-shielding. The negative aspects of flexible implants appear at high shear stresses.

The transition between bone and implant is commonly realized by bone cement like polymethylmethacrylat. To avoid usage of bone cement, a direct adherence of bone to the implant is desired. Achieving a high surface area to volume ratio of an implant is required to optimize the bone–implant interaction. For the bone cell ingrowth, a specific porosity on the implant surface according to literature is optimal. This is an important point for the colonization of osteoblasts. The ingrowth of bone cells increases the strength between medical device and bone and avoids degeneration of bone due to stress shielding. This connectivity amends the durability. Mismatch of the moduli between the implant and surrounding bone can cause stress shielding in bone. This eventually leads to bone resorption and is one of the primary causes of implant loosening, which requires painful revision surgery. The pore size is a crucial factor of influencing the bone ingrowth.

A case study has proven that samples with a pore size of 5–20 µm, 20–50 µm, and 50–200 µm show good results. In this book, the considered samples with pore sizes of 50–200 µm give best results in total strength. A comparison of several case studies has shown that an increased ossification occurs at a strut diameter of 300 µm.

Bones are comparable to a composite material. Their mechanical properties are defined by the external/internal and shape/structure as well as the properties of the material. The design of bone is a natural process that is mainly steered by the loading conditions and optimized to withstand them with minimal usage of cellular material.

Bone cores are made of a fine frame of spongiosa. This frame is coated by an outer layer called substantia corticalis with varying wall thicknesses. A bone represents an excellent example of composite materials because it is optimized very well to the loading conditions or more simply expressed not over engineered.

A very important influencing factor of the strength and stiffness is the level of mineralization of a bone. In addition to this factor, the density or rather the porosity of bone augmentation is crucial. Typical Young's moduli are in the range of 10–24 GPa. This magnitude suits for tissue of the cortical and spongiosi bone. The frame of spongiosi bone has a stiffness depending exponentially on the porosity. Values are arranged in a wide field of approximately 10–2000 MPa. Solid metallic medical devices have Young's moduli of more than 100 GPa. This value is significantly higher than that of bones. Different dimensions of stiffness implicate a change in loading conditions on the bone. In principle, the force flows within the bone change dramatically and the implant shields most of the appearing stresses from the bone. This reduction is called stress-shielding and occurs

most prominently on the transition loadings that are reflected by the implant. Depending on loading conditions, bone structure alters or degenerates.

For preventing bone resorption, implants with lower stiffness are advantageous. A reduction in the durability is affected through the loss of stiffness, smaller elastic strain, and the hysteresis of solid metallic medical devices. Fast bone ingrowth and following consistent connections are required because relative movements between medical device and bone might appear. In this case, the ossification can be disturbed and only a weak connection between tissue and implant grows, which is not efficient enough and will never mineralize correctly. For a better biocompability and better connection of the bone–implant interface, both surfaces are usually coated with hydroxyapatite.

4.6 $TiAl_6V_4$

EOS Ti64 is a material with selectable characteristics depending on the application field. The ratio of two phases in microstructure plays a crucial role. The titanium alloys are divided according to their phases (α-Ti : β-Ti) in different classes (Figure 4.20).

The various elements of titanium alloy can be divided in two different charts for characterization (Table 4.1).

Alloys with high percentage of *α*-stabilizer are characterized by good strength, creep resistance, weldability, and low temperature resistance. In contrast to this, β-stabilizers cause low temperature brittleness (Figure 4.21).

$TiAl_6V_4$ is the most common alloy over all industries. The chemical composition of this material is shown in Table 4.2**.**

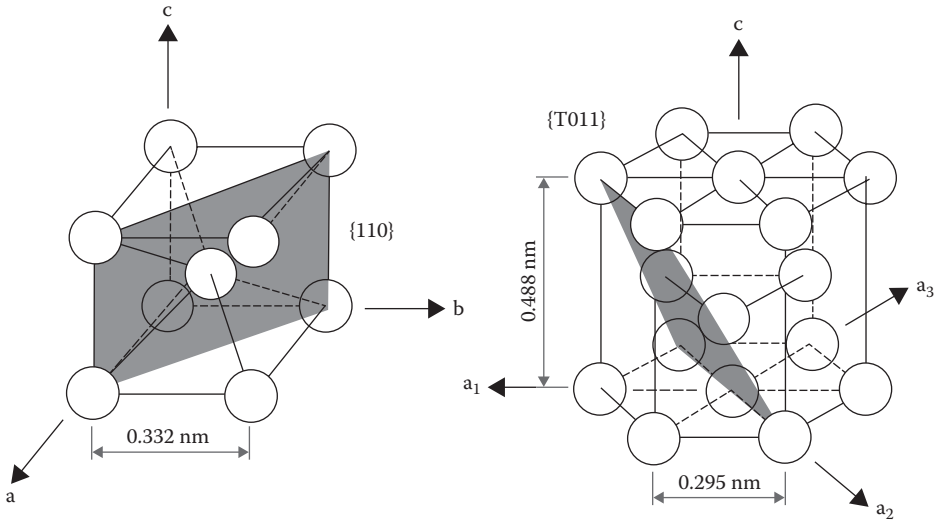

FIGURE 4.20
Possible microstructure of titanium with different microstructural phases: β-titanium krz (left side) and α-titanium hdp (right side). With particular main glide plane.

TABLE 4.1

Different Types of Stabilizers

α-Stabilizer	β-Stabilizer
Aluminum (Al)	Molybdenum (Mo)
Tin (Sn)	Ferrite (Fe)
Zircon (Zr)	Vanadium (Va)
Oxygen (O)	Chromium (Cr)
Nitrogen (N)	Niobium (Nb)

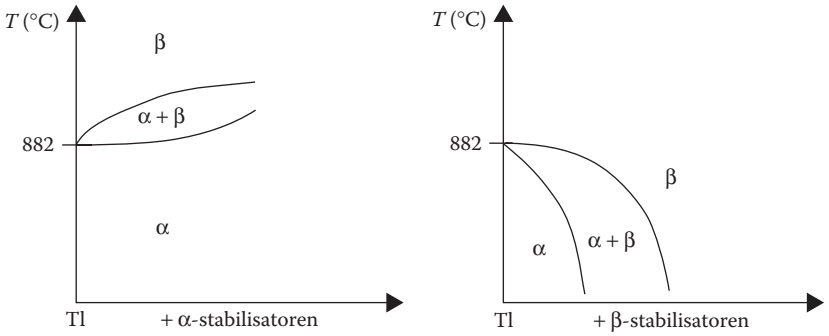

FIGURE 4.21
Possible influence of the α-β-phase transition by allowing elements.

TABLE 4.2

Chemical Composition as per ISO 5832-3: 1996

Element	Compositional Limits (%)
Aluminum	5.5–675
Vanadium	3.5–4.5
Iron	Max. 0.3
Oxygen	Max. 0.2
Carbon	Max. 0.08
Nitrogen	Max. 0.05
Hydrogen	Max. 0.015
Titanium	Balance

Source: DIN ISO 5832–3: 1996, Implants for surgery—Metallic materials, Part 3: Wrought titanium 6-aluminium 4-vanadium alloy, August 2000.

Due to a titanium oxide layer formation on the surface, this alloy has an excellent corrosion resistance. The material exhibits high strength at low density. Ti64 is often used as a high-strength lightweight material in the aerospace and medical industries [10].

Table 4.3 shows the mechanical properties of the EOS Ti6Al4V alloy. Because of an excellent biocompatibility, the material is often used for medical implants, for example, knees, hips, and other joints. Biocompatibility is the ability of a material to perform with an appropriate

TABLE 4.3

Extract of Mechanical Properties of the EOS Ti6Al4V Acc. to EOS-Datasheet

Density (g/cm³)	Tensile Strength (MPa)	Modulus of Elasticity (GPa)
4.41	1230 ± 50	110 ± 10

host response in a specific application. For biomaterials, special requirements exist like corrosion resistance, biocompatibility, bioadhesion, and good mechanical properties.

4.7 Standards for Porous Structures

Adjustments to mechanical properties of lattice structures being used for medical devices are also applied for lightweight parts.

The use of lattice structures and foam-cores sandwich structures is also advantageous. The ratio of mass and stiffness can be increased of this hybrid material.

The most influencing factor of mechanical properties for 3D lattice structures and porous structures is the relative density $\left(\rho_{rel}\right)$ [11]. It describes the quotient of porous material's density and used raw material's density [12].

$$\rho_{rel} = \frac{\rho^*}{\rho_s} = [\%] \tag{4.9}$$

Relative density

where:

ρ^* is the density of the porous material [g/cm³]

ρ_s is the density of the raw material [g/cm³]

Due to the lack of former manufacturing processes, it was only possible to build fine porous structures using stochastic procedures like foams. An influence of internal structure is often restricted to the relative density. With the latest manufacturing technologies, it is possible to build these fine internal geometries with full control over density, strut distribution, shape, stiffness, and flexibility, among others. The disadvantages are usually higher costs per part but adding value by technical details can compensate these increased manufacturing costs.

The easiest form of lattice structures is providing a shell or design space. It is filled with a framework and designed using unit cells or rather tessellations. In the best case, frameworks have constant cross sections. This is the reason why it is possible to allow a description of the linear elastic behavior by analytical approaches [13].

The mechanical properties depend upon the basis of the cross section, number, and configuration of the struts like connectivity.

This parameter corresponds to the number of beams which interacts in one nodal point. In the 3D case with a number of 12, only tensile forces and compressive forces occur instead of bending moments within the struts.

The primary stretching structures are more efficient than the primary bending structure and contain higher peeks of strength.

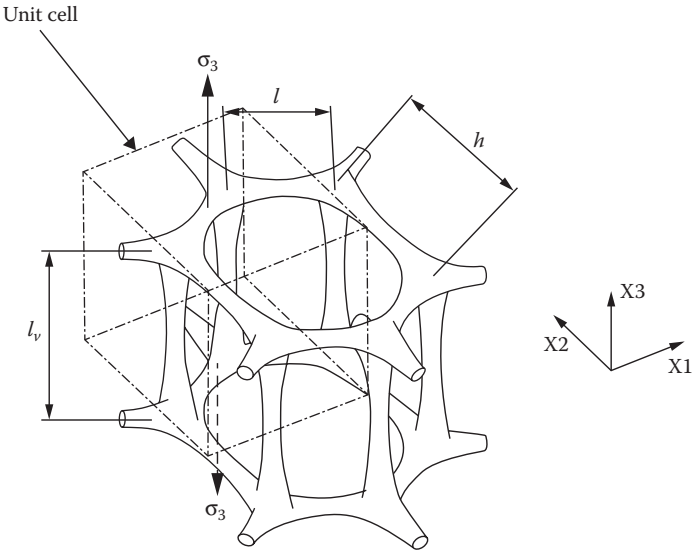

FIGURE 4.22
Hexagonal model of rod-like columnar structure. (Data from Kim, H., *Inte. J. Mechan. Sci.*, 43, S1027–S1060, 2001.)

An important aspect is the occurring failure after reaching the yield point. In contrast to this, primary bending foams can adjust higher strain [14].

Further developments of unit cells are optimized with variable cross sections of load flow within the struts. For hexagonal unit cells, an analytical description is still possible. More material is needed at nodal points to increase effectiveness of the structures. All optimizations of lattice designs are considering design rules for feasibility of build and osseointegration (Figure 4.22).

Most analytical methods only consider types of single unit cells. But it is much more important to consider interactions of several cells. For this case, finite element analysis (FEA) is used [16]. With these programs, it is possible to optimize grids regarding their desired properties such as the Poisson modulus.

Furthermore, it is possible to compare unit cells regarding various loading conditions. It is possible to define mechanical properties in correlation with their relative density. Case studies have revealed that structures with very high porosities may fail, due to buckling, whereas materials with high relative density fail by yielding.

4.8 Design of Porous Structures

For the design of porous structures, different methods are known. All of them have advantages and disadvantages. Most of them are very time consuming and need large-scale computing power.

It is important to find a manufacturing process for these porous structures that combines reproducibility and profitability/economy.

The following different manufacturing processes are described briefly:

- Titanium dross
- Fiber depositioning
- Tissue engineering
- EBM
- Direct metal laser sintering

The first possibility for designing open porous structures for medical devices is sintering of *titanium dross*.

For the creation of porous structures, *placeholders* are filled in. A disadvantage is the loss of the models being required for the manufacturing. These moulds are created by a wax printer. For every process, new forms are necessary, and it is an expensive and time-consuming method.

An alternative manufacturing process is *fiber depositioning*. In this case, a mixture of powder binder is extruded. It can produce strut thicknesses of <100 µm. With the extrusion of the mixture, the process is not finished. A second step is necessary–a sintering process in which the strength is enhanced.

Another type of manufacturing process is an AM process named direct metal laser sintering in which layer upon layer of metal powder is selectively melted by a laser. An advantage is almost no limits in design are given.

Further terms are *SLM* and the *direct laser forming*. These are competitive technologies using in principle the same methods.

4.9 Design of Lattice Structures

In this chapter, two different software tools are used for the design of lattice structures. These are netfabb® and Within Enhance. Since the market is evolving very rapidly, more and more software providers appear like Materialise metal structures, Simpleware, and Uformia.

4.9.1 Design of Lattice Structures Using Netfabb

For generating lattice structures, netfabb Studio Professional with 3S module from netfabb GmbH, Lupburg (version 4.8) was used. The user interface is shown in Figure 4.23.

The principle operation of the program consists of filling and cutting a design space with unit cells (Figure 4.24).

The first step is loading a design space as an STL file. If no model is available, simple geometries can be created. The second step is applying desired unit cells. For this purpose, either a default unit cell can be used or a new cell can be created via an editor. Single elements, such as beams or plates, can be created this way and can be positioned and spread within the cell volume. For beams, supplementary two-dimensional cross sections of polygons need to be created and assigned. Alternatively, for the creation of trabeculae, STL files can be uploaded into the unit cell like micro CT scanned spongiosa bone. The first step is

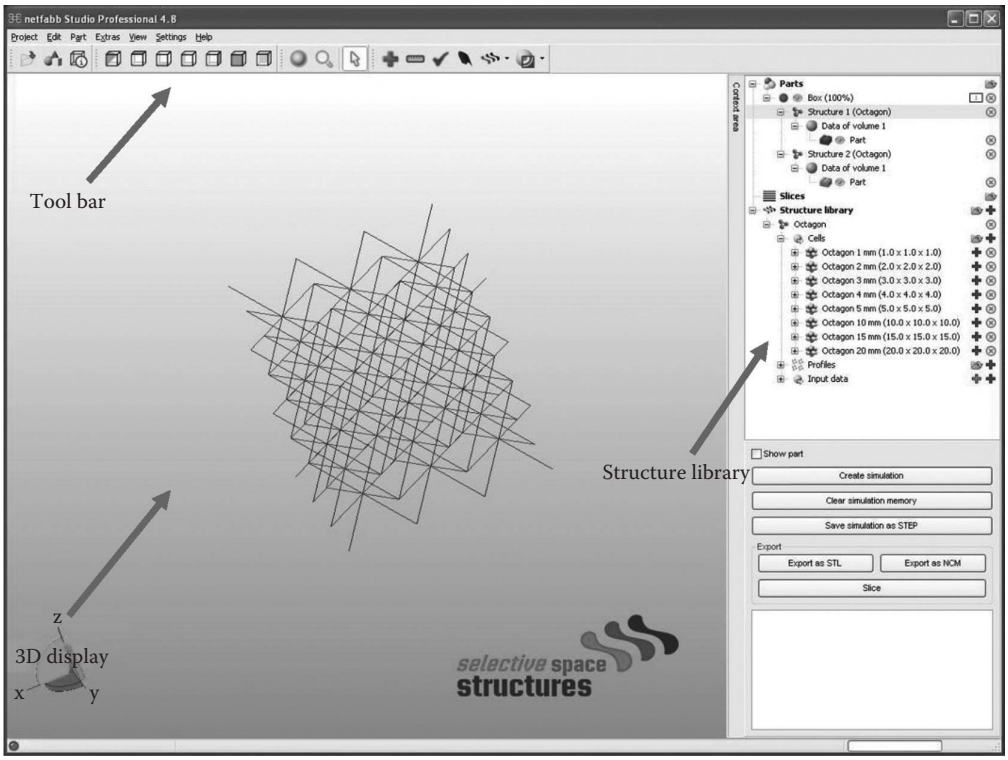

FIGURE 4.23
User interface of netfabb.

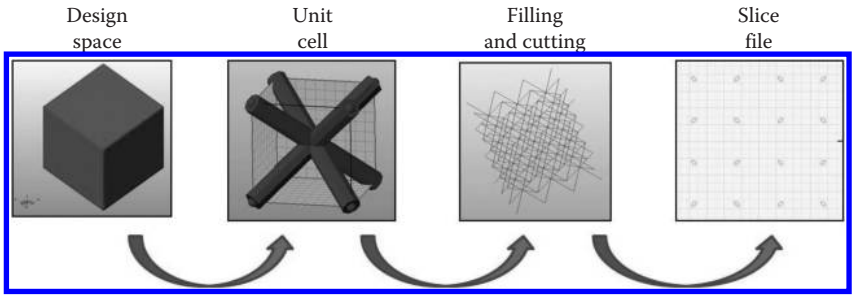

FIGURE 4.24
Lattice structure generating using netfabb.

assigning the unit cell's size and struts' thickness to a single elementary cell. Afterward, this cell is populated all over the design space. It is possible to use different elementary cells to increase diversity within the design space. It is necessary to define the layer thickness of the building process as well. After assigning, data can be saved and exported to an SLI file.

4.9.1.1 Unit Cells

All used unit lattices are created via netfabb. These are unit cells with struts. The first one is a diamond unit cell with the shape of a diamond crystal (Figure 4.25).

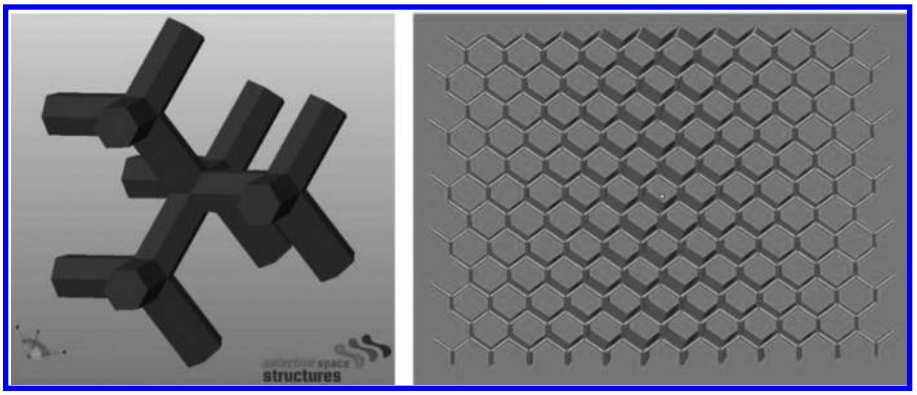

FIGURE 4.25
Diamond unit cell.

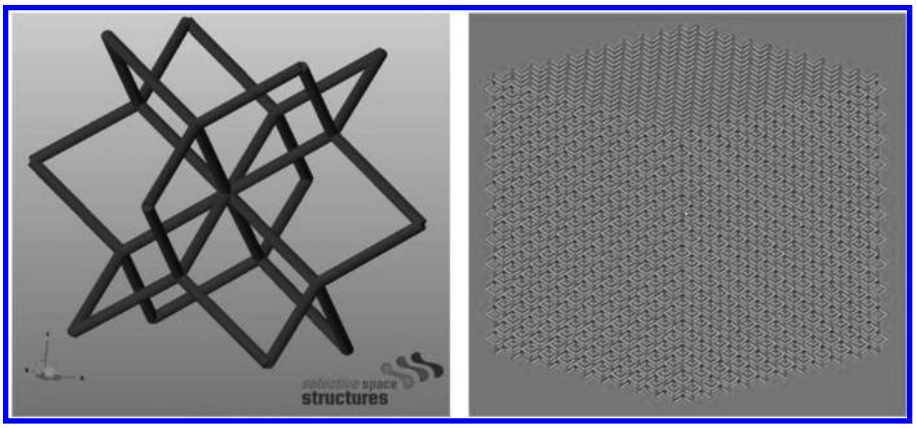

FIGURE 4.26
Dodecahedron unit cell.

A superposition of the diamond unit cells with 90° rotated copies creates a dodecahedron structure (Figure 4.26). Furthermore, a simple cubic structure with diagonal bars, named octagon, is investigated (Figure 4.27).

In order to explore special lattice structure properties, a unit cell is created only containing beams in a certain vertical plane. Horizontal struts are a disadvantage for the DMLS process due to exposure into the bulk powder bed. For this reason, only hexagonal structures with vertical and diagonal beams are used. The occurring anisotropy of these unit cells is, however, a disadvantage.

4.9.2 Design of Lattice Structure Using within Enhance

A second approach for designing lattice structures is a software, named Within Enhance. This program is a special tool for optimizing parts for lightweight. It can be used to enhance parts assigning lattices of various sizes, shapes, thicknesses, and densities. The revised 3D part will be optimized in reference to lightweight components in one direction but also

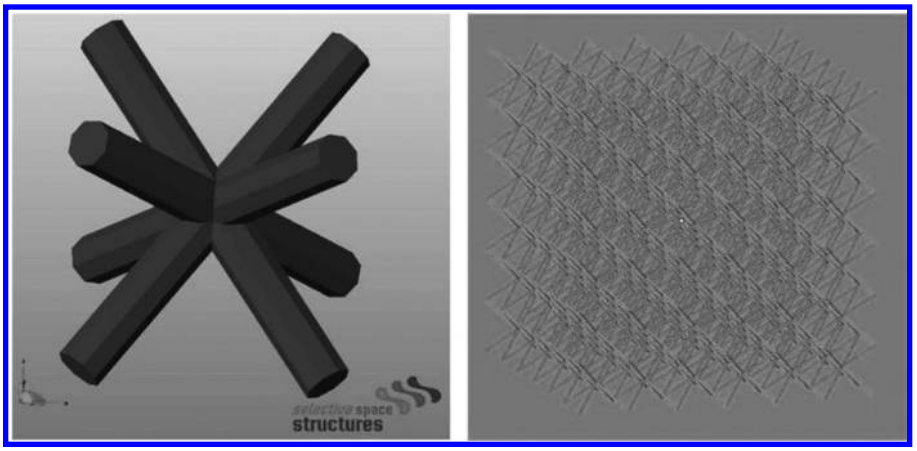

FIGURE 4.27
Octagon unit cell.

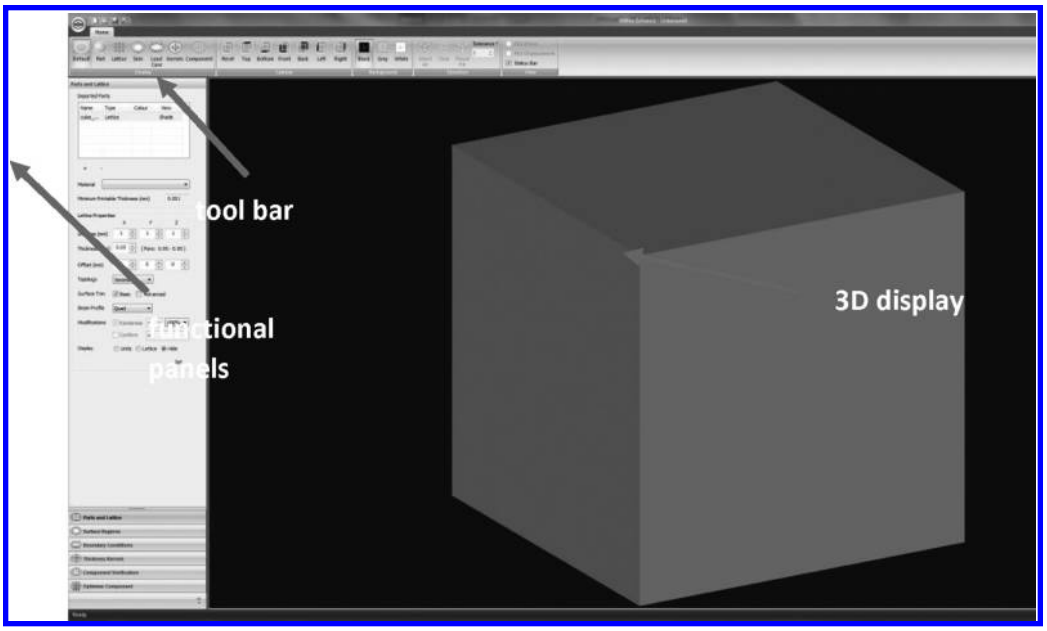

FIGURE 4.28
Within enhance interface.

flexibility of stiffness in others. A big advantage of Within Enhance is its ability to create irregular lattice structures inspired by Voronoi tessellations [17].

Strand7® is embedded in Within Enhance and provides an FEA solver. It can be used to verify the feature characteristics of the modified part.

Within Enhance provides functionality (Figure 4.28) to carry out the following tasks:

- Multiple 3D parts in the STL format can be displayed.
- Lattices of various types and sizes for the 3D parts can be created.

- Skins of varying thickness can be created for loaded 3D files.
- By using thickness kernels, lattices and skins with varying density can be defined.
- All optimized changes of the 3D part regarding the defined lattice, skin, boundary conditions, thickness kernel, and optimized properties can be FEA simulated and optimized according to freely applicable loading conditions.

The process of creating a trabecular lattice cube is divided into three main steps:

Figure 4.29 shows the first step of generating trabecular lattice parts. The cube is loaded as an STL file into the Within Enhance interface. The surface has an FEA conformal triangulation that is necessary for the creation of the defined pore sizes and struts.

The second step (Figure 4.30) is to define parameters of the lattice structure. In this case, modified parameters are pore size and struts thickness. Each of these factors can be changed individually and to a preliminarily prohibitive level of detail.

After allocating values to the defined lattice structure, cubes can be created. This preview gives a first overview of the defined parameters and a visual check can be done.

After defining all necessary parameters (Figure 4.31), the part is ready for export to an STL file. It can be saved to a new file without the design space.

The volume of the used cube is 1000 mm^3. It is calculated via [18]:

$$V = a * a * a \tag{4.10}$$

Volume of a cube

$$V = 10 * 10 * 10$$

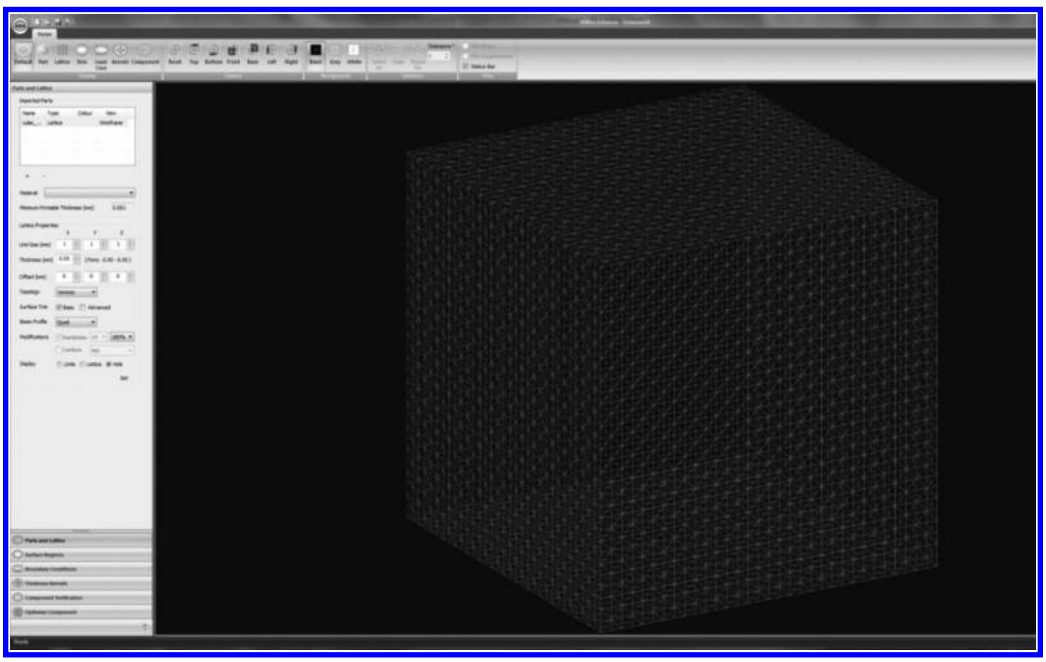

FIGURE 4.29
Step 1: STL file with surface mesh.

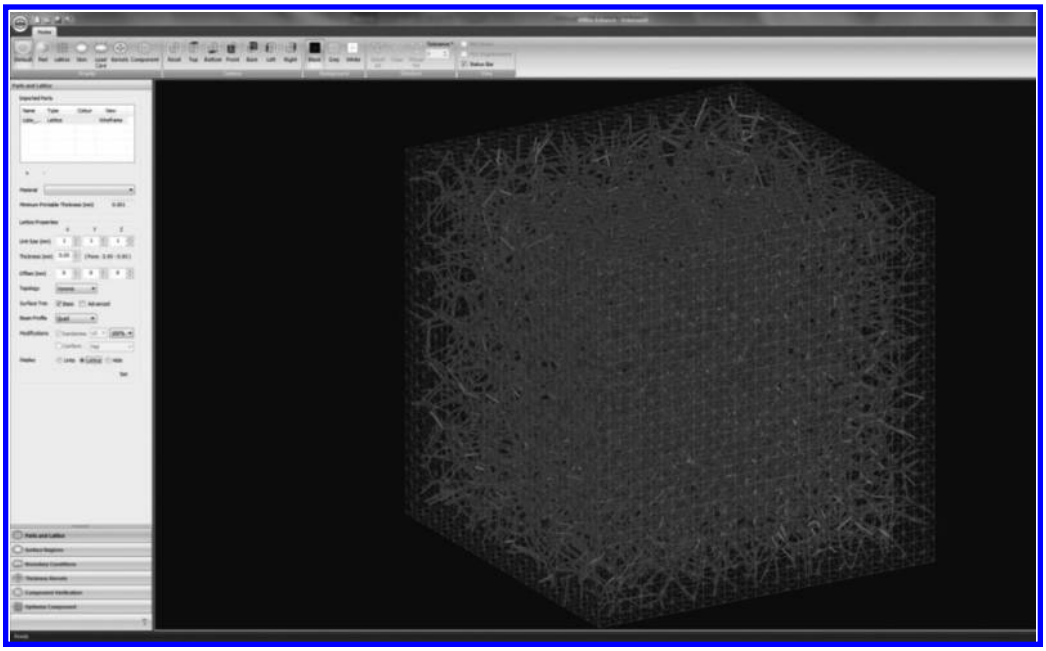

FIGURE 4.30
Step 2: Trabecular lattice structure with defined parameters.

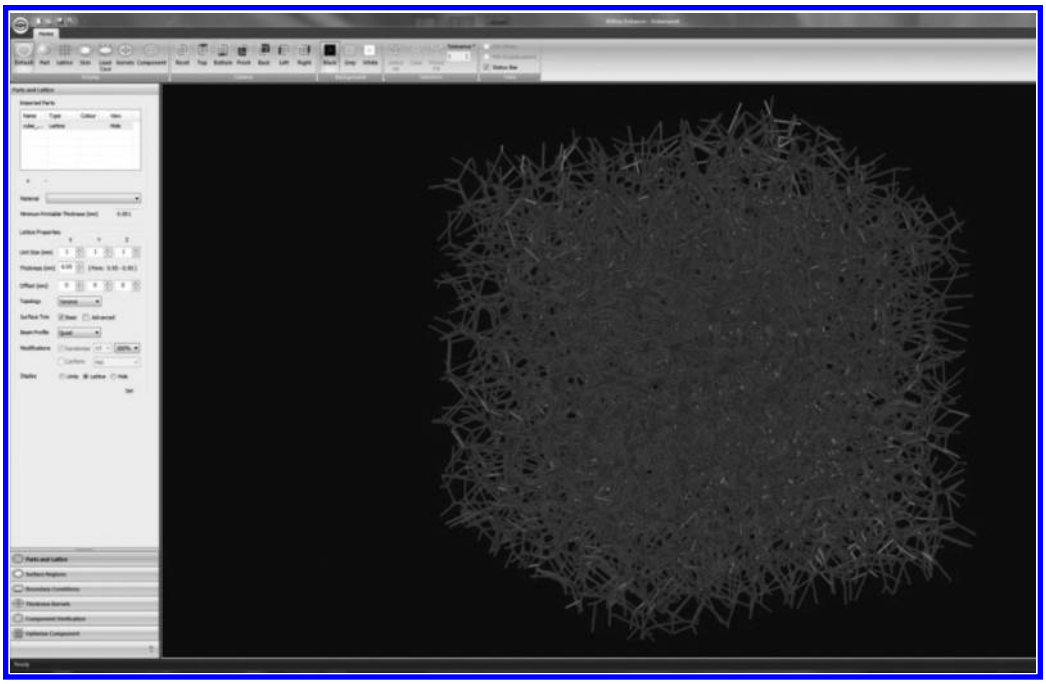

FIGURE 4.31
Step 3: Created lattice structure cube with defined sizes and parameters.

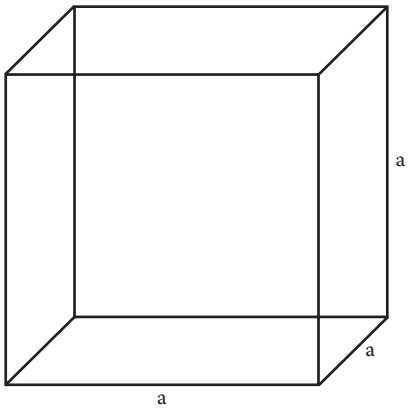

FIGURE 4.32
Example of a cube.

$$V = 1000 \text{ mm}$$

where:
V is the volume
a is the length of the edges

The design space created using Magics has edges of length 10 mm (Figure 4.32).

The pore size depends on the requested sizes. They vary between 300 and 1350 µm (Figure 4.33). Through the use of different pore sizes, different mechanical properties can be achieved.

The current minimal struts size is around 200 µm. It defines the struts thickness and is in contrast to the pore size constant in the whole part.

All used options are shown in Table 4.4.

A special feature of this program is the use of thickness kernels. These kernels make it possible to create a lattice structure with varying densities within the design space.

The example in Figure 4.34 shows a design space with different types of thickness kernels. The highlighted layers show the varying density within the design space.

In the created model, the difference of the various struts can be seen (Figure 4.35). The thicker sections are in the upper, lower, and middle area of the cube (Figure 4.35a). The thinner sections are located between the thicker sections of the part (Figure 4.35b).

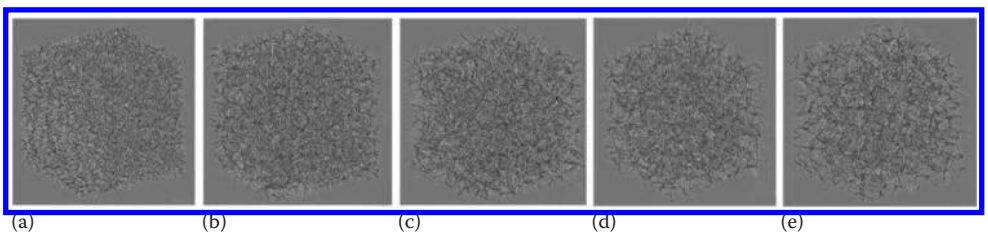

FIGURE 4.33
Varying densities of trabecular lattice (a) type 1, (b) type 2, (c) type 3, (d) type 4, (e) type 5 (Table 4.4).

TABLE 4.4

Different Trabecular Lattice Types

Trabecular Lattice Part Number	Design Space (mm^3)	Pore Size(µm)	Struts Thickness (µm)
1	Cube 10 × 10 × 10	300–700	200
2		450–1250	
3		600–1400	
4		115–1725	
5		1350–2025	

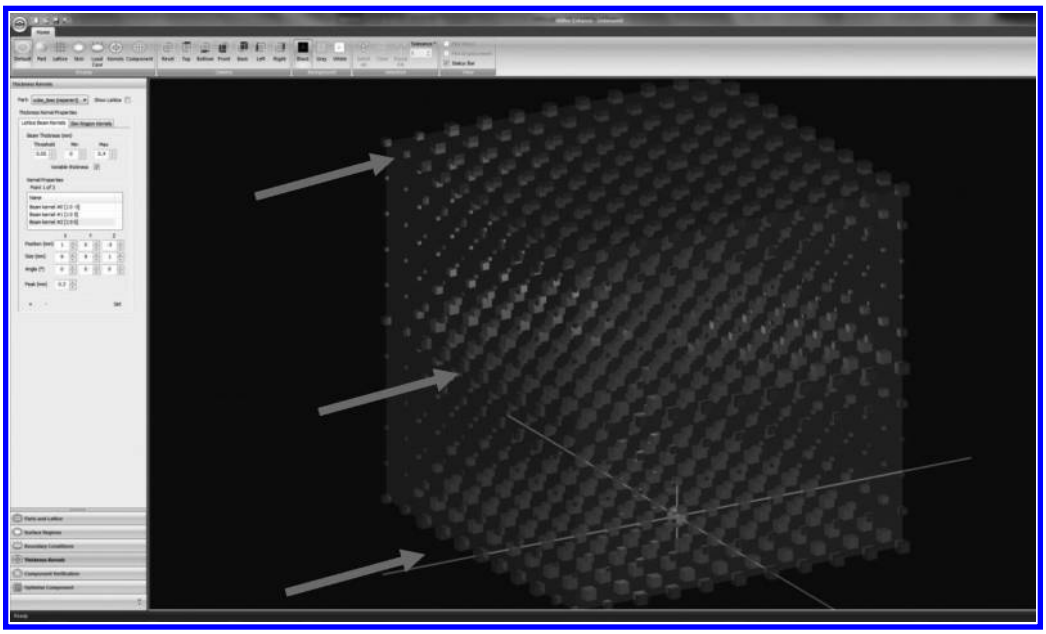

FIGURE 4.34
Example for using thickness kernels.

4.10 Influencing Factors of the Process

All present evaluations have shown that the laser sintering is a very complex manufacturing process. Because of this, it is indispensible to observe all necessary influencing parameters of this process (Figure 4.36).

The factors of concern are those included in the process parameter. Influencing parameters of the mechanical properties and microstructure are as follows:

- Laser power (P)
- Exposure speed (v)
- Hatch distance (h)
- Scanning geometry

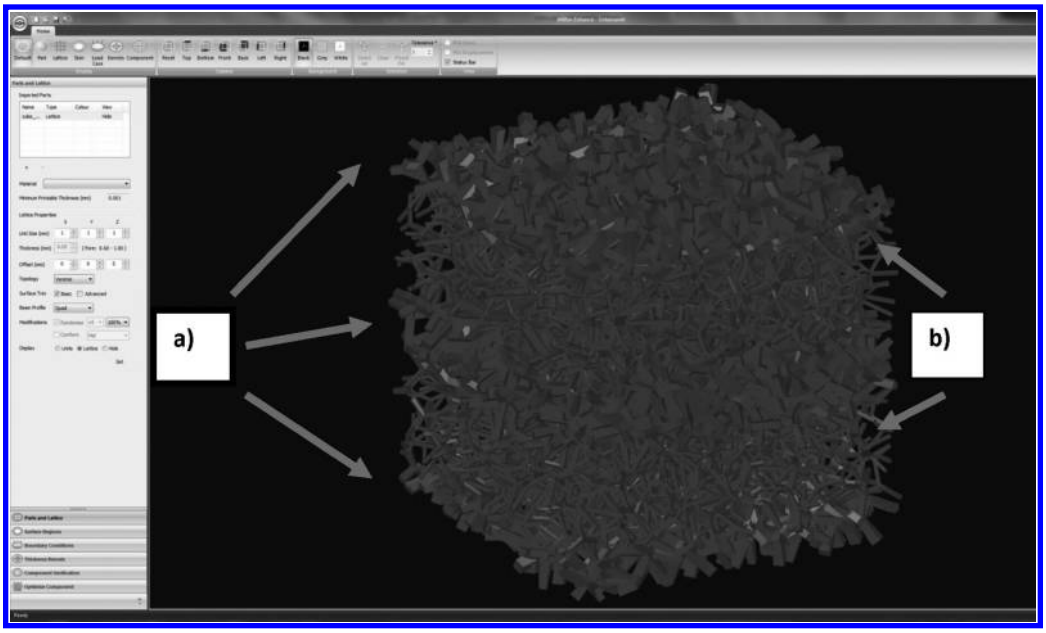

FIGURE 4.35
Result of a lattice cube by using thickness kernels. (a) Sections with thickness kernels and (b) sections without thickness kernels.

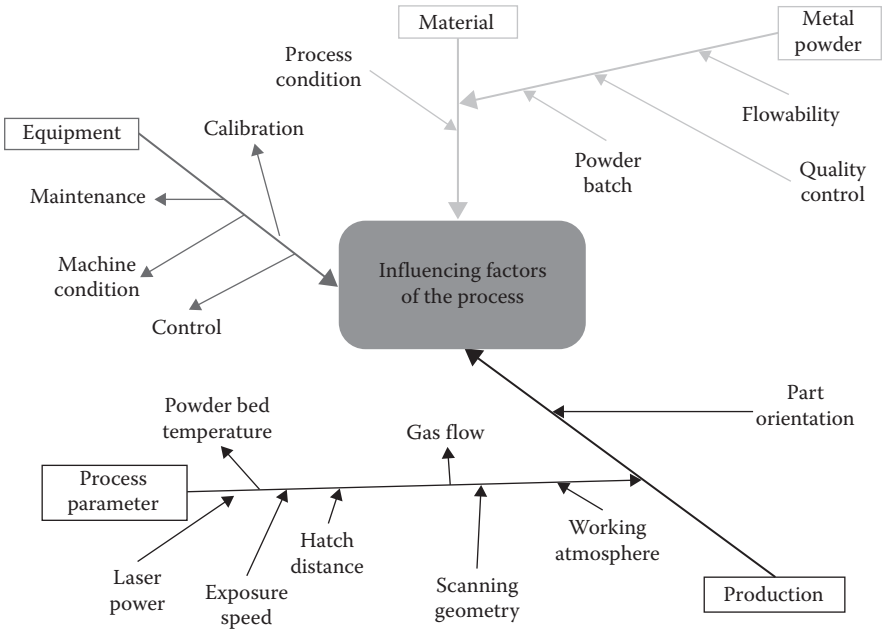

FIGURE 4.36
Overview of the main influencing factors.

- Working atmosphere
- Powder bed temperature
- Gas flow

4.10.1 Exposure Strategies

The slice files loaded into the machine are describing the parts contours as slice stacks. Every manufacturer of AM machines has different approaches on the exposure strategies. For this reason, the different approaches are detailed in Subsections 4.10.1.1 through 4.10.1.9.

4.10.1.1 Exposure

During the exposure of a layer for a part, the laser beam moves over the surface of the bed of powder. In relation to the exposure, a differentiation is made between exposing the part contour and hatching of the enclosed area of the layer.

- Exposing the part contour

  During contour exposure, which defines the subsequent geometrical shape, by default beam shaping is used for high detail resolution and as a result optimal surface properties. The contour of the part in each layer is predefined by polygons.
- Hatching of the enclosed area of the layer

  Hatching of the enclosed areas of the layer within the contour produces a solidified layer. During the exposure of the internal areas of layers to be solidified, by default a high process speed and optimized strength properties have priority. During this process, the laser beam moves within the cross section of the part along parallel paths (hatch lines) with the constant application of energy.

4.10.1.2 Curing Zone

During the exposure, a curing zone of melted metal powder forms around the laser beam (Figure 4.37).

For the dimensional accuracy of parts, the size of the curing zone must be taken into account during exposure. It is dependent on the material used and the exposure type selected. To compensate for dimensional variations, values for a beam offset can be entered at various points in the process software. These corrections are cumulative.

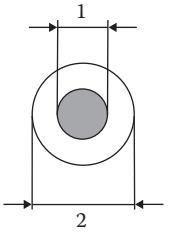

FIGURE 4.37
Illustration of the curing zone.

1 Diameter of the laser beam
2 Diameter of the curing zone

4.10.1.3 Beam Offset

- Beam offset on exposure of the contour

  If the path of the center of the laser beam moves along the nominal contour of the part during exposure, the contour of the part is enlarged by the radius of the curing zone of the laser beam. The beam offset compensates for this contour enlargement. It displaces the center of the path of the laser beam inward (Figure 4.38).
- Beam offset on exposure of the enclosed areas of the layer

  During exposure, the beam offset displaces the path of the center of the laser beam from the nominal contour by the value entered toward the inside (Figure 4.39).

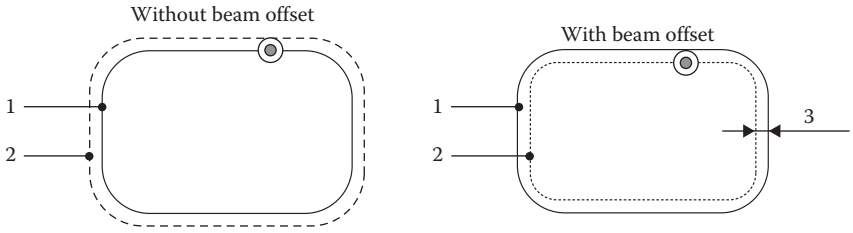

1 Nominal contour
2 Actual contour

1 Nominal contour = Actual contour
2 Center of the path of the laser beam
3 Beam offset

FIGURE 4.38
Exposure with and without beam offset.

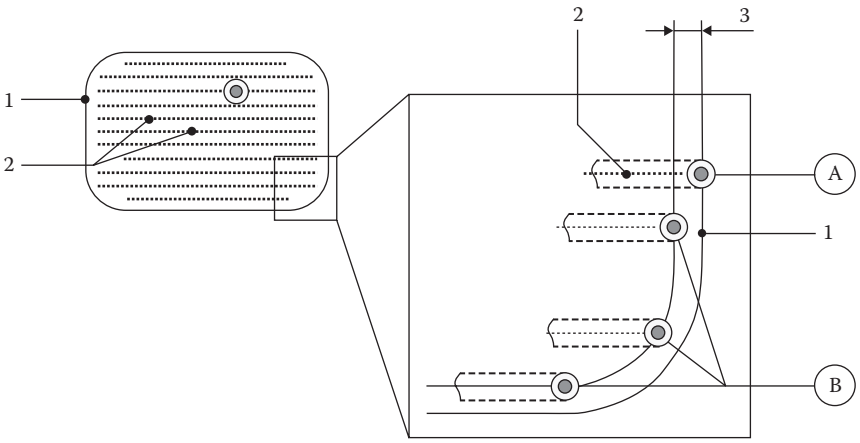

1 Nominal contour
2 Center of the path of the laser beam
3 Beam offset

A Without beam offset
B With beam offset

FIGURE 4.39
Exposure strategy.

- Correcting beam offset to suit the specific material

  The effect of the beam offset on the dimensional accuracy of the parts is dependent on the diameter of the curing zone of the material. Different values for the beam offset for specific materials are qualified by EOS.
- Correcting beam offset to suit specific parts

  If a part for special applications, for example, for a fit, is to be oversize or undersize, this change can be achieved using the value for the part-specific beam offset. The default setting for the value is 0. On the entry of a positive value, the contour is offset in the direction of the inside of the part. The entry of a negative value will produce an oversize.
- Correct beam offset via exposure parameters (exposure editor module)

  The beam offset in the exposure parameters defines the offset between the individual exposure processes. The default value for the outer contour and the related edges is 0. The same exposure parameters will produce the same results independent of the machine.

4.10.1.4 Basic Exposure Type ChessRotLx

In the case of the exposure type, ChessRotLx exposure is in the form of squares and gaps. First, all squares in one direction of exposure are exposed in the defined sequence, then all squares in the other exposure direction. The gaps are exposed last.

The squares and gaps in the hatching are rotated by 67° in each layer prior to the next exposure (Figure 4.40).

The arrangement of the squares in the part is always the same, even on displacement of the part. Unexposed gaps are left between the squares. After the exposure of the entire surface area with squares, the remaining gaps are exposed at a second speed. The laser beam moves over the entire width of the part during this process.

The width of the overlap between the squares and the gaps is set in the process software.

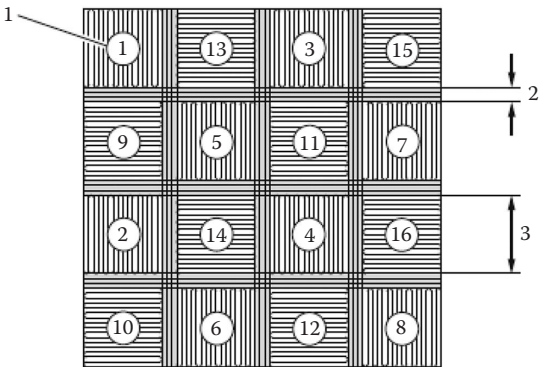

FIGURE 4.40
Chess exposure strategy.

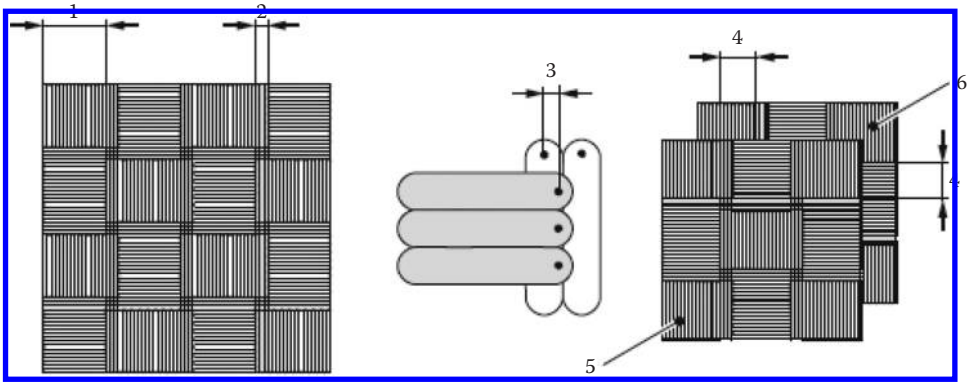

1 Square width
2 Gap width
3 Overlapping
4 Offset
5 1st, 3rd, 5th layer
6 2nd, 4th, 6th layer

FIGURE 4.41
Chess exposure strategy variations.

It is possible to build with an offset both in the *X* and in the *Y* direction from layer to layer (Figure 4.41).

4.10.1.5 Basic Exposure Type Contours

With the exposure type contours, the contour is exposed and optimized for the geometry. The process software compares the contour to be exposed with a contour already exposed in a defined layer below the contour to be exposed (comparison contour). If the contour to be exposed or part of the contour

- Is exactly over the corridor for the comparison contour, the contour or the part of the contour is exposed using the values for the standard exposure parameters;
- Is within the exposure area enclosed by the comparison contour, the contour or the part of the contour is exposed using the values for the OnPart exposure parameters;
- Is outside the corridor for the comparison contour in loose metal powder, the contour or the part of the contour is exposed using the values for the downskin exposure parameters (Figure 4.42).

4.10.1.6 Basic Exposure Type SkinCore

The exposure type SkinCore divides a part into skin and core. The skin and the core can be allocated different exposure types to obtain shorter building times but still obtain resilient parts (Figure 4.43).

4.10.1.7 Basic Exposure Type SLI_HatchLx

With this exposure type, defined exposure requirements are included in the SLI file.

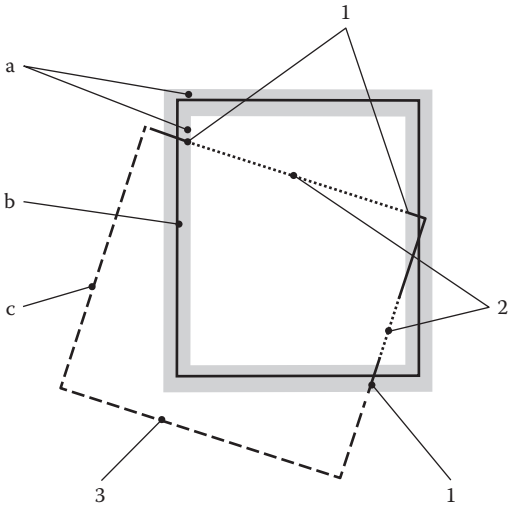

a Corridor
b Comparison contour
c Contour to be exposed
1 Standard
2 OnPart
3 Downskin

FIGURE 4.42
Upskin and Downskin.

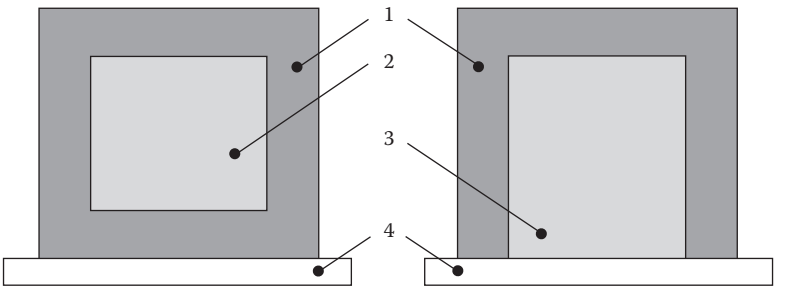

1 Skin
2 Core
3 Core open to the building platform
4 Building platform

FIGURE 4.43
SkinCore exposure.

4.10.1.8 Basic Exposure Type UpDownStripesAdaptiveLx

The exposure type UpDownStripesAdaptiveLx comprises the exposure forms UpDown, stripes, and Lx combined.

The stripes in the hatching are rotated by 90° in relation to the layer underneath on every second layer prior to the next exposure.

- UpDown

  For each layer to be exposed, the process software checks whether the area under the area to be exposed has been exposed or is to be exposed and whether there is overlapping.

  - Upskin

    Area to be exposed over which there is no area to be exposed
  - Inskin

    Area to be exposed over and under which there is an area to be exposed or that has been exposed
  - Downskin

    Area to be exposed under which there is no area exposed
  - Overlap with inskin

    Area to be exposed between an inskin area and an upskin or downskin area that can be individually exposed for improved attachment to the related neighboring areas (Figure 4.44).

    Exposure without overlap:
- Stripes

  Inskin areas are exposed in stripes (Figure 4.45).
- Lx

  Inskin areas are skipped on each alternate layer during exposure and then exposed in the next layer with double exposure depth (Figure 4.46).

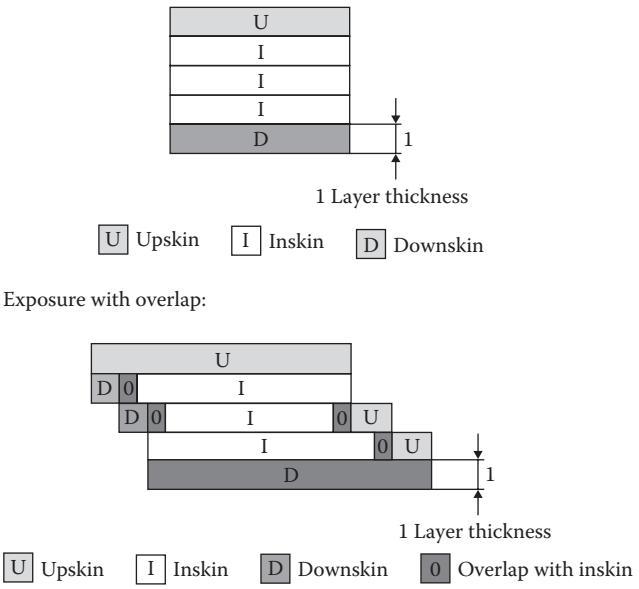

FIGURE 4.44
Description of Upskin and Downskin.

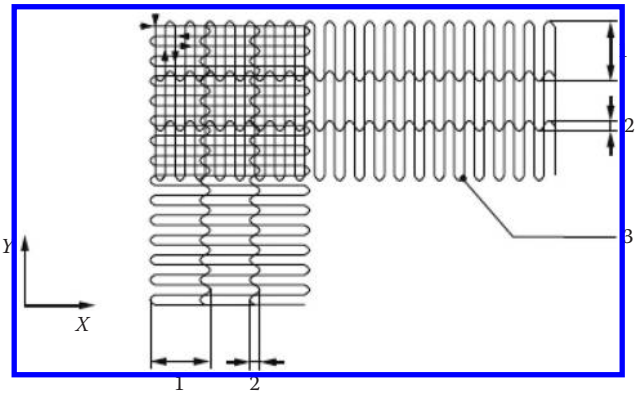

1 Stripe width
2 Stripes overlap
3 Center of the path of the laser beam

FIGURE 4.45
Stripe exposure.

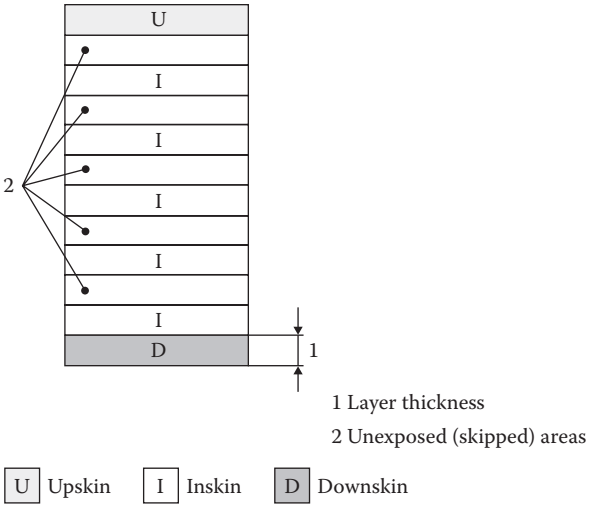

FIGURE 4.46
Skip layer.

4.10.1.9 Basic Exposure Type UpDownStripesAdaptiveRotLx

The exposure type UpDownStripesAdaptiveRotLx differs from the exposure type UpDownStripesAdaptiveLx in that the stripes for the hatching on every layer are rotated by 67° prior to the next exposure.

Exposure types from the Initial values for parameters module

- *Exposure type _Default_DirectPart*

  The exposure type _Default_DirectPart is used for the production of complex parts, e.g. for gear wheels, turbine wheels, and so on. It can comprise several subexposure types for skin and core areas.

- *Exposure type _Default_DirectTool*

  The exposure type _Default_DirectTool is used for the production of tools for injection moulding, die casting, and so on. It can comprise several sub-exposure types for skin and core areas.
- *Exposure type _Default_ExternalSupport*

  The exposure type _Default_ExternalSupport exposes support structures that are necessary to support parts with large overhangs during the building process.
- *Exposure type _Default_OuterSkin_DirectPart*

  The exposure type _Default_OuterSkin_DirectPart is used for the exposure of a skin for parts in DirectPart applications.
- *Exposure type _Default_OuterSkin_DirectTool*

  The exposure type _Default_OuterSkin_DirectTool is used for the exposure of a skin for parts in DirectTool applications.
- *Exposure type _Default_Postcontours*

  Using the exposure type _Default_Postcontours contour exposure is undertaken after the exposure of the hatching for the part.
- *Exposure type _Default_Precontours*

  Using the exposure type _Default_Precontours contour exposure is undertaken before the exposure of the hatching for the part.

4.11 Summary

With the relatively young technology (compared to conventional machining) of AM the industry is still facing acceptance problems in the industry. People often just have a hard time to imagine that additively manufactured components can be from mechanical properties standpoint of view competes with classical machining. Standards for AM are not well enough defined yet. However with time the general acceptance and trust into the technology is growing. With recent releases of additive manufactured products in highly regulated industries such as aerospace and medical the technology awareness of the industry has significantly raised.

References

1. Gebhardt, A., *Generative Fertigungsverfahren, Rapid Prototyping—Rapid Tooling—Rapid Manufacturing*, 3. Auflage, Germany, Hanser Verlag, 2007.
2. EOS Unterlagen. EOS documentation (non-public).
3. N., N. www.calraminc.com/services.htm.
4. Gibson, I., Rosen, D.W., Stucker, B., *Additive Manufacturing Technologies, Rapid Prototyping to Direct Digital Manufacturing*, Germany, Springer-Verlag, 2010.
5. N., N. http://www.laserfocusworld.com/articles/2008/04/beam-characterization-camera-based-sensors-characterize-laser-beams.html.

6. Boyan, B.D. et al., Titanium—Bone Cell Interface. *Titanium in Medicine*, D. Brunette et al. (eds.), Berlin, Germany, Springer, 2001, pages 562–579.
7. N., N. www.laser-journal.de, Strahlqualität von Lasern.
8. N., N. http://www.rp-photonics.com/gaussian_beams.html.
9. DIN ISO 5832–3: 1996, Implants for surgery—Metallic materials, Part 3: Wrought titanium 6-aluminium 4-vanadium alloy, ISO standard, August 2000.
10. N., N. http://www.ifw.tu-bs.de/ifw/deutsch/lehre/fachlabore/titanlabor.pdf.
11. Gibson, L.J. et al., *Cellular Materials in Nature and Medicine*, Cambridge, Cambridge University Press, 2010.
12. Gibson, L., Ashby, M.F., *Cellular Solids*. 2. Auflage, Germany, Cambridge University Press, 199.
13. Chen, J., Fracture analysis of cellular materials: A strain gradient model. *Journal of the Mechanics and Physics of Solids*, 46(5), 1998, pages 789–828.
14. Deshpande, V., Foam topology: bending versus stretching dominated architectures. *Acta Materialia*, 49(6), 2001, pages 1035–1040.
15. Kim, H., A morphological elastic model of general hexagonal columnar structures. *International Journal of Mechanical Sciences*, 43(4), 2001, pages S1027–S1060.
16. Alkhader, M., Vural, M., Mechanical response of cellular solids: Role of cellular topology and microstructural irregularity. *International Journal of Engineering Science*, 46(10), 2008, pages 1035–1051.
17. *Within Enhance Technical Manual*, For version 3.2, London, Within Technologies, 2011.
18. Stöcker, *Taschenbuch der Physik*, 5. korrigierte Auflage, Germany, Verlag, Harri Deutsch, 2007, page 371.
19. Wintermantel, E., Ha, S.-W., *Medizintechnik mit biokompatiblen Werkstoffen und Verfahren*, 3. Auflage, Germany, Springer-Verlag, 2001, pages 5–8.
20. Huiskes, R. et al., The relationship between stress shielding and bone resorption around total hip stems and the effects of flexible materials. *Clinical Orthopedics and Related Research*, (274), 1992, pages 124–134.
21. Cheah, C. et al., Development of a Tissue Engineering Scaffold Structure Library for Rapid Prototyping. Part 1: Parametric Library and Assembly Program. *The International Journal of Advanced Manufacturing Technology*, 21(4), 2003, pages 302–312.
22. Frenkel, S.R. et al., Bone response to a novel highly porous surface in a canine implantable chamber. *Journal of Biomedical Materials Research. Part B, Applied Biomaterials*, 71(2), 2004, pages 387–397.
23. Ha, S., Werkstoffe in der Medizintechnik—Einleitung. *Mediztintechnik*, 5. Auflage, E. Wintermantel, S. Ha (eds.), Berlin, Germany, Springer-Verlag, 2009, page 189.
24. Cheah, C., Hayes, W., The compressive behaviour of bone as two—phase porous structure. *Journal of Bone and Joint Surgery*, 59(7), 1977, pages 954–962.
25. Karageorgiou, V., Kaplan, D., Porosity of 3D biomaterial scaffolds and osteogenesis. *Biomaterials*, 26(27), 2005, pages 5474–5491.
26. Seemanm, E., Modeling and Remodeling. *Principle of Bone Biology*, Volumes 1, 3, J.P. Bilezikian et al. (eds.), Amsterdam, the Netherlands, Academic Press, 2008, pages 3–28.
27. Morgan, E.F., Bouxsein, M.L., Biomechanics of Bone and Age—Related Fractures. *Principle of Bone Biology*, Volumes 1, 3, J.P. Bilezikian et al. (ed.), San Amsterdam, the Netherlands, Academic Press, 2008, pages 29–51.
28. Rho, J., Mechanical properties and the hierarchical structure of bone. *Medical Engineering & Physics*, 20(2), 1998, pages 92–102.
29. Rho, J.Y. et al., Young's modulus of trabecular cortical bone material: Ultrasonic and microtensile measurements. *Journal of Biomechanics*, 26(2), 1993, pages 111–119.
30. Turner, C., The elastic properties of trabecular and cortical bone tissue are similar: results from two microscopic measurement techniques. *Journal of Biomechanics*, 32(4), 1999, pages 437–441.

31. Li, X. et al., Fabrication and compressive properties of Ti6Al4V implant with honeycomb—like structure for biomedical applications. *Rapid Prototyping Journal*, 16(1), 2010, pages 44–49.
32. Ryan, G. et al., Fabrication methods of porous metals for use in orthopedic applications. *Biomaterials*, 27(13), 2006, pages 2651–2670.
33. Shah-Derler, B. et al., Gewebe. *Medizintechnik*, 5. Auflage, E. Wintermantel, S. Ha (eds.), Berlin, Germany, Springer-Verlag, 2009, page 175.
34. Turner, T. et al., A comparative study of porous coatings in a weight-bearing total hip-arthroplasty model. *Journal of Bone and Joint Surgery*, 68(9), 1986, pages 1396–1409.
35. Zhang, L.C. et al., Manufacture by selective laser melting and mechanical behaviour of a biomedical Ti-24Nb-4Zr-8Sn alloy, *Scripta Materialia*, 2011.
36. Sumner, D.R., Galante. J.O., Determinants of stress shielding: Design versus materials versus interface. *Clinical Orthopedics and Related Research*, (274), 1992, pages 202–212.
37. Vamsi Krishna, B. et al., Engineered porous metals for implants. *JOM*, 60(5), 2008, pages 45–48.
38. Kienapfel, H. et al., Implant fixation by bone ingrowth. *The Journal of Arthroplasty*, 14(3), 1999, pages 355–368.
39. Ha. S., Wintermantel, E., Biokompabilität Keramischer Werkstoffe. *Medizintechnik*, 5. Auflage, E. Wintermantel, S. Ha (eds.), Berlin, Germany, Springer-Verlag, 2009.
40. Kooistra, G., Compressive behaviour of age hardenable tetrahedral lattice truss structures made from aluminium. *Acta Materialia*, 52(14), 2004, pages 4229–4237.
41. Harrysson, O.L. et al., Direct metal fabrication of titanium implants with tailored materials and mechanical properties using electron beam melting technology. *Material and Biological Issues*, ASTM STP 1272, S.A. Brown, J.E. Lemons (eds.), Germany, American Society for Testing and Materials, 1996, pages 136–149.
42. Sigmund, O., Tailoring materials with prescribed elastic properties. *Mechanics of Materials*, 20(4), 1995, pages 351–369.
43. Christensen, R., Mechanics of cellular and other low-density materials. *International Journal of Solids and Structures*, 37(1/2), 2000, pages 93–104.
44. Sigmund, O., Tailoring materials with prescribed elastic properties. *Mechanics of Materials*, 20(4), 1995, pages 351–369.
45. Christensen, R., Mechanics of cellular and other low-density materials. *International Journal of Solids and Structures*, 37(1/2), 2000, pages 93–104.
46. Cheah, C. et al., Development of a tissue engineering scaffold structure library for rapid prototyping. Part 2: Parametric library and assembly program. *The International Journal of Advanced Manufacturing Technology*, 21(4), 2003, pages 302–312.
47. Baksh, D. et al., Three-dimensional matrices of calcium polyphosphates support bone growth in vitro and in vivo. *Journal of Materials Science: Materials in Medicine*, 9(12), 1998, pages 743–748.
48. N., N. http://www.datlof.com/8Axamal/docs/Marketing/jhu/JE/index.htm.
49. Traini, T. et al., Direct laser metal sintering as a new approach to fabrication of an isoelastic functionally graded material for manufacture of porous titanium dental implants. *Dental Materials: Official Publication of the Academy of Dental Materials*, 24(11), 2008, pages 1525–1533.
50. Warnke, P.H. et al., Rapid prototyping: porous titanium alloy scaffolds produced by selective laser melting for bone tissue engineering. *Tissue Engineering. Part C, Methods*, 15(2), 2009, pages 115–124.
51. Hollander, D.A. et al., Structural, mechanical and in vitro characterization of individually structured Ti-6Al-4V produced by direct laser forming. *Biomaterials*, 27(7), 2006, pages 955–963.
52. Meiners, W., Direktes selektives Laser-Sintern einkomponentiger metallischer Werkstoffe. Dissertation, RWTH Aachen, Aachen, Germany, 1999.
53. Wagner, C., Untersuchung zum Slektiven Lasersintern von Metalen. Dissertation, RWTH Aachen, Aachen, Germany, 2003.

54. Wolf, D., Entwicklung von Prozessparametern für das Lasersintern von 3D-Gitterstrukturen in Titan, Diplomarbeit, EOS GmBH International Diploma Thesis, 2010.
55. Breme, J., Titanlegierungen in der Medizintechnik. *Titan und Titanlegierungen*, 3., D.M. Peters et al. (eds.), Weinheim, Germany, Wiley-VCH Verlag GmbH, 2002, pages 205–227.
56. N., N. www.m-pore.de/download/veroeff-mechanik_4.pdf.
57. Ryan, G.E. et al., Porous titanium scaffolds fabricated using a rapid prototyping and powder metallurgy technique. *Biomaterials*, 29(27), 2008, pages 3625–3635.
58. Lu, X. et al., Fine lattice structures fabricated by extrusion freeforming: Process variables. *Journal of Materials Processing Technology*, 209(10), 2009, pages 4654–4661.

5

Additive Manufacturing of Ceramics

Susmita Bose, Sahar Vahabzadeh, Dongxu Ke, and Amit Bandyopadhyay

CONTENTS

ABSTRACT Ceramic processing involves multiple steps due to the high melting point and low ductility. Traditionally, ceramics are manufactured from its powder to a green shape followed by densification or sintering at high temperature. Application of additive manufacturing (AM) of ceramics started with the ease of green shape forming that can then be sintered using conventional methods. Later, different AM approaches developed to form ceramic coatings on metallic substrates to improve wear, corrosion, and heat resistance of materials. The following chapter is focused on different AM techniques, how they can be utilized for ceramic processing, and their advantages as well as concerns. Some of

the recent developments and work done over the past 20 years are addressed to understand the history and growth of this field through process descriptions and examples.

5.1 Introduction

The concept of solid freeform fabrication or 3D (three-dimensional) printing (3DP) was first introduced by Chuck Hull in 1986 through stereolithography (SLA) method [1]. Since then, several processes such as selective laser sintering (SLS), fused deposition modeling (FDM), ink-jet printing, and laser engineered net shaping (LENS) have been introduced to fabricate metals, ceramics, polymers, and composites. Among various approaches, AM techniques used to fabricate 3D ceramic structures can be classified as (1) laser assisted sintering (e.g., SLS and LENS), (2) extrusion (e.g., fused deposition of ceramics, FDC), (3) polymerization (e.g., SLA), and (4) direct writing-based processes (e.g., ink-jet 3DP). In all AM techniques, a 3D model is created by computer-aided design (CAD) program and then is converted to an STL (standard tessellation language) file. The 3D object is then sliced to two-dimensional (2D) cross sections and fabrication of the part is started from the base in alternating layers. Manufacturing is continued layer by layer until the entire part is fabricated. Compared to traditional manufacturing processes, the primary advantage of AM is its ability to create complex designs with high accuracy in dimensions and structural features without the need for specific tooling or dies. In addition, almost all AM techniques are faster than traditional processes without the need for further surface finishing. However, not all the AM techniques are useful for fabrication of similar ceramic structure due to the limitations of each technique.

In this chapter, the methodology of these techniques is explained in detail and various ceramic structures processed by each technique for different applications are introduced as examples for readers to understand the process better.

5.2 SLA of Ceramics

5.2.1 SLA: History and Methodology

SLA is an AM process in which an ultraviolet (UV) laser is used to solidify a photocurable polymer [2]. SLA was first used to manufacture polymeric structures; however, further modifications allowed SLA to be used for processing of ceramic materials. Flexibility, high accuracy in dimensions of ceramic structures with different geometries, and efficiency are the main advantages of SLA. However, the need for supporting material during manufacturing is a disadvantage of SLA. In spite of processing limitation, SLA has potential for manufacturing ceramic implants based on patient-specific needs and direct refractory molds fabrication of prototypes prior to defining an expensive mold for injection molding [3].

Ceramic manufacturing using SLA was first introduced in the early 1990s by Griffith et al. from the University of Michigan [4]. They processed 3D ceramic structures of silica (SiO_2) and alumina (Al_2O_3) by dispersing 45–55 v/o of relative powder in a UV-curable aqueous acrylamide solution, followed by curing the ceramic composite solution using high intensity UV lamp (220–450 nm) at different exposure times [4].

The ceramic powder ratio, chemistry and concentration of photocurable polymer, and UV power are important parameters in the success of SLA. Hinczewski et al. reported the

TABLE 5.1

Ceramic—Photocurable Polymer Systems in SLA

Ceramic Powder	Photocurable Polymer	References
Alumina (Al_2O_3)	Di-ethoxylated bisphenol a dimethacrylate (diacryl 101)	[5]
	Hexanediol diacrylate (HDDA)	[12]
	Diacryl 101 and HDDA	[13]
	Acrylamide	[4]
	Acrylic and silicon acrylate	[14]
	Acrylate	[9]
	Zirconate + 3% irgacure 184	[15]
Silica (SiO_2)	Acrylate	[3]
	Acrylamide	[4]
	acrylic and silicone acrylate	[16]
Lead zirconate titanate (PZT)	Acrylates (diacryl 101and HDDA) and epoxy-acrylates (SOMOS 6100)	[10,11]
Hydroxyapatite (HA)	SL5180 resin (Huntsman)	[9]
Barium titanate ($BaTiO_3$)	Hexanediol diacrylate (HDDA)	[17]
Titanium oxide (TiO_2)	Epoxy resin	[18]

effects of dispersant and diluent concentrations on the viscosity and rheological behavior of highly loaded alumina particles in curable acrylate monomer solutions [5]. The effects of exposure conditions, powder characteristics, reactive system, and cured depth and width on SLA process were also reported by Chartier et al. [3].

Different types of polymers along with ceramic powder compositions have been used in SLA, as listed in Table 5.1 for various structures and applications including photonic crystals, piezoelectrics, cellular ceramic structures, and bone scaffolds [6–11].

Figure 5.1 shows the steps to fabricate alumina parts using SLA. Briefly, ceramic particles are added to photoreactive polymers such as acrylate and epoxy resins to form homogeneous ceramic–polymer suspension. Ceramic particles are then cured with photocurable polymer using a UV laser beam. After the curing is completed, the organic phase is removed by an appropriate thermal treatment cycle.

To be suitable for SLA, ceramic–polymer composite solution should be homogenous and stable. It should have appropriate rheological behavior and its viscosity should be similar to conventional SLA resins (<3000 mPa s) to achieve proper flow during layer-by-layer processing [4]. In addition, the ceramic suspension should be photoactive with high cure depth and low cure width to achieve high efficiency and resolution during the manufacturing [3,5,6]. Furthermore, the cured ceramic green part must have high density to prevent crack formation, deformation, or significant shrinkage after polymer removal [4,5].

5.2.2 Stability of Ceramic Suspension and Its Rheological Behavior

Ceramic powders have negligible solubility in polymer solutions. To achieve a homogeneous dispersion of ceramic powders in polymer solution with high ceramic loading, dispersants are needed. Dispersants are widely used to disperse ceramic particles in low-polar organic media through electrostatic and steric repulsion forces [5,13]. Many dispersants have been introduced to improve ceramic powder loading and homogeneity of suspension for SLA process. Using quaternary ammonium acetate as dispersant allows the 50 vol.% of

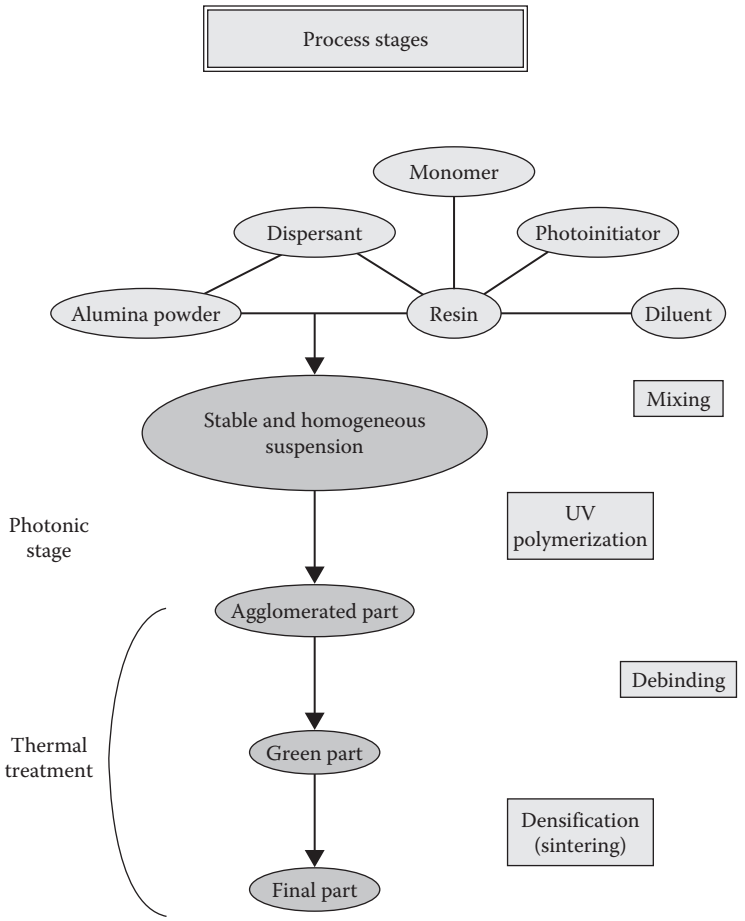

FIGURE 5.1
SLA steps in processing alumina structures. (Data from C. Hinczewski et al., *Rapid Prototyp J*, 4, 104–11, 1998.)

alumina loading in hexanediol diacrylate (HDDA); however, 50 vol.% of alumina loading in HDDA without dispersant results in a stiff paste-like colloidal gel [12]. Triton X-100 is another dispersant used in barium titanate-HDDA (BT-HDDA) resin system. 6 wt.% triton X-100 is the optimized concentration for 30 vol.% BT-HDDA suspension [17].

Viscosity is another crucial factor that decides the rheological behavior of the suspension. The viscosity of an SLA suspension can be calculated using modified Krieger–Dougherty equation [4,19]. Viscosity of the suspension is usually larger than pure photocurable resin.

Viscosity of the suspension for SLA is usually in the range of 2–5 Pa s to assure satisfactory layer recoating [13]. Thus, decreasing the viscosity of the suspension is vital for a successful ceramic SLA. Suspension with low viscosity can be achieved by using an appropriate polymer, dispersant, and diluent [5,13].

Not only the initial viscosity, but also the change in viscosity with regard to shear rate plays a significant role during the SLA. By increasing the shear rate, viscosity may decrease (shear thinning), increase (shear thickening), or remain unchanged (shear immunity). Shear thinning is desired in standard SLA process as it allows the tape casting of

layers prior to UV treatment [13]. Viscosity of the suspensions decreases with increase in temperature as well. However, the temperature should not be higher than polymerization temperature as it causes the undesired polymerization before UV scanning.

5.2.3 SLA of the Ceramic Suspension

In SLA, cured depth and width are important parameters that determine the accuracy and rate of the process. Cured depth (C_d) is the thickness of gelled resin and should be larger than 0–2 mm [5,20]. It can be theoretically calculated using the Beer–Lambert law [21]

$$C_d = D_p \ln\left(\frac{E}{E_c}\right)$$

where

D_p, E_c, and E are penetration depth, minimal energy for polymerization of the monomer, and provided energy, respectively

D_p depends on volume fraction of ceramic powder, particle size, and the refractive index difference between the UV-curable solution and ceramic powder [4,20,22,23]. Ceramic powder characteristics such as particle size and refractive index, the monomer properties such as minimal energy for polymerization and refractive index, and suspension characteristics such as the volume fraction of ceramic powder, inter-particle distance, and UV energy and wavelength of irradiation affect the cured depth of SLA. However, cured width (W_c) should be low enough to ensure high resolution and quality of SLA processed parts. For ceramic SLA, since the addition of ceramic powder, it is much more complicated than the pure polymer SLA due to scattering phenomena. Cured width has been studied with density of energy, photoinitiator concentration, powder concentration, particle diameter, and refractive index difference between powder and monomer. A linear relationship was found between the mean particle diameter and cured width, with slopes depending on the density of energy. Also cured width corresponds to a power law with powder concentration, with an exponent close to –1.

5.2.4 Applications and Further Development

Compared to traditional multilayer ceramic shell, SLA processed alumina/silica molds are more efficient and cost effective for investment casting [24–27]. SLA is also used to process piezoelectric ceramics such as lead zirconate titanate (Pb[Zr,Ti]O_3, PZT) and barium titanate ($BaTiO_3$, BT) due to its flexibility, efficiency, and accuracy [10,11,17,28]. In addition, complex 3D photonic crystals for telecommunication domain applications such as antennas, filters, and resonators have also been manufactured using ceramic-loaded SLA [7,18, 29–32].

Zhou et al. reported a direct fabrication of the ceramic casting mold by SLA, which was shown in Figure 5.2a. For manufacturing this mold, an anti-gravity process was chosen to cast this part, because the thin wall was only 3 mm. This anti-gravity design needed two risers to exhaust air in the mold and one sprue to fill as shown in Figure 5.2b. The advantage of SLA here was that it avoided the middle steps of making a wax pattern and coating shell, which was necessary in traditional investment casting. Meanwhile, this method effectively shortened the time and saved the cost for manufacturing small-batch products [24].

Figure 5.3 showed the design of a dielectric resonant or using SLA by Delhote et al. [30]. This shielded dielectric resonator was made by alumina with high unloaded Q (~3900).

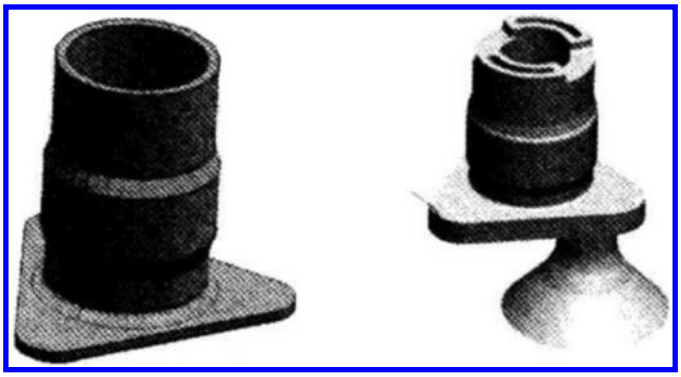

FIGURE 5.2
Three-dimensional model (a) and ceramic casting design scheme according to 3D model (b). (Data from W.Z. Zhou et al., *Proc Inst Mech Eng Part B J Eng Manuf*, 224, 237–43, 2010.)

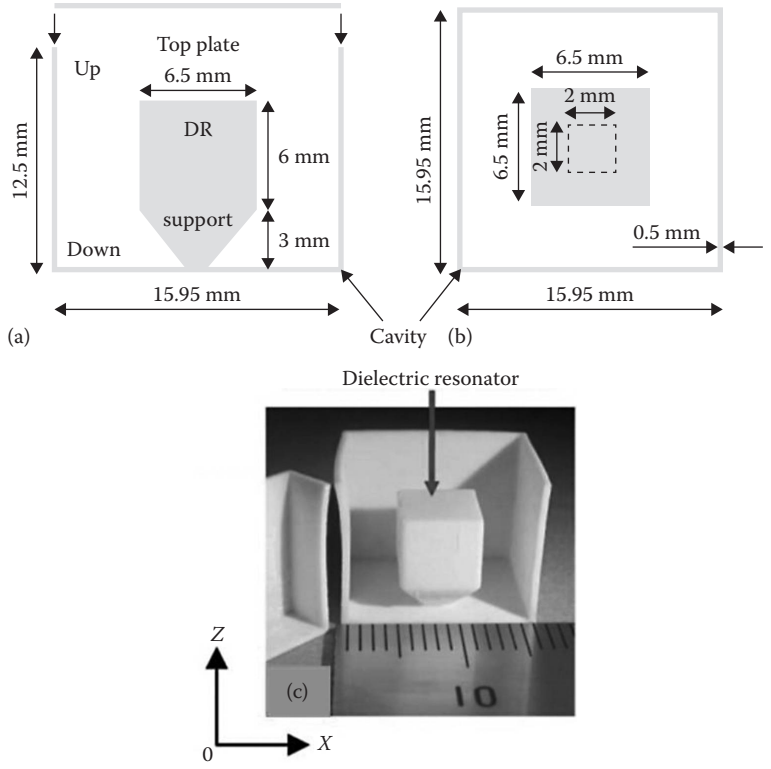

FIGURE 5.3
Design of the alumina resonant or structure with its main dimensions: (a) inside side view, (b) top view, and (c) parts produced by SLA. (Data from N. Delhote et al., *IEEE Microw Wirel Compon Lett*, 17, 433–5, 2007.)

The SLA made it possible for producing electric devices in small dimension and complex structure. This novel resonant or was very compact and able to be integrated on a substrate carrier by standard means (flip-chip or bumps), which made it very interesting for many applications [30].

The future development of this process is to further increase the resolution and decrease the processing time as well as enhanced repeatability. Recently, biocompatible ceramics, such as hydroxyapatite (HA), tricalcium phosphate (TCP), and bioglass, have been processed via SLA for biomedical implants for tissue engineering scaffolds, but there are still lots of challenges that need to be overcome [8,9]. With the development of this technology, SLA has the potential to become a more promising AM method for manufacturing products based on different applications.

5.3 SLS of Ceramics

5.3.1 SLS: History and Methodology

SLS is an AM method in which a pulsed CO_2 laser is used to fuse fine particles together [33]. SLS is the first commercialized powder bed-based manufacturing method, developed and patented by Deckard and Beaman from the University of Texas at Austin [14]. The first commercial SLS machine, SLS Sinterstation 2000, was introduced in 1992 by DTM Corporation. With the development of SLS technology, part accuracy, temperature uniformity, build speed, process repeatability, feature definition, and surface finish are improved, but the basic processing features and system configuration remain unchanged from the description [33].

The schematic of SLS is shown in Figure 5.4. Prior to laser sintering, the powder needs to be preheated just below the melting point/glass transition temperature to minimize thermal distortion and facilitate fusion of new layer to previous layer [33,34]. During the process, chamber should be sealed using nitrogen gas to avoid oxidation and degradation of the powder. The focused CO_2 laser beam is then directed onto the powder bed to form the pattern according to the CAD design. Meanwhile, surrounding powder remains loose and serves as a support for subsequent layers [33]. After sintering each layer, the build platform is lowered and the roller spreads next layer of powder to the build bed. The process is repeated until manufacturing the designed part is complete. At last, the SLS processed part should be kept long enough in the chamber to cool down. This prevents any degradation of powder and shape deformation due to the presence of oxygen and uneven thermal contraction.

Compared to metals or polymers processing, manufacturing of ceramics by SLS is accompanied by challenges mainly due to high melting temperature of ceramics. As a result, more laser energy and longer cooling time are required, which is not efficient and cost effective in many cases. For example, Hagedorn et al. reported an SLS process to manufacture dense Al_2O_3–ZrO_2 parts at the eutectic composition. The electrical heating energy was 7 kW. The powder was preheated to higher than 1700°C to avoid thermal cracks and achieve the sintering [35]. In general, ceramics can be processed by direct or indirect SLS. For direct SLS method, ceramic powders are sintered or melted directly; however, an organic phase is melted for indirect SLS which acts as binder to manufacture green ceramic parts [36].

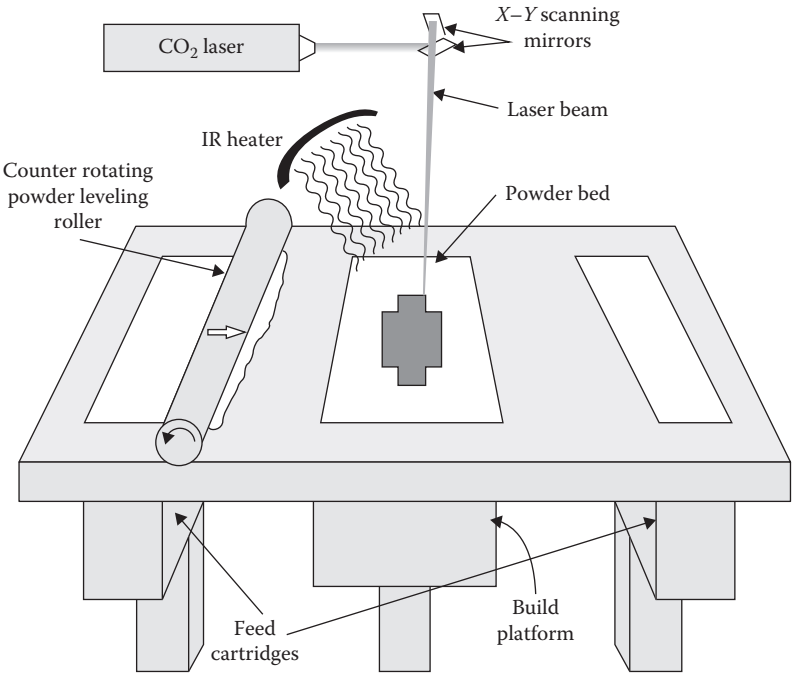

FIGURE 5.4
Schematic of selective laser sintering process. (Data from I. Gibson et al., *Additive Manufacturing Technologies*, Springer, Boston, MA, 2010.)

5.3.2 Direct SLS

Direct SLS of ceramics can be further divided into two subcategories: powder- and slurry-based direct laser sintering. In powder-based direct SLS, a roller spreads a layer of powder from feed bed to build bed. This method allows processing of 3D products with physical, mechanical, and chemical properties different from original properties of those powder compositions [37]. However, low packing density in powder bed is a drawback which may lead to low sintered density and crack formation due to thermal stresses [36]. In addition, sometimes the laser energy must be high enough to directly sinter the ceramic powder with high temperature resistance.

Shishkovsky et al. reported the manufacturing process of dense aluminum and zirconium mixture using SLS. This high-speed laser sintering creates ceramics with high density and uniform distribution of stable phases. It showed great potential to be used as thermal and electrical insulators and wear resistant coating for the application of solid oxide fuel cells, crucibles, heating elements, and medical tools [37]. Yttria–zirconia has also been processed by powder-based direct SLS. Figure 5.5 illustrated the CAD design and how accurate this method could be for manufacturing complex structures. However, the preparation of powder with appropriate characteristics suitable for SLS process is still challenging [38]. Table 5.2 summarizes some of the ceramic compositions processed by powder-based direct SLS, along with their potential applications.

Slurry-based direct SLS, however, starts from homogeneous slurry as feeding layers. Unlike powder-based SLS, slurry suspension is commonly fed to the build platform by

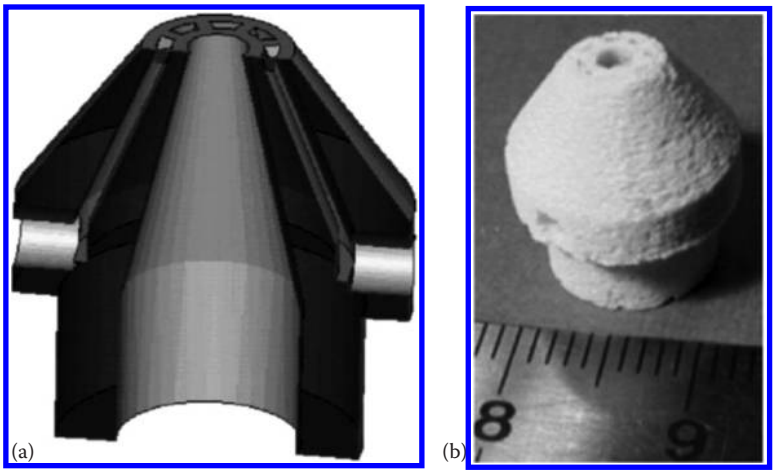

FIGURE 5.5
Objects manufactured by direct SLS technology. (a) CAD design, (b) real manufactured part. (Data from P. Bertrand et al., *Appl Surf Sci*, 254, 989–92, 2007.)

TABLE 5.2

Ceramic Materials Processed by Powder-Based Direct SLS and Their Potential Applications

Ceramic Composition	Potential Applications	References
Alumina (Al_2O_3) and zirconia (ZrO_2)	Automotive, aerospace or biomedical sector, and implant	[35,37]
Yttria (Y_2O_3) and Zirconia (ZrO_2)	Ceramic shell molds and solid oxide fuel cells	[38]
Tricalcium phosphate (TCP)/ hydroxyapatite (HA)	Implant materials in tissue engineering	[39]
Nano-hydroxypatite	Bone tissue engineering scaffolds	[40,41]
Cu–Ni and ZrB_2	Electrical discharge machining (EDM) electrodes	[42]
45S5 bioactive glass	Bone tissue engineering scaffolds	[43]
PZT (PbO, ZrO_2, and TiO_2)	Piezoelectric material	[44]

doctor blade or spray deposition followed by subsequent drying and laser processing [36]. High density of final product is one the most important advantages of this method. This is mainly due to the possibility of using smaller ceramic particles in slurry [45,46].

Tian et al. reported a slurry-based SLS for making 3D porcelain parts with sintered density of ~86%; however, the mechanical strength of parts was low due to microstructural inhomogeneities and thermal cracks [36,47]. Recently, Liu reported a novel slurry-based SLS using HA, silica sol, and sodium tripolyphosphate (STPP) as slurry suspension for biomedical scaffolds preparation. Sintering at 1300°C resulted in scaffolds with porosity of ~14% and compressive strength of 43 MPa. As shown in Figure 5.6, scaffolds have high resolution and dimensional accuracy, which indicated the great potential for applying this method for bone tissue engineering scaffolds manufacture [48]. Table 5.3 summarizes the details of some of the slurry-based direct SLS systems.

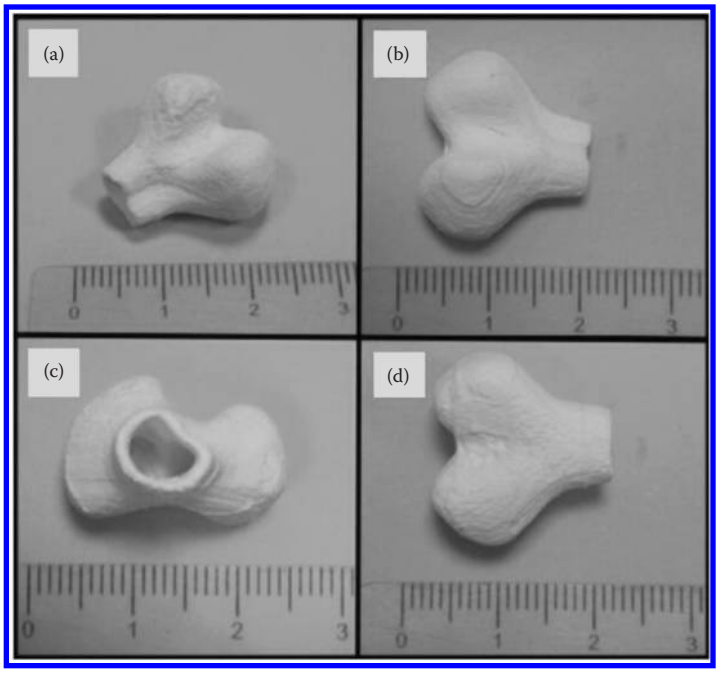

FIGURE 5.6
(a) Green body, (b) front view, (c) top view, and (d) back view of scaffold parts obtained by direct slurry-based SLS via a laser scan speed of 300 mm/s and laser energy of 10 W. (Data from H.C. Yen, H.H. Tang, *Int J Adv Manuf Technol*, 60, 1009–15, 2012.)

TABLE 5.3
Slurry-Based Direct Selective Laser Sintering Systems

Suspension Composition	Layer Feeding Method	Application	Reference
SiO_2 powder and silica sol	Doctor blade	Manufacturing ceramic shell mold with high permeability	[49]
3 mol.% yttria stabilized ZrO_2	Spray deposition	Ceramic shell mold	[46]
Al_2O_3/SiO_2 powder mixtures	Doctor blade	Ceramic dental components	[50]
HA, silica sol, and sodium tripolyphosphate (STPP)	Doctor blade	Bone tissue engineering scaffolds	[48]
HA and silica	Doctor blade	Implant devices for biological and abiological interfaces	[51]

5.3.3 Indirect SLS for Ceramics

In the case of indirect SLS, ceramic powders coated with an organic phase are used as the feedstock material. Due to lower melting point compared to that of ceramics, polymers act as binder to fuse ceramic particles using the laser beam. They also consolidate ceramic layers. Similar to direct SLS, indirect SLS is categorized into powder-based and slurry-based processes [52]. Powder-based indirect SLS makes it possible for using conventional SLS equipment to produce ceramic parts with high melting points [36,53–56]. For the selection of the polymer, since semi-crystalline polymers had a higher density than amorphous polymers, semi-crystalline polymers are preferred to be used as binder phase for indirect

SLS process [36,52]. However, powder-based indirect SLS via semi-crystalline polymers as binder phase might show volume shrinkage during solidification, which will lead to distortion of the whole part.

Various polymers have been used with ceramic particles for powder-based indirect SLS manufacture. Liu et al. reported an AM process using selective laser processed, cold isostatic pressing (CIP) followed by sintering. Alumina indirect SLS parts were prepared using epoxy resin E06 and polyvinyl alcohol (PVA) as organic binder. CIP was performed after the laser sintering to eliminate the pores and increase the density of green ceramics. The final SLS alumina parts achieved a relative density more than 92% after sintering [53]. Another alumina indirect SLS processing was introduced by Cardon et al. The powder was coated with polystyrene (PS) as binder to fabricate products via SLS. Interestingly, the binder was not just blended with alumina by simple stir mixing. The author applied an in situ polymerization method for mixing ceramic powder and binder together. This study demonstrated the processing feasibility of different 3D geometries via PS-coated alumina powders, but only parts with small dimension do not have crack formation [54]. The optimization of the indirect SLS had been studied as well by Deckers et al. Three operating parameters (laser remelting, warm isostatic pressing [WIP], and ceramic suspension infiltration) were manipulated to increase the green density of the indirect SLS parts using alumina–polyamide composite powder. Remelting was found to be effective in improving the green density during SLS processing due to the unwanted *dross formation* when too high laser energies were applied. WIP tended to reduce the final dimensional shrinkage of the parts, but not to increase the final density. Finally, ceramic suspension could increase the final density up to 71% without introducing unwanted cracks [55].

Like slurry-based direct SLS, the slurry-based indirect SLS was applied to make up for the low density of ceramic parts manufactured by powder-based indirect SLS as well. However, the part building efficiency was decreased a lot for this method because of the additional drying step. Waetjen et al. reported a novel slurry indirect SLS processing method by airbrush spray for spreading the slurry on the substrate. This airbrush technique was proved to be successful for producing homogeneous slurry layers suitable for the laser sintering process. And the green density of the part was increased by this way [56]. For achieving high density and mechanical strength of ceramic parts, Tian et al. also invented a slurry indirect SLS system using hydrolyzed PVA as organic binder [57]. Alumina parts of about 98% density were successfully made by this manufacturing process. A 3D lion was produced using this processing procedure. The part shrunk a lot without crack formation. The facial and hair detail of the lion were exquisite, which is shown in Figure 5.7. In addition, a mean flexural strength of about 363.5 MPa was achieved, because there were no delamination and crack formation through this slurry-based process [57]. Some more indirect selective laser sinter information is shown in Table 5.4.

5.3.4 Application and Future Development

SLS is an advanced AM process that is excellent for complex geometry because no support structure is needed during the process. Hence, this method has been used in many fields based on their specific requirements. It has been adopted to produce PZT ceramics from precursor powders. The property of the part was manipulated to match the requirements of some medical ultrasonic equipment such as hydrostatic charge and voltage [63]. Bone tissue engineering scaffolds were also prepared by SLS. Bioceramics, such as HA and TCP, were manufactured by SLS with high processing accuracy and biocompatibility, which is excellent for bone regeneration [39,40,62,64,65].

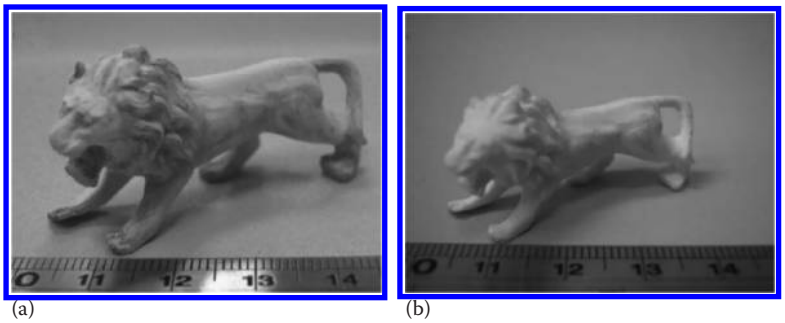

(a) (b)

FIGURE 5.7
(a) 3D green part and (b) 3D sintered part using indirect selective laser sintering. (Data from H.-H. Tang et al., *J Eur Ceram Soc*, 31, 1383–8, 2011.)

TABLE 5.4

Ceramic Composition, Binder, and Feeding Layer Phase of Some Reported Indirect SLS Processing

Ceramic Composition	Polymer Binder Composition	Feeding Layer Phase	Reference
3 mol% Y_2O_3–ZrO_2	Isotactic polypropylene (PP)	Powder	[36]
Cordierite ($Mg_2Al_4Si_5O_{18}$) and aluminum titanate (Al_2TiO_5) or magnesia-partially stabilized zirconia (Mg-PSZ)	Polyvinyl alcohol (PVA)	Slurry	[56]
Silicon carbide (SiC) powder	Poly(methy1 methacrylate) (PMMA)	Powder	[58]
Castable glass (SiO_2–Al_2O_3–P_2O_5–CaO–CaF_2)	Acrylic binder	Powder	[59]
13-93 bioactive glass	Stearic acid polymeric binder	Powder	[60]
α-Al_2O_3 powder	Epoxy resin and polyvinyl alcohol	Powder	[53]
α-Al_2O_3 powder	Polystyrene by dispersion polymerization	Powder	[54]
Al_2O_3 powder	Hydrolyzed PVA	Slurry	[47]
Alumina	PA composite	Powder	[55]
Si_3N_4 and Al_2O_3 powders	self-made copolymer, which polymerized by MMA and BMA	Powder	[61]
Tricalcium phosphate (β-TCP)	Epoxy resin and nylon	Powder	[62]

There are three main challenges for SLS process:

1. The density of parts is usually modest, which will cause poor mechanical strength.
2. Due to the high processing temperature, the cooling cycle is an important issue. An inappropriate cooling might cause failure of the whole part.
3. Ceramic parts in large dimension are hard to manufacture.

The future development will move forward to adjust the processing parameters to overcome these drawbacks.

5.4 Ink-Jet 3DP for Ceramics

5.4.1 Ink-Jet 3DP: History and Methodology

In the late 1980s, Sachs et al. invented the 3DP technology that was later patented to *print* plastic, ceramic, and metallic parts [66]. 3DP is a powder-based freeform fabrication method, similar to the ink-jet technology that is used in 2D printers.

Figure 5.8 shows the schematic of the 3DP process from Bose et al. [67]. Prior to printing, the powder should be fully packed in the powder feed bed. A roller then spreads a layer of powder with predetermined thickness to the powder build bed. Usually, a few primary layers are spread to build a foundation layer as a support for the final part. These layers may get dried for longer time than the main part layers, to assure a stable foundation. According to the CAD file, a regular ink-jet printhead selectively sprays the binder to the build powder layer [67]. Binder, water or organic based, starts a hydraulic setting reaction or binds the particles together [68–70]. The printed layer is then moved under the heater to allow the binder to dry out and prevent its spreading between layers. This process is repeated until the completion of the final part printing [67].

In this method, binder and powder characteristics should be determined prior to printing. Binder and powder characteristics such as powder packing density, particle size, powder flowability, powder wettability, layer thickness, binder drop volume, binder saturation as well as drying time and heating rate play crucial roles toward the success of this method. Powder packing density is the relative density of the powder after spreading into the build bed. Binder drop volume is the volume of binder drop, released from each nozzle. Binder saturation can be obtained by coordinating the relative bulk density of the powder and binder drop volume. Binder saturation is calculated according to the following equation [71]:

$$S = \frac{V_b}{\left[1-\left(\mathrm{PR}/100\right)\%\right]\times a\times b\times LT}$$

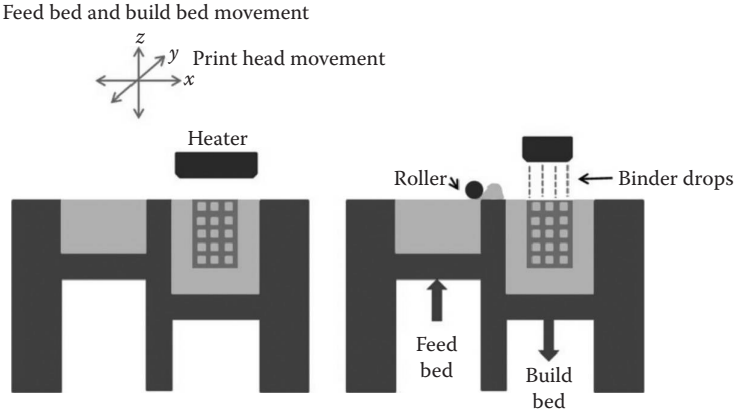

FIGURE 5.8
Schematic of ink-jet 3DP processing. (Data from S. Bose et al., *Mater. Today*, 16, 496–504, 2013.)

where:
S is the relative binder saturation
V_b is the binder drop volume (pL)
PR is the relative bulk density of the powder bed
$a \times b$ is the lateral pixel area of one droplet on substrate (μm^2)
LT is the thickness of the spread layer (μm)

Tarafder et al. reported that high binder saturation can cause binder spreading over multiple layers of powder as well as bumping appearance in build layers, whereas low binder saturation causes the layer displacement and/or unhandleable parts [72].

Powder flowability is another critical parameter that is regulated by powder particle size, size distribution, shape, and surface roughness. Flowability is enhanced by using large particles; however, the densification and sinterability of the ceramic part is compromised due to smaller surface area. On the other hand, use of fine particles causes severe agglomeration. Flowability is determined according to the Hausner ratio, H, using the following equation [73]:

$$H = \frac{\rho_{Tap}}{\rho_{Bulk}}$$

where
ρ_{Tap} and ρ_{Bulk} are the tapped and freely settled bulk densities of the powder, respectively

Similarly, powder wettability is related to particle characteristics such as chemistry and surface energy. Low wettability causes the weak integration between particle and binder; however, high wettability results in binder spreading among different layers [74,75].

One of the main advantages of the ink-jet 3DP is the simplicity of the technology. Ink-jet 3DP is categorized as one of the low-cost AM methods. In addition, it does not require any external platform or support, and the powder bed supports the structure during the printing [76]. Furthermore, this method does not demand liquid with modified viscosity or photopolymerizable material [77].

However, ink-jet 3DP processed parts suffer from considerable amount of porosity because of the high friction between particles, lack of external compression force to provide better packing, and random agglomeration [76,78]. In addition, using the toxic polymeric binder is harmful for specific applications such as drug delivery and tissue engineering. This is due to the fact that not all the ceramic powders can be printed by a biocompatible polymer/printing solution [79]. As a result, this method has limitation over printing biocompatible ceramics. Post-processing including depowdering (loose powder removal) and sintering are also the other challenges of this method. Due to low green density of printed ceramic, depowdering can crack the part [80]. 3D printed ceramics need to be sintered to enhance the densification and mechanical properties [72,81].

5.4.2 Ink-Jet 3DP Processed Ceramics

Several ceramic materials have been printed using ink-jet 3DP for high temperature applications, electronic devices, tissue engineering, and drug delivery. Nan et al. processed Ti_3SiC_2-based ceramics using a combination of 3DP and liquid silicon infiltration (LSI). TiC powder and dextrin were used as the printing feedstock and binder, respectively. LSI was performed in Ar atmosphere at 1600°C–1700°C followed by annealing at 1400°C. The obtained Ti_3SiC_2-$TiSi_2$-SiC composite at 1700°C presented relatively high bending strength of 293 MPa and Vickers hardness of 7.2 GPa [82].

SiOC polymer-derived ceramics (PDCs) have been processed using 3DP of a pre-ceramic polymer. Generally, PDCs have unique oxidation resistance and thermomechanical properties up to relatively high temperatures, in addition to specific properties such as luminescence and piezoresistivity. In this study, a polymethylsilsesquioxane pre-ceramic polymer powder (MK) was used. Two different approaches were applied to print the parts: (1) MK powder was mixed with isopropanol and zirconium acetylacetonate (ZrAcAc) as catalyst. This mixture was used after drying as the base powder precursor and isoropanol was used as the printing media. (2) Tin-octoate (TinOc) was dissolved in 1-hexanol and hexylacetate mixture and used as the printing media. The 3D printed Kagome lattice of polymer and subsequent ceramic was printed with high accuracy of local features as shown in Figure 5.9 [83].

Maleksaeedi et al. fabricated 3D alumina scaffolds using the ink-jet printing. To achieve the flowability and uniform shape of powders, alumina aqueous slurry was milled and spray dried. The powder was then mixed with PVA as binder, and the mixture of alcohol and deionized water was used as the printing ink to activate the binder. After sintering at 1000°C, the vacuum infiltration was done using high concentrated alumina. This resulted in increase in density from 37% to 86%. It was found that slurry concentration plays a critical role in final properties of parts and depends on feature size, complexity of the part, and its thickness [76].

Silicon nitride (Si_3N_4) is widely used at high temperatures due to low coefficient of thermal expansion, good mechanical properties, and resistance to thermal shock. For some applications, porous structure with precise control over the pore size and pore distribution

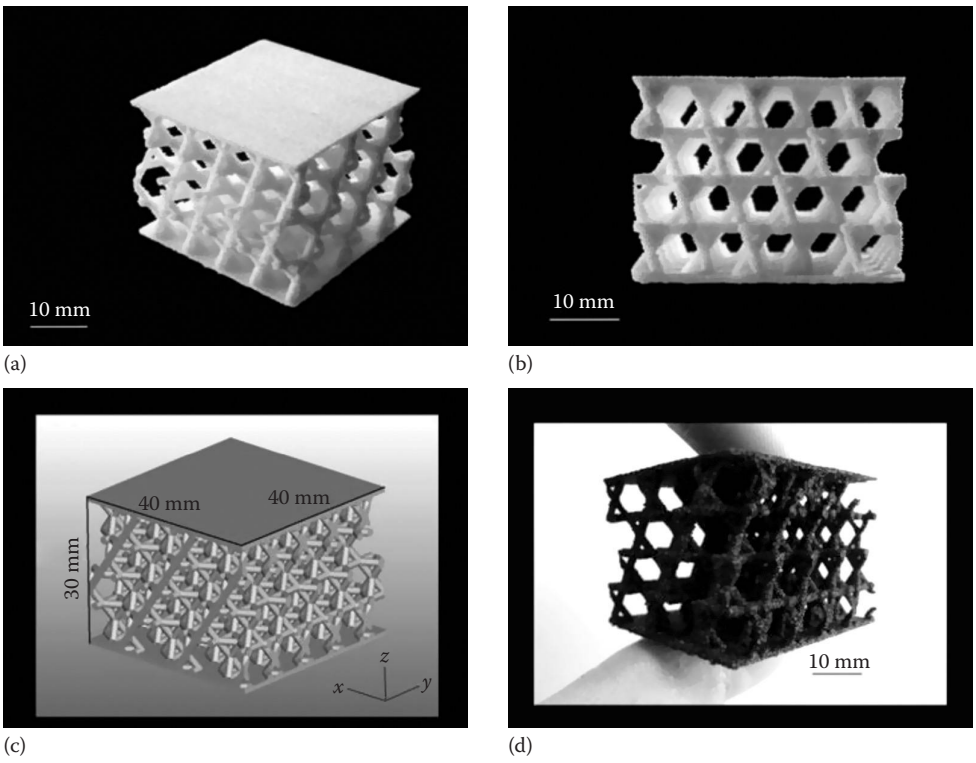

FIGURE 5.9
(a) Lateral view of the polymeric printed Kagome structure, (b) front view of the polymeric printed Kagome structure, (c) CAD model of the Kagome structure, and (d) SiOC ceramic structure ceramized at 1200°C. (Data from A. Zocca et al., *J Mater Res*, 28, 2243–52, 2013.)

demands unique fabrication method. Li et al. printed a 3D structure of Si_3N_4 using a powder-based printer. Si_3N_4 was mixed with Lu_2O_3 and dextrin in water. After drying and crushing, printing was performed using a water-based printer solution. By this method, structure with 68% porosity and low fracture toughness of 0.3 MPa $m^{1/2}$ and Vickers hardness of 0.4 GPa was achieved [84].

Ink-jet 3DP has been widely used in tissue engineering and drug delivery applications. HA scaffolds have been printed using water-based solutions as binder [85,86]. Tetracalcium phosphate (TTCP), dicalcium phosphate, and TCP have also been fabricated using citric acid as binder [69]. Winkel et al. processed 13–93 bioactive glass/HA composite with complex porosity structure by 3DP, using 7:1 water:glycerol as printing solution, as shown in Figure 5.10 [87].

As mentioned before, post-processing of 3D printed ceramics is essential to achieve handleability and higher mechanical strength, specifically in bone tissue engineering [88].

Due to low mechanical properties of porous 3D printed scaffolds, the effects of sintering condition [72], dopant addition [89,90], and polymer infiltration [91] on their final properties are well studied. Khalyfa et al. found that infiltration of bismethacrylated oligolactide macromer (DLM-1) increases the compressive strength of TTCP/β-TCP from 0.7 to 76.1 MPa [80]. Compressive stiffness of starch increased from 11.15 to 55.19 MPa through PCL/PLLA infiltration [92]. Silica/zinc oxide incorporation in TCP resulted in increase in compressive strength from 5.5 to 10.2 MPa [93].

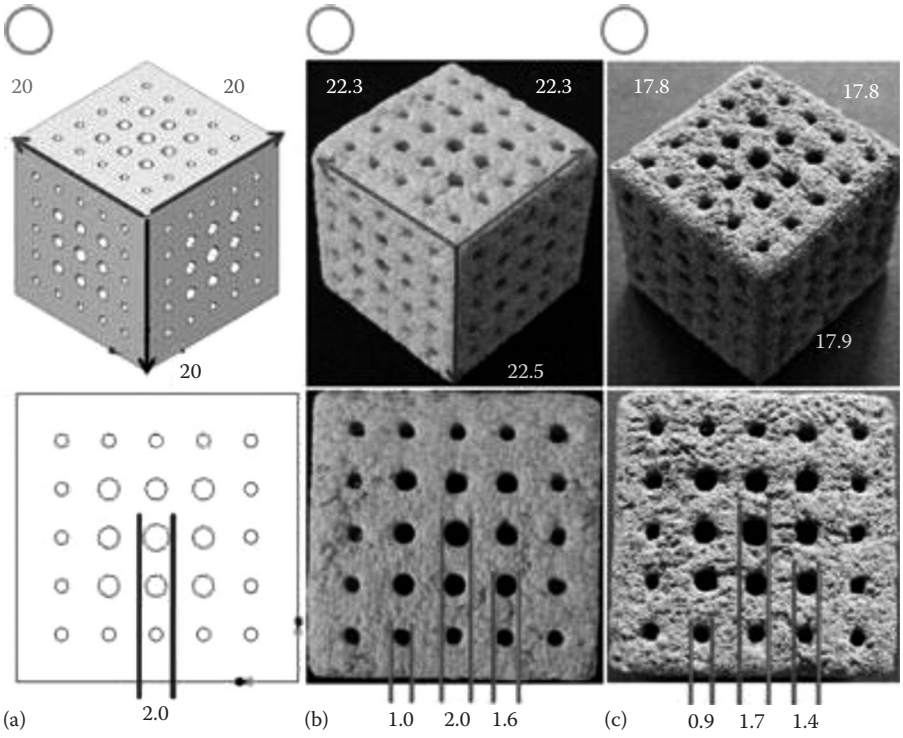

FIGURE 5.10
(a) Computer model, (b) photograph of 3D-printed green body, and (c) sintered glass/HAp composite structure after heating to 750°C at 2 K/min. Labels indicate dimensions in mm. (Data from A. Winkel et al., *J Am Ceram Soc*, 95-11, 3387–93, 2012.)

Due to its unique control over pore size, connectivity, and geometry, ink-jet 3DP is widely used in local delivery of drugs and growth factors to control drug release kinetics and reduce the dosage. Several drugs and growth factors such as vancomycin, ofloxacin, tetracycline hydrochloride, and bone morphogenic protein have been locally delivered using 3DP scaffolds [94–96]. Tarafder et al. studied the alendronate release kinetics from 3D printed TCP. Drug release kinetics was controlled by polycaprolactone coating and enhanced osteogenesis in vitro and in vivo [91].

5.5 Fused Deposition of Ceramics

5.5.1 FDC: History and Methodology

FDC is a modified FDM process. FDM was first introduced in 1991 by Stratasys (Eden Prairie, MN) [97]. In 1996, FDC was introduced by researchers at Rutgers University as a modified FDM process and patented later in 1998 to process 3D ceramic structures including novel ceramic materials, ceramic/polymer composites, oriented/radial piezoelectrics, and photonic band-gap structures [98–103]. Figure 5.11 shows the schematic of FDC. In this process, a filament of a semi-solid thermoplastic polymer is fed into a liquefier by two rollers, extruded through the liquefier and then a nozzle, and finally gets deposited on a platform. The heaters in liquefier heat up the polymer at temperatures above but close to the melting temperature, so that the extruded filament can move easily through the nozzle. Based on the CAD file, the nozzle moves in *X*–*Y* direction and *roads* or *rasters* get deposited [104,105]. Solidification starts from the outer surface of the roads and then continues radially to the core [106]. After deposition of the first layer, the platform moves downward and the second layer gets deposited on the first one. This process continues until the whole part is built.

In this process, rollers provide the needed pressure for extrusion of the molten material through nozzle [107]. Liquefier plays two distinct roles: (1) due to its high temperature compared to that of binder, strong interlamellar and interlaminar bindings are provided,

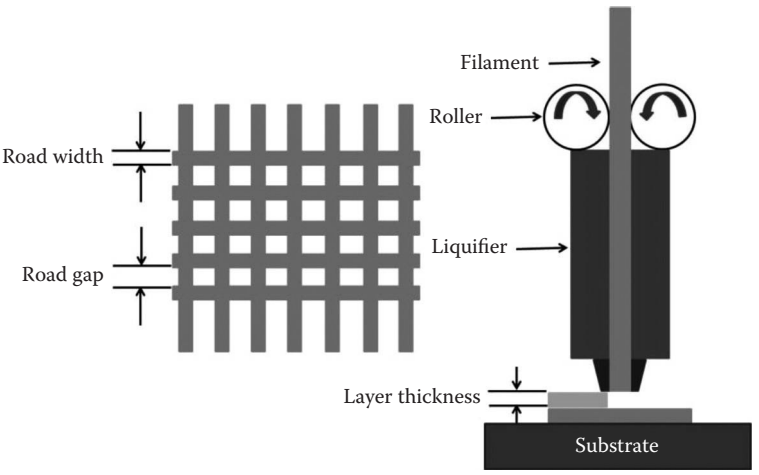

FIGURE 5.11
Schematic of FDC.

and (2) due to the pressure and shear of molten mixture exerted by liquefier nozzle, better bonding is achievable [108]. In addition, extruder die diameter controls the accuracy of dimension and layer thickness [109].

In FDC, the semi-solid thermoplastic polymer mixture, including binder, plasticizer, and dispersant, acts as the ceramic powder carrier [110]. The ceramic is dispersed and mixed with the polymer between 50 and 65 vol.% [111]. During this step, pretreatment of powder with organic dispersant/surfactant is a critical step to obtain an extrudable material [107]. Road width, thickness, gap between the roads, and the angle between layers govern the size, shape, and volume of the pores in FDC (shown in Figure 5.11) [105]. In addition, the flow rate of the process can be controlled by the rate of feedstock entrance to the heated liquefier. Molten material temperature and deposition speed should match the cooling and solidification rate to prevent any discontinuity or destruction of the structure [106].

Filament fabrication is one of the main obstacles in this method as it is one of the most time-consuming steps [111]. Filament should be compositionally homogeneous and agglomerate-free to prevent the clogging of the FDC nozzle. In addition, to ensure the accuracy in deposition and final size of the part, the high dimensional tolerance of the filament is required [108]. In case of brittle materials, optimization of filament composition and processing parameters is required to prevent filament buckling during the extrusion [107].

Stiffness of the filament, viscosity of the ceramic and semi-solid polymer mixture, and binder chemistry are the important parameters in FDC that determine the success of the process [112]. In addition, extrusion, vectoring, and layering are important factors determining the final part isotropy and homogeneity. Inappropriate vector spacing or road width, insufficient bonding between the roads (interlamellar) or build layers (interlaminar), and inaccurate filling between vectors and perimeter (subperimeter voids) can cause the formation of structure with defects in FDC method [108].

Apart from the filament preparation, developing a suitable binder-ceramic formulation as well as large amount of binder is another obstacle in FDC. To remove the binder and sinter the ceramic part, the post-processing of the part including binder removal and ceramic sintering is needed to achieve a densified part. Removing all the binder and organic components, as well as not damaging the structure of the part, is the key requirement for the post-processing of the ceramics [106]. Relaxation of viscoelastic stresses during post-processing causes the major shrinkage [113]. To minimize the shrinkage during the binder removal, low viscosity of the mixture and high solid loading are required. To meet these requirements, ceramic powder should be well dispersed in polymer [114]. Finally, samples should be sintered to achieve the desired density. Compared to binder removal step, the major shrinkage happens in this step. Warping in parts fabricated by FDC is an important issue. Many parameters can cause the warping but the thermal stresses and relaxation in binder are the main reasons. During deposition, binder cools and shrinks. High coefficient of thermal expansion of binder causes the tensile stresses in each building layer. Due to constraint in bottom built layers, the tensile stresses cause the warping. These residual stresses are due to viscoelasticity of the binder, and the relaxation is possible if enough time or temperature is given to the system [108].

5.5.2 FDC Processed Ceramics

FDC has been used as a unique processing tool for piezoelectric materials fabrication. Compared to traditional methods, FDC allows the fabrication of composites with complex internal structure and symmetry. Bandyopadhyay et al. processed 3D PZT ceramics with ladder and honeycomb structures through direct and indirect FDC process, respectively [115].

Turcu et al. processed PZT-epoxy composites with volume fraction of solid phase of 0.3 using FDC and studied the effect of deposition angle on piezoelectric properties of PZT [116]. Panda et al. also processed PZT/polymer piezoelectric with different structures as shown in Figure 5.12a. Piezoelectric material with ladder structure was processed using ceramic volume fraction of 70%. The achieved uniformity and repeatability of the structure with road diameter of 300 μm presents the FDC as a unique method for piezoelectric fabrication [117]. Si_3N_4 ceramic parts have been processed using FDC at different conditions [108,110]. Oley alcohol and a commercially available investment casting wax (ICW) were used as surfactant and binder, respectively. The effects of build process parameters on final part homogeneity and isotropy were studied using different angles of 0°, 90°, and ±45° between the roads and long axis of the bar in alternating layers. They found, in the first two cases, significant warping occurred in samples; however, using the +45° or −45° of vector angles resulted in no warping. Binder removal resulted in ~1% shrinkage, and major shrinkage, 16%–18%, happened during the sintering. During binder removal, shrinkage was significantly higher in the direction of road vectors than across the roads in parts using 0° and 90° of building [108].

MgO-doped alumina with honeycomb structure was processed using indirect FDM. Ceramic slurry was developed using 1-butanol and Darvan 821 as antifoaming agent and

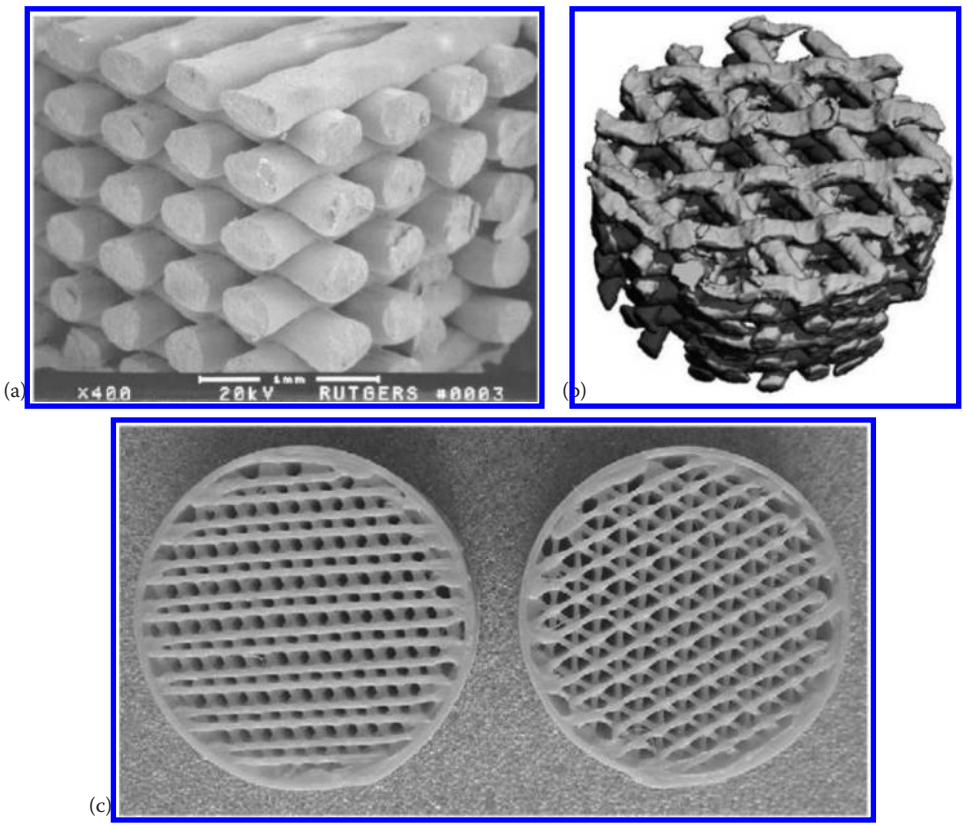

FIGURE 5.12
(a) Ladder structure of PZT processed by FDC. (Data from A. Safari et al., *Mater Sci*, 41, 177–98, 2006.) (b) PCL-CaP scaffold architecture observed under micro-computed tomography. (Data from J.T. Schantz et al., *J Mater Sci: Mater Med*, 16, 807–19, 2005.) (c) PP-TCP composite scaffolds with different internal architecture. (Data from S.J. Kalita et al., *Mater Sci Eng C*, 23, 611–20, 2003.)

dispersant, respectively. The slurry was then infiltrated to FDM processed ICW mold, followed by drying, binder removal, and final sintering at 1600°C [118]. Using the same technique, alumina bone graft with horse knuckle structure was also processed [119]. Bandyopadhyay et al. processed in situ Al/Al_2O_3 composites with controlled microstructure using FDC processed silica structures followed by Al infiltration at 1150°C [120].

HA and TCP structures have also been fabricated using direct and indirect FDC. In direct process, HA powder was first coated by stearic acid as surfactant and then mixed with binder solution including polyolefin-based binder, polyethylene wax, hydrocarbon resin tackifier, and polybutylene plasticizer. The HA scaffolds were fabricated using filament with 55 vol.% ceramic. Binder burnout (BBO) was performed at 550°C, followed by final sintering at 1100°C [121]. Using indirect process, various designs of ICW molds were fabricated and infiltrated with slurries containing food graded TCP powder to fabricate the 3D TCP with different pore size and volume [122].

Schantz et al. reported the osteogenic properties of CaP/PCL scaffolds prepared by FDM using mesenchymal progenitor cells. CaP/PCL filaments were fabricated through melt extrusion of CaP/PCL pellets containing 25 wt.% CaP. The fabricated part had the lay-down pattern of 0/60/120° (a honeycomb-like design), as shown in Figure 5.12b. Results showed circular and centripetally directed arrangement of the cells in pores, whereas multiple focal adhesions of elongated cells were observed in angles [123].

In case of ceramic-polymer composites for biomedical applications, polymer selection in which both non-toxic and extrudable properties should be achieved is an important step. Kalita et al. processed biocompatible composite of TCP/polypropylene (PP) using vegetable oil as plasticizer and VESTOWAX SH 105 pallets (Crenova, NJ) as viscosity modulator, including 20.5 vol.% TCP in filament. Scaffolds with different internal architecture were fabricated as shown in Figure 5.12c. Results showed that fused deposition process allows the precise control of pore volume, and increases the pore volume from 36% to 40% and 52%, and decreases the strength gradually from 12.7 to ~10 MPa [105].

Pilleux et al. used fused deposition of multi-materials (FDMM) to fabricate 3D alumina photonic band-gap structure. This approach allows the fabrication of complex designs with periodic structure. Compared to traditional methods where structures are fabricated by making bulk pieces followed by etching and/or machining to achieve the desired dielectric properties, FDMM allows better control over the structure. Alumina feedstock was prepared by mixing the 60 and 62 vol.% of alumina powder in stearic acid solution in toluene and ECG-9 as surfactant and thermoplastic binder, respectively. ICW-06 was used as the support for the alumina and deposition was performed in layer-by-layer manner of alumina and the wax. The dewaxing was done for 10 minutes. During dewaxing, zirconia powder was used as a refractory mechanical support for the alumina to prevent the bending of the rods during BBO [124].

5.6 Laminated Object Manufacturing of Ceramics

5.6.1 LOM: History and Methodology

Laminated object manufacturing (LOM) was first introduced in 1991 by Helisys, USA. LOM offers the manufacturing of 3D parts using green ceramic tapes [125]. In this method, multiple laminations are stacked to manufacture a 3D object. The system, as shown in Figure 5.13, includes a work table, which can move vertically; a feeder, which is a continuous roll of the

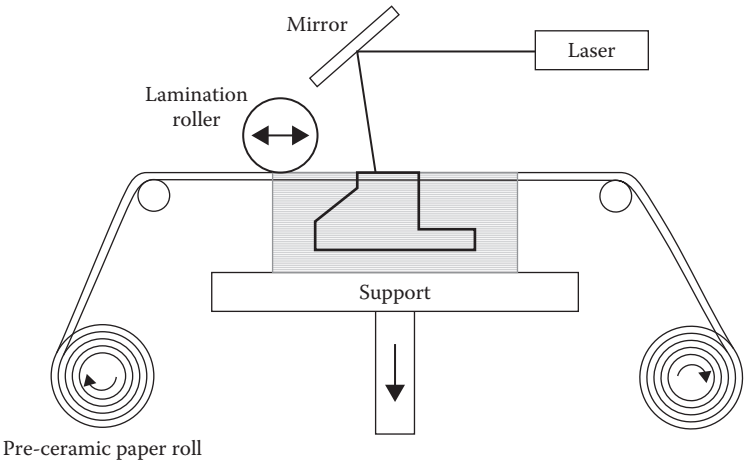

FIGURE 5.13
Schematic of LOM process. (Data from N. Travitzky et al., *J Am Ceram Soc*, 91, 3477–92, 2008.)

material; and an *X–Y* plotter. The feeder sends the laminations/sheets over the build platform on work table. The bottom side of the sheets is covered with a heat sensitive adhesive. Using a hot lamination roller, the adhesive melts and sheet gets bonded to the below layer. The *X–Y* plotter uses a laser beam to cut the outline of the part at each layer. The excess part is also cut into *cubes* to facilitate its removal after manufacturing [126]. During the building process, this excess part remains in the building block to support the structure [127]. After completion of each layer, the build platform moves downward by a depth of sheet thickness. This process continues layer by layer until the whole part is made. Once the part is manufactured, *decubing* is applied to remove any excess material [126,128].

Prior to fabrication of the ceramic roll, a suspension including the ceramic precursor, plasticizer, binder, and dispersant should be prepared. Rheological properties of the suspension determine the success of paper preparation, possibility of crack formation during drying process, green density, and homogeneity of the final structure [129]. The viscosity and shear thinning of suspensions are determined using the Herschel–Bulkley model [130].

The dispersant content has significant effect on the viscosity of suspension [131]. High amount of dispersant increases the viscosity significantly, which is undesirable due to decrease in green density and increase in firing shrinkage [125]. Suspension with viscosity lower than 20 Pa s results in a fluid system, while higher viscosity causes the paste system formation, which is not helpful in LOM process [132].

The next step is paper formation. To form a continuous sheet of paper, prepared suspensions including fibers, binder, and retention agents are transferred to papermaking machine and ceramic paper gets prepared through sheet formation, pressing, drying, calendaring, and rolling, as shown in Figure 5.14 [133]. Pre-ceramic paper roll is then transferred to LOM machine to fabricate the 3D structure as discussed earlier. After decubing, post-processing including resin infiltration or polishing are applied to enhance the strength and surface quality of the part [134,135].

In LOM, the laser line energy is calculated using the following equation:

$$E_L = \frac{P_L}{V_L}$$

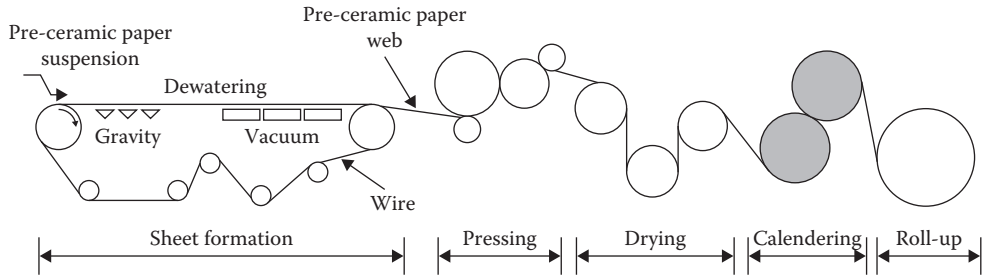

FIGURE 5.14
Schematic of pre-ceramic paper roll preparation for LOM. (Data from N. Travitzky et al., *J Am Ceram Soc*, 91, 3477–92, 2008.)

where:

P_L and V_L are laser power and scanning speed, respectively

E_L is a critical factor in cutting and decubing process. High E_L causes the cutting of the lower sheets and oxidation of the organic components in pre-ceramic papers, whereas low E_L causes the insufficient cutting of the papers. As a result, E_L optimization is necessary to control the cutting depth and facilitate the decubing process [128].

Compared to other rapid prototyping methods, LOM is a high speed method. In addition, its low operation cost is another advantage. Although the LOM is a fast method, the decubing process is time consuming, and depending on geometry and complexity of the part, labor work is needed [126,136].

5.6.2 LOM Processed Ceramics

Windsheimer et al. processed dense Si-SiC using LOM. Using Rapid Köthen aqueous handsheet-forming process, pre-ceramic papers including 76.8 wt.% SiC powder, 20 wt.% cellulose pulp, and 3.2 wt.% retention agent and binder were fabricated. A thermosetting polymeric adhesive with softening point of 60°C was used to coat the sheets. LOM was performed using a 25 W CO_2 laser at a wavelength of 10.6 μm [128].

Al_2O_3 was manufactured using 7 wt.% polyvinyl butyral (PVB) and polyvinyl acetate as binder and adhesive, respectively. Binder was removed at 240°C–300°C and samples were sintered at 1580°C. Although binder removal did not cause any damage, sintering and cooling processes led to distortion and cracking. This shows the effective role of heating and cooling rates to obtain damage-free parts [137].

LOM has been used to manufacture LiO_2–ZrO_2–SiO_2–Al_2O_3 (LZSA) glass ceramics. Suspensions were prepared through dispersion of glass powder in distilled water with ammonium polyacrylate as dispersant, followed by mixing with PVA, polyethylene glycol, and blend of modified fatty and alkoxylated compound as binder, plasticizer, and antifoaming agent, respectively. Glass ceramic roll was fabricated using a tape caster. A continuous wave CO_2 laser with the power of 16.8 W was used during the LOM process. Figure 5.15 shows the manufactured parts with homogeneous distribution of the porosity within the microstructure [125,129].

Weisensel et al. processed SiSiC composites using LOM technique. The pre-ceramic papers were prepared through pyrolysis of a commercially available filter paper made of cellulose fibers. The adhesive tape including phenolic resin, PVB, benzyl butyl phthalate,

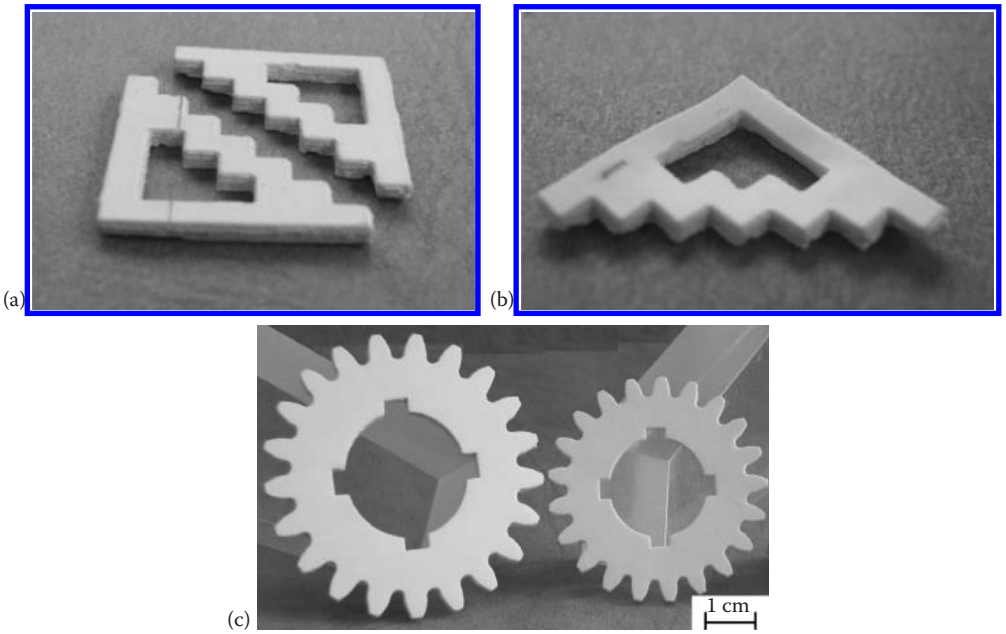

FIGURE 5.15
LOM processed LZSA glass ceramics: (a) stair-like green sample, (b) stair-like sintered sample, and (c) gear wheel structure (left: green sample, right: sintered sample). (Data from C.M. Gomes et al., *J Mater Process Tech*, 206, 194–201, 2008; C.M. Gomes et al., *J Am Ceram Soc*, 92, 1186–91, 2009.)

and ethanol was bonded to pyrolysed paper. Followed by laminating step, an additional pyrolysis step was performed at 800°C. Finally, Si infiltration was performed at 1500°C in vacuum [134].

Though LOM is a simple process, it is only useful for fiber reinforced composite fabrication. Even then, if there is curved surfaces, it is very difficult to control warpage in LOM processed and cured components. At present, there is no commercial vendor for LOM-based process for ceramic structures. However, a cheaper version of the same concept using sticky paper and knife is still available to produce 3D parts from CAD files.

5.7 Laser Engineered Net Shaping™

5.7.1 LENS: History and Methodology

LENS is a commercially available AM process to fabricate metallic parts. In this method, a focused neodymium-doped yttrium aluminum garnet (Nd:YAG) laser up to 2 kW is used to melt the substrate [138]. As shown in Figure 5.16, the focused beam produces a small molten area on the substrate and metal powder is injected through a gas stream into the molten part. By moving the laser beam away, the molten area cools down and solidifies rapidly, and forms a strongly bonded solid material to the substrate. In this method, the cooling rate depends on processing parameters such as transverse velocity and laser output energy [139]. After deposition of the first layer, the laser head moves upward and second layer gets deposited. This process continues layer by layer until the whole part is fabricated.

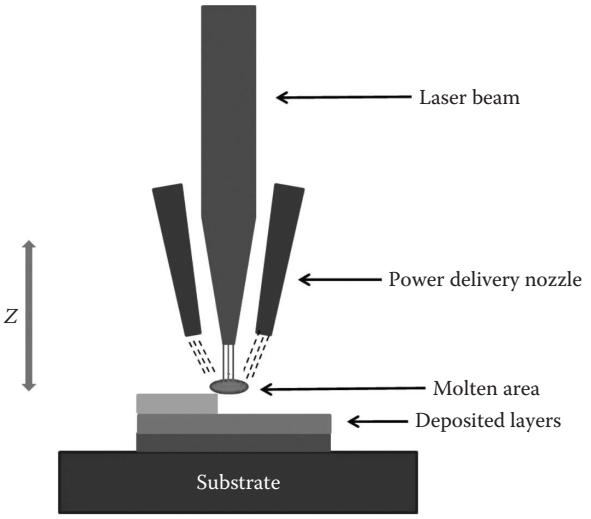

FIGURE 5.16
Schematic of LENS™ processing.

Success in this method depends on the interaction between the laser beam and the powder [140]. Generally, increasing the power of laser beam and decreasing the laser beam diameter and the scan speed increase the specific laser energy input using the following equation [141]:

$$I = \frac{P}{vD}$$

where:
I is laser energy input
P is power of laser beam
v is scan speed
D is laser beam diameter

Small heating zone and high cooling rate result in fine microstructure of deposited material [139]. Controlling the microstructure in this method is easily possible by altering the cooling rate [142,143]. During solidification, thermal gradient (G) and solidification velocity (R) determine the cooling rate ($\partial T/\partial t$) [144]:

$$R = \frac{1}{G}\frac{\partial T}{\partial t}$$

In addition, $\partial T/\partial t$ is related to the processing parameters according to the following equation [145]:

$$\frac{\partial T}{\partial t} \propto \frac{k\left(T - T_0\right)^2}{P/V}$$

where
k is the thermal conductivity of the material
T_0 is the temperature of the substrate

P is the power of the laser beam
V is the transverse speed

Unlike other AM processes, LENS allows the fabrication of fully dense structures [146]. Another advantage of this method is the possibility of gradient deposition of various materials in a single component [147,148].

Presence of thermal stresses is one of the main drawbacks of this method. Due to the nature of LENS, small volume of material is heated at a certain time, resulting in an intense temperature gradient within the sample in each layer. In addition, there are thermal stresses/strains between the solid deposited at first layer and the solidifying second layer. Due to heat transfer from the top layer, there is a thermal expansion in solidified layer, and as a result, compressive and tensile stresses develop in solidified first layer and solidifying top layer, respectively. Depending on processing parameters and the magnitude of the stresses, distortion and possible failure may happen due to delamination or cracking [138]. Not all the ceramic materials can be processed using the LENS technique due to high thermal stresses [149]. Post-processing of LENS fabricated structures is needed in many cases. In addition, if the substrate is not a part of the final product, it should be removed [144].

5.7.2 LENS Processed Ceramics

The LENS process is able to fabricate complex prototypes in near net shape, leading to time and machining cost savings. Various ceramics with different shapes have been processed using LENS.

Liu et al. used LENS to fabricate crack-free functionally graded TiC/Ti composite. Using two separate powder feeders with controllable rotational speed, the functionally graded composite was processed. This was achieved by regulating the rotational speed of one material's powder feeder from zero to maximum, and the second material's feeder from maximum to zero, as the number of layers increased. Figure 5.17a shows the light microscope image of the structure. The bottom layer consists of α-Ti with small amount of TiC. TiC concentration increases from bottom layer to the top with dendritic or equiaxed particulate structure. The TiC concentration at top was 95 vol.%. Figure 5.17b–g shows the SEM microstructure of sample at different layers [147]. Compositionally graded aluminum oxide coating on stainless steel substrate with crack-free microstructure and high hardness was also fabricated using two optimized power levels of 400 and 500 W. Bond coating of Ni-20 wt.% Cr was deposited at first layer. Powder feed rate decreased from 13 g/min to 0 over the first three layers, while the aluminum oxide feed rate increased from 0 to 14 g/min and remained constant for four more layers [150].

LENS has also been used to produce particle reinforced metallic matrix composites (MMCs) [139,149,151]. MMCs cannot be easily processed by conventional processes such as powder metallurgy techniques or casting. In conventional powder metallurgical processes, the product geometry is limited due to the complexity of the process. On the other hand, casting causes the particle segregation and undesirable interfacial reactions. Compared to these methods, LENS is a time, energy and cost-effective approach for the processing of MMCs [139,149]; however, use of very fine and irregular particles is still a challenge in the fabrication of MMCs by LENS. Zheng et al. used the Ni-coated TiC particles with size up to 45 μm as reinforcement in Ni-based IN625 superalloy. The process was performed using the laser with power of 650 W in Ar environment to prevent oxidation. During the process, Ni coating remained on the surface of TiC and the strength of the matrix increased significantly due to the presence of the reinforcement. In addition, Ni coating resulted in

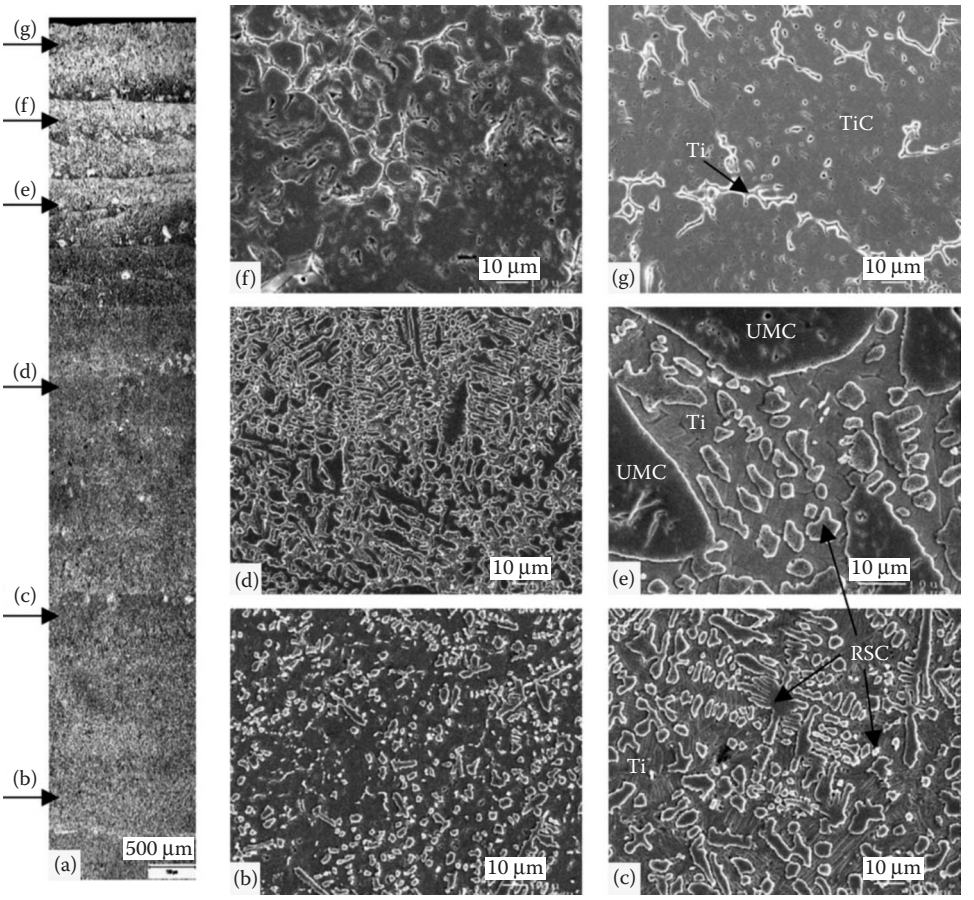

FIGURE 5.17
Microstructures of the FGM deposit: (a) light optical microscopy photomicrograph of the deposit; (b)–(g) SEM photomicrographs with increasing TiC contents in different locations (UMC and RSC denote unmelted and resolidified TiC carbide, respectively). (Data from W. Liu, J.N. DuPont, *Scripta Mater*, 48, 1337–42, 2003.)

better flowability of powders and interaction between laser beam and TiC particles [149]. They have also processed Ni-coated TiC particles in Ti6V4Al matrix MMCs as shown in Figure 5.18a. Formation of the intermetallic phase of Ti-Ni resulted in significant increase in strength but decrease in toughness [139].

LENS has been used to fabricate ceramic coatings on metallic structures for biomedical applications. High crystallinity of coatings, controllable thickness, and good adherence between the coatings and substrate are the advantages of using LENS compared to other methods such as sol-gel, dip coating, biomimetic coating, and plasma spraying where one or more of the mentioned characteristics cannot be achieved. Laser beam power, laser scan speed, and powder feed rate control the coating thickness [140,148]. Roy et al. showed that increasing the power from 400 to 500 W resulted in increase in coating thickness from 250 to 400 µm (Figure 5.18b and c). As shown in Figure **5.**18d and e, keeping the laser power at 500 W and decreasing the scan speed increased the coating thickness. Increasing the powder feeding rate from 9 to 13 g/min increased the coating thickness from 220 to 375 µm (Figure 5.18e and f). In addition to coating thickness, microstructure and TCP

content in coating varied by powder feed rate, laser beam power, and scan speed. Ti grains had columnar and equiaxed structures at the bottom and top of the coating, respectively. Increase in powder feeding rate increased the TCP content in coatings, whereas increase in scan speed decreased the TCP volume fraction [140]. In addition, although the HA and Ti interaction was minimum, some $CaTiO_3$ was formed in this coating. Comparing the single and multilayer coatings, HA layer was formed on top of the multilayer coatings, representing a significant drop in heat transformation from molten Ti to HA [148].

Balla et al. reported the processing of functionally graded Ti-TiO_2 structures using LENS. Compositionally graded TiO_2 coating with 50% TiO_2 on top surface of porous Ti increased the hardness and the wettability of Ti implants, which enhanced their wear resistance and cell–material interactions [152]. They also reported the LENS processed functionally graded yttria-stabilized zirconia coating on stainless steel. The composition varied from 100% bond coat on top of the stainless steel substrate to 100% YSZ top coat at the

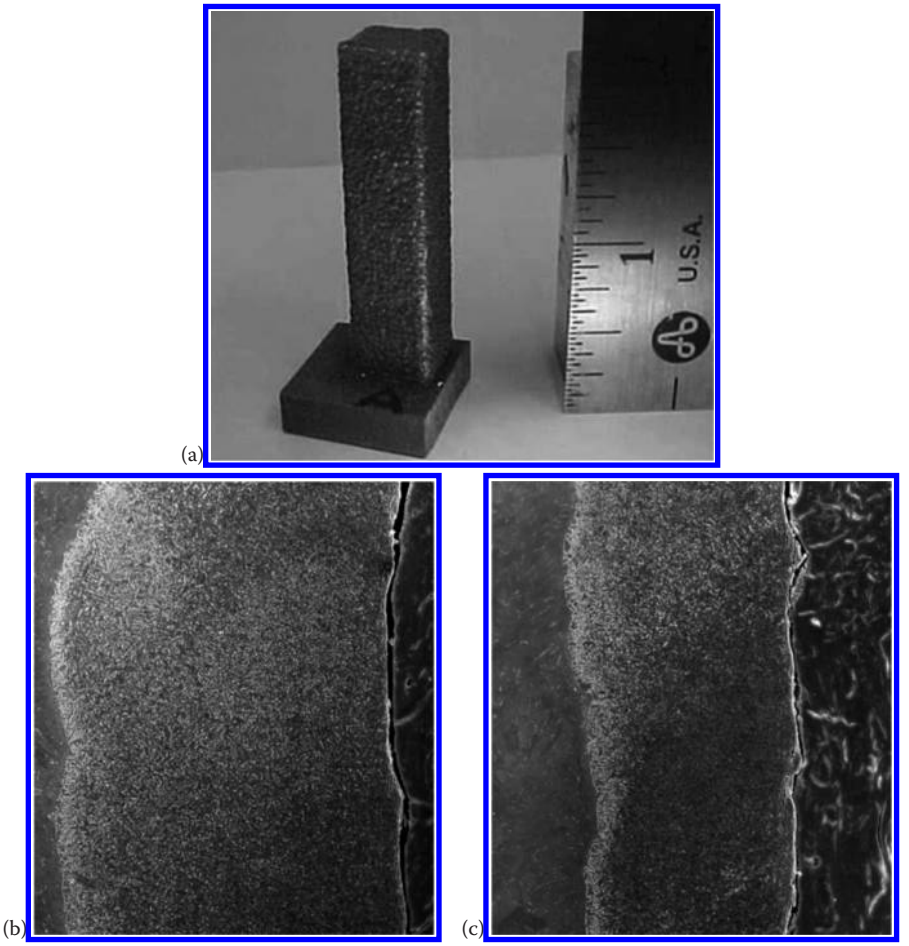

FIGURE 5.18
(a) Laser-deposited Ti6Al4V + 10 wt.% TiC/Ni cubic samples with LENS. (Data from B. Zheng et al., *Metall Mater Trans A*, 39, 1196–205, 2008.) (b–g) SEM micrographs of TCP coatings on Ti fabricated using LENS™: (b) at a scan speed of 15 mm/s with powder feed rate of 13 g/min and 500 W, (c) at a scan speed of 15 mm/s with powder feed rate of 13 g/min and 400 W. (*Continued*)

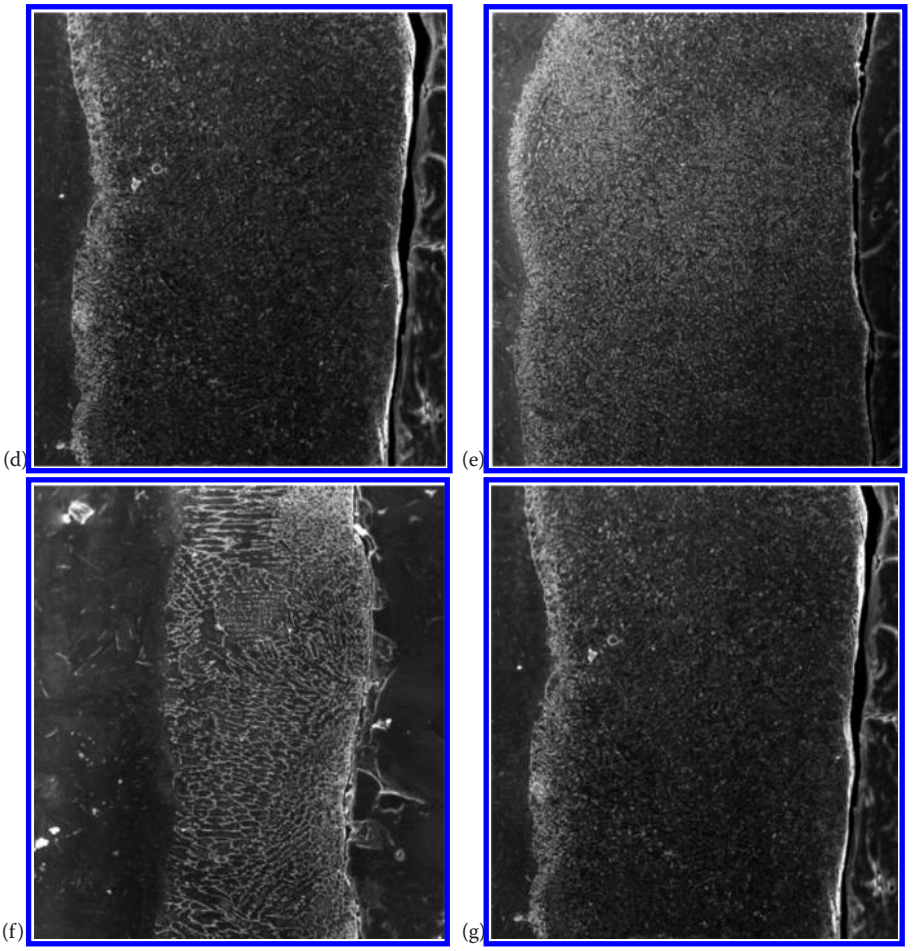

FIGURE 5.18 (Continued)
(b–g) SEM micrographs of TCP coatings on Ti fabricated using LENS™, (d) 500 W power with a powder feed rate of 13 g/min and scan speed of 15 mm/s, (e) 500 W power with a powder feed rate of 13 g/min and scan speed of 10 mm/s, (f) 500 W power at a scan speed of 10 mm/s with a powder feed rate of 9 g/min, and (g) 500 W power at a scan speed of 10 mm/s with a powder feed rate of 13 g min^{-1}. (Data from M. Roy et al., *Acta Biomater*, 4, 324–33, 2008.)

third layer. Coatings were prepared at laser power of 250 W and scan speed of 40 mm/s. The gradation in composition was achieved by altering the YSZ powder feed rate from 0 to 14 g/min, and bond coat powder feed rate from 13 g/min to 0 over the first three layers. The microstructural analysis revealed that the columnar grain-oriented structure included few segmented cracks along the coating thickness, which made the obtained structure suitable for thermal barrier applications [153].

LENS has been used to fabricate dense and crack-free Al_2O_3 parts. Using a laser power of 125 W, scan speed of 10 mm/s, and powder feed rate of 14 g/min, bulk Al_2O_3 parts with density of 94% were achieved. Smooth surface of the parts, as shown in Figure 5.19a, indicates that the Al_2O_3 particles were completely melted and resolidified using the mentioned LENS working parameters [138].

Dense and porous PZT can also be fabricated by LENS. Using the laser power of 150 W, scan speed of 5 mm/s and powder feed rate of 1.3 g/min, crack-free and dense PZT with

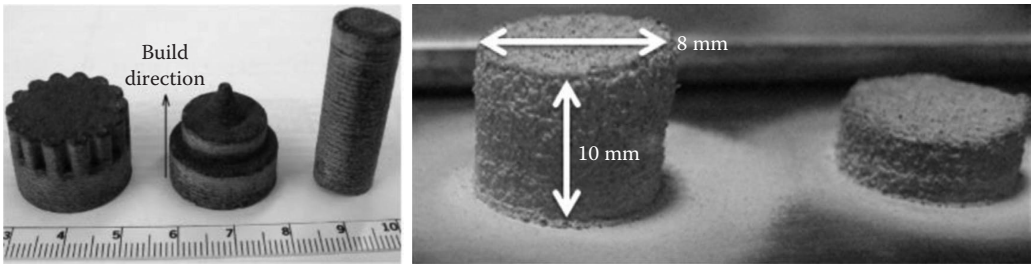

FIGURE 5.19
LENS™ processed structures: (a) Al_2O_3 (Data from V.K. Balla e al., *Int J Appl Ceram Technol*, 5, 234–42, 2008), and (b) PZT. (Data from S.A. Bernard et al., *Mater Sci Eng B–Adv*, 72, 85–8, 2010.)

reasonable dielectric properties was achieved (Figure 5.19b). In addition, at very low energy density, the porous structure was obtained by incomplete melting and presence of unbound particles [146].

5.8 Robocasting

Robocasting is an AM process that depends on robotics for computer-designed deposition of ceramic slurry, containing water, trace amounts of chemical modifiers, and ceramic powder through a syringe. Figure 5.20 illustrated the schematic for a robocasting process. Basically, the ceramic mixture, including water content of only about 15%, flows like a

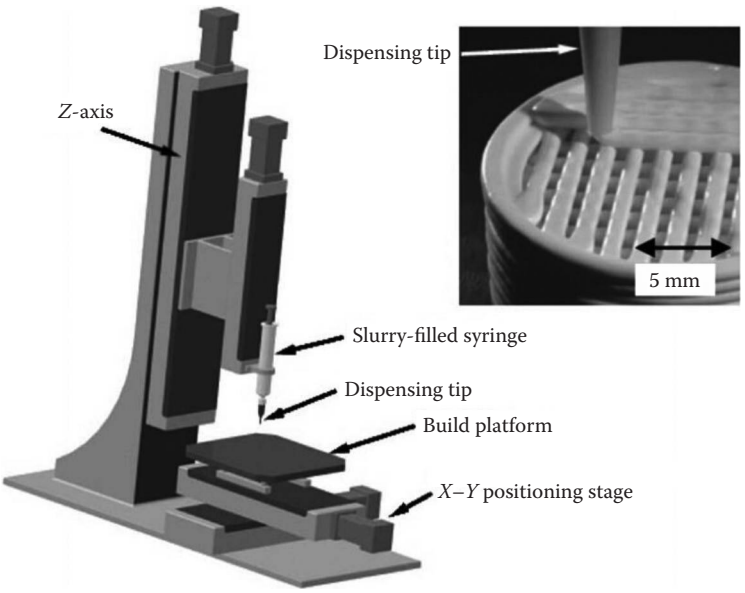

FIGURE 5.20
Schematic of robocasting process. (Data from J.N. Stuecker et al., *J Mater Process Technol*, 142, 318–25, 2003.)

milkshake and then is deposited onto a heated build platform for constructing 3D ceramic parts layer by layer [154]. This new AM technique was developed at Sandia National Laboratories, Albuquerque, New Mexico. Compared with other AM technologies, the most obvious advantage of robocasting is that the entire process, including fabrication, drying, and sintering, can be complete in less than 24 hours [154,155]. By this way, engineers can modify the design of a part as soon as possible to make sure it is working.

Stuecker et al. used robocasting technique to fabricate parts via aqueous mullite suspensions with an organic polyelectrolyte as dispersant. Interparticle forces were characterized by sedimentation and viscometry data. The pH and counter-ion addition of the suspension were controlled to optimize mullite suspensions for use of robocasting process. Figure 5.21 showed the structure of the green part after the robocasting process. The robocasted part was also sintered up to 1650°C resulting in parts with greater than 96% density [156]. More recently, a kind of concentrated, aqueous colloidal ceramic slurry consisting of SiC, Al_2O_3, and Y_2O_3 was used to build parts with complex geometry via robocasting. After robocasting, drying, and calcining processes, green parts were fired at 1700°C in argon by SPS. The sintered structures displayed average grain size around 1–2 μm and above 97% of theoretical density, which is outstanding compared with other AM techniques [157].

With the development of this new technology, robocasting has also been applied to construct medical devices and scaffolds for tissue engineering. Calcium phosphate is one of the most common ceramic used for robocasting because of its excellent biocompatibility.

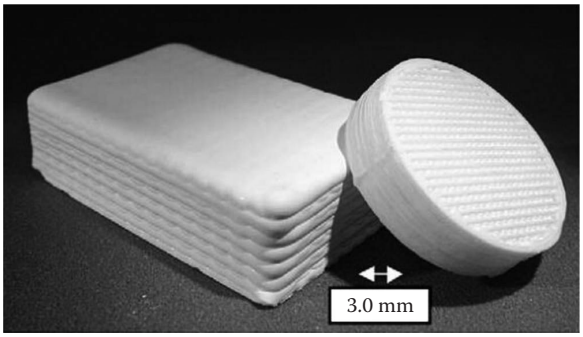

(a)

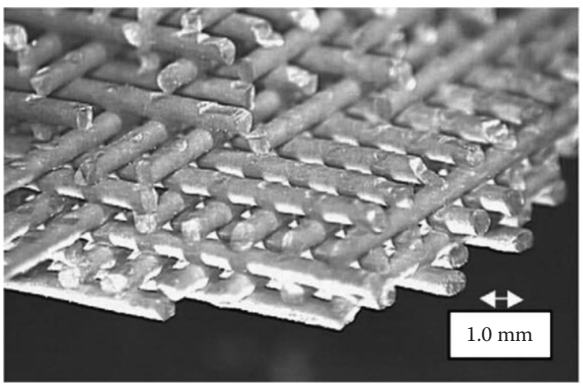

(b)

FIGURE 5.21
(a and b) Examples of robocasting process by mullite suspension (from a 52 vol.% suspension with a yield-pseudoplastic rheology). (Data from J.N. Stuecker et al., *J Mater Process Technol*, 142, 318–25, 2003.)

TABLE 5.5

Ceramic Slurry for Robocasting

Ceramic Particle	Other Compositions	Relative Density	References
Mullite	Polyelectrolyte	> 96% dense	[158]
Tricalcium phosphate	Darvan® C dispersant, hydroxypropyl methylcellulose and polyethylenimine	< 92% dense	[158,160]
HA, Bioglass 4S35, and metallic alloys (6P53B)	Polylactide or polycaprolactone (PCL)	Not mentioned	[159]
Hydroxyapatite	Darvan® C dispersant, hydroxypropyl methylcellulose and polyethylenimine (PEI)	Not mentioned	[160,161]
Nanobioactive glass (nBG)	Chitosan (Chit)	Not mentioned	[162]
β-SiC, Al_2O_3, and Y_2O_3	H-PEI (high molecular weight) (polyethylenimine) and L-PEI	> 97% dense	[157]
HA	PCL and CNTs	Not mentioned	[163]
Bioglass 45S5	Carboxymethyl cellulose (CMC)	Not mentioned	[164]

TCP has been exploited by Miranda et al. to produce scaffolds using robocasting for orthopedic applications. The particle size and morphology of TCP were optimized in order to prepare suspension suitable for robocasting. It turned out that TCP powders with reduced particle size and low specific surface area were more appropriate for slurry preparation. Meanwhile, through the analysis of microstructure and heat treatment, scaffolds fabrication via robocasting with tailored performance could be achieved for bone tissue engineering applications as well [158]. Russias et al. also reported tissue engineering scaffolds prepared via robocasting with HA or bioglass/polylactide or polycaprolactone slurry. The mechanical property was characterized before and after submerging in simulated body fluid for 20 days. It was strongly dependent on the ratio of the organic and inorganic phase and could be controlled based on different applications [159]. Various ceramic composite slurries were used for robocasting. More ceramic suspension systems are shown in Table 5.5.

The challenge for robocasting is how to develop ceramic slurries that are suitable for the deposition process. Excellent ceramic slurries should contain more solid than liquid but exhibit a fluid like consistency, which can also minimize the amount of drying and shrinkage [154]. The research for new ceramic slurry system has never stopped. Moreover, storing these slurries for long time is also a challenge.

5.9 Future Trends for Ceramic Additive Manufacturing

Among different materials, manufacturing of ceramics is probably the most challenging due to their high melting points, low thermal shock resistance, and inherent brittleness. Processing of ceramics using additive manufacturing is exciting because it can combine multiple steps in one operation. However, most of the AM processes produce green ceramic structures that require further post-processing such as binder removal and sintering. Since cracking and warping of large ceramic parts are of serious concern during thermal post-processing treatment of large ceramic parts, application of additive manufacturing is most useful for parts that are either smaller in size or porous in nature. One such application is bone grafts, and fabrication of porous bone grafts using additive manufacturing is

becoming a very popular research field. Bone tissue engineering requires bioactive and bioresorbable ceramics with complex porous network mimicking the bone architecture. Use of additive manufacturing can help in processing these structures with controlled pore size, pore–pore interconnectivity, and tailored volume fraction porosity. Additive manufacturing can also be helpful to make these structures patient specific based on individual's bone defect captured in a computed tomography or magnetic resonance imaging scans [119]. When implanted in vivo, those structures can also be used for guided tissue integration. Typical pore size of >300 μm and pore volume between 10% and 80% with extensive interconnectivity are considered ideal. Such structures help to induce new tissue ingrowth and blood vessel formation such as angiogenesis or vasculogenesis that can enhance osseointegration and reduce healing time. Apart from the size and the shape of the bone tissue engineering scaffolds, compositions can also be tailored for these structures including multi-material constructs with sharp or gradient compositional variations. Bose et al. reported a novel 3D printed porous TCP scaffolds with SiO_2 and ZnO as dopants for bone tissue engineering, shown in Figure 5.22 [89]. In vivo results showed scaffold that had excellent biocompatibility with enhanced osteogenesis and angiogenesis capability due to dopants addition. Figure 5.22 shows powder-bed-based inkjet 3D printed ceramic scaffolds with improved osteogenesis and angiogenesis when used in rat and rabbit distal femur model [165, 166]. These 3D printed structures can be further modified with the addition of cells to improve in vivo bone biology and healing. Further addition of drugs and proteins to these structures are also of interest to many. Overall, it is anticipated that additive manufacturing of various bioceramics and bioceramic–polymer composites for bone tissue engineering will grow rapidly in the coming years.

Apart from bioceramics, porous ceramic structures can also be used for other applications such as filtration, sensors, and scaffolds for composites, which are all expected to benefit from the growth of ceramic additive manufacturing, where simultaneously both the micro- and the macrostructures can be controlled. Additive manufacturing is also expected to impact ceramic coatings for structural and functional applications, though these coatings may not be many layers thick, but can be placed on demand in specific locations with tailored composition to only change surface properties. Such surface property change may be needed to enhance high temperature resistance, increase resistance to wear and corrosion, or add charge storage ability. In fact, some of these coatings can also be used to repair existing devices. The inherent agility of additive manufacturing with added benefit of composition control is expected to have a significant impact on manufacturing ceramic coatings.

In addition to the mentioned AM techniques, some other processes are gaining attractions in recent years such as Lithoz, large area maskless photopolymerization (LAMP), and

FIGURE 5.22
(a) 3D printed controlled porosity ceramic scaffolds with (b) improved osteogenesis and (c) angiogenesis when used in rat and rabbit distal femur model.

Ceradrop. Most of these processes are currently in development stage or recently introduced in the market, therefore limited data is available to independently evaluate their scientific contributions. In the Lithoz' lithography-based ceramic manufacturing (LCM) process, high performance ceramic parts can be achieved through selective curing of a photosensitive resin which contains homogeneously dispersed ceramic particles. The photopolymer acts as the binder and allows the high density of the green body. The LED-technology being used in this method followed by conventional debinding and sintering steps results in fabrication of ceramic parts with high density, fine details, exceptional surface quality, and material properties comparable to that in serial production. In the case of LAMP, a stereolithography-based process, a thin layer of ceramic resin is cured by UV light based on the CAD file. Similar to other AM processes, LAMP will be continued layer by layer until the entire part is fabricated. Compared to the traditional investment casting, LAMP is significantly more efficient from both time and cost aspects. Ceradrop has developed printers with multiple options of printheads from different manufacturers, such as Dimatix, Minolta, Konica as well as various options of post-processing such as UV, IR, photonics, and so on.

Finally, additive manufacturing techniques for ceramics are still at its infancy. While novel techniques are becoming popular for thin microscale structures for flexible electronics and semiconductor devices, ceramic processing for large-scale bulk structures is still quite difficult. Further research and development is needed to make ceramic additive manufacturing a popular approach for direct low-volume manufacturing of structural, functional, or bioceramic parts.

5.10 Summary

In this chapter, seven different AM processes for ceramics are discussed in detail. Table 5.6 summarizes the processing steps for these methods, as well as some of their advantages and disadvantages. Though ceramic processing using AM techniques started in early 1990s, its widespread applications are still sparse. The primary reason is extensive process optimization necessary from one powder to another powder due to changes in particle size, shape, and surface energy. Moreover, large ceramics parts are almost impossible to densify due to cracking or delamination. Finally, no dedicated machine is available even today that can be used to print only ceramics. However, need for ceramic-based AM techniques are

TABLE 5.6

AM Techniques for Ceramic Materials

Technique	Processing Steps	Advantages and Disadvantages
Stereolithography	• Mix ceramic particle with photocurable material • Apply UV light to the area based on the design • Debind the parts from the build platform and densify the parts by sintering	Advantages: • The manufacture of this method is flexible and efficient. • The geometry and dimension are accurate. Disadvantages: • Support material is need when producing parts with complex geometry. • Poor density and mechanical strength. • It cannot manufacture large ceramic parts.

(*Continued*)

TABLE 5.6 (*Continued*)

AM Techniques for Ceramic Materials

Technique	Processing Steps	Advantages and Disadvantages
Selective laser sintering	• Preheat the ceramic powder • Fill the chamber with nitrogen gas to avoid oxidation and then use CO_2 laser to scan • Cool down the part for removing	Advantages: • Excellent for complex geometry. • No support material is needed. Disadvantages: • The density of the part is usually low. • Part with large dimension is hard to manufacture this way.
Ink-jet three-dimensional printing	• Spreading the powder on build bed using a roller • Selective spraying of binder/printing solution on built layer • Drying, depowdering, and sintering of part	Advantages: • No need for support. • Possible for wide range of materials. Disadvantages: • Low mechanical strength. • Difficult depowdering process. • Limitation over ceramic/binder system.
Fused deposition of ceramics	• Mixing the ceramic powder with a polymer carrier • Deposition of strands on substrate using a liquefier and a nozzle • Polymer removal and sintering	Advantages: • High ceramic loading without trapping in voids. • Complete bonding between layers. Disadvantages: • Filament fabrication. • Polymer/ceramic system optimization. • Challenging post-processing steps.
Laminate object manufacturing	• Pre-ceramic paper preparation • Cutting the paper using laser beam • Decubing of final part and sintering	Advantages: • Processing fully dense structure with control on microstructural features. • High speed process. • Low cost. Disadvantages: • Need for post-processing, including decubing, surface finishing, and sintering.
Laser engineered net shaping	• Melting the substrate using Nd:YAG laser • Injection of ceramic powders to the molten area • Cooling the structure by moving the laser	Advantages: • Processing fully dense structure with control on microstructural features. • Control over the composition. • Gradient deposition of materials. Disadvantages: • Need for post-processing. • Poor resolution and surface finish.
Robocasting	• Prepare ceramic slurry • Deposit on heated build platform • Drying and sintering	Advantages: • Efficient, the whole process can be done less than 24 hours. Disadvantages: • Logpile structure makes this method not so accurate.

growing, and it is our hope that more research and development work will focus on ceramic AM techniques in the coming days. Apart from green freeform fabrication, direct densification of ceramics structures via laser-based AM is also quite exciting and holds a lot of promise. Finally, approaches toward fabrication of ceramic-loaded composites will probably see more real-world applications in the near future using a variety of AM techniques.

References

1. C.W. Hull, Apparatus for production of three-dimensional objects by stereolithography, US Patent # 4,575,330, 1986.
2. 3D Printing Process—What is Stereolithography (SLA)? THRE3D n.d.
3. T. Chartier, C. Chaput, F. Doreau, M. Loiseau, Stereolithography of structural complex ceramic parts. *J Mater Sci* 2002;37:3141–7.
4. M.L. Griffith, J.W. Halloran, Ultraviolet curable ceramic suspensions for stereolithography of ceramics. *Manuf Sci Eng* 1994;68-2:529–34.
5. C. Hinczewski, S. Corbel, T. Chartier, Ceramic suspensions suitable for stereolithography. *J Eur Ceram Soc* 1998;18:583–90.
6. S. Kanehira, S. Kirihara, Y. Miyamoto, Fabrication of TiO_2-SiO_2 photonic crystals with diamond structure. *J Am Ceram Soc* 2005;88:1461–4.
7. T. Chartier et al., Fabrication of millimeter wave components via ceramic stereo- and microstereolithography processes. *J Am Ceram Soc* 2008; 91:2469–74.
8. R. Felzmann et al., Lithography-based additive manufacturing of cellular ceramic structures. *Adv Eng Mater* 2012;14:1052–8.
9. J.Y. Kim, J.W. Lee, S.-J. Lee, E.K. Park, S.-Y. Kim, D.-W. Cho, Development of a bone scaffold using HA nanopowder and micro-stereolithography technology. *Microelectron Eng* 2007;84:1762–5.
10. O. Dufaud, S. Corbel, Stereolithography of PZT ceramic suspensions. *Rapid Prototyp J* 2002;8:83–90.
11. O. Dufaud, P. Marchal, S. Corbel, Rheological properties of PZT suspensions for stereolithography. *J Eur Ceram Soc* 2002;22:2081–92.
12. G.A. Brady, J.W. Halloran, Stereolithography of ceramic suspensions. *Rapid Prototyp J* 1997;3:61–5.
13. C. Hinczewski, S. Corbel, T. Chartier, Stereolithography for the fabrication of ceramic three-dimensional parts. *Rapid Prototyp J* 1998;4:104–11.
14. A. Greco, A. Licciulli, A Maffezzoli, Stereolithography of ceramic suspensions. *J Mater Sci* 2001;36:99–105.
15. A. Licciulli, C. Esposito Corcione, A. Greco, V. Amicarelli, A. Maffezzoli, Laser stereolithography of ZrO_2 toughened Al_2O_3. *J Eur Ceram Soc* 2005;25:1581–9.
16. C.E. Corcione, A. Greco, F. Montagna, A. Licciulli, A. Maffezzoli, Silica moulds built by stereolithography. *J Mater Sci* 2005;40:4899–904.
17. J.H. Jang, S. Wang, S.M. Pilgrim, W.A. Schulze, Preparation and Characterization of Barium Titanate Suspensions for Stereolithography. *J Am Ceram Soc* 2000;83:1804–6.
18. S. Kirihara, Y. Miyamoto, K. Takenaga, M.W. Takeda, K. Kajiyama, Fabrication of electromagnetic crystals with a complete diamond structure by stereolithography. *Solid State Commun* 2002;121:435–9.
19. I.M. Krieger, T.J. Dougherty, A mechanism for non-Newtonian flow in suspensions of rigid spheres. *Trans Soc Rheol* 1957–1977 1959;3:137–52.
20. M.L. Griffith, J.W. Halloran. Freeform fabrication of ceramics via stereolithography. *J Am Ceram Soc* 1996;79:2601–8.
21. P.F. Jacobs, *Rapid Prototyping & Manufacturing: Fundamentals of Stereolithography*. Dearborn, MI: Society of Manufacturing Engineers; 1992.
22. W. Zimbeck, M. Pope, R.W. Rice, Microstructures and strengths of metals and ceramics made by photopolymer-based rapid prototyping. *Solid Free Fabr Proc* 1996:411–18.
23. M.L. Griffith, T.-M. Chu, W. Wagner, J. W. Halloran, Ceramic stereolithography for investment casting and biomedical applications. *Proc Solid Free Fabr Symp Austin Tex,* Edited by H. L. Marcus, J. J. Beaman, J. W. Barlow, D. L. Bourell and R. H. Crawford, The University of Texas at Austin, Austin, TX, 1995:31–8.
24. W.Z. Zhou, D. Li, Z.W. Chen, S. Chen, Direct fabrication of an integral ceramic mould by stereolithography. *Proc Inst Mech Eng Part B J Eng Manuf* 2010;224:237–43.

25. H. Wu, D. Li, N. Guo, Fabrication of integral ceramic mold for investment casting of hollow turbine blade based on stereolithography. *Rapid Prototyp J* 2009;15:232–7.
26. H. Wu, D. Li, Y. Tang, B. Sun, D. Xu, Rapid fabrication of alumina-based ceramic cores for gas turbine blades by stereolithography and gelcasting. *J Mater Process Technol* 2009;209:5886–91.
27. C.E. Corcione, F. Montagna, A. Greco, A. Licciulli, A. Maffezzoli, Free form fabrication of silica moulds for aluminium casting by stereolithography. *Rapid Prototyp J* 2006;12:184–8.
28. O. Dufaud, S. Corbel, Oxygen diffusion in ceramic suspensions for stereolithography. *Chem Eng J* 2003;92:55–62.
29. A. Buerkle, K. Brakora, K. Sarabandi, Fabrication of a DRA array using ceramic stereolithography. *Antennas Wirel Propag Lett* 2006;5:479–82.
30. N. Delhote, D. Baillargeat, S. Verdeyme, C. Delage, C. Chaput, Innovative shielded high dielectric resonator made of alumina by layer-by-layer stereolithography. *IEEE Microw Wirel Compon Lett* 2007;17:433–5.
31. K.F. Brakora, J. Halloran, K. Sarabandi. Design of 3-D monolithic MMW antennas using ceramic stereolithography. *IEEE Trans Antennas Propag* 2007;55:790–7.
32. N. Delhote, D. Baillargeat, S. Verdeyme, C. Delage, C. Chaput, Ceramic layer-by-layer stereolithography for the manufacturing of 3-D millimeter-wave filters. *IEEE Trans Microw Theory Tech* 2007;55:548–54.
33. I. Gibson, D.W. Rosen, B. Stucker, *Additive Manufacturing Technologies*. Boston, MA: Springer, 2010.
34. D.T. Pham, R.S. Gault, A comparison of rapid prototyping technologies. *Int J Mach Tools Manuf* 1998;38:1257–87.
35. Y.-C. Hagedorn, N. Balachandran, W. Meiners, K. Wissenbach, R. Poprawe, SLM of net-shaped high strength ceramics: New opportunities for producing dental restorations. *Proc Solid Free Fabr Symp*, Edited by J. J. Beaman and D. L. Bourell, The University of Texas at Austin, Austin, TX, 2011:536–46.
36. K. Shahzad, J. Deckers, Z. Zhang, J.-P. Kruth, J. Vleugels, Additive manufacturing of zirconia parts by indirect selective laser sintering. *J Eur Ceram Soc* 2014;34:81–9.
37. I. Shishkovsky, I. Yadroitsev, P. Bertrand, I. Smurov, Alumina–zirconium ceramics synthesis by selective laser sintering/melting. *Appl Surf Sci* 2007;254:966–70.
38. P. Bertrand, F. Bayle, C. Combe, P. Goeuriot, I. Smurov, Ceramic components manufacturing by selective laser sintering. *Appl Surf Sci* 2007;254:989–92.
39. C. Shuai, P. Li, J. Liu, S. Peng, Optimization of TCP/HAP ratio for better properties of calcium phosphate scaffold via selective laser sintering. *Mater Charact* 2013;77:23–31.
40. C. Shuai, C. Gao, Y. Nie, H. Hu, Y. Zhou, S. Peng, Structure and properties of nano-hydroxyapatite scaffolds for bone tissue engineering with a selective laser sintering system. *Nanotechnology* 2011;22:28:5703.
41. C. Shuai, C. Gao, Y. Nie, H. Hu, H. Qu, S. Peng, Structural design and experimental analysis of a selective laser sintering system with nano-hydroxyapatite powder. *J Biomed Nanotechnol* 2010;6:370–4.
42. T. Czelusniak, F.L. Amorim, A. Lohrengel, C.F. Higa, Development and application of copper–nickel zirconium diboride as EDM electrodes manufactured by selective laser sintering. *Int J Adv Manuf Technol* 2014;72:905–17.
43. J. Liu, H. Hu, P. Li, C. Shuai, S. Peng, Fabrication and characterization of porous 45S5 glass scaffolds via direct selective laser sintering. *Mater Manuf Process* 2013;28;6:610–15
44. E.Y. Tarasova, G.V. Kryukova, A.L. Petrov, I.V. Shishkovsky, Structure and properties of porous PZT ceramics synthesized by selective laser sintering method. *SPIE Proc* 2000;3933:502–4
45. H.-C. Yen, A new slurry-based shaping process for fabricating ceramic green part by selective laser scanning the gelled layer. *J Eur Ceram Soc* 2012;32:3123–8.
46. F. Klocke, C. Derichs, C. Ader, A. Demmer, Investigations on laser sintering of ceramic slurries. *Prod Eng* 2007;1:279–84.
47. X. Tian, D. Li, J.G. Heinrich, Rapid prototyping of porcelain products by layer-wise slurry deposition (LSD) and direct laser sintering. *Rapid Prototyp J* 2012;18:362–73.
48. F.-H. Liu, Synthesis of biomedical composite scaffolds by laser sintering: Mechanical properties and in vitro bioactivity evaluation. *Appl Surf Sci* 2014;297:1–8.

49. H.C. Yen, H.H. Tang, Study on direct fabrication of ceramic shell mold with slurry-based ceramic laser fusion and ceramic laser sintering. *Int J Adv Manuf Technol* 2012;60:1009–15.
50. A. Gahler, J.G. Heinrich, J. Günster, Direct laser sintering of Al_2O_3-SiO_2 dental ceramic components by layer-wise slurry deposition. *J Am Ceram Soc* 2006;89:3076–80.
51. F.-H. Liu, Y.-K. Shen, J.-L. Lee, Selective laser sintering of a hydroxyapatite-silica scaffold on cultured MG63 osteoblasts in vitro. *Int J Precis Eng Manuf* 2012;13:439–44.
52. D. Drummer, D. Rietzel, F. Kühnlein, Development of a characterization approach for the sintering behavior of new thermoplastics for selective laser sintering. *Phys Procedia* 2010;5:533–42.
53. K. Liu, Y. Shi, C. Li, L. Hao, J. Liu, Q. Wei, Indirect selective laser sintering of epoxy resin-Al_2O_3 ceramic powders combined with cold isostatic pressing. *Ceram Int* 2014;40:7099–106.
54. L. Cardon et al., Polystyrene-coated alumina powder via dispersion polymerization for indirect selective laser sintering applications. *J Appl Polym Sci* 2013;128:2121–8
55. J. Deckers, J.-P. Kruth, K. Shahzad, J. Vleugels. Density improvement of alumina parts produced through selective laser sintering of alumina-polyamide composite powder. *CIRP Ann—Manuf Technol* 2012;61:211–14.
56. A.M. Waetjen, D.A. Polsakiewicz, I. Kuhl, R. Telle, H. Fischer, Slurry deposition by airbrush for selective laser sintering of ceramic components. *J Eur Ceram Soc* 2009;29:1–6.
57. H.-H. Tang, M.-L. Chiu, H.-C. Yen, Slurry-based selective laser sintering of polymer-coated ceramic powders to fabricate high strength alumina parts. *J Eur Ceram Soc* 2011;31:1383–8.
58. J.C. Nelson, N.K. Vail, J.W. Barlow, J.J. Beaman, D.L. Bourell, H.L. Marcus, Selective laser sintering of polymer-coated silicon carbide powders. *Ind Eng Chem Res* 1995;34:1641–51.
59. R.D. Goodridge, D.J. Wood, C. Ohtsuki, K.W. Dalgarno, Biological evaluation of an apatite–mullite glass-ceramic produced via selective laser sintering. *Acta Biomater* 2007;3:221–31.
60. K.C.R. Kolan, M.C. Leu, G.E. Hilmas, R.F. Brown, M. Velez, Fabrication of 13-93 bioactive glass scaffolds for bone tissue engineering using indirect selective laser sintering. *Biofabrication* 2011;3:025004.
61. J. Zhao, W.B. Cao, J.T. Li, Z. Han, Y.H. Li, C.C. Ge, Selective laser sintering of Si_3N_4 and Al_2O_3 ceramic powders ceramic powders. *Key Eng Mater* 2008;368–372:858–61.
62. B. Ma, L. Lin, X. Huang, Q. Hu, M. Fang, Bone tissue engineering using beta-tricalcium phosphate scaffolds fabricated via selective laser sintering. *Knowl Enterp Intell Strateg Prod Des Manuf Manag* 2006;207:710–16.
63. D.M. Gureev, R.V. Ruzhechko, I.V. Shishkovskii, Selective laser sintering of PZT ceramic powders. *Tech Phys Lett* 2000;26:262–4.
64. D. Liu, J. Zhuang, C. Shuai, S. Peng, Mechanical properties' improvement of a tricalcium phosphate scaffold with poly-l-lactic acid in selective laser sintering. *Biofabrication* 2013;5:025005.
65. C. Shuai, J. Zhuang, H. Hu, S. Peng, D. Liu, J. Liu, In vitro bioactivity and degradability of β-tricalcium phosphate porous scaffold fabricated via selective laser sintering: Properties of β-TCP Porous Scaffold. *Biotechnol Appl Biochem* 2013;60:266–73.
66. E.M. Sachs et al., Three-dimensional printing techniques, US Patent # 5,204,055, 1993.
67. S. Bose, S. Vahabzadeh, A. Bandyopadhyay, Bone tissue engineering using 3D printing. *Mater. Today* 2013;16:496–504.
68. P.H. Warnke et al., Ceramic scaffolds produced by computer-assisted 3D printing and sintering: Characterization and biocompatibility investigations. *J Biomed Mater Res* 2010;93B:212–17.
69. E. Vorndran et al., 3D powder printing of β-tricalcium phosphate ceramics using different strategies. *Adv Eng Mater* 2008;10:B67–B71.
70. B. Leukers et al., Biocompatibility of ceramic scaffolds for bone replacement made by 3D printing. *Mater Wiss Werkstofftech* 2005;36:781–7.
71. A. Zocca, C.M. Gomes, E. Bernardo, R. Müller, J. Günster, P. Colombo, LAS glass–ceramic scaffolds by three-dimensional printing. *J Eur Ceram Soc* 2013;33:1525–33.
72. S. Tarafder et al., Microwave-sintered 3D printed tricalcium phosphate scaffolds for bone tissue engineering. *J Tissue Eng Regen Med* 2013;7:631–41.
73. H. Hausner, Powder characteristics and their effect on powder processing. *Powder Technol* 1981;30:3–8.

74. S.A. Uhland et al., Strength of green ceramics with low binder content. *J Am Ceram Soc* 2001;84:2809–18.
75. S. Amirkhani, R. Bagheri, A. Zehtab Yazdi, Effect of pore geometry and loading direction on deformation mechanism of rapid prototyped scaffolds. *Acta Mater* 2012;60:2778–89.
76. S. Maleksaeedi, H. Eng, F.E. Wiria, T.M.H. Ha, Z. He, Property enhancement of 3D-printed alumina ceramics using vacuum infiltration. *J Mater Process Tech* 2014;214:1301–6.
77. B.C. Gross, J.L. Erkal, S.Y. Lockwood, C. Chen, D.M. Spence, Evaluation of 3D printing and its potential impact on biotechnology and the chemical sciences, *Anal Chem* 2014;86:3240–3253.
78. J. Suwanprateeb, R. Sanngam, T. Panyathanmaporn, Influence of raw powder preparation routes on properties of hydroxyapatite fabricated by 3D printing technique. *Mater Sci Eng C* 2010;30:610–17.
79. A. Doraiswamy, T.M. Dunaway, J.J. Wilker, R.J.J. Narayan, Inkjet printing of bioadhesives, *Biomed Mater Res, Part B: Appl Biomater* 2009;89B:28–35.
80. A. Khalyfa et al., Development of a new calcium phosphate powder-binder system for the 3D printing of patient specific implants. *J Mater Sci: Mater Med* 2007;18:909–16.
81. J. Suwanprateeb, R. Sanngam, T.W. Suvannapruk, Panyathanmaporn. Mechanical and in vitro performance of apatite-wollastonite glass ceramic reinforced hydroxyapatite composite fabricated by 3D-printing. *J Mater Sci: Mater Med* 2009;20:1281–9.
82. B. Nan, X. Yin, L. Zhang, L. Cheng, Three-dimensional printing of Ti3SiC2-based ceramics. *J Am Ceram Soc* 2011;94-4:969–72.
83. A. Zocca et al., SiOC ceramics with ordered porosity by 3D-printing of a preceramic polymer. *J Mater Res* 2013;28:2243–52.
84. X. Li, L. Zhang, X. Yin, Microstructure and mechanical properties of three porous Si_3N_4 ceramics fabricated by different techniques. *Mat Sci Eng A-Struct* 2012;549:43– 9.
85. B. Leukers, H. Gulkan, SH. Irsen, S. Milz, C. Tille, H. Seitz, M. Schieker, Biocompatibility of ceramic scaffolds for bone replacement made by 3D printing. *Mater Wiss Werkstofftech* 2005;36:781–7.
86. J. Suwanprateeb, R. Chumnanklang, Three-dimensional printing of porous polyethylene structure using water-based binders. *J Biomed Mater Res B* 2006;78B:138–45.
87. A. Winkel et al., Sintering of 3D-printed glass/HAp composites. *J Am Ceram Soc* 2012; 95-11:3387–93.
88. S. Bose, M. Roy, A. Bandyopadhyay, Recent advances in bone tissue engineering scaffolds. *Trends Biotechnol* 2012;30:546–54.
89. S. Bose and G. Fielding, SiO_2 and ZnO dopants in 3D printed TCP scaffolds enhances osteogenesis and angiogenesis in vivo *Acta Biomater* 2013;9:9137–48.
90. S. Tarafder, N.M. Davies, A. Bandyopadhyay, S. Bose, 3D printed tricalcium phosphate scaffolds: Effect of SrO and MgO doping on in vivo osteogenesis in rat distal femoral defect model. *Biomater Sci* 2013;1:1250–9.
91. S. Tarafder, S. Bose, Polycaprolactone-coated 3D printed tricalcium phosphate scaffolds for bone tissue engineering: In vitro alendronate release behavior and local delivery effect on in vivo osteogenesis. *ACS Appl Mater Interfaces* 2014;6:9955–65.
92. C.X.F. Lam, X.M. Mo, S.H. Teoh, D.W. Hutmacher, Scaffold development using 3D printing with a starch-based polymer. *Mater Sci Eng C* 2002;20:49–56.
93. G.A. Fielding, A. Bandyopadhyay, S. Bose, Effects of silica and zinc oxide doping on mechanical and biological properties of 3D printed tricalcium phosphate tissue engineering scaffolds. *Dent Mater* 2012;28:113–22.
94. U. Gbureck, E. Vorndran, F.A. Müller, J.E. Barralet, Low temperature direct 3D printed bioceramics and biocomposites as drug release matrices. *J Control Release* 2007;122:173–80.
95. R. Gauvin et al., Microfabrication of complex porous tissue engineering scaffolds using 3D projection stereolithography. *Biomater* 2012;33:3824–34.
96. E. Vorndran et al., Simultaneous immobilization of bioactives during 3D powder printing of bioceramic drug-release matrices. *Adv Funct Mater* 2012;20:1585–2159.
97. Stratasys Inc. http://www.stratasys.com.
98. M. Agarwala, A. Bandyopadhyay, S.C. Danforth, V.R. Jamalabad, N. Langrana, W.R. Priedeman, A. Safari, R. van Weeren, Solid freeform fabrication methods, US Patent # 5,900,207, 1999.

99. M. Agarwala, A. Bandyopadhyay, S.C. Danforth, V.R. Jamalabad, N. Langrana, A. Safari, R. van Weeren, Solid freeform fabrication methods, US Patent # 5,738,817, 1998.
100. M. Agarwala, A. Bandyopadhyay, S.C. Danforth, V.F. Janas, R.K. Panda, A. Safari, Novel ceramic composites and methods for producing same, US Patent # 6,004,500, 1999.
101. A. Bandyopadhyay, S.C. Danforth, T. McNulty, R.K. Panda, A. Safari, Radial ceramic piezoelectric composites, US Patent # 6,049,160, 2000.
102. A. Bandyopadhyay, S.C. Danforth, V.F. Janas, R.K. Panda, A. Safari, Oriented piezoelectric ceramics and ceramic polymer composites, US Patent # 5,796,207, 1998.
103. J. Ballato, A. Bandyopadhyay, S.C. Danforth, A. Safari, R. van Weeren, Process for forming of photonic band-gap structures, US Patent # 5,997,795, 1999.
104. E.A. Griffin, S. McMillin, Selective laser sintering and fused deposition modeling processes for functional ceramic parts, *Solid Freeform Fabrication Proceedings*, University of Texas, Austin, TX, 1995;25–30.
105. S.J. Kalita, S. Bose, H.L. Hosick, A. Bandyopadhyay, Development of controlled porosity polymer-ceramic composite scaffolds via fused deposition modeling, *Mater Sci Eng C* 2003; 23:611–20.
106. J.A. Lewis, J.E. Smay, J. Stuecker, J. Cesarano, Direct ink writing of three-dimensional ceramic structures, *J Am Ceram Soc* 2006;89-12:3599–609.
107. A. Safari, M. Allahverdi, E.K. Akdogan, Solid freeform fabrication of piezoelectric sensors and actuators, *J Mater Sci* 2006;41:177–98.
108. S. Iyer et al., Microstructural characterization and mechanical properties of Si_3N_4 formed by fused deposition of ceramics, *Int J Appl Ceram Technol* 2008;5-2:127–37.
109. H.Y. Yang, X.P. Chi, S. Yang, J.R.G. Evans, Mechanical strength of extrusion freeformed calcium phosphate filaments, *J Mater Sci: Mater Med* 2010;21:1503–10.
110. M. K. Agarwala, R. van Weeren, R. Vaidyanathan, A. Bandyopadhyay, G. Carrasquillo, V. Jamalabad, N. Langrana, et al. Structural ceramics by fused deposition of ceramics, *Proceedings of the Solid Freeform Fabrication Symposium*, Edited by H. L. Marcus, J. J. Beaman, J. W. Barlow, D. L. Bourell and R. H. Crawford, The University of Texas at Austin, Austin, TX, 1995: 1–8.
111. L. Shor et al., Fabrication of three-dimensional polycaprolactone/hydroxyapatite tissue scaffolds and osteoblast-scaffold interactions in vitro. *Biomaterials* 2007;28:5291–7.
112. S. Onagoruwa, S. Bose, A. Bandyopadhyay. Fused deposition of ceramics (FDC) and composites. *Proc. SFF*, Austin, TX, 2001;224–31.
113. A. Bellini, Fused deposition of ceramics: A comprehensive experimental, analytical and computational study of material behavior, fabrication process and equipment design, PhD Thesis, Drexel University, Philadelphia, PA, 2002.
114. T.F. McNulty, D.J. Shanefield, S.C. Danforth, and A. Safari, Dispersion of lead zirconate titanate for fused deposition of ceramics. *J Am Ceram Soc* 1999;82:1757–60.
115. A. Bandyopadhyay, R.K. Panda, V.F. Janas, M.K. Agarwala, S.C. Danforth and A. Safari, Processing of piezocomposites by fused deposition technique. *J Am Ceram Soc* 1997;80:1366–72.
116. S. Turcu, B. Jadidian, S.C. Danforth, A. Safari, Piezoelectric properties of novel oriented ceramic-polymer composites with 2-2 and 3-3 connectivity. *J Electroc* 2002;9, 165–71.
117. R.K. Panda, Development of novel piezoelectric composites by solid freeform fabrication techniques, Ph.D. Thesis, Rutgers University, New Brunswick, NJ, 1998.
118. S. Bose, S. Sugiura, A. Bandyopadhyay, Processing of controlled porosity ceramic structures via fused deposition process. *Scripta Mater* 1999;41-9:1009–14.
119. J. Darsell, S. Bose, H. Hosick, A. Bandyopadhyay, From CT scans to ceramic bone grafts. *J Am Ceram Soc* 2003;86-7:1076–80.
120. A. Bandyopadhyay, K. Das, J. Marusich, S. Onagoruwa, Application of fused deposition in controlled microstructure metal-ceramic composites, *Rapid Prototyp J* 2006;12-3:121–8.
121. T.F. McNulty, F. Mohammadi, A. Bandyopadhyay, D.J. Shanefield, S.C. Danforth, A. Safari, Development of binder formulation for fused deposition of ceramics, *Rapid Prototyp J* 1998;4-4:144–50.
122. S. Bose, J. Darsell, M. Kintner, H. Hosick, A. Bandyopadhyay, Pore size and pore volume effects on calcium phosphate based ceramics, *Mat Sci Eng C* 2003;23:479–86.

123. J.T. Schantz et al., Osteogenic differentiation of mesenchymal progenitor cells in computer designed fibrin-polymer-ceramic scaffolds manufactured by fused deposition modeling. *J Mater Sci: Mater Med* 2005;16:807–19.
124. M.E. Pilleux et al., 3-D photonic bandgap structures in the microwave regime by fused deposition of multimaterials. *Rapid Prototyp J* 2002;8:46–52.
125. C.M. Gomes, A.P.N. Oliveira, D. Hotza, N. Travitzky, P. Greil, LZSA glass-ceramic laminates: Fabrication and mechanical properties. *J Mater Process Tech* 2008;206:194–201.
126. K. Schindler, A. Roosen, Manufacture of 3D structures by cold low pressure lamination of ceramic green tapes, *J Eur Ceram Soc* 2009;29:899–904.
127. I. Cho, K. Lee, W. Choi, Y.A. Song, Development of a new sheet deposition type rapid prototyping system. *Int J Mach Tools Manuf* 2000;40:1813–29.
128. H. Windsheimer, N. Travitzky, A. Hofenauer, P. Greil, Laminated object manufacturing of preceramic-paper-derived Si-SiC composites. *Adv Mater* 2007;19:4515–19.
129. C.M. Gomes, C.R. Rambo, A.P. Novaes de Oliveira, D. Hotza, D. Gouvea, Colloidal processing of glass–ceramics for laminated object manufacturing. *J Am Ceram Soc* 2009;92-6:1186–91.
130. C.W. Macosko, *Rheology: Principles, Measurements and Applications*. New York: VCH Publishers, 1993.
131. J.S. Reed, *Principles of Ceramics Processing*, 2nd edn., New York: Wiley Interscience Publications, 1988.
132. R.E. Mistler, E.R. Twiname, *Tape Casting—Theory and Practice*. The American Ceramic Society, Westerville, OH, 2000.
133. N. Travitzky, H. Windsheimer, T. Fey, P. Greil, Preceramic paper-derived ceramics, *J Am Ceram Soc* 2008;91-11:3477–92.
134. L. Weisensel, N. Travitzky, H. Sieber, P. Greil, Laminated object manufacturing (LOM) of SiSiC composites. *Adv Eng Mater* 2004;6-11:899–903.
135. S. Yi, F. Liu, J. Zhang, S. Xiong, Study of the key technologies of LOM for functional metal parts. *J Mater Process Technol* 2004;150:175–81.
136. B. Mueller, D. Kochan, Laminated object manufacturing for rapid tooling and patternmaking in foundry industry. *Comput Ind* 1999;39:47–53.
137. Y. Zhang, X. He, S. Du, J. Zhang, Al_2O_3 ceramics preparation by LOM (laminated object manufacturing). *Int J Adv Manuf Technol* 2001;17:531–4.
138. V.K. Balla, S. Bose, A. Bandyopadhyay, Processing of bulk alumina ceramics using laser engineered net shaping. *Int J Appl Ceram Technol* 2008;5-3:234–42.
139. B. Zheng, J.E. Smugereky, Y. Zhou, D. Baker, E.J. Lavernia, Microstructure and properties of laser-deposited Ti6Al4V metal matrix composites using Ni-coated powder, *Metall Mater Trans A* 2008;39-5:1196–205.
140. M. Roy, V.K. Balla, A. Bandyopadhyay, S. Bose, Laser processing of bioactive tricalcium phosphate coating on titanium for load-bearing implants. *Acta Biomater* 2008;4:324–33.
141. J. Mazumder, A. Schifferer, J. Choi, Direct materials deposition: designed macro and microstructure. *Mater Res Innovations* 1999;3:118–31.
142. S.P. Harimkar, A.N. Samant, A.A. Khangar, B.D. Narendra, Prediction of solidification microstructures during laser dressing of alumina- based grinding wheel material. *J Phys D: Appl Phys* 2006;39:1642–9.
143. M. Das, V.K. Balla, T.S.S. Kumar, I. Manna, Fabrication of biomedical implants using laser engineered net shaping (LENS™). *Trans Ind Ceram Soc* 2013;72-3:169–74.
144. I. Gibson, D.W. Rosen, B. Stucker, *Additive Manufacturing Technologies Rapid Prototyping to Direct Digital Manufacturing*, New York: Springer-Verlag, 2009.
145. S. Kou. *Welding Metallurgy*. New York: John Wiley & Sons, 1987, p. 46.
146. S.A. Bernard, V.K. Balla, S. Bose, A. Bandyopadhyay, Direct laser processing of bulk lead zirconate titanate ceramics, *Mater Sci Eng B–Adv* 2010;72:85–8.
147. W. Liu, J.N. DuPont, Fabrication of functionally graded TiC/Ti composites by laser engineered net shaping, *Scripta Mater* 2003;48:1337–42.
148. M. Roy, V.K. Balla, A. Bandyopadhyay, S. Bose, Compositionally graded hydroxyapatite/tricalcium phosphate coating on Ti by laser and induction plasma, *Acta Biomater* 2011;7:866–73.

149. B. Zheng, T. Topping, J.E. Smugeresky, Y. Zhou, A. Biswas, D. Baker, E.J. Lavernia, The influence of Ni-coated TiC on laser-deposited IN625 metal matrix composites, *Metall Mater Trans A* 2010;41A:568–73.
150. P.P. Bandyopadhyay, V.K. Balla, S. Bose, A. Bandyopadhyay, Compositionally graded aluminum oxide coatings on stainless steel using laser processing. *J Am Ceram Soc* 2007;90-7:1989–91.
151. W. Liu, J.N. DuPont, Fabrication of carbide-particle-reinforced titanium aluminide–matrix composites by laser-engineered net shaping. *Metall Mater Trans A* 2004;35A:1133–40.
152. V.K. Balla, P.D. DeVasConCellos, W. Xue, S. Bose, A. Bandyopadhyay, Fabrication of compositionally and structurally graded Ti–TiO2 structures using laser engineered net shaping (LENS). *Acta Biomater* 2009;5:1831–7.
153. V.K. Balla, P.P. Bandyopadhyay, S. Bose, A. Bandyopadhyay, Compositionally graded yttria-stabilized zirconia coating on stainless steel using laser engineered net shaping (LENS™). *Scripta Mater* 2007;57:861–4.
154. J. Cesarano. Robocasting: New way to fabricate ceramics, n.d. http://www.sandia.gov/media/robocast.htm (accessed August 31, 2014).
155. J. Cesarano. Recent developments in robocasting of ceramics and multimaterial deposition. *Solid Free Fabr Proc*, Austin, TX, 1998:697–703.
156. J.N. Stuecker, J. Cesarano, D.A. Hirschfeld, Control of the viscous behavior of highly concentrated mullite suspensions for robocasting. *J Mater Process Technol* 2003;142:318–25.
157. K. Cai et al., Geometrically complex silicon carbide structures fabricated by robocasting. *J Am Ceram Soc* 2012;95:2660–6.
158. P. Miranda, E. Saiz, K. Gryn, A.P. Tomsia, Sintering and robocasting of β-tricalcium phosphate scaffolds for orthopaedic applications. *Acta Biomater* 2006;2:457–66.
159. J. Russias et al., Fabrication and in vitro characterization of three-dimensional organic/inorganic scaffolds by robocasting. *J Biomed Mater Res A* 2007;83A:434–45.
160. P. Miranda, A. Pajares, E. Saiz, A.P. Tomsia, F. Guiberteau, Mechanical properties of calcium phosphate scaffolds fabricated by robocasting. *J Biomed Mater Res A* 2008;85A:218–27.
161. P. Miranda, A. Pajares, E. Saiz, A.P. Tomsia, F. Guiberteau, Fracture modes under uniaxial compression in hydroxyapatite scaffolds fabricated by robocasting. *J Biomed Mater Res A* 2007;83A:646–55.
162. B. Dorj, J.-H. Park, H.-W. Kim, Robocasting chitosan/nanobioactive glass dual-pore structured scaffolds for bone engineering. *Mater Lett* 2012;73:119–22.
163. B. Dorj, J.-E. Won, J.-H. Kim, S.-J. Choi, U.S. Shin, H.-W. Kim, Robocasting nanocomposite scaffolds of poly(caprolactone)/hydroxyapatite incorporating modified carbon nanotubes for hard tissue reconstruction. *J Biomed Mater Res A* 2013;101A:1670–81.
164. S. Eqtesadi, A. Motealleh, P. Miranda, A. Pajares, A. Lemos, J.M.F. Ferreira, Robocasting of 45S5 bioactive glass scaffolds for bone tissue engineering. *J Eur Ceram Soc* 2014;34:107–18.
165. S. Tarafder, W. Dernell, A. Bandyopadhyay, S. Bose, SrO and MgO doped microwave sintered 3D printed tricalcium phosphate scaffolds: Mechanical properties and in vivo osteogenesis in a rabbit model. *J Biomed Mater Res B* 2015;103(3):679–90.
166. A. Bandyopadhyay, S. Bose, S. Das, 3D printing of biomaterials. *MRS Bull* 2015;40(02):108–15.

6

Design Issues in Additive Manufacturing

Gaurav Ameta

CONTENTS

ABSTRACT This chapter discusses design and modeling issues that are present in additive manufacturing (AM). AM, due to its specific process capabilities, has the ability to produce unique shapes that are either not feasible or cost inefficient with traditional manufacturing. Current traditional design practices are compared with respect to design activities related to AM. Data representation schemes and processing steps for AM are reviewed. Current research challenges and opportunities are summarized, including use of design rules, specification, and verification of quality of AM parts.

6.1 Introduction

Computer-aided design (CAD) systems are software tools that are used to create digital mock-ups of products before manufacturing the product. Such digital mock-ups aid in planning for function, material, shapes, quality, costs, and so on. Such a planning involves studying and developing the design requirements and performing conceptual, preliminary, and detail design. In today's manufacturing, all products are first digitally created using CAD systems and verified for proper function, performance, and assembly. These digital mock-ups are then used to create a manufacturing plan for the product based on materials and shapes specified in the digital mock-ups of the product.

Unlike traditional manufacturing processes, AM is a technique that builds parts layer by layer. AM presents several advantages over traditional manufacturing. These are mass-customizations, aesthetics, part consolidation, weight reduction, functional customizations, and so on [1]. This chapter discusses design for AM and then presents technological and computational challenges in developing tools that can aid in design for AM. Design for AM is a notion that implies considering AM constraints early in the design, viz., preliminary design. Design for AM, if implemented correctly, will reduce the iterations a design needs to undergo before it can be manufactured, thus saving time and money. The next section presents a review of design for AM. Research challenges and opportunities are presented in Section 6.3 followed by conclusion in Section 6.4.

6.2 Design and Processing for AM: Review

Traditionally, AM parts are created by sending digital mock-ups to the AM machine which then creates the parts. The overall flow of traditional design to production compared with the use of AM as prototyping technology is shown in Figure 6.1.

The digital mock-ups sent to the AM machine usually follow a standard format. The digital mock-up is then processed by the AM machine in order to create the product layer by layer based on the specific technology used by the AM machine. In this section, we will

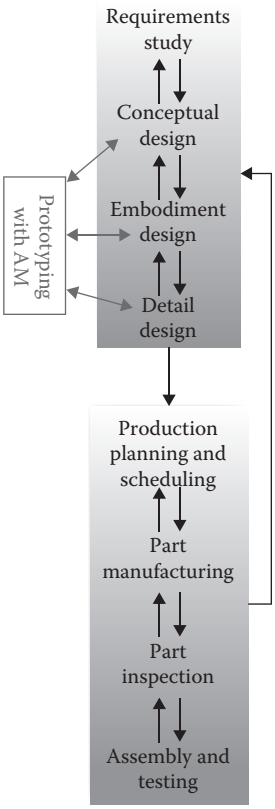

FIGURE 6.1
Traditional design to production processes and use of AM as prototyping technology.

discuss the standards for digital mock-ups and a few examples of the type of processing that the AM machine does. Then, we will discuss the notion of design for AM.

6.2.1 Design Representations for AM

Commonly used standard format for digital mock-ups used in AM is called stereolithography (STL) file format [2]. This format basically consists of triangulated geometry for the part to be created. Each triangle has unit normal and three vertices ordered to follow the right hand rule to find the direction of the normal. The co-ordinates of the vertices are represented in 3D Cartesian coordinates.

The precision of the triangulation and number of triangles in the STL defines the precision with which the part will be produced. Usually large numbers of triangles are needed to approximately represent a freeform surface than a flat surface. Figure 6.2 shows an example of coarse and fine triangulations approximating a section of an adapter tube in an STL file.

The coarse (Figure 6.2a) triangulation has 1,658 triangles, while the fine (Figure 6.2b) triangulation has 19,320 triangles. Variations of STL format include color information in the file for each triangle.

To overcome this limitation of the STL format, the ASTM (American Society of Testing and Materials) standards committee has developed a new standard called AM file (AMF) format. AMF is eXtended Markup Language (XML)-based format and is part of ASTM 2915 standard [3]. XML has the advantage that it can be easily interpreted by computers and can be expanded without affecting backward compatibility of the files. The basic advantage of AMF over STL is the capability to include the following additional information (from STL) regarding the object in the digital file:

- *Color specification*: To support colors in AM parts for the technologies that can utilize colors.
- *Texture maps*: To support different surface textures. This will be used with AM technologies that can utilize textures or colors.
- *Material specification*: To make parts with different materials. This will be used with AM technologies that can use multiple materials for part production.

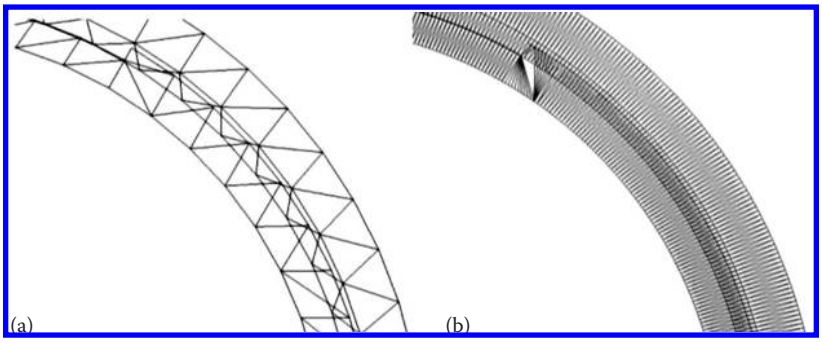

FIGURE 6.2
(a) Coarse and (b) fine triangulations approximating a section of an adapter tube in an STL file. Usually triangulations work well with flat surfaces. For freeform surfaces, large numbers of triangles are needed to approximate the surface.

- *Constellations*: These represent multiple groups of parts manufactured at one time. Constellations can also be used to specify the orientations of the parts when they are manufactured.
- *Additional meta-data*: Meta-data can contain any kind of information that the designer would like to include with the file.
- *Formulas*: Any equations representing surface geometry or equations that should govern the construction of support structures for AM production can be included.
- *Curved triangles*: To specify the surface accurately with less number of triangles. Curved Bezier or b-spline triangles can be used to mathematically represent different types of freeform surfaces in the AMF file.

Although AMF is developed keeping backward compatibility with STL, industry adoption of AMF will be a critical issue in the success of AMF format [4].

Another format for AM was proposed by 3D Systems in 1994 and was called SLiCe (SLC) format [5]. SLC format consists of contours of the digital model for each slice that needs to be made in using AM [6]. The main disadvantage was that such slice information was not sufficient for all types of AM technologies.

6.2.2 Processing for AM

Overall steps required to create a given part after receiving STL file are shown in Figure 6.3. The digital mock-up in the form of STL file is imported in the native application for the AM technology. Usually, the user can now visualize in the native application to input desired orientation and location of the part with respect to the build volume in the particular

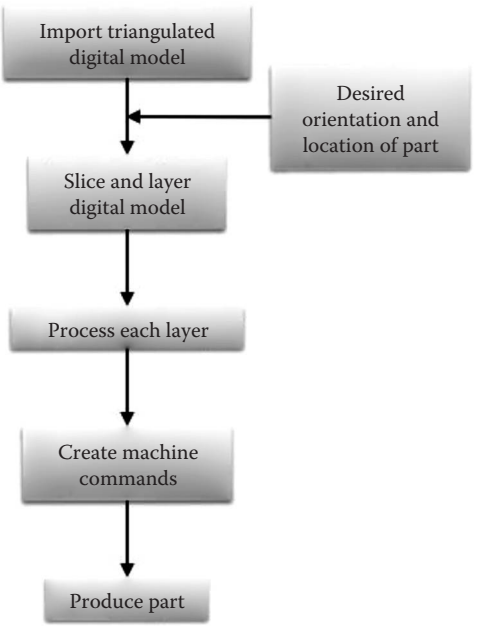

FIGURE 6.3
Steps for processing a digital model into a physical part using AM technology.

AM process. The STL file and the user input are taken together in order to build slices of the digital mock-up. These slices create layers to be used in the AM process for producing the part. Although there are techniques to create the slices directly from CAD model [7–10] without creating a STL file, these techniques are not commercially popular. Further processing of each layer may be required based on the particular AM technology. Some AM technology requires building support structures with same materials as the part while others can use different materials. Other AM technologies need to process each layer to create profile of the path that would be traversed by the AM technology.

These processed layers and related information are then used to create machine commands that will be passed to the AM technology in order to produce the part. In this process, there are usually issues with slicing and support structure building from the STL file. These issues are further discussed in the subsections 6.2.2.1 and 6.2.2.2.

6.2.2.1 Slicing and Layering

Slicing of STL representation of the digital model is done to create layers. The basic method of slicing is by using two parallel planes based on the orientation of the digital model. The STL representation is then intersected with these two parallel planes. The distance between the two parallel planes is usually the desired layer thickness for AM part. The intersection of each plane with triangles from STL file will result in a set of lines and/or points. The set of lines and/or points is then used to generate a contour of the slice. This contour is the layer that needs to be created by the AM process. Various algorithms and issues in this area have been addressed by researchers in the last two decades (e.g., [11–14]). Examples of the issues are (1) two intersecting contour in one layer, (2) thin features in a layer, and (3) non-manifold objects created as a result of intersection process. These three issues are highlighted in Figure 6.4. A 3D model of Utah Teapot [15] is shown in Figure 6.4a. Slices of the 3D model result in different types of issues, which are shown in Figure 6.4b–d. Figure 6.4b shows three contours that are 2d surfaces. Two

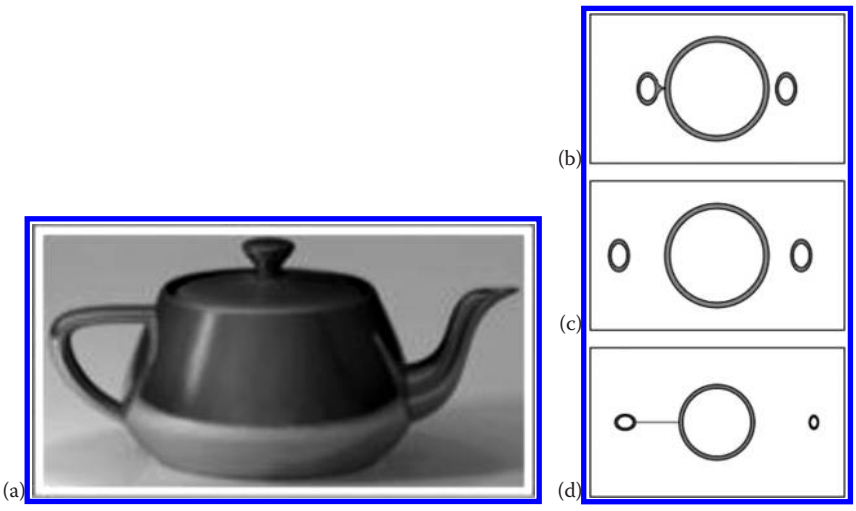

FIGURE 6.4
(a) A 3D model of Utah Teapot (Data from "Utah Teapot," http://commons.wikimedia.org/wiki/File:Utah_teapot_simple_2.png, 2014.); (b), (c), and (d) slices at different positions of the Utah Teapot showing two intersecting contours, three disjoint contours, and a non-manifold line connecting two contours, respectively.

of the contours are connected or attached together by a point. A point is a dimensionless entity and therefore cannot be made in AM technology. Figure 6.4d shows three contours (2d surfaces), two of which are connected or attached together by a line (1d geometric entity), leading to a non-manifold set of shapes.

Furthermore, if these slices were generated using approximated triangles (STL format) of the model, various issues of connectivity of the triangles and creation of contours due to the number of floating points handled by the computers arise. Some of these issues are disjointed triangles, open contours, and so on [16,17].

These issues are currently handled using heuristics by the processing software based on the choices made by the programmer. Certain choices may work in some scenarios, while the same choices may not work in others [18].

6.2.2.2 Support Structure Generation

After generating the layers using slices as discussed in the previous section, the next task may involve generating support structures based on the particular AM technology (e.g., fused deposition modeling, STL). For generating support structure, information regarding the material properties (usually strength and weight) and geometry of subsequent layers at the time of layer construction has to be computed beforehand. If there are overhang features in consecutive layers, the weight and strength are used to identify if a support structure will be needed or not [19,20]. This is demonstrated in Figure 6.5.

6.2.3 Design for AM

AM is unique in the fact that it can produce surfaces and features that are not feasible using traditional manufacturing techniques. Examples of such features include lattice structures, internal cavities of different shapes and forms, assembly parts manufactured at once, and porous parts [21]. Due to these additional capabilities, designers need tools to be able to utilize the capabilities in optimizing their design. One such technique used by designers is topology optimization [22,23]. Topology optimization utilizes different mathematical techniques to identify the location of material and holes from a preliminary identification of location of loads and constraints in a part or assembly. Various examples of application of topology optimization for AM are present in the literature [24–26]. An example of a

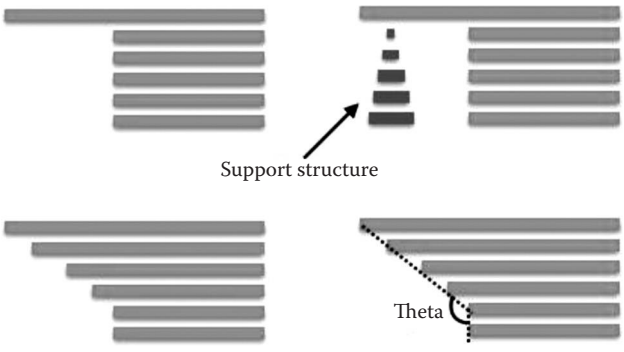

FIGURE 6.5
Examples showing how decisions are made regarding support structure creation. Either support structure is needed based on the geometry and design or based on the angle of overhang in subsequent layers, weight of overhang, and strength of the material support structure may be avoided.

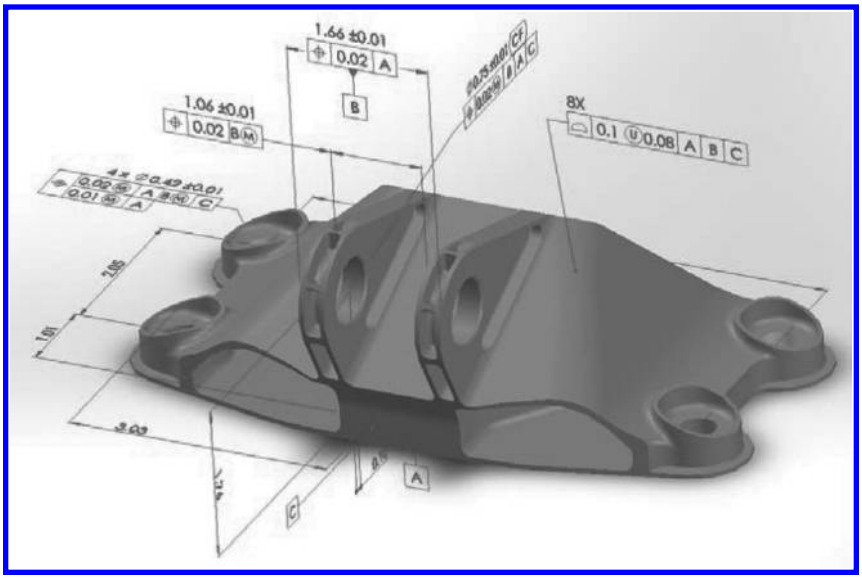

FIGURE 6.6
Bracket design based on topology optimization. (Design inspired from Keulen, F.V., Langelaar, M., and Baars, G.E., "Topology optimization and additive manufacturing, natural counterparts for precision systems—State-of-the-art and challenges," *29th American Society of Precision Engineering Annual Meeting*, 2014, http://www.aspe.net/publications/Short%20Abstracts%2014SP/3946.pdf.)

bracket designed using topology optimization for AM is shown in Figure 6.6. The surfaces of this topology optimized part will be very time consuming and highly cost inefficient using traditional manufacturing techniques.

6.3 Research Challenges and Opportunities

To represent research challenges and opportunities in AM, two aspects are considered in this section: first, design rules and tools for AM and second, specification and verification for AM.

6.3.1 Design Rules and Tools for AM

Currently, CAD designers use meshed results from topology optimized parts to create realistic shapes based on their intuition. Lack of design tools to directly validate, analyze, and utilize topology optimized shapes in AM hampers faster progress in this field. To create CAD tools to enable design for AM will require development of process- and product-level understanding of variations related to AM technologies. Seepersad in [28] lays down the main guidelines to develop design for AM rules. These rules are focused on the stage of the design. In conceptual design, the designers are asked to avoid fixation on current designs and avoid considering current design for manufacturing and assembly rules. In embodiment design, the designers need tools that can model and optimize part topology, can model material distributions, and can model complex shapes and structures. Furthermore, these tools need to include AM process-specific constraints while designing parts.

6.3.2 Porous Parts and Lattice Structures

Many researches in AM have pointed toward the capability of manufacturing porous, scaffolds, and lattice structures that are lightweight and strong. Porous and scaffolds have been demonstrated for biomaterials application using AM techniques for more than a decade [29–31]. Figure 6.7 [30] shows a sample part with porous and solid ceramic section. This part is made for bio-applications.

Lattice-based structures have recently been proposed with the main consideration in automotive and aerospace industry. [32] shows an optimized lattice structure for hull created to be manufactured using AM technology. Design tools for creating optimal lattice structures are currently not available.

6.3.3 Multi-Material Parts

Recently, multi-material-based fabrication using AM has been demonstrated [33–35]. Even commercial plastics-based 3D printers are available in the market [36]. These types of multi-material parts can have different materials at different locations of a single part. These parts are not alloys, are not welded together, and are not even categorized as composites. The multi-material parts are built using AM. Researchers from MIT have demonstrated in [37] production of parts that are multi-material, that can follow a given deformation profile, and that can even have a given texture on the surface.

In [37], the authors have demonstrated a simple but powerful design tool to create these multi-material basic parts. Design tools that can provide the flexibility of using different materials and different lattice/cellular structures at different locations of complex parts are not yet available. There is a need for such tools in order to facilitate further innovations in the application of AM technology.

6.3.4 Quality Specification and Verification for AM

In traditional manufacturing, quality of each part is very critical in proper functioning of the product. Due to the capability of AM to produce complex shapes and internal

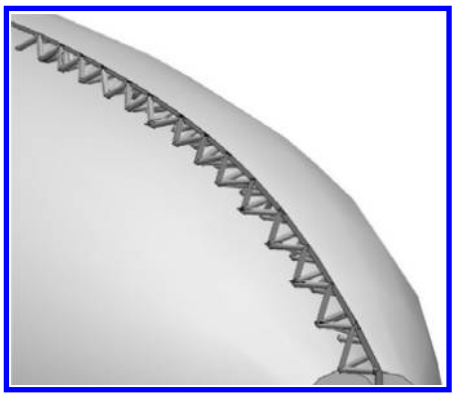

FIGURE 6.7
Lattice structure of hull designed for AM. (Data from Nguyen, J.M., "A heuristic optimization method for the design of meso-scale truss structure for complex-shaped parts," M.S. Thesis, Georgia Institute of Technology, Atlanta, GA, 2012. https://smartech.gatech.edu/bitstream/handle/1853/44810/nguyen_jason_n_201208_mast.pdf.)

structures, the quality specification and verification methods need to be modified so that they can be applied to AM. Part quality implies many aspects, such as material, dimensional, geometric, and surface. The quality of a part in these aspects is specified by a designer, is followed by a manufacturing, and then, is verified by a part/product inspector. Material quality is verified through ASTM standards [38]. Dimensional, geometric [39,40], and surface [41] quality is specified and verified [42] using ASME (American Society of Mechanical Engineers) and ISO (International Standards Organization) standards. These standards are developed for parts that are produced using traditional manufacturing. Since AM can produce shapes, material, and structures that are not feasible in traditional manufacturing, new methods of specifying quality (by a designer) and verifying the quality (by a part/product inspector) are needed for AM parts. Furthermore, in-process AM quality techniques need to be developed so a manufacturer can keep his parts within the specified quality required.

6.4 Conclusions

AM is a technique that has been in existence for several decades. Technological innovations have enabled the use of AM for metals at lower costs and have brought this process into small businesses. Due to different capabilities of AM process, it can create shapes and parts that are not feasible through traditional manufacturing. Therefore, design methods need to be adapted for AM. Specifically, new design rules and tools are needed to (1) utilize topology optimization directly for part design, (2) use lattice and cellular structures in part design, and (3) use multi-material and different material distributions in part design. Current methods of specifying and verifying product quality are not sufficient to specify and verify the shapes and parts that can be produced using AM. Therefore, product quality specification and verification methods should be adapted to include the capabilities of AM techniques.

References

1. Quarshie, R., Machachlan, S., Reeves, P., Whittaker, D., and Blake, R., *Shaping Our National Competency in Additive Manufacturing*. The Additive Manufacturing Special Interest Group for the Technology Strategy Board, 2012. https://connect.innovateuk.org/documents/2998699/3675986/UK+Review+of+Additive+Manufacturing+-+AM+SIG+Report+-+September+2012.pdf/a1e2e6cc-37b9-403c-bc2f-bf68d8a8e9bf.
2. 3D Systems, *Stereolithography Interface Specification*, 3D Systems, Valencia, CA, 1988.
3. ASTM ISO/ASTM52915-13, *Standard Specification for Additive Manufacturing File Format (AMF) Version 1.1*, ASTM International, West Conshohocken, PA, 2013, http://www.astm.org/.
4. Climatro Limited Press Release, *ClimatronE to Support AMF Format for 3D Printing*, January 21, 2014. http://www.cimatron.com/Group/pressreleases.aspx?FolderID=3099&docID=23413&lang=en.
5. 3D Systems, *SLC File Format Information*, p/n 50065-S03-00, 3D Systems, Valencia, CA, 1994.
6. SLC-SLiCe Format, Web article, http://paulbourke.net/dataformats/slc/, accessed April 2014.
7. Sun, S.H., Chiang, H.W., and Lee, M.I., "Adaptive direct slicing of a commercial CAD model for use in rapid prototyping," *International Journal of Advanced Manufacturing Technology*, Vol. 34, 2007, pp. 689–701.

8. Cao, W. and Miyamoto, Y. "Direct slicing from autoCAD solid models for rapid prototyping," *International Journal of Advanced Manufacturing Technology*, Vol. 21, 2003, pp. 739–742.
9. Jamieson, R. and Hacker, H., "Direct slicing of CAD models for rapid prototyping," *Rapid Prototyping Journal*, Vol. 1(2), 1995, pp. 4–12.
10. Starly, B., Lau, A., Sun, W., Lau, W., and Bradbury, T., "Direct slicing of STEP based NURBS models for layered manufacturing," *Computer-Aided Design*, Vol. 37, 2005, pp. 387–397.
11. Pandey, P.M., Reddy, N.V., and Dhande, S.G., "Slicing procedures in layered manufacturing: A review," *Rapid Prototyping Journal*, Vol. 9(5), 2003, pp. 274–288.
12. Fadel, G.M. and Kirschman, C., "Accuracy issues in CAD to RP translations," *Rapid Prototyping Journal*, Vol. 2(2), 1996, pp. 4–17.
13. Wang, P., Xiang, C., and Li, Z.H., "Optimization and application of STL model slicing algorithm in rapid prototyping," *Advanced Materials Research*, Vol. 605, 2013, pp. 669–672.
14. Gupta, V., Bajpai, V.K., and Tandon, P., "Slice generation and data retrieval algorithm for rapid manufacturing of heterogeneous objects," *Computer-Aided Design and Applications*, Vol. 11(3), 2014, pp. 255–262.
15. Dhatfield., "Utah Teapot," http://commons.wikimedia.org/wiki/File:Utah_teapot_simple_2.png, accessed April 2014.
16. Szilvsi-Nagy, M., "Analysis of STL files," *Mathematical and Computer Modeling*, Vol. 38(7–9), 2003, pp. 945–960.
17. Yau, H.-T., Kuo, C.-C., and Yeh, C.-H., "Extension of surface reconstruction algorithm to the global stitching and repairing of STL models," *Computer-Aided Design*, Vol. 35(5), 2003, pp. 477–486.
18. Huang, Pu, Wang, C.C.L., and Chen, Y., *Algorithms for Layered Manufacturing in Image Space*. ASME Press, 2014.
19. Huang, X., Ye, C., Wu, S., Guo, K., and Mo, J., "Sloping wall structure support generation for fused deposition modeling," *International Journal of Advanced Manufacturing Technology*, Vol. 42(11–12), 2009, pp. 1074–1081.
20. Kirschman, C.F., Jara-Almonte, C.C., Bagchi, A., Dooley, R.L., and Ogale, A.A., "Computer aided design of support structures for stereolithographic components," *Proceedings of the ASME Computers in Engineering Conference*, Santa Clara, CA, pp. 443–448, 1991.
21. "Additive manufacturing: opportunities and constraints: A summary of a roundtable forum held on May 23, 2013 hosted by the Royal Academy of Engineering," http://www.raeng.org.uk/publications/reports/additive-manufacturing.
22. Bendsoe, M.P. and Sigmund, O., *Topology Optimization: Theory, Methods, and Applications*, Springer, Berlin, Germany, 2011, 370pp.
23. Brackett, D., Ashcroft, I., and Hague, R., "Topology optimization for additive manufacturing," *Proceedings of the Solid Freeform Fabrication Symposium*, Austin, TX, 2011, pp. 348–362.
24. Keulen, F.V., Langelaar, M., and Baars, G.E., "Topology optimization and additive manufacturing, natural counterparts for precision systems—State-of-the-art and challenges," *29th American Society of Precision Engineering Annual Meeting*, 2014, http://www.aspe.net/publications/Short%20Abstracts%2014SP/3946.pdf.
25. Meisel, N.A., Gaynor, A., Williams, C.B., and Guest, J.K., "Multiple-material topology optimization of compliant mechanisms created via polyjet 3d printing," *24th International Solid Freeform Fabrication Symposium*, 2013, http://utwired.engr.utexas.edu/lff/symposium/proceedingsArchive/pubs/Manuscripts/2013/2013-78-Meisel.pdf.
26. Vayre, B., Vignat, F., and Villeneuve, F., "Designing for additive manufacturing," *Procedia CIRP*, Vol. 3, 2012, pp. 632–637.
27. http://grabcad.com/library/topology-optimized-bracket-v5-official-1, accessed June 26, 2015.
28. Seepersad, C.C., "Design for additive manufacturing: Opportunities, barriers and democratization," National Academy of Engineering, Irvine, CA, April 26–28, 2013. http://www.naefrontiers.org/File.aspx?id=39135, accessed June 2014.
29. Bose, S., Roy, M., and Bandyopadhyay, A., "Recent advances in bone tissue engineering scaffolds," *Trends in Biotechnology*, Vol. 30(10), 2012, pp. 546–554.

30. Bose, S., Suguira, S., and Bandyopadhyay, A., "Processing of controlled porosity ceramic structures via fused deposition," *Scripta Materialia*, Vol. 41(9), 1999, pp. 1009–1014.
31. Hutmacher, D.W., "Scaffold design and fabrication technologies for engineering tissues—State of the art and future perspectives," *Journal of Biomaterials Science, Polymer Edition*, Vol. 12(1), 2001, pp. 107–124.
32. Nguyen, J.M., "A heuristic optimization method for the design of meso-scale truss structure for complex-shaped parts," M.S. Thesis, Georgia Institute of Technology, Atlanta, GA, 2012. https://smartech.gatech.edu/bitstream/handle/1853/44810/nguyen_jason_n_201208_mast.pdf.
33. Hofmann, D.C., Roberts, S., Otis, R., Kolodziejska, J., Dillon, R.P., Suh, J., Shapiro, A.A., Liu, Z., and Borgonia, J., "Developing gradient metal alloys through radial deposition additive manufacturing," Scientific Reports, 2014/06/19/online, Vol. 4, Macmillan Publishers. http://www.nature.com/srep/2014/140619/srep05357/abs/srep05357.html.
34. Ott, M. and Zaeh, M.F., "Multi-material processing in additive manufacturing," *21st International Solid Freeform Fabrication Symposium*, 2010, http://utwired.engr.utexas.edu/lff/symposium/proceedingsArchive/pubs/Manuscripts/2010/2010-18-Ott.pdf.
35. SpaceX, "Dragon version 2: Spacex's next generation manned spacecraft," 2014, *SpaceX News Article*, http://www.spacex.com/news/2014/05/30/dragon-v2-spacexs-next-generation-manned-spacecraft.
36. Stratasys, "Object Connex 500 3D printer," http://www.stratasys.com/3d-printers/design-series/precision/objet-connex500.
37. Chen, D., Levin, D.I.W., Didyk, P., Sitthi-Amorn, P., and Matusik, W., "Spec2Fab: A reducer-tuner model for translating specifications to 3D prints," *ACM Transactions on Graphics*, Vol. 32(4), 2013, pp. 135:1–135:10.
38. American Society of Testing and Materials, www.astm.org/Standards.
39. ASME. *Dimensioning and Tolerancing*, ASME Y14.5–2009 standard, ASME, New York, 2009.
40. ISO 1101:2012, "Geometrical product specifications (GPS)—Geometrical tolerancing—Tolerances of form, orientation, location and run-out," International Organization for Standardization, Geneva, Switzerland, 2012.
41. ASME. *Surface Texture (Surface Roughness, Waviness, and Lay)*, ASME B46.9–2009 standard, ASME, New York, 2009.
42. ASME. *Measurement Uncertainty Standards and Guidelines*. ASME B89.7, ASME, New York. http://files.asme.org/Catalog/Codes/PrintBook/25586.pdf.

7

Bioprinting: Application of Additive Manufacturing in Medicine

Forough Hafezi, Can Kucukgul, S. Burce Ozler, and Bahattin Koc

CONTENTS

ABSTRACT The main goal of tissue or organ engineering is to reconstruct a damaged or diseased tissue or organ with cells, biomaterials, and bioactive molecules. Recently, many tissue engineering approaches are based on developing highly porous tissue scaffolds and seeding cells into the scaffold with or without biologically active molecules to reinstate damaged tissue or organ. Various additive manufacturing (AM) methods have been used successfully to develop scaffolds with controlled microarchitecture and geometry. However, scaffold-based approaches still face some challenges such as difficulty in seeding different cells spatially in a scaffold, limited vascularization and blood vessel formation, and weak cell adhesion to scaffold material. This chapter focuses on bioprinting, a special AM technique, for tissue/organ engineering. Bioprinting or biofabrication creates complex living and non-living biological products from living cells, biomolecules, and biomaterials. Various bioprinting techniques are discussed and contrasted in this chapter.

7.1 Introduction

Over the past few decades, tissue engineering has grown as a new inter- and multidisciplinary scientific field to reinstate damaged or diseased tissue with the combination of functional cells and/or biodegradable scaffolds with engineered biomaterials (Langer and Vacanti 1993). The basic concept of traditional tissue engineering methods is to seed living cells and/or

biologically active molecules into a highly porous scaffold to fix and/or regenerate damaged tissues (Bonassar and Vacanti 1998). A highly porous scaffold is required to make both mass transfer and cell incorporation possible. Traditionally, particulate leaching, solution casting, gas foaming, phase separation, freeze–drying, and melt molding processes have been used for scaffold fabrication (Leong et al. 2003; Pham et al. 2006; Hafezi et al. 2012). However, these methods generally lack no or little control over pore size, geometry, and interconnectivity. Recently, various AM techniques have been used to produce scaffolds with controlled microarchitecture and geometry (Yeong et al. 2004; Lee et al. 2008; Peltola et al. 2008; Khoda et al. 2011; 2013a, 2013b; Ozbolat and Koc 2011). Regardless of the successful scientific outcomes of scaffold-based approaches, these methods still face some challenges. First, the cell growth and proliferation in a scaffold might take long time because of weak cell adhesion to the scaffold. Second, organs and tissues are generally complex structures containing different cell types. Placement of cells within scaffolds is essentially random process. It is very challenging to seed different cell types spatially into a scaffold and provide necessary cell-to-cell interaction to form desired tissue. Moreover, most of scaffold-based approaches suffer from the absence of built-in vascularization. Vascularization and new blood vessel formation are compulsory to provide nutrients and oxygen to the cells for a successful tissue or organ engineering. Hence, living cells alone or in combination of biomolecules and biomaterials need to be assembled in three dimensions for a successful tissue or organ engineering.

This chapter focuses on bioprinting, a special AM technique, for tissue/organ engineering. Bioprinting or biofabrication is defined as the production of complex living and nonliving biological products from living cells, biomolecules, and biomaterials (Derby 2008; Mironov et al. 2009). Bioprinting combines both fundamental science and technologies of AM, materials, and biological sciences (Figure 7.1).

In spite of the extensive variety of AM techniques, just few of them are suitable for bioprinting. Similar to other AM processes, 3D living structures are built layer by layer using bioprinting methods. Most of the bioprinting methods employ ink-jet (Nakamura et al. 2005; Xu et al. 2005; Calvert 2007), photolithography/two photon polymerization (2PP) (Cooke et al. 2003; Arcaute et al. 2006; Schade et al. 2010), direct laser printing

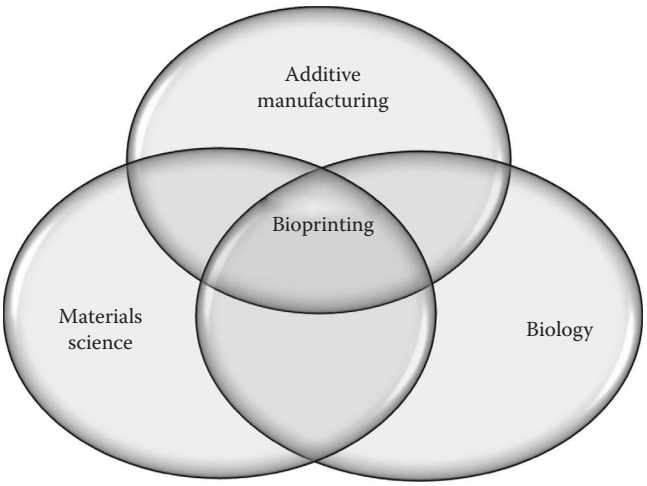

FIGURE 7.1
The main disciplines contributing to the emergence of bioprinting: additive manufacturing, cell and developmental biology, and biomaterials science

(Barron et al. 2004a, b; Yuan et al. 2008; Guillotin et al. 2010), extrusion/deposition (Smith et al. 2007; Skardal et al. 2010) or direct cell printing, and self-assembly (Mironov et al. 2003, 2008; Norotte et al. 2009) techniques. Figure 7.2 shows the schematic representation of various bioprinting methods. The details of each of these methods are discussed below.

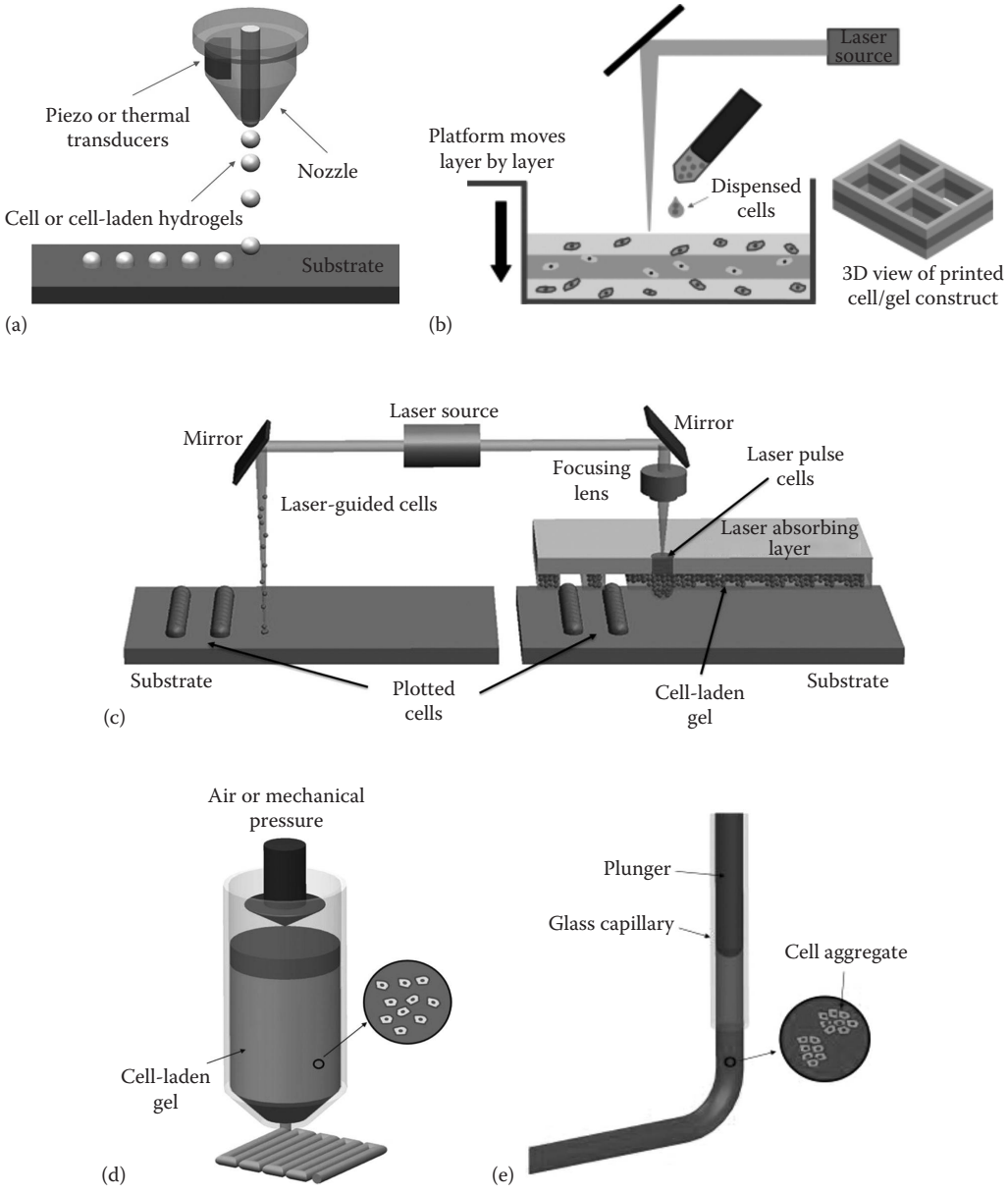

FIGURE 7.2
(See color insert.) (a) Thermal and piezoelectric ink-jet bioprinting. (b) Stereolithography-based bioprinting. (c) Laser-based bioprinting setup. Left: Laser-guided direct cell printing. Right: The cell–hydrogel compound is propelled forward as a jet by the pressure of a laser-induced vapor bubble. (d) Extrusion/deposition-based bioprinting. (e) Direct cell-aggregate deposition.

7.2 Bioprinting Methods

7.2.1 Ink-Jet Printing

Ink-jet bioprinting is likely one of the most commonly used biofabrication methods because of its distinctive characteristics of high-throughput efficiency, cost-effectiveness, and full automation (Boland et al. 2006). Traditionally, ink-jet printing is used to reproduce digital image data on a substrate through applying picoliter ink droplets. The technique can be classified into continuous ink-jet (CIJ), where a stable flow of small droplets made by fluid instability on a passage through a nozzle is either deviated by an electrostatic field onto a substrate or not deviated and gathered for reutilization, and drop-on-demand (DOD) ink-jet, where ink droplets are only produced when needed. Since CIJ needs electrically conducting ink formulations, there is a contamination risk on ink recycling so that makes the technique not useful cell printing. Therefore, only DOD ink-jet as shown in Figure 7.2a has been used in bioprinting up to now.

Boland and his colleagues (2003) used thermosensitive gels to make consecutive layers on top of each other for 3D cellular assemblies with bovine aortal endothelial cells. They observed that during consecutive culture of the tissue engineered construct, cells fused to each other within the hydrogel. Cooper and colleagues demonstrated that spatial control of osteoblast differentiation in vitro and bone formation in vivo is possible via applying ink-jet bioprinting technology. They showed that it is possible to create 3D persistent bio-ink patterns of bone morphogenetic protein-2 (BMP-2) and its modifiers inactivated within microporous scaffolds via using ink-jet bioprinting techniques. Semicircular patterns of BMP-2 were printed within human allograft scaffold constructs. They demonstrated that patterns of bone formation in vivo were comparable with patterned responses of osteoblastic differentiation in vitro (Cooper et al. 2010). Ink-jet printers can also be used to deliver drugs or other active biomolecules along with cells. However, shear stress during the process could cause degradation of enzyme activity corresponding to the voltage applied for printing (Cook et al. 2010). Ola Hermanson and colleagues used an ink-jet printer to print biologically active macromolecules on polyacrylamide-based hydrogels, which were subsequently seeded with primary fetal neural stem cells. They observed that ink-jet printing can successfully be combined with gene delivery to achieve effective control of stem cell differentiation (Ilkhanizadeh et al. 2007). Although ink-jet bioprinting has been one of the most commonly used method in printing living cells and biomaterials, the technology still faces many challenges. Considering the fact that inkjet printers need cells to be suspended in liquid, cell aggregation and sedimentation are intrinsic weaknesses of the system (Parsa et al. 2010). Because of the high shear stress during printing, cell survivability and degradation of biomolecule activity are other drawbacks related to ink-jet-based bioprinting.

7.2.2 Photolithography and 2PP

Photolithography or stereolithography (SLA) is another AM technique used for bioprinting (Melchels et al. 2010). Most of the SLA-based bioprinting setups used are similar to the ones first developed (Cooke et al. 2003; Dhariwala et al. 2004). Applying a computer-controlled laser beam to sketch a pattern, cell-laden structures are built bottom-up from a support platform that lies beneath the resin surface as shown in Figure 7.2b.

Arcaute and her research group (2006) showed that it is possible to change the resolution of the cure depth by changing the laser energy, the concentration of poly(ethylene glycol)

dimethyacrylate (PEG-DMA) as photocross-linkable material, and the type and concentration of the photoinitiator. In Arcaute et al. (2010), the same group later fabricated a bioactive scaffold via using SLA techniques. Human dermal fibroblast cells were seeded on top of the fabricated scaffolds. They applied fluorescent microscopy so that they could observe specific localization of cells in the regions patterned with bioactive PEG (Arcaute et al. 2010).

2PP is another emerging photolithography-based technique. In this process, light is applied to trigger a chemical reaction leading to polymerization of a photosensitive material. 2PP initiates the polymerization through irradiation with near-infrared femtosecond laser pulses of 800 nm (Liska et al. 2007).

Recently, Ovsianikov and the colleagues (2011a, b) fabricated 3D poly(ethylene glycol) diacrylate (PEG-DA) scaffolds for tissue engineering by means of 2PP. Fabricated scaffold was reproducible and it was suitable for investigation of cellular processes in three dimensions and for better understanding of in vitro tissue formation. The results of their work suggest that 2PP may be used to polymerize PEG-based materials into 3D structures with well-defined geometries that mimic the physical and biological properties of native cell environment (Ovsianikov et al. 2011b). The researchers also fabricated methacrylamide modified gelatin (GelMOD) scaffolds for tissue engineering applications through using 2PP. The results demonstrated that the fabricated scaffolds are suitable to support porcine mesenchymal stem cell adhesion and subsequent proliferation (Ovsianikov et al. 2011a).

7.2.3 Direct Laser Printing

Patterning cells with the help of laser light has been one of the first methods for 2D cell patterning. Various methods by use of laser have been used to move cells for patterning (Figure 7.2c). The most commonly used laser-based direct-write techniques for cellular applications are laser-induced forward transfer (LIFT), absorbing film-assisted LIFT (AFALIFT), laser-guided direct writing (LG DW), matrix-assisted pulsed laser evaporation direct writing (MAPLE DW), and biological laser processing (BioLP). LIFT, AFA-LIFT, BioLP, and MAPLE DW have some distinct similarities in methodology for the direct writing of cells. These direct-write techniques utilize laser transparent print ribbons on which one side is coated with cells that are either adhered to a biological polymer through initial cellular attachment or uniformly suspended in a thin layer of liquid (usually cell culture medium mixed with glycerol) or a hydrogel. A receiving substrate is coated with a biopolymer or cell culture medium to maintain cellular adhesion and sustained growth, mounted on motorized stages, and positioned facing the cell-coated side of the ribbon. A pulsed laser beam is transmitted through the ribbon and is used to propel cells from the ribbon to the receiving substrate. The rapid volatilization of the cellular support layer on the ribbon creates the force necessary to allow the cells to cross the small (700–2000 μm) gap between the ribbon and receiving substrate.

Ovsianikov and colleagues (2010) applied LIFT for cell printing purposes. They demonstrated that in order to control cell migration and cellular interactions within the scaffold, novel technologies capable of producing 3D structures in accordance with predefined design are required. Hence, they first used 2PP technique for the fabrication of scaffolds. Cells were then seeded into the scaffold by means of LIFT. They showed that with this technique printing of multiple cell types into 3D scaffolds is possible. Combination of LIFT and 2PP provides a route for the realization of 3D multicellular tissue constructs and artificial extracellular matrix (ECM) engineered at a microscale. Guillemot and colleagues (2011) applied AFALIFT for cell printing. They demonstrated that applying AFALIFT technique avoids the printing of undesired debris produced by a metallic interlayer because of potential harm to cell biology in the long term.

LGDW of living cells was developed in 1999 (Odde 1999; Odde et al. 2000). Here, cells drifting by natural convection in the fluid medium were directly deposited onto an untreated glass surface by the laser. The laser beam continuously captures cells as they drifted into the light path, pulls the cells into the center of the beam where the intensity is maximal, and pushes them through the fluid medium along the beam axis onto the target surface. When the desired amount of cells, either a single cell or a number of cells, had been deposited in one spot with a spot size of 10 μm, the focusing lens was translated to move the focal point to a new spot. The terminology *direct writing* indicates that no mask or similar film is used in this process. In 2005, Yaakov Nahmias and colleagues demonstrated that the LGDW can pattern multiple cell types with micrometer resolution on arbitrary surfaces including biological gels. They applied LGDW in order to seed human umbilical vein endothelial cells (HUVEC) in two and three dimensions with micrometer accuracy. Via patterning HUVEC on matrigel, they could direct their self-assembly into vascular structures along the desired pattern. Finally, co-culturing the vascular structures with hepatocytes resulted in an aggregated tubular structure similar in organization to a hepatic sinusoid (Nahmias et al. 2005). Jason A. Barron and colleagues (2004a, b) applied another laser-based writing, MAPLE DW, to rapidly and accurately deposit mammalian cells. Recently, Bruce and colleagues also used a similar method, cell deposition microscope based on the laser-guidance technique, in which they can micropattern individual cells to specific points on a substrate with high spatial resolution. Their deposition microscope was capable of patterning different cell types onto and within standard cell research devices and providing on-stage incubation for long-term cell culturing (Ma et al. 2011). Similar to other laser-based writing methods, Wu and colleagues applied biological laser printing (BioLP) in order to fabricate branch/stem structures of HUVEC and human umbilical vein smooth muscle cells. They mimicked vascular networks in natural tissue but also allow cells to develop new and finer structures away from the stem and branches (Wu et al. 2010). Guillotin and his research group (2011) also printed human endothelial cells from an alginate ink as well as deposition of nano-particulate hydroxyapatite by BioLP. Pirlo et al. (2006) designed a laser cell deposition system where they apply laser to locate single cells at particular points in a multiplicity of in vitro environments. Finally, from the results they reached to this point that laser cell deposition system can achieve time-specific placement of an individual cell in a cell culture for the systematic investigation of cell–cell and cell–ECM interactions (Pirlo et al. 2006).

Laser-based cell writing methods are very versatile and can precisely pattern the cells. However, most of these methods are limited to 2D patterning and it is difficult to fabricate 3D tissue constructs. Another drawback of laser-based cell writing methods is cell injury due to the process-induced mechanical stress during the cell droplet formation and landing processes. The thermal stress and ultraviolet radiation caused by laser printing could also affect the cell viability.

7.2.4 Extrusion Printing

7.2.4.1 Cell-Laden Printing

The main principle of extrusion-based bioprinting techniques is to force continuous filaments of a material through a nozzle in a controlled manner to construct a 3D structure (Figure 7.2d). For the purpose of extrusion printing of cells, the material normally includes an extremely viscous cell-laden hydrogel (Fedorovich et al. 2007), which have the ability to flow from the nozzle without applying high temperatures. After the material is deposited

and become a solid via thermal, physical, or chemical methods, it provides adequate mechanical integrity to fabricate 3D structures. The bioprinter design here is normally simple, including a three-axis robot that controls the motions of either pneumatically or volumetrically driven displacement pens or syringes with a typical nozzle diameter of 150–500 μm. Landers and Mülhaupt (2000) at the Freiburg Research Center developed an extrusion-based bioprinting process called bioplotting. Bioplotting is a biofabrication technology based on the extrusion of continuous filaments. The 3D fabrication happens in layer-by-layer fashion through the computer-controlled deposition of material on a surface. The dispensing head moves in three dimensions, whereas the fabrication platform is immobile. It is feasible to carry out either discontinuous dispensing of microdots or a continuous dispensing of microstrands. Landers and his colleagues used the developed bioplotter for printing hydrogel scaffolds with encapsulated cells. Fedorovich and his research group (2008) also used the similar bioplotter for bone tissue engineering. They showed the maintenance of spatially organized, osteo and endothelial progenitor cells in printed grafts after in vivo implantation for the first time (Fedorovich et al. 2011). This 3D bioplotter technology is commercialized by Envisiontec (envisiontec.com).

Smith and his colleagues also used a commercial extrusion-based printer developed by nScrypt (nscrypt.com) and they deposited cold (2°C–10°C) solutions of either human fibroblasts encapsulated in Pluronic-F127, or bovine aortic endothelial cells in type I collagen, onto heated substrates where solidification of the printed structures was induced by thermal gelation of the biopolymers. Applying low temperatures has resulted in low cell viabilities (Smith et al. 2004). Significantly, Smith's work indicated that CAD/CAM technology could be used to deposit cell-laden structures mimicking a vascular structure.

Butcher and colleagues applied 3D bioprinting to fabricate living alginate/gelatin hydrogel valve conduits with anatomically correct architecture and direct incorporation of dual cell types. The researchers used a modified fab@home printer for printing hydrogels encapsulated with cells. After bioprinting, encapsulated aortic root sinus smooth muscle cells and aortic valve leaflet interstitial cells (VIC) were viable within alginate/gelatin hydrogel discs over 7 days in culture (Duan et al. 2013) (Figure 7.3).

Extrusion-based bioprinters have also been used for printing stem cell-laden hydrogels. Xu et al. (2009) demonstrated that adipose-derived stem cells (ASCs) printed in gelatin/alginate/fibrinogen gels have the ability to differentiate into endothelial cells at the walls of printed channels. They used a bioprinter with two nozzles controlled by a computer called cell-assembler for printing a 3D structure, which consisted of square grids and orderly channels. The same group also used adipose-derived stromal cells combined within a gelatin/alginate/fibrinogen hydrogel to form a vascular-like network, and hepatocytes combined gelatin/alginate/chitosan were placed around it for the fabrication of complex 3D structures mimicking a liver (Shengjie et al. 2009) (Figure 7.4).

Khademhosseini and his group used cell-laden printing technique for fabricating microfluidic channels from cell-laden hydrogels (Ling et al. 2007). They demonstrated that the encapsulation of mammalian cells within the bulk material of microfluidic channels may be beneficial for applications ranging from tissue engineering to cell-based diagnostic assays. They presented a technique for fabricating microfluidic channels from cell-laden agarose hydrogels. The channels of different dimensions were generated, and it was shown that agarose, though highly porous, is a suitable material for performing microfluidics. Cells embedded within the microfluidic molds were well distributed, and media pumped through the channels allowed the exchange of nutrients and waste products. While most cells were found to be viable upon initial device fabrication, only those cells near the

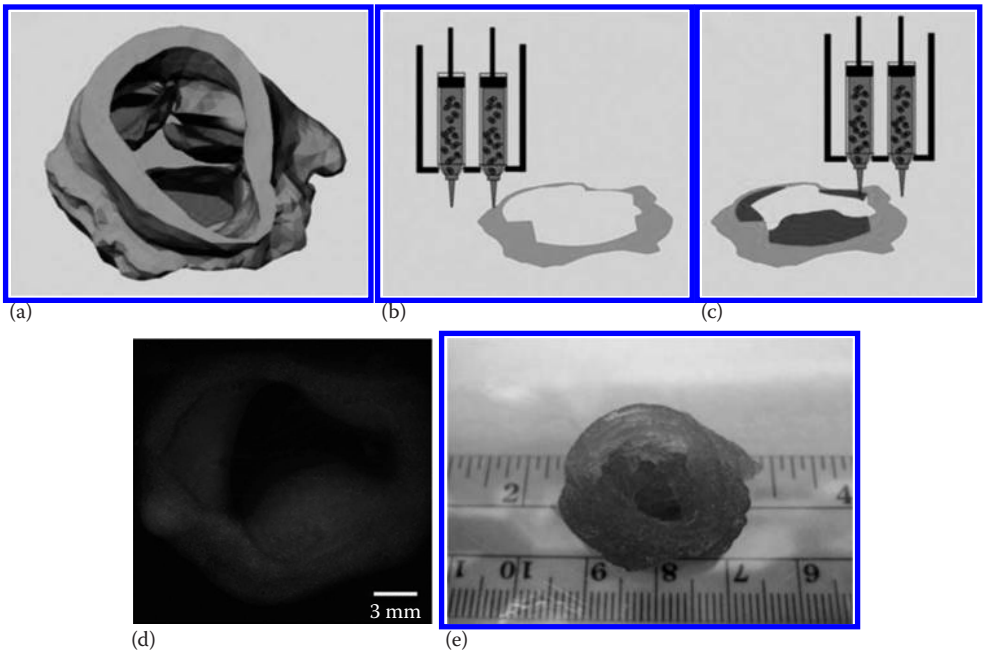

FIGURE 7.3
Bioprinting of aortic valve conduit. (a) Aortic valve model reconstructed from micro-CT images. The root and leaflet regions were identified with intensity thresholds and rendered separately into 3D geometries into STL format (lighter shade indicates valve root and darker shade indicates valve leaflets); (b, c) schematic illustration of the bioprinting process with dual cell types and dual syringes: (b) root region of first layer generated by hydrogel with SMC; (c) leaflet region of first layer generated by hydrogel with VIC; (d) fluorescent image of first printed two layers of aortic valve conduit; SMC for valve root were labeled by cell tracker lighter shade and VIC for valve leaflet were labeled by cell tracker darker shade; (e) as-printed aortic valve conduit. (Reproduced with permission from Duan, B. et al., *J. Biomed. Mater. Res. A*, 101, 1255–1264, 2013.)

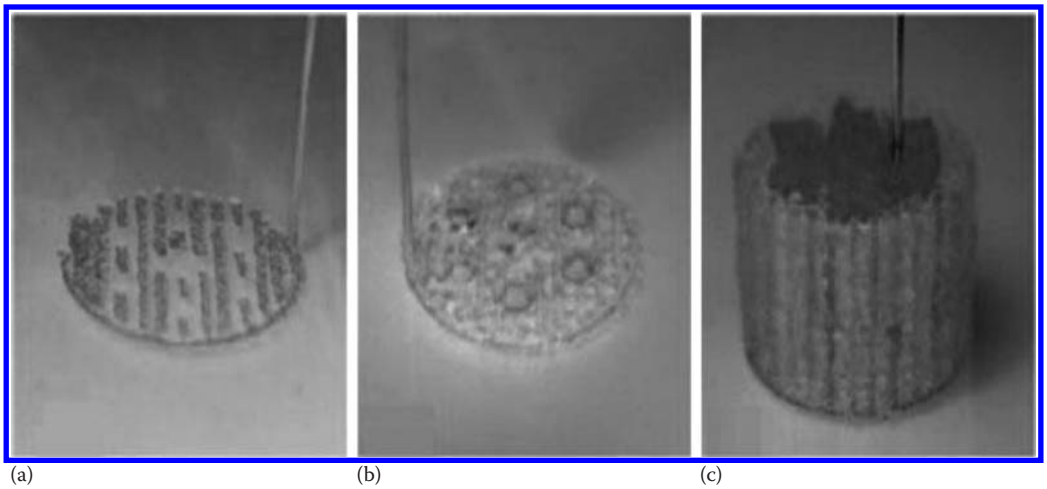

FIGURE 7.4
Sequential deposition of hepatocytes in gelatin/alginate/collagen (a, clear) and ASCs in gelatin/alginate/fibrinogen (b, darker shade) to produce a 3D liver construct (c). (Adapted from Shengjie, L. et al., *J. Bioact. Compat. Polym.*, 24, 249–265, 2009.)

microfluidic channels remained viable after three days, demonstrating the importance of a perfused network of microchannels for delivering nutrients and oxygen to maintain cell viability in large hydrogels.

There are several challenges related to extrusion-based printing of cell-laden hydrogels. First, hydrogel material used for cell encapsulation could limit cell–cell interaction and ECM formation. Because of weak mechanical properties of hydrogel, the printed structures lack mechanical integrity. This could limit scale of the constructs printed and make the implantation as well as the maintenance of the printed structure difficult. Hydrogels used for printing tissue constructs could also cause immunogenic reactions after implantation.

7.2.4.2 Direct Cell Printing/Self-Assembly

The concepts of tissue fusion and tissue fluidity are fundamental for the modern organ printing technology based on self-assembly (Steinberg 1963; Foty et al. 1994). Direct cell printing, also called self-assembly or scaffold-free bioprinting, employs layer-based printing of multicellular aggregates or self-assembling tissue spheroids as building blocks (Mironov 2003; Mironov et al. 2003, 2008) (Figure 7.2e). The main idea of this technique is formation of tissue fusion of closely placed multicellular aggregates or tissue spheroids without using any scaffolds. Tissue fusion is an omnipresence process during embryonic development (Perez-Pomares et al. 2006), and hence, this biofabrication technology is considered biomimetic. Cell aggregates or microtissues can be fabricated in pre-designed shapes by seeding and culturing in micromolded well plates and serve as building blocks to assembly multicellular tissues at a higher level of organization. With the help of computer-controlled automated bioprinting methods, tissue or organ printing technology can be completely automated. Fully developed organ bioprinting could make 3D vascularized functional human organs or living functional organ constructs possible for surgical implantation (Rivron et al. 2009).

Forgacs and colleagues (Norotte et al. 2009) developed a fully biological self-assembly approach through an extrusion-based bioprinting method for scaffold-free small diameter vascular reconstruction. Various vascular cell types, including smooth muscle, endothelial, and fibroblasts cells, were aggregated into discrete units, either multicellular spheroids or cylinders of controllable diameter (300–500 mm). These were printed layer by layer concurrently with agarose rods, used here as a molding template. The post-printing fusion of the discrete units resulted in single- and double-layered small diameter vascular tubes (outer diameters ranging from 0.9 to 2.5 mm). A unique aspect of the method was the ability to engineer vessels by directly printing multicellular aggregates scaffold-free as shown in Figure 7.5. The developed bioprinting technology was commercialized by Organovo (organovo.com).

Chang and colleagues (2011) developed a hybrid bioprinting process to create a 3D microorgan, which biomimics the cell's natural microenvironment with enhanced functionality. The researchers used an automated syringe-based direct cell writing hybrid bioprinting process. They first dispensed gel lines and then used the dispensed gels as mold to bioprint microvascular cells and isolated microvessel fragments into composite 3D structures. The printed cells and vessel fragments remained viable after incorporation into biohybrid structures.

In direct cell printing, complex tissue constructs with multiple cells can be printed spatially. Since live cells are directly printed without mixing with hydrogels or seeding into scaffolds, there will not be any immunogenic rejection or inflammation problems.

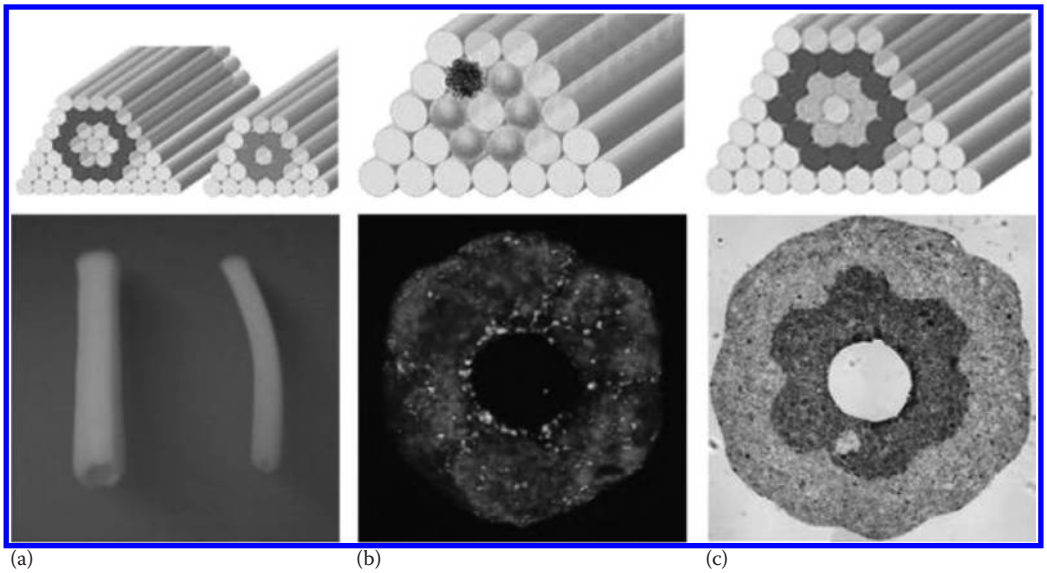

FIGURE 7.5
(a) Design templates (top) and fused constructs (bottom) of different vessel diameters built with cylindrical bioink. (b) The top image shows a template to build a construct with spheroids composed of SMC (darker shade) and ECs (lighter shade). A transversal section after fusion (bottom) shows that the lumen is composed predominantly of endothelial cells. (c) Template to construct a double-layered vascular tube (top). The inner layer is constructed of SMC building blocks (lighter shade), the second of fibroblast building blocks (darker shade). The transversal section (bottom) shows fusion and the segregation of the two cell types mimicking the media and adventitia of blood vessels. (Reproduced with permission from Jakab et al., Tissue engineering by self-assembly and bio-printing of living cells, *Biofabrication*. Copyright 2010, IOP Publishing.)

Cells can be patterned easily with automated bioprinting processes. However, the printed tissue constructs need vascularization to survive and to form tissue or organ substitutes in vitro. Another challenge is keeping the form of mechanically weak cells or cell aggregates in 3D during printing process.

7.2.4.3 Direct Cell Printing of Macrovascular Constructs

Scaffold-free tissue engineering of small-diameter tubular grafts has been studied in literature (Norotte et al. 2009). However, the previous research is limited to fabrication of simple small-diameter tubular vascular conduits. We developed novel computer-aided algorithms and strategies to model and 3D bioprint a human aortic tissue construct biomimetically (Kucukgul et. al. 2014). Cylindrical mouse embryonic fibroblast (MEF) cell aggregates and agarose-based support structures (hydrogels) were 3D bioprinted using Novogen MMX Bioprinter as shown in Figure 7.6. The 3D bioprinter has two deposition heads equipped with glass capillaries for cell aggregates and hydrogel biomaterials, respectively. MEF cells were cultured based on general cell culturing protocols. In order to obtain cell pellets for printing, cells were centrifuged at relatively high speed following the detachment of them from the cell culture flask. Once the dense cell pellet was obtained, it was transferred into capillaries for continuous bioprinting.

Since the primary objective of this work is to 3D bioprint an anatomically correct blood vessel, the original geometry of the vessel needs be obtained and converted into a computer

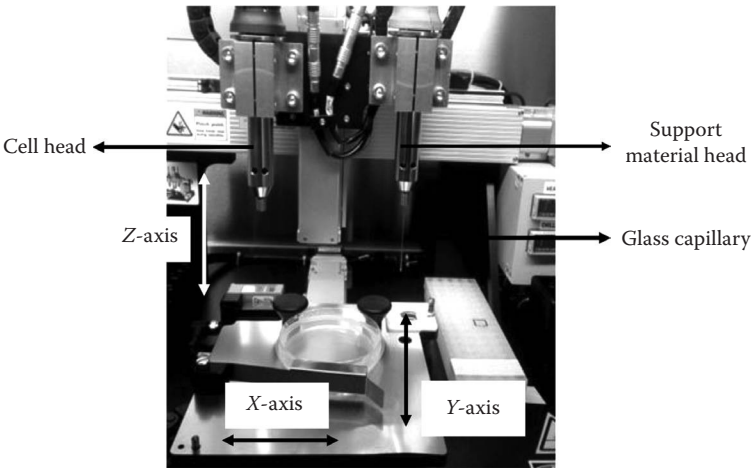

FIGURE 7.6
(See color insert.) Organovo Novogen MMX Bioprinter.

model. Hence, the correct form of the vascular structures can be exactly mimicked in biofabrication process. A part of human abdominal aorta model was chosen to illustrate the proposed methods for 3D bioprinting of macrovascular structures. The geometry of the aorta was captured from a sample medical image using imaging and segmentation process and then transformed into 3D computer model as an STL model. STL files are constructed with numerous triangles that tessellate the outside surface of the object, here, a part of abdominal aorta. To be able to optimize 3D bioprinting and generate tool path planning, the obtained STL model of the abdominal aorta needs to be represented with parametric surfaces. A novel biomodeling method was developed to create smooth parametric surfaces using the geometric information of these mesh (triangular facet) structures. The developed method generates section curves as well as the center points from the mesh model, then approximates a centerline curve from those center points. Smooth parametric surfaces are then generated along with this centerline curve (Figure 7.7).

After the biomodeling phase, the aorta model was then 3D bioprinted layer by layer vertically, with microcapillaries of specific diameter (450 μm), using hydrogel as supportive material and MEF cells as bioink. Tool path planning for the biofabrication step was generated by developed computer algorithms so the entire printing process could be carried out without any human intervention.

To bioprint an anatomically correct aorta model, mechanically weak cellular aggregates need to be supported by hydrogels in order to preserve the desired/exactly mimicked shape. As shown in Figure 7.8, a novel self-supporting method was developed so that both cellular aggregates (lighter shade cylinders) and hydrogels (darker shade cylinders) are placed on the valleys of the preceding layer to form 3D construct.

After path planning and optimization, cylindrical cellular aggregates and their support structures were printed layer by layer using the 3D bioprinter (Figure 7.6). As shown in Figure 7.9, MEF cell aggregates were successfully printed at the valleys formed by the support material (hydrogel). The cells were printed directly by controlling the bioprinter's cell and support heads using the generated scripts. After bioprinting, the printed tissue construct were kept in an incubator until the cell aggregates are fused and formed the tissue construct.

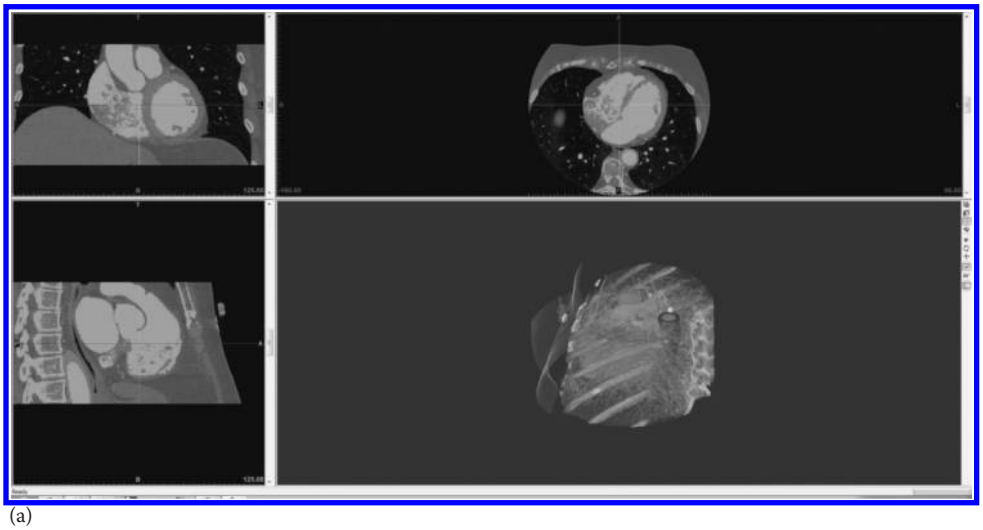

(a)

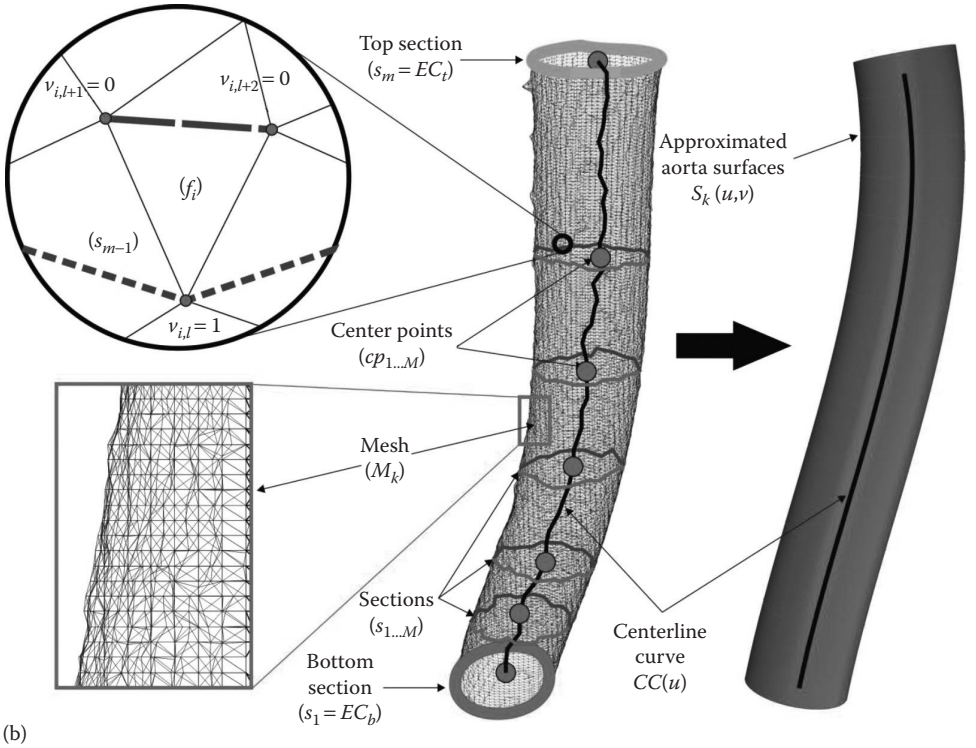

(b)

FIGURE 7.7
(See color insert.) Proposed methods for 3D bioprinting of macrovascular structures. (a) Capturing accurate geometry of the aorta from a sample magnetic resonance imaging (MRI) data. (b) Segmentation and then transformation of the data into a 3D surface as a stereolithography (STL) model.

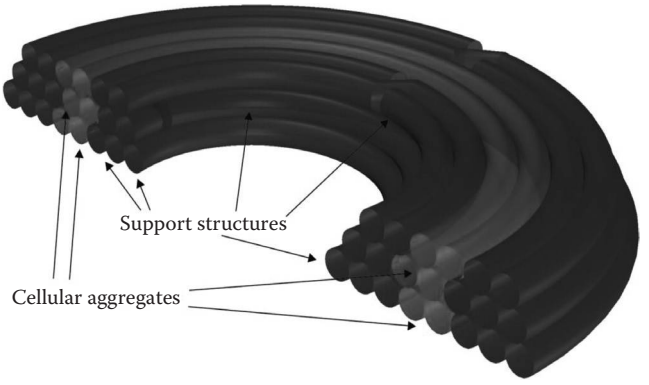

FIGURE 7.8
Three consecutive example layers showing support structures (darker shade) and cellular aggregates (lighter shade).

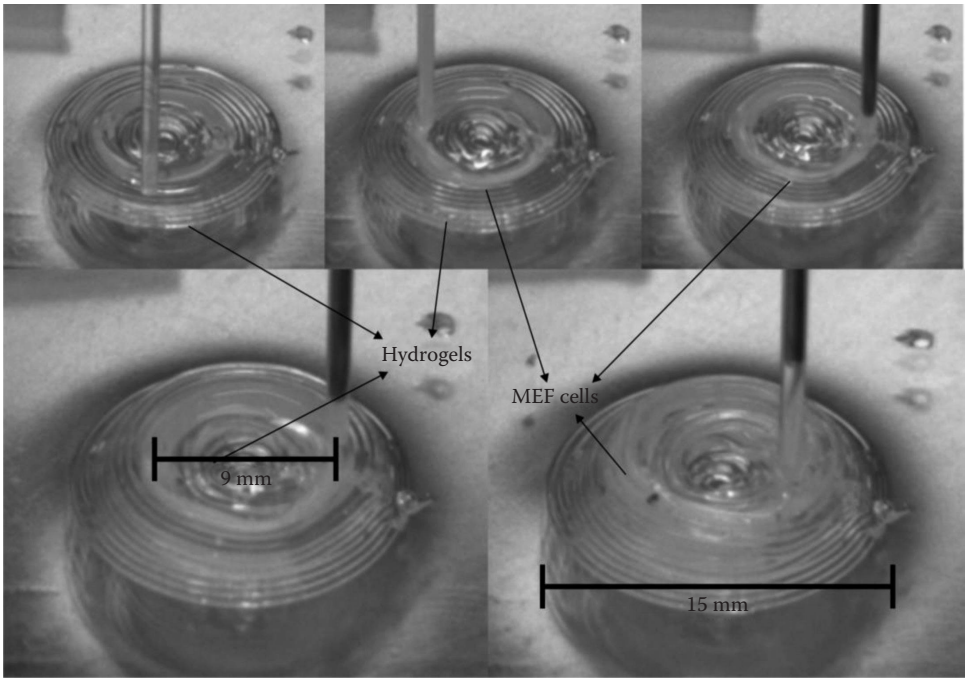

FIGURE 7.9
3D printed MEF cell aggregates of originally mimicked aorta.

7.3 Conclusion

In this chapter, a novel use of AM for bioprinting tissue or organs is presented. Various AM techniques have been successfully used for developing tissue scaffolds with controlled geometry and microarchitecture. However, possible immunogenic reactions of scaffold materials, difficulty in cell seeding, and vascularization problems lead researcher

to develop scaffold-free bioprinting methods with live cells for tissue or organ printing. We have discussed several bioprinting processes for engineering replacements for diseased or damaged tissues. For any scaffold-based or scaffold-free bioprinting processes, vascularization of printed tissue constructs to allow oxygen and nutrition delivery and waste removal must be considered. Tissues or organs are complex structures, and new methods should also biomimick the geometry and multicellular architecture including ECM for a successful formation of tissues and organs. Newly developed bioprinting processes should allow not only printing regular cells but also stem cells as well as active biomolecules to stimulate cells for possible organogenesis. Finally, the developed tissue engineering technologies will have to consider the feasibility of printed 3D tissue constructs for clinical applications to move from bench to bedside.

Acknowledgment

This work is supported by The Scientific and Technological Research Council of Turkey (TUBITAK) under the grant number 112M094.

References

Arcaute, K., Mann, B., Wicker, R. "Stereolithography of spatially controlled multi-material bioactive poly(ethylene glycol) scaffolds." *Acta Biomater* 6(3)(2010): 1047–1054.

Arcaute, K., Mann, B.K., Wicker, R.B. "Stereolithography of three-dimensional bioactive poly(ethylene glycol) constructs with encapsulated cells." *Ann Biomed Eng* 34(9)(2006): 1429–1441.

Barron, J.A., Ringeisen, B.R., Kim, H., Spargo, B.J., Chrisey, D.B. "Application of laser printing to mammalian cells." *Thin Solid Films* 453–454(2004a): 383–387.

Barron, J.A., Wu, P., Ladouceur, H.D., Ringeisen, B.R. "Biological laser printing: a novel technique for creating heterogeneous 3-dimensional cell patterns." *Biomed Microdevices* 6(2)(2004b): 139–147.

Boland, T., Mironov, V., Gutowska, A., Roth, E.A., Markwald, R.R. "Cell and organ printing 2: fusion of cell aggregates in three-dimensional gels." *Anat Rec A Discov Mol Cell Evol Biol* 272(2)(2003): 497–502.

Boland, T., Xu, T., Damon, B., Cui, X. "Application of inkjet printing to tissue engineering." *Biotechnol J* 1(9)(2006): 910–917.

Bonassar, L.J., Vacanti, C.A. "Tissue engineering: the first decade and beyond." *J Cell Biochem Suppl* 30–31(1998): 297–303.

Calvert, P. "Materials science. Printing cells." *Science* 318(5848)(2007): 208–209.

Chang, C.C., Boland, E.D., Williams, S.K., Hoying, J.B. "Direct-write bioprinting three-dimensional biohybrid systems for future regenerative therapies." *J Biomed Mater Res B Appl Biomater* 98(1)(2011): 160–170.

Cook, C.C., Wang, T., Derby, B. "Inkjet delivery of glucose oxidase." *Chem Commun (Camb)* 46(30)(2010): 5452–5454.

Cooke, M.N., Fisher, J.P., Dean, D., Rimnac, C., Mikos, A.G. "Use of stereolithography to manufacture critical-sized 3D biodegradable scaffolds for bone ingrowth." *J Biomed Mater Res B Appl Biomater* 64(2)(2003): 65–69.

Cooper, G.M., Miller, E.D., Decesare, G.E. et al. "Inkjet-based biopatterning of bone morphogenetic protein-2 to spatially control calvarial bone formation." *Tissue Eng Part A* 16(5)(2010): 1749–1759.

Derby, B. "Bioprinting: inkjet printing proteins and hybrid cell-containing materials and structures." *J Mater Chem* 18(47)(2008): 5717.

Dhariwala, B., Hunt, E., Boland, T. "Rapid prototyping of tissue-engineering constructs, using photopolymerizable hydrogels and stereolithography." *Tissue Eng* 10(9/10)(2004): 1316–1322.

Duan, B., Hockaday, L.A., Kang, K.H., Butcher, J.T. "3D bioprinting of heterogeneous aortic valve conduits with alginate/gelatin hydrogels." *J Biomed Mater Res A* 101(5)(2013): 1255–1264.

Fedorovich, N.E., Alblas, J., de Wijn, J.R. et al. "Hydrogels as extracellular matrices for skeletal tissue engineering: state-of-the-art and novel application in organ printing." *Tissue Eng* 13(8)(2007): 1905–1925.

Fedorovich, N.E., De Wijn, J.R., Verbout, A.J., Alblas, J., Dhert, W.J. "Three-dimensional fiber deposition of cell-laden, viable, patterned constructs for bone tissue printing." *Tissue Eng Part A* 14(1)(2008): 127–133.

Fedorovich, N.E., Wijnberg, H.M., Dhert, W.J., Alblas, J. "Distinct tissue formation by heterogeneous printing of osteo- and endothelial progenitor cells." *Tissue Eng Part A* 17(15/16)(2011): 2113–2121.

Foty, R.A., Forgacs, G., Pfleger, C.M., Steinberg, M.S. "Liquid properties of embryonic tissues: measurement of interfacial tensions." *Phys Rev Lett* 72(14)(1994): 2298–2301.

Guillemot, F., Guillotin, B., Fontaine, A. et al. "Laser-assisted bioprinting to deal with tissue complexity in regenerative medicine." *MRS Bulletin* 36(12)(2011): 1015–1019.

Guillotin, B., Guillemot, F. "Cell patterning technologies for organotypic tissue fabrication." *Trends Biotechnol* 29(4)(2011): 183–190.

Guillotin, B., Souquet, A., Catros, S. et al. "Laser assisted bioprinting of engineered tissue with high cell density and microscale organization." *Biomaterials* 31(28)(2010): 7250–7256.

Hafezi, F., Hosseinnejad, F., Fooladi, A.A. et al. "Transplantation of nano-bioglass/gelatin scaffold in a non-autogenous setting for bone regeneration in a rabbit ulna." *J Mater Sci Mater Med* 23(11)(2012): 2783–2792.

Ilkhanizadeh, S., Teixeira, A.I., Hermanson, O. "Inkjet printing of macromolecules on hydrogels to steer neural stem cell differentiation." *Biomaterials* 28(27)(2007): 3936–3943.

Jakab, K., Norotte, C., Marga, F., Murphy, K., Vunjak-Novakovic, G., and Forgacs, G. "Tissue engineering by self-assembly and bio-printing of living cells," *Biofabrication*.

Khoda, A.K., Ozbolat, I.T., Koc, B. "Engineered tissue scaffolds with variational porous architecture." *J Biomech Eng* 133(1)(2011): 011001.

Khoda, A.K.M., Ozbolat, I.T., Koc, B. "Designing heterogeneous porous tissue scaffolds for additive manufacturing processes." *Comput Aided Design* 45(12)(2013a): 1507–1523.

Khoda, A.K.M.B., Koc, B. "Functionally heterogeneous porous scaffold design for tissue engineering." *Comput Aided Des* 45(11)(2013b): 1276–1293.

Kucukgul, C., Ozler S.B., Inci, I., Karakas E., Irmak S., Gozuacik D., Taralp, A., Koc B. "3D bioprinting of biomimetic aortic vascular constructs with self-supporting cells." *Biotechnol Bioeng* 112(4)(2014): 811–821.

Landers, R., Mülhaupt, R. "Desktop manufacturing of complex objects, prototypes and biomedical scaffolds by means of computer-assisted design combined with computer-guided 3D plotting of polymers and reactive oligomers." *Macromol Mater Eng* 282(1)(2000): 17–21.

Langer, R., Vacanti, J.P. "Tissue engineering." *Science* 260(5110)(1993): 920–926.

Lee, J., Cuddihy, M.J., Kotov, N.A. "Three-dimensional cell culture matrices: state of the art." *Tissue Eng Part B Rev* 14(1)(2008): 61–86.

Leong, K.F., Cheah, C.M., Chua, C.K. "Solid freeform fabrication of three-dimensional scaffolds for engineering replacement tissues and organs." *Biomaterials* 24(13)(2003): 2363–2378.

Ling, Y., Rubin, J., Deng, Y. et al. "A cell-laden microfluidic hydrogel." *Lab Chip* 7(6)(2007): 756–762.

Liska, R., Schuster, M., Inführ, R. et al. "Photopolymers for rapid prototyping." *J Coating Techn Res* 4(4)(2007): 505–510.

Ma, Z., Pirlo, R.K., Wan, Q. et al. "Laser-guidance-based cell deposition microscope for heterotypic single-cell micropatterning." *Biofabrication* 3(3)(2011): 034107.

McGuigan, A.P., Sefton, M.V. "Modular tissue engineering: fabrication of a gelatin-based construct." *J Tissue Eng Regen Med* 1(2)(2007): 136–145.

Melchels, F.P., Feijen, J., Grijpma, D.W. "A review on stereolithography and its applications in biomedical engineering." *Biomaterials* 31(24)(2010): 6121–6130.
Mironov, V. "Printing technology to produce living tissue." *Expert Opin Biol Ther* 3(5)(2003): 701–704.
Mironov, V., Boland, T., Trusk, T., Forgacs, G., Markwald, R.R. "Organ printing: computer-aided jet-based 3D tissue engineering." *Trends Biotechnol* 21(4)(2003): 157–161.
Mironov, V., Kasyanov, V., Drake, C., Markwald, R.R. "Organ printing: promises and challenges." *Regen Med* 3(1)(2008): 93–103.
Mironov, V., Trusk, T., Kasyanov, V. et al. "Biofabrication: a 21st century manufacturing paradigm." *Biofabrication* 1(2)(2009): 022001.
Nahmias, Y., Schwartz, R.E., Verfaillie, C.M., Odde, D.J. "Laser-guided direct writing for three-dimensional tissue engineering." *Biotechnol Bioeng* 92(2)(2005): 129–136.
Nakamura, M., Kobayashi, A., Takagi, F. et al. "Biocompatible inkjet printing technique for designed seeding of individual living cells." *Tissue Eng* 11(11/12)(2005): 1658–1666.
Norotte, C., Marga, F.S., Niklason, L.E., Forgacs, G. "Scaffold-free vascular tissue engineering using bioprinting." *Biomaterials* 30(30)(2009): 5910–5917.
Odde, D. "Laser-guided direct writing for applications in biotechnology." *Trends Biotechnol* 17(10)(1999): 385–389.
Odde, D.J., Renn, M.J. "Laser-guided direct writing of living cells." *Biotechnol Bioeng* 67(3)(2000): 312–318.
Ovsianikov, A., Deiwick, A., Van Vlierberghe, S. et al. "Laser fabrication of three-dimensional CAD scaffolds from photosensitive gelatin for applications in tissue engineering." *Biomacromolecules* 12(4)(2011a): 851–858.
Ovsianikov, A., Gruene, M., Pflaum, M. et al. "Laser printing of cells into 3D scaffolds." *Biofabrication* 2(1)(2010): 014104.
Ovsianikov, A., Malinauskas, M., Schlie, S. et al. "Three-dimensional laser micro- and nano-structuring of acrylated poly(ethylene glycol) materials and evaluation of their cytoxicity for tissue engineering applications." *Acta Biomaterialia* 7(3)(2011b): 967–974.
Ozbolat, I.T., Koc, B. "A continuous multi-material toolpath planning for tissue scaffolds with hollowed features." *Comput Aided Des Appl* 8(2)(2011): 237–247.
Parsa, S., Gupta, M., Loizeau, F., Cheung, K.C. "Effects of surfactant and gentle agitation on inkjet dispensing of living cells." *Biofabrication* 2(2)(2010): 025003.
Peltola, S.M., Melchels, F.P., Grijpma, D.W., Kellomaki, M. "A review of rapid prototyping techniques for tissue engineering purposes." *Ann Med* 40(4)(2008): 268–280.
Perez-Pomares, J.M., Foty, R.A. "Tissue fusion and cell sorting in embryonic development and disease: biomedical implications." *Bioessays* 28(8)(2006): 809–821.
Pham, Q.P., Sharma, U., Mikos, A.G. "Electrospinning of polymeric nanofibers for tissue engineering applications: a review." *Tissue Eng* 12(5)(2006): 1197–1211.
Pirlo, R.K., Dean, D.M., Knapp, D.R., Gao, B.Z. "Cell deposition system based on laser guidance." *Biotechnol J* 1(9)(2006): 1007–1013.
Rivron, N.C., Rouwkema, J., Truckenmuller, R. et al. "Tissue assembly and organization: developmental mechanisms in microfabricated tissues." *Biomaterials* 30(28)(2009): 4851–4858.
Schade, R., Weiss, T., Berg, A., Schnabelrauch, M., Liefeith, K. "Two-photon techniques in tissue engineering." *Int J Artif Organs* 33(4)(2010): 219–227.
Shengjie, L., Zhuo, X., Xiaohong, W. et al. "Direct fabrication of a hybrid cell/hydrogel construct by a double-nozzle assembling technology." *J Bioact Compat Polym* 24(3)(2009): 249–265.
Skardal, A., Zhang, J., McCoard, L. et al. "Photocrosslinkable hyaluronan-gelatin hydrogels for two-step bioprinting." *Tissue Eng Part A* 16(8)(2010): 2675–2685.
Smith, C.M., Christian, J.J., Warren, W.L., Williams, S.K. "Characterizing environmental factors that impact the viability of tissue-engineered constructs fabricated by a direct-write bioassembly tool." *Tissue Eng* 13(2)(2007): 373–383.
Smith, C.M., Stone, A.L., Parkhill, R.L. et al. "Three-dimensional bioassembly tool for generating viable tissue-engineered constructs." *Tissue Eng* 10(9/10)(2004): 1566–1576.
Steinberg, M.S. "Reconstruction of tissues by dissociated cells." *Science* 141(3579)(1963): 401–408.

Whitesides, G.M., Boncheva, M. "Beyond molecules: self-assembly of mesoscopic and macroscopic components." *Proc Natl Acad Sci USA* 99(8)(2002): 4769–4774.

Wu, P.K., Ringeisen, B.R. "Development of human umbilical vein endothelial cell (HUVEC) and human umbilical vein smooth muscle cell (HUVSMC) branch/stem structures on hydrogel layers via biological laser printing (BioLP)." *Biofabrication* 2(1)(2010): 014111.

Xu, M., Yan, Y., Liu, H., Yao, R., Wang, X. "Controlled adipose-derived stromal cells differentiation into adipose and endothelial cells in a 3D structure established by cell-assembly technique." *J Bioact Compat Polym* 24(1 Suppl)(2009): 31–47.

Xu, T., Jin, J., Gregory, C., Hickman, J.J., Boland, T. "Inkjet printing of viable mammalian cells." *Biomaterials* 26(1)(2005): 93–99.

Yeong, W.Y., Chua, C.K., Leong, K.F., Chandrasekaran, M. "Rapid prototyping in tissue engineering: challenges and potential." *Trends Biotechnol* 22(12)(2004): 643–652.

Yuan, D., Lasagni, A., Shao, P., Das, S. "Rapid prototyping of microstructured hydrogels via laser direct-write and laser interference photopolymerisation." *Virtual Phys Prototyp* 3(4)(2008): 221–229.

8

Multifunctional Printing: Incorporating Electronics into 3D Parts Made by Additive Manufacturing

Dishit Paresh Parekh, Denis Cormier, and Michael D. Dickey

CONTENTS

8.1 Introduction

This chapter discusses the use of additive manufacturing (AM) for creating three-dimensional (3D) objects that contain electronic components.

According to the ASTM definition,[1] AM or rapid prototyping (RP) is the process of joining materials to make objects from 3D model data, usually layer upon layer. More colloquially, AM and RP are referred to as *3D printing*. In addition to layer-based AM processes, there are *direct-writing* techniques (DW) in which functional and/or structural materials are precisely deposited onto a substrate in digitally defined locations.[2,3] DW

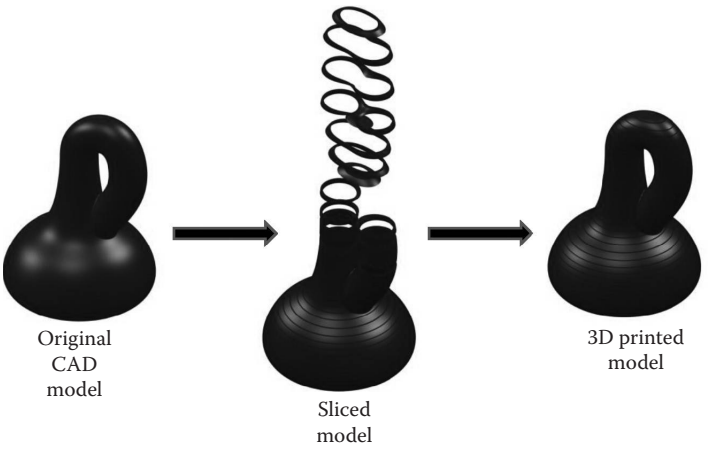

FIGURE 8.1
Example of an additive process. A 3D CAD model is broken up into thin slices, which are then printed in an additive manufacturing process in a layer-by-layer fashion to create a 3D printed part.

techniques are most often used to print electronic elements onto the surface of an existing part, although there is growing interest in hybrid techniques that allow printed electronics within the bulk of additively manufactured parts. In this chapter, we use the term AM to describe the general field of layer-based manufacturing, and we use DW when describing methods used to deposit functional electronic materials.[4]

Although many AM techniques exist, they all employ the same basic steps. These steps are as follows: (1) create a computer model of the design; (2) slice the model into thin cross-sectional layers; (3) construct the model physically one layer atop another; and (4) clean and finish the part, as shown in Figure 8.1.

Most commercial AM machines are designed to create objects from a specific class of material (typically either polymers,[5] ceramics, or metals). There are exceptions, such as tools that print polymers that contain ceramic or metal particles. Constructing 3D parts with electronic functionality often requires integrating multiple types of materials, which causes fabrication challenges for AM processing. We call these processes *multifunctional 3D printing* because of the need to incorporate multiple materials to achieve multiple functions (typically a synergistic combination of electrical functionality with either form factor or mechanical properties).

The approach for integrating electronics into a 3D object depends entirely on the desired function and the level of sophistication of the electronics involved. In this chapter, we categorize three broad approaches that utilize AM for integrating electronics with 3D printed parts: (1) hybrid chip-insertion approaches, (2) surface DW approaches, and (3) freeform multi-material 3D printing approaches. Most AM techniques are not able to print electronic materials with satisfactory properties (e.g., purity, crystallinity, doping, and charge mobility) at high enough resolution to compete with conventional electronic devices such as integrated circuits (ICs), light emitting diodes (LEDs), transistors, and solar cells among others. Thus, sophisticated electronics are often fabricated separately and then integrated into a 3D printed part by robot, by hand, or by some other transfer technique. This approach (Category 1) can provide sophisticated functionality, but does not fall within the spirit of AM and requires methods to connect the individual components. DW techniques are capable of 2D printing moderate quality, passive electronic

structures (resistors, inductors, capacitors). In principle, these processes (Category 2) could print electronic components as layers in 3D objects, but there are significant challenges with using these 2D techniques in 3D space. It is not the intent of this chapter to review DW techniques since excellent resources exist on this topic.[2,6–12] Instead, we will introduce DW techniques within the context of 3D printing and highlight the challenges. Finally, we review some emerging techniques for printing electronic materials in a manner that is truly 3D (Category 3).

To appreciate the challenges associated with multifunctional printing, we first briefly review what *electronics* means. We discuss the merits of electronics made by AM, the reasons for incorporating electronics into 3D objects, and the new possibilities for electronics made possible by AM. To help motivate the challenges of integrating electronics into 3D parts, we describe briefly the conventional methods for making sophisticated electronics. We then discuss printed electronics, which offer inexpensive approaches for creating low-grade electronics. DW techniques are a subset of printed electronic strategies and the only ones that align conceptually with AM. Thus, we focus most of our discussion on these techniques and discuss challenges of using these techniques within the context of AM. We categorize three general strategies for integrating electronics into 3D objects and spend the remainder of the chapter discussing these strategies. We discuss the capabilities of each technique for depositing materials to achieve the final desired component with appropriate feature sizes and resolution along with the required electronic functionality.

Finally, there are many resources on DW and AM, including this book. For this reason, several sections are intentionally concise and we point the reader to appropriate references in these instances. In contrast, there has been very little work in the academic literature on integrating electronics into 3D printed objects. A theme of this chapter is elucidating the challenges and opportunities associated with the various approaches for integrating electronics into 3D objects constructed by AM to inspire and guide future work on this topic.

8.2 What Are Electronics and Why Do We Need Them in 3D Objects?

Electronics are devices that provide one or more electrical functions (e.g., communications, sensing, computation, memory) via the use of circuits and electrical components. Examples of electronic components include the fundamental passive circuit elements (resistor, inductor, capacitor, memristor), conductors (wires, interconnects, antennas), insulators, transistors, sensors, and microelectromechanical systems (MEMS) devices (useful for switching, actuating, and sensing).

Electronics are ubiquitous in modern society in the form of cell phones and computers, and are incorporated in many appliances, cars, and toys, to name but a few examples. The electronics industry is driven by products that are smaller, thinner, lighter, faster, and more cost-effective. Because of the importance of electronics in our society and the growing interest in the *Internet of things* (IoT) (i.e., the notion that objects of interest will someday be interconnected wirelessly), it is natural to understand there is—and will continue to be—a great demand for electronics in 3D printed objects. AM is a growing market in every manufacturing sector with a global AM market of $1.8 billion in 2012 that is expected to reach $3.5 billion by 2017[13] and $7 billion by 2025[14]; the integration of electronics will hence only add more value.

AM has several capabilities that are, in principle, well-suited for building electronic components. First, AM generates minimal waste and allows for RP of new designs. Second, it can create complex form factors, spanning structures, out-of-plane geometries, and embedded electronics. Hence, AM enables the creation of intricate and conformal electronics that are structurally integrated into a manufactured part. This attribute may minimize cable interconnects and redundant electronics packaging, resulting of a reduction of mass and assembly complexity in the final electronic component. It may also allow for the creation of entirely new objects containing electronics[15] that simply are not possible to form using 2D approaches.

More than a half-century has gone into the art of building sophisticated components for computers and electronics. It is sensible to consider these mature approaches as a way to integrate electronics into 3D objects. In the next section, we describe these methods briefly to illustrate why it is not straightforward to use these advanced techniques for integrating electronics into 3D objects.

8.3 Conventional Fabrication of Electronics

Since the invention of ICs in 1959,[16] the electronics industry has focused on miniaturization, which has faithfully followed Moore's Law.[17,18] Miniaturization lowers the cost per unit (e.g., per number of transistors) and therefore allows the consumer more buying power. Miniaturization also allows devices, such as cell phones, to be possible by fitting large amounts of computing power into a small form factor.

ICs consist of conductors, resistors, insulators, and semiconductors integrated and patterned spatially into complex circuits and devices on a planar substrate. The techniques to build these devices are inherently 2D and involve a number of steps such as deposition (e.g., physical vapor deposition, sputtering), removal (e.g., etching, sputtering), patterning (e.g., photolithography), and modification (e.g., ion implantation for doping) of electronic materials. The quest for miniaturization corresponds with an increase in complexity and sophistication of the fabrication processes used to build ICs. There are several excellent monographs and reviews on fabrication methods utilized to create electronics.[19–26]

Photolithography is the cornerstone process utilized to pattern the components in a computer chip. AM is effectively a patterning technique, and thus, it is prudent to briefly discuss photolithography as a basis for comparison. An example of the photolithographic process is shown in Figure 8.2.[27] Photolithography utilizes patterns of light to chemically modify the solubility of thin polymer films coated on a surface. Photolithography is an inherently 2D process because the light used to expose the polymer has a single focal plane. This limitation, along with the need to coat, expose, and remove polymer, makes photolithography essentially incompatible with AM. Although academic research provides many unconventional approaches[8,25,28–35] to pattern electronic materials to overcome some of the limitations of photolithography, it still remains the backbone of the semiconductor industry.

There are several reasons conventional electronic fabrication techniques are not compatible with AM. State-of-the-art electronics (e.g., ICs, hard drives) rely critically on ultra-pure materials, well-defined interfaces, and crystalline semiconductors with precise doping

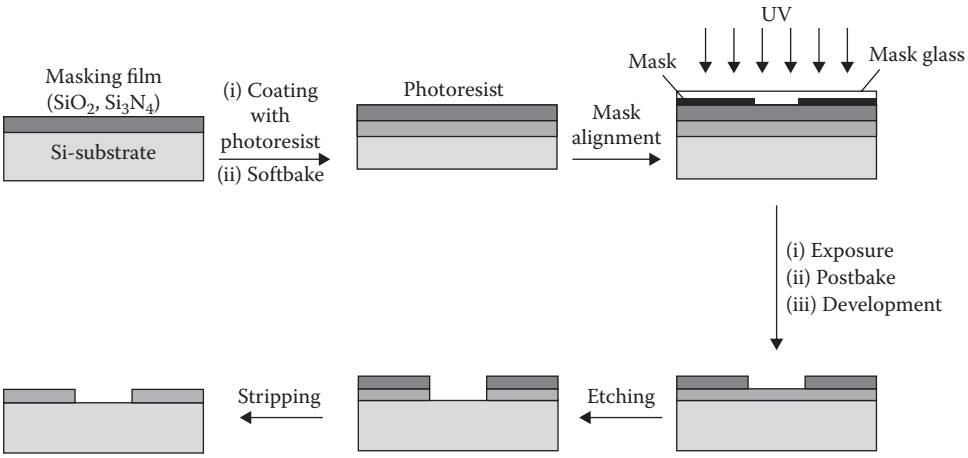

FIGURE 8.2
A schematic of photolithography, which is a conventional subtractive manufacturing process used to make ICs. (Adapted from Optical Issues in Photolithography. *Connexions*. http://cnx.org/content/m25448/latest/.)

concentration. To date, AM has not been capable of meeting any of these requirements. In addition, these sophisticated planar processes are carried out in a clean room environment on flat substrates (typically precisely engineered silicon wafers), whereas AM is often done under ambient conditions on complex substrates. Also, most AM techniques produce features with resolutions (of ~10–100 μm) that are nearly 3–4 orders of magnitude larger than those produced by photolithography. For these reasons, sophisticated electronic components are typically built separately and then placed onto or into 3D objects; we refer to this approach as *Category 1*. For example, cell phones are currently built in this modular manner in which the case, display, battery, and electronics are all built separately and assembled. There is, however, a need to interconnect these electronic components to other components in the object. Passive components (capacitors, resistors, and inductors) are commonly connected to printed circuit boards (PCBs) by soldering using surface mount technologies (SMTs) or are embedded into multilayered low-temperature co-fireable ceramic packages (LTCC).[36] In the case of a cell phone, these connections can be made using wires, solder, and flexible circuit boards in the void space of the phone, but AM has the potential to directly define these connections in a continuous process to minimize assembly and create more complex, customizable parts.

In summary, conventional electronics processing uses expensive, sophisticated equipment in clean room environments to pattern ultra-pure materials onto planar substrates of a limited geometry using numerous processing steps including those requiring large temperature excursions. There is a need for additional tools to directly and inexpensively print electronic materials by eliminating the masking and etching steps, even if there is a trade-off in quality relative to the state of the art.

The ability to additively print electronics reduces the material waste, energy consumption,[38] and processing time and steps relative to IC processing, as shown in Figure 8.3.[37] The next section describes this class of printed electronics. These inherently 2D methods have features that may be useful for integrating electronics into 3D objects.

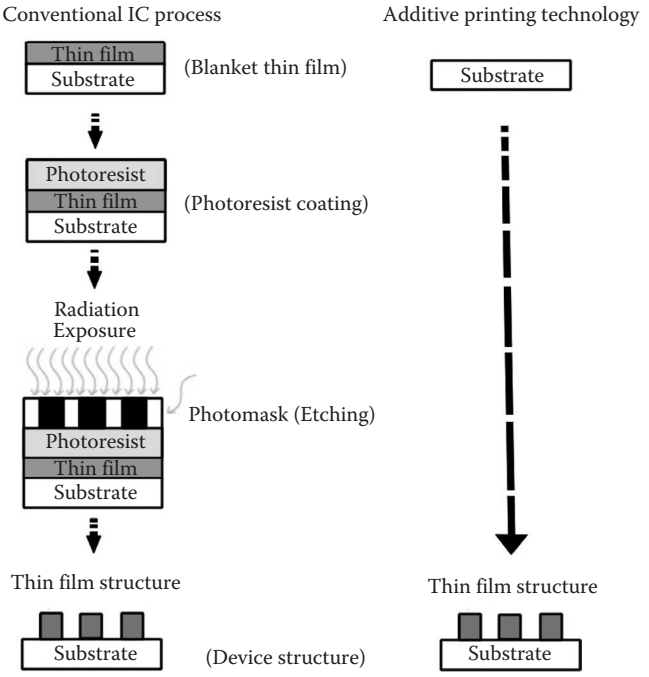

FIGURE 8.3
Process comparison of subtractive IC processing and additive printing approach for thin film device development. (Adapted from Joshi, P.C. et al., Direct digital additive manufacturing technologies: Path towards hybrid integration, In *Future Instrum. Int. Workshop*, 1–4, 2012, doi:10.1109/FIIW.2012.6378353.)

8.4 Printed Electronics

Printed electronics are formed by directly dispensing or patterning functional inks to define electronic components onto a wide range of substrates. The main aim of printed electronics is to reduce the manufacturing cost of electronics per unit area using less-expensive, all-additive printing methods. Low-cost printed electronics[39,40] have gained a great deal of interest over the past 10 years because of their promise to greatly reduce the cost of many electronic applications and the ability to print on larger, unconventional surfaces (e.g., flexible substrates, large displays). The Flexible Electronics Forecast report projects that the market size for printed electronics will grow from $2.2 billion in 2011 to $6.5 billion in 2017 and to $44.2 billion in 2021.[41]

Printed electronics present a trade-off between cost and performance relative to conventional electronics, as described in Table 8.1.[42] There are several challenges associated with printed electronics. First, the materials must start in the form of an ink that can be deposited. Once deposited, most of these inks need some post-processing, such as thermal treatments, to obtain the final desired properties, which limits the substrate onto which the features are printed and creates additional processing steps. The deposition techniques are much lower in resolution than photolithography (typically tens of microns or larger). There is a general trade-off between the feature size and throughput of printed electronic processes (Figure 8.4).[43]

TABLE 8.1

Printed and Conventional Electronics as Complementary Technologies

Printed Electronics	Conventional Electronics
Long switching times	Extremely short switching times
Low integration density	Extremely high integration density
Large printing area	Small printing area
Process compatible with flexible substrates	Process compatible with rigid substrates
Simple and cheap fabrication process	Sophisticated and expensive fabrication process

Source: Wikipedia. File:ComplementaryTechnologies.png. *Wikipedia Free Encycl.* http://en.wikipedia.org/wiki/File:ComplementaryTechnologies.png.

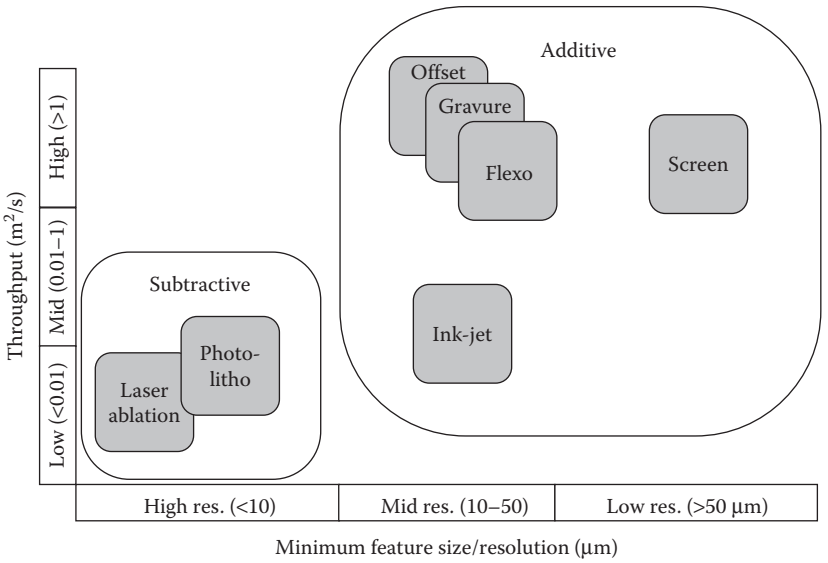

FIGURE 8.4
Comparison of various printing technologies. (Adapted from Chang, J. et al., Challenges of printed electronics on flexible substrates, In *2012 IEEE 55th Int. Midwest Symp. Circuits Syst.*, 582–585, 2012.)

Despite the inferior performance of printed electronics relative to conventional electronics, there are several applications for low-cost printed electronics including radio frequency identification (RFID) tags,[44] chemical and electronic sensors,[45] displays,[46] smart cards,[47] packaging,[48,49] and PCBs/keypads.[50,51] The common element among all these applications is the fact that they do not need either ultra-fast circuitry or ultra-dense circuitry such as that in ICs.

The selection of the appropriate printing method is determined by the physical specifications and resolution of the printed materials that comprise the electronic devices, the substrate size and composition, the desired throughput, and economic and technical considerations of the final printed products. Two of the most promising printing technologies for fabricating low-cost printed electronics include ink-jet printing and gravure printing. Ink-jet printing[52–55] is a well-known technology that makes use of multiple droplet dispensers that deposit individual drops to form patterns on a substrate. Gravure printing[56–58] uses a cylinder featuring an etched pattern, onto which the ink is deposited. Rolling the cylinder

over a substrate transfers the pattern from the cylinder to the substrate in a manner that is compatible with high throughput roll-to-roll processing. There are a number of other methods for printing electronics including screen printing,[59,60] flexography,[61,62] and offset lithography[63] that are utilized to fabricate devices such as solar cells, organic light-emitting diodes (OLEDs), and RFIDs.[39]

It is possible to print both organic and inorganic materials as inks to form conductors, semiconductors, dielectrics, or insulators. These ink materials must be available as either a liquid, solution, dispersion, or suspension.[64]

Organic ink materials include conjugated polymers[65] or small molecules that possess conducting, semiconducting, electroluminescent, photovoltaic, and other properties that can be exploited in printed electronics. These organics[66–69] are commercially available in different formulations and have been deposited using ink-jet printing,[70] gravure printing,[71] flexography,[72] screen printing,[73] and offset lithography.[74] Organic electronics are used commercially in OLEDs and organic molecules are also used in liquid crystal displays.[75] There are several excellent reviews and books on organic electronics.[76–83] Although organic materials offer appealing properties such as mechanical flexibility and tunability of properties via chemical modifications (e.g., light color in OLEDs),[84] they offer poor charge carrier mobility[65] and hence the electrical performance lags behind that of conventional silicon-based electronics. In addition, organic materials are prone to oxidation,[85] which limits the longevity of devices built using these materials.

Inorganic ink materials such as dispersions of metallic or semiconductor micro- and nano-particles including silver and silicon[86] may also be printed. The silver and gold particles can be deposited using, for example, ink-jet printing,[87,88] flexography,[89] and offset lithography.[90] After deposition, these particles need to be sintered to form stable conductive structures using either conventional heating (often at temperatures >200°C[91]), laser sintering,[92,93] flash exposure to light, or microwave sintering.[94] The resulting sintered structures generally cannot match the electrical properties of equivalent bulk materials, but can be deposited relatively easily using these techniques.

There is also a growing interest in printed carbon nanotubes[95–99] and graphene[100–104] because of their remarkable electrical properties. These materials can serve as conductors or semiconductors, but there are challenges with making, purifying, and patterning these materials on a large scale. There are several excellent reviews and books on carbon-based electronic materials.[98,105–112]

Many of the techniques introduced in this section—such as gravure printing—are not directly compatible with the AM of 3D objects because they are not *digital* (i.e., they cannot dispense inks into arbitrary patterns on demand). In addition, most of the methods discussed in this section are intended only for 2D substrates such as plastic films, foils, and paper and cannot be used for AM on complex, non-planar, or 3D substrates. Thus, we limit our focus to only the subset of printed electronics techniques that are digital (i.e., DW techniques, such as ink-jet printing) because of their potential to be compatible with 3D printing.

8.5 Direct-Writing of Electronics

DW techniques[2,3,12,113] are a subset of printed electronics processes to precisely deposit functional and/or structural materials on to a substrate in *digitally defined* locations to form simple 2D or complex conformal (3D) structures. These locations are determined

by a computer-controlled translation stage, which moves a pattern-generating device, for example, ink deposition nozzle or laser writing optics, to create materials with controlled architecture and composition. DW technologies complement the conventional manufacturing techniques such as photolithography for applications that need rapid turnaround and/or pattern iteration, for reducing the environmental impact,[38] for conformal patterning and modeling intricate components, circuits, and sub-assemblies.[114]

DW methods can be used for both conductive and non-conductive materials[2,7,10,12,115–119] including many of the materials introduced in the previous section. DW does not require expensive tooling, dies, or lithographic masks required in conventional electronics fabrication making it a low-cost, consumer-friendly process. In general, DW techniques have the following attributes:

1. The resolution of the features printed by DW ranges from ~250 to 0.1 μm.
2. DW techniques are compatible with various classes of materials including metals, ceramics, polymers, and biological materials such as cells. These materials can be used as powders, slurries, or suspensions depending on the technique employed for printing.
3. DW can print directly passive components such as conductors, resistors, inductors, and dielectrics.
4. DW can increase the reliability of electronic components since no soldering is needed to connect the circuitry.
5. DW can print directly on a variety of substrates including flexible surfaces such as paper and plastics.
6. Since DW deposits materials on-demand, it produces minimal waste and has a small environmental footprint. It can also achieve dramatic weight, cost, space, and inventory savings.
7. DW requires fewer steps compared to conventional subtractive processing and thereby reduces the prototyping time, which is helpful in products with short life-cycle (e.g., electronics).
8. DW allows for front-end inventiveness (due to reduction in the turnaround time) and back-end processing for design revisions thus reducing the time to market of parts from weeks to days.
9. Specialty parts can be built *on the fly* in small volumes without the need for mass production setup and capital investments.

Although DW techniques have many desirable attributes, there exist some key challenges when using it to print electronics into or onto 3D objects.

8.6 Why Does DW Not Translate Readily to 3D Printing?

AM is based on depositing and stacking materials one layer at a time. It therefore seems intuitive that DW techniques—which have been developed to printing electronics in 2D—could be utilized for depositing layers of electronic materials as part of the AM process of building

a 3D device. DW processes have several limitations that make it challenging to translate into 3D printing electronics:

1. Electronics are composed of multiple materials and therefore would necessitate multiple nozzles for dispensing. Each material may have different processing requirements.
2. The minimum feature size of DW is about 4–5 orders of magnitude poorer than photolithography (c.f. Figure 8.4)[43] and therefore cannot produce circuitry as sophisticated as conventional electronics.
3. DW requires fluidic inks that can be dispensed with controlled viscosity, surface tension, and solid content. Dispersions of inorganic or metal inks have the tendency to clog creating non-uniform depositions on the substrate.
4. DW inks often contain solvents and additives that require time to dry, which can slow processing speeds. These solvents can also interact with the underlying substrate in an undesirable manner and the ink needs to be tuned to properly wet the underlying substrate. Additives can improve the printability of inks, but can also affect the electronic functionality of the printed structures.[66]
5. DW inks often require thermal post-processing for attaining the desired electrical and mechanical properties, which limits the variety of substrates onto which the inks may be printed and adds processing steps.
6. Adhesion of DW materials to the AM substrates and external circuitry is decided by factors such as substrate swelling, surface energy and wettability, roughness, and chemical interactions between them.
7. The thickness of layers of *electronic materials* patterned by DW is often much thinner than the layers of polymer deposited by AM, which leads to incommensurate length scales and the need to do multiple layers of printing by DW to equal one by AM.
8. DW techniques are generally poor at making self-supporting or spanning structures. Features printed by DW usually need an underlying substrate for support.
9. DW techniques are intended primarily for smooth 2D, planar substrates, whereas 3D parts produced by AM are often rough.
10. Multifunctional materials often have different physical properties. For example, materials with different thermal expansion coefficients can lead to stress and ultimately delamination.
11. The feature quality obtained after DW printing multiple layers of a single material in 3D can suffer due to factors such as unstable print head temperatures or possible smearing, which can occur due to unsolidified previous layers.

8.7 Categories for Generating Electronics in 3D Objects

Up to this point, the chapter has focused on the reasons why existing strategies for fabricating electronics do not easily translate to 3D printing. These challenges motivate the categorization of approaches for integrating electronics in 3D parts into three categories as follows:

1. *Hybrid chip insertion approach:* Section 8.3 established that conventional electronic processing is capable of fabricating complex circuitry, but in a manner that is not compatible with AM. Thus, one approach is to create the electronic components separately using high-throughput, high-resolution processing and then to insert the resulting components (which are usually *off-the-shelf* and commercially available) onto or into a 3D printed object. This hybrid approach is disruptive to the printing process and breaks away from the spirit of 3D printing, but it has the advantage of providing sophisticated circuitry into 3D parts. There are, however, two challenges: (1) How does one transfer the electronics? and (2) How does one connect the electronic components?
2. *Surface DW approach:* This technique uses DW methods to print electronic components directly onto the surface of 3D objects created by AM. Typically, approaches in this category have additional challenges that go beyond those encountered while writing onto 2D substrates. It also requires the ability to print multiple (two or more) materials in parallel or sequence.
3. *Freeform multi-material 3D printing approach:* These techniques can produce true, self-supporting 3D parts (e.g., arches, out-of-plane structures, spanning structures) on their own using DW, but are often used in conjunction with other techniques to make useful parts because of the limited materials pallet that exists today.

We first briefly discuss hybrid chip insertion methods (Category 1) and then organize the remainder of this chapter by relevant DW techniques (Categories 2 and 3).

8.7.1 Hybrid Chip Insertion Approach (Category 1)

8.7.1.1 Pick and Place

Conventional electronics (e.g., ICs) provide sophisticated functionality using fabrication techniques that are not compatible with AM processing. One strategy for integrating electronics is to simply take off-the-shelf parts and place them into a 3D printed part. Although this approach is disruptive to the printing process and the least scalable approach, it is the simplest. There are few examples of academic research that focus on this technique.[15,120–125] The main challenge is finding ways to connect individual components (e.g., batteries, LEDs, CPUs, memory elements) within a 3D printed device beyond the conventional means of wire bonding and soldering. The approaches of Category 2 have the potential to address these challenges using processes that are compatible with AM.

8.7.1.2 Ultrasonic Consolidation for Embedding Electronic Structures

Ultrasonic consolidation (UC)[126–128] deposits metallic foils using ultrasonic energy to make metallic parts that could potentially contain electronic structures. UC[129] bonds each foil layer to the substrate (or previously deposited layers) using an oscillating sonotrode as shown in Figure 8.5[130,131] that applies heat, pressure, and friction to produce solid-state bonds. After bonding, an integrated three-axis CNC milling machine may be used to produce the desired contours for each layer.

Most metal parts fabricated by conventional AM techniques use powder bed fusion (PBF) processes, which sinter metal powders to form a coherent solid structure.[132] These processes require large processing temperatures that are not compatible with most electronic components. UC can make complex metal parts with high-dimensional accuracy and surface

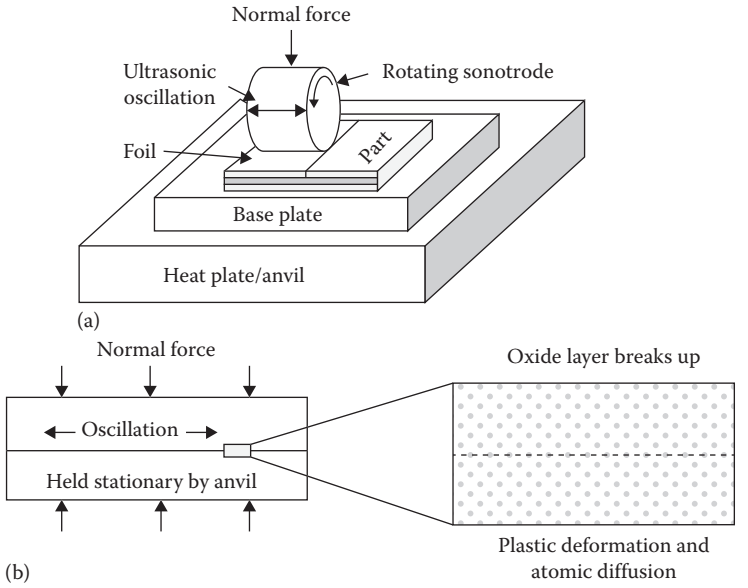

FIGURE 8.5
Schematic showing the UC process. (a, b) UC works by vibrating a foil material against a base substrate with a sonotrode layer by layer. (Adapted from Obielodan, J.O. et al., *J. Mater. Process Technol*., 211, 988–995, 2011.)

finish at low temperatures without the need for high temperature sintering. The UC process can be performed at various temperatures ranging from room temperature to ~200°C. Generally, a temperature of 150°C is used, which is a relatively low temperature compared to other metal fabrication processes.[132] In addition, PBF processes are often done in inert environments to avoid powder explosions or undesired oxidative reactions[132]; UC does not require an inert enclosure. Since UC does not involve melting/sintering; the dimensional errors due to shrinkage, residual stresses, and distortion that are typically caused by high temperature processing[133] are less pronounced than with some other processes.

Electronic components can be manufactured directly into a solid metal structure (using DW)[126] and subsequently completely enclosed to form an embedded structure (using UC).[134] Although these two processes are usually done separately, it could, in principle, be possible to integrate a DW deposition head onto a UC apparatus, which would eliminate the need to move the part between apparatuses. UC can construct various metallic objects with complex internal passageways, objects made up of multiple materials (engineering materials such as SiC fibers; Fe; Ni; Cu; and dissimilar combinations such as Al/brass, Al/stainless steel, and Al/Ni),[133,135] and objects integrated with wiring, fiber optics, and sensors.

8.7.1.3 Integrating Circuitry Using Transfer Printing

Transfer printing techniques are motivated by the desire to independently fabricate electronics using the most suitable conventional fabrication techniques on the most appropriate substrate (called a *donor* substrate), transfer them temporarily onto a elastomeric stamp (this stamp is sometimes called a *transfer* substrate—TS), and then later transfer

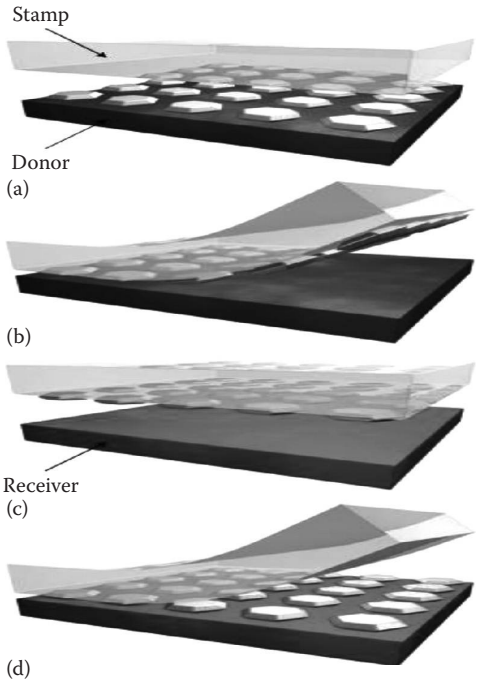

FIGURE 8.6
(See color insert.) Schematic illustration of the generic process flow for transfer printing solid objects. (a) Laminating a stamp (TS) against a donor substrate and then quickly peeling it away, (b) pulling the microstructures (PL) from the donor substrate onto the stamp (TS), (c) contacting the stamp (TS) to another substrate (DS), and then (d) slowly peeling it away transfers the microstructures (PL) from the stamp (TS) to the receiver (DS). (Adapted from Meitl, M.A. et al., *Nat. Mater.*, 5, 33–38, 2006.)

them onto a less conventional *receiver* or *device* substrate (DS—i.e., the substrate where the electronics will ultimately reside). This technique transfers only the thin active layer of electronic components, which differs from the pick-and-place (Section 8.7.1.1) transfer of electronics in relatively bulky, finished packaging.

Figure 8.6[136] describes the transfer printing process. The transferred components are called the *printed layer* (PL); the PL is not actually *printed*; rather, it is fabricated using conventional fabrication techniques on the donor substrate. For example, electronic components (PL) may be created on a silicon wafer (a donor substrate) and then later transferred as a thin film onto a plastic sheet (DS) using an elastomeric stamp (TS). To our knowledge, little work has been done using transfer techniques to deposit electronics onto or into 3D objects, but it is possible in principle. Many of the transfer techniques rely on fabricating circuits on donor substrates that allow the features to be released to a temporary polymer TS.[136–140] The transfer printing process is relatively simple and thus compatible with many different materials.

There are a number of methods to release the patterned features that reside as a thin, top layer on the donor substrate including undercutting via etching. The transfer of a PL from a TS to a DS is done via conformal contact, which is driven by generalized adhesion forces that are typically dominated by van der Waals interactions[141–143] but may also be controlled by the viscoelastic properties of the TS.

Transferring a PL from one surface to another requires differential adhesion. If the work of adhesion (W_A) at the DS/PL interface is larger than the TS/PL interface, the printable layer will remain on the device substrate upon removing the TS. However, if the work of cohesion (W_C) of the PL is less than the work of adhesion for the printable layer with both substrates, that is, $W_C(PL) < W_A(DS/PL)$ and $W_A(TS/PL)$, then the printable layer will be only partially transferred. Furthermore, if during the transfer printing process, the transfer substrate makes contact with the device substrate, then, in addition, the work of adhesion between the substrates must be less than the work of cohesion of both the substrates.

A practical implementation of the above requirements can be established using chemical surface treatments. Adhesion between two surfaces can also be controlled kinetically,[136] that is, the peeling rate of the TS from the DS impacts the adhesion of the PL owing to the viscoelastic behavior of the TS. A limitation of such an approach is the possible pattern distortion from using soft stamp materials. This method is similar to the parallel pick-and-place technology[144–147] that is compatible with extremely thin, fragile device components, originally developed for manipulating individual silicon transistors.

8.7.1.4 Laser-Assisted Transfer

Transfer printing of electronic materials from a donor film to the device substrate can also be carried out using laser-assisted transfer. Transfer printing can be assisted by high power lasers,[148–152] which serve as a precision thermal source to locally heat regions of the substrate to high temperatures. The donor film is comprised of several components—a laser transparent substrate (e.g., polystyrene, polyvinyl acetate, or polyethylene), a thin polymeric film, which has a high optical coefficient of absorption to the wavelength of the laser, and a thin layer of metals (e.g., nickel, gold, silver, among others) deposited by physical vapor deposition.

A schematic of this transfer method is shown in Figure 8.7.[148] During exposure to a laser, the absorptive layer is vaporized and propels the metal composite toward the target substrate. When the film reaches the substrate, it forms a cold weld or pressure bond.

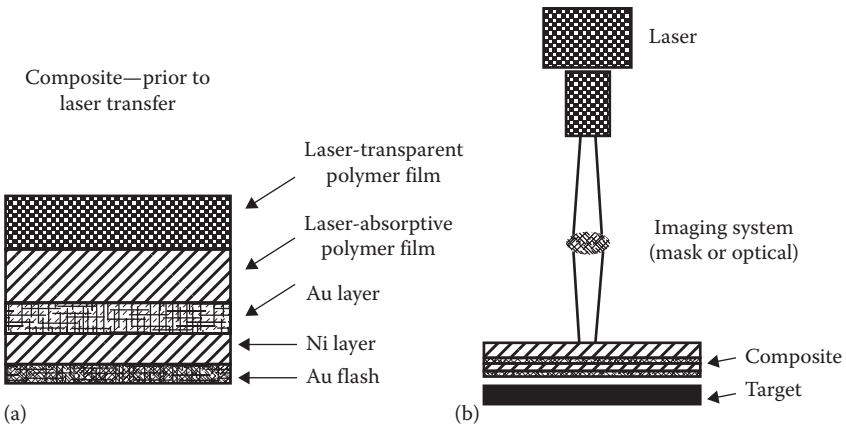

FIGURE 8.7
(a, b) Schematic of laser-assisted transfer technology. (Adapted from Zhang, J. et al., In *Direct-Write Technol. Rapid Prototyp.*, Piqué, A., 33–54, Academic Press, 2002. http://www.sciencedirect.com/science/article/pii/B9780121742317500543.)

This method can transfer a variety of electronic-grade materials for microelectronics manufacturing such as passive components, conductors, and batteries by supplying materials on a ribbon or donor film. The feature sizes are of the order of 25 μm due to the small spot size and high energy possible with commercial laser systems. An appeal of this approach is that it delivers quality electronic materials onto a target substrate without the need to heat the substrate. It does, however, require expensive optics and control systems for maintaining the appropriate gap between the ribbon and the target substrate.

8.7.1.5 Connecting the Transferred Components

The techniques within this section place or transfer electronic components onto a target substrate, but these components often still need to be interconnected. The next section discusses DW techniques that, in principle, could be used to connect discrete components electrically.

8.7.2 Surface DW Approach (Category 2)

One approach for building electronics into a 3D object is to use AM to fabricate parts (typically composed of plastic or ceramic) that have surfaces onto which the electronics circuits may be printed or patterned using DW techniques. This combination of AM approaches to form multifunctional 3D structures of arbitrary and complex form with directly integrated printed electronics offers unique functionality while addressing the cost/performance demands of the manufacturing technology. There are in general two categories of DW techniques: (1) those that can deposit functional materials in a single deposition step, and (2) those that deposit materials that have to be subsequently processed (at low/high temperatures) to induce controlled and reproducible functionality. DW techniques are usually classified based on the deposition mechanism. Figure 8.8 shows the classification of the various DW techniques.[2]

We only discuss DW techniques that have been utilized for electronics. Each technique differs in resolution, writing speed, 3D and multi-material capabilities, operational environment (gas requirement, pressure, and temperature), and what kind of final structures can be built. The common feature to all techniques is their dependence on high-quality

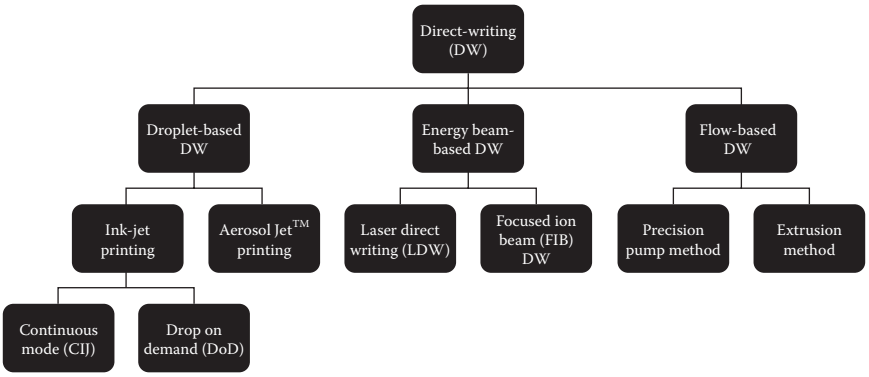

FIGURE 8.8
Classification of surface direct-write (DW) methods. (Adapted from Hon, K.K.B. et al., *CIRP Ann.—Manuf. Technol.*, 57, 601–620, 2008.)

starting materials, with specially tailored chemistries and/or physical properties such as viscosity, density, rheology, surface tension/wetting properties, mean particle geometry, size and distribution, coefficient of thermal expansion, solids loading, and porosity. The selection of materials must be based on additional chemical and process factors such as solvent and binder removal, the reactivity, chemical compatibility, stress development, sintering rate, and the direct-write tool used.

The starting materials termed as *pastes* or *inks* may consist of combinations of powders, nanopowders, flakes, surface coatings, organic precursors, binders, vehicles, solvents, dispersants, and surfactants. These materials can serve as conductors[153,154] (based on silver/gold/copper/palladium/copper or alloys), resistors[155,156] (based on polymer thick film and ruthenium oxide), and dielectrics[157,158] to make various passive electronic components on low-temperature flexible substrates such as plastics, paper, and fabrics. The field is advancing rapidly, and no single source covers all the different technologies. We will briefly discuss the most relevant techniques and point the reader to additional resources as needed.

8.7.2.1 Droplet-Based DW

Droplet-based DW consists mainly of two techniques: (1) Ink-jet printing and (2) Aerosol Jet™ printing.

8.7.2.1.1 Ink-Jet Printing

8.7.2.1.1.1 Process Ink-jet-based DW[6,12,54,132,159,160] is a highly advanced technique. Ink-jet printing is a droplet-based technology that places materials where they are needed via the ejection of liquid material from a single nozzle or multiple nozzles to precise locations by thermal or piezoelectric actuation. For this process, the jetted material must be a liquid with appropriate physical properties including viscosity, surface tension, and density. Ink-jet printing is appealing because it is low cost, high speed and involves non-contact processing. There are two key types of ink-jet printing technologies, continuous ink jetting (CIJ) and drop on demand (DoD). In case of CIJ printing, the ink reservoir is pressurized to ensure that a continuous stream of material passes through a nozzle which breaks up into individual uniform droplets as it issues from the orifice according to the waveform generated by the piezoelectric transducer. In the case of DoD printing, droplets may be ejected from the nozzle using a joule heater to heat and volatilize ink or by deforming a piezoelectric material in the print head. Both methods create the required pressure difference for dispensing the droplet on demand. Thermal and piezoelectric techniques are the most common approaches for DoD printing, but although the droplets can also be ejected by other methods such as electrostatic and acoustic actuation.[161] Both CIJ and DoD have four stages of development[162] when a droplet impacts the substrate (kinematic, spreading, relaxation, and wetting), which are time-dependent and controlled by physical forces like inertia, viscosity, and surface tension. In the earlier stages of impact, inertial forces dominate and viscous forces are weak. After impact, capillary (surface tension) forces become more important. Thus, these factors must be considered when designing new ink-jet printing applications.

8.7.2.1.1.2 Materials, Writing Speed, and Resolution Ink-jet systems usually work best with low viscosity materials (up to 100 mPa-s) that have low interfacial tension[6,163–167] (~20 dynes/cm). Various materials are compatible with ink-jet printing including metal particle suspensions (gold/silver/copper/aluminum), ceramic particle suspensions, and electronic/

optical materials such as epoxies, solders, and organometallics, among others. Since ink-jet printing is a non-contact deposition method, it is compatible with a variety of substrates including metals, ceramics, polymers, and silicon. The volumetric dispense rate[2,113,168] of a single nozzle is typically on the order of 0.3 mm^3/s (DoD) and 60 mm^3/s (CIJ), which can be increased by using an array of nozzles. The resolution of ink-jet-based DW[2,113,132,169] is measured in terms of the droplet size that can range from ~20 μm to 1 mm for CIJ printing and ~15 to 200 μm for DoD printing.

8.7.2.1.1.3 Applications in Electronics Ink-jet-based DW has been used in the field of electronic manufacturing since the 1980s and recently in printed electronics[55,170–176] such as solar cells, transistors, OLEDs, RFIDs, MEMS, and wireless communication, among others. For example, the DoD ink-jet approach can microdeposit organic light-emitting polymers[70] and phosphors, solder bumps,[177,178] spacer balls, electrical interconnects, and adhesive sealant/bond lines in the manufacture of display panels.[179,180] Both CIJ and DoD methods have been used to achieve solder drops from tens to hundreds of micrometers in diameter, with the capability to produce continuous lines and tracks as well as discrete spheres or dots as shown, for example, in Figure 8.9.[177] Figure 8.10[181] shows an electrostatic rotary motor where the electrodes are printed in five layers of silver nanoparticle ink with a 100 μm line trace width and the diameter of the whole device is 25 mm. Using a mixture of metal nanoparticles to form a core-shell dispersion, ink-jet printing has also been able to print RFID antennas onto photo paper.[182]

8.7.2.1.1.4 Challenges The major challenge in ink-jet printing is to control the four stages of development, which are dynamic in nature, using process parameters like impact velocity and initial drop diameter in order to achieve uniform printing. The drop formation is also affected by inertia, viscosity, and surface tension.[166] For example, undesirable splashing can occur if the drop formed is large with high impact velocity and the fluid has low surface tension and viscosity. Hence, it becomes necessary to study these parameters[162,183] in detail. The development stages decide whether we obtain homogenous CIJ/DoD or a mixture of these processes, which directly affects the quality of the printed structure.

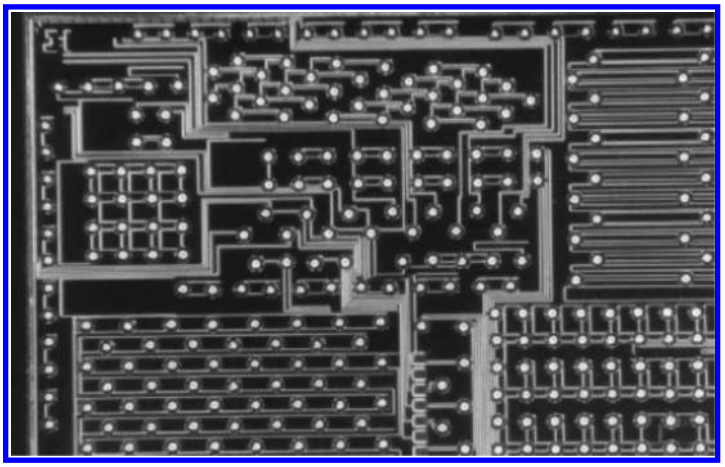

FIGURE 8.9
Image showing solder bumps (70 μm diameter) deposited by DoD ink-jet printing onto an IC test substrate. (Adapted from Hayes, D.J. et al., *MicroJet Printing of Solder and Polymers for Multi-Chip Modules and Chip-Scale Packages*.)

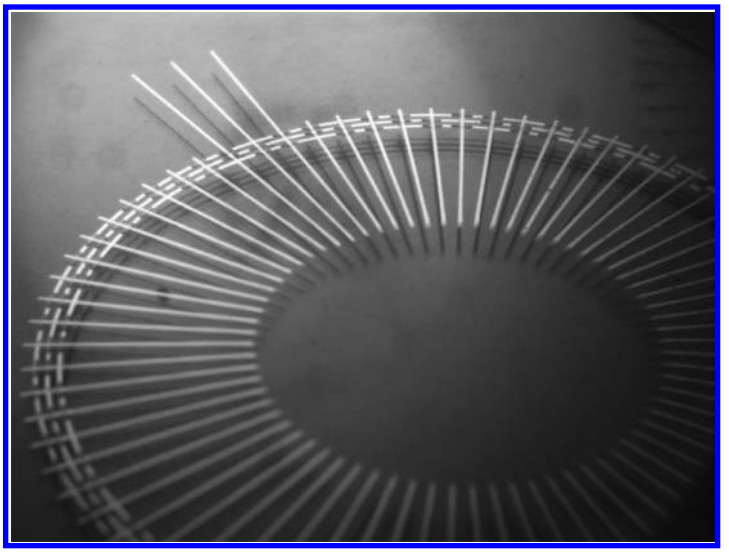

FIGURE 8.10
Optical micrograph of an ink-jet printed electrostatic rotary motor. (Adapted from Fuller, S.B. et al., *J. Microelectromechanical Syst.*, 11, 54–60, 2002.)

Electronic features with high conductivity need high concentrations of metal particles; however, high concentrations make the ink more viscous and therefore difficult to jet.[164] Typical formulations contain 30%–40% metal by weight although up to 50% loadings can be found. These higher percent loadings implement very small particle sizes which create the challenge of agglomeration that reduces jetting reliability. Ink-jet printing can also be carried out by the direct deposition of bulk metals in liquid form using elevated temperatures to melt the metals. Bulk metals with higher melting points pose significant challenges for print head design since they have large surface tensions, they tend to oxidize, and they can easily ruin the piezoelectric transducer. This problem can be avoided by using other actuation methods such as direct pneumatic ejection[184] via DoD printing. Metallic particles suspended in a suitable fugitive liquid can be printed by ink-jet processes and are used for both structural and electrical applications. In these applications, small particles are usually favored as the suspensions formed are more stable (i.e., the particles do not sediment), which lowers the chance of nozzle clogging. In addition, these particles have a high surface area-to-volume ratio which thus requires lower post-processing sintering temperatures.[153,181] Nanoparticle metal ink (Ag/Cu/Al/Ni) suspensions in which the solvent does not evaporate but cures to form a binder usually have lower conductivity than bulk metal inks, which affects the electrical performance in the final device.[37] Other challenges exists as covered in Section 8.6.

8.7.2.1.2 Aerosol Jet™ Printing

8.7.2.1.2.1 Process As the name implies, Aerosol Jet™ is the spraying of inks composed of small droplets dispersed in a liquid as seen in Figure 8.11.[2]

The process contains two main components: the atomizer and the deposition head. The atomizer is either an ultrasonic or pneumatic device that generates a dense vapor (mist) of

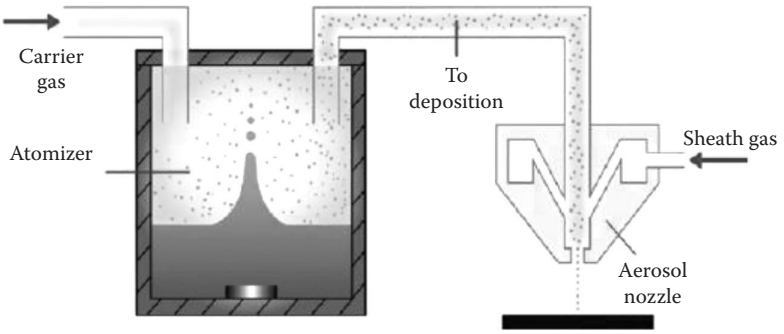

FIGURE 8.11
Schematic of Aerosol Jet™ printing system. (Adapted from Hon, K.K.B. et al., *CIRP Ann.—Manuf. Technol.*, 57, 601–620, 2008.)

material droplets. A carrier gas such as nitrogen passes through the atomizer to transfer the mist into the deposition head. The resulting annular flow leaves the deposition head through a nozzle onto the substrate. Aerosol Jet™ printing is particularly well suited to 3D applications as its deposition head can be mounted to a five-axis positioning stage to follow the contour of the substrate at a fixed stand-off distance (typically 1 to 5 mm).[113] In addition, it is possible to obtain fine feature definition as the aerosol consists of a high density of micro-droplets that are aerodynamically focused to produce lines as narrow as ~10 μm.[185] The features can deposit easily and conformally over non-planar surfaces.

8.7.2.1.2.2 Materials, Writing Speed, and Resolution An appeal of Aerosol Jet™ printing is that it can print features with fine resolution using a variety of processing materials and more clog-resistant nozzles, which is challenging in ink-jet printing systems. Aerosol Jet™ systems can handle materials in a wide viscosity range, that is, between 0.001 and 2.5 Pa-s, and thus enables a wide range of materials[186] that can be deposited including metals, alloys, polymers, adhesives, and organic electronics, among others. The deposition rate obtainable from a single nozzle is about 0.25 mm^3/s, which can be increased by using an array of nozzles. The resolution of Aerosol Jet™ printing is measured in terms of line width that ranges from 10 to 150 μm with thickness ranging from 10 nm to 5 μm.[2,185,186]

8.7.2.1.2.3 Applications in Electronics Aerosol Jet™ printing is widely used to print conductive traces using gold, silver, or other nanoparticles inks. Conductors can be formed by printing a seed layer, followed by electroless plating.[187] Embedded resistors can be fabricated by printing polymer thick film pastes. Figure 8.12 shows an example of a strain gauge sensor.[188] For 3D surfaces with larger surface profiles, the Aerosol Jet™ system makes use of three-axis printing as shown in Figure 8.13.[186]

8.7.2.1.2.4 Challenges This printing technique requires inks that can form aerosols, which may present a limitation for certain materials. For substrates with high coefficient of thermal expansion, thermal mismatch between the ink and substrate material can lead to cracking or delamination of the printed metallic circuit material, although this is a challenge of all multifunctional printing processes. Rough and porous surfaces can severely affect the behavior of the deposited ink as such surfaces have relatively high surface energy, which makes it difficult to form a clean and uniform deposit. This effect is aggravated when

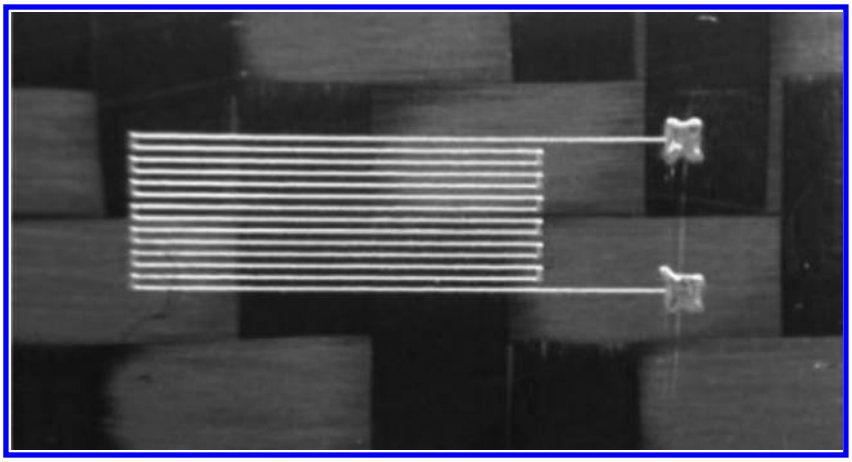

FIGURE 8.12
Image of an aerosol jet printed silver strain gauge on carbon fiber composite. (Courtesy of Optomec, Inc.; Adapted from Hedges, M. & Marin, A.B., 3D aerosol jet® printing-adding electronics functionality to RP/RM, In *Proc DDMC 2012 Conf*, Berlin, Germany, 2012. http://aerosoljet.com/downloads/Optomec_NEOTECH_DDMC_3D_Aerosol_Jet_Printing.pdf.)

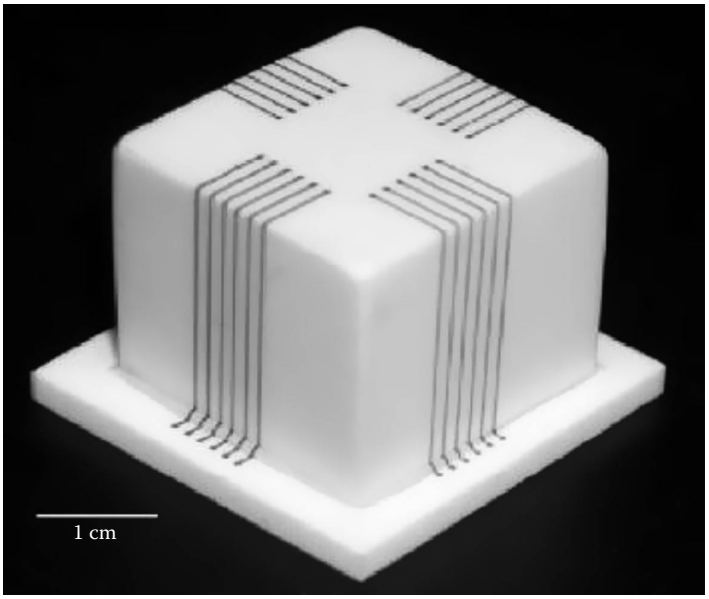

FIGURE 8.13
Image of 3D silver interconnects (150 μm line width) written over an alumina cube. (Courtesy of Optomec, Inc; Adapted from King, B. & Renn, M., Aerosol jet® direct write printing for mil-aero electronic applications. In *Palo Alto Colloq. Lockheed Martin*, 2009. http://www.optomec.com/downloads/Optomec_Aerosol_Jet_Direct_Write_Printing_for_Mil_Aero_Electronic_Apps.pdf.)

the surface roughness is much larger than the ink thickness as it affects the quality of the printed lines. This issue can be avoided by pre-machining the rough areas where the electrical circuit is to be printed, although that adds extra processing steps.

8.7.2.2 Energy Beam-Based DW

Energy beam-based DW consists of all those processes that use high-power laser/ion/electron beam sources[148–152,189] as a mode for deposition of a variety of electronic-grade materials on the substrate. These sources precisely heat local regions of the substrate to high temperatures for sintering and curing while taking care to avoid melting of the substrate. The feature sizes are of the order of 25 μm due to the small spot size and high energy made possible by commercial laser systems. These techniques are divided into two broad categories depending on the source of the energy beam used for DW: (1) laser DW (LDW), which uses photons, and (2) focused ion beam (FIB) DW (discussed in Category 3), which uses ions as the energy source. There are many different varieties of these techniques, but almost none of them have been used for electronics in 3D objects. These methods have not been used for integrating electronics due to large processing temperatures involved which can easily affect any surrounding electronic circuitry. This disadvantage also puts a limitation on materials and substrates used in the deposition process.

8.7.2.2.1 Laser DW

8.7.2.2.1.1 Process LDW uses a laser beam to create complex 3D structures with self-supporting features having fine resolutions without the use of expensive masks or lithographic methods. Laser writing techniques[9,190–202] create patterned materials through gas-phase deposition, ablation, selective sintering, or reactive chemical processes that include several methods such as thin film consolidation,[203,204] laser chemical vapor deposition[199] (LCVD), laser ablation,[193,194] laser-enhanced electroless plating[205,206] (LEEP), laser-induced forward transfer[207,208] (LIFT) and backward transfer[209] (LIBT), laser-guided DW[12] (LGDW), flow-guided DW[12] (FGDW), matrix-assisted pulsed laser direct-write[195,196] (MAPLE), two/multi-photon polymerization (MPP),[191,201] and selective laser sintering[9,197,198] (SLS), among others. All of these techniques utilize lasers to localize energy as a means to modify, deposit, or remove material.

8.7.2.2.1.2 Materials, Writing Speed, and Resolution Each technique places different demands on the laser writing tools and the physicochemical properties of the material being patterned. A wide range of materials can be deposited including metals, ceramics, polymers, semiconductors, and composites, among others which have been reviewed in the methods referenced earlier. The deposition rate or the writing speed is different for each method and the precursor or feed material used at the start of the process. With the exception of ablative approaches, most of the other techniques are capable of generating complex 3D structures with self-supporting features[191,210] at resolutions comparable to those achieved by various ink-based techniques.

8.7.2.2.1.3 Applications in Electronics LDW was introduced in the 1980s to enable the fabrication of micro-electronic circuits with 1D to 2D features and it was then developed in the 1990s to enable the creation of 3D features for applications such as photonic crystals and MEMS. More recently, these techniques have been employed in various devices such as microcapacitors, interconnects, phosphor displays, co-planar transistors, and resistors, among others. An example of a spiral inductor[36] fabricated using contact transfer is shown

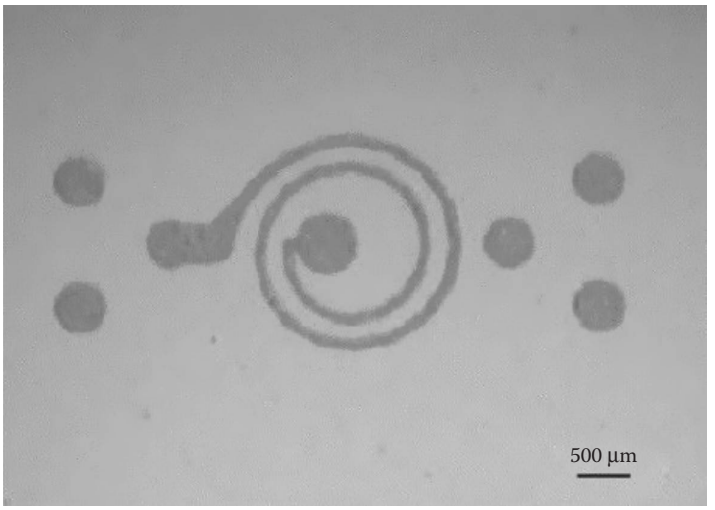

FIGURE 8.14
Photograph showing a spiral inductor deposited by contact transfer technique (derivative of MAPLE DW). (Adapted from Zhang, C. et al., *Microelectron. Eng.*, 70, 41–49, 2003.)

in Figure 8.14. Contact transfer is a derivative of MAPLE in which the mixture material is coated onto a flexible transparent backing film and dried at low temperatures (normally below 100°C) to form a dry, flexible ribbon that is vacuum chucked and placed in direct contact with the receiving substrate in a conformal manner. After the laser irradiation, the ribbon is peeled off and materials remain on the substrate in the laser-defined areas.

8.7.2.2.1.4 Challenges Most of the LDW techniques are limited by the availability of volatile metal-organic or inorganic materials, contamination of the deposited materials, and the need for expensive and specialized reaction chambers, vacuum equipment, and lasers. The processing temperatures (≤400°C) are not suitable for the fabrication of high-quality crystalline materials required for state-of-the-art electronic performance of the final device, even with laser sintering. The presence of porosity in the powders used for DW processes can severely affect the electric performance as it can reduce the effective dielectric constant by almost an order of magnitude.[211] Also, in gas-phase deposition, the morphology and the electrical conductivity of the deposited features are generally inferior when compared with the bulk material and the adhesion of the material to the substrate can be poor and difficult to control.

8.7.2.3 Flow-Based DW

Flow-based DW methods consist of processes that require positive mechanical pressure using a pump, air pressure, or extrusion to achieve precise micro-dispensing through a syringe tip leading to a continuous flow of ink, paste, or slurries on to the substrate. Extrusion systems are favorable for integration with AM because the DW tool tip is maneuverable, can dispense in different orientations, and can process high volumes of material. Flow-based DW approaches consist of two main techniques: (1) precision pump method, and (2) extrusion method.

8.7.2.3.1 Precision Pump Method

8.7.2.3.1.1 Process The precision pump method is a direct-dispensing tool integrated with nScrypt's novel pump called smart pump.[212] This pump is based on Sciperio's micro-dispense direct-write technology developed through the DARPA (US Defence Advanced Research Projects Agency) MICE program (Mesoscopic Integrated Conformal Electronics) in 2002. With this pump, dispensing is initiated via the opening of a valve that allows the material to be dispensed through the dispensing tip onto the substrate. The valve retracts to stop dispensing, and this retraction results in suction of material back into the dispensing nozzle thus resulting in cleaner, more precise printed features.

8.7.2.3.1.2 Materials, Writing Speed, and Resolution The pump is capable of dispensing very small volumes of the materials down to 20 pL and within a wide range of viscosities from 1 to 1,000,000 mPa-s, which makes it highly versatile with respect to the materials that can be used and the patterns that can be drawn with them. The maximum writing speed can be varied from 0.1 to 300 mm/s depending on the material and the application. The resolution measured in terms of the line width varies from ~25 μm to 3 mm depending on the material and the ceramic tip orifice diameter.

8.7.2.3.1.3 Applications in Electronics The process has a wide range of applications including, conductors, resistors, optics, adhesives, sealants, frit, solders, encapsulants, wire bonding, underfilling, flip-chip bumping, and MEMS. This system is capable of writing on highly non-conformal surfaces to make 3D structures. An example of non-conformal writing is shown in Figure 8.15.[212]

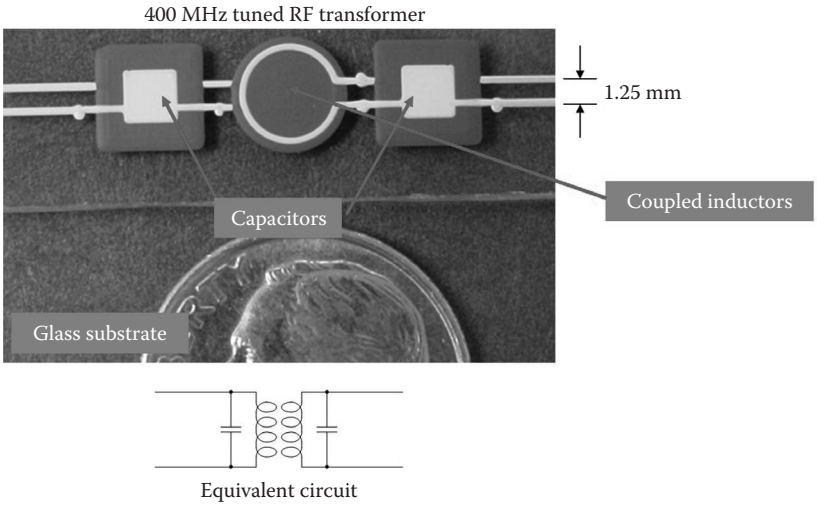

FIGURE 8.15
Image showing capacitors and coupled inductors dispensed on an uneven surface by the precision pump method to fabricate a printed RF device. (Adapted from Li, B. et al., Robust direct-write dispensing tool and solutions for micro/meso-scale manufacturing and packaging, In *ASME 2007 Int. Manuf. Sci. Eng. Conf.*, 715–721, American Society of Mechanical Engineers, 2007. http://proceedings.asmedigitalcollection.asme.org/proceeding.aspx?articleid = 1598546.)

8.7.2.3.1.4 Challenges The line width obtained from the pump is directly dependent on the material, which is often a slurry or paste, as well as the nozzle diameter. Generally, the minimum line width is at least 10 times larger than the average particle size in the specific paste.[213] Second, the flow rate is sensitive to the dispensing height (distance between the substrate and the dispensing tip) for a constant applied pressure. Thus, in order to maintain the line width, consistency, and accuracy, the dispensing height must be maintained at a constant value. This is generally accomplished by laser scanning the substrate and then dynamically adjusting the tool path's *z*-axis height based upon measured variations in surface height.

8.7.2.3.2 Extrusion Method

8.7.2.3.2.1 Process In this method, the flowable material/ink—typically in the form of liquid, particulate slurry, or molten polymer filament—is loaded into a syringe which is then connected to the writing head that moves with the help of a computer-controlled transition stage to create materials with controlled architecture and composition. Depending on the material used for deposition, several methods are available for patterning materials in 3D, which includes robotic deposition,[214] 3D printing,[215] fused deposition modeling[216,217] (FDM), curved-layer FDM (CLFDM),[218] and micropen writing,[219] among others.

8.7.2.3.2.2 Materials, Writing Speed, and Resolution The extrusion systems can dispense fluidized materials with viscosities up to 5000 Pa-s and are mostly used to dispense metal-based inks consisting of metal particles or flakes dispersed in a volatile solvent that evaporates after being dispensed. The metals used are most commonly gold or silver due to their resistance to oxidation. Less expensive carbon-based inks can also be dispensed with these systems, although these inks are less conductive than metal inks. Typical writing speeds are of the order of 300 mm/s and the resolution measured in terms of the line width varies from 50 μm to 2.5 mm depending on the method employed for DW.

8.7.2.3.2.3 Applications in Electronics Extrusion methods for DW can be used to fabricate functional electronics on AM substrates. These devices include embedded, wearable and conformal electronics,[220] batteries,[221] and discrete electronics.[125] Electronics can also be printed on flexible substrates such as paper[222] to form functional electronic components,[223] including thermochromic displays,[224] disposable RFID tags,[225,226] and cellulose-based batteries,[227] to name but a few examples.

Figure 8.16[117] shows an application of conductive strain gauge devices formed by extruding liquid metal on a glass. Because the metal is liquid, these strain gauges can also be directly written and encapsulated in elastomeric substrates such as polydimethylsiloxane (PDMS) to obtain stretchable electronics.

8.7.2.3.2.4 Challenges For extrusion DW applications, the metal content of the ink is a critical factor. Higher loading results in higher particle density and thus better conductivity. However, inks with high metal loadings are more viscous and require more pressure to dispense. Their high particle content can lead to clogging issues in the dispensing nozzles and limit the minimum feature size. Thus, using larger nozzle tip diameters represents a trade-off; it reduces clogging but increases the minimum achievable feature size. The printing quality is also affected by several other factors such as the surface energy, ink formulations, roughness, and wettability of the substrate, which have been enlisted in Section 8.6. An additional difficulty is the fabrication of multifunctional complex electronic devices due to non-conformal geometry of these devices which helps to focus the discussion to the next section where we discuss techniques for 3D printing electronics.

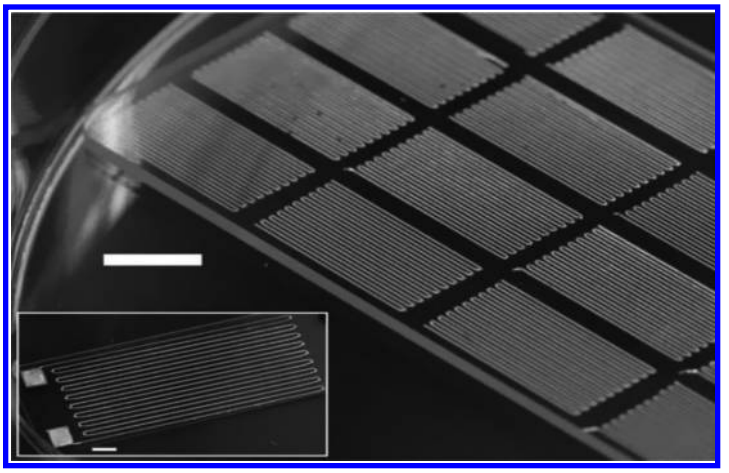

FIGURE 8.16
A photograph of multiple strain gauge devices made up of gallium–indium on glass. These patterns were written using a 119-μm inner diameter nozzle. Inset shows a larger scale directly written strain gauge on glass. Scale bars are 5 mm in length. Device and pads were written using a 379-μm inner diameter nozzle. (Adapted from Boley, J.W. et al., *Adv. Funct. Mater.*, 2014. doi:10.1002/adfm.201303220.)

8.7.3 Freeform Multi-Material 3D Printing Approach (Category 3)

Freeform multi-material 3D printing approaches are capable of producing free-standing, out-of-plane structures with electronic functionality. Most of the techniques are inspired by DW extrusion techniques. The use of inks that can form out-of-plane structures distinguishes the examples in Category 3 from those in Category 2. The resulting structures—typically metals—can be encased in different materials such as polymers, elastomers, or ceramics to obtain functional electronic devices.

8.7.3.1 Omnidirectional Printing

8.7.3.1.1 Process

Colloidal suspensions (e.g., silver nanoparticles in water) are extruded from a syringe.[10,116,221,228–232] Due to the shear yielding rheology of these inks, the material only flows when it is sheared and the printed structures stabilize due to the rheological properties of the inks. As a result, this process can create mechanically stable, out-of-plane structures. As the solvent (e.g., water) evaporates, the structures become even more stable. The structures become conductive as the particles move closer together, but ultimately need to be sintered to improve the conductivity closer to that of bulk metal.

Metal 3D structures can also be electrodeposited[233] to write pure copper and platinum in an ambient air environment to fabricate high density and high quality, complex, microscale and nanoscale metallic structures like interconnects. The electrodeposition relies on an electrolyte-containing micropipette with a microscopic dispensing nozzle as the working toolbit. The electrodeposition is initiated within the substrate surface confined by the meniscus between the dispensing nozzle and the substrate surface using an appropriate electrical potential between the electrolyte contained in the micropipette and the substrate surface.

8.7.3.1.2 Materials, Writing Speed, and Resolution

3D structures consisting of continuous solids, with high aspect ratio (e.g., parallel walls), or self-supporting features that must span gaps in the underlying layers can be fabricated through controlled ink composition, rheological behavior, and printing parameters. This emerging technique has been demonstrated with inks that are typically formulated from shear-thinning concentrated colloidal suspensions or gels,[10,116,234–238] fugitive organic/polymeric[10,238–242] melts, composites,[10,243–245] polyelectrolyte,[10,239,241,246–248] and sol-gel[249,250] building blocks suspended or dissolved in a liquid or heated to create a stable, homogeneous ink with the desired rheological (or flow) behavior. The important rheological parameters for a given ink design include its apparent viscosity, yield stress under shear and compression, and viscoelastic properties (i.e., the shear loss and elastic moduli), which are tailored for the specific direct-write technique of interest. The writing speed is usually decided by the DW method chosen. The DW of 3D periodic architectures with filamentary features ranges from hundreds of micrometers (~250 μm) to sub-micrometer in size (~0.1 μm).

8.7.3.1.3 Applications in Electronics

The omnidirectional structures can be utilized in wire bonding to fragile 3D devices,[116,251] spanning antennas,[228] batteries,[221] and interconnects[116,252] for solar cell and LED arrays. These structures can also act as functional composites,[253] microfluidic networks,[240] and templates for photonic band-gap materials[254] and inorganic–organic hybrid structures.[239] Figure 8.17 demonstrates the conformal printing of a small 3D antenna.[228] A 100-μm metal nozzle is used to print meander-line patterns on the surface of a glass hemisphere.

Omnidirectional printing has also been exploited to create free-standing interconnects as shown in Figure 8.18[116] for commercially available gallium nitride LED arrays. This ability to print out-of-plane enables the microelectrodes to directly cross pre-existing patterned features through the formation of spanning arches. Such conformal printing of conducting features enables several applications, including flexible,[173,255] implantable[256] and wearable[257] antennas, electronics, and sensors.

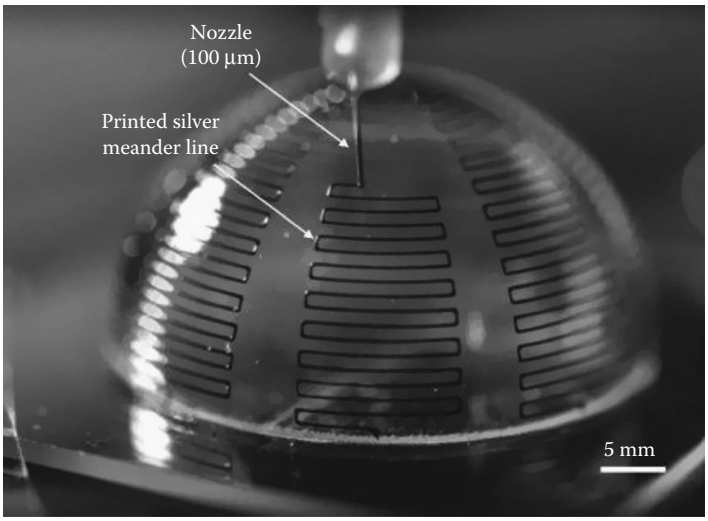

FIGURE 8.17
Optical image captured during conformal printing of electrically small antennas on a hemispherical glass substrate. (Adapted from Adams, J.J. et al., *Adv. Mater.*, 23, 1335–1340, 2011.)

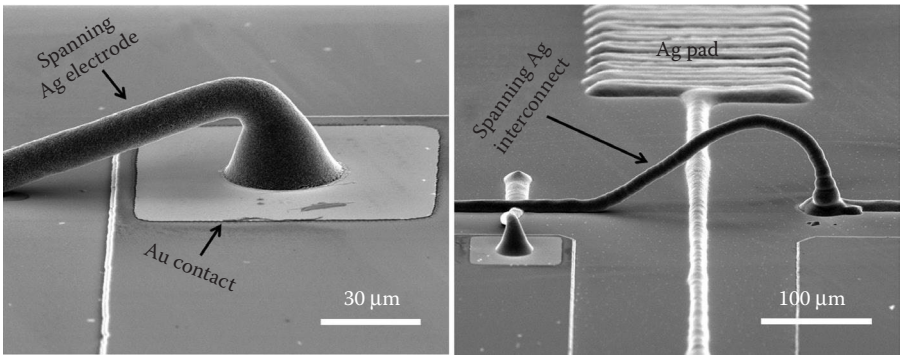

FIGURE 8.18
SEM images of a silver interconnect arch printed on a gold contact pad (80 by 80 µm) (left) and over an electrode junction (right). (Adapted from Ahn, B.Y. et al., *Science*, 323, 1590–1593, 2009.)

It is also possible to direct write 3D microvasculature networks out of polymers as fugitive inks, which can then be backfilled or infiltrated with electronic inks.[240] First, these inks must flow through a fine deposition nozzle under high shear, yet be self-supporting under ambient conditions. Second, the ink scaffold must maintain its shape during resin infiltration and curing. Finally, the ink scaffold must liquefy at modest temperatures to facilitate its removal from the polymer matrix, leaving behind an interconnected network of microchannels.

8.7.3.1.4 Challenges

Most of the challenges faced with omnidirectional printing are the same as those observed in DW extrusion-based techniques discussed in Section 8.7.2.3.2. Most of the shortcomings are unique to the ink. For example, colloidal gel-based inks require significant applied pressures to induce flow during deposition and suffer clogging problems when the nozzle-to-particle diameter is reduced to below ~100.[235,236] Most of the materials used for omnidirectional printing need sintering at high temperatures for densification and reduction of porosity in the final structure. The resulting structures can be quite conductive, but are not at the same level as bulk metals.

8.7.3.2 Liquid Metal Printing

8.7.3.2.1 Process

Liquid metals offer the electrical and thermal benefits of metals combined with ease of printing to enable the 3D printed fabrication of soft, flexible, and stretchable devices at room temperature. It is possible to direct write a low viscosity liquid metal (e.g., gallium and its alloys, such as eutectic gallium–indium alloy[258]) at room temperature into a variety of stable free-standing 3D microstructures[259,260] (cylinders with aspect ratios significantly beyond the Rayleigh stability limit,[261] 3D arrays of droplets, out-of-plane arches, wires as shown in Figure 8.19). These liquid metals have low viscosities (similar to water) at room temperature and are therefore easy to extrude. They form mechanically stable structures despite being liquids due to the presence of a surface oxide that forms spontaneously and rapidly.

The general approach for printing these liquid metal microstructures is by applying modest pressures to a syringe needle that extrudes the liquid metal wire onto a substrate controlled by a motorized translation stage. In addition to extruding wires, it is possible to form free-standing liquid metal microstructures using three additional methods:

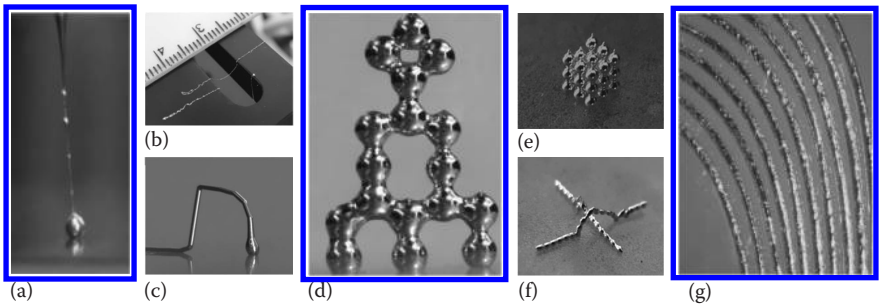

FIGURE 8.19
DW of liquid metal 3D structures. Photographs of the diverse free-standing, liquid metal microstructures that can be direct printed at room temperature. (a) Liquid metal ejected rapidly from a glass capillary forms a thin wire. (b) These fibers are strong enough to suspend over a gap despite being composed of liquid. (c) A free-standing liquid metal arch. (d) A tower of liquid metal droplets. (e) A 3D cubic array of stacked droplets. (f) A metal wire and an arch composed of liquid metal droplets. (g) An array of in-plane lines of free-standing liquid metal fabricated by filling a microchannel with the metal and dissolving away the mold. Scale bars represent 500 μm. (Adapted from Ladd, C. et al., *Adv. Mater.*, 25, 5081–5085, 2013.)

(1) rapidly expelling the metal to form a stable liquid metal filament, (2) stacking droplets, and (3) injecting the metal into microchannels and subsequently removing the channels chemically.

8.7.3.2.2 Materials, Writing Speed, and Resolution

The writing is done using a binary eutectic alloy of gallium and indium (EGaIn, 75% Ga 25% In by wt.), but in principle, any alloy of gallium will work. EGaIn is liquid at room temperature (m.p. ~15.7°C) with metallic conductivity one order less than silver and copper.[262] The liquid metal exhibits a negligible vapor pressure and low toxicity. Upon exposure to air, the metal instantaneously forms a thin passivating *skin* composed of gallium oxide,[258] and the electrical resistance remains largely unaffected because the skin is thin.[263] In addition, the liquid metal adheres to most surfaces and alloys with many metals to form ohmic contacts. The writing speed or the draw rate is not yet known. The smallest components fabricated to date are ~10 μm.

8.7.3.2.3 Applications in Electronics

These techniques are used in conjunction with other methods to 3D print conductive devices[117,264–269] that are soft, flexible, and stretchable—properties that may be useful for creating stretchable electronics, soft robotics, and electronic skins. These extrusion methods can also be used for connecting electronic devices by embedding the microstructures in various substrates such as PDMS to form flexible and stretchable electronic devices. An example of such a structure is shown in Figure 8.20.[259]

8.7.3.2.4 Challenges

This approach is relatively new, and the process is not yet well understood. In the context of ink-jet printing, the combination of surface tension and the surface oxide makes these alloys non-printable without modifying either the material or the atmosphere. Additionally, the fast-forming oxide layer can potentially clog a nozzle orifice, further increasing the difficulty of printing Ga–In alloys. Finally, the resulting structures are liquid and therefore have to be embedded in a supporting structure for practical applications.

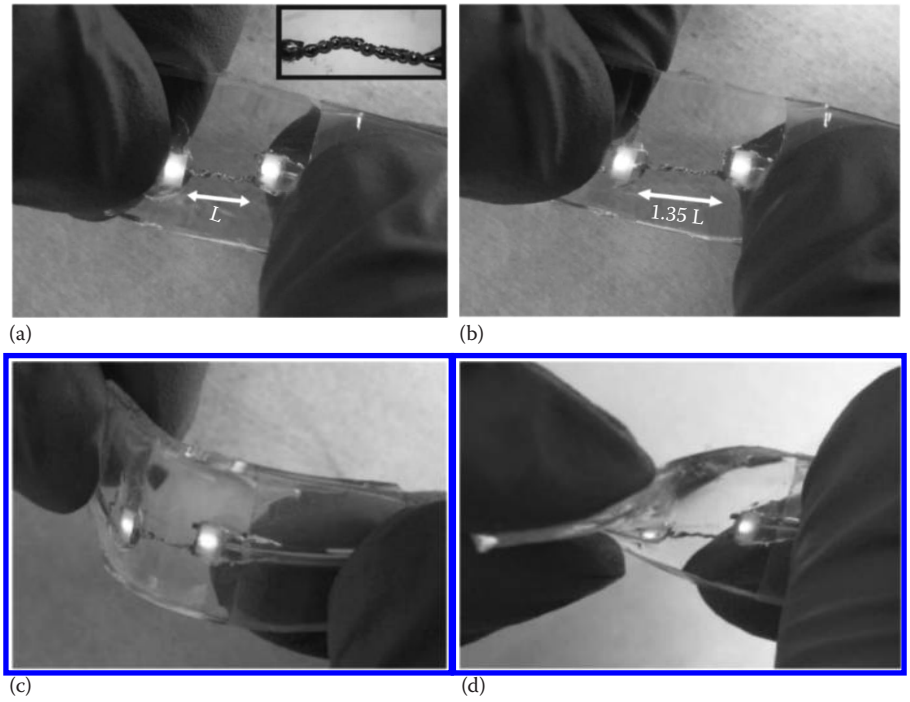

FIGURE 8.20
(See color insert.) Stretchable interconnects formed by DW. (a) A prototype device composed of two LEDs connected by a stretchable wire bond and embedded in PDMS (Inset: Microscopy image of the liquid metal wire bonds). (b–d): The fluidic property of the metal wire in the elastomer allows elasticity (b) and flexibility (c, d) of the device and keeps its electrical continuity. (Adapted from Ladd, C. et al., *Adv. Mater.*, 25, 5081–5085, 2013.)

8.7.3.3 Focused Ion Beam DW

8.7.3.3.1 Process

In FIB DW, a low energy ion beam (10–50 keV) generated from a liquid gallium source is used to bombard the precursor gas on the surface of the substrate in a vacuum environment. The precursor gas breaks down, resulting in the deposition of material (typical metals). The deposition method is capable of conformal deposition and forming 3D microstructures.[270–279] At larger energies, the ions can also be utilized to etch the substrate.

8.7.3.3.2 Materials, Writing Speed, and Resolution

FIB DW is usually used for depositing conductors such as gold, aluminum, copper, and platinum along with insulators using organometallic precursor gases. The deposition rate is lower than the LDW methods but it offers higher resolution with the minimum feature that can be produced being of the order of 80 nm. The minimum thickness is about 10 nm and the aspect ratios are between five and ten.[270]

8.7.3.3.3 Applications in Electronics

FIB systems are used for micromachining due to their ability to precisely add or remove the materials. This allows thermographic *in situ* process monitoring and imaging for

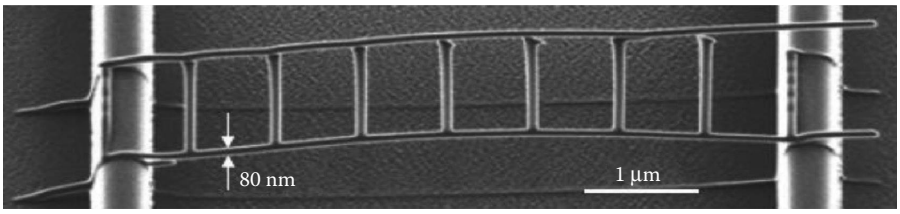

(a)

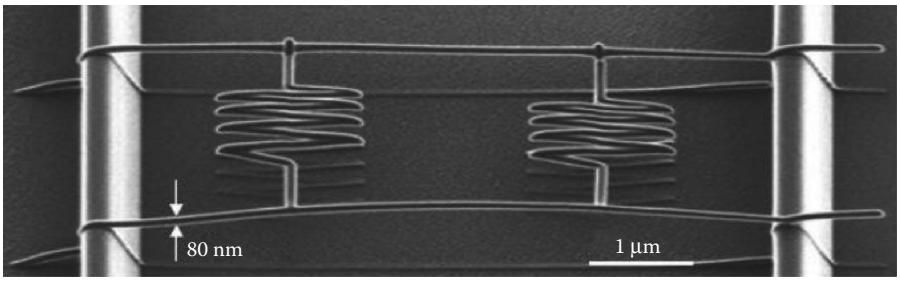

(b)

FIGURE 8.21
SIM images of carbon nanostructures prepared by FIBID: (a) free-space wiring with a bridge shape, (b) free-space wiring with parallel resistances. (Adapted from Morita, T. et al., *J. Vac. Sci. Technol. B*, 21, 2737–2741, 2003.)

navigation, alignment, and inspection using electron-beam melting (EBM) technology.[280,281] This feature is extremely important in the semiconductor industry for mask repair, failure analysis, and IC prototype rewiring. Figure 8.21[276] shows scanning ion microscopy (SIM) images of two nanostructures: a bridge and a parallel-resistance component made of amorphous diamond-like carbon containing a Ga core deposited using FIB-induced deposition (FIBID). This result demonstrates that a 3D electrical circuit can be fabricated in free-space by FIB.

8.7.3.3.4 Challenges

FIB is done in a vacuum environment in a tool that has limited space and can therefore typically only accommodate small substrates. It is therefore not compatible with 3D printing. Features deposited by FIB are not pure because of the organic contaminants that arise primarily from the organometallic precursors used for the deposition of metal. The resistivity of these deposits is about one or two orders of magnitude higher than those of pure metal. Due to the slow writing process, the applications are restricted to low volume production like repair works. Ions from the FIB process can also induce damage of underlying layers.

8.8 Conclusion

This chapter discusses approaches to integrate electronics into 3D printed objects. We characterized these approaches into three categories which have been summarized in Tables 8.2 and 8.3.

TABLE 8.2

Comparison of All the Approaches Used for Integrating Electronics into 3D Parts Excluding Laser Direct-Write Techniques

Approach	Deposition Method	Mechanism for Integration	Deposition Rate/ Writing Speed	Materials and Viscosity (μ)	Resolution or Minimum Feature Size	3D Periodic Structures
Hybrid chip insertion (Category 1)	Ultrasonic Consolidation (UC)	Deposition of metallic foils using ultrasonic energy	To 50 mm/s	Metals and alloys like Ni, Fe, Cu, brass, and steel	Foil thickness ~0.1 mm	N/A
	Transfer printing	Transfer patterns from TS to DS via differential adhesion	To 10 cm/s	Metallo-organics and conductive polymers	Pattern size ~12 μm	N/A
Surface DW (Category 2)	Ink-jet printing (CIJ)	Deposition of liquid droplets by break-up of continuous jet	To 60 mm^3/s with a single nozzle	Liquid with μ ~2 to 10 mPa-s; can contain small particles	Droplet size ~20 μm to 1 mm (typically 150 μm)	No
	Ink-jet printing (DoD)	Deposition of individual liquid droplets when required	To 0.3 mm^3/s with a single nozzle	Liquid with μ ~10 to 100 mPa-s; can contain small particles	Droplet size ~15 to 200 μm	No
	Aerosol jet printing	Kinetic bombardment of atomized droplets	To 0.25 mm^3/s with a single nozzle	Materials with μ < 2.5 mPa-s that can be atomized	Line width ~10 to 150 μm, thickness ~10 nm to 5 μm	Yes
	Precision pump	Precision micro-dispensing pump with suck-back action	Typically 50 mm/s (up to 300 mm/s)	Liquid, paste and slurry materials with μ up to 1000 Pa-s	Line width ~25 μm to 3 mm	Yes
	Extrusion	Deposition of materials via syringe-based flow	Typically 25 mm/s	Liquid, paste and slurry materials with μ up to 500 Pa-s	Line width ~50 μm to 2.5 mm	Yes
Freeform multi-material 3D printing (Category 3)	Omnidirectional printing	Extrusion of concentrated inks through fine cylindrical nozzles	Typically 6 mm/s	Liquid, paste, and slurry materials with μ up to 500 Pa-s	0.1 to 250 μm	Yes
	Liquid metal printing	Deposition of microstructures via extrusion of liquid metals at room temperature	Not yet known	Gallium-based alloys with μ up to 2 mPa-s	~10 μm	Yes
	Focused ion beam (FIB) DW	Ion-induced deposition of precursor gas molecules	Typically 0.05 $\mu m^3/s$	Metals and insulators	Line width ~80 nm to 20 μm	Yes

TABLE 8.3

Comparison of All Laser Direct-Write Techniques

Deposition Method	Mechanism	Deposition Rate/ Writing Speed	Materials and Viscosity (μ)	Resolution or Minimum Feature Size	3D Periodic Structures
Thin film consolidation	Melting, fusion onto substrates	10 to 2000 μm/s	Metals/ceramics on metal/ ceramic substrates	10 to 50 μm	No
LIFT and MAPLE DW	Transfer of material by kinetic energy of vaporizing organic binders	Typically 3 to 50 mm/s (up to 500 mm/s)	Metals, ceramics, semiconductors, polymers, composites	10 to 100 μm	No
LEEP	Thermal decomposition of the liquid	0.1 to 80 μm/s	Metals and ceramics on inorganic substrates	2 to 12 μm	No
Laser-activated electroplating	Accelerated chemical reaction by local high temperatures	Typically 0.1 to 10 m/s (up to 2.5 m/s)	Metals on metallic substrates	0.1 to 300 μm	No
LCVD	Decomposition of gases after vaporization and condensation takes place	Typically 50 to 100 μm/s (up to 5 mm/s)	Metals, semiconductors and ceramic such as Al, W, Si, Al_2O_3, WC	1 to 20 μm	Yes
LIBT	Physical vapor/liquid deposition after laser irradiation through transparent medium	10 to 100 mm/s	Metals and ceramics on transparent substrates	5 to 200 μm	No
LGDW	Laser-assisted deposition of generated aerosol using optical forces	To 1 m/s	Non-absorbent droplets and solid particulates with $\mu < 2.5$ mPa-s	2 μm	No
FGDW	Gas flow-assisted deposition of generated aerosol using hydrodynamic forces	To 0.25 mm^3/s	Atomizable fluids and colloids with $\mu < 2.5$ mPa-s	25 μm	No
TPP	Photopolymerization of UV-curable resin at laser focus within matrix	To 100 μm/s	Photo-sensitive acrylate polymers	≤100 nm	Yes
SLS	Locally sinters and binds the powder bed	To 35 mm/h	Polymers, metals, alloy mixtures and composites in powder form	100 μm	No

The first category builds electronic components separately and places them into the 3D printed object. This hybrid approach goes against the spirit of 3D printing, but provides the sophistication of modern electronics. It remains a challenge to find ways to connect these components using AM principles.

The second category is inspired by the variety of DW techniques developed originally to print electronic materials onto 2D substrates. Because AM is accomplished by building a 3D object one layer at a time, it seems sensible that these techniques could be adapted for 3D printing, yet there are many challenges that arise as discussed in this chapter.

The third category captures emerging techniques that can print freeform 3D electronic components. These techniques have yet to be implemented commercially, but may inspire new approaches to 3D printing electronic materials.

In summary, there has been very little work done on 3D printing of electronics—particularly those with high levels of sophistication—and it is the hope that this chapter will inspire new approaches to enable new electronic components built using AM. An ultimate goal of this field would be to develop a single system capable of rapid (in scale of hours or less) prototyping/manufacturing that can deposit a wide variety of materials (conductors, insulators, semiconductors, ferrites, ruthenates, metals, ferroelectrics, glasses, polymers, etc.) for customized, robust, electronic components at low substrate temperatures in a conformal manner on virtually any substrate (paper, plastic, ceramics, metals, etc.).

References

1. F42 Committee. *Terminology for Additive Manufacturing Technologies* (ASTM International, 2012). http://enterprise.astm.org/SUBSCRIPTION/filtrexx40.cgi?+REDLINE_PAGES/F2792.htm.
2. Hon, K.K.B., Li, L. & Hutchings, I.M. Direct writing technology—Advances and developments. *CIRP Ann.—Manuf. Technol.* **57,** 601–620 (2008).
3. Church, K.H., Fore, C. & Feeley, T. Commercial applications and review for direct write technologies. *MRS Online Proc. Libr.* **624,** null–null (2000).
4. Holshouser, C. et al. Out of bounds additive manufacturing. *Adv. Mater. Process.* **171,** 15–17 (2013).
5. Hofmann, M. 3D printing gets a boost and opportunities with polymer materials. *ACS Macro, Lett.* **3,** 382–386 (2014).
6. Calvert, P. Inkjet printing for materials and devices. *Chem. Mater.* **13,** 3299–3305 (2001).
7. Morissette, S.L., Lewis, J.A., Clem, P.G., Cesarano, J. & Dimos, D.B. Direct-write fabrication of Pb(Nb,Zr,Ti)O_3 devices: Influence of paste rheology on print morphology and component properties. *J. Am. Ceram. Soc.* **84,** 2462–2468 (2001).
8. Piner, R.D., Zhu, J., Xu, F., Hong, S.H. & Mirkin, C.A. "Dip-pen" nanolithography. *Science* **283,** 661–663 (1999).
9. Bourell, D., Marcus, H., Barlow, J. & Beaman, J. Selective laser sintering of metals and ceramics. *Int. J. Powder Metall.* **28,** 369–381 (1992).
10. Lewis, J.A. Direct ink writing of 3D functional materials. *Adv. Funct. Mater.* **16,** 2193–2204 (2006).
11. Kim, N.-S. & Han, K.N. Future direction of direct writing. *J. Appl. Phys.* **108,** 102801 (2010).
12. Piqué, A. & Chrisey, D.B. *Direct-write Technologies for Rapid Prototyping Applications: Sensors, Electronics, and Integrated Power Sources* (Academic Press, San Diego, CA, 2002).
13. MarketsandMarkets. Additive Manufacturing Market—Forecasts 2012–17: (MarketsandMarkets) (2013). http://www.marketsandmarkets.com/Market-Reports/additive-manufacturing-medical-devices-market-843.html.
14. IDTechEx. Applications of 3D Printing 2014–2024 (IDTechEx) (2014). http://www.idtechex.com/research/reports/applications-of-3d-printing-2014-2024-000385.asp.

15. Macdonald, E. et al. 3D Printing for the rapid prototyping of structural electronics. *IEEE Access* **2,** 234–242 (2014).
16. Powers, T.R. *The Integrated Circuit Hobbyist's Handbook* (Newnes, High Text Publications, Inc., Solana Beach, CA, 1995).
17. Moore, G.E. Cramming more components onto integrated circuits. *Proc. IEEE* **86,** 82–85 (1998).
18. Schaller, R.R. Moore's law: Past, present and future. *IEEE Spectr.* **34,** 52–59 (1997).
19. Madou, M.J. *Manufacturing Techniques for Microfabrication and Nanotechnology* (CRC Press, Boca Raton, FL, 2011).
20. Qin, D., Xia, Y. & Whitesides, G.M. Soft lithography for micro- and nanoscale patterning. *Nat. Protoc.* **5,** 491–502 (2010).
21. Xia, Y. & Whitesides, G.M. Soft lithography. *Annu. Rev. Mater. Sci.* **28,** 153–184 (1998).
22. Colburn, M. et al. Step and flash imprint lithography: A new approach to high-resolution patterning. *SPIE Proc. Emerg. Lithogr. Tech. III.* **3676,** 379–389 (1999).
23. Resnick, D.J. et al. Imprint lithography for integrated circuit fabrication. *J. Vac. Sci. Technol. B* **21,** 2624–2631 (2003).
24. Thompson, L.F. et al. Introduction to microlithography (1983). http://pubs.acs.org/isbn/9780841207752.
25. Gates, B.D. et al. New approaches to nanofabrication: Molding, printing, and other techniques. *Chem. Rev.* **105,** 1171–1196 (2005).
26. Costner, E.A., Lin, M.W., Jen, W.-L. & Willson, C.G. Nanoimprint lithography materials development for semiconductor device fabrication. *Annu. Rev. Mater. Res.* **39,** 155–180 (2009).
27. Barron, A.R. & Ball, Z. Optical Issues in Photolithography. *Connexions.* http://cnx.org/content/m25448/latest/
28. Xia, Y.N., Rogers, J.A., Paul, K.E. & Whitesides, G.M. Unconventional methods for fabricating and patterning nanostructures. *Chem. Rev.* **99,** 1823–1848 (1999).
29. Rogers, J.A. & Lee, H.H. *Unconventional Nanopatterning Techniques and Applications* (John Wiley & Sons, Hoboken, NJ, 2008).
30. Gates, B.D., Xu, Q.B., Love, J.C., Wolfe, D.B. & Whitesides, G.M. Unconventional nanofabrication. *Annu. Rev. Mater. Res.* **34,** 339–372 (2004).
31. Zhao, X.-M., Xia, Y. & Whitesides, G.M. Soft lithographic methods for nano-fabrication. *J. Mater. Chem.* **7,** 1069–1074 (1997).
32. Odom, T.W., Thalladi, V.R., Love, J.C. & Whitesides, G.M. Generation of 30–50 nm structures using easily fabricated, composite PDMS masks. *J. Am. Chem. Soc.* **124,** 12112–12113 (2002).
33. Kim, K.-H., Moldovan, N. & Espinosa, H.D. A nanofountain probe with sub-100nm molecular writing resolution. *Small* **1,** 632–635 (2005).
34. Lewis, A. et al. Fountain pen nanochemistry: Atomic force control of chrome etching. *Appl. Phys. Lett.* **75,** 2689–2691 (1999).
35. Hwang, K., Dinh, V.-D., Lee, S.-H., Kim, Y.-J. & Kim, H.-M. Analysis of line width with nano fountain pen using active membrane pumping. In *2nd IEEE Int. Conf. NanoMicro Eng. Mol. Syst.* 759–763 (2007). http://yadda.icm.edu.pl/yadda/element/bwmeta1.element.ieee-000004160431.
36. Zhang, C. et al. Laser direct-write and its application in low temperature Co-fired ceramic (LTCC) technology. *Microelectron. Eng.* **70,** 41–49 (2003).
37. Joshi, P.C. et al. Direct digital additive manufacturing technologies: Path towards hybrid integration. In *Future Instrum. Int. Workshop.* 1–4 (2012). doi:10.1109/FIIW.2012.6378353.
38. Williams, E.D., Ayres, R.U. & Heller, M. The 1.7 kilogram microchip: Energy and material use in the production of semiconductor devices. *Environ. Sci. Technol.* **36,** 5504–5510 (2002).
39. Cantatore, E. *Applications of Organic and Printed Electronics: A Technology-Enabled Revolution* (Springer, Spring street, NY, 2012).
40. Chang, J., Zhang, X., Ge, T. & Zhou, J. Fully printed electronics on flexible substrates: High gain amplifiers and DAC. *Org. Electron.* 15, 701–710 (2014).
41. Das, R., Harrop, P. & Printed, O. Flexible Electronics Forecasts. *Play. Oppor.* **2021,** (2011).
42. Wikipedia. File:ComplementaryTechnologies.png. *Wikipedia Free Encycl.* (2008). http://en.wikipedia.org/wiki/File:ComplementaryTechnologies.png.

43. Chang, J., Ge, T. & Sanchez-Sinencio, E. Challenges of printed electronics on flexible substrates. In *IEEE 55th Int. Midwest Symp. Circuits Syst.* Boise, ID, Circuits and Systems, 582–585 (2012).
44. Subramanian, V. et al. All-printed RFID tags: Materials, devices, and circuit implications. *19th Int. Conf. VLSI Des. 2006 Held Jointly 5th Int. Conf. Embed. Syst. Des.* 6 (2006). doi:10.1109/VLSID.2006.34.
45. Subramanian, V., Lee, J.B., Liu, V.H. & Molesa, S. Printed electronic nose vapor sensors for consumer product onitoring. *Solid-State Circuits Conf. 2006 ISSCC 2006 Dig. Tech. Pap. IEEE Int.* 1052–1059 (2006). doi:10.1109/ISSCC.2006.1696148.
46. Curling, C.J. Prototype line for manufacturing flexible active matrix displays. In *5th Annu. Flex. Disp. Conf.* USDC Flexible Displays & Microelectronics, Plastic Logic Unlimited, Cambridge, 6–9. (February 2006)
47. Finkenzeller, K. In *RFID Handb.* 347–359 (John Wiley & Sons, Chichester, UK, 2010). http://onlinelibrary.wiley.com/doi/10.1002/9780470665121.ch12/summary.
48. Berggren, M., Nilsson, D. & Robinson, N.D. Organic materials for printed electronics. *Nat. Mater.* **6,** 3–5 (2007).
49. Blackwell, G.R. *The Electronic Packaging Handbook* (CRC Press, Boca Raton, FL, 1999).
50. Siegel, A.C. et al. Foldable printed circuit boards on paper substrates. *Adv. Funct. Mater.* **20,** 28–35 (2010).
51. Subramanian, V. et al. Printed electronics for low-cost electronic systems: Technology status and application development. *Solid-State Circuits Conf. 2008 ESSCIRC 2008 34th Eur.* 17–24 (2008). doi:10.1109/ESSCIRC.2008.4681785.
52. Yin, Z., Huang, Y., Bu, N., Wang, X. & Xiong, Y. Inkjet printing for flexible electronics: Materials, processes and equipments. *Chin. Sci. Bull.* **55,** 3383–3407 (2010).
53. Molesa, S., Redinger, D.R., Huang, D.C. & Subramanian, V. High-quality inkjet-printed multilevel interconnects and inductive components on plastic for ultra-low-cost RFID applications. *PROC 769 H831* **769,** 2003.
54. Singh, M., Haverinen, H.M., Dhagat, P. & Jabbour, G.E. Inkjet printing—Process and its applications. *Adv. Mater.* **22,** 673–685 (2010).
55. Ko, S.H. et al. All-inkjet-printed flexible electronics fabrication on a polymer substrate by low-temperature high-resolution selective laser sintering of metal nanoparticles. *Nanotechnology* **18,** 345202 (2007).
56. Hrehorova, E. et al. Gravure printing of conductive inks on glass substrates for applications in printed electronics. *J. Disp. Technol.* **7,** 318–324 (2011).
57. Gravure Association America; Gravure Education Foundation, *Gravure: Process and Technology* (Gravure Association of America, Gravure Education Foundation, Denver, NC, 1991). http://catalog.lib.ncsu.edu/record/NCSU2266370.
58. Pudas, M. Gravure-offset printing in the manufacture of ultra-fine-line thick-films for electronics (2004). http://jultika.oulu.fi/Record/isbn951-42-7303-6.
59. Krebs, F.C. et al. A complete process for production of flexible large area polymer solar cells entirely using screen printing—First public demonstration. *Sol. Energy Mater. Sol. Cells* **93,** 422–441 (2009).
60. Pardo, D.A., Jabbour, G.E. & Peyghambarian, N. Application of screen printing in the fabrication of organic light-emitting devices. *Adv. Mater.* **12,** 1249–1252 (2000).
61. White, A. High quality flexography—A literature review. (1998).
62. Blayo, A. & Pineaux, B. Printing processes and their potential for RFID printing. *Proc. 2005 Jt. Conf. Smart Objects Ambient Intell. Innov. Context-Aware Serv. Usages Technol.* 27–30 (ACM, New York, 2005). doi:10.1145/1107548.1107559.
63. Ramsey, B.J., Evans, P.S.A. & Harrison, D. A novel circuit fabrication technique using offset lithography. *J. Electron. Manuf.* **7,** 63–67 (1997).
64. Bao, Z. Materials and fabrication needs for low-cost organic transistor circuits. *Adv. Mater.* **12,** 227–230 (2000).
65. Heeger, A.J., MacDiarmid, A.G. & Shirakawa, H. The Nobel Prize in chemistry, 2000: Conductive polymers. *Stockh. Swed. R. Swed. Acad. Sci.* (2000).

66. Krebs, F.C. Fabrication and processing of polymer solar cells: A review of printing and coating techniques. *Sol. Energy Mater. Sol. Cells* **93,** 394–412 (2009).
67. Krebs, F.C. *Polymeric Solar Cells: Materials, Design, Manufacture* (DEStech Publications, Lancaster, PA, 2010).
68. Søndergaard, R., Hösel, M., Angmo, D., Larsen-Olsen, T.T. & Krebs, F.C. Roll-to-roll fabrication of polymer solar cells. *Mater. Today* **15,** 36–49 (2012).
69. Søndergaard, R.R., Hösel, M. & Krebs, F.C. Roll-to-Roll fabrication of large area functional organic materials. *J. Polym. Sci. Part B Polym. Phys.* **51,** 16–34 (2013).
70. Bharathan, J. & Yang, Y. Polymer electroluminescent devices processed by inkjet printing: I. Polymer light-emitting logo. *Appl. Phys. Lett.* **72,** 2660–2662 (1998).
71. Mäkelä, T., Jussila, S., Vilkman, M., Kosonen, H. & Korhonen, R. Roll-to-roll method for producing polyaniline patterns on paper. *Synth. Met.* **135–136,** 41–42 (2003).
72. Mäkelä, T. et al. Utilizing roll-to-roll techniques for manufacturing source-drain electrodes for all-polymer transistors. *Synth. Met.* **153,** 285–288 (2005).
73. Bock, K. Polymer Electronics Systems—Polytronics. *Proc. IEEE* **93,** 1400–1406 (2005).
74. Zielke, D. et al. Polymer-based organic field-effect transistor using offset printed source/drain structures. *Appl. Phys. Lett.* **87,** 123508 (2005).
75. Sheraw, C.D. et al. Organic thin-film transistor-driven polymer-dispersed liquid crystal displays on flexible polymeric substrates. *Appl. Phys. Lett.* **80,** 1088 (2002).
76. Klauk, H. *Organic Electronics: Materials, Manufacturing, and Applications* (John Wiley & Sons, Weinheim, Germany, 2006).
77. So, F. *Organic Electronics: Materials, Processing, Devices and Applications* (CRC Press, Boca Raton, FL, 2010).
78. Iwamoto, M., Kwon, Y.-S. & Lee, T. *Nanoscale Interface for Organic Electronics* (World Scientific, Singapore, 2011).
79. Klauk, H. *Organic Electronics II: More Materials and Applications* (John Wiley & Sons, Weinheim, Germany, 2012).
80. Forrest, S.R. & Thompson, M.E. Introduction: Organic electronics and optoelectronics. *Chem. Rev.* **107,** 923–925 (2007).
81. Kelley, T.W. et al. Recent progress in organic electronics: Materials, devices, and processes. *Chem. Mater.* **16,** 4413–4422 (2004).
82. Shaw, J.M. & Seidler, P.F. Organic electronics: Introduction. *IBM J. Res. Dev.* **45,** 3–9 (2001).
83. Dimitrakopoulos, C.D. & Malenfant, P.R.L. Organic thin film transistors for large area electronics. *Adv. Mater.* **14,** 99–117 (2002).
84. Moliton, A. & Hiorns, R.C. Review of electronic and optical properties of semiconducting π-conjugated polymers: Applications in optoelectronics. *Polym. Int.* **53,** 1397–1412 (2004).
85. De Leeuw, D.M., Simenon, M.M.J., Brown, A.R. & Einerhand, R.E.F. Stability of n-type doped conducting polymers and consequences for polymeric microelectronic devices. *Synth. Met.* **87,** 53–59 (1997).
86. Britton, D.T. & Härting, M. Printed nanoparticulate composites for silicon thick-film electronics. *Pure Appl. Chem.* **78,** 1723–1739 (2009).
87. Perelaer, J., de Gans, B.-J. & Schubert, U.S. Ink-jet printing and microwave sintering of conductive silver tracks. *Adv. Mater.* **18,** 2101–2104 (2006).
88. Noh, Y.-Y., Zhao, N., Caironi, M. & Sirringhaus, H. Downscaling of self-aligned, all-printed polymer thin-film transistors. *Nat. Nanotechnol.* **2,** 784–789 (2007).
89. Siden, J., Olsson, T., Koptioug, A. & Nilsson, H.-E. Reduced amount of conductive ink with gridded printed antennas. In *5th Int. Conf. Polym. Adhes. Microelectron. Photonics Polytronic,* 86–89 (2005). doi:10.1109/POLYTR.2005.1596493.
90. Harrey, P.M., Evans, P.S.A., Ramsey, B.J. & Harrison, D.J. Interdigitated capacitors by offset lithography. *J. Electron. Manuf.* **10,** 69–77 (2000).
91. Cheng, K. et al. Ink-jet printing, self-assembled polyelectrolytes, and electroless plating: Low cost fabrication of circuits on a flexible substrate at room temperature. *Macromol. Rapid Commun.* **26,** 247–264 (2005).

92. Chung, J., Ko, S., Bieri, N.R., Grigoropoulos, C.P. & Poulikakos, D. Conductor microstructures by laser curing of printed gold nanoparticle ink. *Appl. Phys. Lett.* **84,** 801–803 (2004).
93. Choi, T.Y., Poulikakos, D. & Grigoropoulos, C.P. Fountain-pen-based laser microstructuring with gold nanoparticle inks. *Appl. Phys. Lett.* **85,** 13–15 (2004).
94. Nüchter, M., Ondruschka, B., Bonrath, W. & Gum, A. Microwave assisted synthesis—a critical technology overview. *Green Chem.* **6,** 128–141 (2004).
95. Kordás, K. et al. Inkjet printing of electrically conductive patterns of carbon nanotubes. *Small* **2,** 1021–1025 (2006).
96. Zhou, Y., Hu, L. & Grüner, G. A method of printing carbon nanotube thin films. *Appl. Phys. Lett.* **88,** 123109 (2006).
97. Meitl, M.A. et al. Solution casting and transfer printing single-walled carbon nanotube films. *Nano Lett.* **4,** 1643–1647 (2004).
98. Ishikawa, F.N. et al. Transparent electronics based on transfer printed aligned carbon nanotubes on rigid and flexible substrates. *ACS Nano* **3,** 73–79 (2009).
99. Rowell, M.W. et al. Organic solar cells with carbon nanotube network electrodes. *Appl. Phys. Lett.* **88,** 233506 (2006).
100. Eda, G., Fanchini, G. & Chhowalla, M. Large-area ultrathin films of reduced graphene oxide as a transparent and flexible electronic material. *Nat. Nanotechnol.* **3,** 270–274 (2008).
101. Liang, X., Fu, Z. & Chou, S.Y. Graphene transistors fabricated via transfer-printing in device active-areas on large wafer. *Nano Lett.* **7,** 3840–3844 (2007).
102. Allen, M.J. et al. Soft transfer printing of chemically converted graphene. *Adv. Mater.* **21,** 2098–2102 (2009).
103. Song, L., Ci, L., Gao, W. & Ajayan, P.M. Transfer printing of graphene using gold film. *ACS Nano* **3,** 1353–1356 (2009).
104. Chen, J.-H. et al. Printed graphene circuits. *Adv. Mater.* **19,** 3623–3627 (2007).
105. Tans, S.J., Verschueren, A.R.M. & Dekker, C. Room-temperature transistor based on a single carbon nanotube. *Nature* **393,** 49–52 (1998).
106. Baughman, R.H., Zakhidov, A.A. & Heer, W.A. de. Carbon nanotubes—The route toward applications. *Science* **297,** 787–792 (2002).
107. Werth, J., O'Donnell, S., Lamensdorf, D., Marshall, J. & Teig, L. Carbon nanotube-based electronic devices (2011). http://www.google.com/patents/US8013247.
108. Fecht, H.J. & Brühne, K. *Carbon-based Nanomaterials and Hybrids: Synthesis, Properties, and Commercial Applications* (CRC Press, Boca Raton, FL, 2014).
109. Capano, M. *Special Section: Carbon-based Electronic Materials* (Springer, Pennsylvania, 2009).
110. McEuen, P.L., Fuhrer, M.S. & Park, H. Single-walled carbon nanotube electronics. *IEEE Trans. Nanotechnol.* **1,** 78–85 (2002).
111. Avouris, P., Chen, Z. & Perebeinos, V. Carbon-based electronics. *Nat. Nanotechnol.* **2,** 605–615 (2007).
112. Snow, E.S., Novak, J.P., Campbell, P.M. & Park, D. Random networks of carbon nanotubes as an electronic material. *Appl. Phys. Lett.* **82,** 2145–2147 (2003).
113. Zhang, Y., Liu, C. & Whalley, D. Direct-write techniques for maskless production of microelectronics: A review of current state-of-the-art technologies. in *Int. Conf. Electron. Packag. Technol. High Density Packag. 2009 ICEPT-HDP 09*, 497–503 (2009). doi:10.1109/ICEPT.2009.5270702.
114. Chrisey, D.B. The power of direct writing. *Science* **289,** 879–881 (2000).
115. Aydemir, N. et al. Direct writing of conducting polymers. *Macromol. Rapid Commun.* (2013). doi:10.1002/marc.201300386.
116. Ahn, B.Y. et al. Omnidirectional printing of flexible, stretchable, and spanning silver microelectrodes. *Science* **323,** 1590–1593 (2009).
117. Boley, J.W., White, E.L., Chiu, G.T.-C. & Kramer, R.K. Direct writing of gallium-indium alloy for stretchable electronics. *Adv. Funct. Mater.* (2014). doi:10.1002/adfm.201303220.
118. Farahani, R.D. et al. Direct-write fabrication of freestanding nanocomposite strain sensors. *Nanotechnology* **23,** 085502 (2012).
119. Gao, Y., Li, H. & Liu, J. Direct writing of flexible electronics through room temperature liquid metal ink. *PLoS One* **7,** e45485 (2012).

120. Lopes, A.J., MacDonald, E. & Wicker, R.B. Integrating stereolithography and direct print technologies for 3D structural electronics fabrication. *Rapid Prototyp. J.* **18,** 129–143 (2012).
121. Navarrete, M. et al. *Integrated Layered Manufacturing of a Novel Wireless Motion Sensor System with GPS, Presented at 18th Symposium on Solid Freeform Fabrication*, Austin, TX. vii-ix, 1-609, U.S. Government or Federal Rights License. August 6–8(2007).
122. Palmer, J.A. et al. Realizing 3-d interconnected direct write electronics within smart stereolithography structures. *ASME 2005 International Mechanical Engineering Congress and Exposition on Electronic and Photonic Packaging, Electrical Systems Design and Photonics, and Nanotechnology*, Orlando, FL, November 5–11, 287–293 (2005). doi:10.1115/IMECE2005-79360.
123. Medina, F. et al. Hybrid manufacturing: Integrating direct-write and stereolithography. In *Proc. 2005 Solid Free. Fabr.* (2005). http://edge.rit.edu/edge/P10551/public/SFF/SFF%202005%20Proceedings/Manuscripts%202005/05-Medina.pdf.
124. Espalin, D., Muse, D.W., MacDonald, E. & Wicker, R.B. 3D Printing multifunctionality: Structures with electronics. *Int. J. Adv. Manuf. Technol.* **72,** 963–978 (2014).
125. Medina, F. et al. Integrating multiple rapid manufacturing technologies for developing advanced customized functional devices. In *Rapid Prototyp. Manuf. 2005 Conf. Proc.* , Michigan, Emerald Group Publishing Limited, Bingley, 10–12 (2005).
126. Robinson, C.J., Stucker, B., Lopes, A.J., Wicker, R.B. & Palmer, J.A. Integration of direct-write (DW) and ultrasonic consolidation (UC) technologies to create advanced structures with embedded electrical circuitry. In *Proc. 17th Annu. Solid Free. Fabr. Symp.*, University of Texas, Austin, TX, 60–69 (Society of Manufacturing Engineers, Austin, TX, 2006).
127. Siggard, E.J., Madhusoodanan, A.S., Stucker, B. & Eames, B. Structurally embedded electrical systems using ultrasonic consolidation (UC). In *Proc. 17th Solid Free. Fabr. Symp.* Austin, TX, August (American Welding Society, Austin, TX, 2006). http://edge.rit.edu/edge/P10551/public/SFF/SFF%202006%20Proceedings/Manuscripts/07-Siggard.pdf.
128. Siggard, E.J. *Investigative Research Into the Structural Embedding of Electrical and Mechanical Systems Using Ultrasonic Consolidation (UC)* (ProQuest, 2007). http://books.google.com/books?hl = en&lr = &id = AH1f7mmAGAcC&oi = fnd&pg = PR3&dq = Structurally+embedded+electrical+systems+using+ultrasonic+consolidation+(UC)&ots = BxodKLQaKt&sig = hUxyjagNV7Iikx9GiYhsFjNDkLc.
129. White, D.R. Ultrasonic consolidation of aluminum tooling. *Adv. Mater. Process.* **161,** 64–65 (2003).
130. Ram, G.J., Yang, Y., George, J., Robinson, C. & Stucker, B. Improving linear weld density in ultrasonically consolidated parts. In *Proc. 17th Solid Free. Fabr. Symp.* 692–708 (WH Freeman, Austin, TX, 2006). http://utwired.engr.utexas.edu/lff/symposium/proceedingsArchive/pubs/Manuscripts/2006/2006-60-Ram.pdf.
131. Obielodan, J.O. et al. Optimization of the shear strengths of ultrasonically consolidated Ti/Al 3003 dual-material structures. *J. Mater. Process. Technol.* **211,** 988–995 (2011).
132. Gibson, I., Rosen, D.W. & Stucker, B. *Additive Manufacturing Technologies: Rapid Prototyping to Direct Digital Manufacturing* (Springer, Spring street, NY, 2010).
133. Ram, G.D.J., Robinson, C., Yang, Y. & Stucker, B.E. Use of ultrasonic consolidation for fabrication of multi-material structures. *Rapid Prototyp. J.* **13,** 226–235 (2007).
134. Mosher, T. & Stucker, B. In *Space 2004 Conf. Exhib* (American Institute of Aeronautics and Astronautics, Reston, VA, 2004). http://arc.aiaa.org/doi/abs/10.2514/6.2004-6117.
135. Janaki Ram, G.D., Yang, Y. & Stucker, B.E. Effect of process parameters on bond formation during ultrasonic consolidation of aluminum alloy 3003. *J. Manuf. Syst.* **25,** 221–238 (2006).
136. Meitl, M.A. et al. Transfer printing by kinetic control of adhesion to an elastomeric stamp. *Nat Mater* **5,** 33–38 (2006).
137. Lee, C.H., Kim, D.R. & Zheng, X. Fabricating nanowire devices on diverse substrates by simple transfer-printing methods. *Proc. Natl. Acad. Sci.* **107,** 9950–9955 (2010).
138. Lee, C.H., Kim, D.R. & Zheng, X. Fabrication of nanowire electronics on nonconventional substrates by water-assisted transfer printing method. *Nano Lett.* **11,** 3435–3439 (2011).
139. Weisse, J.M., Lee, C.H., Kim, D.R. & Zheng, X. Fabrication of flexible and vertical silicon nanowire electronics. *Nano Lett.* **12,** 3339–3343 (2012).

140. Keum, H. et al. Silicon micro-masonry using elastomeric stamps for three-dimensional microfabrication. *J. Micromech. Microeng.* **22,** 055018 (2012).
141. Hsia, K.J. et al. Collapse of stamps for soft lithography due to interfacial adhesion. *Appl. Phys. Lett.* **86,** 154106 (2005).
142. Huang, Y.Y. et al. Stamp Collapse in Soft Lithography. *Langmuir* **21,** 8058–8068 (2005).
143. Chen, H., Feng, X., Huang, Y., Huang, Y. & Rogers, J.A. Experiments and viscoelastic analysis of peel test with patterned strips for applications to transfer printing. *J. Mech. Phys. Solids* **61,** 1737–1752 (2013).
144. Huang, Y., Duan, X., Wei, Q. & Lieber, C.M. Directed assembly of one-dimensional nanostructures into functional networks. *Science* **291,** 630–633 (2001).
145. Smith, P.A. et al. Electric-field assisted assembly and alignment of metallic nanowires. *Appl. Phys. Lett.* **77,** 1399–1401 (2000).
146. Collins, P.G., Arnold, M.S. & Avouris, P. Engineering carbon nanotubes and nanotube circuits using electrical breakdown. *Science* **292,** 706–709 (2001).
147. Whang, D., Jin, S., Wu, Y. & Lieber, C.M. Large-scale hierarchical organization of nanowire arrays for integrated nanosystems. *Nano Lett.* **3,** 1255–1259 (2003).
148. Zhang, J., Szczech, J., Skinner, J. & Gamota, D. In *Direct-Write Technol. Rapid Prototyp.* (Piqué, A.) 33–54 (Academic Press, San Diego, CA, 2002). http://www.sciencedirect.com/science/article/pii/B9780121742317500543.
149. Williams, R.T., Wrisley, D.B., Jr & Wu, J.C. Pressure bonding layer of noble metal to base metal substrate (1991).
150. Drew, R.F., Jr, Schmidt, F.J.S. & Vanduynhoven, T.J. Laser deposition of metal upon transparent materials. (Defensive publication 1979). http://www.google.tl/patents/CA1105093A1?cl=en.
151. Owen, M.D. Laser system and method for plating vias (1997). https://www.google.com/patents/US5614114.
152. Chrisey, D.B. & Hubler, G.K. Pulsed laser deposition of thin films. In *Pulsed Laser Depos. Thin Films* (Chrisey D.B & Hubler, G.K) 648 (Wiley-VCH 2003).
153. Park, B.K., Kim, D., Jeong, S., Moon, J. & Kim, J.S. Direct writing of copper conductive patterns by ink-jet printing. *Thin Solid Films* **515,** 7706–7711 (2007).
154. Woo, K., Kim, D., Kim, J.S., Lim, S. & Moon, J. Ink-jet printing of Cu–Ag-based highly conductive tracks on a transparent substrate. *Langmuir* **25,** 429–433 (2009).
155. Modi, R., Wu, H.D., Auyeung, R.C.Y., Gilmore, C.M. & Chrisey, D.B. Direct writing of polymer thick film resistors using a novel laser transfer technique. *J. Mater. Res.* **16,** 3214–3222 (2001).
156. Pique, A. et al. A novel laser transfer process for direct writing of electronic and sensor materials. *Appl. Phys. Mater. Sci. Process.* **69,** S279–S284 (1999).
157. Kaydanova, T. et al. Direct-write inkjet printing for fabrication of barium strontium titanate-based tunable circuits. *Thin Solid Films* **515,** 3820–3824 (2007).
158. Young, D. et al. Dielectric properties of oxide structures by a laser-based direct-writing method. *J. Mater. Res.* **16,** 1720–1725 (2001).
159. Sirringhaus, H. et al. High-resolution inkjet printing of all-polymer transistor circuits. *Science* **290,** 2123–2126 (2000).
160. De Gans, B.J., Duineveld, P.C. & Schubert, U.S. Inkjet printing of polymers: State of the art and future developments. *Adv. Mater.* **16,** 203–213 (2004).
161. Hudd, A. Inkjet printing technologies. In *Chem. Inkjet Inks*, 3–18 (World Scientific Publishers, Singapore, 2010).
162. Rioboo, R., Marengo, M. & Tropea, C. Time evolution of liquid drop impact onto solid, dry surfaces. *Exp. Fluids* **33,** 112–124 (2002).
163. Derby, B. & Reis, N. Inkjet printing of highly loaded particulate suspensions. *MRS Bull.* **28,** 815–818 (2003).
164. Tekin, E., Smith, P.J. & Schubert, U.S. Inkjet printing as a deposition and patterning tool for polymers and inorganic particles. *Soft. Matter.* **4,** 703–713 (2008).
165. Wang, T. & Derby, B. Ink-jet printing and sintering of PZT. *J. Am. Ceram. Soc.* **88,** 2053–2058 (2005).

166. Magdassi, S. Ink requirements and formulations guidelines. In *Chem. Inkjet Inks* (Word Scietific Publishers, Singapore 2010). http://www.worldscientific.com/doi/pdf/10.1142/9789812818225_0002
167. Kodas, T.T. et al. Low viscosity precursor compositions and methods for the deposition of conductive electronic features (2010). http://www.google.com/patents/US20070120096.
168. Perez, K.B. & Williams, C.B. *Combining Additive Manufacturing and Direct Write for Integrated Electronics—A Review.* (2013). http://utwired.engr.utexas.edu/lff/symposium/proceedingsArchive/pubs/Manuscripts/2013/2013-77-Perez.pdf.
169. Wallace, D.B., Royall Cox, W. & Hayes, D.J. In *Direct-Write Technol. Rapid Prototyp.* (Piqué, A.) 177–227 (Academic Press, San Diego, CA, 2002). http://www.sciencedirect.com/science/article/pii/B9780121742317500609.
170. Nir, M.M. et al. Electrically conductive inks for inkjet printing. In *Ink Jet Inks* (2010). http://http://www.worldscientific.com/doi/pdf/10.1142/9789812818225_0012.
171. Korvink, J.G., Smith, P.J. & Shin, D.-Y. *Inkjet-Based Micromanufacturing* (John Wiley & Sons, Weinheim, Germany, 2012).
172. Magdassi, S. *The Chemistry of Inkjet Inks.* **20** (World Scientific Publishers, Singapore, 2010).
173. Forrest, S.R. The path to ubiquitous and low-cost organic electronic appliances on plastic. *Nature* **428,** 911–918 (2004).
174. Van Osch, T.H.J., Perelaer, J., de Laat, A.W.M. & Schubert, U.S. Inkjet printing of narrow conductive tracks on untreated polymeric substrates. *Adv. Mater.* **20,** 343–345 (2008).
175. Perelaer, J., Klokkenburg, M., Hendriks, C.E. & Schubert, U.S. Microwave flash sintering of inkjet-printed silver tracks on polymer substrates. *Adv. Mater.* **21,** 4830–4834 (2009).
176. Magdassi, S., Grouchko, M. & Kamyshny, A. Copper nanoparticles for printed electronics: Routes towards achieving oxidation stability. *Materials* **3,** 4626–4638 (2010).
177. Hayes, D.J., Wallace, D.B. & Cox, W.R. *MicroJet Printing of Solder and Polymers for Multi-Chip Modules and Chip-Scale Packages, Journal of International Microelectronics and Packaging Society* (1999) http://microfab.com/images/papers/imaps99.pdf.
178. Liu, Q. & Orme, M. High precision solder droplet printing technology and the state-of-the-art. *J. Mater. Process. Technol.* **115,** 271–283 (2001).
179. Cox, W.R. et al. Microjetted lenslet triplet fibers. *Opt. Commun.* **123,** 492–496 (1996).
180. Hayes, D.J., Grove, M.E., Wallace, D.B., Chen, T. & Cox, W.R. Inkjet printing in the manufacture of electronics, photonics, and displays. in **4809,** 94–99 (2002).
181. Fuller, S.B., Wilhelm, E.J. & Jacobson, J.M. Ink-jet printed nanoparticle microelectromechanical systems. *J. Microelectromechanical Syst.* **11,** 54–60 (2002).
182. Grouchko, M., Kamyshny, A. & Magdassi, S. Formation of air-stable copper–silver core–shell nanoparticles for inkjet printing. *J. Mater. Chem.* **19,** 3057–3062 (2009).
183. Yarin, A.L. in *Annu. Rev. Fluid Mech.* **38,** 159–192 (2006).
184. Cheng, S.X., Li, T. & Chandra, S. Producing molten metal droplets with a pneumatic droplet-on-demand generator. *J. Mater. Process. Technol.* **159,** 295–302 (2005).
185. Kahn, B.E. The M3D aerosol jet system, an alternative to inkjet printing for printed electronics. *Org. Print. Electron.* **1,** 14–17 (2007).
186. King, B. & Renn, M. Aerosol jet® direct write printing for mil-aero electronic applications. in *Palo Alto Colloq. Lockheed Martin* (2009). http://www.optomec.com/wp-content/uploads/2014/04/Optomec_Aerosol_Jet_Direct_Write_Printing_for_Mil_Aero_Electronic_Apps.pdf.
187. Vongutfeld, R., Acosta, R. & Romankiw, L. Laser-enhanced plating and etching—Mechanisms and applications. *Ibm J. Res. Dev.* **26,** 136–144 (1982).
188. Hedges, M. & Marin, A.B. 3D aerosol jet® printing-adding electronics functionality to RP/RM. In *Proc DDMC 2012 Conf.*, Berlin, Germany (2012). http://aerosoljet.com/downloads/Optomec_NEOTECH_DDMC_3D_Aerosol_Jet_Printing.pdf.
189. Horais, B., Love, L. & Dehoff, R. The use of additive manufacturing for fabrication of multi-function small satellite structures. *AIAAUSU Conf. Small Satell.* (2013). http://digitalcommons.usu.edu/smallsat/2013/all2013/64.

190. Arnold, C.B., Serra, P. & Piqué, A. Laser direct-write techniques for printing of complex materials. *Mrs Bull.* **32,** 23–31 (2007).
191. Cumpston, B.H. et al. Two-photon polymerization initiators for three-dimensional optical data storage and microfabrication. *Nature* **398,** 51–54 (1999).
192. Campbell, M., Sharp, D.N., Harrison, M.T., Denning, R.G. & Turberfield, A.J. Fabrication of photonic crystals for the visible spectrum by holographic lithography. *Nature* **404,** 53–56 (2000).
193. Lim, D., Kamotani, Y., Cho, B., Mazumder, J. & Takayama, S. Fabrication of microfluidic mixers and artificial vasculatures using a high-brightness diode-pumped Nd:YAG laser direct write method. *Lab. Chip* **3,** 318–323 (2003).
194. Takesada, M. et al. Micro-character printing on a diamond plate by femtosecond infrared optical pulses. *Jpn. J. Appl. Phys.* **42,** 4613 (2003).
195. Chrisey, D.B. et al. Direct writing of conformal mesoscopic electronic devices by MAPLE DW. *Appl. Surf. Sci.* **168,** 345–352 (2000).
196. Wu, P.K. et al. Laser transfer of biomaterials: Matrix-assisted pulsed laser evaporation (MAPLE) and MAPLE direct write. *Rev. Sci. Instrum.* **74,** 2546–2557 (2003).
197. Deckard, C.R. Method and apparatus for producing parts by selective sintering (1989). http://www.google.com/patents/US4863538.
198. Kumar, S. Selective laser sintering: A qualitative and objective approach. *IOM* **55,** 43–47 (2003).
199. Wallenberger, F.T. Rapid prototyping directly from the vapor phase. *Science* **267,** 1274–1275 (1995).
200. Zhang, X., Jiang, X.N. & Sun, C. Micro-stereolithography of polymeric and ceramic microstructures. *Sens. Actuators Phys.* **77,** 149–156 (1999).
201. Kawata, S., Sun, H.B., Tanaka, T. & Takada, K. Finer features for functional microdevices—Micromachines can be created with higher resolution using two-photon absorption. *Nature* **412,** 697–698 (2001).
202. Provin, C., Monneret, S., Le Gall, H. & Corbel, S. Three-dimensional ceramic microcomponents made using microstereolithography. *Adv. Mater.* **15,** 994–997 (2003).
203. Gross, M.E., Appelbaum, A. & Schnoes, K.J. A chemical and mechanistic view of reaction profiles in laser direct-write metallization in metallo-organic films. *J. Appl. Phys.* **60,** 529–533 (1986).
204. Gross, M.E., Appelbaum, A. & Gallagher, P.K. Laser direct-write metallization in thin palladium acetate films. *J. Appl. Phys.* **61,** 1628–1632 (1987).
205. Chen, Q.J., Imen, K. & Allen, S.D. Laser enhanced electroless plating of micron-scale copper wires. *J. Electrochem. Soc.* **147,** 1418–1422 (2000).
206. Shrivastva, P.B., Boose, C.A., Kolster, B.H., Harteveld, C. & Meinders, B. Selective metallization of alumina by laser. *Surf. Coat. Technol.* **46,** 131–138 (1991).
207. Bohandy, J., Kim, B. & Adrian, F. Metal-deposition from a supported metal-film using an excimer laser. *J. Appl. Phys.* **60,** 1538–1539 (1986).
208. Bohandy, J., Kim, B., Adrian, F. & Jette, A. Metal-deposition at 532-nm using a laser transfer technique. *J. Appl. Phys.* **63,** 1158–1162 (1988).
209. Mir-Hosseini, N., Schmidt, M.J.J. & Li, L. Growth of patterned thin metal oxide films on glass substrates from metallic bulk sources using a Q-switched YAG laser. *Appl. Surf. Sci.* **248,** 204–208 (2005).
210. Kuebler, S.M. et al. Optimizing two-photon initiators and exposure conditions for three-dimensional lithographic microfabrication. *J. Photopolym. Sci. Technol.* **14,** 657–668 (2001).
211. McNeal, M.P., Jang, S.-J. & Newnham, R.E. Particle size dependent high frequency dielectric properties of barium titanate. *Proc 10th IEEE Int Symp Appl Ferroelectr* **2,** 837–840 (1996).
212. Li, B., Clark, P.A. & Church, K.H. Robust direct-write dispensing tool and solutions for micro/meso-scale manufacturing and packaging. In *ASME Int. Manuf. Sci. Eng. Conf.* 715–721 (American Society of Mechanical Engineers, 2007). http://proceedings.asmedigitalcollection.asme.org/proceeding.aspx?articleid=1598546.
213. Mott, M. & Evans, J.R.G. Zirconia/alumina functionally graded material made by ceramic ink jet printing. *Mater. Sci. Eng. A* **271,** 344–352 (1999).

214. Cesarano III, J.C. & Calvert, P.D. Freeforming objects with low-binder slurry (2000). http://www.google.com/patents/US6027326.
215. Sachs, E., Cima, M., Williams, P., Brancazio, D. & Cornie, J. Three dimensional printing: Rapid tooling and prototypes directly from a CAD model. *J. Eng. Ind.* **114,** 481–488 (1992).
216. Crump, S.S. Apparatus and method for creating three-dimensional objects (1992). http://www.google.com/patents/US5121329.
217. Mireles, J. et al. Development of a fused deposition modeling system for low melting temperature metal alloys. *J. Electron. Packag.* **135,** 011008–011008 (2013).
218. Diegel, O., Singamneni, S., Huang, B. & Gibson, I. Curved layer fused deposition modeling in conductive polymer additive manufacturing. *Adv. Mater. Res.* **199–200,** 1984–1987 (2011).
219. Cai, Z., Li, X., Hu, Q. & Zeng, X. Study on thick-film PTC thermistor fabricated by micro-pen direct writing. *Microelectron. J.* **39,** 1452–1456 (2008).
220. Castillo, S., Muse, D., Medina, F., MacDonald, E. & Wicker, R. Electronics integration in conformal substrates fabricated with additive layered manufacturing. In *Proc. 20th Annu. Solid Free. Fabr. Symp.*, University of Texas, Austin TX, 730–737 (2009).
221. Sun, K. et al. 3D printing of interdigitated LI-ion microbattery architectures. *Adv. Mater.* **25,** 4539–4543 (2013).
222. Russo, A. et al. Pen-on-paper flexible electronics. *Adv. Mater.* **23,** 3426–3430 (2011).
223. Ahn, B.Y., Lorang, D.J. & Lewis, J.A. Transparent conductive grids via direct writing of silver nanoparticle inks. *Nanoscale* **3,** 2700–2702 (2011).
224. Siegel, A.C., Phillips, S.T., Wiley, B.J. & Whitesides, G.M. Thin, lightweight, foldable thermochromic displays on paper. *Lab. Chip* **9,** 2775–2781 (2009).
225. Dragoman, M., Flahaut, E., Dragoman, D., Al Ahmad, M. & Plana, R. Writing simple RF electronic devices on paper with carbon nanotube ink. *Nanotechnology* **20,** 375203 (2009).
226. Jung, M. et al. All-printed and roll-to-roll-printable 13.56-MHz-operated 1-bit RF tag on plastic foils. *IEEE Trans. Electron Devices* **57,** 571–580 (2010).
227. Nyström, G., Razaq, A., Strømme, M., Nyholm, L. & Mihranyan, A. Ultrafast all-polymer paper-based batteries. *Nano Lett.* **9,** 3635–3639 (2009).
228. Adams, J.J. et al. Conformal printing of electrically small antennas on three-dimensional surfaces. *Adv. Mater.* **23,** 1335–1340 (2011).
229. Ahn, B.Y. et al. Planar and three-dimensional printing of conductive inks. *J. Vis. Exp. JoVE* (2011). doi:10.3791/3189.
230. Lewis, J.A. & Gratson, G.M. Direct writing in three dimensions. *Mater. Today* **7,** 32–39 (2004).
231. Walker, S.B. & Lewis, J.A. Reactive silver inks for patterning high-conductivity features at mild temperatures. *J. Am. Chem. Soc.* **134,** 1419–1421 (2012).
232. Lewis, J.A., Smay, J.E., Stuecker, J. & Cesarano, J. Direct ink writing of three-dimensional ceramic structures. *J. Am. Ceram. Soc.* **89,** 3599–3609 (2006).
233. Hu, J. & Yu, M.-F. Meniscus-confined three-dimensional electrodeposition for direct writing of wire bonds. *Science* **329,** 313–316 (2010).
234. Lewis, J.A. Colloidal processing of ceramics. *J. Am. Ceram. Soc.* **83,** 2341–2359 (2000).
235. Smay, J.E., Cesarano, J. & Lewis, J.A. Colloidal inks for directed assembly of 3-D periodic structures. *Langmuir* **18,** 5429–5437 (2002).
236. Smay, J. e., Gratson, G. m., Shepherd, R. f., Cesarano, J. & Lewis, J. a. Directed colloidal assembly of 3D periodic structures. *Adv. Mater.* **14,** 1279–1283 (2002).
237. Guo, J.J. & Lewis, J.A. Aggregation effects on the compressive flow properties and drying behavior of colloidal silica suspensions. *J. Am. Ceram. Soc.* **82,** 2345–2358 (1999).
238. Therriault, D., Shepherd, R.F., White, S.R. & Lewis, J.A. Fugitive inks for direct-write assembly of three-dimensional microvascular networks. *Adv. Mater.* **17,** 395–399 (2005).
239. Xu, M., Gratson, G.M., Duoss, E.B., Shepherd, R.F. & Lewis, J.A. Biomimetic silicification of 3D polyamine-rich scaffolds assembled by direct ink writing. *Soft Matter* **2,** 205–209 (2006).
240. Therriault, D., White, S.R. & Lewis, J.A. Chaotic mixing in three-dimensional microvascular networks fabricated by direct-write assembly. *Nat. Mater.* **2,** 265–271 (2003).

241. Gratson, G.M., Xu, M. & Lewis, J.A. Microperiodic structures: Direct writing of three-dimensional webs. *Nature* **428,** 386–386 (2004).
242. Lebel, L.L., Aissa, B., Khakani, M.A.E. & Therriault, D. Ultraviolet-assisted direct-write fabrication of carbon nanotube/polymer nanocomposite microcoils. *Adv. Mater.* **22,** 592–596 (2010).
243. Michna, S., Wu, W. & Lewis, J.A. Concentrated hydroxyapatite inks for direct-write assembly of 3-D periodic scaffolds. *Biomaterials* **26,** 5632–5639 (2005).
244. Smay, J.E., Cesarano, J., Tuttle, B.A. & Lewis, J.A. Directed colloidal assembly of linear and annular lead zirconate titanate arrays. *J. Am. Ceram. Soc.* **87,** 293–295 (2004).
245. San Marchi, C., Kouzeli, M., Rao, R., Lewis, J.A. & Dunand, D.C. Alumina–aluminum interpenetrating-phase composites with three-dimensional periodic architecture. *Scr. Mater.* **49,** 861–866 (2003).
246. Cesarano III, J. & Calvert, P.D. US Patent 6,027,326, 2000; Li, Q. & Lewis, J.A. *Adv Mater* **15,** 1639 (2003).
247. Li, Q. & Lewis, J. a. Nanoparticle inks for directed assembly of three-dimensional periodic structures. *Adv. Mater.* **15,** 1639–1643 (2003).
248. Gratson, G.M. & Lewis, J.A. Phase behavior and rheological properties of polyelectrolyte inks for direct-write assembly. *Langmuir* **21,** 457–464 (2005).
249. Ahn, B.Y., Lorang, D.J., Duoss, E.B. & Lewis, J.A. Direct-write assembly of microperiodic planar and spanning ITO microelectrodes. *Chem. Commun.* **46,** 7118–7120 (2010).
250. Duoss, E.B., Twardowski, M. & Lewis, J.A. Sol-gel inks for direct-write assembly of functional oxides. *Adv. Mater.* **19,** 3485–3489 (2007).
251. Guo, X. et al. Two- and three-dimensional folding of thin film single-crystalline silicon for photovoltaic power applications. *Proc. Natl. Acad. Sci. U. S. A.* **106,** 20149–20154 (2009).
252. Yoon, J. et al. Ultrathin silicon solar microcells for semitransparent, mechanically flexible and microconcentrator module designs. *Nat. Mater.* **7,** 907–915 (2008).
253. Smay, J.E., Iii, J.C., Tuttle, B.A. & Lewis, J.A. Piezoelectric properties of 3-X periodic Pb(ZrxTi1–x) O3–polymer composites. *J. Appl. Phys.* **92,** 6119–6127 (2002).
254. Gratson, G.M. et al. Direct-write assembly of three-dimensional photonic crystals: Conversion of polymer scaffolds to silicon hollow-woodpile structures. *Adv. Mater.* **18,** 461–465 (2006).
255. Sun, Y. & Rogers, J.A. Inorganic semiconductors for flexible electronics. *Adv. Mater.* **19,** 1897–1916 (2007).
256. Kim, D.-H. et al. Dissolvable films of silk fibroin for ultrathin conformal bio-integrated electronics. *Nat. Mater.* **9,** 511–517 (2010).
257. Hamedi, M., Forchheimer, R. & Inganäs, O. Towards woven logic from organic electronic fibres. *Nat. Mater.* **6,** 357–362 (2007).
258. Dickey, M.D. et al. Eutectic gallium-indium (EGaIn): A liquid metal alloy for the formation of stable structures in microchannels at room temperature. *Adv. Funct. Mater.* **18,** 1097–1104 (2008).
259. Ladd, C., So, J.-H., Muth, J. & Dickey, M.D. 3D printing of free standing liquid metal microstructures. *Adv. Mater.* **25,** 5081–5085 (2013).
260. Trlica, C., Parekh, D. P., Panich, L., Ladd, C. & Dickey, M. D. 3-D printing of liquid metals for stretchable and flexible conductors. **9083**, 90831D–90831D–10 (2014).
261. Rayleigh, Lord. On the capillary phenomena of jets. *Proc. R. Soc. Lond.* **29,** 71–97 (1879).
262. French, S.J., Saunders, D.J. & Ingle, G.W. The system gallium-indium. *J. Phys. Chem.* **42,** 265–274 (1937).
263. Cademartiri, L. et al. Electrical resistance of Ag-TS-S(CH_2)(n-1)CH_3//Ga_2O_3/EGaIn tunneling junctions. *J. Phys. Chem. C* **116,** 10848–10860 (2012).
264. Baldwin, D.F., Deshmukh, R.D. & Hau, C.S. Gallium alloy interconnects for flip-chip assembly applications. *IEEE Trans. Compon. Packag. Technol.* **23,** 360–366 (2000).
265. Chiechi, R.C., Weiss, E.A., Dickey, M.D. & Whitesides, G.M. Eutectic gallium-indium (EGaIn): A moldable liquid metal for electrical characterization of self-assembled monolayers. *Angew. Chem. Int. Ed.* **47,** 142–144 (2008).

266. Cheng, S., Rydberg, A., Hjort, K. & Wu, Z. Liquid metal stretchable unbalanced loop antenna. *Appl. Phys. Lett.* **94,** 144103–144103–3 (2009).
267. Palleau, E., Reece, S., Desai, S.C., Smith, M.E. & Dickey, M.D. Self-healing stretchable wires for reconfigurable circuit wiring and 3d microfluidics. *Adv. Mater.* **25,** 1589–1592 (2013).
268. Tabatabai, A., Fassler, A., Usiak, C. & Majidi, C. Liquid-phase gallium–indium alloy electronics with microcontact printing. *Langmuir* **29,** 6194–6200 (2013).
269. Lu, T., Finkenauer, L., Wissman, J. & Majidi, C. Rapid prototyping for soft-matter electronics. *Adv. Funct. Mater.* (2014). doi:10.1002/adfm.201303732.
270. Nagel, D.J. In *Direct-Write Technol. Rapid Prototyp.* (Piqué, A.) 557–679 (Academic Press, 2002). http://www.sciencedirect.com/science/article/pii/B9780121742317500725.
271. Campbell, A.N. et al. *Electrical and Chemical Characterization of FIB-Deposited Insulators* (Sandia National Labs, Albuquerque, NM, 1997). http://www.osti.gov/bridge/product.biblio.jsp?osti_id = 532558.
272. Edinger, K., Melngailis, J. & Orloff, J. Study of precursor gases for focused ion beam insulator deposition. *J. Vac. Sci. Technol. B* **16,** 3311–3314 (1998).
273. Edinger, K. in *Direct-Write Technol. Rapid Prototyp.* (Piqué, A.) 347–383 (Academic Press, 2002). http://www.sciencedirect.com/science/article/pii/B9780121742317500658.
274. Tjerkstra, R.W., Segerink, F.B., Kelly, J.J. & Vos, W.L. Fabrication of three-dimensional nanostructures by focused ion beam milling. *J. Vac. Sci. Technol. B* **26,** 973–977 (2008).
275. Olivero, P. et al. Ion-beam-assisted lift-off technique for three-dimensional micromachining of freestanding single-crystal diamond. *Adv. Mater.* **17,** 2427–2430 (2005).
276. Matsui, S. in *Springer Handb. Nanotechnol.* (Bhushan, P.B.) 211–229 (Springer, Berlin, Germany, 2010). http://link.springer.com/chapter/10.1007/978-3-642-02525-9_7.
277. Matsui, S. in *Springer Handb. Nanotechnol.* (Bhushan, P.B.) 179–196 (Springer, Berlin, Germany, 2007). http://link.springer.com/referenceworkentry/10.1007/978-3-540-29857-1_6.
278. Matsui, S. Three-dimensional nanostructure fabrication by focused-ion-beam chemical vapor deposition. *SPIE Conf. Optomech. Micro/Nano Devices Comp. II*. Boston, MA, October 01, **6376,** 637602–637602–15 (2006). http://proceedings.spiedigitallibrary.org/proceeding.aspx?articleid=1332448.
279. Morita, T. et al. Free-space-wiring fabrication in nano-space by focused-ion-beam chemical vapor deposition. *J. Vac. Sci. Technol. B* **21,** 2737–2741 (2003).
280. Dinwiddie, R.B., Dehoff, R.R., Lloyd, P.D., Lowe, L.E. & Ulrich, J.B. Thermographic in-situ process monitoring of the electron-beam melting technology used in additive manufacturing. SPIE Proc. Thermo. Therm. Infra. Appl XXXV. **8705,** 87050K–87050K–9 (2013). http://spie.org/Publications/Proceedings/Paper/10.1117/12.2018412.
281. Dehoff, R. et al. Case study: Additive manufacturing of aerospace brackets. *Adv. Mater. Process.* **171,** 19–22 (2013).

9

Industrial Implementation of Additive Manufacturing

Edward D. Herderick and Clark Patterson

CONTENTS

ABSTRACT The rapid maturation of additive manufacturing (AM) technologies is accelerating a transition from the traditional *design for manufacturing* model to a new paradigm of *manufacturing by design*. In this new paradigm, industrial designers are fully enabled to design components based on functionality, rather than limits of assembly technologies. For the AM suite of technologies to realize their full potential, materials and process specialists must continue to innovate and provide tailored solutions for industrial end users. This chapter explores innovation space presented in three parts: first, a brief analysis of AM technologies with respect to industrial needs; second, relevant industrial case studies demonstrating potential areas for implementation; and third, a view of where things are headed over the coming years.

9.1 Introduction

Over the past 30 years, AM technology has matured beyond rapid prototyping to become a viable route to producing industrial parts in high-performance metals and polymers.

The maturation of AM technologies is accelerating a transition from the traditional *design for manufacturing* model to a new paradigm of *manufacturing by design*. In this new paradigm, industrial designers are fully enabled to design components based on functionality, rather than limits of assembly technologies.

The goal of this chapter is to present the current state of the art, seed ideas for where the technology can be implemented today, and provide thoughts on where the technology will

be in the future. The scope is for industrial applications using structural properties of the materials with an emphasis on metal and polymers owing to their high level of technology readiness.

9.2 Application of Additive Technologies for Industrial Products

There are three key tenets for creating an industrial product: design, materials, and manufacturing processes.[1] The shape-making capability of AM technologies has captured the imagination of the design community since its earliest days for rapid creation of form, fit, and function prototypes. The key hurdle toward industrial implementation is the availability of engineering materials and corresponding technical data that designers can use to create products. Manufacturing processes and materials are firmly linked and share a synergistic interaction where innovation in one leads to further innovation in the other.[2] It is this link for innovation that is driving industrial applications for AM.

Table 9.1 is a brief review of the ASTM designated AM technologies including advantages and disadvantages with respect to industrial implementation.[3] A clear demarcation can be made between those technologies that are currently able to manufacture engineering materials. Practically speaking, for engineering classes of polymers those technologies are material extrusion and powder bed fusion. For metals, those processes are binder jetting, powder bed fusion, directed energy deposition, and sheet lamination.

9.3 Direct Part Fabrication in Engineering Thermoplastics

The largest current application set for industrial implementation of AM for direct parts is for parts manufactured using thermoplastics.[4] Polymeric air moving duct work made of engineering polyamides manufactured using laser powder bed fusion 3D system's selective laser sintering (3DS SLS) has been implemented by Boeing for several years.[5] That example demonstrated that air moving applications are ideal candidates for AM implementation. The parts are non-load bearing, limiting their structural requirements, and include complex shapes that are difficult to machine or injection mold.

Figures 9.1 through 9.3 show examples of generic ducts made of Ultem 9085 and manufactured using material extrusion on a Stratasys Fortus fused deposition modeling (FDM™) industrial grade AM platform. Ultem 9085 made using FDM has a high tensile strength (10,390 psi), has a high heat deflection temperature of 333°F, and is flame-smoke-toxicity certified.[6] Efforts are underway to provide designers a statistically significant data set for Ultem 9085 FDM to support further implementation.[7]

Figure 9.1 shows an image of a thin-walled hot air moving duct. The wall thickness is only a few tool path passes thick, on the order of 0.050″. Parts can be made leak tight using post-process vapor smoothing that joins any incongruities and smooths *z*-axis roughness. Parts can be made lighter and more complex than those that could be injection molded. Figure 9.2 shows an air-guiding grate. The vanes in the center of this duct have internal curvature that could not be machined or would be die-locked using traditional injection molding. Figure 9.3 is a high temperature duct attachment interfacing between a round

TABLE 9.1

ASTM Defined AM Processes, Example Vendors, and Pros/Cons of Technology Class

ASTM Defined Technology Category	Description	Example Vendor Technology	Advantages for Industrial Parts Production	Challenges for Industrial Parts Production
Binder jetting	Liquid bonding agent is selectively deposited to join powder metal	ExOne M-Flex, Voxeljet	Broadest range of materials, cost effective	Composite microstructure (usually), intensive post-processing may be required
Directed energy deposition	Focused thermal energy is fuses materials by melting as material is deposited	Optomec LENS, Lincoln Electric Hybrid Laser-Arc, Sciaky EBDM	In situ alloying, hardfacing, repair	Difficult to manufacture direct parts
Powder bed fusion	Thermal energy selectively fuses regions of powder bed	EOS DMLS, 3D Systems SLS, Arcam EBM	Engineering materials coupled with high resolution, highest density structures (as printed metals with >99.5% density achievable	Relatively slow, relatively expensive, limited build volume of parts
Material extrusion	Material is selectively dispensed through a nozzle or orifice	Stratasys Fused Deposition Modeling	Engineering polymers, large builds, fast	Surface roughness due to raster, requires support material
Material jetting	Droplets of build material are selectively deposited	Objet Connex, Optomec Aerosol Jet	Fast, high resolution, multiple materials, inexpensive	Requires materials compatible with jetting (stricter for structural than functional)
Sheet lamination	Sheets of material are bonded to form an object	Fabrisonic VHP-UAM, CAM-LEM	Very large builds (6ft x 6ft x 6ft possible), composites of metal alloys and electronic materials	*z*-Axis strength penalty, maturing technology
Vat photopolymerization	Liquid photopolymer in vat is selectively cured by light-activated polymerization	3D Systems Stereolithography	Fast, very high resolution, inexpensive	Lack of engineering polymers

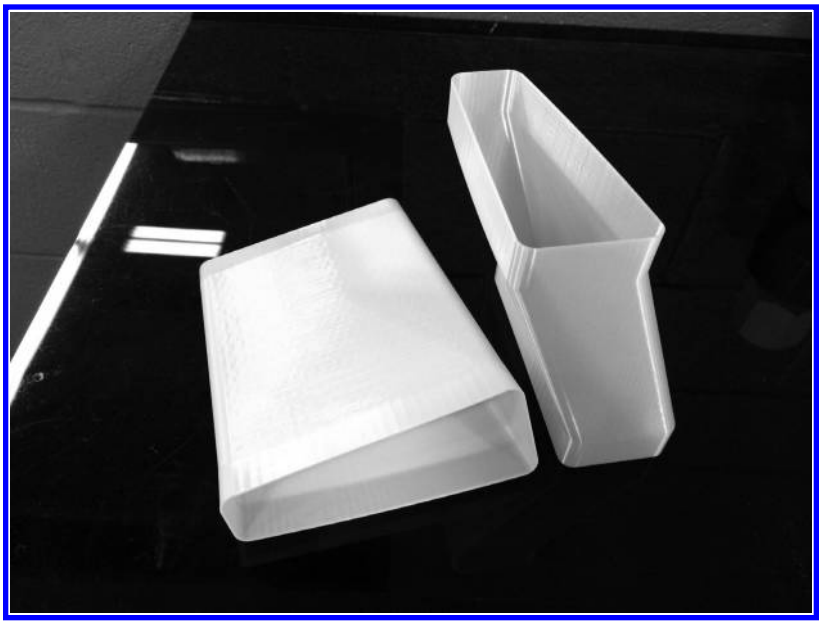

FIGURE 9.1
Thin walled hot air moving duct made from Ultem 9085 using Stratasys FDM™. (Copyright Rapid Prototype and Manufacturing, LLC, Avon Lake, Ohio, 2014.)

FIGURE 9.2
Air guiding grate made from Ultem 9085 using Stratasys FDM™. (Copyright Rapid Prototype and Manufacturing, LLC, Avon Lake, Ohio, 2014.)

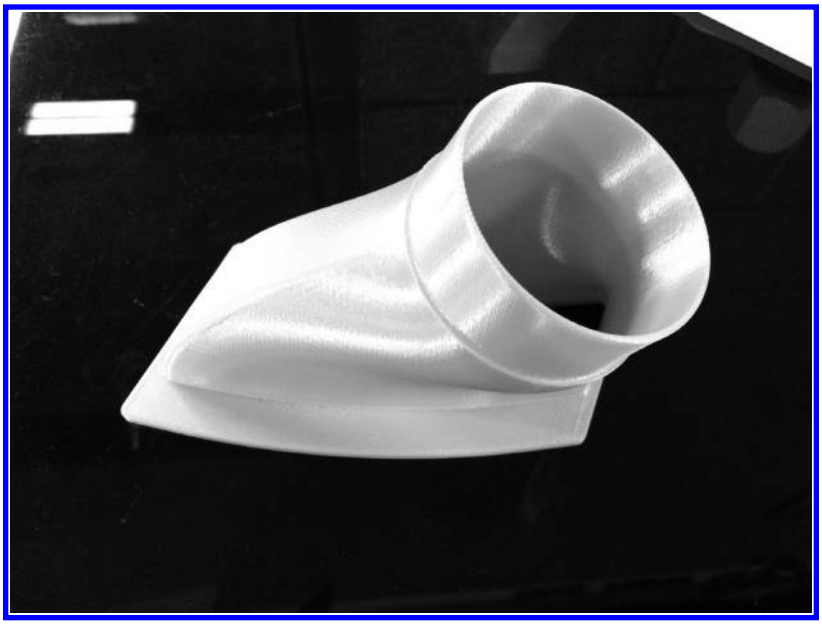

FIGURE 9.3
High temperature duct attachment interfacing between a round and a flat, rectangular shape made from Ultem 9085 using Stratasys FDM™. (Copyright Rapid Prototype and Manufacturing, LLC, Avon Lake, Ohio, 2014.)

and a flat, rectangular shape. Similar to Figure 9.2, this part would be difficult to machine or difficult to injection mold and is enabled by the shape-making capability of AM.

The ability to select and manufacture different materials is key attribute of AM. Using the same digital file, with modified tool paths, the same part design can be made more economically using commodity materials or with a higher performance material in low volumes to serve different markets on an as-needed basis without dramatic impacts on inventory. Figure 9.4 demonstrates this principle for product design, in it are three single to four-port nozzles showing shape-making capability of AM. On the left is a part made using standard white acrylonitrile butadiene styrene (ABS), on the center is Ultem 9085, and on the right is carbon fiber filled poly-ether-imide all manufactured using FDM. In this way, design teams can source and select properties of components specifically for their application need without significant manufacturing process changes.

There are other emerging applications for manufacturing polymers using AM for functional applications. Many of these are in the medical device space, Figures 9.5 and 9.6 include examples for medical imaging applications. During normal operation, computed tomography (CT) and positron emission tomography (PET) scanners emit X-rays used to create images that require shielding and filtering. Historically, this has been done using lead or other high *z* metal shielding made using casting or machining. These applications show a strong value proposition for AM because of their relatively low volumes and complex geometries. The medical imaging components in Figures 9.5 and 9.6 were made from tungsten-loaded polycarbonate printed using FDM. Figure 9.5 is a mounting bracket and Figure 9.6 is a mounting cup for electronics in a CT scanner. In this case, the tungsten metal in the composite shields the X-rays and the overall material has been tailored to match the shielding characteristics of lead metal castings. AM offers reduced inventory costs, manufacturing without tooling, and higher shape complexity allowing for reduced footprint in the medical imaging devices.

FIGURE 9.4
(See color insert.) Three single- to four-port nozzles showing shape-making capability of additive manufacturing. On the left is a part made using standard white ABS, center is Ultem 9085, and on the right is carbon-fiber-filled poly ether imide all manufactured using FDM™. (Copyright Rapid Prototype and Manufacturing, LLC, Avon Lake, Ohio, 2014.)

FIGURE 9.5
Mounting bracket made from tungsten loaded polycarbonate printed using FDM™. (Copyright Rapid Prototype and Manufacturing, LLC, Avon Lake, Ohio, 2014.)

Industrial applications for printed thermoplastics will continue to emerge as more engineering materials are introduced. There are more than 8,000 commercially available injection moldable thermoplastics[8]; however, there are less than 20 commercially available AM polymers. This implementation will be particularly valuable for loaded composites and other high-value polymers. An example of an AM composite material component is shown

FIGURE 9.6
Mounting cup for electronics in a CT scanner made from tungsten loaded polycarbonate printed using FDM™. (Copyright Rapid Prototype and Manufacturing, LLC, Avon Lake, Ohio, 2014.)

in Figure 9.7, which is a forming tool set made from chopped carbon fiber loaded polyether-imide. This material has higher stiffness, a lower CTE (more closely matched to aluminum), and higher thermal conductivity than the related Ultem 9085 and demonstrates the types of materials that are in product development now and will be commercially available over the next 1–3 years.

9.4 Approaches to Indirectly Manufacturing Parts

Applications where AM built parts are indirectly used to manufacture industrial products, such as injection molding and casting, present ripe areas for implementation since the new processes themselves do not need to be recertified.

Injection molding is a mature industry that is highly competitive on performance, cost, and delivery schedule. The core and cavity tool that provide the shape-making capability are themselves expensive to manufacture and require long lead times on the order of months in many cases and therefore require strong business cases to fulfill orders. This means that in general, injection molding is only economical for large volumes of parts on the order of 1,000s or more where the tool cost and schedule can be amortized over many parts. This makes short runs of parts below 1,000 on quick turnaround timelines a high-value niche market that innovative businesses are driven to serve. AM has a strong value proposition for these applications.

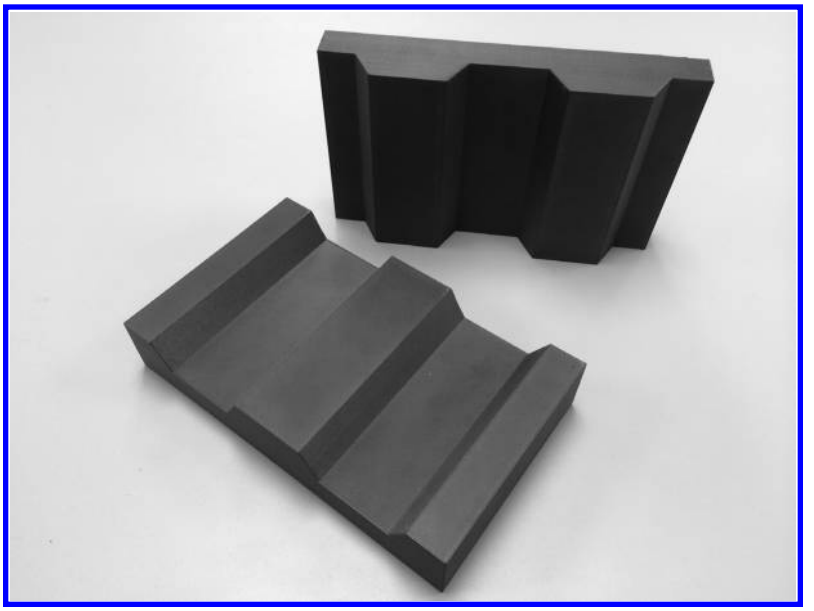

FIGURE 9.7
Forming tool set made from chopped carbon fiber loaded poly-ether-imide. (Copyright Rapid Prototype and Manufacturing, LLC, Avon Lake, Ohio, 2014.)

Figure 9.8 is an example short-run tool made using objet material jetting technology. The two pieces form the cavity into which a polymer is injected thereby forming a component. The material jetting technology uses ABS-like polymers that can be printed in a few hours and can last for a short run of 100–200 parts. The main challenge is that the thermal conductivity of the polymer is lower than standard metal tools increasing cycle times so that the tool is not damaged. For short-run parts, cycle time is typically not a deciding factor when compared to delivery time. When higher temperature or chemical resistance is required, Ultem 9085 manufactured using FDM can be used for higher stress molds and longer part runs. Figure 9.9 is a core and cavity set for thermoplastic elastomer molding. In this example, there are rails on the cavity set that allow for changing the tab features on the top and bottom of the rubber piece.

Although useful, there are many applications where polymer molds will not effectively meet injection molding requirements. For the right value proposition, printed metal injection mold tooling, this includes when tooling is not available quickly enough or with difficult to mold polymers or part geometries. The cost to manufacture may be higher for the printed tool, but printing the tool allows integration of cooling channels that speed cycle times and improve quality leading to holistic life cycle cost reduction. Figure 9.10 shows an example injection molding tool for a fitting made of maraging steel using laser powder bed fusion on an EOS DMLS platform.

Another industrial application of AM technology for indirectly making components is printing of sand molds and cores for metal casting using the binder jetting process. Figures 9.11 and 9.12 are images of an aluminum sand casting mold made using binder jetting on a Voxeljet vx200 platform. This application is particularly appealing for AM implementation as the same materials, that is, foundry sand and foundry resin, used in the standard process are used in the printing process. Of particular interest are complex core structures used for casting of aluminum fluid moving pump housings.

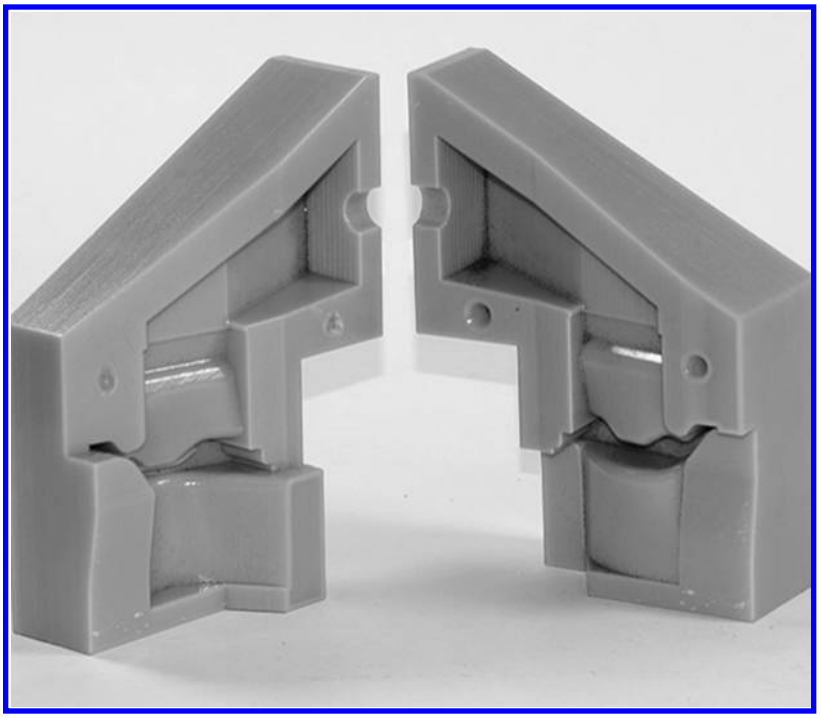

FIGURE 9.8
(See color insert.) Example of a short-run injection molding tool made from ABS using Objet material jetting technology. (Copyright Rapid Prototype and Manufacturing, LLC, Avon Lake, Ohio, 2014.)

FIGURE 9.9
(See color insert.) Injection mold core and cavity set for thermoplastic elastomer molding made from Ultem 9085 using Stratasys FDM™. (Copyright Rapid Prototype and Manufacturing, LLC, Avon Lake, Ohio, 2014.)

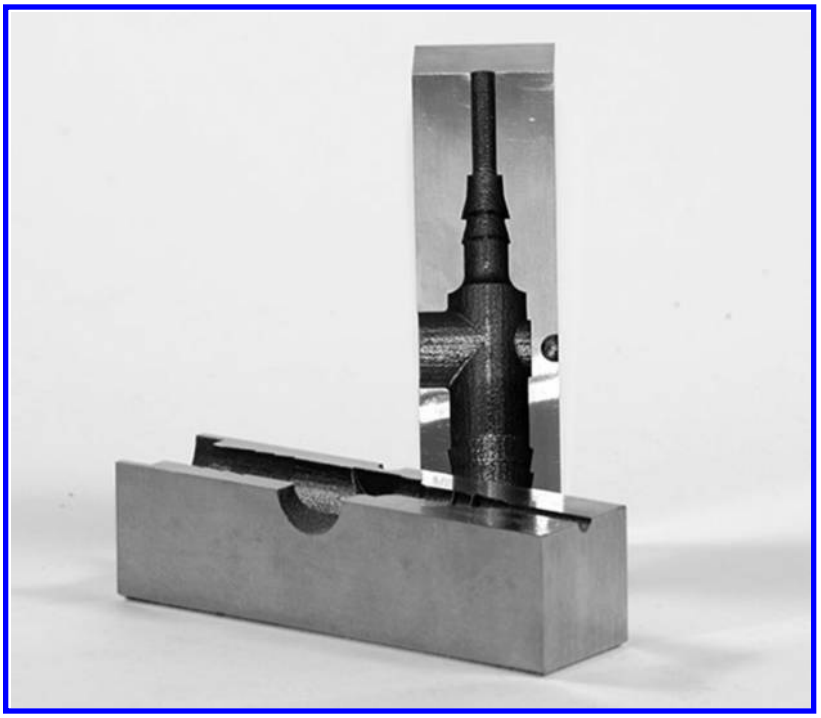

FIGURE 9.10
Example injection molding tool for a fitting made of maraging steel using laser powder bed fusion on an EOS DMLS™ platform. (Copyright Rapid Prototype and Manufacturing, LLC, Avon Lake, Ohio, 2014.)

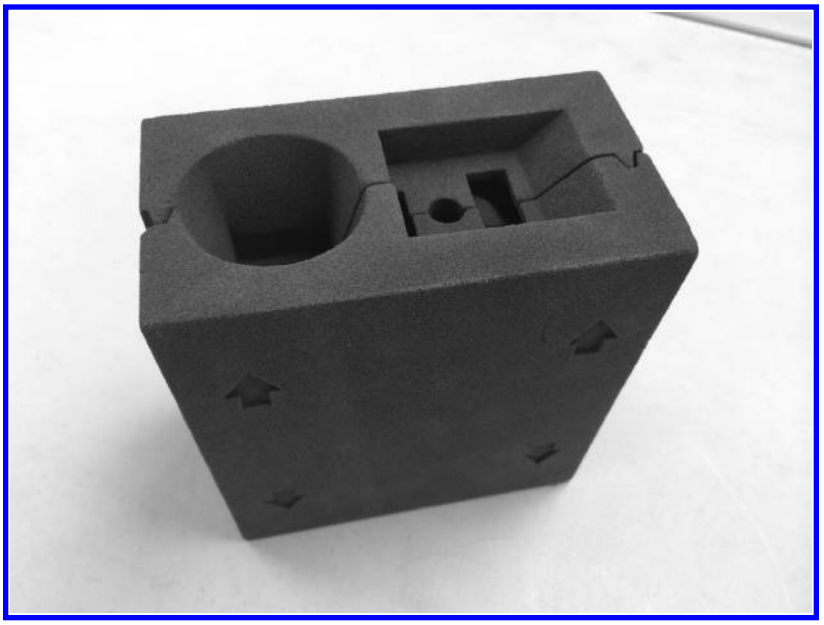

FIGURE 9.11
Closed aluminum sand casting mold made using binder jetting on a Voxeljet vx200 platform. (Copyright Rapid Prototype and Manufacturing, LLC, Avon Lake, Ohio, 2014.)

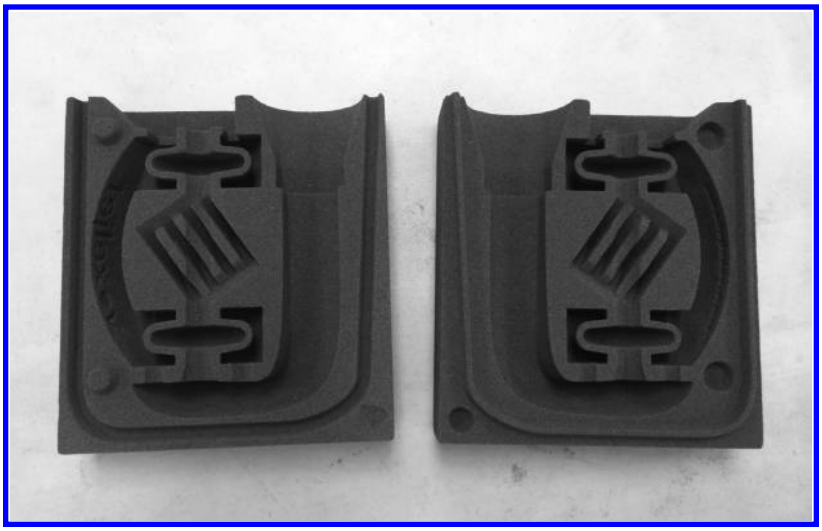

FIGURE 9.12
Open aluminum sand casting mold made using binder jetting on a Voxeljet vx200 platform. (Copyright Rapid Prototype and Manufacturing, LLC, Avon Lake, Ohio, 2014.)

9.5 Direct Part Fabrication in Metals

The ability to directly produce metal alloy parts using AM is among the fastest growing sectors for the technology and has captured the popular imagination.[9] As the technology has matured, industrial manufacturers have developed a series of use cases where metal parts are difficult or expensive to source with long lead times due to complex castings, machining costs, and diminished supply chain capacity. AM enables turnaround times on the order of weeks without several months long wait for tooling. Furthermore, part consolidation provides a huge benefit as metal assemblies that were originally brazed or joined together can be made in a single piece allowing for greater design flexibility.

In the laser powder bed fusion process for manufacturing metal parts, the use of support materials and structures relative to part orientation is a key determinant of part manufacturability. Figure 9.13 shows several stainless steel PH1 (15-5 Cr-Ni) impeller prototypes bonded to the build plate in the build chamber. The parts are welded to the build plate and support materials are used to promote thermal conduction of heat away from the build layer and prevent warping due to residual stresses. Figure 9.14 is a high-performance automotive rocker arm made from maraging steel MS1 (a Ni precipitation hardened tool steel alloy). The lighter areas are support material left on the part to demonstrate how supports are required to manufacture open areas in the z direction. The value proposition for this particular application is rapid turnaround time to meet race deadlines and design freedom for new and spare parts.

Figure 9.15 is a functional gear prototype made from PH1 stainless steel. This application use case for laser powder bed fusion is driven by the ability to print a build plate with varying parts for rapid testing of different designs. The conventional method would require machining each design from rod stock. Furthermore, initial production runs could be completed using AM prior to full-scale tooling implementation.

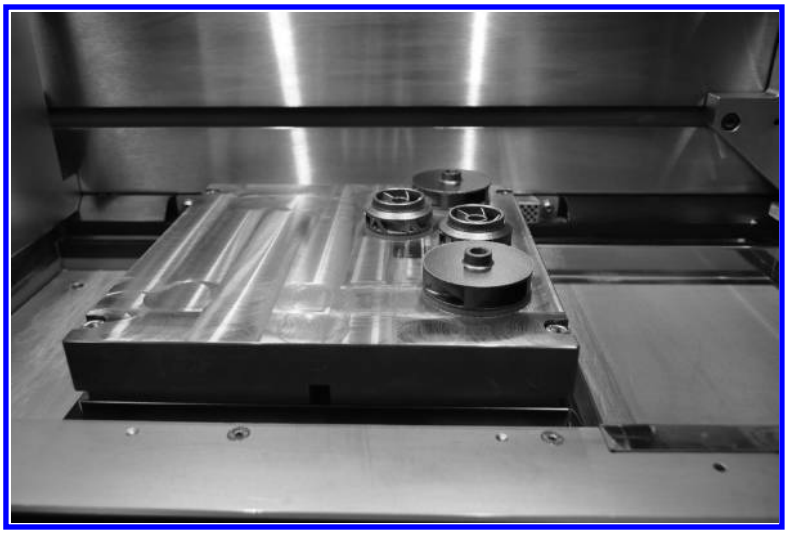

FIGURE 9.13
(See color insert.) Stainless steel PH1 (15-5 Cr-Ni) impeller prototypes bonded to the build plate in an EOS DMLS™ M280 build chamber. (Copyright Rapid Prototype and Manufacturing, LLC, Avon Lake, Ohio, 2014.)

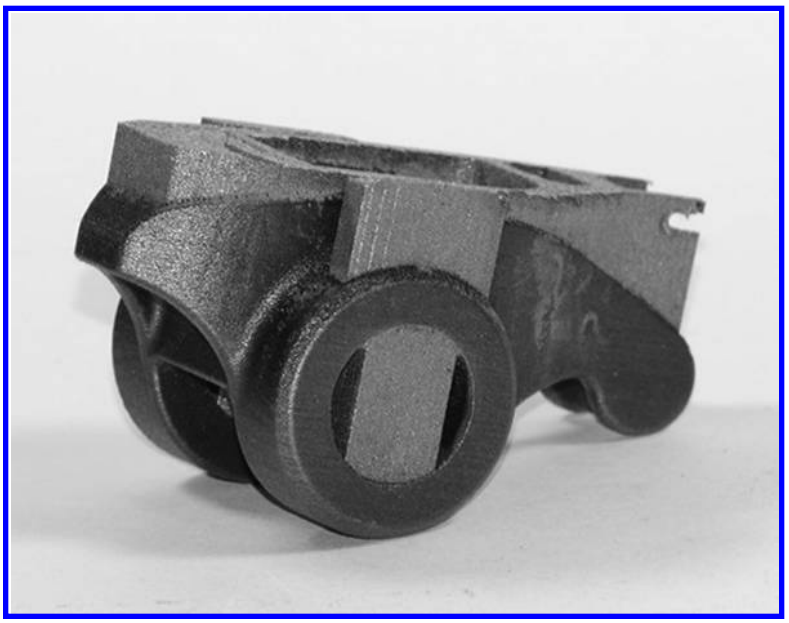

FIGURE 9.14
High-performance automotive rocker arm made from maraging steel MS1 on an EOS DMLS™ platform. (Copyright Rapid Prototype and Manufacturing, LLC, Avon Lake, Ohio, 2014.)

Metal AM parts are also finding strong use cases for fluid moving applications for similar reasons as engineered polymers as discussed in the previous section. Figure 9.16 is a pair of water cooling channels in MS1 using laser powder bed fusion. The original part design was cast in three separate components and brazed together, where this is printed in a single part. Special considerations like chamfers on edges and part orientation are required to

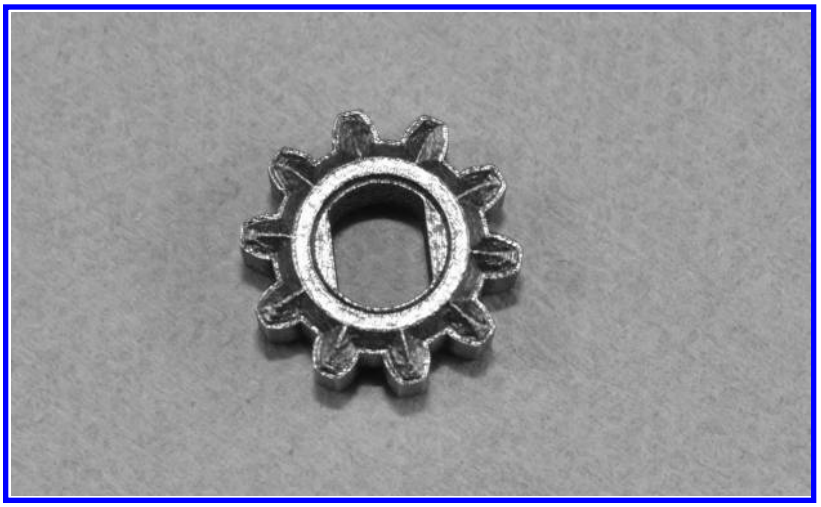

FIGURE 9.15
Functional gear prototype made from PH1 stainless steel on an EOS DMLS™ platform. (Copyright Rapid Prototype and Manufacturing, LLC, Avon Lake, Ohio, 2014.)

FIGURE 9.16
Pair of water cooling channels made from MS1 on an EOS DMLS™ platform. (Copyright Rapid Prototype and Manufacturing, LLC, Avon Lake, Ohio, 2014.)

print with open cooling channels inside the part for water flow because of support material considerations as demonstrated in Figures 9.13 and 9.14. Figure 9.17 is another more complex water cooling assembly that was printed in a single part using laser powder bed fusion. The original design called for six cast components that were then welded together, which was cost prohibitive. In this case, using AM to eliminate the joining steps to make a single part actually made the part cost effective in a way that conventional processes could not.

FIGURE 9.17
Complex water cooling assembly made from MS1 on an EOS DMLS™ platform. (Copyright Rapid Prototype and Manufacturing, LLC, Avon Lake, Ohio, 2014.)

Another fluid moving application for metal AM parts is high-performance impellers in industrial pumping systems. Figure 9.18 shows an example PH1 impeller from Figure 9.13 after removal of support material and finishing steps. AM allows mechanical designers to select the number and shape of individual impeller vanes with more extreme angles that conventional casting or joining techniques do not allow, which enable higher performance, lighter weight pumping systems. In cases of higher volume, lower margin markets like automotive and heavy truck applications, impellers can be built using stainless steel–bronze composite materials using binder jetting. Where these metal–metal composites are appropriate materials, the binder jetting approach is appealing as it can make larger parts than laser powder bed fusion roughly 10x faster and 1/10th the cost. Figure 9.19 shows an example of a hydraulic fluid moving impeller for a heavy truck application manufactured using binder jetting on an ExOne M-Flex platform.

For materials that are difficult to process using fusion techniques, binder jetting AM offers the capability to make parts that could not be easily printed. One example of this capability is for tungsten polymer composites for medical imaging applications. Figure 9.20 shows an X-ray shielding bracket and Figure 9.21 an X-ray collimator, both printed using binder jetting on an ExOne M-Flex platform. These materials are being used to replace lead components that shield and direct radiation to reduce patient dose and improve resolution and clarity of imaging techniques. The AM use case is focused on the reduction of costly materials like tungsten polymer, while managing inventory and producing precision parts on an as-needed basis.

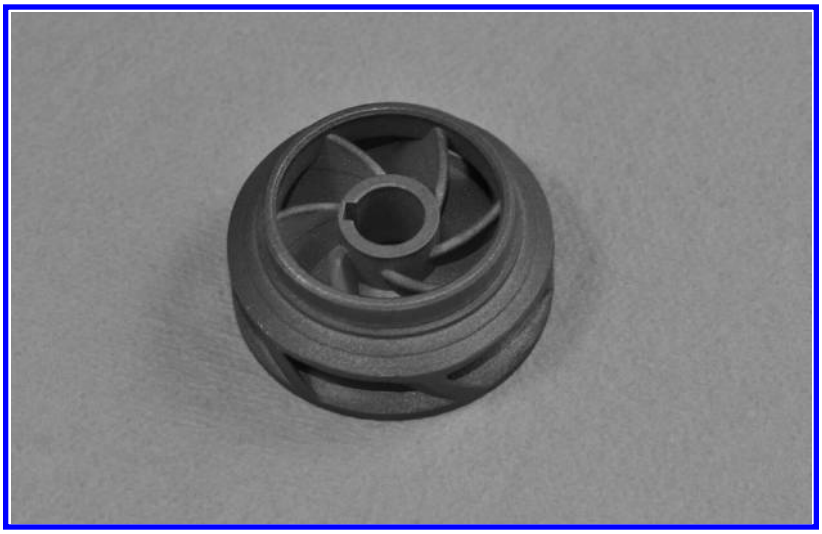

FIGURE 9.18
Example of a fluid moving impeller made from PH1 on an EOS DMLS™ platform. (Copyright Rapid Prototype and Manufacturing, LLC, Avon Lake, Ohio, 2014.)

FIGURE 9.19
Example of a hydraulic fluid moving impeller for a heavy truck application made from 410 stainless steel–bronze composite using binder jetting on an ExOne M-Flex platform. (Copyright Rapid Prototype and Manufacturing, LLC, Avon Lake, Ohio, 2014.)

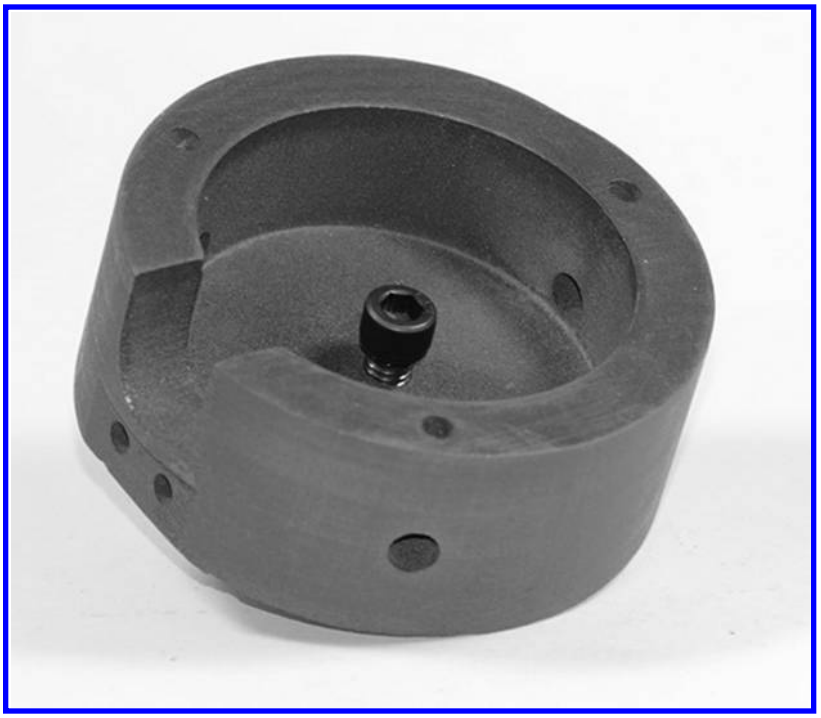

FIGURE 9.20
X-ray shielding bracket made from tungsten—polymer using binder jetting on an ExOne M-Flex platform. (Copyright Rapid Prototype and Manufacturing, LLC, Avon Lake, Ohio, 2014.)

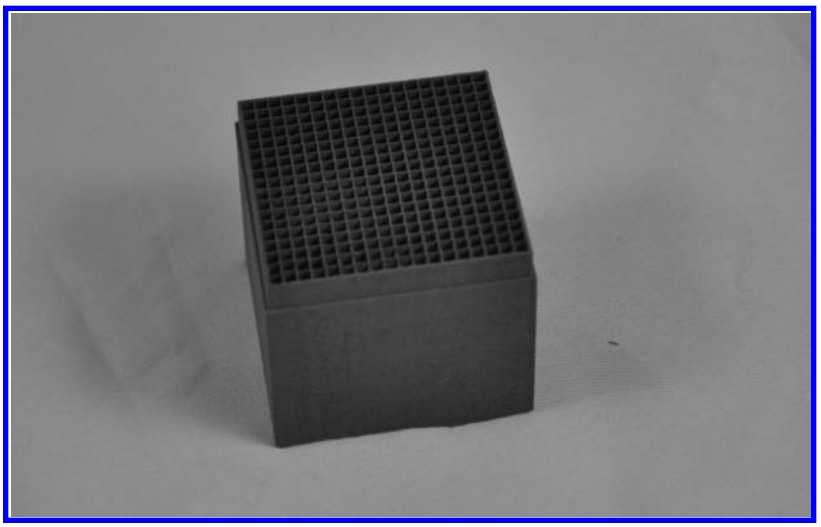

FIGURE 9.21
X-ray collimator made from tungsten—polymer using binder jetting on an ExOne M-Flex platform. (Copyright Rapid Prototype and Manufacturing, LLC, Avon Lake, Ohio, 2014.)

9.6 Summary and Future Trends

AM is perhaps the disruptive manufacturing technology being implemented by industrial manufacturers today. As more engineering materials are introduced, the supply chain will continue to develop use cases to provide greater value to clients. There are still key needs to improve quality and capability of technologies, and corresponding needs for standards development, accreditation, and certification by relevant bodies.[10]

As the suite of AM technologies continues to mature, it is breaking the traditional *design for manufacturing* model and providing the foundation for a new paradigm of *manufacturing by design*. In this new paradigm, industrial designers are fully enabled to design components based on functionality, rather than limits of assembly technologies. In this future paradigm, integrated computational materials engineering will be leveraged to develop new materials for these new processes in parallel to their development and for specific applications. Similarly, the fine line between structural and functional AM will be merged and new devices that support customized medicine and the *Internet of things* will begin to emerge.

References

1. National Research Council. *Retooling Manufacturing: Bridging Design, Materials, and Production*. Washington, DC: The National Academies Press, 2004.
2. Schafrik, R. and Sprague, R. Superalloy technology—A perspective on critical innovations for turbine engines. *Key Engineering Materials*, 380, 113, 2008.
3. ASTM Standard F2792, Standard terminology for additive manufacturing technologies, ASTM International, West Conshohocken, PA, 2012, www.astm.org.
4. Wohlers Report. 3D printing and additive manufacturing state of the industry. Annual Worldwide Progress Report, 2014.
5. Lyons, B., Deck, E., and Bartel, A. Commercial aircraft applications for laser sintered polyamides, SAE Technical Paper ATC-0387, Warrendale, PA: Society of Automotive Engineers International, 2009. doi:10.4271/2009-01-3266.
6. Stratasys. Ultem 9085 FDM™ data sheet, Stratasys, http://www.stratasys.com/~/media/Main/Secure/Material%20Specs%20MS/Fortus-Material-Specs/Fortus-MS-ULTEM9085-01-13-web.ashx, accessed January 7, 2014.
7. Maturation of fused depositing modeling (FDM™) component manufacturing, https://americamakes.us/engage/projects/item/455-maturation-of-fused-depositing-modeling-fdm-component-manufacturing, accessed January 7, 2014.
8. Rosato, D.V. et al. *Injection Molding Handbook*, 3rd edition. Norwell, MA: Kluwer Academic Partners, 2000.
9. The Economist. Print me a jet engine. *The Economist*, November 22, 2012. http://www.economist.com/node/21567145, accessed January 7, 2014.
10. Energetics Incorporated. *Measurement Science Roadmap for Metal-Based Additive Manufacturing Workshop Summary Report*. Columbia, MA: National Institute of Standards and Technology, U.S. Department of Commerce, 2013.

10

Additive Manufacturing for the Space Industry

Christian Carpenter

CONTENTS

10.1 Introduction

Space exploration is a captivating endeavor, not only for discovering the unknown, but also for overcoming difficult technical challenges. We must take a moment to understand the culture, objectives, and technical challenges of the space industry in order to understand how additive manufacturing can be infused for the benefit of space exploration.

One of the main reasons that we are currently experiencing an infrequent increase in space exploration capabilities is that the culture has become afraid to fail. A culture with a strong aversion to risk accepts long development and production schedules and high life-cycle cost because they are incorrectly perceived to be associated with heightened safety and mission assurance. Improved approaches are forfeited for continuing the status quo or *heritage* processes because new approaches are perceived to increase risk, even though new approaches often reduce risk when infused properly. In order to reinvigorate space exploration and develop robust space exploration programs, this culture must be changed. Technology is unlikely to drive change in the cultural acceptance of risk; however, additive manufacturing is a revolutionary technology that, when infused properly, can significantly reduce development and production schedules and life-cycle cost, thereby causing an opportunity to change what is viewed as normal and acceptable. In his book *Leading Change*, John Kotter recommends eight steps for developing lasting and meaningful change. In addition to describing the potential technical impacts of additive manufacturing on space exploration, this chapter will discuss three of Kotter's steps as applied to the

adoption of additive manufacturing including development of a change vision, generation of short-term wins, and incorporation of changes into culture.

The vision for space exploration is in constant flux; however, a few constant themes can be identified which are summarized in the so-called von Braun paradigm. Simply put, the vision for space exploration is the realization of four main objectives:

1. Establishment of a capability to reach low Earth orbit (LEO) routinely and affordably
2. Establishment of a near-Earth, space-based research station
3. Colonization of the Moon
4. Colonization of Mars

To accomplish the vision, we must develop a safe and affordable space transportation architecture. This architecture must encourage rapid development and infusion of new technologies that maximize our potential for exploration and ultimately colonization. The transportation architecture must support a range of mission classes including robotic surveying and science missions, crewed missions, and cargo logistics missions that support crewed missions and pre-deployment of crewed systems. A modular transportation architecture that separates mission phases is required to enable demonstration and adoption of new vehicles (versus the all-up missions of the past) and new business models (e.g., government and commercial space launch providers). Exploration of small bodies such as asteroids and the moons of Mars may well be included in future endeavors; however, a transportation architecture that supports the four vision objectives also efficiently supports exploration of these small bodies.

Within the mission architecture, a variety of vehicles are required including launch vehicles, space vehicles, landers, and Moon- and Mars-based infrastructure elements such as habitats and laboratories. Vehicle service life will range from one to five years for small satellite demonstrations to over 20 years of service life for missions such as colonization of Mars. We need to develop serviceable vehicles and subsystems, replacement components, and a logistics infrastructure capable of supporting a long duration supply chain. Modular vehicles that support demonstration and infusion of new vehicle subsystems as well as in situ servicing and replacement will be required to support the architecture and the vision objectives in an affordable and timely manner. The International Space Station (ISS) project has shown how a modular vehicle architecture supports widespread collaboration and incremental building, which enables sustainable long-term exploration and capability development.

There is probably no more significant technical challenge or contributor to cost in space exploration than the simple logistics of moving mass from origin to destination. The reality of gravity and rocket propulsion physics is that significant mass is required to move a payload from Earth to a location in space. The total mass of a mission at the beginning of life is generally treated as mass on the launch pad (pad mass) that includes all launched mass or initial mass in LEO (IMLEO), which includes all mass released from the launch vehicle into LEO. Due to a number of cultural factors ranging from certification paperwork to complexity of systems, to low volume production, one can generally estimate the cost of a space mission based solely on the pad mass or IMLEO. Barring physics breakthroughs such as wormholes and warp drives, the matter of launched mass must be addressed in order to reduce the cost of space exploration.

The dry mass of a space system includes everything except propellant. The rocket equation shows that dry mass, mission ΔV (change in velocity), acceleration due to gravity, and specific impulse (or I_{sp}, which is a measure of propulsive efficiency similar to gas mileage) determine how much propellant is required to perform a mission. The result of these physics is that a

typical mission results in propellant accounting for over 98% of pad mass with the remaining 2% being dry mass. An average satellite IMLEO consists of 50% propellant and 50% dry mass. There are four fundamental technology development areas that one can explore to minimize the mass and thus the cost of space missions. These are listed below in order of increasing impact to space mission cost:

1. *Low-cost systems*: This approach focuses on simply reducing the production cost of space systems.
2. *Low-mass (lightweight) systems*: This approach focuses on reducing dry mass, usually through lightweight materials or designs, but as noted previously reductions in dry mass have a significant effect on required propellant mass.
3. *Advanced propulsion*: This approach focuses on reducing propellant mass through increased specific impulse, but can also result in reduced dry mass through smaller propellant tanks and structural elements, which are a significant component of dry mass.
4. *In Situ Resource Utilization (ISRU)*: This approach reduces propellant mass and dry mass by developing technologies that allow missions to live off the land so that less material needs to be shipped to the destination.

Now that we have a basic understanding of space exploration culture and vision and have defined characteristics for the vehicles and technologies required, we can begin to evaluate additive manufacturing as a solution that enables affordable and sustainable space exploration.

10.1.1 Low-Cost Systems

Space systems are highly complex and manufactured in low volumes, and these characteristics align well with scenarios where additive manufacturing offers great cost benefit. Demonstrated metrics of 50% reduction in cost and schedule for complex, low volume components simply cannot be ignored and even the most risk-averse space product manufacturers have to take notice. Many manufacturers are likely to take advantage of the cost savings offered by switching from subtractive to additive manufacturing, but the real innovators that will help ensure a robust future of space exploration are those that adopt a design-for-additive-manufacturing philosophy. This design philosophy surpasses the basic concept of replacing machined parts with printed parts and transitions to designing systems that fully utilize the capabilities of additive manufacturing including the following:

- Reduced machining cost enabled through designs that minimize the need for build supports and post-machining
- Reduced tooling costs enabled through designs that integrate tooling required for post-machining and assembly
- Reduced labor costs enabled through designs that combine parts to reduce total parts count, joining operations, and assembly hours

Development phase systems are likely the best infusion opportunity for these additive manufacturing philosophies, because the aforementioned culture presents a significant barrier to changing existing fielded systems, even for the sake of cost improvements. Let us now consider the process of transforming a preexisting space product designed for

subtractive manufacturing into an additively manufactured product and examine the associated cost benefits and technical challenges. Let us consider a rocket engine subassembly that includes an injector and a thrust chamber, and for the sake of simplicity, let us assume that these components are both made of the same metallic alloy and that the parts fit into the build volume of several existing additive manufacturing machines.

The preexisting fabrication process might begin by procuring a metal plate for the injector and a casting for the thrust chamber. As we transition to the additive manufacturing approach, we have an opportunity to cut the number of procurements in half by procuring a common powder batch. Additionally, the powder can be purchased in volume to accommodate subsequent production of these parts or others that might use the same powder. In addition to reducing the cost of labor to place the orders, we have also reduced the cost of tracking material certification and inventory by aligning the parts on a common material. Rather than inventorying and tracking several sizes of metal, we can track a single powder part number with certifications by lot. This feature of additive manufacturing will likely reduce standing inventories at manufacturers, reducing the costs of holding this inventory. Another key aspect of cost savings in the procurement cycle is the reduced impact of the government specialty metals clause. Because additive processes use powder, it is much easier to locate compliant materials, greatly reducing sensitivity to material sourcing, availability, and price volatility.

An additive manufacturing approach clearly offers us significant cost and schedule in the procurement phase for this scenario. However, several barriers to adopting this process will surface that drive non-recurring costs including, but not limited to the following:

- A need to qualify a new supplier.
- A need to qualify a new material.
- The company may not own the 3D printing machine and therefore must qualify a 3D printing vendor and their process.
- Changing materials and fabrication processes could drive a requirement to re-qualify the product.

These non-recurring cost drivers must be included in the consideration in order to determine if there is actual cost benefit for our scenario. It is possible that these challenges will present significant non-recurring costs and these must be evaluated with several other factors in the broader context of cost savings. Taken alone, the procurement phase may not provide cost savings for a single feature of a product and it may make sense to consider application to several products or product lines to amortize the non-recurring cost impact. However, in a risk-averse culture the need to drive significant change through many products will likely be seen as an insurmountable task and could damage the potential of future infusion of additive manufacturing if a cultural perception develops that suggests additive manufacturing as something that requires significant non-recurring cost or sweeping application. It is therefore highly important to consider all factors and ensure that additive manufacturing is applied to the right product at the right time to realize the significant benefits and gain cultural acceptance. It is clear that the procurement phase presents both opportunity for benefit and risk of implementation for additive manufacturing.

Next, let us assume that the procurement phase analysis presents no show-stoppers and we are now ready to dig into the design improvements. First, we might simply compare the cost of manufacturing the components between the two processes. It would not be

surprising to find a 50% cost and schedule reduction and this has been demonstrated previously in real scenarios. While we could stop here and declare success, our intent is to affect systemic cost reductions. In our next step of design considerations, we might consider joining the parts together in CAD and then printing them as a single piece. Eliminating joining processes, such as welding and brazing, can carry significant cost schedule savings while also reducing quality risks and improving mechanical performance. It is important to note here that for new product designs, the elimination of joining processes can also reduce non-recurring costs.

At this point, our design improvements have significantly improved cost and schedule, but we can go further still by designing to reduce tooling and post-machining. Space products often require at least some features with tight tolerances, such as joints, seals, or flow passages, that are not achievable with additive manufacturing. As such post-machining of the parts may be necessary. With our legacy subtractive machining approach, we may find that a significant amount of cost is spent designing, producing, verifying, and tracking tooling. As we transition to additive manufacturing, we have the opportunity to reduce non-recurring and recurring costs of tooling in the following ways:

- Identify critical features that must be machined, but allow loose tolerances and rougher surfaces for non-critical features
- Identify build direction and minimize overhangs and the need for build supports that will require subsequent removal
- Integrate post-machining tooling into the design so that this tooling can be scrap material that does not require inventorying or tracking

At this point, we have developed a design that significantly streamlines production and results in significant life-cycle cost and schedule savings. However, as in the procurement phase we are likely to encounter several barriers to design acceptance that must be addressed including the following:

- How will we verify the new design for thermomechanical performance?
- Do we have sufficient material data to believe our analyses?

These types of questions arise with any new material or manufacturing process, and determining how to qualify the analysis for a specific part will be dependent on the maturity of the analysis methods and material databases. These issues will be discussed later in the chapter, but for now it is appropriate to note that there is significant ongoing investment to answer these questions for additive manufacturing processes. Let us now assume that we have completed our design and are ready to proceed with the manufacturing process development.

With our legacy subtractive manufacturing processes, a significant amount of time was spent creating g-code for machining operations and concerns of non-recurring costs for new code may arise. However, with additive manufacturing the cost of generating machine code is significantly reduced through the use of slicing programs that autogenerate this code making the non-recurring costs quite low. With subtractive processes, there was a significant amount of setup due to required tooling; however, with additive manufacturing, this setup cost is greatly reduced due to the reduced or eliminated tooling accomplished in the design phase. With subtractive manufacturing, there was a cost of waste rejection associated with cutting fluids and scrap material; however, with the

additive manufacturing, the cutting fluid is eliminated and scrap material is minimized. In addition, scrap material associated with build supports can be made crushable enabling efficient packaging for lower cost waste disposal. Finally, the cost to rework our subtractively manufactured parts was significant and included difficulties in scheduling queues across several machines to work the parts. With the new additive manufacturing process, we find the cost impact of rework is significantly reduced and may times it is possible to place a rework part into empty space in already-planned builds. It is clear that the fabrication phase offers many benefits, but like other phases there are barriers to implementation including the following:

- How will we develop and control the build configuration? For instance, if build supports are required do they need to be configuration controlled?
- How will we inspect the additively manufactured parts? For instance, the injector holes are critical features and may be difficult or impossible to inspect if inseparable from the thrust chamber.
- How will we qualify, handle, use, and reuse feedstock (powder)? For instance, are we allowed to reuse unconsumed powder from a build and if so, under what conditions?

Resolution of these issues will be discussed later in the chapter, and like the design and analysis phase, there is significant ongoing investment to answer these questions. It is critical to note, however, that these considerations must be taken into account during the design phase even though they are not encountered until the manufacturing phase.

Let us now assume that we have successfully completed development phase and are ready to transition into production of several units. For space products in transition from development to production, there is typically a significant cost to develop controlled drawings, work instructions, and material traceability. At this point, additive manufacturing provides significant benefits as the major quality parameters are captured in the build files providing an intrinsic quality control set that significantly reduces the cost of transitioning to production.

The single-material printing processes assumed for the presented scenario are currently the most mature and prolific with capabilities ranging from plastics to aerospace metals. Development and production of either replacement parts for legacy systems or new components for development phase systems can be accomplished with these processes. There are few plastics in space systems, but aerospace metals such as steels, aluminum (primarily 6061 T6), and titanium are of high interest. For high-performance components, Inconel and exotics such as moly/rhenium are required. Because components are traditionally machined from a single billet of material, we can reasonably expect, and in fact it is already being realized, that the first infusion of additive manufacturing will be single-material manufacturing. Selective laser melting, electron beam melting, and other powder bed single-material processes are sufficiently accurate that they are already being infused. Freeform fabrication processes such as laser freeform fabrication (LF3) and electron beam freeform fabrication (EBF3) provide capabilities for larger parts, but have some progress to make in feature size before wide infusion is possible for intricate space systems.

Infusion of single material additive manufacturing will certainly have a significant impact on the cost of space products, but we can go farther. In the previously presented scenario, we made the assumption that the injector and thrust chamber were constructed

of the same metallic alloy, whereas a more realistic scenario would be that the two are composed of differing alloys. Let us now explore for a moment the next tier of cost savings that can only be achieved with multi-material additive manufacturing. Akin to color printing versus black and white, multi-material additive manufacturing is likely to replace most current additive manufacturing approaches because when qualified, it should reduce or eliminate joining and assembly of components that are some of the largest areas of risk in the manufacturing life cycle. A few additive manufacturing processes, such as LF3 and EBF3, currently offer this capability in metals and some studies have begun to demonstrate significant successes blending and transitioning between dissimilar materials. Multi-material printing complicates the design and analysis phase because development of models capable of analyzing transitions between materials is still in its infancy and there is a wide range of potential combinations of materials that must be characterized and tested to ensure a path to qualification. Due to the significant opportunity for cost and schedule reductions enabled by multi-material additive manufacturing, as technology progresses we are likely to see significant effort put into establishing tools and validation processes that support this complex capability.

Valves are one of the most expensive and long lead elements of space systems, and as such, a 3D printed valve is currently considered a sort of Holy Grail for space additive manufacturing. Achieving this feat requires a system with characteristics of tight tolerances and the ability to deposit metallic and soft good material systems. Even with the advent of multi-material systems, it is likely that tolerances will require post-machining of printed components. Therefore, the next tier of cost savings may be achieved with multi-material additive and subtractive manufacturing, which we call additive–subtractive manufacturing, or ASM. Here we find a very small base of capability where the limitations of additive manufacturing machines are addressed by integrating some subtractive machining that can be done in-process. The ASM approach enables most of the benefits of additive manufacturing while maintaining high tolerances and smooth surface finish of machined parts.

In summary, additive manufacturing presents significant opportunities to reduce cost and schedule for space systems through the implementation of a design-for-additive-manufacturing philosophy. Many technical challenges also exist to capture these savings and many organizations are working to overcome these challenges. In the next section, we will explore how to take these benefits even further by reducing the mass of space systems, which translates into significant mission level cost savings.

10.1.2 Low-Mass Systems

Let us again consider the scenario of transforming an existing product into an additive manufactured product, but this time we will focus on how additive manufacturing can be used to reduce the mass of the product. It is important to remember that launch costs are approximately $10,000 per pound of mass launched into space, so saving dry mass can significantly reduce cost. For this example, we will consider a notional rocket propulsion system consisting of the following elements:

- Structure
- Propellant tank
- Gimbal
- Rocket engine

Let us first focus on using additive manufacturing to reduce the mass of the structure. The first approach taken with design for additive manufacturing would be to replace solid structure with less dense infill layers such as a honeycomb pattern encapsulated with a thin outer wall. From the outside, the part might look identical to a machined part, but could be over 80% lighter. Modern freeform fabrication machines can implement this approach directly and powder bed machines simply require incorporation of a powder removal method. Algorithms exist that automate the process of creating low density infill layers, and it is likely that in the future, more complex infill algorithms will be developed to optimize the infill for structural strength, stiffness, and mass. This approach to mass reduction can have a significant and immediate impact on spacecraft structure and mechanisms, which typically comprise 10%–20% of dry mass. The same philosophy can be applied to every aspect of the vehicle to enable significant mass reductions throughout a space system.

Next let us focus on the propellant tank, which is a thin-walled pressure vessel, typically made of a metallic alloy. Here we cannot implement the infill approach used on the structure, so the next step in reducing mass is to highly engineer the shape of the tank for optimal mass. Highly coupled CAD, structural, and thermal analysis tools must be employed to determine how to shape the part for maximum strength, stiffness, and mass. The addition of goal-seeking tools, such as genetic algorithms, capable of developing non-intuitive designs could enable highly engineered parts with reduced non-recurring costs. The same tools could be used to engineer subtractively manufactured parts; however, the resulting designs would likely be too expensive to produce using subtractive manufacturing alone making the additive manufacturing community the likely driver of development of these advanced tools. The result of this design philosophy might include areas of thicker or thinner solid material coupled to areas with low infill or complex open-cell shapes. Alternatively, we might find that it is best to implement a thin-walled vessel with an exoskeleton. In this case, merging the structure with the propellant tank may reduce parts count and eliminate areas that would typically carry extra material for attachment between the two system elements. All of the above processes can be applied using single material processes, but as we move into consideration of multi-material additive manufacturing we can expect to see tools that enable the blending or transitioning of materials along our tank wall to optimize mass. Complex algorithms that take into account variables of shape, strength, mass, temperature, alloy, and cost would need to be employed to optimize material systems throughout the part. New alloys are likely to be designed during this process that enable continuous transitions from one metal to another enabling even more highly engineered designs.

This philosophy, like the ones mentioned previously, can be applied throughout the vehicle and is likely to result in substantially increased performance not only for mass, but especially for thermal and cost as well. In the particular case of cryogenic propellant tanks, the industry has the significant challenge of balancing propellant boil-off with tank mass and use of cryocoolers. The ability to design the propellant tank to minimize heat flow into the propellant could have savings not only on the tank mass itself, but on the amount of cryocoolers support needed and the amount of propellant lost due to boil-off. In this case, additive manufacturing may be able to offer new solutions to a difficult and significant challenge.

Next we will consider the engine gimbal and we can certainly apply the aforementioned design philosophies to reduce mass of the component, but with additive manufacturing the most significant mass reductions occur when we consider the system as a whole and it follows that multifunctional system designs will begin to emerge quickly as additive

manufacturing design philosophies are applied at the system level. The engine gimbal has a unique requirement for propellant lines and wiring to cross movable joints, which is a problem that we have yet to consider. If one were to imagine a highly engineered beam structure with a significant amount of free space inside, such as we would likely find in our gimbal, the designer is likely to make us of this space by incorporating flow passages, wiring, and so on into the free space in order to leverage the existing structural capabilities of the parent part to reduce the overall mass of the multifunctional system. One example would be embedding the propellant tubes in the wall of the gimbal structure. Another example would be elimination of circular wire sheaths through a sandwich of center conductor, insulator, and then gimbal structure. While elimination of a wire sheath might seem a small mass savings, the amount of wire harnessing in spacecraft is not insignificant and one can expect both mass and cost to significantly decrease. Finally, development of additively manufactured slip rings and propellant swivel joints that allow electricity or fluids to pass through the rotating joints would be both a significant challenge and benefit. If we consider an entire space vehicle, we can find many systems and components that could implement these design philosophies especially solar power systems and environmental control and life support systems.

Finally, let us briefly consider the last component in the system, the rocket engine. Rocket engines operate at high temperature and pressure over many cycles. They are highly complex components that can include valves, turbopumps, injectors, combustion chambers, and nozzles. Optimizing rocket engine mass will require implementing all of the aforementioned processes and will require multi-material design and analysis tools covering metals, ceramics, softgoods, composites, and coatings. The rocket engine optimization will bring the added complexity of incorporation of performance models required to analyze engine performance over a range of conditions to ensure that the additive manufacturing design philosophies are applied in a way that considers all extremes of operation. It is likely that such design and analysis tools are years away, but we can begin by applying our philosophies to rocket engine components with a knowledge of our vision for the future we can make significant near-term progress.

Significant challenges are likely to occur as additive manufacturing design philosophies are applied to space systems. The evolution and validation of complex design and analysis tools must occur in order to enable progress. First, we must improve tools to allow consideration of infilled, open-celled, and exoskeletal designs. Next we must add capabilities for consideration of material transitions such as joint and blended materials. The addition of blended materials brings a complication of requiring some way to qualify the new alloys used in these parts as well as the processes used to fabricate the parts. Typically, qualification of new material systems is a very costly activity. Additive manufacturing can reduce the cost of qualification through low-cost and rapid fabrication of samples; however, in this case we are discussing highly engineered material systems that will have varying lengths, repeatability, and mixture from design to design. Qualification of materials used in this way will present a significant challenge to the culturally accepted norms. It is possible that the cost of space missions will be so significantly reduced that it may become acceptable to fly new materials with validation by protoflight testing only, but alternate methods to qualification are likely required. As components and systems are combined to save mass and cost, the perceived risk of failure is likely to increase. It will be critically important for innovators to consider failure modes and effects when determining what components and systems to merge. All of these considerations point to a common theme that has been propagated for decades, which is that we are moving into a time where systems engineering disciplines and tools will need drastic and significant improvements to enable success.

It should now be clear that additive manufacturing has much to offer in the way of reducing space system dry mass and that the benefits are as significant as the challenges. Efforts made to develop the significant design and analysis tools required to enable new paradigms in space systems will also have great impact on other terrestrial markets, and as such, we should expect that many markets will drive development and implementation of these types of tools enabling space-focused manufacturers a significant opportunity to collaborate and focus on unique problems to the space industry. Next we will consider how additive manufacturing can affect significant propellant mass reductions through the development of more efficient propulsion systems.

10.1.3 Advanced Propulsion

Excluding exotic and theoretical transportation systems such as wormholes and warp drives, the primary types of propulsion that are available to support space exploration are either thermal or electric. In the previous sections, we considered how reducing the cost and mass of propulsion systems through additive manufacturing can provide revolutionary improvements. However, aspects of additive manufacturing can also be brought to bear to improve propulsive efficiency that reduces propellant mass. Because propellant mass can account for up to 98% of pad mass, any improvements in propulsive efficiency can have drastic impacts on the affordability and sustainability of space exploration.

Thermal propulsion systems (sometimes referred to as high thrust propulsion) where specific impulse (gas mileage) is dependent on combustion temperature are limited by the material systems employed within the rocket engine. Storable monopropellants produce a specific impulse typically from 220s to 250s and operate with combustion temperatures ranging from 800°C to 1800°C. At the high end of this range, exotic materials such as rhenium and iridium are required to contain combustion. For these systems, highly engineered additive manufactured components with new alloys can not only improve cost and lead time, but also improve temperature capability and structural strength of rocket engine components, thereby enabling higher temperature propellants and thus higher specific impulse. Storable and cryogenic bipropellants produce specific impulse in the range of 300s to 452s and combustion temperatures rise to over 2700°C where ablative or regeneratively cooled components must be implemented. Here, additive manufacturing can be used to embed coolant passages that would be unaffordable or impossible to implement in subtractively manufactured components. This capability can enable improved specific impulse and there is potential to increase cooling efficiency to the point that lower cost materials could be implemented. At the highest range of thermal propulsion is nuclear thermal propulsion where nuclear fuel heats a working fluid, typically hydrogen, to create thrust and produce specific impulse in the 900s range. Here additive manufacturing of regeneratively cooled passages as well as incorporation of engineered radiation shielding could significantly improve not only the performance of these engines, but also safety of the system.

Solar electric propulsion systems employ electrostatic or electromagnetic forces to produce very high specific impulse ranging from 400s to >10,000s. These systems are sometimes referred to as low thrust propulsion because they are dependent on solar power to create thrust, and modern solar power systems only provide kilowatts of power, which results in thrust levels of millinewtons. As a result of power limited thrust, electric propulsion systems require long duration firings (non-Hohmann), which result in less efficient thrusting and increased total ΔV (typically 2×) compared with high thrust thermal systems. As we discussed previously, increased ΔV requires more propellant; however,

electric propulsion systems typically offer 4× increased specific impulse resulting in a net 50% reduction in propellant mass for a typical mission. A 50% propellant mass reduction has an enormous impact on space mission affordability, and as a result, we are seeing a significant increase in the use of electric propulsion. Additive manufacturing can improve electric propulsion system efficiency through 3D printing of improved magnetic structures, electrical insulators, and ion optics increasing engine efficiency. However, electric propulsion systems are already highly efficient typically in the >50% range. The most significant impact to the performance of these systems is improvement in the spacecraft level power to mass ratio that increases the total thrust potential (reducing ΔV and trip time) of the solar electric propulsion system. 3D printed lightweight structures for solar arrays, and high reliability slip rings and SADA drives would all provide significant improvements in solar electric propulsion systems, but the most significant impact to solar electric propulsion system efficiency is the solar cells themselves. 3D printed, high-efficiency, radiation-hardened, low-mass solar cells are the key to significant propellant savings. Additionally, solar electric propulsion systems operate best at high voltage levels, which presents a problem for space solar arrays as voltage increases result in significant risk of arcing and plume interactions. Additive manufacturing processes can provide for fully encapsulated solar cells and solar arrays that eliminate this risk and enable high voltage solar electric propulsion systems to operate at higher efficiency and reduce mass. These benefits could easily drive propellant savings of 10%–20% resulting in significant reductions in space mission mass and cost.

Additive manufacturing has many potential benefits to thermal and electric propulsion systems that we are just beginning to explore, but the net result is the potential for substantial propellant mass reductions. Up to this point, we have focused on how terrestrial additive manufacturing can reduce the mass and cost of space logistics, but in the next section we will consider how space-based additive manufacturing can fundamentally address the root of the problem by reducing the overall need for these logistics operations.

10.1.4 In Situ Resource Utilization

ISRU is a space architecture design philosophy wherein raw materials located at the destination are leveraged to support a mission or campaign rather than solely depending on supplies shipped from the mission origin. This approach transports only what is needed to perform manufacturing at the destination, thereby drastically reducing cargo mass, pad mass, and space mission cost. An extension of this philosophy is in situ manufacturing wherein raw materials and manufacturing equipment are shipped to the destination rather than transporting all components that might be needed. This approach provides lesser, but still significant, mass and cost reductions for destinations where needed materials may not exist. Space-based additive manufacturing processes could play a significant role in both approaches; however, these processes will exist in a different environment from ground-based process including low gravity, vacuum pressure levels, wide temperature ranges, and electrostatic charging, just to name a few. In this section, we will explore what is likely the most significant value proposition for additive manufacturing to long-term space exploration.

Manned space missions are currently confined to LEO where the ISS serves as the primary laboratory for research. The internal environment of the ISS requires consideration of low gravity, but eliminates vacuum pressure and temperature variables. As such, it is not surprising that the first use of space-based in situ additive manufacturing will be demonstrated onboard the ISS. Made In Space, a company located at the NASA Ames

Research Park, is currently flying a plastic extrusion 3D printer on the ISS to validate and demonstrate low gravity 3D printing. If successful, the demonstration could have a significant impact on ISS logistics by enabling researchers to ship material to the ISS for in situ manufacturing versus shipping and maintaining an inventory of spare parts. This capability would reduce the total mass shipped to the ISS. Additionally, the ability to print in situ would enable researchers to change their experiments after launch and allow them to be more responsive to research results enabling more value for a given experiment. In the far term, this capability has a significant impact on long duration crewed missions to destinations such as Mars where replacement parts will need to be fabricated en route destinations and during the exploration mission operations.

Powder bed processes are likely to have an issue with the low gravity environment. Spinning the device to create an artificial gravity might be a solution, but loading material and removing parts from the spinning platform could complicate the situation. Electrostatic approaches that provide force onto the powder might be another approach, but could encounter issues in electron beam devices. Powder spray approaches such as LENS™ could also be used; however, the physics of ensuring the powder is delivered to the intended target with no effect of residual spray would be critical. Freeform fabrication techniques such as EBF3 and LF3 use a wire feed approach and appear well suited to handling the low gravity environment. As low gravity additive manufacturing matures, it is likely that external applications will become a desire. The ISS is equipped with external research points and robotics that could be used for space-based additive manufacturing demonstrations.

The external environment of the ISS adds variables such as changing thermal environments, vacuum pressures (though the ISS does outgas compared to a true deep-space mission and there is a higher level of atomic oxygen in the ISS orbit), and electrostatic charging. As the ISS circles the Earth every 90 minutes, it encounters approximately 60 minutes in Sun and 30 minutes in eclipse. These alternating thermal conditions could cause significant thermal stresses to build up as additive manufactured parts are produced. Initially, it will be possible to perform demonstrations in Sun or eclipse to limit these variations, but eventually they will have to be overcome. Layer-by-layer thermal image recording is being developed for quality purposes in terrestrial applications, but space-based applications my actually need to react to these data in order to produce good parts. The machine may have to rotate or have a rotating build plate in order to more uniformly distribute solar and Earth-reflected heat influx to the part. Forms of composition analysis such as residual gas analysis may be required in order to ensure that contaminants are not introduced during a build due to atomic oxygen levels or outgassing. As the part is fabricated, differential charging could occur on the part or in the machine, and as such, special equipment grounding or charge mitigation devices may be required. Automatic part removal is also likely required in order to simplify the logistics of moving the part to its intended point of use. There are many new variables that will need to be taken into account, but the ISS research platform provides an excellent test bed to develop space-based additive manufacturing. As space-based additive manufacturing technologies are demonstrated, there will be a desire to use them in support of spacecraft servicing.

Spacecraft servicing generally means the on-orbit repair or upgrade of a satellite or spacecraft. This technology will likely be proven in LEO and then later applied to medium Earth orbit and geosynchronous orbit satellites. Modular spacecraft systems are being developed to enable in situ repairs or upgrades to a satellite by a servicing vehicle. Some repair or upgrade operations will be accomplished through replacement or addition of modules; however, in situ manufacturing can provide a capability to create components that the

servicing mission did not anticipate, repair non-modular components, or repair damaged components. In situ manufacturing for spacecraft servicing and life extension can significantly reduce pad mass and mission cost by enabling lower cost servicing missions and by reducing the number and mass of satellites put into orbit. Examples might include patching holes created by micrometeorite damage or repair of faulty wiring. In one form of satellite servicing, a life extension spacecraft attaches itself to an existing host satellite in order to provide propulsion and power that enable significantly longer missions for the host satellite. Many existing satellites are not designed for grappling, and the process of a life extension vehicle grappling with a host satellite is highly complex. Additive manufacturing can play a significant role for this mission by enabling in situ fabrication of custom grappling points that enable life extension and/or servicing missions.

Large-scale missions require grand structures that we cannot affordably fabricate on Earth, test, and then deploy into space. One example is the James Webb Space Telescope that has large structures, but must be packaged into the launch vehicle fairing requiring complicated spacecraft design and intricate deployment mechanisms. As space-based additive manufacturing matures, it is probable that low gravity production of optimized mass elements can significantly contribute to reduced pad mass and cost. Space-based additive manufacturing could enable the in situ manufacturing of such spacecraft, and this capability would enable an entirely new approach to space architecture from both a design and a logistics philosophy. In this scenario, raw materials for the spacecraft structure would be shipped to LEO where the spacecraft would be fabricated. Modular system components such as solar array panels, electronics boxes, propulsion systems, and so on would be installed on orbit, possibly prior to close out of the structure similar to how buildings are fabricated on Earth. When complete, a skin could be applied, or even printed into place to close out the spacecraft. In addition to structure, this approach to spacecraft manufacturing would have a significant impact on the specific mass of solar arrays, radiators, and antennas. Additionally, launch loads, which typically drive a significant portion of spacecraft component cost and mass, could be handled much more easily as parts could be optimally packaged, oriented, and protected during launch. Upon arrival in orbit, the components could be unpacked and installed into the satellite. This approach also poses significant benefits for manned missions where large volume habitats are ideal for the crew. Presently, inflatable structures are being explored to create the large volumes, but an in situ manufacturing approach may provide an optimal solution in the future.

It stands to reason that the continued push by mankind to explore space will eventually lead to small space-based research stations, outposts, and settlements beyond LEO. The enormous cost and schedule of the logistics systems required to transport materials from Earth to likely targets such as the Moon, asteroids, and Mars offers a strong business case for ISRU. The benefits highly depend on the materials found at the destination, but the net result is reduced pad mass and mission cost. Assessments of the impacts of ISRU propellant generation have shown that ISRU has the highest impact to mission mass of any other technology. Few studies have explored ISRU for generation of structures, but it is reasonable to think that the impact of building exploration outposts using ISRU would enable maximum reductions to the mass and cost of space exploration. Additive manufacturing processes, especially freeform processes, are likely to play a major role in ISRU structure generation. To date, most space architecture studies have focused on structures shipped to a destination and then assembled on-site. A more affordable approach would be to send robotic scouting missions (called prospectors) to analyze the materials that can be found at a destination as well as the terrain. Following identification of the material types and locations for facilities, Earth-based analogs can be performed to validate

additive manufacturing processes required. Once validated, robotic missions can be sent to the destination that would excavate materials that would be fed into freeform additive manufacturing machines. These machines could then print (probably in thick layers) the structures required for the exploration mission. Both the Moon and Mars are covered in fine dust, which may prove useful for powder-based freeform additive manufacturing processes, or for processing into feedstock for extruder processes. The regolith of Earth's Moon and Mars contains silicon dioxide, titanium dioxide, aluminum oxide, iron oxide, magnesium oxide, and calcium oxide, all of which could be processed and used for construction of outposts. Separation and storage of oxygen from the base material would be beneficial for crew air supplies or oxidizer for propulsion.

Destinations such as the Moon and Mars add new variables to the space-based additive manufacturing processes. The new variables are too numerous to mention in this section, but we will briefly explore a few examples. As most destinations of interest are farther away from the sun, it is important to note that larger thermal gradients than typical will be experienced during additive manufacturing. This will have to be taken into account and will likely complicate Earth-based experiments to prove out additive manufacturing processes for these locations. Additionally, destinations such as Earth's Moon present issues of dust accumulation as machines move about on the surface. This effect will require additive manufacturing systems that are tolerant to the dust and will also require some consideration of dust accumulation onto the structure being fabricated. Systems to remove dust during the build may be required. In the case of Mars, which has both dust and significant atmosphere, weather effects will have to be taken into account if processes are to be conducted outside enclosures, which is probable if we are manufacturing structure for an outpost. Finally, the signal delay at these destinations will require that all of these processes be conducted autonomously. This presents an additional complication as on Earth we can pause a crashed build, perform a fix, and then continue or restart; however, this type of capability will have to be included in additive manufacturing machines designed for ISRU applications. On a positive note, solving many of these issues also translates into more robust machines that can be implemented to benefit Earth-based additive manufacturing.

10.2 Developing Cultural Acceptance

Space products are typically required to operate in extreme environments driving a need for exotic materials and complex designs. The market for space products is characterized by low volumes and long life cycles. The severe cost and reputation impacts of space product failures require thorough qualification of product designs and processes before manufacturers can adopt them for flight use. These characteristics of the space product market have resulted in long development schedules and high costs. In fact, it is not uncommon for a space product to take 10 years to progress from concept to first flight. As a result, new technologies are traditionally infused into space products at a low rate. This has resulted in a large gap between the demand for low cost, fast delivery products and the supply chain's characteristically high cost, long lead products. Manufacturers of space products are experiencing ever increasing pressure from government and commercial customers to conform to the commercial electronics paradigm of delivering smaller, faster, and cheaper products on increasingly shorter timescales. When customer expectations significantly

contrast with the capability of a supply base, such as is the case with space products, a revolutionary change must be made to resolve the gap between supply and demand. The development of additive manufacturing technology enables a new paradigm of significantly reduced cost and lead time for space products. It is expected that additive manufacturing for many complex space products will result in greater than 50% reduction in both cost and schedule. Additionally, the ability to fabricate parts in an additive fashion and/or with new materials could enable new designs with improved performance capabilities. As a result, it is not surprising to see space product manufacturers rushing to adopt and infuse additive manufacturing and in some cases emerging as leaders in additive manufacturing processes. This behavior is a testament not only to the technology of additive manufacturing, but to the willingness of space product manufacturers to return to the innovative culture demonstrated in the Apollo era. Additive manufacturing has a unique opportunity to change the paradigm of space products, but cultural acceptance of the design, analysis, manufacturing, and test processes must be developed.

In a risk-averse culture, safety issues are the most costly impact to a program. Resolution of safety issues drives lengthy and costly investigations and ultimately results in more lengthy and costly production processes. Therefore, the most important step that additive manufacturing advocates can take to develop cultural acceptance is to demonstrate and communicate that the processes are safe. The resolution of quality issues has a similar impact in that they require lengthy and costly investigations and generally result in increased production cost and schedules. Therefore, the second most important step in developing cultural acceptance is to demonstrate that additive manufacturing processes reliably produce high-quality components. Long schedules are typically accepted based on a combination of technical challenges associated with development and the lead time to produce a system. However, the length of a program schedule drives a certain standing army cost and therefore shorter schedules can intrinsically reduce mission cost and this standing army can have a more significant than the production cost of the hardware. Additive manufacturing advocates will know that 50% schedule savings are possible, but many used to long schedules will likely see these claims as unrealistic, naive, or impossible. It is therefore highly important for advocates to develop case studies that clearly demonstrate the greatly compressed development and production schedules enabled by additive manufacturing to overcome the preconceived notions and prior experiences of the culture. Last is the actual system development and production cost where cheaper materials and manufacturing approaches have much to offer. Like the schedule scenario, it will be difficult for many that are used to high-cost products to believe that it is possible to achieve 50% cost savings. Again, advocates should develop and communicate case studies to demonstrate the cost-saving metrics to the community. It is important for additive manufacturing advocates to consider safety, quality, schedule, and cost aspects as well as cultural norms in order to determine what change will drive improvements in space mission schedules and life-cycle costs.

10.2.1 Ensuring Safety and Quality: Qualification of Additive Manufacturing Processes

The qualification process is the way in which a product or process demonstrates that it is safe and of high quality. The qualification process must be comprehensive while also ensuring minimum impact to the product schedule and cost. In an ideal scenario, each product to be used in a space mission would be able to demonstrate through test that it is able to successfully complete the mission with significant margin. However in reality,

we must also find ways to qualify though inspection and analysis in order to minimize schedule and cost. Space product qualification is a rigorous process and the requirements are highly dependent on the type of product, the launch and operating environments, and, in many cases, the specific end user. When compared to the commercial electronics paradigm that is being requested of the space industry, one begins to discover that a lack of standards exists in the space product market that drives enormous scope, schedule, and cost into the products. For example, each satellite manufacturer may have their own operating voltage and electrical interfaces and one can imagine the high cost that household appliances might attain if not for a standard operating voltage and physical interface. The lack of standards will require additive manufacturing process advocates to consider how to qualify a general process, yet be able to accommodate particular requirements of specific end users. We will now explore some of the requirements for qualification of additive manufacturing processes.

Material and manufacturing processes must also be qualified. Material vendors for additive manufacturing materials must develop and document standards for powder or feedstock composition and physical properties. Lot traceability of materials must be maintained. Processes for proper handling and reclamation of the materials must be established. Data from extensive testing will be required before designers can consider incorporation of a material system into the overall product development process.

Design and analysis processes must be qualified. Initially, design and analysis software used for subtractive manufacturing will suffice for single material additive manufacturing processes with subtractive style designs, but as designs begin to take full advantage of additive manufacturing it is probable that structural and thermal analysis codes will not be able to accurately model the complex geometries, especially in an efficient manner. New codes will likely need to be developed and validated through testing to ensure that produced parts match analysis results. Companies and government organizations are already beginning to understand these challenges and are starting to make progress toward resolutions. A few multi-material printers have already been brought to market; however, the complexity of the design and qualification process along with the cost of these machines is likely to delay their infusion into the aerospace market. Additionally, the usually risk-averse aerospace companies investing in qualification of single-material processes over the next decade are unlikely to make a subsequent large investment to make the technology leap to multi-material machines. Despite the likely delayed infusion, multi-material additive manufacturing has the potential for far greater impacts to aerospace products than single-material printers over the next 10–20 years. As multi-material processes evolve an added dimension of material property, transitions will need to be incorporated and similarly qualified through validation testing. The range of possible geometries and material compositions is significant and acceptance of qualification data would and should be scrutinized for accuracy and range applicability.

Additive manufacturing process qualifications should be conducted in parallel with material, design, and analysis qualifications. Processes need to define and document all build parameters such as speed and power settings. During the build, data on part temperature, composition, build chamber gas levels, and so on need to be captured and saved for later analysis. Completed parts need to be tested for porosity and mechanical strength. Initially, simple geometries may be tested similar to castings, but as geometries become more complex, lot testing may be required. Build supports and infill geometry are currently variables in many processes, but space manufacturers will likely require that these become fixed process parameters as variability in these could significantly affect resulting part mechanical properties.

Qualification of materials, design, analysis, and manufacturing processes is likely to be costly and tedious tasks, but must be completed to ensure high-quality space products. Involvement of all levels of the supply chain including insurance groups, spacecraft operators, spacecraft manufacturers, and component suppliers should be strongly encouraged to ensure buy-in for qualification activities. On the long road to process qualification, near-term flight demonstrations can be accomplished to help improve cultural acceptance.

10.2.2 Demonstrating Short-Term Wins: Enabling Shorter Development Schedules

It is an exciting time in the field of space exploration because CubeSat and SmallSat standards have enabled routine, low–cost access to space. In 2010, over 100 CubeSats were launched, most from Universities. In 2014, the company Planet-Labs alone expected to launch a constellation of 100 units, the largest satellite constellation in history. If this growth trend continues, we can expect >200 deployments per year in the very near future. Because CubeSat and SmallSat systems are low cost and packaged inside a dispenser, more risk can be accepted and lengthy and costly material process analyses can be deferred in favor of test and flight demonstrations. These small platforms enable opportunities for rapid demonstration of additive manufacturing materials and designs on real missions that will generate data and experience required for cultural acceptance by larger spacecraft manufacturers.

At the simplest level, one can use CubeSats to begin exposing additive manufactured materials to the environment of space. The ISS acts as a possible platform wherein a CubeSat can be exposed to space and then brought back into the ISS for subsequent analysis or return to Earth. Follow-on missions might include demonstrating through flight that additive manufactured materials can be used for CubeSat and SmallSat structure. The next step in this evolution might be inclusion of additive manufactured functional components such as circuit boards and valves. High pressure and liquid propellant systems will likely be one of the pinnacles of CubeSat and SmallSat demonstrations due to severe consequences of a failure scenario. Further still, swarms of CubeSats or SmallSats equipped with additive manufacturing heads and proximity operations capabilities could be used to demonstrate freeform space-based additive manufacturing.

CubeSats and SmallSats provide additive manufacturing advocates with an excellent opportunity to develop cultural acceptance with real flight missions at low–cost and on fast–paced schedules. While skeptics may still present scaling challenges, data collected from these small-scale missions will ultimately prove invaluable in the push toward adoption of additive manufacturing for space exploration.

10.2.3 Instilling the Culture: Training the Workforce in Additive Manufacturing

The final step of any change effort is to engrain the change into the culture. This is a difficult task as there are many ways in which this is accomplished. For space missions, there are two ways to accomplish this task. The first method is to fly additive manufactured components on a major mission. Once a component is successfully flown on a major mission, the risk-averse culture kicks in and making any change to the incumbent system is almost impossible and certainly expensive. This approach is good, but highly dependent on a small number of long timescale and high-cost missions. However, a second and highly impactful method is to train the emerging workforce to adopt the new way of doing things. For additive manufacturing, several functional areas will need to have training in order to engrain the process into the culture.

Design and analysis engineers need to be trained on how to design systems and components for additive manufacturing. It can be expected that the resistance to change will be driven by some of the previously mentioned qualification issues. One can expect that designers will be concerned that parts will be too complex and that design costs will increase as specialized build support tooling is added to the work scope. Additionally, designers may become frustrated as processes emerge and they find that redesigns are required to account for process development or incorporation of alternate processes to existing designs. Additive manufacturing advocates can facilitate this change by working early to train designers on the philosophies of design for additive manufacturing, available processes, and case studies showing long-term cost and schedule savings. Additionally, managers can facilitate change by incorporating training on new CAD tools that are being designed with additive manufacturing in mind.

Thermal and structural analysts will share many of the same concerns as design engineers; however, it is likely that analysis tools will lag design tools. Additionally, the design and analysis process is likely to merge in the future and analysts will need to learn more about the design process to develop, capture, and communicate suggestions for improvement as well as risks to quality. Analysts will require training similar to that of designers and it may be necessary to develop common training for both design and analysis functions.

Manufacturing and industrial engineers are likely champions for adoption of additive manufacturing, but incorporating any new processes will be met with at least some level of skepticism. For many additive manufactured parts, there is a reduced ability to inspect parts including porosity, features located inside a part, and surface properties driving difficulty in implementing traditional NDT methods. Additionally, it is probable that many parts will require some level of post-machining driving some to conclude there are minimal cost savings. Advocates will need a clear manufacturing plan that incorporates printing, post-machining, inspection, and assembly in order to convince others that the ideas are sound. Cost assessments will also be needed and as aforementioned may require consideration of more than one part before cost savings are evident. Early training on available processes, pitfalls, new inspection methods, and so on will be critical for gaining acceptance and advocates should be patient while new training is conducted.

Standards and qualification programs will be key to development of cultural acceptance as will early flight demonstrations on low-cost platforms. Despite qualification and flight demonstrations, space product manufacturers will likely take a long time before cultural acceptance of additive manufacturing is attained and pervasive, but early adopters and advocates can take steps to expedite the infusion of additive manufacturing technology through immersive cross-cutting training plans that include coverage of new tools, risks and mitigation methods, detailed manufacturing, inspection and test plans, and through case studies. Working together to develop robust training programs, space industry advocates can drive accelerated cultural acceptance of additive manufacturing processes.

10.3 Summary

Space products are currently expensive and require a decade or more to infuse new technologies. Additive manufacturing enables >50% cost and schedule reduction for most parts driving affordable space exploration. Additive manufacturing enables improved system designs and space mission architectures that drive further toward

sustainable and affordable space exploration. Over the next five to ten years, we can expect to see single material processes gain acceptance. In the next 10 to 20 years we can expect to see multi-material processes infused into space products. In the far term, we can expect to see space-based additive manufacturing in wide use. With robust industry training, qualification programs, and low-cost flight demonstrations, advocates can greatly accelerate cultural acceptance and develop a new paradigm of affordable and sustainable space exploration.

11

Additive Manufacturing and Innovation in Materials World

Mitun Das and Vamsi Krishna Balla

CONTENTS

11.1 Introduction

During the last two decades, significant progress has been made in the development of complex, near net shape structures with novel materials such as composites and functionally graded materials (FGMs). Some of the products have also been commercialized for various applications in automotive, aerospace, and consumer products. More than 20 additive manufacturing (AM) techniques have been developed while most frequently used techniques are stereolithography (SLA), three-dimensional printing (3DP), fused deposition modeling (FDM), selective laser sintering (SLS), selective laser melting (SLM), and laser metal deposition (LMD) (Guo and Leu 2013). As shown in Table 11.1, several materials including polymers, ceramics, metals, and their composites have been successfully used in these AM technologies. For example, photocurable resins in liquid form are used as feedstock in SLA, and FDM uses thermoplastics, thermosetting plastics, and waxes in filament form. Feedstock materials in powder forms are suitable for SLS, 3DP, and LMD.

TABLE 11.1

Important AM Processes and Materials Used for Fabricating Complex Components

AM Process	Feedstock Form	Materials Type	Materials
SLA	Liquid	Polymers	Photocurable resins
		Ceramics	Suspensions of SiO_2, ZrO_2, Al_2O_3, and other ceramics
3DP	Powder	Polymers	Acrylic plastics, wax
		Ceramics	ZrO_2, SiO_2, Al_2O_3, CaP ceramics, sands, mullite
		Composites	Polymer matrix, ceramic matrix, short fiber-reinforced composites
SLS	Powder	Polymers	Polyamide 12, GF polyamide, polystyrene
		Ceramics	SiO_2, ZrO_2, Al_2O_3, ZrB_2, CaP ceramics, graphite, bioglass, mullite, sand
		Composites	Metal matrix, ceramic matrix, polymer matrix, fiber-reinforced composites
FDM	Filament or paste	Polymers	PC, ABS, PC-ABS, ULTEM
		Ceramics	PZT, Si_3N_4, Al_2O_3, SrO_2, SiO_2, CaP ceramics, mullite
		Composites	Polymer matrix and short fiber-reinforced composites
LMD/SLM	Powder	Metals	Stainless steels, CoCrMo, Ti and Ti alloys, Ni-based alloys, Al alloys, Cu alloys
		Composites	Metal matrix, ceramic matrix, particulate-reinforced composites
		Functionally graded materials	Metal–metal, metal–ceramic, ceramic–ceramic FGMs

Source: Guo, N., Leu, M.C., *Front. Mech. Eng.*, 8, 215–243, 2013.

The process of fabricating net shape components with commercially available single materials (polymers, metals, and ceramics) using AM techniques has been mostly optimized by respective equipment manufacturers. Therefore, the users simply use process parameters that are prescribed by the manufacturer while fabricating the components. Further, use of custom materials in some of these AM machines appears to be difficult, and as a result, developing structures with novel materials such as composites and FGMs becomes difficult. For example, for high performance and properties, composites should be fabricated with high volume fraction of reinforcements having controlled alignment/orientation (with respect to the load) and appropriate connectivity, and exhibit microstructural hierarchy if desired. Further, these composites should be manufactured to near net shape to eliminate problems associated with conventional machining. Such new composite materials are difficult to fabricate using conventional manufacturing routes.

Apart from providing geometrical design flexibility, recent developments in AM technologies enabled tailored materials design (such as composites, meso-scale compositional variations, functional variation in composition in three dimensions, and multifunctional materials) and their effective incorporation in the complex geometrical designs. These capabilities of AM technologies in developing novel materials/structures can be effectively utilized to reduce materials innovation gestation period. Therefore, several research groups across the globe are focusing on creating new and designed materials for variety of applications with increased functionality, performance, and reduced environmental

impact. Considering above, the first part of the chapter is focused on the use of AM techniques in creating novel materials such as composites, nanocomposites, and multifunctional materials structures. In the second part, we discuss novel designs enabled via AM technologies.

11.2 Composites by AM

The use of AM capabilities for composite materials fabrication has started in last decade but its full potential has yet to be explored. Combining AM with composite fabrication has opened up new possibilities to explore unique tailored materials (Wohlers 2010). Among many available AM technologies, only a few technologies have shown their potential in composites fabrication, which include SLS/SLM, LENS™, laminated object manufacturing (LOM), SLA, FDM, 3DP, and ultrasonic consolidation (Kumar and Kruth 2010). However, a majority of the efforts are focused on polymer composites, while studies on metal matrix composites (MMCs) are limited. There has not been much progress reported in the area of manufacturing ceramic matrix composites (CMCs) using AM due to numerous materials and processing challenges. Therefore, herein we emphasize more on MMCs and CMCs fabrication using various AM technologies, but briefly discuss polymer composites as well.

11.2.1 Metal Matrix Composites

MMCs with ceramic reinforcements exhibit properties of both the ceramic and metal (Tjong and Ma 2000). The addition of ceramic reinforcements to metallic matrix is known to improve specific strength, fracture toughness, stiffness, fatigue, and wear resistance, compared to their metallic counterparts (Mortensen and Llorca 2010). Among continuous or discontinuous reinforcements, discontinuously reinforced MMCs, include both particulates and whiskers or short fibers, have drawn considerable attention due to their relatively lower costs and isotropic properties of composites (Tjong and Ma 2000).

In the recent years, laser-based AM has been attempted extensively to fabricate MMC 3D structures or coatings to improve materials properties (Kumar and Kruth 2010). These techniques include direct laser fabrication (DLF) (Li et al. 2009), LENS™ (Banerjee et al. 2003b; Balla et al. 2012), direct metal deposition (DMD) (Hong et al. 2013), and powder bed-based techniques such as SLS/SLM (Lu et al. 2000). The properties of the MMCs depend on the size, distribution and volume fraction of the reinforcements as well as the nature of the matrix-reinforcement interfaces (Tjong and Ma 2000). One unique feature of these techniques is their ability to incorporate reinforcements either ex situ (where reinforcing phases are prepared separately and added to the matrix during composite fabrication) or in situ (where reinforcing phases are synthesized/prepared during composite fabrication) (Tjong and Ma 2000). In ex situ MMCs, the size of reinforcing phase depends on the starting powder, whereas in situ synthesized MMCs contain homogeneously distributed finer ceramic phases, which provide enhanced mechanical properties. Further, AM techniques enable creation of functionally graded composites in complex shaped bulk MMC components with finer microstructure due to very fast cooling associated with laser processing.

The SLS/SLM technique has been used to study different ex situ reinforced MMCs such as WC–Co composite (Laoui et al. 2000; Maeda and Childs 2004; Kumar 2009), WC–10%

Co particulate-reinforced Cu matrix composites (Gu and Shen 2006, 2007), (Fe,Ni)–TiC composites (Gåård, Krakhmalev, and Bergström 2006), Al–7Si–0.3Mg/SiC composites (Simchi and Godlinski 2008), and SiC particulates-reinforced Al-MMCs (Ghosh, Saha, and Kishore 2010; Ghosh and Saha 2011). Gu and Shen (2007) prepared submicron WC–10% Co particulate-reinforced Cu matrix composites using direct metal laser sintering. With increasing reinforcement, densification of Cu matrix composite deteriorated (at 20 wt.%) and heterogeneous microstructure with significant particulate aggregation was found at 40 wt.% reinforcement. Laser sintering has been used to fabricate ultra-high-temperature ceramic composites. High density (>92%) multilayer Ti–ZrB_2 mixtures with hardness up to 11.4 GPa were fabricated by laser sintering (Sun and Gupta 2011). Furthermore, in situ synthesis of reinforcement via the reaction between the constituent elements of composites during fabrication process is regarded as a more promising method to obtain more homogeneous microstructures (Tjong 2007). Dadbakhsh and Hao (2012) and Dadbakhsh et al. (2012) studied SLS of Al matrix composite part from Al/Fe_2O_3 powder mixture. It was observed that incorporation of Fe_2O_3 significantly influences the SLM process ability of particulate-reinforced Al matrix composite. At present, multi-material reinforcements are being proposed for betterment of Al-MMCs. Ghosh, Bandyopadhyay, and Saha (2014) used direct metal laser sintering of a premixed powder containing Al, TiO_2, and B_4C which reacted in situ to form Al_2O_3, TiC, and TiB_2 reinforcements in Al matrix. Gu, Shen, and Meng (2009) and Gu et al. (2009) prepared in situ formed TiC-reinforced ($TiAl_3$+Ti_3AlC_2) matrix composites from high-energy ball milled Ti–Al–C composite powder. In situ TiC-reinforced Cu matrix composite synthesized from Cu–Ti–C and Cu–Ni–Ti–C powder mixtures showed that addition of Ni has improved wettability between Cu and TiC particulates, thus resulted in improved microstructure and surface quality of the laser-fabricated parts (Lu et al. 2000). While above studies show SLM capabilities in fabricating net shape MMCs, one major drawback of SLM process is high porosity, which is detrimental to mechanical properties. In order to achieve full density, trace amounts of rare-earth elements have been added to reduce surface tension of melt (Gu et al. 2007) or the porous product is infiltrated (Kumar 2009). Another processing difficulty associated with SLM of MMCs is the balling effect, where fresh molten materials do not wet underlying substrate leading to the formation of broken liquid cylinders and rough surface after consolidation (Dadbakhsh et al. 2012). The tendency of balling effect can be reduced by increasing energy input by increasing laser power, lowering scan speed, or decreasing powder layer thickness (Gu and Shen 2009).

In case of DMD techniques, a high power laser locally melts the top surface of the work piece, and simultaneously, a powder (ceramic or metal) is injected into the melt pool. Depending on interaction with the laser beam and melt pool temperature, the injected particles may react in situ with molten matrix or entrapped in the matrix with minimal chemical reaction. Processing parameters, such as laser power, scan speed, and powder flow, have an influence on the resulting composite microstructure and hence the properties. Several ex situ-reinforced MMC coatings have been deposited using LENS™. Table 11.2 summarizes various materials system used to create ex situ-reinforced MMC via laser-based DMD techniques.

DMD techniques have also been used to deposit in situ synthesized MMCs. In situ synthesized ceramic-reinforced titanium matrix composites (TMCs) have been studied extensively. Among different types of reinforcements, TiB has been considered the best material for titanium matrix due to its high elastic modulus, similar thermal expansion coefficient that minimizes residual stress, and excellent interfacial bonding with titanium matrixes (Banerjee et al. 2003b). Earlier studies on TiB-reinforced TMC coatings fabricated via DMD method, using Ti, B, or TiB_2 as feedstock powders, showed considerable

TABLE 11.2

Materials Used for the Direct Fabrication of Ex Situ-Reinforced MMC in LENS™

Sl No.	Materials	Composites	References
1	WC–Co	MMC	Xiong et al. 2008
2	WC–12% Co	MMC	Balla, Bose, and Bandyopadhyay 2010a
3	Ti, SiC	TMC	Das et al. 2010
4	Ti, SiC	TMC	Das et al. 2011
5	Ti, TiN	TMC	Balla et al. 2012
6	Ni, TiC	MMC	Zheng et al. 2010
7	Ni, SiC Ni, Al_2O_3 Ni, TiC	MMC	Cooper et al. 2013
8	Inconel 718, TiC	MMC	Hong et al. 2013

improvement in tribological properties (Banerjee et al. 2003b; Wang, Mei, and Wu 2008). Samuel et al. (2008) demonstrated in situ formed boride-reinforced Ti–Nb–Zr–Ta alloy for orthopedic application using LENS™ technique. They found substantial improvement in the wear resistance due to homogeneous distribution of very fine boride reinforcement in Ti–Nb–Zr–Ta alloys.

In situ synthesized TiB + TiN-reinforced Ti6Al4V alloy composite coatings were successfully deposited on Ti using premixed Ti6Al4V and BN powder using LENS™ (Das et al. 2012). In situ reaction of BN with Ti formed a novel microstructure with homogeneously distributed fine reinforcements of TiB and TiN. The microstructures shown in Figure 11.1 consist of TiB nanorods, are locally concentrated in the matrix, and formed quasi-continuous network architecture. These LENS™ processed in situ synthesized TiB-TiN-reinforced TMCs exhibited high hardness, high modulus, and wear resistance (Das et al. 2014). Zhang, Sun, and Vilar (2011) studied in situ (TiB + TiC)/TC4 composites by laser direct deposition of coaxially fed TC4 and B_4C mixed powders. The microstructure showed needle-like and prismatic TiB, granular TiC with small amount of unreacted B_4C. Authors found that

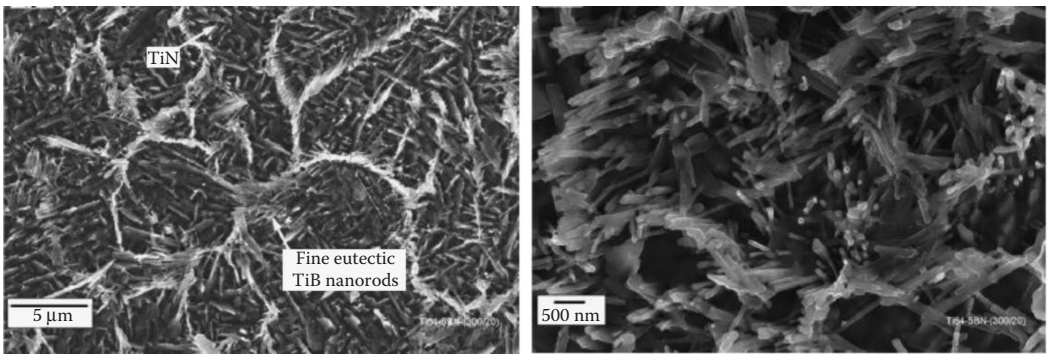

FIGURE 11.1
FESEM microstructure of laser processed TiB-TiN-reinforced titanium matrix composite coatings containing TiB nanorods. (Reprinted with permission from Das, M. et al., *J. Mech. Behav. Biomed. Mater.*, 29, 259–271, 2014.)

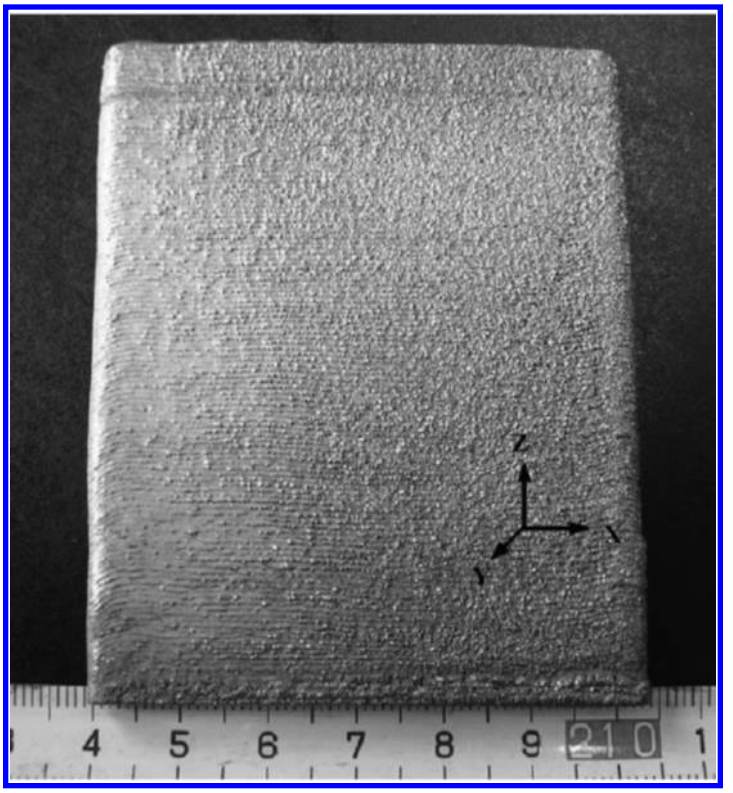

FIGURE 11.2
Laser direct deposited (TiB + TiC)/TC4 composite thin wall. (Reprinted with permission from Zhang, Y.Z. et al., *J. Mater. Process. Technol.*, 211, 597–601, 2011.)

unreacted B_4C weakened its interface bonding with the titanium matrix leading to deterioration of mechanical properties. Thin wall structure of the composite was shown in Figure 11.2.

In situ formed TiC-reinforced Ni-based MMCs were studied by Li et al. (2009) and Gopagoni et al. (2011). In situ reaction between elemental titanium and carbon (graphite) within the molten nickel pool allowed Ni–TiC composites formation with refined, homogeneously distributed carbide precipitates. This novel in situ composite showed enhanced microhardness and tribological properties with comparisons to laser-deposited pure Ni. In situ synthesized MMCs showed homogeneously distributed hard ceramic phases, which provide hardness and metal matrix gives the toughness. LENS™ technique has also been used for creating functionally graded composite coatings as well as coatings on complex shaped parts in single step, which are not possible in conventional processing.

11.2.2 Ceramic Matrix Composites

CMCs have numerous applications as high-temperature and high-performance materials in defense, aerospace, and energy conservation sectors (Sommers et al. 2010). However, AM of CMCs is not well investigated and very limited data have been reported in the literature. The most popular AM methods for fabricating dense and porous ceramic parts are

3DP, LOM, SLS, and selective laser gelation (SLG). Among different ceramics, AM of SiC-based CMCs has been reported widely (Griffin, Mumm, and Marshall 1996). LOM is a promising AM technique used for fiber-reinforced CMCs. For ceramic fabrication using LOM, ceramic tapes usually produced by tape casting method are bonded with an adhesive in layer-by-layer fashion. The bonding between the layers is activated by a heated plate or roller during the LOM process. Klosterman et al. (1999) produced monolithic SiC ceramics as well as SiC/SiC composites using LOM. They reported the use of ceramic-grade Nicalon fiber-based phenolic prepregs with alternating layers of monolithic ceramic tapes. However, flexural strength of these CMCs was found to be low due to weak interlayer bonding. Weisensel et al. (2004) studied the fabrication of biomorphous Si/SiC composites using LOM. Porous carbon preforms were made from pyrolysed paper sheets, and phenolic resin was used as an adhesive, which was subsequently pyrolysed. The net-shaped structure was later infiltrated with liquid silicon (Si) to form Si/SiC composite. The composite exhibited bending strength between 123 ± 8 MPa and 130 ± 10 MPa.

SLS is a popular AM approach since the early 1990s to fabricate ceramic parts. However, ceramic part fabrication using SLS is more challenging due to their high melting temperature, low or no plasticity, and low thermal shock resistance. Ceramic parts fabrication using SLS can be broadly divided as direct and indirect techniques. In direct SLS technique, laser beam heat up the ceramic powder creating solid-state sintering or melting of the loose powder bed. In indirect SLS processing, the bonding is achieved via polymer binder. The green ceramic parts are subsequently debinded and sintered to enhance density and strength. Stevinson, Bourell, and Beaman (2008) studied an indirect SLS technique to fabricate silicon/silicon carbide (Si/SiC) composite structures. The resulting net shape Si/SiC composites were observed to be thermally stable. Liu, Shen, and Liao (2011) demonstrated SLG technique that combines SLS and sol–gel technique to fabricate CMC green parts. In this process, stainless steel (316L) powders are mixed with the silica sol and subsequently silica sol is evaporated using a laser beam, which yields gel that links particles together to form a composite green part. Figure 11.3 shows the metal–ceramic composite green parts fabricated using SLG with surface finish of 32 µm (R_z) and a dimensional variation of 10%.

3DP is another approach for ceramic composites fabrication. Different ceramic-based composites such as Al_2O_3/Cu–O (Travitzky and Shlayen 1998; Melcher et al. 2006), Si/SiC

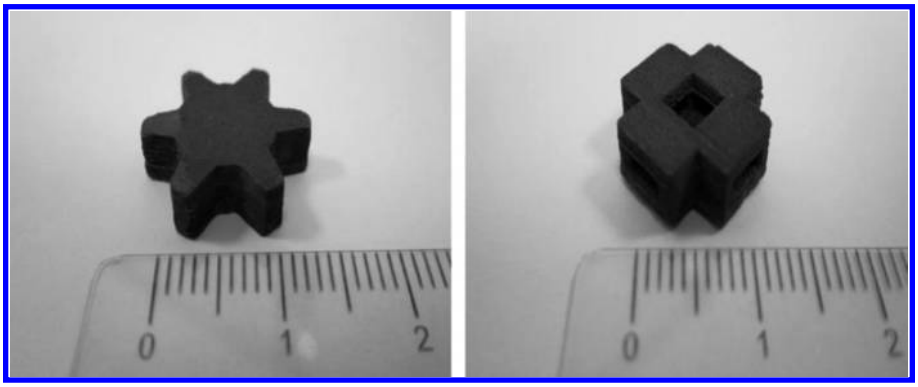

FIGURE 11.3
Ceramic matrix composite parts obtained by SLG. (Reprinted with permission from Liu, F.-H. et al., *Compos B*, 42, 57–61, 2011.)

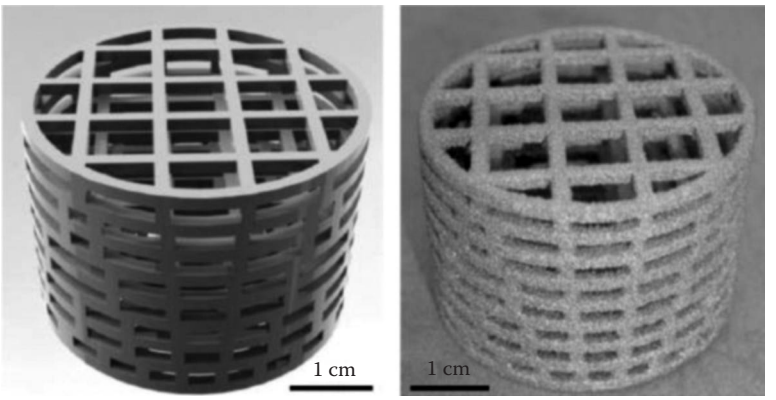

FIGURE 11.4
3D printing of SiSiC ceramics with starting composition of 49.2 vol.% Si, 32.8 vol.% SiC, and 18 vol.% dextrin: (a) CAD design of the lattice structure; (b) reactive infiltrated SiSiC part. (Reprinted with permission from Fu, Z. et al., *Mater. Sci. Eng. A*, 560, 851–856, 2013.)

(Moon et al. 2001), $TiAl_3/Al_2O_3$ (Yin et al. 2006), $Ti_3AlC_2/TiAl_3/Al_2O_3$ (Yin, Travitzky and Greil 2007), $NbAl_3/Al_2O_3$ (Zhang, Travitzky, and Greil 2008), and Al_2O_3/glass (Zhang et al. 2009) have been successfully fabricated using 3DP and subsequent post-processing. In addition, designed porous ceramic preforms fabricated using 3DP are processed further using reactive metal melt infiltration to create complex CMCs with tailored distribution of reinforcement/matrix. In the reactive melt infiltration process, the microstructure of ceramic preforms, for example, pore size, shape, and interconnectivity, strongly affects the wettability of infiltrating metal melt on the ceramic preform (Zhang, Travitzky, and Greil 2008). Fu et al. (2013) demonstrated a gradient macrocellular lattice truss structure (Figure 11.4) from Si/SiC ceramic composites. The composite structure was fabricated by the 3DP from Si/SiC/dextrin powder blends.

11.2.3 Polymer Matrix Composite

Polymer matrix composites using AM are receiving attention to simultaneously build hierarchical materials and net shape structures. In general, to improve mechanical properties as well as functionality in the polymer, various fillers (fibers, whiskers, platelets, or particles) are incorporated to form polymer matrix composites. Wide range of polymeric materials such as photosensitive resin, nylon, elastomer, acrylonitrile butadiene styrene (ABS), and wax has been successfully used in SLA, FDM, SLS/SLM, LOM, and 3DP to create complex structures. Among these techniques, SLA, FDM, and LOM enable processing fiber-reinforced polymer matrix composites.

In FDM process, several attempts have been made to incorporate metal and ceramic filler into the feedstock filament for composite fabrication (Zhong et al. 2001; Masood and Song 2004; Nikzad, Masood, and Sbarski 2011). Zhong et al. (2001) studied a method of forming a short glass fiber (GF)-reinforced ABS polymer feedstock filament with GF contents up to 18 wt.% for use in FDM. It was found that the addition of GFs resulted in higher tensile strength along longitudinal direction but interlayer adhesive strength was

low compared to ABS without reinforcement. Singh and Singh (2014) have introduced varying concentration of aluminum oxide (Al_2O_3) in nylon fibers to fabricate feedstock for FDM.

SLS/SLM is another highly employed AM technique for polymer matrix composites. Polycarbonate (PC) (Ho, Cheung, and Gibson 2003), polystyrene (PS) (Yang et al. 2009), and polyamide (PA) (Caulfield, McHugh, and Lohfeld 2007) have been widely used as SLS materials. PA-based polymer is found to be the most frequently studied material for composites. Different micron-scale particles, such as glass beads (Chung and Das 2006), SiC (Hon and Gill 2003), aluminum powders (Mazzoli, Moriconi, and Pauri 2007), and hydroxyapatite (HA) (Zhang et al. 2008a), have been developed for SLS process. Hon and Gill (2003) demonstrated SiC/PA composites for SLS and found a reduced tensile strength, but improved stiffness for the composite parts when compared with pure PA parts. Mazzoli, Moriconi, and Pauri (2007) developed a mechanically mixed aluminum/PA composite powder for SLS. These composite SLS parts showed metallic appearance with higher dimensional accuracy and stiffness, smoother surface, and better finishing properties, with respect to pure PA SLS parts. Commercially available carbon fiber/PA composite powder called CarbonMide® was developed by EOS (Munich, Germany) from mechanical mixing of pure PA powder and carbon fibers (Yan et al. 2011). However, SLS of these composite powders is expected to form agglomeration of carbon fibers, which causes poor mechanical properties. Yan et al. (2011) developed a new route for carbon fiber/PA-12 (CF/PA) composite powders preparation and showed manufacturing of high performance components by SLS. Surface modified carbon fibers with layer of PA-12 on surface has been prepared by the dissolution–precipitation process and found to provide uniform dispersion and good interfacial bonding with the matrix (Figure 11.5). Results indicated that the addition of carbon fibers with good interfacial bonding greatly enhanced the flexural strength and flexural modulus of sintered components. Kenzari et al. (2012) developed and commercialized nylon-based composites reinforced by Al-based quasicrystals (QC) for SLS process. This composite showed promising applications in rapid manufacturing of complex functional parts with high dimensional accuracy, wear resistance, and reduced friction coefficients. Figure 11.6 shows QC-reinforced PA-based composite parts processed by SLS.

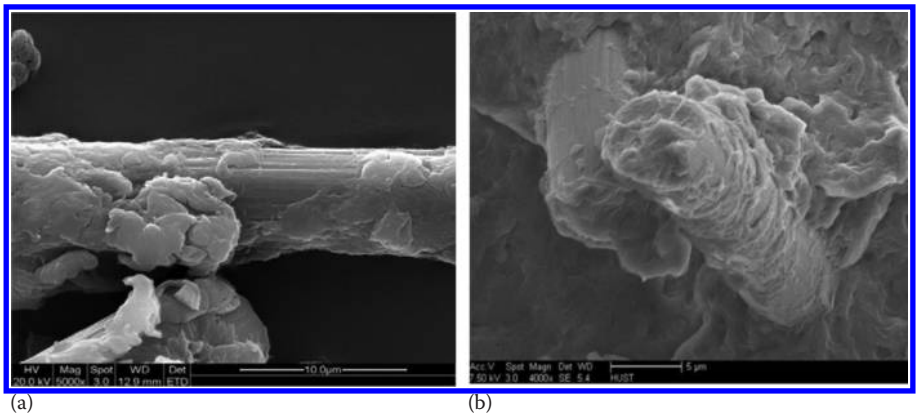

FIGURE 11.5
SEM micrographs of (a) 30% CF/PA composite powder and (b) the fractured surfaces of the 30% CF/PA SLS parts. (Reprinted with permission from Yan, C. et al., *Compos. Sci. Technol.*, 71, 1834–1841, 2011.)

FIGURE 11.6
Examples of freeform SLS composite parts of a polymer matrix reinforced by quasicrystalline AlCuFeB particles. This SLS part has a volume fraction of porosity lower than 2% and is directly leak-tight without post-impregnation of resin. (Courtesy of Ateliers CINI SA, Tomblaine, France and MV2T; Reprinted with permission from Kenzari, S. et al., *Mater. Des.*, 35, 691–695, 2012.)

11.3 Nanocomposite Structures by AM

The field of nanocomposites brought the attention of the scientific world because of their improved material properties. The mechanical, electrical, thermal, optical, electrochemical, and catalytic properties of nanocomposites differ significantly from that of the component materials. The concept of multifunctionality and improved properties in nanocomposites is attributed to homogeneous distribution of nanoscale phases in the matrix. However, key challenges remain for nanocomposites production, including processing, cost, consistency in volume production, high lead time, and oxidative and thermal instability of nanomaterials. The application of AM manufacturing in the production of nanocomposite parts is expected be a promising approach to alleviate some of these limitations (Campbell and Ivanova 2013). The development of nanocomposites using AM has started very recently and reported literature is very limited. Moreover, most of the work concentrated on polymer-based nanocomposites where AM techniques were used to add nanomaterials such as carbon nanotubes (CNTs), nanowires, quantum dots, and metal or ceramic nanoparticles in the host polymer matrix. This early development in polymer matrix nanocomposites is due to ease of incorporating nanomaterials and enormous progress in polymer-based AM techniques. However, limited work has been reported in the area of metal matrix nanocomposites due to its inherent difficulties for incorporating nanoparticles in metal powder-based AM techniques such as SLS, LENS™, and 3DP.

Despite few successes of nanocomposites development using AM, there are several issues unanswered such as interaction of nanoparticles with printing material, optimization of process parameters, and synthesis methods for different nanomaterials. Further, thermal stability and tendency of agglomeration of nanomaterials in the printing media and subsequent modification of AM processing conditions are huge challenges to integrate nanomaterials and AM (Ivanova, Williams, and Campbell 2013). The limited choice of materials has restricted the wider adoption of these technologies, which can be overcome by developing innovative materials and processes.

11.3.1 Metal Matrix Nanocomposites

Among different nanomaterials, metal nanoparticles possess attractive optical, thermal, and electrochemical properties. First metal nanoparticles were used in solid freeform fabrication process to densify porous metallic parts prepared using 3DP and SLS (Crane et al. 2006). The porous test specimens were printed using 410 SS powders with particle size ranging from 63 to 90 µm. Nanoparticles suspension was used to infiltrate the porous part which showed to strengthen the bonds between particles and also to reduce creep and sintering shrinkage up to 60%.

Particulate reinforcement in TMCs greatly improved the performance of titanium alloys. The size of the ceramic particle strongly affects strength, ductility, and failure mode of TMCs. Generally, decreasing the size of ceramic particles to nanometer level can lead to a substantial improvement in mechanical properties of TMCs (Mortensen and Llorca 2010). The nanoscale dispersion of ceramic phase in TMCs tends to introduce novel behaviors owing to high surface-to-volume ratio, which are absent in the conventional composites. Homogeneous distribution and restricting grain coarsening of nanoscale ceramic reinforcements during processing is the main criterion for enhanced performance of the nanocomposites. Nanocrystalline TiC-reinforced Ti matrix composites parts were fabricated using SLM by Gu et al. (2011). Figure 11.7 shows cubic specimens of nanoTiC (50 nm)-reinforced composites fabricated using SLM. The coarsening of the TiC phase was found to depend on laser energy density and nanoscale TiC reinforcements were observed when laser energy density was below 120 J/mm^3. The SLM-processed TiC/Ti nanocomposite part showed significantly high nanohardness (90.9 GPa), elastic modulus (256 GPa), and wear resistance.

LENS™, a DMD-based AM technique, has flexibility to deposit different TMCs with additional flexibility in terms of functional gradation in composition. Das et al. (2014) has synthesized TiB–TiN-reinforced Ti6Al4V alloy composite using LENS where a premixed Ti6Al4V and BN powder was used. They found formation of TiB nanorods in the matrix when composites were deposited at lower laser energy density (38 J/mm^2). Similar nanometer-scale TiB precipitates were also observed in case of Ti6Al4V–TiB composites, which have been laser-deposited from a premixed powder consisting of Ti6Al4V and elemental boron powder (Banerjee et al. 2005). Fabrication of multiwalled CNTs dispersed nickel matrix composites has been attempted using LENS™ (Hwang et al. 2008). Bhat et al. (2011) fabricated multiwall CNT-reinforced Cu–10Sn alloy composites using LENS™. Composites containing 12 vol.% CNTs showed more than 80% increase in the Young's modulus and 40% increase in the thermal conductivity of Cu–10Sn alloy.

Furthermore, the addition of metal nanoparticles was found to reduce shrinkage and distortion of 3DP processed parts. Bai, Creehan, and Kuhn (2007) showed that incorporating silver nanoparticles, through water-based binder system, onto 3DP of microsilver powder significantly reduced the sintering temperature and improved sintering

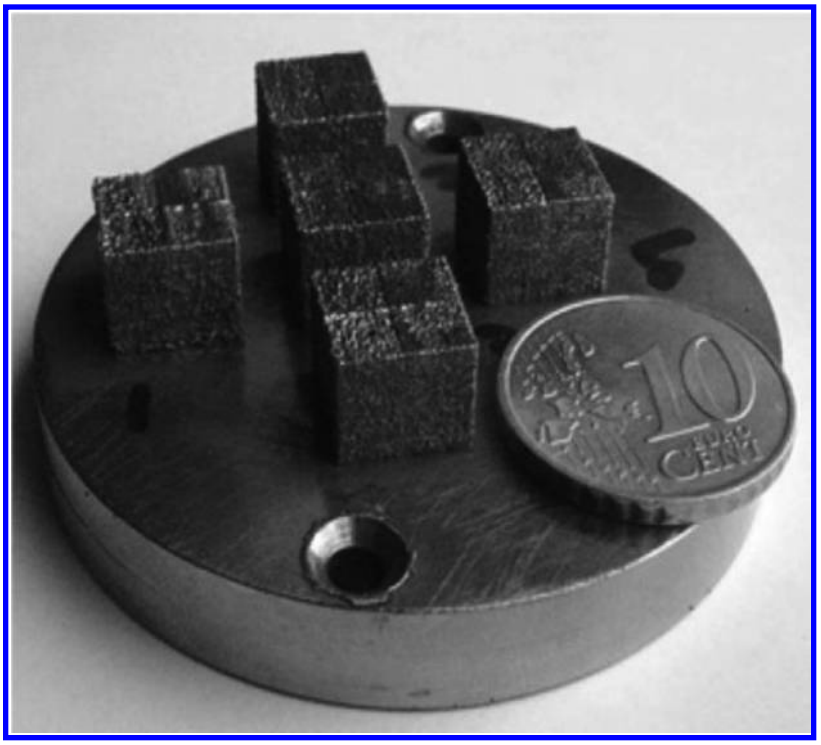

FIGURE 11.7
TiC-reinforced titanium matrix nanocomposite parts prepared using SLM. (Reprinted with permission from Gu, D. et al., *Compos. Sci. Technol.*, 71, 1612–1620, 2011.)

characteristics part. Direct ink-jet printing is an attractive technique of making desired conductive pattern or electrodes in printed electronic and optoelectronic devices. Further, the addition of nanoparticles in printing medium could change the rheology of the material, which is very important for AM processing. Ahn et al. (2009) showed printing of Ag microelectrodes using omnidirectional printing of concentrated silver nanoparticles inks. The ink with high solids loading (≥70 wt.%) was achieved by optimizing silver nanoparticles concentration, size, and distribution. Such ink was found suitable for printing of self-supporting microelectrode with complex shapes.

11.3.2 Polymer Matrix Nanocomposites

Selective laser sintering (SLS/LS) is quite popular in fabricating polymer matrix nanocomposites with high accuracy. LS polymer parts have huge demand in the aerospace, automotive, defense, and medical industries. However, anisotropic mechanical behavior and limited choice of materials have restricted its progress (Kruth et al. 2007). Several attempts have been made to improve mechanical or physical properties of LS polymer using nanofillers such as clay (Kim and Creasy 2004; Jain, Pandey, and Rao 2009; Wahab et al. 2009), nanosilica (Chung and Das 2008), nano-Al_2O_3 (Zheng et al. 2006), and carbon nanofiber (Goodridge et al. 2011). Incorporating nanofillers not only significantly enhance mechanical properties, but also improve other properties such as optical properties, thermal

conductivity, heat resistance, and flame retardancy or to accelerate biodegradability or increase bioactivity of the polymer composite. However, the success of a polymer nanocomposite for SLS is highly dependent on uniform dispersion of the nanoparticles and good interfacial adhesion between filler and polymer matrix (Goodridge et al. 2011). Therefore, preparation of starting powder for SLS is most important. Coating the filler materials with base polymer was found to be successful. Zheng et al. (2006) used PS coating on nano-Al_2O_3 particles by emulsion polymerization technique and used the polymer-coated fillers to reinforce PS-based composites using SLS. The nanoparticles were found dispersed homogeneously in the matrix, and the tensile strength of the nanocomposites improved significantly (300%) than the unfilled PS.

It was observed by Chung and Das (2008) that mechanical mixing of nylon-11 and nanosilica powders used for SLS causes agglomeration of nanosilica particles in the sintered part. Yan et al. (2009) used a dissolution–precipitation technique to prepare a nanosilica/nylon-12 composite powder for SLS. The nanosilica particles (3 wt.%) were found homogeneously dispersed in the sintered part. The tensile strength, tensile modulus, and impact strength of the nanocomposites increased by 20.9%, 39.4%, and 9.54%, respectively, compared to the neat nylon-12 prepared using an identical dissolution–precipitation technique. Athreya, Kalaitzidou, and Das (2010) used 4 wt.% nanosized carbon black powder reinforcement in nylon-12 to process an electrically conductive polymer nanocomposite using SLS. Flexural modulus of nylon-12/carbon black composites was observed to be lower than pure nylon-12 due to segregation of carbon black in the composite and a weak polymer–filler interface. Electrical conductivity of the nanocomposite was five orders of magnitude higher than that of pure nylon-12 processed by SLS.

Further, owing to exceptional mechanical, thermal, and electrical properties, CNTs and nanofibers have inspired their use as filler in polymers. A study by Goodridge et al. (2011) demonstrated that the reinforcement of laser-sintered PAs with carbon nanofibers can increase the strength of a base PA. The composite powder containing 3 wt.% carbon nanofibers was prepared using melt mixing and cryogenic milling, which facilitates homogeneous dispersion of nanofibers within the polymer matrix after sintering. Mechanical behavior of the nanocomposites showed 22% increase in the storage modulus compared to the base material.

AM techniques have achieved more and more attention for scaffold fabrication in recent decades due to the unique advantages such as possibility of defined external and internal architectures of scaffolds, computer-controlled fabrication processes, higher accuracy, and reproducibility. Duan et al. (2010) successfully fabricated three-dimensional nanocomposite scaffolds using SLS. Calcium phosphate (Ca-P) and carbonated HA (CHAp) nanoparticles were incorporated into poly(hydroxybutyrate-co-hydroxyvalerate) (PHBV) and poly(L-lactic acid) (PLLA), respectively, to prepare nanocomposite microspheres. These nanocomposite microspheres (Ca-P/PHBV and CHAp/PLLA) were used to fabricate 3D scaffolds. Figure 11.8 shows four kinds of scaffolds, namely, PHBV, Ca-P/PHBV, PLLA, and CHAp/PLLA, which were fabricated using microsphere powders. The compressive strength and modulus of the nanocomposite scaffolds were found to be higher than their polymer counter parts in dry condition. Cell proliferation and alkaline phosphatase (ALP) expression by SaOS-2 cells were enhanced in the case of Ca-P/PHBV scaffolds compared to pure PHBV, while no difference was observed in cell proliferation between CHAp/PLLA and pure PLLA scaffolds.

SLA can be used to build 3D nanocomposite parts using light-curable photopolymer. In SLA process, a thin layer of photosensitive resin with nanoparticles is cured on the surface of a resin bath using localized UV exposure, which allows the nanoparticles to reinforce in

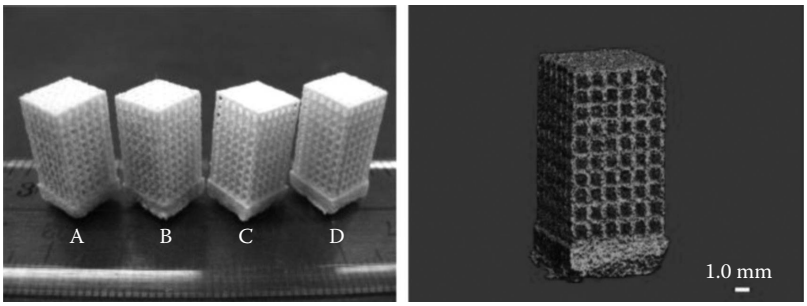

FIGURE 11.8
(a) 3D scaffolds with different composition (A) PHBV, (B) Ca-P/PHBV, (C) PLLA, (D) CHAp/PLLA produced by SLS; (b) MicroCT image of a Ca-P/PHBV scaffold. (Reprinted with permission from Duan, B. et al., *Acta Biomater.*, 6, 4495–4505, 2010.)

the polymer. The viscosity of the resin can significantly increase by the addition of nanoparticles. Micro-SLA (MSL) was used to fabricate porous scaffolds by mixing nanosized HA powder in a photo-crosslinkable PDLLA-diacrylate resin (Ronca, Ambrosio, and Grijpma 2013). With increasing concentration of nanoparticles, viscosity of the resin increases and stiffness increases in the cured composites. In a study, Gurr et al. (2010) showed in situ synthesized calcium phosphate/layered silicate hydride nanoparticles dispersed in acrylic resin. The nanocomposite was prepared using rapid prototype process based on photopolymerization of acrylic resin to improve property of resins. Nanocomposite materials showed significantly increased stiffness with increasing filler contents both in the green and post-cured state. Duan et al. (2011) used SLA to improve the mechanical and thermal properties of photosensitive resin by incorporating nano-TiO_2. The mechanical and thermal stability of the resin was found significantly high when nano-TiO_2 content was at 0.25%. It was observed that the tensile strength was increased by 89% from 25 to 48 MPa, the tensile modulus increased by 18% from 2,001 to 2,362 MPa, the flexural strength and the hardness increased by 6% and 5%, respectively. Moreover, the presence of nanomaterials in photopolymer suspension has changed the absorption or refraction ability of UV light, which subsequently alters cure depth and cure shape profile (Ivanova, Williams, and Campbell 2013). Therefore, process optimization is required for different nanomaterials when incorporated in SLA system.

11.4 Functional Materials

11.4.1 Functionally Graded Materials

FGMs are materials in which the composition and microstructure change gradually (gradient) or stepwise (graded) from one side to the other, resulting in a corresponding variation in the properties (Liu and DuPont 2003). Various fabrication techniques such as chemical vapour deposition (CVD)/physical vapour deposition (PVD), plasma spraying, powder metallurgy, and self-propagating high-temperature synthesis are generally used for producing FGMs (Kieback, Neubrand, and Riedel 2003). Most of these techniques are

not able to manufacture complex shape parts in single step, which is highly desirable. In recent years, AM of dissimilar and graded structures has been receiving more attention due to its huge demand for different applications. AM processes, more specifically the processes which are capable to deliver multiple materials at a time, are potentially suitable to manufacture complex shaped FGM parts. DMD processes have demonstrated its potential for manufacturing FGMs due to its flexibility in powder feeding mechanism that can change or mix materials when fabricating multi-material structures (Yakovlev et al. 2005). Several attempts have been made in FGM deposition of different metals and alloys such as stainless, nickel base superalloys, CoCrMo alloy, and titanium using LENS technique.

Collins et al. (2003) and Banerjee et al. (2003a) deposited a graded binary Ti-V and Ti-Mo alloy using LENS™ process from a blend of elemental Ti and V (or Mo) powders. Several researchers studied functionally graded TiC-reinforced MMCs by adjusting processing parameters and real-time variation of the feeding ratio of metal powder to TiC during laser direct deposition process (Liu and DuPont 2003; Zhang et al. 2008b; Wilson and Shin 2012). Crack-free functionally graded TiC/Ti composite, from pure Ti to approximately 95 vol.% TiC, was fabricated using LENS™ by Liu and DuPont (2003). Functionally graded TiC/Inconel 690 composite coating having TiC particles varied from 0 to 49 vol.% showed significant improvement in hardness and wear resistance (Wilson and Shin 2012). Compositionally graded alumina coating (Bandyopadhyay et al. 2007) and yttria-stabilized zirconia coating (Balla et al. 2007) on steel and Ti-TiO_2 structure (Balla et al. 2009) with composition and structural gradation were fabricated using LENS™ technique. These graded coatings were found superior to conventional homogeneous coatings as they provide better bonding strength between the coating and the substrate and relatively less residual stress due to gradual compositional variation. As a result, there are no sharp interfaces and the microstructure and hardness change smoothly leading to lower stress intensity at the interface. Laser deposition of full CoCrMo coating on titanium was difficult to produce crack free, possibly because of brittle intermetallic formation and residual stresses generation. Krishna et al. (2008a) demonstrated crack- and defect-free deposition of functionally graded, hard and wear-resistant CoCrMo alloy coating on Ti6Al4V using LENS™. The cross-sectional microstructure of the functionally graded coating is shown in Figure 11.9. In laser direct deposition, multiple powder hoppers were used to deliver different elemental powders individually and their feed rates are controlled separately to adjust the composition in FGMs. Wang, Mei, and Wu (2007) and Farayibi, Folkes, and Clare (2013) prepared titanium-based FGM components by combining powder (TiC or WC) and wire (Ti6Al4V) for DLF. During the process, by gradually increasing the powder feed rate and/or decreasing the wire feed rate, the graded composition was fabricated. This technique has advantage of less wastage due to no mixing of the feedstock materials.

FGM by SLS has been reported by Chung and Das (2006). They created glass bead particulate-filled nylon-11 composites with filler volume fraction vary from 0% to 30%. In this work, a macroscopic 3D polymer composite part with a one-dimensional material gradient in the build direction was demonstrated in single uninterrupted SLS run. Schematic of the FGM part with change in filler concentration and the corresponding cross-sectional SEM micrographs are shown in Figure 11.10. Smooth interfacial region indicates successful fabrication of nylon-11 and glass beads FGM.

11.4.2 Materials for Hydrogen Storage

Laser-based AM was found to be an attractive technique for the deposition of multicomponent high entropy alloys. This laser processing technique has the advantage of rapid

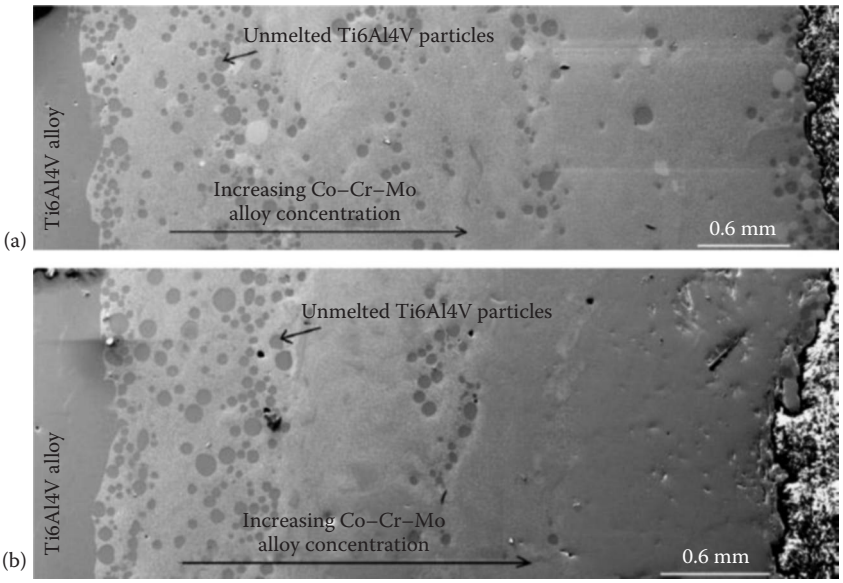

FIGURE 11.9
SEM micrograph of graded CoCrMo coatings on Ti6Al4V alloy: (a) 50% CoCrMo alloy at the surface and (b) 86% CoCrMo alloy at the surface. (Reprinted with permission from Krishna, B.V. et al., *JOM*, 60, 45–48, 2008b.)

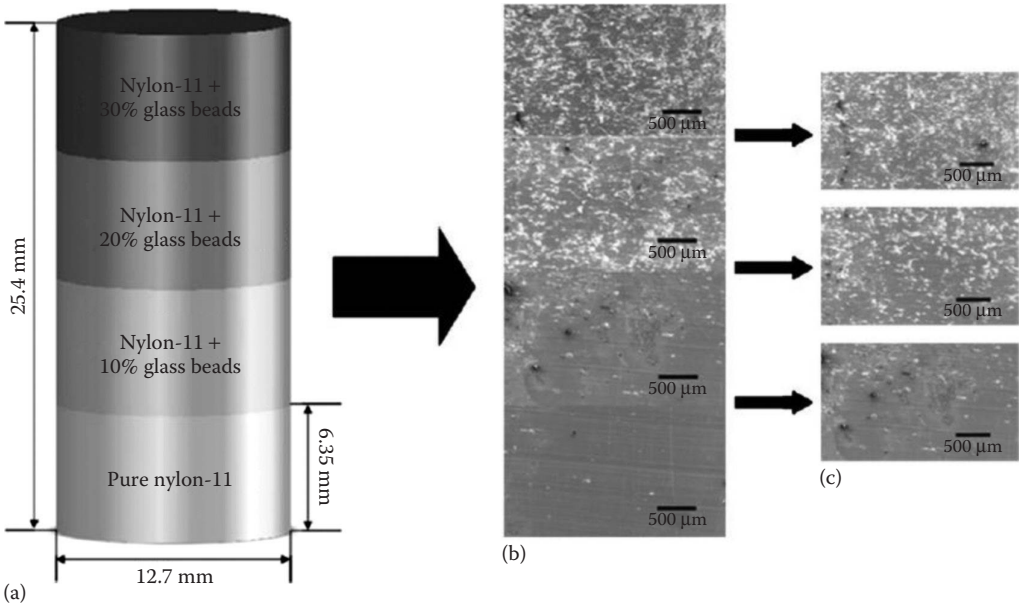

FIGURE 11.10
(a) Schematic description of graded compositions, (b) SEM micrographs of each composition in the fabricated FGM specimen, and (c) SEM micrographs of interface of two different compositions.

cooling velocity, leading to a significant non-equilibrium solute-trapping effect that avoids component segregation and overcome solubility limitations. Kunce, Polanski, and Bystrzycki (2013) successfully synthesized high entropy alloy (ZrTiVCrFeNi) from elemental powders in a near equimolar ratio using LENS™ technology. The synthesized alloy exhibited good chemical composition after laser deposition, compared to the nominal composition. The as-deposited alloy showed maximum hydrogen capacity of 1.81 wt.% and reduced to 1.56 wt.% after the additional heat treatment (for work on compositional-graded samples see Polanski et al. [2013] and Müller et al. [2014]).

11.5 Design Freedom/AM-Enabled Designs

Design optimization is very essential for manufacturing optimized products. This is because many of the novel design benefits/aims are compromised due to conventional manufacturing constraints. For example, design and manufacturing of lightweight structures is one of the most important requirements of components for use in aerospace. To achieve this, optimization of geometrical structure of components is required and is mostly done by mathematical means. Typical optimized design thus obtained is shown in Figure 11.11, which is not possible to manufacture using traditional manufacturing techniques.

Emergence of AM technologies enables manufacture of optimized products with improved functionality, in some cases multifunctionality, reduced weight and wastage, and associated energy savings. These product designs are normally of complex shapes, materials combinations, and hierarchy (in composition, internal architecture, and microstructure), some of which could possibly be achieved using current AM technologies. Some of the complex designs enabled by AM technologies are shown in Figure 11.12.

11.5.1 Design and Development of Lattice Structures

For more effective mechanical performance and weight reduction, periodic arrangement of load-bearing cross sections (struts) has been developed. Such structures/materials are known as lattice structures and exhibit more predictable mechanical behavior (Parthasarathy, Starly, and Raman 2011). These lattice structures exhibit several useful

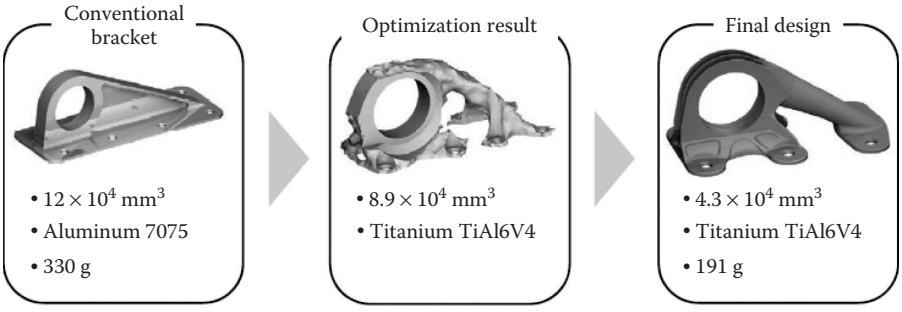

FIGURE 11.11
Mathematic design optimization process. (Reprinted with permission from Emmelmann, C. et al., *Phys. Procedia*, 12, 364–368, 2011.)

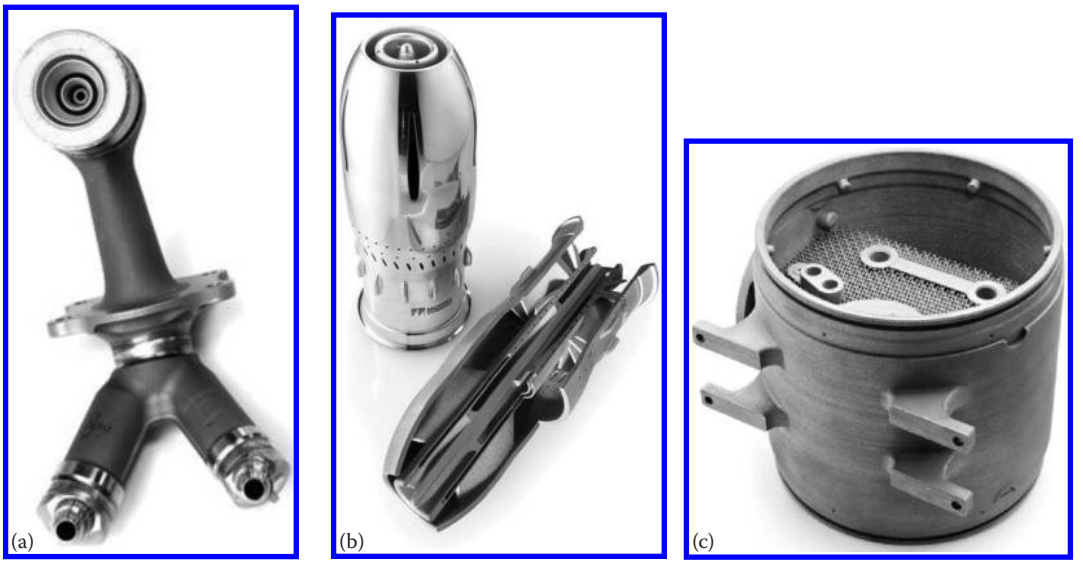

FIGURE 11.12
(a) GE Leap engine fuel nozzle fabricated using DMLS (Courtesy of www.industrial-lasers.com.); (b) component with complex internal cooling channels manufactured by SLS (Courtesy of www.mmsonline.com.); (c) metal housing with integrated solid and lattice structures. (Courtesy www.arcam.com.)

properties (Gibson and Ashby 1997) such as acoustic and thermal insulation, and energy absorption, and these properties can be easily tailored by changing size and shape of struts and total porosity (Gibson and Ashby 1982). Further, these designed materials with lattice structure type internal macrostructure/architecture are placed in different area too far from conventional materials in terms of their elastic modulus as a function of density (Figure 11.13). Therefore, lattice structures enable more design options to achieve desired mechanical or functional properties.

The internal unit cell structure has been tailored to achieve negative Poisson's ratio (Rehme and Emmelmann 2009). The honeycomb structures analyzed for their Poisson's ratio are shown in Figure 11.14. Both designs exhibited negative Poisson's ratio and cubic chiral architecture had a highest negative Poisson's ratio of −0.2835. The results are primarily dictated by diameter of the nodes and should be balanced with length of the struts. Yang et al. (2012a, 2012b) successfully fabricated auxetic mesh structures, shown in Figure 11.15, using electron beam melting (EBM). They found that desired strength or stiffness can be achieved by changing the strut length and these properties are high for the structures with high negative Poisson's ratio. The Poisson's ratio has been tailored changing the reentrant strut angle and/or ratio of vertical-to-reentrant strut length (Yang et al. 2012b). Compression and bending tests performed on these structures demonstrated that the bending strength without solid skin is significantly higher than conventional sandwich structures (Yang et al. 2012a). The EBM process-induced defects reduced the compressive strength and energy absorption capacity but the structures with negative Poisson's ratio may compensate this (Yang et al. 2012a). These experimental results suggest that lattice structures with negative Poisson's ratio show strong potential for use in applications such as shock/impact absorbers and artificial intervertebral discs, where high shear strength and low resistance to compression are primary requirements (Rehme and Emmelmann 2009).

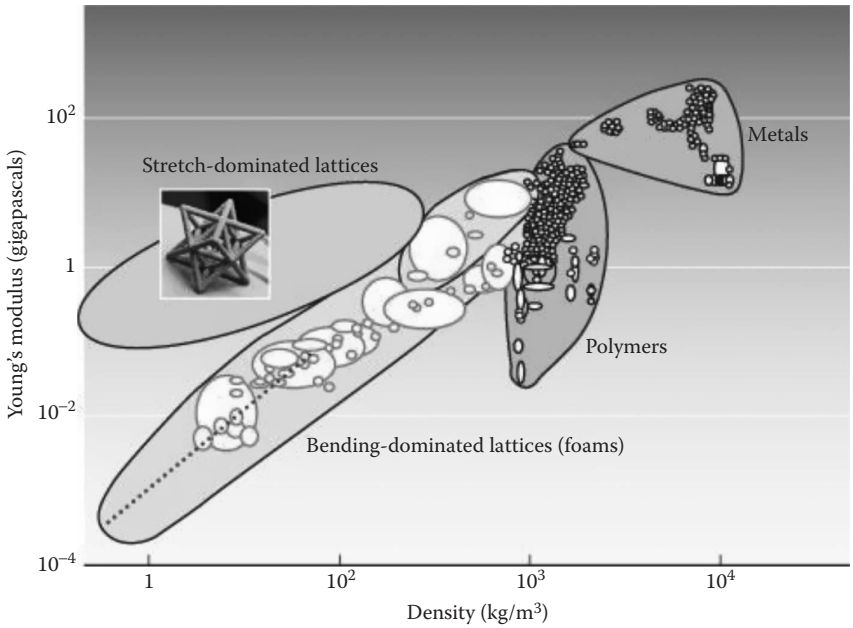

FIGURE 11.13
Lattice structures position compared to conventional materials. (Courtesy of https://manufacturing.llnl.gov/additive-manufacturing/designer-engineered-materials.)

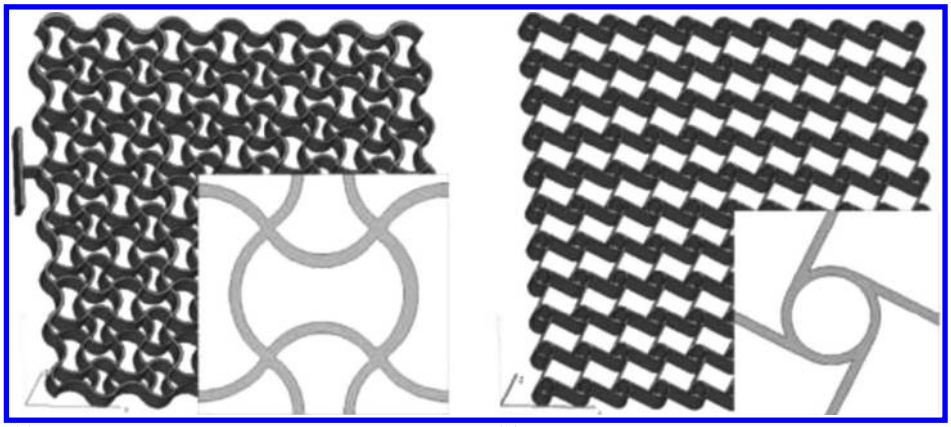

FIGURE 11.14
Tailored honeycomb structures (a) cubic sinus wave design, (b) cubic chiral design. (Reprinted with permission from Rehme, O., Emmelmann, C., *J. Laser. Micro. Nanoen.*, 4, 128–134, 2009.)

The effect of unit cell strut edge design on impact absorption of lattice structures has also been reported (Brennan-Craddock et al. 2012). Structures with two types of unit cell struts were fabricated using FDM and were compression tested to delineate the differences. The compression behavior of these structures is presented in Figure 11.16. It can be clearly seen that the energy absorption capacity (area under the curve) of helix strut

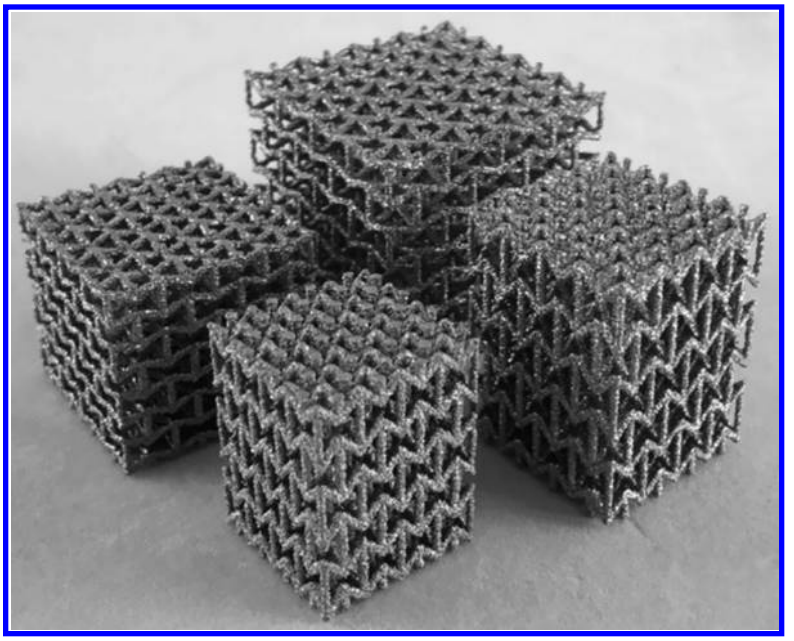

FIGURE 11.15
Ti6Al4V alloy auxetic structures fabricated using EBM. (Reprinted with permission from Yang, L. et al., *Mater. Sci. Eng. A*, 558, 579–585, 2012a.)

structure is significantly higher than other structures. This is primarily due to the ability of helical design to increase in strut overall length allowing more deformation before collapse (Brennan-Craddock et al. 2012). These results demonstrate the potential of complex tailored lattice structures fabricated using AM as efficient energy absorbing structures.

Another unique design that uses this lattice architecture is conformal lattice structures or spatially variant structures. These structures offer valuable properties such as high strength-to-weight ratio, predictable load and stress distributions, better mechanical performance, noise and vibration dampening. The effective use of such conformal lattice structures has been in the reduction of losses in directional dependent self-collimation (Rumpf et al. 2013). In this report, a spatially variant device was fabricated using FDM to control electromagnetic waves. Figure 11.17a shows such a device which can direct an unguided beam without significant loss due to conformal positioning and orientation of unit cells without variations in their size and shape. The device has been experimentally tested between 14.8 and 15.8 GHz and found to exhibit 6.5% fractional bandwidth (Rumpf et al. 2013). The structures with conformal lattice architecture possibly enable effective control of electromagnetic waves in various applications/devices.

11.5.2 Design Innovations for Medical Applications

It is well known that the natural bone is highly complex composite comprising different materials and functional gradation in microstructure, macrostructure, and composition. Therefore, the mechanical properties of bone also change accordingly—elastic modulus of 20 GPa for dense cortical bone and 0.5 GPa for highly porous cancellous bone. However, the current artificial implants that replace this natural bone are fully dense and also have

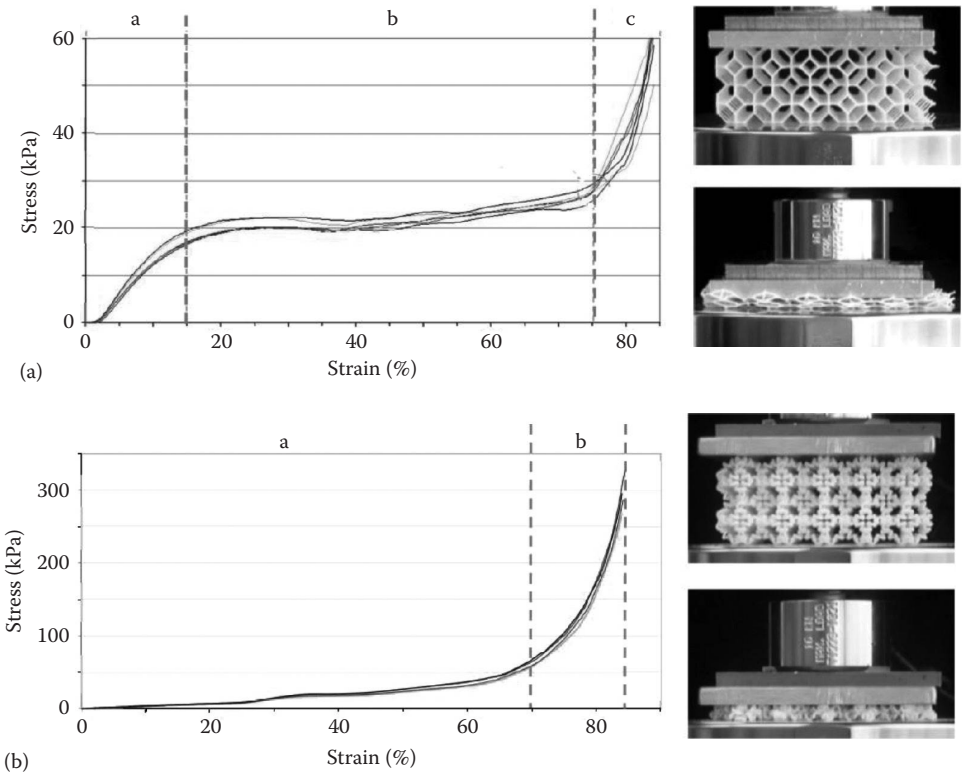

FIGURE 11.16
Compression deformation behavior of lattice structures: (a) structure with straight struts; (b) structure with helical strut—please note significantly high compression stress. (Reprinted with permission from Brennan-Craddock, J. et al., *J. Phys. Conf. Ser.*, 382, 012042, 2012.)

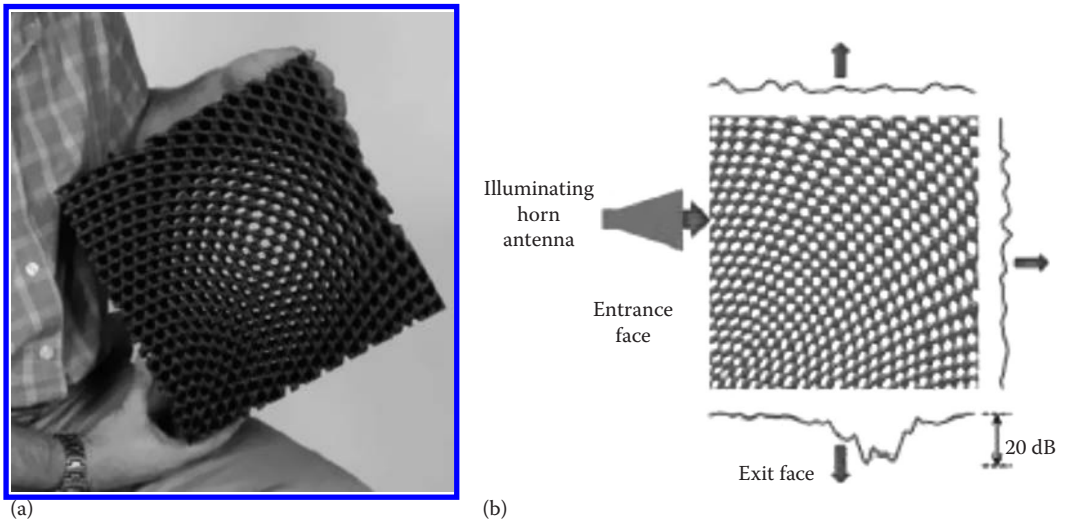

FIGURE 11.17
(a) Spatially variant structured fabricated using FDM; (b) measured profile of the waves around the device. (Reprinted with permission from Rumpf, R.C. et al., *Prog. Electromag. Res.*, 139, 1–14, 2013.)

elastic modulus significantly higher than natural bone. This modulus mismatch results in stress shielding leading to bone loss. Therefore, ideal bone replacement material must have identical geometry and site-specific mechanical and functional properties to that of natural bone. For example, monoblock acetabular shell, shown in Figure 11.18a, with porous surface on one side (to improve osseointegration) and wear resistant surface on the other side (articulating against femoral head) can potentially improve overall in vivo performance and life of artificial implants (España et al. 2010). Functional gradation in porosity, similar to natural bone, is also beneficial for implant's long-term stability (Figure 11.18b). Artificial implants with complex internal and external architectures can also be designed to obtain site-specific functions at different locations of the same implant as shown in Figure 11.18c. However, manufacturing these implants is not possible with traditional manufacturing routes but with AM processes such unique implants can be easily fabricated (Figure 11.19).

Porous metals have been proposed to address stress shielding problem (Krishna, Bose, and Bandyopadhyay 2007, 2009; Xue et al. 2007, Krishna et al. 2008b; Bandyopadhyay et al. 2009, 2010; Balla et al. 2010; DeVasConCellos et al. 2012) but with drop in mechanical properties. However, regular arrangement of pores in these porous structures was found to greatly improve mechanical properties while maintaining desired elastic modulus close to nature bone (Balla, Bose, and Bandyopadhyay 2010b).

Fabrication, deformation behavior, and mechanical properties of cellular materials with tailored internal micro-architecture for different applications, fabricated using AM technologies, have been reported by several authors (Ahmadi et al. 2014; Yan et al. 2012, 2014a, 2014b). These internal architectures have also been incorporated in artificial load-bearing implants with an aim to reduce weight, match stiffness with natural bone, improve osseointegration and overall long-term stability (Kusakabe et al. 2004; Heinl et al. 2008; Stoica 2009; Ghiba, Prejbeanu and Vermesan 2010; Ovidiu et al. 2010). Earlier simulations on implants with internal tailored lattice structures showed clear reduction in stress shielding (Ovidiu et al. 2010) in addition to favorable bone ingrowth into open pores. Another novel approach proposed by Mueller et al. (2012) involves incorporation of functional cavities and channels in to current load-bearing implants such as hip and knee. One such design is presented in Figure 11.20. Such a design features provide local supply of desired materials such as drugs, filler materials, and post-operative inspection of the implants (Muller et al. 2012). EBM-fabricated functional implants with complex lattice structures have been reviewed in Murr et al. (2012a). These implants have been demonstrated to have excellent biocompatibility and provide paths for osseointegration. Further, the inclusion of lattice architecture in the implants eliminates stress shielding thereby improving the long-term implant survivability. Tibial components of knee with incorporated lattice structures are shown in Figure 11.21. The capabilities of AM technologies also enable fabrication of functionally graded lattice structures mimicking natural bone. Mechanical properties of cellular implants have been reported by Murr et al. (2012b). These research investigations shown strong application potential of these novel implants but require significant efforts in terms of in vitro, in vivo trials and testing before these can be used for clinical use.

Being CAD-based manufacturing technologies, the AM processes enable design and development of custom devices and implants directly from computed tomography or MRI scan data of a patient. Clinical and experimental results clearly demonstrate that custom fit implants ensure mechanical stability and long-term in vivo success (McCarthy, Bono, and O'Donnel 1997; Fitzpatrick et al. 2011). AM technology has been successfully used to fabricate customized amputation prosthesis with functional gradation in porosity (DeVasConCellos et al. 2012). Figliuzzi, Mangano, and Mangano (2012) employed direct

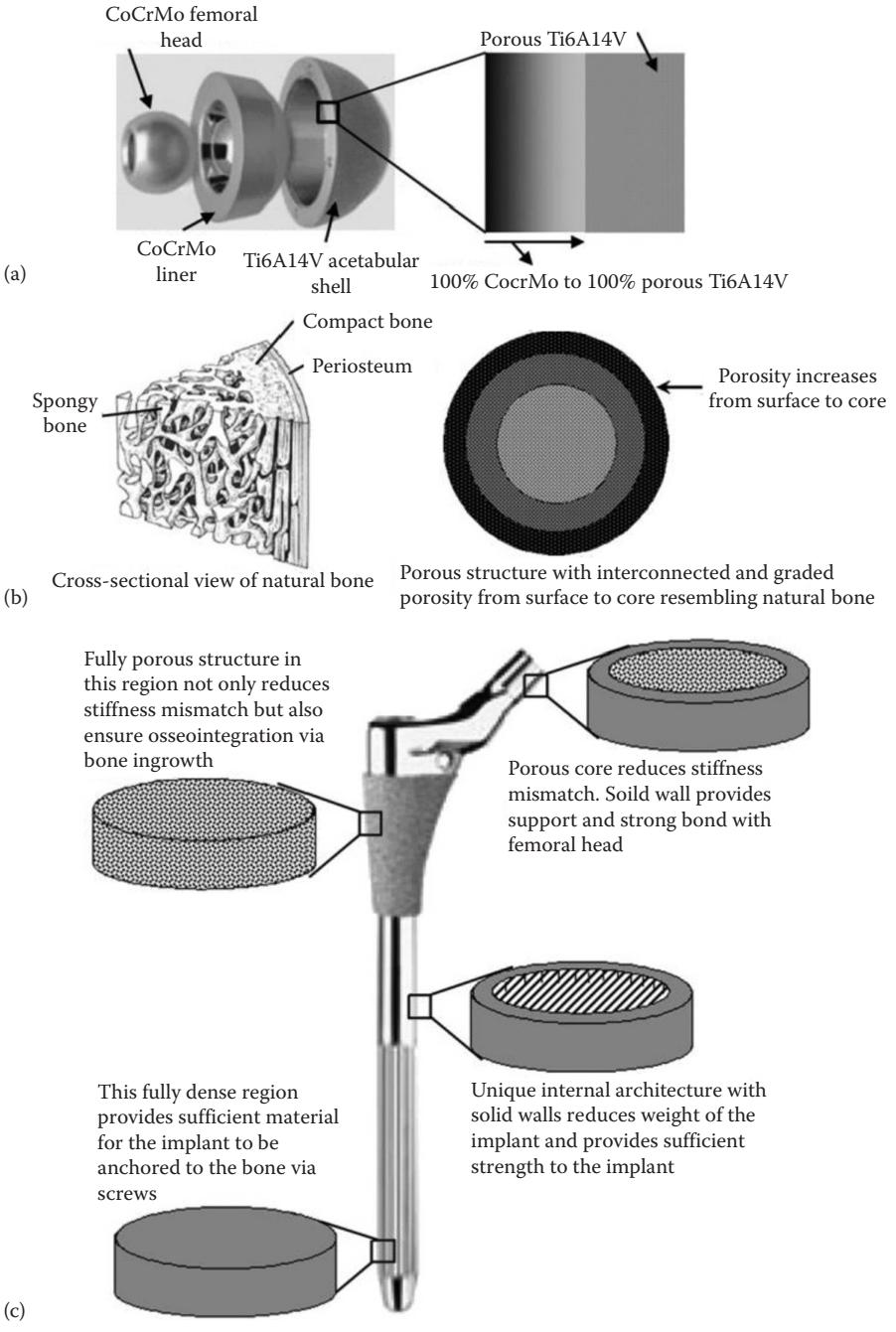

FIGURE 11.18
Schematic showing (a) monoblock acetabular shell, (b) graded porous structures, and (c) site-specific design of artificial implants. (Reprinted with permission from España, F.A. et al., *Mater. Sci. Eng. C*, 30, 50–57, 2010.)

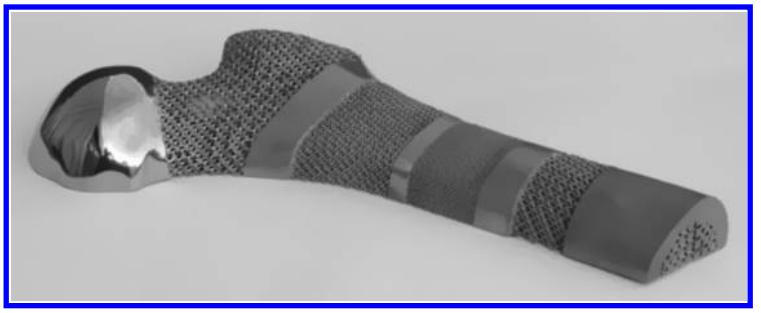

FIGURE 11.19
Typical femoral prototype with different internal architecture manufactured using AM. (Courtesy of www.tctmagazine.com.)

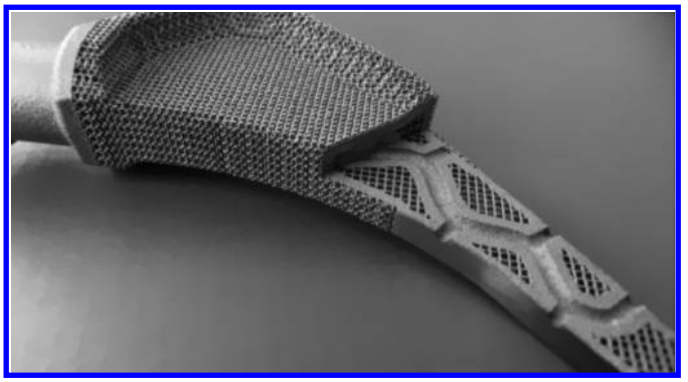

FIGURE 11.20
Hip stem with complex internal and external architecture. (Reprinted with permission from Mueller, B. et al., Innovative features in implants through beam melting—A new approach for additive manufacturing of endoprostheses, In *Innovative Developments in Virtual and Physical Prototyping*, Leira, Portugal, 519–523, 2012.)

laser metal forming technique to fabricate root-analogue implant designed using 3D projections of the maxilla and residual root (Figure 11.22). The Ti6Al4V alloy implant was manufactured using direct laser metal forming and has been implanted. Perfect matching between the implant and the root was observed, thus improving the stability of the implant after one year of follow-up. The implant did not show any indication of pain or infection. Figure 11.22c shows good bone-implant integration and stability of nature bone. The AM capabilities can be effectively exploited to include functional gradation in cellular structures, which can potentially mimic nature bone structure and hence enable favorable vascularization and early bone formation (Murr et al. 2012a). Typical implant with functional variation in porosity from core to shell fabricated using EBM is presented in Figure 11.23. More efficient mathematical designs for effective mechanical and flow ability properties can also be incorporated in desired components (Khoda, Ozbolat, and Koc 2013). Future development in AM technologies is expected to enable fabrication of complex artificial organs as well (Wang et al. 2013). AM has also been extensively exploited to fabricate tailored and designed tissue constructs (Melchels et al. 2012). Complex structures with desired cell seeding enable fundamental studies to understand cellular behavior during tissue formation.

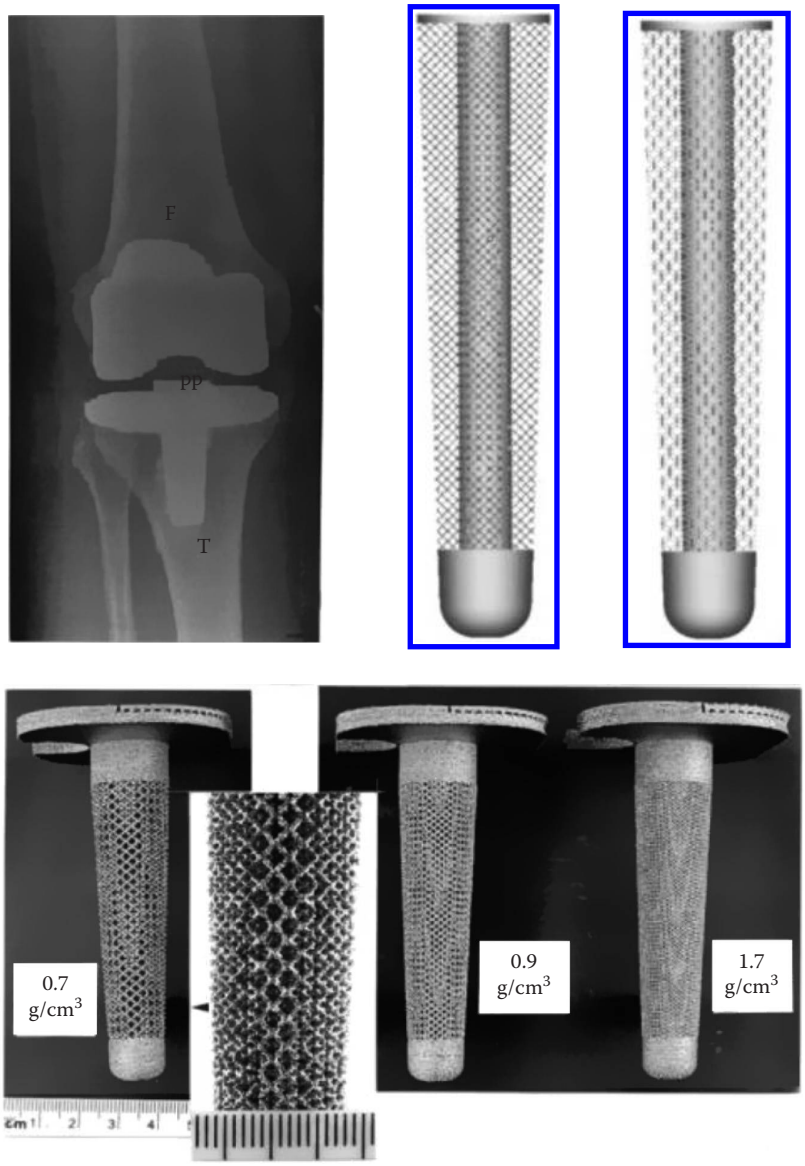

FIGURE 11.21
CAD models of tibial tray showing solid core for mechanical support and cellular shell for bone ingrowth (above); EBM fabricated components with complex architectures (below). (Reprinted with permission from Murr, L.E. et al., *J. Biotechnol. Biomaterial.*, 2, 1000131, 2012a.)

11.5.3 Multifunctional Devices

Recently, advances in AM-enabled fabrication of integrated systems such as embedded electronics, electrical circuits, and sensors in mechanical structure/parts. Further, these new systems may also consist of complex/conformal shapes made with variety of materials (multi-materials) with/without functional gradation in composition (Vaezi et al. 2013). Such multifunctional devices can be designed and manufactured on demand using a

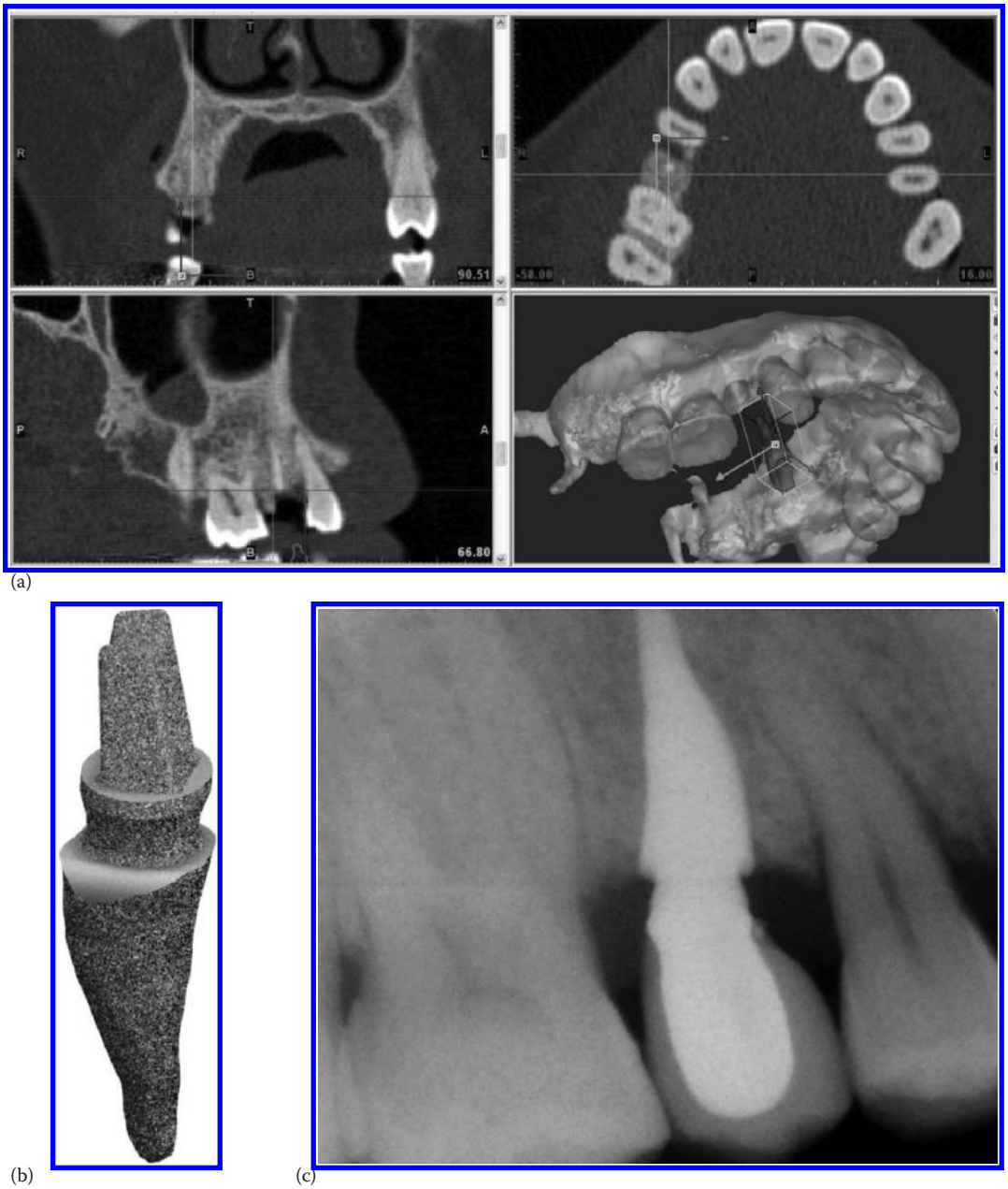

(a)

(b)

(c)

FIGURE 11.22
(See color insert.) (a) Designing dental implant using image data of maxilla and the residual root; (b) custom-designed dental root-analogue implant model; and (c) one year post-surgery radiograph of custom dental implant with crown. (Reprinted with permission from Figliuzzi, M. et al., *Int. J. Oral Maxillofac. Surg.*, 41, 858–862, 2012.)

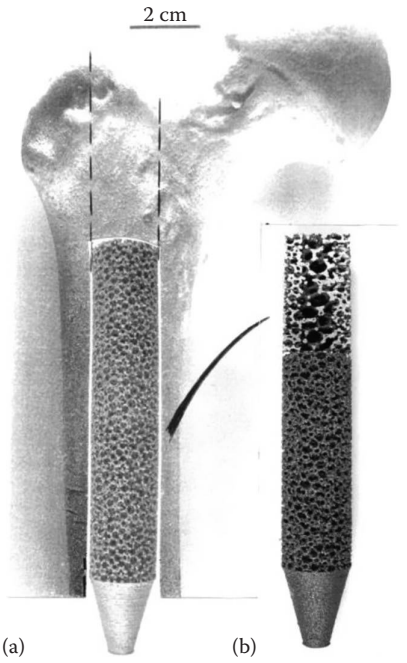

FIGURE 11.23
Intramedullary implant fabricated using EBM (a) and cross section showing the variation in porosity from core to surface (b). (Reprinted with permission from Murr, L.E. et al., *J. Biotechnol. Biomaterial.*, 2, 1000131, 2012a.)

combination of current AM technologies. For example, Lopes, MacDonald, and Wicker (2012) attempted to integrate SLA and direct printing (DP) processes in creating 3D polymeric structures with up to 555 embedded timer circuits. The overall process consists of multiple starts and stops between SLA, DP and intermediate processes where SLA has been used to create main supporting structure and DP for conductive circuits. Several processing steps are currently manual and therefore require further developments to enable automatic fabrication of complex 3D structure with embedded circuits and interconnects (Lopes, MacDonald, and Wicker 2012).

Very recently, the problems associated with materials used in SLA, for producing structures with electronic circuits, such as long-term durability, functionality, and conductive inks with low curing temperatures, have been addressed by a novel technology that uses FDM and DP or thermal embedding technology (Espalin et al. 2014). The use of FDM replaces polymers with thermoplastics having high strength and conductive copper wires embedded into the substrates using thermal technology enabled fabrication of devices with superior performance and robustness compared to SLA-based processes (Lopes, MacDonald, and Wicker 2012). However, it was found that FDM-based process requires other techniques such as direct wire technology for printing electronic circuits in addition to subtractive processes such as micromachining to achieve desired feature resolution (Espalin et al. 2014). The capability of such multi-3D system has been effectively used to fabricate CubeSat module (Figure 11.24), and the system has been found to provide significant improvements in overall performance (Espalin et al. 2014).

Ink-jet printing was used to fabricate split-ring resonator (SRR) arrays on a flexible polyimide substrate (Walther et al. 2009). This study demonstrated that ink-jet printing is an

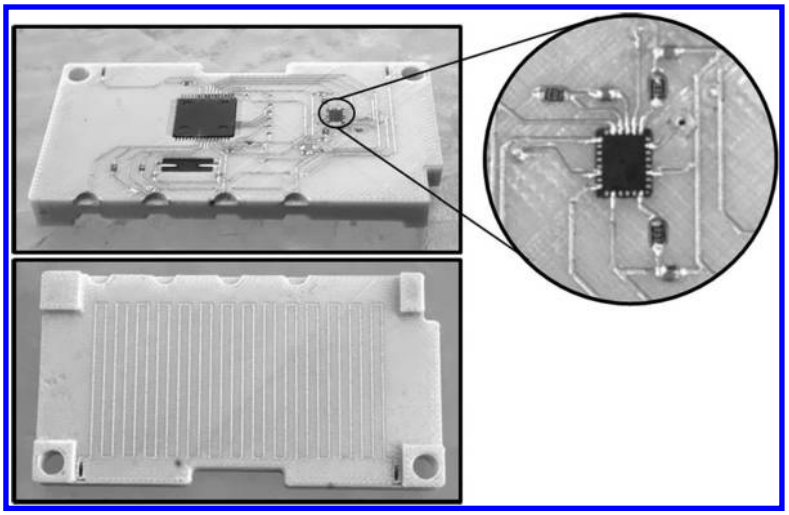

FIGURE 11.24
Typical CubeSat module fabricated using hybrid technique (FDM, direct printing and micromachining). (Reprinted with permission from Espalin, D. et al., *Int. J. Adv. Manuf. Technol.*, doi:10.1007/s00170-014-5717-7, 2014.)

agile processing route to deposit meta-material structures on a variety of substrates for gigahertz to terahertz frequencies (Figure 11.25). The circuits were printed using 20 wt.% silver nanoparticle suspension and the printed polyimide substrates were then heated at 220°C before testing. The performance of these SRR arrays was comparable to that of conventionally processed arrays but the variation was relatively high.

In medical field, there is a growing interest and demand for minimally invasive and even noninvasive surgeries. In fact, for ideal minimally invasive surgeries, the surgical tools must be as small as possible, sometimes the dimensions could be in micrometers.

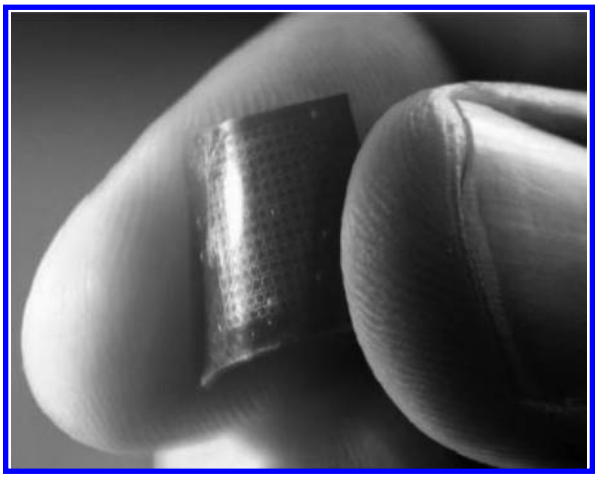

FIGURE 11.25
Conductive circuits on a flexible substrate printed using ink-jet printing process. (Reprinted with permission from Walther, M. et al., *Appl. Phys. Lett.*, 95, 251107, 2009.)

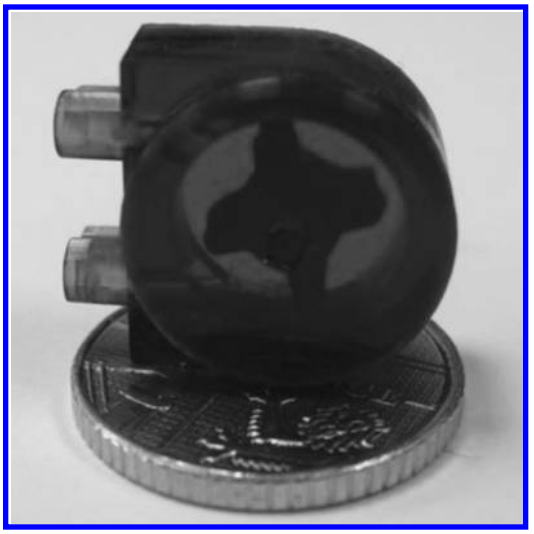

FIGURE 11.26
Miniature flow sensor with functional composite rotor made using MSL. (Reprinted with permission from Leigh, S.J. et al., *Sens. Actuators A*, 168, 66–71, 2011.)

Conventionally manufacturing technologies are not suitable for fabricating miniature surgical devices or tools. Recently, electrochemical fabrication (EFAB) technology has been identified as one suitable manufacturing technology for miniature surgical tools. This technology found to have extremely high geometrical resolution and is capable of producing micro-devices with several individual moving and assembled parts (Cohen et al. 2010). It was demonstrated that device with small feature up to 4 μm can be easily fabricated using EFAB and is the only technology that can produce miniature metal devices with micron-level features and moving mechanisms (Cohen et al. 2010). The technology can also produce miniature sensors for military applications, microfluidic devices, and so on.

MSL is another AM technique that has the capability to produce micro-devices. With an ability to use multiple materials and extremely fine feature resolution, the technology has been effectively used in the development of microelectromechanical systems. In addition to structural support, the resins have been added with desired filler material to achieve desired functionality. A functional composite material consisting of magnetic nanoparticle added to the resin has been reportedly used to build micro-flow sensor device (Leigh et al. 2011). Such micro devices find applications where space restrictions are very high (Figure 11.26). The details and capabilities of other micro-AM processes are discussed by Vaezi, Seitz, and Yang (2013) in greater detail.

11.6 Summary

Existing AM techniques have demonstrated their capabilities to create novel structures with unique geometrical design as well as incorporation of tailored/designed materials into the structures. In particular, cellular structures and components with embedded lattice

structures show strong application potential in various sectors. For example, large structures with designed internal lattice structures provide significant weight savings while maintaining strength and other service requirements of aerospace industries. These structures are also good candidate materials to energy absorption systems in automobiles. Such structures provide site-specific functional requirements for orthopedic implants thus improving their in vivo life. Ideal combination of multiple AM technologies appears to be an effective approach in creating multifunctional devices and structures with embedded sensors.

In spite of significant developments and improvements in AM technologies, materials innovation using AM appears to be still in its embryonic stage. Comprehensive processing, microstructure, and property correlations are required. Major hurdle in designed materials development using AM is nonavailability of desired materials. Promising results have been reported in developing metal, ceramic, and polymer matrix composites via AM techniques utilizing existing and new feedstock materials, several materials-related challenges remain to be addressed. Even existing materials are not optimized or designed for AM technologies. Important requirement in the development of new materials for AM is preparation of feedstock materials with desired characteristics suitable for specific AM technique. Finally, as with challenges the rewards are also extremely high for the integration of nanomaterials and AM.

References

Ahmadi, S.M., Campoli, G., Yavari, G.A., Sajadi, B., Wauthle, R., Schrooten, J., Weinans, H., Zadpoor, A.A. 2014. Mechanical behavior of regular open-cell porous biomaterials made of diamond lattice unit cells. *J. Mech. Behav. Biomed. Mater.* 34:106–115.

Ahn, B.Y., Duoss, E.B., Motala, M.J. et al. 2009. Omnidirectional printing of flexible, stretchable, and spanning silver microelectrodes. *Science* 323:1590–1593.

Athreya, S.R., Kalaitzidou, K., Das, S. 2010. Processing and characterization of a carbon black-filled electrically conductive nylon-12 nanocomposites produced by selective laser sintering. *Mater. Sci. Eng. A* 527:2637–2642.

Bai, J.G., Creehan, K.D., Kuhn, H.A. 2007. Inkjet printable nanosilver suspensions for enhanced sintering quality in rapid manufacturing. *Nanotechnology* 18:185701–185705.

Balla, V.K., Bandyopadhyay, P.P., Bose, S., Bandyopadhyay, A. 2007. Compositionally graded yttria-stabilized zirconia coating on stainless steel using laser engineered net shaping (LENS™). *Scripta Mater.* 57:861–864.

Balla, V.K., Bhat, A., Bose, S., Bandyopadhyay, A. 2012. Laser processed TiN reinforced Ti6Al4V composite coatings. *J. Mech. Behav. Biomed. Mater.* 6:9–20.

Balla, V.K., Bodhak, S., Bose, S., Bandyopadhyay, A. 2010. Porous tantalum structures for bone implants: Fabrication, mechanical and in vitro biological properties. *Acta Biomater.* 6(8):3349–3359.

Balla, V.K., Bose, S., Bandyopadhyay, A. 2010a. Microstructure and wear properties of laser deposited WC–12%Co composites. *Mater. Sci. Eng. A* 527(24–25):6677–6682.

Balla, V.K., Bose, S., Bandyopadhyay, A. 2010b. Understanding compressive deformation in porous titanium. *Philos. Mag.* 90(22):3081–3094.

Balla, V.K., DeVasConCellos, P.D., Xue, W., Bose, S., Bandyopadhyay, A. 2009. Fabrication of compositionally and structurally graded Ti–TiO_2 structures using laser engineered net shaping (LENS). *Acta Biomater.* 5(5):1831–1837.

Bandyopadhyay, A., España, F.A., Balla, V.K., Bose, S., Ohgami, Y., Davies, N.M. 2010. Influence of porosity on mechanical properties and in vivo response of Ti6Al4V implants. *Acta Biomater.* 6(4):1640–1648.

Bandyopadhyay, A., Krishna, B.V., Xue, W., Bose, S. 2009. Application of laser engineered net shaping (LENS) to manufacture porous and functionally graded structures for load bearing implants. *J. Mater. Sci. Mater. Med*. 20(S1):S29–S34.

Bandyopadhyay, P.P., Balla, V.K., Bose, S., Bandyopadhyay, A. 2007. Compositionally graded aluminum oxide coatings on stainless steel using laser processing. *J. Am. Ceram. Soc*. 90(7):1989–1991.

Banerjee, R., Collins, P.C., Bhattacharyya, D., Banerjee, S., Fraser, H.L. 2003a. Microstructural evolution in laser deposited compositionally graded α/β titanium-vanadium alloys. *Acta Mater*. 51:3277.

Banerjee, R., Collins, P.C., Genc, A., Fraser, H.L. 2003b. Direct laser deposition of in situ Ti-6Al-4V-TiB composites. *Mater. Sci. Eng. A* 358:343–349.

Banerjee, R., Genc, A., Collins, P.C., Fraser, H.L. 2005. Nanoscale TiB precipitates in laser deposited Ti-Matrix composites. *Scripta Mater*. 53:1433–1437.

Bhat, A., Balla, V.K., Bysakh, S., Basu, D., Bose, S., Bandyopadhyay, A. 2011. Carbon nanotube reinforced Cu–10Sn alloy composites: Mechanical and thermal properties. *Mater. Sci. Eng. A* 528(22–23):6727–6732.

Brennan-Craddock, J., Brackett, D., Wildman, R., Hague, R. 2012. The design of impact absorbing structures for additive manufacture. *J. Phys. Conf. Ser*. 382:012042.

Campbell, T.A., Ivanova, O.S. 2013. 3D printing of multifunctional nanocomposites. *Nano Today* 8:119–120.

Caulfield, B., McHugh, P.E., Lohfeld, S. 2007. Dependence of mechanical properties of polyamide components on build parameters in the SLS process. *J. Mater. Process. Technol*. 182:477–88.

Chung, H., Das, S. 2006. Processing and properties of glass bead particulate-filled functionally graded nylon-11 composites produced by selective laser sintering. *Mater. Sci. Eng. A* 437:226–34.

Chung, H., Das, S. 2008. Functionally graded nylon-11/Silica nanocomposites produced by selective laser sintering. *Mater. Sci. Eng. A* 487:251–257.

Cohen, A., Chen, R., Frodis, U., Wu, M.-T., Folk, C. 2010. Microscale metal additive manufacturing of multi-component medical devices. *Rapid Prototyping J*. 16(3):209–215.

Collins, P.C., Banerjee, R., Banerjee, S., Fraser, H.L. 2003. Laser deposition of compositionally graded titanium–vanadium and titanium–molybdenum alloys. *Mater. Sci. Eng. A* 352(1):118–128.

Cooper, D.E., Blundell, N., Maggs, S., Gibbons, G.J. 2013. Additive layer manufacture of Inconel 625 metal matrix composites, reinforcement material evaluation. *J. Mater. Process. Technol*. 213(12):2191–2200.

Crane, N.B., Wilkes, J., Sachs, E., Allen, S.M. 2006. Improving accuracy of powder-based SFF processes by metal deposition from a nanoparticle dispersion. *Rapid Prototyping J*. 12:266–274.

Dadbakhsh, S., Hao, L. 2012. in situ formation of particle reinforced Al matrix composite by selective laser melting of Al/Fe_2O_3 powder mixture. *Adv. Eng. Mater*. 14:45–48.

Dadbakhsh, S., Hao, L., Jerrard, P.G.E., Zhang, D.Z. 2012. Experimental investigation on selective laser melting behaviour and processing windows of in situ reacted Al/Fe_2O_3 powder mixture. *Powder Tech*. 231:112–121.

Das, M., Balla, V.K., Basu, D., Bose, S., Bandyopadhyay, A. 2010. Laser processing of SiC-particle-reinforced coating on titanium. *Scripta Mater*. 63(4):438–441.

Das, M., Balla, V.K., Basu, D., Manna, I., Kumar, T.S.S., Bandyopadhyay, A. 2012. Laser processing of in situ synthesized TiB–TiN-reinforced Ti6Al4V alloy coatings. *Scripta Mater*. 66(8):578–581.

Das, M., Bhattacharya, K., Dittrick, S.A. et al. 2014. in situ synthesized TiB–TiN reinforced Ti6Al4V alloy composite coatings: Microstructure, tribological and in-vitro biocompatibility. *J. Mech. Behav. Biomed. Mater*. 29:259–271.

Das, M., Bysakh, S., Basu, D., Kumar, T.S.S., Balla, V.K., Bose, S., Bandyopadhyay, A. 2011. Microstructure, mechanical and wear properties of laser processed SiC particle reinforced coatings on titanium, *Surf. Coat. Tech*. 205(19):4366–4373.

DeVasConCellos, P., Balla, V.K., Bose, S., Bandyopadhyay, A., Fugazzi, R., Dernell, W.S. 2012. Patient specific implants for amputation prostheses: Design, manufacture and analysis. *Vet. Comp. Orthop. Traumatol*. 25(4):286–296.

Duan, B., Wang, M., Zhou, W.Y., Cheung, W.L., Li, Z.Y., Lu, W.W. 2010. Three-dimensional nanocomposite scaffolds fabricated via selective laser sintering for bone tissue engineering. *Acta Biomater*. 6:4495–4505.

Duan, Y., Zhou, Y., Tang, Y., Li, D. 2011. Nano-TiO_2-modified photosensitive resin for RP. *Rapid Prototyping J*. 17(4):247–252.

Emmelmann, C., Sander, P., Kranz, J., Wycisk, E. 2011. Laser additive manufacturing and bionics: Redefining lightweight design. *Phys. Procedia* 12:364–368.

Espalin, D., Muse, D.W., MacDonald, E., Wicker, R.B. 2014. 3D Printing multifunctionality: Structures with electronics. *Int. J. Adv. Manuf. Technol.* doi:10.1007/s00170-014-5717-7.

España, F.A., Balla, V.K., Bose, S., Bandyopadhyay, A. 2010. Design and fabrication of CoCrMo based novel structures for load bearing implants using laser engineered net shaping. *Mater. Sci. Eng. C* 30(1):50–57.

Farayibi, P.K., Folkes, J.A., Clare, A.T. 2013. Laser deposition of Ti-6Al-4V wire with WC powder for functionally graded components. *Mater. Manuf. Process*. 28:514–518.

Figliuzzi, M., Mangano, F., Mangano, C. 2012. A novel root analogue dental implant using CT scan and CAD/CAM: Selective laser melting technology. *Int. J. Oral Maxillofac. Surg*. 41:858–862.

Fitzpatrick, N., Smith, T.J., Pendegrass, C.J., Yeadon, R., Ring, M., Goodship, A.E., Blunn, G.W. 2011. Intraosseous transcutaneous amputation prosthesis (ITAP) for limb salvage in 4 dogs. *Vet. Surg.* 40(8):909–925.

Fu, Z., Schlier, L., Travitzky, N., Greil, P. 2013. Three-dimensional printing of SiSiC lattice truss structures. *Mater. Sci. Eng. A* 560:851–856.

Gåård, A., Krakhmalev, P., Bergström, J. 2006. Microstructural characterization and wear behavior of (Fe, Ni)–TiC MMC prepared by DMLS. *J. Alloys Compd*. 21:166–71.

Ghiba, M.O., Prejbeanu, R., Vermesan, D. 2010. The mechanical behavior of a mini hip endoprosthesis with a lattice structure tail. *Revista de ortopedie si traumatologie a Asociatiei de ortopedie Romano-Italiano-Spaniole* [Journal of Orthopaedic Trauma of the Romanian – Italian - Spanish Orthopedic Association] 2(18):101–104.

Ghosh, S.K., Bandyopadhyay, K., Saha, P. 2014. Development of an in-situ multi-component reinforced Al-based metal matrix composite by direct metal laser sintering technique—Optimization of process parameters. *Mater. Charact*. 93:68–78.

Ghosh, S.K., Saha, P. 2011. Crack and wear behavior of SiC particulate reinforced aluminium based metal matrix composite fabricated by direct metal laser sintering process. *Mater. Des*. 32:139–45.

Ghosh, S.K., Saha, P., Kishore, S. 2010. Influence of size and volume fraction of SiC particulates on properties of ex situ reinforced Al–4.5Cu–3Mg metal matrix composite prepared by direct metal laser sintering process. *Mater. Sci. Eng. A* 527:4694–701.

Gibson, L.J., Ashby, M.F. 1982. The mechanics of three-dimensional cellular materials. *P. Roy. Soc. Lond. A Mat*. 382:43–59.

Gibson, L.J., Ashby, M.F. 1997. *Cellular Solids: Structure and Properties*. Cambridge: Cambridge University Press.

Goodridge, R.D., Shofner, M.L., Hague, R.J.M., McClelland, M., Schlea, M.R., Johnson, R.B., Tuck, C.J. 2011. Processing of a polyamide-12/carbon nanofibre composite by laser sintering. *Polym. Test*. 30:94–100.

Gopagoni, S., Hwang, J.Y., Singh, A.R.P. et al. 2011. Microstructural evolution in laser deposited nickel–titanium–carbon in situ metal matrix composites. *J. Alloy. Compd*. 509:1255–60.

Griffin, E.A., Mumm, D.R., Marshall, D.B. 1996. Rapid prototyping of functional ceramic composites. *The Amer. Ceram. Soc. Bull*. 75(7):65–68.

Gu, D., Hagedorn, Y.-C., Meiners, W., Wissenbach, K., Poprawe, R. 2011. Nanocrystalline TiC reinforced Ti matrix bulk-form nanocomposites by selective laser melting (SLM): Densification, growth mechanism and wear behavior. *Compos. Sci. Technol*. 71:1612–1620.

Gu, D., Shen, Y. 2006. WC–Co particulate reinforcing Cu matrix composites produced by direct laser sintering. *Mater. Lett*. 60(29–30):3664–8.

Gu, D., Shen, Y. 2007. Influence of reinforcement weight fraction on microstructure and properties of submicron WC–Co_p/Cu bulk MMCs prepared by direct laser sintering. *J. Alloys Compd*. 431(1/2):112–120.

Gu, D., Shen, Y. 2009. Balling phenomena in direct laser sintering of stainless steel powder: Metallurgical mechanisms and control methods. *Mater. Des*. 30(8):2903–2910.

Gu, D., Shen, Y., Meng, G. 2009. Growth morphologies and mechanisms of TiC grains during selective laser melting of Ti–Al–C composite powder. *Mater. Lett.* 63(29):2536–2538.

Gu, D., Shen, Y., Zhao, L., Xiao, J., Wu, P., Zhu, Y. 2007. Effect of rare earth oxide addition on microstructures of ultra-fine WC–Co particulate reinforced Cu matrix composites prepared by direct laser sintering. *Mater. Sci. Eng. A* 445–446:316–322.

Gu, D., Wang, Z., Shen, Y., Li, Q., Li, Y. 2009. In-situ TiC particle reinforced Ti–Al matrix composites: Powder preparation by mechanical alloying and selective laser melting behavior. *Appl. Surf. Sci.* 255(22):9230–9240.

Guo, N., Leu, M.C. 2013. Additive manufacturing: Technology, applications and research needs. *Front. Mech. Eng.* 8(3):215–243.

Gurr, M., Thomann, Y., Nedelcu, M., Kübler, R., Könczöl, L., Mülhaupt, R. 2010. Novel acrylic nanocomposites containing in-situ formed calcium phosphate/layered silicate hybrid nanoparticles for photochemical rapid prototyping, rapid tooling and rapid manufacturing processes. *Polymer* 51:5058–5070.

Heinl, P., Müller, L., Körner, C., Singer, R.F., Müller, F.A. 2008. Cellular Ti–6Al–4V structures with interconnected macro porosity for bone implants fabricated by selective electron beam melting. *Acta Biomater.* 4(5):1536–1544.

Ho, H.C.H., Cheung, W.L., Gibson, I. 2003. Morphology and properties of selective laser sintered Bisphenol: A polycarbonate. *Ind. Eng. Chem. Res.* 42:1850–1862.

Hon, K.K.B., Gill, T.J. 2003. Selective laser sintering of SiC/polyamide composites. *CIRP Ann. Manuf. Technol.* 52:173–6.

Hong, C., Gu, D., Dai, D., et al. 2013. Laser metal deposition of TiC/Inconel 718 composites with tailored interfacial microstructures. *Opt. Laser. Technol.* 54:98–109.

Hwang, J.Y., Neira, A., Scharf, T.W., Tiley, J., Banerjee, R. 2008. Laser-deposited carbon nanotube reinforced nickel matrix composites. *Scripta Mater.* 59(5):487–490.

Ivanova, O., Williams, C., Campbell, T. 2013. Additive manufacturing (AM) and nanotechnology: Promises and challenges. *Rapid Prototyping J.* 19(5):353–364.

Jain, P.K., Pandey, P.M., Rao, P.V.M. 2009. Selective laser sintering of clay reinforced polyamide. *Polym. Compos.* 31(4):732–743.

Kenzari, S., Bonina, D., Dubois, J.M., Fournée, V. 2012. Quasicrystal–polymer composites for selective laser sintering technology. *Mater. Des.* 35:691–695.

Khoda, A.K.M.B., Ozbolat, I.T., Koc, B. 2013. Spatially multi-functional porous tissue scaffold. *Procedia Eng.* 59:174–182.

Kieback, B., Neubrand, A., Riedel, H. 2003. Processing techniques for functionally graded materials. *Mater. Sci. Eng. A* 362:81–106.

Kim, J., Creasy, T.S. 2004. Selective laser sintering characteristics of nylon6/clay reinforced nanocomposite. *Polym. Test.* 23:629–636.

Klosterman, D.A., Chartoff, R.P., Osborne, N.R., et al. 1999. Development of a curved layer LOM process for monolithic ceramics and ceramic matrix composites. *Rapid Prototyping J.* 5(2):61–71.

Krishna, B.V., Bose, S., Bandyopadhyay, A. 2007. Low stiffness porous Ti structures for load bearing implants. *Acta Biomater.* 3(6):997–1006.

Krishna, B.V., Bose, S., Bandyopadhyay, A. 2009. Fabrication of porous NiTi shape memory alloy structures using laser engineered net shaping. *J. Biomed. Mater. Res. B* 89B(2):481–490.

Krishna, B.V., Xue, W., Bose, S., Bandyopadhyay, A. 2008a. Functionally graded Co–Cr–Mo coating on Ti–6Al–4V alloy structures. *Acta Biomater.* 4:697–706.

Krishna, B.V., Xue, W., Bose, S., Bandyopadhyay, A. 2008b. Engineered porous metals for implants. *JOM* 60(5):45–48.

Kruth, J.-P., Levy, G., Klocke, F., Childs, T.H.C. 2007. Consolidation phenomena in laser and powder-bed based layered manufacturing. *CIRP Ann. Manuf. Technol.* 56(2):730–759.

Kumar, S. 2009. Manufacturing of WC–Co moulds using SLS machine. *J. Mater. Process. Technol.* 209(8):3840–3848.

Kumar, S., Kruth, J.-P. 2010. Composites by rapid prototyping technology. *Mater. Des.* 31:850–56.

Kunce, I., Polanski, M., Bystrzycki, J. 2013. Structure and hydrogen storage properties of a high entropy ZrTiVCrFeNi alloy synthesized using laser engineered net shaping (LENS). *Int. J. Hydrogen Ener.* 38:12180–12189.

Kusakabe, H., Sakamaki, T., Nihei, K., Oyama, Y., Yanagimoto, S., Ichimiya, M., Kimura, J., Toyama, Y. 2004. Osseointegration of a hydroxyapatite-coated multilayered mesh stem. *Biomaterials* 25(15):2957–2969.

Laoui, T., Froyen, L., Kruth, J.P. 2000. Effect of mechanical alloying on selective laser sintering of WC–9CO powder. *Powder Metal* 42(3):203–205.

Leigh, S.J., Purssell, C.P., Bowen, J., Hutchins, D.A., Covington, J.A., Billson, D.R. 2011. A miniature flow sensor fabricated by micro-stereolithography employing a magnetite/acrylic nanocomposite resin. *Sens. Actuators A* 168:66–71.

Li, Y., Bai, P., Wang, Y., Hu, J., Guo, Z. 2009. Effect of TiC content on Ni/TiC composites by direct laser fabrication. *Mater. Des.* 30:1409–1412.

Liu, F.-H., Shen, Y.-K., Liao, Y.-S. 2011. Selective laser gelation of ceramic–matrix composites. *Compos B* 42:57–61.

Liu, W., DuPont, J.N. 2003. Fabrication of functionally graded TiC/Ti composites by laser engineered net shaping. *Scripta Mater.* 48(9):1337–1342.

Lopes, A.J., MacDonald, E., Wicker, R.B. 2012. Integrating stereolithography and direct print technologies for 3D structural electronics fabrication. *Rapid Prototyping J.* 18(2):129–143.

Lu, L., Fuh, J.Y.H., Chen, Z.D., Leong, C.C., Wong, Y.S. 2000. In-situ formation of TiC composite using selective laser melting. *Mater. Res. Bull.* 35:1555–61.

Maeda, K., Childs, T.H.C. 2004. Laser sintering (SLS) of hard metal powders for abrasion resistant coatings. *J. Mater. Process. Technol.* 149(1–3):609–15.

Masood, S.H., Song, W.Q. 2004. Development of new metal/polymer materials for rapid tooling using fused deposition modeling. *Mater Des.* 25:587–594.

Mazzoli, A.G., Moriconi, G., Pauri, M.G. 2007. Characterization of an aluminum-filled polyamide powder for applications in selective laser sintering. *Mater. Des.* 28:993–1000.

McCarthy, J.C., Bono, J.V., O'Donnel, P.J. 1997. Custom and modular components in primary total hip replacement. *Clin. Orthop.* 344:162–171.

Melchels, F.P.W., Domingos, M.A.N., Klein, T.J., Malda, J., Bartolo, P.J., Hutmacher, D.W. 2012. Additive manufacturing of tissues and organs. *Prog. Polym. Sci.* 37:1079–1104.

Melcher, R., Martins, S., Travitzky, N., Greil, P. 2006. Fabrication of Al_2O_3-based composites by indirect 3D-printing. *Mater. Lett.* 60:572–575.

Moon, J., Caballero, A.C., Hozer, L., Chiang, Y.-M., Cima, M.J. 2001. Fabrication of functionally graded reaction infiltrated SiC-Si composite by three-dimensional printing (3DP™) process. *Mat. Sci. Eng. A* 298:110–119.

Mortensen, A., Llorca, J. 2010. Metal matrix composites. *Annu. Rev. Mater. Res.* 40:243–70.

Mueller, B., Toeppel, T., Gebauer, M., Neugebauer, R. 2012. Innovative features in implants through beam melting—A new approach for additive manufacturing of endoprostheses. In *Innovative Developments in Virtual and Physical Prototyping*, Leira, Portugal; Taylor & Francis, London, 519–523.

Müller, M., Huynh, Q.-U., Uhlmann, E., Wagner, M.H. 2014. Study of inkjet printing as additive manufacturing process for gradient polyurethane material. *Prod. Eng.* 8(12):25–32.

Murr, L.E., Gaytan, S.M., Martinez, E., Medina, F.R., Wicker, R.B. 2012a. Fabricating functional Ti-alloy biomedical implants by additive manufacturing using electron beam melting. *J. Biotechnol. Biomaterial.* 2(3):1000131.

Murr, L.E., Gaytan, S.M., Martinez, E., Medina, F.R., Wicker, R.B. 2012b. Next generation orthopaedic implants by additive manufacturing using electron beam melting. *Int. J. Biomater.* 2012:245727.

Nikzad, M., Masood, S.H., Sbarski, I. 2011. Thermo mechanical properties of a highly filled polymeric composites for fused deposition modeling. *Mater. Des.* 32:3448–3456.

Ovidiu, G.M., Mirela, T., Radu, P., Dinu, V. 2010. Influence of the lattice structures on the mechanical behavior of hip endoprostheses. In *Proceeding of the 2010 Advanced Technologies for Enhancing Quality of Life, IEEE*, Washington, DC, 6–11.

Parthasarathy, J., Starly, B., Raman, S. 2011. A design for the additive manufacture of functionally graded porous structures with tailored mechanical properties for biomedical applications. *J. Manuf. Process*. 13:160–170.

Polanski, M., Kwiatkowska, M., Kunce, I., Bystrzycki, J. 2013. Combinatorial synthesis of alloy libraries with a progressive composition gradient using laser engineered net shaping (LENS): Hydrogen storage alloys. *Int. J. Hydrogen Energ*. 38(27):12159–12171.

Rehme, O., Emmelmann, C. 2009. Selective laser melting of honeycombs with negative Poisson's ratio. *J. Laser. Micro. Nanoen*. 4(2):128–134.

Ronca, A., Ambrosio, L., Grijpma, D.W. 2013. Preparation of designed poly(D,L-lactide)/nanosized hydroxyapatite composite structures by stereolithography. *Acta Biomater*. 9:5989–5996.

Rumpf, R.C., Pazos, J., Garcia, C.R., Ochoa, L., Wicker, R. 2013. 3D printed lattices with spatially variant self-collimation. *Prog. Electromag. Res*. 139:1–14.

Samuel, S., Nag, S., Scharf, T.W., Banerjee, R. 2008. Wear resistance of laser-deposited boride reinforced Ti-Nb–Zr–Ta alloy composites for orthopedic implants. *Mater. Sci. Eng. C* 28:414–420.

Simchi, A., Godlinski, D. 2008. Effect of SiC particles on the laser sintering of Al–7Si–0.3Mg alloy. *Scripta Mater*. 59(2):199–202.

Singh, R., Singh, S. 2014. Development of Nylon based FDM filament for rapid tooling application. *J. Inst. Eng. C*. doi:10.1007/s40032-014-0108-2.

Sommers, A., Wang, Q., Han, X., T'Joen, C., Park, Y., Jacobi, A. 2010. Ceramics and ceramic matrix composites for heat exchangers in advanced thermal systems—A review. *Appl. Therm. Eng*. 30(11–12):1277–1291.

Stevinson, B., Bourell, D.L., Beaman, F.F. 2008. Over-infiltration mechanisms in selective laser sintered Si/SiC performs. *Rapid Prototyping J*. 14(3):149–54.

Stoica, A. 2009. Robotic Scaffolds for Tissue Engineering and Organ Growth. In *Proceedings of Advanced Technologies for Enhanced Quality of Life*, *IEEE,* Washington, DC, 47–51.

Sun, C.-N., Gupta, M.C. 2011. Effect of laser sintering on Ti–ZrB_2 mixtures. *J. Am. Ceram. Soc*. 94(10):3282–3285.

Tjong, S.C. 2007. Novel nanoparticle-reinforced metal matrix composites with enhanced mechanical properties. *Adv. Eng. Mater*. 9:639–53.

Tjong, S.C., Ma, Z.Y. 2000. Microstructural and mechanical characteristics of in situ metal matrix composites. *Mater. Sci. Eng. R* 29:49–113.

Travitzky, N.A., Shlayen, A. 1998. Microstructure and mechanical properties of Al_2O_3/Cu-O composites fabricated by pressureless infiltration technique. *Mater. Sci. Eng. A* 244:154–60.

Vaezi, M., Seitz, H., Yang, S. 2013. A review on 3D micro-additive manufacturing technologies. *Int. J. Adv. Manuf. Technol*. 67:1721–1754.

Vaezi, M., Srisit, C., Brian, M., Shoufeng, Y. 2013. Multiple material additive manufacturing—Part 1: A review. *Virtual Phys. Prototyp*. 8(1):19–50.

Wahab, M.S., Dalgarno, K.W., Cochrane, R.F., Hassan, S. 2009. Development of polymer nanocomposites for rapid prototyping process. *Proceedings of the World Congress on Engineering*, vol. II, WCE, London, 2009.

Walther, M., Ortner, A., Meier, H., Löffelmann, U., Smith, P.J., Korvink, J.G. 2009. Terahertz metamaterials fabricated by inkjet printing. *Appl. Phys. Lett*. 95:251107.

Wang, F., Mei, J., Wu, X. 2007. Compositionally graded Ti6Al4V + TiC made by direct laser fabrication using powder and wire. *Mater. Design*. 28(7):2040–2046.

Wang, F., Mei, J., Wu, X. 2008. Direct laser fabrication of Ti6Al4V/TiB. *J. Mater. Process. Technol*. 195:321–326.

Wang, X., Tuomi, J., Mäkitie, A.A., Paloheimo, K-S., Partanen, J., Yliperttula, M. 2013. The integrations of biomaterials and rapid prototyping techniques for intelligent manufacturing of complex organs. In *Advances in Biomaterials Science and Biomedical Applications*, 437–463, Rosario Pignatello (Ed.). InTech, Croatia.

Weisensel, L., Travitzky, N., Sieber, H., Greil, P. 2004. Laminated object manufacturing (LOM) of SiSiC composites. *Adv. Eng. Mater*. 6(11):899–903.

Wilson, J.M., Shin, Y.C. 2012. Microstructure and wear properties of laser-deposited functionally graded Inconel 690 reinforced with TiC. *Surf. Coat. Tech*. 207:517–522.

Wohlers, T. 2010. Additive manufacturing a new frontier for composites. Composites Technology. http://www.compositesworld.com/columns/additive-manufacturing-a-new-frontier-for-composites (accessed May 22, 2014).

Xiong, Y., Smugeresky, J.E., Ajdelsztajn, L., Schoenung, J.M. 2008. Fabrication of WC–Co cermets by laser engineered net shaping. *Mater. Sci. Eng. A* 493(1–2):261–266.

Xue, W., Krishna, B.V., Bandyopadhyay, A., Bose, S. 2007. Processing and biocompatibility evaluation of laser processed porous titanium. *Acta Biomater.* 3(6):1007–1018.

Yakovlev, A., Trunova, E., Grevey, D., Pilloz, M., Smurov, I. 2005. Laser-assisted direct manufacturing of functionally graded 3D objects. *Surf. Coat. Tech*. 190:15–24.

Yan, C., Hao, L., Hussein, A., Bub, S.L., Young, P., Raymont, S. 2014a. Evaluation of light-weight AlSi10Mg periodic cellular lattice structures fabricated via direct metal laser sintering. *J. Mater. Process. Technol*. 214:856–864.

Yan, C., Hao, L., Hussein, A., Raymont, D. 2012. Evaluations of cellular lattice structures manufactured using selective laser melting. *Int. J. Mach. Tool. Manu*. 62:32–38.

Yan, C., Hao, L., Hussein, A., Young, P., Raymont, D. 2014b. Advanced lightweight 316L stainless steel cellular lattice structures fabricated via selective laser melting. *Mater. Design*. 55:533–541.

Yan, C., Hao, L., Xu, L., Shi, Y. 2011. Preparation, characterisation and processing of carbon fibre/polyamide-12 composites for selective laser sintering. *Compos. Sci. Technol*. 71:1834–1841.

Yan, C.-Z., Shi, Y.-S., Yang, J.-S., Liu, J. 2009. Nanosilica/Nylon-12 composite powder for selective laser sintering. *J. Reinf. Plast. Compos*. 28(23):2889–2902.

Yang, J.S., Shi, Y.S., Shen, Q.W., Yan, C.Z. 2009. Selective laser sintering of HIPS and investment casting technology. *J. Mater. Process. Technol*. 209:1901–8.

Yang, L., Cormier, D., West, H., Harrysson, O., Knowlson, K. 2012a. Non-stochastic Ti–6Al–4V foam structures with negative Poisson's ratio. *Mater. Sci. Eng. A* 558:579–585.

Yang, L., Harrysson, O., West, H., Cormier, D. 2012b. Compressive properties of Ti–6Al–4V auxetic mesh structures made by electron beam melting. *Acta Mater.* 60:3370–3379.

Yin, X.W., Travitzky, N., Greil, P. 2007. Three-dimensional printing of nanolaminated Ti_3AlC_2 toughened $TiAl_3$-Al_2O_3 composites. *J. Am. Ceram. Soc*. 90(7):2128–34.

Yin, X.W., Travitzky, N., Melcher, R., Greil, P. 2006. Three-dimensional printing of $TiAl_3/Al_2O_3$ composites. *Int. J. Appl. Ceram. Technol*. 97(5), 492–8.

Zhang, W., Melcher, R., Travitzky, N., Bordia, R.K., Greil, P. 2009. Three-dimensional printing of complex shaped alumina/glass composites. *Adv. Eng. Mater.* 11(12):1039–43.

Zhang, W., Travitzky, N., Greil, P. 2008. Formation of $NbAl_3/Al_2O_3$ Composites by pressureless reactive infiltration. *J. Am. Ceram. Soc*. 91(9):3117–3120.

Zhang, Y., Hao, L., Savalani, M.M., Harris, R.A., Tanner, K.E. 2008a. Characterization and dynamic mechanical analysis of selective laser sintered hydroxyapatite-filled polymeric composites. *J. Biomed. Mater. Res. A* 86A:607–16.

Zhang, Y., Wei, Z., Shi, L., Xi, M. 2008b.Characterization of laser powder deposited Ti–TiC composites and functional gradient materials. *J. Mater. Process. Technol*. 206:438–444.

Zhang, Y.Z., Sun, J.C., Vilar, R. 2011. Characterization of (TiB+TiC)/TC4 in situ titanium matrix composites prepared by laser direct deposition. *J. Mater. Process. Technol*. 211:597–601.

Zheng, B.L., Topping, T., Smugeresky, J.E., Zhou, Y., Biswas, A., Baker, D., Lavernia, E.J. 2010. The Influence of Ni-coated TiC on Laser-deposited IN625 metal matrix composites. *Metall. Mater. Trans. A* 41:568–73.

Zheng, H., Zhang, J., Lu, S., Wang, G., Xu, Z. 2006. Effect of core-shell composite particles on the sintering behaviour and properties of nano-Al_2O_3/polysterene composites prepared by SLS. *Mater. Lett*. 60(9–10):1219–1223.

Zhong, W., Li, F., Zhang, Z., Song, L., Li, Z. 2001. Short fiber reinforced composites for fused deposition modeling. *Mater. Sci. Eng. A* 301(2):125–130.

12

Additive Manufacturing in Education

Kirk A. Reinkens

CONTENTS

ABSTRACT Engineering education consistently has a goal to produce innovative, hands-on engineers who are familiar with the latest technologies and have the ability and skill to implement them in their work places. Additive manufacturing techniques continue to be a growing consideration and a necessary experience that students should incorporate into their problem-solving and design strategies. The steps demonstrated here share the experience involved in transforming a portion of a design experience through incorporation of additive manufacturing. The author's prior experiences and strategies are described in detail. The key considerations of curricular, equipment, and instructional goals are shared in the context of modifying an energy conversion experiment. The successes and challenges of implementating a more thorough design activity, which includes student printed and evaluated solutions, are discussed in detail. The student rotor-impeller designs proved to be a good modification to the previous project. It continues the exploration of energy conversion concepts and adds a meaningful element of student-driven design choices. The activity provides a highly quantifiable comparison of original and student impeller designs. Additional samples of how additive manufacturing has been applied in classrooms as a part of student projects and to extend research opportunities are also discussed. Additive manufacturing continues to have a transformative effect on engineering and engineering education. Our efforts to explore and incorporate these techniques into our classrooms and make them more readily available to students will continue to enhance their education. Students with meaningful hands-on and design experiences, including the use of additive manufacturing, will be engaged and well prepared for the work place.

12.1 Introduction

As a relative newcomer to the application of additive manufacturing in education, I am consistently amazed by the nearly weekly requests I have for a *quick tutorial* on using the 3D printer I happen to have at my disposal. I'll share the details of my own transition from copycat to an unexpected resource. I had been away from engineering for several years and my exposure to 3D printing was limited. In the late 1980s, I had observed an early stereolithography machine implemented in a model shop at The Boeing Company. More recently, I had visited Louisiana Tech University to gather ideas for my course and they had implemented 3D printing into their efforts successfully. Since then I have been fortunate enough to have access to equipment available on campus and subsequently was able to purchase a good quality Dimension uPrint SE machine. The printer has added to both my experience and that of those around me. In my work throughout the college, I have had the chance to offer its use to individual students, clubs, and teams, as well as graduate and faculty researchers. The ways in which others are working to learn more about the processes and are applying them in their teaching and projects is invigorating. I hope you will consider these descriptions as samples of how I have been drawn into additive manufacturing and consider how you might explore possibilities in your own situation. I hope you will look for the ways in which additive manufacturing might expand learning in your classroom and provide opportunities for students to explore key concepts and their own innovations.

12.2 Application of Additive Manufacturing in Engineering Education: An Example

12.2.1 ENGR 120: Innovation in Design

Washington State University (WSU) continues its adaptation and development of the content and experiences within the context of our "ENGR 120: Innovation in Design" course. This course serves approximately 500 students a year. Students are a majority of our entering engineering majors whose interests include bioengineering, civil, mechanical, and electrical engineering disciplines. The instructors often include a variety of staff, graduate students, and faculty from these disciplines. This course meets weekly for students as a part of a typical first year program of introductory calculus and general chemistry. Over the previous five semesters, the program has been adapting curriculum more heavily toward a hands-on experience. Course modifications offer students the opportunity to take more ownership of their learning by increasing hands-on experiences. The course format and delivery continues to adjust. The most recent structure adopts a flipped classroom approach. Online lectures and other resource materials provide the foundation for students' initial exposure to the covered materials and laboratory activities. A traditional, weekly 2 hour 50 minute laboratory emphasizes the hands-on experiences necessary for students to explore their understanding as well as design and test their solutions. Each section of the course supports up to 42 students working in three person teams. This leads to a high level of interaction within and among the teams. To address some of the challenges that arise in management, the laboratory incorporates the use of peer mentors in the

classroom to enhance the support structure for the students. These peer mentors are junior and senior level certified majors who serve as resources for new students and support instructional expectations.

The incorporation of additive manufacturing began with the replication of the pump impeller design activities of Louisiana Tech University. These have since been modified for our implementation and extended to a student-driven design challenge. Work continues to identify ways in which students' understanding and individual ideas can be further promoted through new experiences in additive manufacturing.

12.2.1.1 Course Content

WSU had previously implemented a group of two-week projects and activities that addressed concepts across a variety of disciplines in a more traditional classroom. These experiences were selected to address the interests of our programs and faculty. Among the topics were; material properties, energy efficiency of geared mechanical systems, programming and control of small robots, and electrical concepts of sensors. Our adoption of a "Fish Tank Control System" project brought many of these concepts together as part of a larger system. One of the attributes of this system exploration is the connectedness that can be demonstrated to students across content and programs. Here concepts and experiences that cut across disciplines are provided in hopes of highlighting the individual value of the knowledge and understanding. This project allows students to explore a subsystem within the larger system and consider the influence of design choices on overall performance of a system. The performance of a motor and pump subsystem is often characterized by its efficiency with respect to the factors that influence its operation. Additive manufacturing offers the opportunity for students to make design choices and implement them for performance comparison reasonably quickly.

12.2.1.2 First Efforts

In summer 2009, WSU's course coordinator attended the National Science Foundation (NSF)-funded workshop hosted by Louisiana Tech University. The workshop provided an introduction to how the "Living with the Lab" program can be implemented. Although exciting, the path to this level of change would take time and a spring 2011 pilot was planned. Over the following year, curriculum development and activity modifications were made to fit within WSU course format. Included in the curriculum were the following: materials testing and beam design, programming of LEGO® microcontroller-based robots, electrical circuits and cascaded switching, motor and pump performance, and temperature and salinity sensor calibration. Final work of the students included explanation and demonstration of the control systems ability to maintain and adjust the tank temperature and salinity within a specified range.

Additive manufacturing was incorporated at a very modest level during the initial work. Figure 12.1 shows the original configuration of the motor and centrifugal pump. Pump performance activities were postponed until later in the term to provide time to prepare pumps and test fixtures consistent with that demonstrated during the original workshop. The centrifugal pump configurations allow students to easily visualize the performance of the pump and relate directly to the experimental data. Students were introduced to 3D using Google's SketchUp Make. Figure 12.2 shows a sample SketchUp Make drawing of the pump housing and impeller. This activity allowed students to disassemble, practice measurement, and reassemble the motor and pump. Using those measurements, students

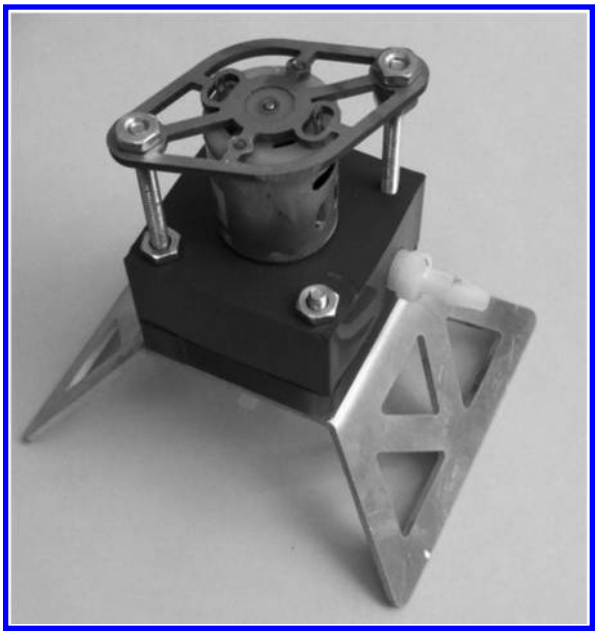

FIGURE 12.1
Original motor and centrifugal pump configuration.

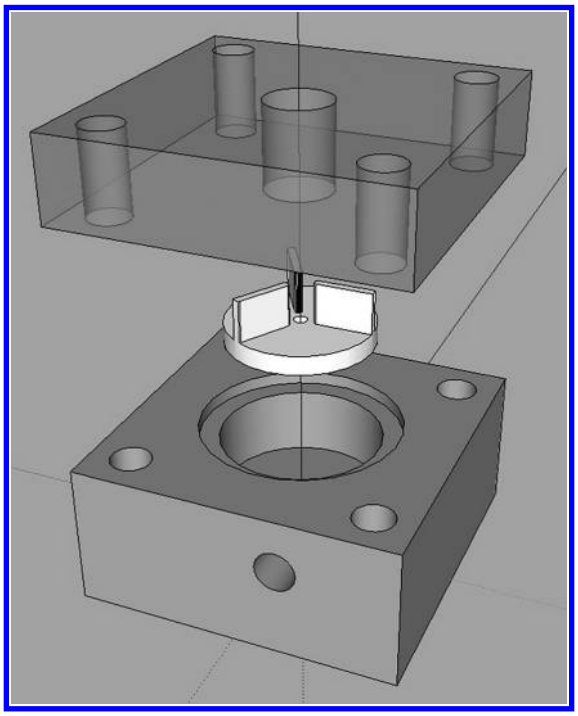

FIGURE 12.2
Sample pump housing drawing, created using SketchUp.

worked through the drawing process. Without the committed use of a 3D printer, we could not offer the opportunity for students to print their own impellers. The impellers used by students were printed on campus using equipment typically used for research. Figure 12.3 shows the motor and pump test configuration. The test fixture provided students the opportunity to complete an experiment characterizing the efficiency of motor–pump system. Electrical measurements of the applied power to the motor–pump combination were taken while also measuring the mechanical energy transfer to the water in the form of kinetic and potential energy. The resulting efficiency and flow rates were presented as functions of the varying head height of the system under test. Figure 12.4 shows sample efficiency and flow rate performance data.

The difficulties with the activity were centered on areas that drew emphasis away from the connections between design and performance. Typical student observations from the experiments noted the difficulties in completing the electrical measurements of voltage and current. Also mentioned were the sometimes prominent leaks that occurred at the pump assembly. From the instructor perspective, these kinds of concerns can be qualified as *good experiences* for students, helping them recognize that the design of the entire

FIGURE 12.3
Efficiency and flow rate test configuration.

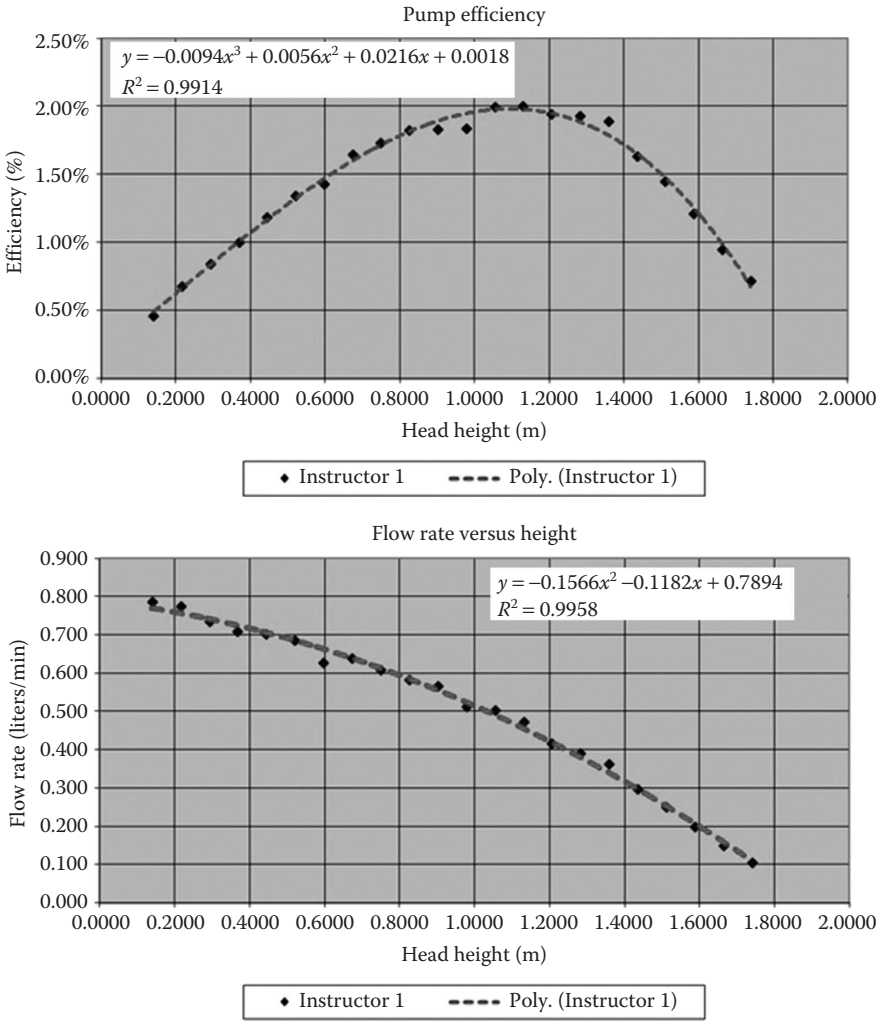

FIGURE 12.4
Example efficiency and flow rate graphs.

system contributes to more successful solutions. Alternatively, when problems occur with the equipment it can be seen as an obstacle to students' learning. As an obstacle, it can draw attention away from the concepts, which are the underdevelopment in the course. These weaknesses provided an opportunity to expand the adoption of additive manufacturing and an initial design experience.

12.2.1.3 Continuing Efforts

This activity was originally intended to emphasize energy conversion concepts. This focus was emphasized over the next few semesters. Data collected by students were usually of a quality and consistency that allowed them to arrive at interpretations of efficiency and flow rate consistent with key concepts. The availability of a new uPrint SE 3D printer brought new opportunities to address some of the activity's weaknesses.

During testing, the increased head pressure often created significant leaks that clearly impacted performance and would also intrude on the electric motor causing damage to the system. Time constraints of the class prevented us from handing over development of a solution for these problems to the students as an activity.

The instructors chose to practice with the new printer and develop their own solutions to some of the classroom equipment problems. The redesign addressed three areas observed as problems to our classroom activities: (1) the need to create separation between the motor and impeller to help avoid water contamination of the motor; (2) the tendency of students to make electrical connections on the motors that created short circuits for operation or measurement; and (3) the inability for students to easily replace original impeller with their own designs. The simplicity with which SketchUp Make allowed the creation of a solution and the export of the design for printing was a great experience for the instructors. Figure 12.5 shows the new configuration with three printed parts: an elevated motor mount to separate the motor from the pump housing, a non-conductive retainer to prevent the motor from spinning and unwanted electrical shorts during student measurement, and a shaft coupler incorporating set screws. As with most designs it met with varied success. The electrical concerns were eliminated while the mechanical solutions produced tradeoffs. The motor mount worked very well while the coupler between the motor and impeller shafts was more difficult to configure for testing and the 3D printed material of the coupler was not well suited for the set screw applications. Again, this experience was an engaging effort for instructors.

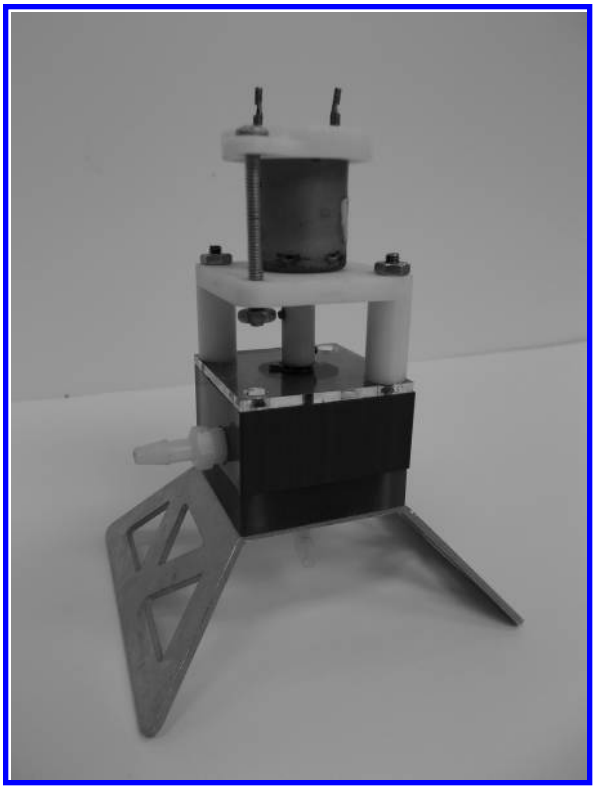

FIGURE 12.5
Instructor designed motor pump configuration.

An initial design experience was also incorporated for students. Drawing exercises focused on the replication and/or redesign of the impellers for these pumps. This did include the expectations that the parts would be 3D printed and available for testing along with the original impellers. The experience and demonstrated skills in creating drawings and preparing the necessary stereolithography files were both engaging and reinforcing to the goals of the course. The printing experience was very well received by students. Three-student teams selected a single impeller design for printing. Students were not directly involved in the printing process. The success of the printed items varied but many impellers were suitable for use in the pumps. Figure 12.6 shows an example of the variety of designs produced by students. Pitfalls arose in combination with the installation and pump operation. Student teams were rarely able to configure, install, and test their impellers during the available class time. The mechanical assembly of the impeller, pump, and motor was more difficult to configure for successful operation.

In parallel with this activity, performance testing of simple commercial fountain pumps was also incorporated. These pumps would be used during other activities the remainder of the semester. This choice addressed the leaking water problems of the classroom pumps and simplified the necessary electrical connections. This allowed students to focus on the other concepts and programming the final demonstration of their ability to monitor and control both temperature and salinity within the system model.

Having students experience the clear influence of their design choices was still a goal for curricular changes. The difficulties of electrical wiring and measurement, along with time limitations that prevented this, led to consideration of other options. The simplicity of the commercial fountain pumps and our new experiences with the 3D printer led us to bring the two together.

12.2.1.4 Simple, Manageable, Measureable

A small variety of commercial fountain pumps were in preliminary use. These submersible pumps have sealed electrical connections and incorporate a magnetically coupled rotor and impeller design. Figure 12.7 shows an example of the fountain pump in use

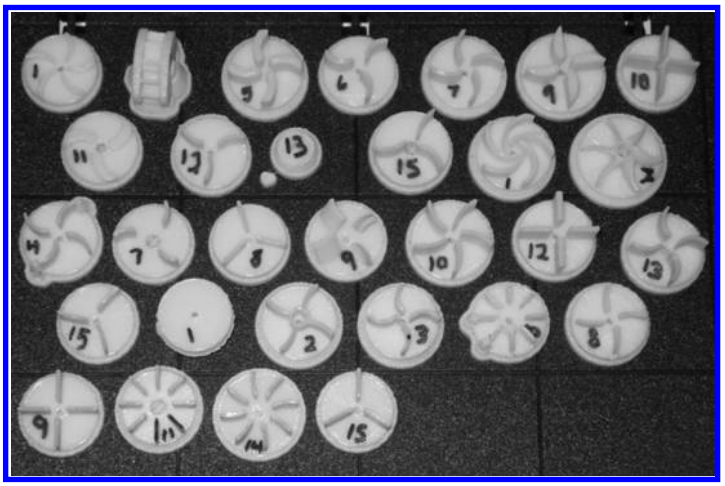

FIGURE 12.6
Example student impeller designs.

FIGURE 12.7
Sample fountain pump with stock impeller.

and the stock impeller design. The rotor-impeller assembly consists of a cylindrical ceramic magnet around its rotating shaft. This magnet is polarized across its diameter. The impeller is incorporated on the end of the rotor and aligned with the axis of rotation. The assembly slides neatly on a centering shaft within the motor-pump housing. The larger and more commonly available pumps were selected for classroom use. These pumps also used a larger rotor-impeller assembly and made final student assembly much easier. Some primary design choices were necessary to help ensure students could focus on design and printing of their chosen impeller designs. As a replacement to the cylindrical magnets, we found small inexpensive magnets that worked well with an alternative design for the rotor-impeller shaft. Figure 12.8 shows a SketchUp drawing of the original design for the rotor-impeller assembly and an alternative rotor design planned for

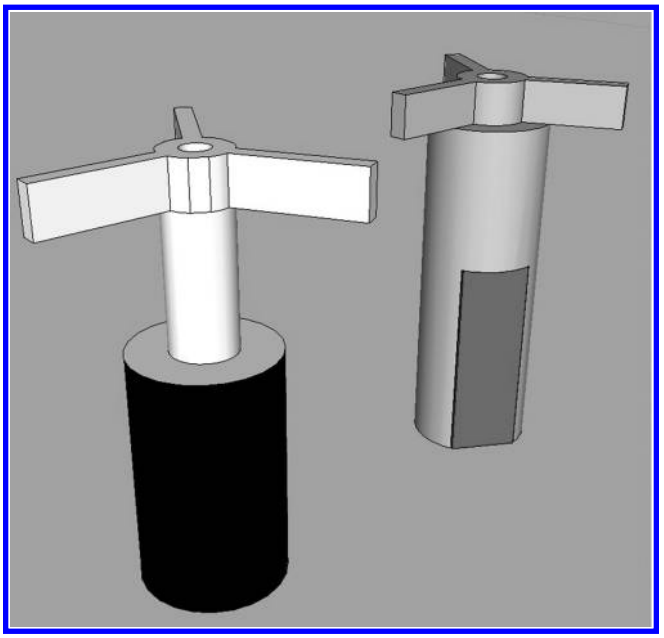

FIGURE 12.8
Sample drawing original rotor-impeller design and planned alternative rotor design.

student use. A few instructor designed practice prints and limited testing proved that the end products could work very well as replacements to the original rotor-impeller assembly. Additionally, these designs could be printed in batches for each course section within a few hours and were of high enough quality and durability to be successful for most student designs.

12.2.1.5 Revised Design Challenge

Starting from the instructor experience, the student experience could be expanded to incorporate a more complete design process, which included individual 3D printing. As a primarily mechanical engineering challenge, the examination of the efficiency and flow rates of the pumps has practical application across the disciplines. The use of the free educational versions of SketchUp Make program as a tool of design helps make 3D drawing highly accessible to all students. The addition of SketchUp Make plug-ins allowing students to export drawings as stereolithography files closes the cycle. The result is that students have the ability to review designs and address errors or defects in form and fit. This is followed by a second opportunity for printing prior to performance testing.

Expectations for the design process now include the following:

1. *Pump concept review*: Students are provided with introductory reading and video materials discussing key concepts to consider in centrifugal pump design. The overview is on primary physical characteristics: volute casing, suction eye, impeller size, vane shape, tongue, and discharge configuration. The emphasis for first design choices is placed on impeller size and vane shape. Extension activities include the possibility of creating inserts to modify the housing for improved performance. Students should demonstrate consideration of these concepts in development of their design modifications.
2. *Measurement*: Students disassemble the fountain pumps and work with digital calipers to capture the measurements necessary for creating drawings of the original impeller and the motor-pump housing. These measurements allow them to recreate the designs and consider the geometry and function of the housing and impeller to determine what changes they might incorporate in a new design. A brief discussion of geometric dimensioning and tolerancing provides an initial exposure to having measurements, drawings, and printing result in working solutions. The tolerances are very flexible in this project and most designs that follow the general guidance can be effectively tested and performance compared. Students' final designs should demonstrate attention to the measurements of the original equipment.
3. *SketchUp Make drawings*: Students apply their measurements and work together to develop individual drawings of the original impeller. This is followed by students recreating the required instructor designed base and subsequently developing their own modifications to the impeller design. This is primarily a software learning experience where students become more comfortable working in computer-aided design and creating meaningful representations of design ideas. Teams review each other's drawings verifying required dimensions and looking for defects that might prevent the part from addressing the form, fit, and function necessary. Students are provided checklists for review, including items such as incorrect dimensions, missing faces, or other items that will affect the quality of the 3D printed part. Students follow the export procedures and file naming

conventions established for the course. The resulting *.stl files are submitted for initial 3D printing.

4. *3D printing, review, and redesign*: Student files are collected and submitted for group printing. Non- *.stl files or files with significant errors are returned to student with comments. Instructor or peer mentor meetings are available to review drawing concerns. Successful prototypes are returned to students. Figure 12.9 shows examples of student-designed impellers. Students complete a review of printed design to verify form, fit, and function. Key features must allow magnets to fit securely on the assembly; rotor-impeller assembly must fit within housing and spin freely on centering shaft; impeller design must fit within the housing cover and accommodate any housing modifications. Designs with file errors or other design concerns are allowed to make corrections and request follow-up printing.
5. *Final assembly, testing, and evaluation*: Students complete individual assembly of prototype designs. Figure 12.10 shows the revised motor-pump test configuration. The changes from the first test configuration (Figure 12.3) allow the original and student-designed rotor-impeller designs to be evaluated quickly. Teams complete efficiency and flow rate data collection across the working head height of the motor-pump assemblies. Figure 12.11 shows a sample of the graphs resulting from student collected data. Graphs compare performance of individual designs alongside the original impeller. Students and teams make observations related to key pumping concepts, highlighting the strengths and weaknesses of designs, and suggest recommendations for design choices that could lead to improved performance.

FIGURE 12.9
(See color insert.) Sample student rotor-impeller designs.

FIGURE 12.10
Revised efficiency and flow rate test configuration.

12.2.1.6 Activity Review

The changes to this portion of the Fish Tank Control System project effectively maintained the emphasis as an experience in energy conversion. The addition of a more thorough design experience was well received by students and managed fairly easily by instructors. The combination of hands-on measurement activities, computer-aided drawing, and 3D printing brought together practical skills and experiences that provide a basis for students to move forward with their own designs more readily.

The modifications of the classroom equipment and procedures helped place an emphasis on conceptual understanding and the student experience in additive manufacturing. The choice to move to commercial fountain pumps addressed weaknesses of previous activities. The electrical energy input measurements can now be completed more easily without the need to incorporate wiring activities, which are covered more carefully at another time during the course. Although the time spent removing and installing impellers in the previous design provided a good hands-on activity, the simplicity of the submersible pump greatly reduced time necessary for students to prepare for and complete the data collection. The reduced pumping characteristics of these pumps also made it possible to move the experience to a desktop configuration.

Evaluation of student performance should focus on goals for the lessons at hand. This is an introductory course that focuses on building and connecting student experiences to introductory concepts. A combination of assessment methods is used in this

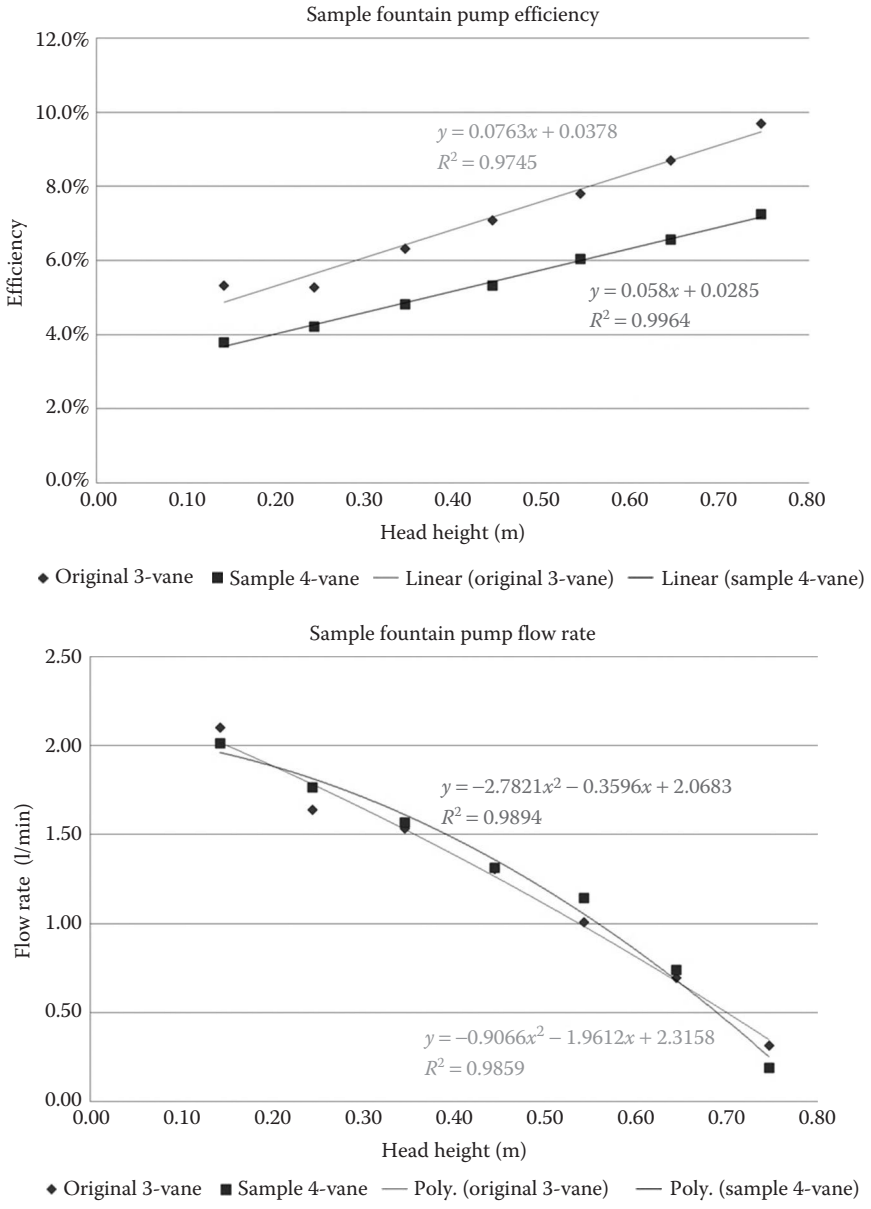

FIGURE 12.11
Example performance comparison graphs.

situation. During classroom activities, students are expected to demonstrate skill with both measurement and drawing with the desired software. The culminating expectations of the project are the preparation of a brief powerpoint slideshow that includes; a summary of the design choices and a connection to the pump concepts, a presentation of test data and the resulting comparison of the original rotor-impeller and the student design, and finally responses to a group of conceptual questions centered on the topics as hand. Included within the project outcomes are the expectation that each student

successfully submit a rotor-impeller design for printing that is distinct from the original design and their teammates' designs.

There are a range of challenges to implementing meaningful additive manufacturing activities into a classroom setting. The selection and availability of equipment is foremost in the challenges for making change. The uPrint SE machine offered much flexibility to the changes in this course. The additional expense for this equipment provided high durability, ease of operation, and the quality of final products that made changes very manageable. The format of this course as primarily an application or laboratory course also offered greater flexibility. Within that structure, there was a need to choose a project or modification whose complexity would fit within the available time constraints. This includes consideration of the scope of the student design portion of the project and selecting the level of *coaching* needed for students to succeed in the activity.

12.3 An Extension Activity: A Robot Design Challenge

This course also continues to adapt the student additive manufacturing experience related to co-curricular projects. In addition to the central Fish Tank Control System content, an element of professional and personal development is included. All students purchase, assemble, and practice programming a simple robot. Figure 12.12 shows the original robot configuration. This robot is used during class to develop and practice programming and

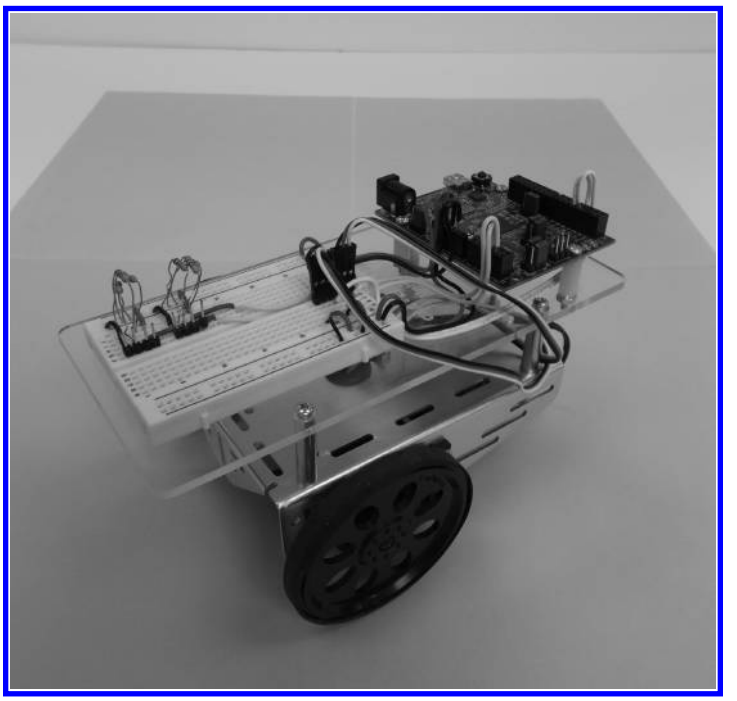

FIGURE 12.12
(See color insert.) Original student robot configuration.

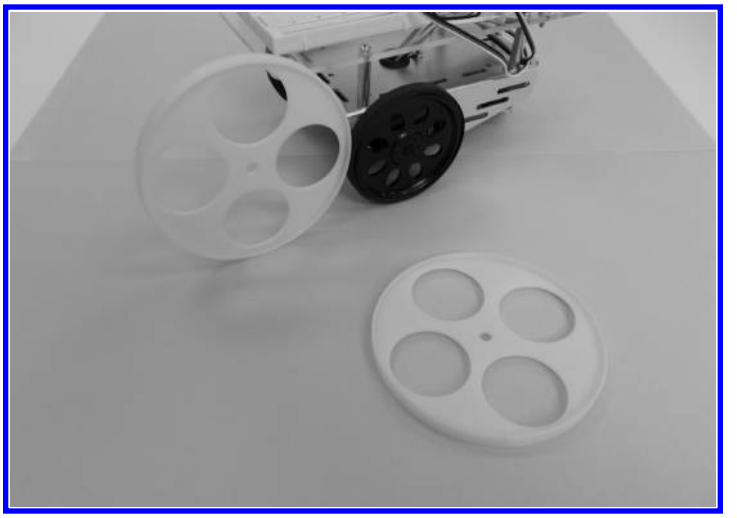

FIGURE 12.13
Example student wheel design.

control methods applied later to the Fish Tank Control System. Additionally, teams of 4–6 students are challenged to complete a line-following robot project. The project involves three areas of design: increasing robot speed through new wheel design, adding sensors and programming for line-following, and design and fabrication of a small bridge to be included in the solution.

The challenge of increasing robot speed is primarily an extension application of additive manufacturing. Team members undertaking this portion of the project must test the original robot to explore the programming, servo rotation characteristics, and wheel dimensions. Students must subsequently design a new wheel, predict the performance of design, and test and compare the results. The project requires that the wheel be designed to work with extra servo arms available with the robot kit. Performance of the design is evaluated by two factors: average vehicle speed measured over a fixed distance and wheel design measured by mass. The performance score is determined by the greatest ratio of speed to wheel mass. Figure 12.13 shows an example student wheel design. The experience and understanding gained as well as the final product must also be combined with the other team designed elements to complete the final line-following challenge for additional performance evaluation.

This activity provides another opportunity for students to engage in design and the application of additive manufacturing. The expectations that performance modeling as a preliminary activity and physical characteristics of the final product are important elements in initial design experiences.

12.4 Beyond This Classroom

In the preparation of new engineers, engineering education is often discussed as a combination of academic and extracurricular experiences. In addition to the example provided here, a few other examples of academically oriented projects have benefited from

application of additive manufacturing. Computer-aided design courses often incorporate the practical experiences of printing a part to bring a design to life. These activities can help validate for students the need for a variety of mechanical design features and develop greater familiarity with form, fit, and function when developing mating components. Machine design and fabrication courses explore and compare traditional manufacturing technique with those involved in additive manufacturing. The course content often explores geometric dimensioning and tolerances concepts at a much more complete level aiding student in understanding of the complete design process. Other faculty have taken advantage of additive manufacturing tools to create equipment for demonstration or laboratory use to update their curriculum in conceptual areas that are more challenging for students. Finally, the wide adoption of senior design projects as graduation requirements continues to benefit from additive manufacturing. The needs in these areas vary significantly. Students without formal computer-aided design (CAD) experience can adopt more simplified tools and prepare prototypes to support the development of the concepts of their design. More advanced students will often go through many iterations employing additive manufacturing. The shortened cycle between design changes help students produce more thoroughly prepared designs and higher-quality final products.

Student participation in extracurricular clubs, teams, competitions, and their own personal projects has long been a recognized benefit to expanding student practical experiences in engineering and problem solving. Producing good quality projects can be very difficult for students with few or no fabrication experiences. Even engaged and eager students might spend hours learning how to use traditional machine fabrication skills and make errors that prevent their finished product from being useful. The rapid prototyping ability of additive manufacturing allows students the luxury of speed with the possibility of some trade-offs in function. Examples include front and rear differential housings for small radio-control vehicles, preliminary designs of paddle shifters for full-size race vehicles, scale prototypes for an aircraft propeller system with variable pitch control, and fixtures to improve quality and streamline assembly of an individual student project. Students across engineering disciplines and across the college or university setting can engage in entrepreneurship, using additive manufacturing to communicate and advance new or novel ideas. Graduate students and researchers are also commonly exploring the fringes of their disciplines in engineering and beyond. When introduced to additive manufacturing, it can become another tool of scientific discovery for their work. Fabrication shops supporting research can often meet unexpected needs for unique designs through these fabrication methods.

12.5 Concluding Remarks

Depending on the classroom format, additive manufacturing provides the opportunity to transform classroom experience. Even a well done experimental laboratory that incorporates significant analysis and connections to practical applications can see real benefits. The availability of the additive manufacturing combined with the simple-to-learn modeling software allows students to develop realistic design solutions for mechanical systems early in their academic career. Restructuring the activities to incorporate and emphasize student development of alternative rotor-impeller designs allows for comparison of solutions with meaningful measurements of design performance. Providing students the

opportunity to put their ideas to work provides greater empowerment and encourages them to consider how their background knowledge and new concepts can be applied.

The impact of additive manufacturing on retention of students in engineering curriculum can be inferred. The factors that affect retention in engineering programs span a wider array of topics including, but not limited to, socioeconomics, demographics, curriculum and instruction, and student engagement and experiences. Additive manufacturing allows programs to incorporate more engaging opportunities to impact students both within the curriculum and beyond. These changes can help contribute to an individual student's desire to continue and obtain their engineering degree. Curricular change that enhances the quality and effectiveness of instruction can be powerful. Additive manufacturing continues to provide the opportunity for faculty to develop inexpensive demonstration and laboratory activities that positively impact the student experience. Most recruiters have heard from well-qualified students that they "… want to work with their hands and design (something)." Often students are discouraged with engineering curriculum and the lack of hands-on experiences, particularly in the first years. Some students have added participation in engineering clubs and teams as an opportunity to enhance their student experience. Additive manufacturing has been, and will continue to be, applied in these extracurricular experiences.

Keeping up with the technology development and propagation of additive manufacturing will likely make it more challenging for institutions to incorporate new equipment in a timely fashion. It can be expected that the speed of development and adoption of additive manufacturing throughout the disciplines will continue. The availability and development in the public sector as commercial enterprises will also continue to power the greater adoption of newer processes for a wider array of applications. The technological advances in the various forms of additive manufacturing will continue to provide exciting opportunities throughout engineering applications. The reach of those opportunities extends to our own educational pedagogy and teaching strategies in engineering education.

13

Personalized Implants and Additive Manufacturing

Mukesh Kumar and Bryan Morrison

CONTENTS

ABSTRACT Additive manufacturing is fast gaining a presence in the manufacturing of personalized medical implants. This chapter discusses the use of additive manufacturing and necessary imaging technology for the generation of custom orthopedic implants with patient-specific designs. The chapter discusses how existing regulations can be adopted to address and mitigate some of the risks associated with medical device manufacturing. However, recognizing that the field of additive manufacturing in orthopedic implant manufacturing is relatively new, the chapter initiates the reader into the realm of medical device regulations. Moreover, the chapter discusses the processing steps necessary in the making of various instruments and implants. Many opponents of the technology raise

the issue of cost as a reason not to embrace this technology. This chapter addresses the question of cost by comparing the processing route of an implant via traditional methods to that via the additive manufacturing method. Such comparison gives the true estimate of cost and therefore the real value of additive manufacturing for personalized medicine. Further, the chapter exposes the reader to various modalities and limitations of imaging techniques and their role in generating the necessary patient-specific designs that will become additive manufactured parts. As the field of additive manufacturing is still relatively new, there is the need for supporting quality control technology that must mature to provide the necessary confidence in implant performance for wider acceptance. This chapter calls out such emerging quality control technology and how supporting technology that exists today could be adapted to help alleviate such misgivings. The chapter closes with the authors' imagination of the future of orthopedics and personalized implants, instruments, and guides.

13.1 Introduction

Additive manufacturing has opened a new manufacturing path to design and manufacture personalized products—this chapter focuses on one such segment of personalized products, namely, medical implants and associated instruments, with greater emphasis on implants for large joints, although great strides have been made and clinically implemented in the field of dentistry. The field of medical implants is not new—implants such as prostheses for joint replacements have been around for a long time. To some extent, some of these have already been personalized using traditional manufacturing methods. For example, the market can already boast of patient-matched implants, although limited to select patients with unusual boney defects or anomalies due to disease, functional deformity, or tumor resection. In these cases, a computed tomography (CT) or magnetic resonance imaging (MRI) scan of the patient is used to assess the dimensions of the bone defect, and a physical bone model of the defect is created. Using this physical model and the patient's CT or MRI scan, a personalized implant is designed and eventually machined using conventional methods. Normally, the machined implant and the physical bone model are shipped to the hospital where the surgeon can use the bone model to help determine the best placement of the implant. While clinically successful, this path to manufacture implant can be time consuming and involves a lot of waste of raw material. Moreover to some extent, the surgical outcome is dependent on the ability of the surgeon to place the implant at the correct location and with the correct orientation, using the provided plastic bone model as a preoperative visual and tactile aid. Additionally, if possible, but perhaps as important as the implant itself, making use of additive manufacturing could better facilitate the design and manufacture of patient-specific instruments and surgical guides that could help the surgeon position the implant accurately.

Recognizing that the field—and regulations—of additive manufacturing is still developing, the intention of this chapter is to expose the reader to the various nuances of medical implants, specifically those related to orthopedics and considerations of various aspects involved in the personalization and manufacture of such devices using additive manufacturing. The chapter closes with some thoughts on the future of additive manufacturing technology specifically as it relates to personalized medical implants and instruments.

13.2 Path to Clinical Use

Prior to clinical use, implantable devices must clear regulatory approval processes that vary by country. The following is a very simplified explanation of medical device regulations and how they could affect personalized medical products. The reader must realize that it takes time to gather information, understand implications of various aspects of new technology, and build consensus between researcher, corporations, and regulatory bodies—regulations almost always tend to follow technology. The reader is cautioned that medical device regulations are vast, complicated, and vary between countries. Additionally, the best place to obtain the latest on regulations, guidance documents, and standards on medical devices is the official Food and Drug Administration (FDA—United States), European Commission, and ISO (International Standardization Organization) websites.

In the United States, medical devices are classified according to the level of risk to patients. Generally, class I devices include tongue depressors; however, orthopedic implants fall under either class II or class III based on the level of risk and potential unknowns. Class II devices require the design holder to demonstrate that the proposed device under scrutiny is *substantially equivalent to* previously cleared device. If the proposed device is *substantially equivalent to a previously cleared device*, the characteristics of the device are relatively well known and thus the level of risk is known and risk mitigation procedures are well understood. At least for orthopedic implants that are not similar to previously cleared devices—and are thus associated with a higher level of risk—a separate classification is used. This class III category has a regulatory path that is extremely challenging and time consuming, sometimes running in years.

Among other things, regulations pose a challenge for the device design holder in adopting the use of additive manufacturing in making patient-specific instruments and devices—how to obtain regulatory approval for personalized implants for patients that generally perform the same function but are potentially shaped different to meet the anatomical and possibly the biomechanical requirements of a particular patient? This regulatory requirement becomes more complicated, as the quest for personalization involves greater complexity—it is conceivable that medical devices can be tailored to the patient's anatomy, bone density, cancellous bone pore structure, and possibly coating with specific antibiotic, peptides, and other personalized biomolecules. Advent of additive manufacturing technology definitely brings close the possibility of making implants that not only match the anatomy of the patient, but can also be used to manufacture implants with density that changes with location, thus effecting mechanical properties and thus the biomechanics of the implant reconstructed site. Implants could be manufactured with variations in porous ingrowth surfaces to achieve varied amounts of biological fixation. One can argue as to the need for such variations—but the fact remains that current state of additive manufacturing technology can deliver such implants. Unfortunately, at the time of writing this chapter, existing regulatory framework is not well tailored to accommodate the potential of this technology. Regulators realize the potential of additive manufacturing and its capability to create personalized implants. Robust and well-crafted regulations will eventually follow. However, a logical approach could be to lay down regulations for *low-risk products* and gradually expand regulations to include higher risk products. It is for this reason that personalized instruments and fixtures to help correctly place implants are currently available, whereas higher risk personalized implants are under development waiting for regulations. Until then, answering the question *what can additive manufacturing techniques make that can be safely used in the operating room (OR) with minimal risk* will help determine

what products can be brought to the market with minimal risk of regulatory rejection. Of course, these devices will still have to meet all existing applicable standards and requirements of the FDA and foreign regulatory agencies to satisfy requirements for sale in those foreign countries.

13.3 Software for Templates: Implant Sizing

In the OR, other than the actual implant, the surgeon makes use of instruments. Prior to surgery, surgeons use a patient-specific X-ray to determine the correct implant size to be used in surgery. The use of an implant overlay on a patient-specific X-ray with implant shape and size information to determine the best fit for the patient is called templating. Templates are device specific and provided by the implant manufacturer, with the intent of helping decide the optimal size of the chosen implant. Additionally, templates help doctors as they determine surgical cut placement and where to position the implant. To some extent, templating is the first step in identifying a personalized product for each patient.

While almost a decade ago, film X-ray was commonly used, many hospitals have moved to digital X-ray systems. Current practice to determine the correct size of implant needed for a particular patient is based on analysis of patient X-ray and implant profile. This is done with proprietary software, currently available from numerous vendors who have gone through the 510K regulatory clearance process as part of a picture archiving and communication system. An X-ray is presented on the screen and calibrated based on a known scaling object. This scaling object could vary in sophistication so much so that in some instances, even a quarter can be used as a marker. We will refer to this aspect later on when describing the various imaging modalities. Obviously, one universal scaling object would be optimal, but generally X-ray technicians use what they have. If no marker or scaling object is seen in the X-ray, some software tools assume that the X-ray was made at 115% scale. This allows for the template to be scaled and placed in the view and moved in to a proper surgical position. Through this procedure, a template is chosen from those available to provide the best fit, as determined by the operating surgeon. This specific template relates to an implant size for that patient.

13.4 Dental Industry: Example of Mass Manufactured Personal Products

Perhaps the most visible advancement in personalized product is the use of digital manufacturing in dentistry. As recent as a decade ago, it was common to make use of bite impressions on a malleable or setting plastic to generate a negative model of the patient's mouth. This was then used to cast a hard model to generate a positive and true impression of the mouth and thus the missing/defective teeth. Using this information, the dentists would prescribe a restorative tooth that was manufactured by milling a stock material in a dental lab. This was sent back to the dentist to evaluate fit. This workflow required the patient to meet with a dentist a few times. Adding to this inconvenience, due to the inherent shrinkage

of setting plastics and hardening plaster, errors in the final part were quite common. While a lot of development work ensued to find malleable setting materials that did not deform or shrink during curing, the field of dentistry saw a sea of change with the advent of a camera wand that could take images of the patient mouth and software that could be used to delineate the defect on the image of the tooth. To elaborate, using a camera system, multiple images of the patient's teeth and mouth are captured. Using specialized software, these images are stitched to create a three-dimensional rendition of the patient's mouth and teeth. On the captured digital image, the dentist demarcates the defect. The software then creates a three-dimensional volume of the defect, taking into account the shape and geometry of the mating teeth to ensure proper bite. The software generates a computer-aided design (CAD) file that is sent to an additive manufacturing machine that prints the implant while the patient waits. The surgeon then implants this additively manufactured personalized product. Comparing the present day workflow to the established workflow from just a decade ago shows the advantage of digital manufacturing—the patient goes home the same day and the quality of the fit of the implant is far superior as the usage of error causing impression materials has been completely eliminated.

13.5 Additive Manufactured Patient-Matched Surgical Guides and Bone Models

A recent push in orthopedics is to ensure that not only the correct implant size is obtained using the templating method described above, but there is growing awareness that placement of the device is critical to restore the biomechanical alignment. In the previous decades and to a large extent even today, the preparation of the surgical site involved the experience of a surgeon to visualize the bony anatomy and prepare the bone bed to achieve the proper orientation to place the implant based on experience and available two-dimensional X-ray films. To appreciate the complexity of this critical step, one must imagine looking at and identifying bony landmarks through a small surgical cut of the intervening soft tissue. To exacerbate the complexity, imagine doing this in a bloody and potentially bleeding environment. It was recognized that if there was a way to use the information on CT or MRI scans, to correctly identify a starting reference plane or line, it would be possible to determine the exact location of the various mechanical axes of the defective site. Further, the availability of a tool in the OR that held onto the bone and guided other tools could help the surgeon quickly and accurately make the necessary surgical cuts on the bony site to prepare for the implant. The recognition of this concept gave birth to the idea of using patient-specific guides to help in orthopedic implant placement.

To elaborate on how patient-specific guides are created, after digital data from CT or MRI of the damaged bone site and possibly other anatomical locations are obtained, the guide design engineering team works with the orthopedic surgeon to identify bony landmarks. Based on these landmarks, the biomechanical axis that the surgeon would want to restore and use in the correct placement of the implant is identified. The operating surgeon approves of this surgical plan, and using this information, a CAD file of a surgical guide is generated. To help the surgeon visualize the damaged bone site, a CAD file of the patient's existing bone structure is also created. In a production environment, where such guides are being manufactured for many patients, one possible method to ensure that there is no mix up of guides during manufacturing is to place unique identifiers on the CAD files,

respecting patient privacy requirements. As the details of bony anatomy vary from patient to patient, it is impractical to write machine codes to turn and mill these guides from bar stock material. These CAD files are converted to stereolithography (STL) files that are used by additive manufacturing machines to make a patient-specific bone model and implant guide. After the making of these bone model and guides, the parts are removed from the machine, cleaned, and undergo quality checks. There can be many different kinds of quality checks but the most common is to ensure dimensional accuracy. The most common method employed is digital scanning where structured light is used to scan the surface of the additive manufactured part. This results in another CAD file that is compared to the original CAD file. These two CAD files must match within the specified tolerances for the guide to be considered to be acceptable for surgical use.

During surgery, the surgeon makes incisions to expose the bone site and uses the guide to make the cuts on the bone or determine the precise location to place standard instruments. If one has chosen a cut-through guide, once the cuts are made, the guide is removed and the implant is placed and secured per the normal surgical procedure. The use of the patient-specific surgical guide enables the surgeon better precision in implant placement. As the bone model and guide is patient specific, after the surgical procedure, these are disposed of as biological hazard materials. A few examples of commercial guides that are being used clinically are (1) Zimmer—Patient Specific Instruments, (2) Biomet—Signature, (3) Depuy—TruMatch, and (4) Conformis—iJig.

As the patient-specific guide is to be placed on the open surgical site, these patient-specific bone models and guides must meet certain regulatory requirements as listed below to ensure biological safety and effectiveness.

1. The material must be biocompatible for short-term exposure meeting the requirements of International Standard ISO–10993, "Biological Evaluation of Medical Devices Part 1: Evaluation and Testing."
2. Mechanical strength requirements as dictated by the surgical procedure to ensure that there is no mechanical failure of the guide during surgery. As these bone models and guides are generally not load bearing, this mechanical strength requirement maybe limited to demonstrating that the construct is strong enough to withstand forces encountered in normal surgical procedures.
3. And depending on the method of delivery to the OR, one or more of the below must be satisfied to ensure the product must meet shipping requirements and is sterile prior to clinical use.
    a. Packaging system integrity testing may include the following:
        i. Package integrity (ASTM F2096: Bubble Test)
        ii. Seal integrity (ASTM F1886: Visual Inspection, ASTM 1929: Dye Test)
        iii. Seal strength (ASTM F88: Peel Test, ASTM F1140: Burst Test)
        iv. Packaging system performance testing/distribution simulation (International Safe Transit Association [ISTA]) procedures
        v. ISO-11607 Packaging for terminally sterilized medical device
    b. Sterility
        i. ANSI/AAMI/ISO: 11137 (Sterilization of health care products—radiation)
        ii. ISO 17665 Steam sterilization for medical devices
        iii. ISO 11135 EtO sterilization for medical devices

Depending on the clinical use of the guides, there may be many other standards and specifications that must be met. The reader is advised to refer to the FDA and ISO websites for more up-to-date guidance or consult a regulatory specialist.

13.6 Additive Manufactured Generic Product

To understand the impetus of additive manufacturing in the orthopedic industry, it is necessary to consider the evolution of bone ingrowth surfaces. Orthopedic implants make use of metallic systems (Ti6Al4V, CoCrMo to name a few common alloys) that allow for integration with surrounding bone (osseointegration) due to the roughened or porous structure on the surface of the metallic implant. Traditional manufacturing methods include sintering of beads or spraying powder particles to generate a porous structure. However, our understanding of the osseointegrating surface has advanced where there is push to make the osseointegrating layer more porous and possibly more biomimetic by making the structure more similar to cancellous bone. The thought being that the presence of large pore volume would provide ample bone integration space. There is a growing clinical need to achieve osseointegration even where bone loss is severe, bone quality is poor, and only focal contacts between implant and host bone are possible. This was evident by the introduction of and with the clinical success of Trabecular Metal™ (Zimmer, Indiana), Tritanium™ (Stryker, Michigan), and Regenerex™ (Biomet, Indiana), among others. The manufacturing methods for these modern porous structures include common processes in powder metallurgy and associated sintering, physical vapor deposition, and chemical vapor deposition. Although the initial clinical use of such porous structures is generally considered clinically successful, the resulting structures were not truly biomimetic. In the quest to make the porous structure biomimetic, additive manufacturing methods are being considered. Further, the advantage would be to make the bone integration layer of variable porosity, modulus, and pore structure to mimic the bone structure of the natural anatomy.

A generic production route may include the following:

1. Generation of the CAD files including that of the solid and porous region
2. Populating the porous region with the details of pore structure, making it as biomimetic as possible
3. Feeding this information to additive manufacturing machines to produce parts that, at least for Ti6Al4V alloy, meet the chemical and mechanical requirements listed in ASTM F2924-14, ASTM F3001-14, and FDA guidance documents (Guidance for industry and for FDA reviewers/staff—Guidance for industry on the testing of metallic plasma sprayed coatings on orthopedic implants to support reconsideration of postmarket surveillance requirements)
4. Machining mating surfaces to ensure that mating components such as ultrahigh molecular weight polyethylene (UHMWPE) fit precisely and the possibility of the inevitable micromotion between the mating parts do not generate polyethylene debris
5. Cleaning the additive manufactured parts of entrapped metal powder and machining additives such as coolant (ASTM F2847)

6. Passivation to meet ASTM A 967-13
7. Final packaging and terminal sterilization (meeting requirements listed in the Section 11.5)

As mentioned previously, substantial regulations dictate risk mitigation on the above workflow. However, at the time of writing this chapter, various underlying regulations are being discussed. The reader is advised to follow FDA-sponsored workshops to get a better perspective on existing and upcoming regulations. Additionally, the reader is advised to refer to the ISO for more up-to-date regulatory guidance.

13.7 Additive Manufactured Patient-Matched Implants

The above workflow does not necessarily create a personalized product or patient-specific implant but can be adapted to create personalized implant utilizing additive manufacturing. To elaborate on the manufacturing route of a patient-specific implant and guide, let us consider the making of components needed for high tibial osteotomy (HTO) surgery. This is a corrective surgery normally used on patients to correct instability due to misalignment of the tibial plateau to the femoral condyles, without compromising or violating the cartilage or menisci of the knee. Patient-specific information is needed to determine the extent of malalignment—so CT or MRI data are required. Based on this information, a surgeon can plan on making a slot in the region inferior to the tibial plateau. This slotted region will receive the implant—thus pushing superior the tibial plateau to correct the misalignment. The design team in collaboration with the operating surgeon would then design the HTO guides that allow the surgeon to position, orient, and make the necessary cuts in the region of the tibia. At the same time, an implant wedge is designed such that the cortical wall of the wedge seamlessly mates with the cortical bone of the receiving bone tissue while correcting the malalignment. Based on the approved design of the wedge, a Ti6Al4V implant, nylon guide, and nylon trial are manufactured. As these components are patient specific, the CAD files could contain patient-specific code identifiers that indicate components are for a particular patient, thus avoiding mix-up with components for other patients. The implant is made per the workflow listing described above, and the guides and trials are made per the procedure described in the earlier section. During surgery, the guide is used to prepare the implant receiving bone bed. Finally, the implant is placed inside the wedge-shaped cavity following normal surgical protocol for HTO. As the guide and trials are patient specific, they are discarded following surgery.

Another example of a personalized product involves flanged acetabular components (i.e., triflange). Essentially this implant looks like an acetabular shell with three continuous flanges designed to mate with the ilium, pubis, and ischium of the pelvis. Surgically restoring function of the hip joint, where there is acetabular bone loss including pelvis discontinuities, presents a challenging situation for the operating surgeon. The problem of where to place the implant and achieve stability and restore functionality is compounded by the fact that there is little bone left in the pelvis to make use of a standard acetabular shell. Currently, a potential treatment option is the use of structural allografts, which may not always be available or may not be viable scaffold for bone integration. While allografts are generally considered safe, there is still an existing risk of disease transmission from the donor to the recipient. The surgeon often has little choice but to order

a patient-specific triflange acetabular component. Using CT scan information of the patient, the sizes of the three flanges, their shapes, and orientation are designed to fit securely with the remaining bones. The orientation of the acetabular cup portion of the triflange implant is established and multiple screw holes are added into the design to accommodate retaining screws. Physical models of the patient's bone and the proposed implant are sent to the operating surgeon for approval. Upon surgeon's approval of the proposed implant, these are shipped back to the manufacturer and serve as a manufacturing tool to aid the manufacturing of the implant. As of now, most such triflanges are milled using traditional manufacturing methods. Subsequently, a porous surface is applied to allow for biologic fixation. Naturally, this process takes time. Additive manufacturing is poised to change this—as with traditional triflange workflow, the new method too will require surgeon's input in implant design and final approval of the implant. However, the manufacturing method will be streamlined where the body of the implant and porous structure are additively manufactured. This is expected to save a lot of wasted material and cut down on manufacturing time as the porous structure will be generated concurrently.

13.8 Hard Tissue Replacement for Cranial Reconstruction

Perhaps the first patient-matched implant approved for clinical use and made by additive manufacturing technology is OsteoFab™ Patient Specific Cranial Device (Oxford Performance Material, CT). While the clinical device was not unique, the use of additive manufacturing technology made the work flow efficient. Additionally, this technology makes use of poly-ether ketone material that is alleged to be more biointeractive compared to the traditional material (poly methyl methacrylate, PMMA). The traditional method and the additive manufacturing method make use of patient CT data. In the older technology, the CT data are used to create a mold where PMMA beads are cast and chemically sintered. In the newer technology, the CT data are used to generate a STL file and an additively manufactured part is generated.

13.9 Manufacturing Cost: Is Additive Manufacturing a Viable Technology?

In spite of the advantages apparent from the descriptions above, currently there are few major disadvantages that limit the wide scale adoption of additive manufacturing to make implants. The first is the prohibitive cost of additive manufacturing machines. At almost three to four times the expense of a generic mill, the capital cost of starting a manufacturing line comprised of additive manufacturing machines becomes steep. However, as with any new technology, the cost of machines is decreasing. There is substantial competition between machine manufacturers—this healthy competition and the rapid adoption in the aerospace, automotive, medical, and other industries are helping to make these machines feature-rich while driving the price down.

The second disadvantage is the speed of build. Additive manufacturing technology has come a long way in achieving better dimensional accuracy and surface finish. But even today it still takes a long time to make an average sized acetabular shell implant—with

some machines, this is measured in hours. In comparison, the time to machine a similar sized acetabular shell is just about 30 minutes and requires machines that are half to a third as expensive. Naturally, there is a camp of manufacturing engineers that highlights the build speed as a deterrent in adopting this technology. However, the argument of build speed as the sole measure of cost of the implant is flawed. One must remember it is the sum of the cost and time of all operational steps that must be considered in estimating or calculating the cost of the implant. In additive manufacturing machines, the solid and the contiguous porous structure is printed concurrently. Therefore, the time to build the porous acetabular shell in additive manufacturing machines covers the time and therefore the cost of building the porous structure as well. In the build time for a generic porous shell via the traditional machining route, one must include the time necessary for post-machining operations such as masking, blasting, and applying a porous structure either via thermal spraying or sintering with beads. Further, as these operations are staged and progress in batches, there is inventory carrying cost as well. Additionally, there is the lead time to deliver the order to market that is quite long with manufacturing via traditional routes.

This difference in work flow for additive manufacturing and traditional machining is explained in detail in Table 13.1.

Recognizing that the cost structure of manufacturing facilities is different, it is imperative that a thorough cost calculation be conducted to ensure that the implant being considered for manufacture via additive manufacturing is economically viable. It is the authors' experience that a combination of design features not possible to achieve via traditional route and the judicious selection of implants that make economic sense usually draws a backing from decision makers.

Though not associated with cost of parts, nevertheless there is yet another deterrent to the adoption of the additive manufacturing technology. This is a perception among

TABLE 13.1

Difference in Work Flow for Additive Manufacturing and Traditional Machining

Traditional Manufacturing Route	Additive Manufacturing Route	Comments
Starting material ASTM F136 bar stock	Starting material ASTM F1584 powder	The cost of powder is generally much higher than the cost of bar stock. However, there is very little material waste in the additive manufacturing route.
Machine inner and outer diameter	Feed CAD files to additive manufacturing machine and build parts	Time to build via AM is longer but this time includes the concurrent building of the porous structure.
Blast and clean outer diameter to prepare surface for thermal spray	Machine ID	
Mask areas that cannot receive thermal spray		
Thermal spray		
Clean and passivate	Clean and passivate	Cleaning procedure must include steps to remove residual powder from porous structure.
Package	Package	

engineers that the printed material is inferior. For the uninitiated in additive manufacturing, this is perhaps natural—after all, the technology makes use of liquid or powder to make a solid part. This concept conjures the possibility of flaws in the parts. Interestingly, the two currently available ASTM standards on Ti6Al4V parts made by additive manufacturing technology specify the minimum strength requirements—these are about the same as that of wrought material. Therefore, processes that have been validated to the ASTM standards ensure strength and counter the belief that additive manufactured parts are not sufficiently strong. Another limitation, which perhaps is most crippling for now, is the lack of standards. While there are now two ASTM standards for Ti6Al4V alloys, there are no standards for CoCrMo alloy. At the time of writing this chapter, the ISO and ASTM committee have recognized these limitations and have signed a Partner Standards Developing Organization cooperative agreement to govern the ongoing collaborative efforts between ASTM International Committee F42 on Additive Manufacturing Technologies and ISO Technical Committee 261 on Additive Manufacturing. The issue of perception of inherent weakness possibly results from earlier and perhaps overzealous attempts by machine manufacturers to sell their technology to implant original equipment manufacturers (OEMs). The earlier versions of the machines were not robust enough resulting in residual porosity or residual unmelted (or partially melted) powder particles. In the last few years, these issues have been corrected by better managing build speed and expectations. Moreover, there is ongoing work on thermal imagining of the build layers where the build layers are thermally imaged for residual porosity or residual unmelted (or partially melted) powder particles. These technologies are still in their infancy and may take time to mature. In the meantime, OEMs must adapt quality control test system similar to that employed by casting facilities. To this end, nondestructive testing methods such as X-ray imaging, ultrasound, and CT scanning would prove most beneficial.

13.10 Role of Imaging Human Anatomy

Custom implants and surgical guides require patient-specific anatomy. Without such data, the immense power of additive manufacturing is worthless as one of the critical inputs in making parts from such technology is STL data, which can only be generated from the 3D medical images. It is of value to note that the accuracy and resolution of existing 3D medical images are magnitudes less than what modern day additive manufacturing machines can deliver. To obtain this patient-specific anatomy, medical scanning devices are utilized. There are four primary modalities that are used to obtain these data. The most common 3D data sources are CT followed by MRI and the most recent ultrasound and X-ray. For CT and MRI, 2D stacked image slices are individually segmented or masked and combined to form a 3D shape. X-ray has been utilized as a 2D templating source and input to make custom sized standard implants. In Sections 13.11.3 and 13.11.4, new uses of ultrasound and X-ray will be discussed. These new uses are typically being utilized as alternatives to their more expensive medical scan counterparts in universities and other research and development environments.

13.11 Most Common Modalities

13.11.1 Computed Tomography

CT is an X-ray-based technology for scanning the body in 3D. These scanners create images in Hounsfield units and are directly related to density of the scanned material. Air has a value of –1000 while bone can range from 700 to 3000, based on the quality of the patient's bone. These scans are relatively fast to generate and are the easiest to reconstruct for orthopedics. There is no soft tissue detail and only bone or calcified ligaments and tendons are visible. They do however expose the patient to radiation.

13.11.2 Magnetic Resonance Imaging

MRI is less dangerous in terms of radiation for patients than X-ray-based scans and provides details on soft tissues. These scanners create images in generic units that can only be compared to details in that current scan. There are methods to calibrate on a scan-by-scan basis but these are time intensive. The resolution of MRI scans is eight times less than CT and takes 10–30 times as long to capture and create the data set. This pushes the boundaries on clinically relevant scans and the patient's ability to sit still long enough to get a good scan. At least for orthopedics, MRIs do provide the most relevant data including that on cartilage and soft tissue. However, these data are much less homogenous and require much more human intervention to determine the 3D shape. There is clinical risk with MRI, but it is closely monitored by specific absorption rate, which is the amount of energy absorbed by the body. All scanners have fail safes to ensure the limit is not exceeded and this can lead to extending the scanning time even longer. A prohibitive aspect of using MRI is the associated high cost. The other modalities do not have issues of volumetric distortion in the 3D image—MRI is the only imaging technique that is encumbered with this issue. If MRI is being used to generate patient-specific CAD data for additive manufacturing, extreme care must be exercised to ensure that these distortions are minimized.

13.11.3 Ultrasound

Ultrasound can be combined with motion capture to create 3D shapes of bones in large point clouds. The 3D shapes can be very accurate, but may have gaps due to other bones or limitations to the motion capture system. This then requires multiple 3D shapes to be registered together in order to have a solid bone.

13.11.4 X-Ray

So far the data generated by the three previous modalities are actual patient three-dimensional data—X-ray image is an image on a single plane with no or little useful information on the third dimension. With X-ray, statistical shape modeling can be utilized to predict patient anatomy from one or more X-rays. Of course, the user must have access to such data. Additionally, this approach has a lot of dependencies on the underlying data that are driving the model. The dependencies are number of data sets, types of data sets, and quality of data sets. So the larger number of data sets one has the more accurate the 3D reconstruction. Having types of data sets that are specific to the anatomy being reconstructed is critical. This means if one wants to address hip orthopedic conditions, then they should have data of hips with similar clinical conditions.

Once the shape is available, it must be formatted to work with commercially available 3D printers. From these 3D point clouds or masks, an STL is typically generated and exported for use.

13.12 Segmentation

This term refers to the act or art of generating 3D shapes from imaging data. This can be done in three different styles—fully manual method, semi-automated, or fully automated.

13.12.1 Manual

Manual segmentation utilizes a trained human to specify pixel by pixel which ones are to be included and which ones are to be excluded from the shape. This method is the most time consuming and can take from minutes on an easy CT with bones of high density to hours or even days on a complicated MRI. This method is still considered the gold standard when evaluating accuracy of segmentations of human anatomy.

13.12.2 Semi-Automated

Semi-automated segmentations rely on algorithms to predict the shape based on guidance from the user. This method can save massive amounts of time on straightforward cases. As the anatomical shape and bone quality of the patient further deviate from normal anatomy, the complexity increases, the time savings decrease, and in extreme cases can actually take longer than manual segmentation.

13.12.3 Automated

Techniques where humans do not interact with the 3D reconstruction are known as automated. These techniques are the least accurate of the three types, but are the most repeatable.

13.12.4 Segmentation Accuracy

There are two components that go into segmentation accuracy—the first component is accuracy of the scanner and the second is the method of segmentation. CT scans are typically your most accurate scans with MRI and ultrasound, depending on how the data are collected from those two modalities coming in second. X-ray is typically the least accurate, due to the fact that it is a predicted model and not enough data sets are usually available to drive the model. This, however, does not mean that X-ray technologies are not clinically relevant.

When creating custom and semi-custom patient-specific products, one needs to look at the accuracy dependencies of the system. As a whole, the scan accuracy is the least accurate component. CT can be run at most facilities somewhere between 1 and 1.25 mm inter-slice distance and around 0.5 mm × 0.5 mm intra-slice pixel dimensions. This gives one a voxel of approximately 0.25 mm^3. MRI scanners produce 2 mm inter-slice distance and 0.8 mm × 0.8 mm intra-slice pixel dimensions for a voxel size of 1.28 mm^3. MRIs are

typically enhanced by interpolation in all three dimensions to an approximate 0.16 mm^3 voxel. Even with this enhancement, one can see that the accuracy of the scanner is the limiting factor.

Besides the differences in accuracy, the other important difference when deciding on a modality is what tissues should be included. If the goal is a long bone with no bearing surface, CT is ideal as it is fast and accurate. If, however, one wants to build a guide for a bearing joint like the hip or knee, one should consider MRI as the mating surface will actually be cartilage which is not visualized in CT. MRI is less accurate, and it takes a lot longer to create a 3D model from the generated data, but includes tissues not seen in the other modalities.

13.13 Software

There are numerous software vendors providing segmentation software or tool kits. For manual segmentation, some of the more popular options are as follows: Amira (FEI, Burlington, MA), ITK (Kitware, Clifton Park, New York), Mimics (Materialise, Leuven, Belgium), ScanIP (Simpleware, Exeter, United Kingdom), 3DSlicer (open source, Harvard, MA), ORS (Object Research Systems, Montreal, Quebec, Canada), or Osirix (Pixmeo, Bernex, Switzerland). Some of these are commercially available, while others are free for noncommercial use or even open source. Depending on the user needs and end goal, a thorough evaluation should be done. Two of the more common medically cleared semi-automated tools are TeraRecon (Foster City, CA) and VitalImages (Minnetonka, MN). They are very robust and handle most CT scans extremely well. With work they can output an STL. Beyond this there are some extremely skilled companies such as Imorphics (Manchester, United Kingdom), ImageIQ (Cleveland, OH), Qmetrics (Rochester, NY), and VirtualScopics (Rochester, NY) that have automated processes and typically work as processing houses or software as a service model (SaaS). Recently, cloud-based tools have been introduced by companies like 3DSystems (Rock Hill, SC)—Bespoke Modeling. All of these options export an STL or finite element analysis (FEA) format that is typically incompatible with many CAD packages.

13.14 STL to CAD

There are CAD packages like SolidWorks (Waltham, MA) that can handle STL files and utilizing them for engineering design. However, if such software packages are unavailable, one is required to stay in the segmentation tool's proprietary design software or use a conversion package like 3D Systems' Geomagic Wrap. Autodesk's Maya (San Rafael, CA) and many other programming languages such as Mathworks MATLAB® (Natick, MA) have scripts available online to perform this conversion as well.

The discussion above is by no means the final word in software necessary in generating patient-specific CAD data, without which additive technology cannot be used to make patient-specific personalized product. Of course, software technology changes at a rapid pace—at the time of writing this chapter, CAD data based on CT scan are considered most prevalent.

13.15 Much Needed Technology

Additive manufacturing involves powder or liquid to be transformed into a physical object with requirements on dimensions and, perhaps more important, on structural integrity. A complex interplay of energy source, raw material quality, and build strategy contributes to the physical and chemical properties of the three-dimensional additive manufactured object. In some instances, finishing operations include thermal treatments as well. The need for devices that determine the dimensional accuracy and presence of structural flaws are apparent. Modern day computers with structured light scanning equipment are becoming indispensable in making additive manufacturing technology address the need for fast checks on dimension on production lines that are catering to personalized products being manufactured in large volumes. The technology has some limitations as it does require some surface preparation, that is, coating the surface with talc and the fact that the method is line of sight dependent so robotics may become necessary to ensure that the entire part is well exposed to the structured light source and camera. If it takes about 15 minutes to coat with talc, fixture the personalized product in the structured light system, make measurements, and compare with the specifications, each such quality control machine can process only 32 parts on an 8-hour work shift. An establishment engaged in mass production of personalized products needing to do 100% inspection on such parts will require multiple such structured light machines to be able to process parts through the quality control group. Suddenly, the cost of running a personalized product manufacturing facility jumps substantially. Newer machines should be able to scan parts regardless of how fixtured, must be faster and work without making use of ad hoc coatings such as talc.

To ensure that there are no structural flaws, common nondestructive tests can be used. The technology here is much more robust as it has had time to mature while addressing the needs of the casting, metal injection molding, and forging industries. However, on personalized products where there is a porous surface layer deliberately added for bone osseointegration, such traditional nondestructive tests may prove inadequate. Of course, process validations, routine monitoring of process parameters, and stringent adherence to preventive maintenance of additive manufacturing machines will help alleviate risk of introducing structural flaw in the additive manufactured part.

13.16 The Future

The future is wide open for mass customization of medical devices. As stated earlier, we will need to start simple, with low-risk medical devices and instruments, and with experience and data, gradually increasing complexity and risk. Regulations currently under development will soon be established and will guide the process in the near term. As the capabilities, creativities, and capacities grow, the then existing regulations will be challenged and hopefully expanded to accommodate this dynamic and prolific field of medical devices.

Some of the most significant advances will come as new materials and alloys are utilized in additive manufacturing machines. This is directly related to multi-material printing and dynamic material property printing. Well-known attributes of today's implants such

as corrosion resistance and biocompatibility will still play an important role. However, design team will tailor make implants such that the biomechanical forces are better channeled to invoke Wolff's laws to ensure strengthening of surrounding remaining bone. Take the hip stem for instance—additive manufacturing a hip stem with strength directly proportional to the bone it is being inserted into and varying the same from the distal end to the proximal seat could potentially be a great advancement. Initially, this may be achieved by simply designing cavities in the body of the stem that do not act as stress riser but help in decreasing the stiffness of the metallic implant. Such design will eventually include organic-shaped cavities as our understanding of form and biomechanics advance. Additive manufactured multi-material will eventually follow but would most likely be limited to metal (or alloy) with ceramic, thus ensuring the elimination of galvanic corrosion. And perhaps well into the future, when collagen printing has advanced with associated and concurrent cross-linking, it is quite possible that metallic parts will eventually be replaced with well-designed composites of collage and calcium phosphates to help with the repair of diseased bone. In the remote future, such composites of collage and calcium phosphates will be seeded with cells obtained from the recipient patient making the implant truly biological and patient specific. There will be procedural controls in place to ensure patient privacy and process controls to ensure that the seeded cells remain biologically viable at the time of surgery. Moreover, quality control using DNA tests will ensure that the patient-specific implant is used with the correct patient. In the meantime, while metal- or alloy-based implants are still the norm, additive manufacturing machines will become a part of traditional subtractive milling or grinding and polishing machines, essentially to obtain better surface finish. Such combination machines will compete with traditional additive manufacturing machine with downstream (electro)chemical-based surface polishing techniques.

The field of additive manufacturing, specially related to medical devices, will be very dynamic—it will enjoy heights of rapid adoption and experience downturns. There will be phenomenal successes and colossal failures. In the future, medical device industry will draw experts from cell and tissue architectural biology, materials scientists and biomechanics, automation, and software. The above portrayal of the future is simply the authors' view—the reader is encouraged to image the future and work to achieve and shape the future.

Disclaimer

The opinions in this chapter are solely of the authors and are not of their employer.

14

Additive Manufacturing: Future of Manufacturing in a Flat World

Amit Bandyopadhyay and Susmita Bose

CONTENTS

ABSTRACT In this final chapter, the editors of this book look at the future to see how AM will influence our everyday life in the coming days and how on-demand manufacturing can influence new product development or community-centric business development or educating our next generation of students with their innovative ideas. It is envisioned that the differences between the manufacturing nations and predominantly consumer nations will decrease in the future due to the use of AM. In combination with Internet-based technologies and the computer-aided designs, AM will make a flat world even more uniform for the generations to come.

14.1 Introduction

The rise of AM is making a significant impact on how parts and products are designed and then manufactured. It is also directed by the part geometry and application need. The focus of this last chapter is to highlight some of these changes that are happening in our society and what the future may look like 10, 15, or 30 years later. Let us start with a simple example—buying a car. In current practice that is being followed for the past many decades, buyers will go to dealership to look at various models and colors and features. Buyers can do most of the same over the Internet as well. Finally, when a buyer makes a decision based on available options, the car will be purchased by the buyer. However, a few weeks back, researchers at Oak Ridge National Lab in Knoxville, TN, worked with a private company to manufacture the world's first functional car using AM.

A large modified fused deposition modeling machine is developed to directly manufacture these parts. All parts of this car were printed using fused deposition-based techniques with carbon fiber-reinforced plastic material. Therefore, it can be envisioned that 10 years down the road, a buyer can go to a showroom and look at various options for new cars and then designs her/his own car and get a quote from the manufacturer who will do the rest of the engineering and make this *customer-designed car* that will be delivered in a few days. Such possibilities are no longer considered as *science fiction* but a reality that is already happening.

Similarly, use of AM technology can have a significant effect on human health, where a physician can have access to a patient-specific or a defect-specific implant to change or improve the patients' lifestyle substantially. Depending on clinical need, this technology can revolutionize today's treatment options and health care routine process. Accepting the fact that more of this kind of transformative changes will happen in our everyday life in the coming days, we like to ask a basic question—how will such changes impact our society? Also, how will that impact the future of manufacturing?

AM or 3D printing is the most exciting news today in the world of manufacturing. Parts can be directly built without any tooling or dies. Most of these parts are near net shape and require only small finishing operation if smooth surface is needed. Unlike 10 years back, when most of these parts only mimic the size and shape of the part, today's AM machines can produce parts that can perform regular operations and replace existing parts in operation. In the first stages on implementation, most companies are looking at low volume parts to see if those can be manufactured using AM-based techniques and reduce to need to stock them for long time. The publishing industry has gone through this transition mostly in the past decade. In today's world, many books are only printed when orders come in. The same concept is currently being implemented by many in manufacturing industries using AM to manufacture on demand. However, if those are multicomponent or multi-material parts, significant challenges still need to be overcome to use AM techniques directly.

14.2 From 3D Printed Car to 3D Printer in Space

The year 2014 marked two important events for the AM—(1) 3D printed functional car and (2) 3D printer in space. NASA launched the first 3D printer in International Space Station to experiment with printing parts in zero gravity. Made-In-Space built the fused deposition-based 3D printer that can operate in zero gravity to manufacture plastic parts that can be produced in space. Though the concept was envisioned by many for the past 20 years, its implementation marks an important new era for AM. The race is now on to use AM technologies to produce functional parts in space using materials other than just polymers. More importantly, can in situ resources be utilized on the surface of Moon or Mars to produce small and large structures for future human explorations? It is envisioned that in the next 10 years, AM in space will see a significant growth. In 2010, we published the first direct fabrication of moon-rock regolith structures using commercially available laser engineered net shaping (LENS) system [1]. In our work, we have shown that direct laser melting of moon-rock regolith is possible due to high silica contents and some simple shapes can be formed, shown in Figure 14.1. Though the parts produced had low strength for tooling, this concept can be utilized to make parts for basic civil infrastructures. For example, it can be envisioned that solar powered 3D printers are busy at work on

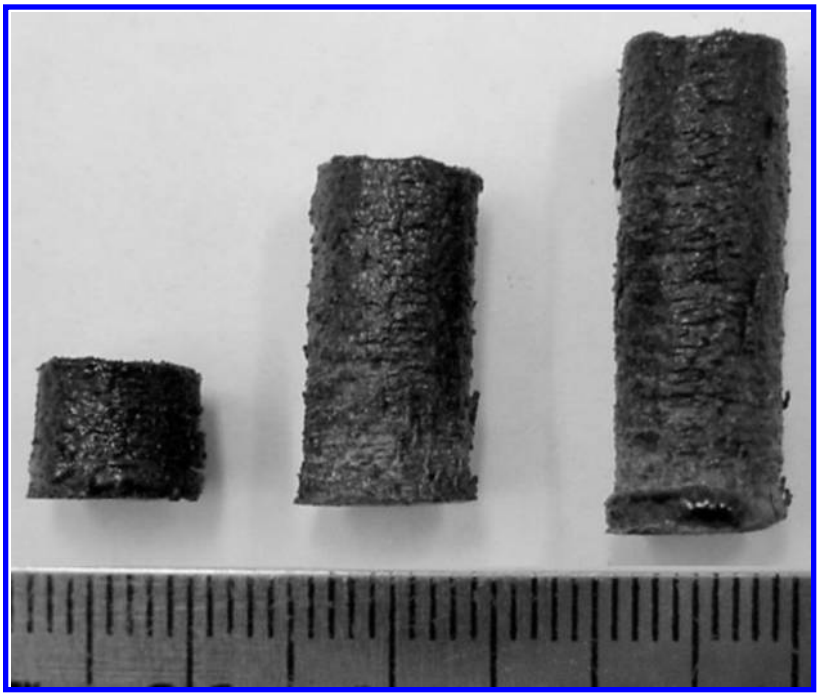

FIGURE 14.1
First demonstration of LENS processed direct fabrication of moon-rock regolith simulants (JSC-1AC). (Data from Balla, V.K. et al., *Rapid Prototyping J.*, 18(6), 451–457, 2012.)

the Moon's or Mars' surface to make bricks that are being used for roads or small buildings or launch pads. Based on recent advances in NASA and European space agency's work with AM, such ideas can soon be a reality. Concept of 3D printed car or 3D printed parts in outer space using in situ resources can be mundane activities in the coming days.

14.3 From Bio-Printing to Flexible Electronics

AM offers significant potential toward solving long-standing challenges related to human health. As discussed in Chapter 7 in detail, there are many facets to bio-printing that are still at research and development stage. However, the basic concept of printing human bone or organs with the help of 3D printing or AM is still a fascinating science. From plastic surgery to cancer treatment, from birth defects to amputees—all are looking for potential breakthrough in the development of tissue engineering to harvest different body parts to enhance quality of life or help patients live longer. In our own research, we have produced metallic implants from computed tomography images of a fractured skull, shown in Figure 14.2, something that is impossible to accomplish using any other means. Our research is also focused in the areas of bone tissue engineering using 3D printing in which we have fabricated defect-specific porous bio-resorbable ceramic scaffolds for bone healing. Scaffolds porous architecture can be tailored to match the bone density of the patient

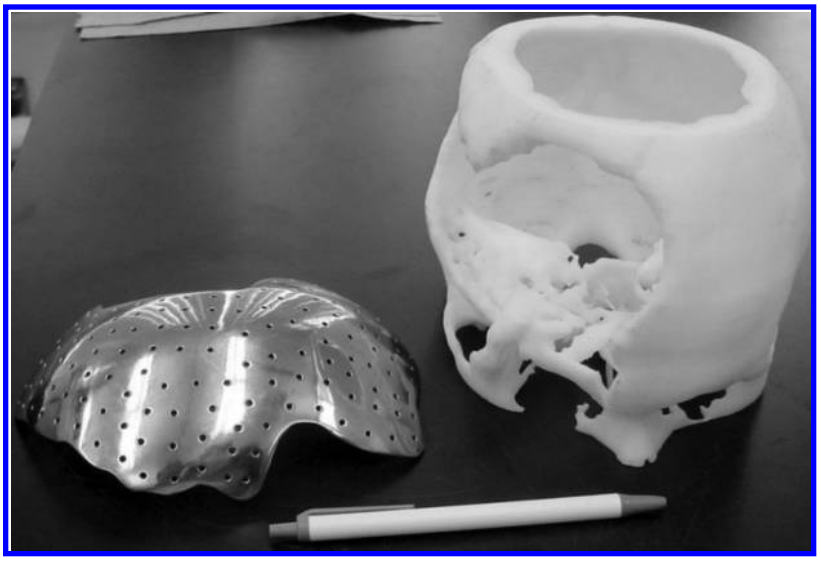

FIGURE 14.2
(See color insert.) LENS processed craniofacial Ti implant and FDM processed polymer prototype of the skull with large defect.

or specific defect location. Such implants can also be used for site-specific drug delivery to enhance healing as discussed in detail in Chapter 5. Researchers are also working on direct deposition of cells on substrate using AM. Although exciting and feasible in small scale, such approaches still need to be developed further to ensure longer shelf life, and cell viability during and after processing. However, the next 10 years will be very exciting in this field and many new products are poised to come to the market with the help of different 3D printing technologies.

Flexible electronics is also an area of significant promise in which AM will play a critical role. As we move beyond 2D structures and enter the domain of 3D structures for various electronic devices, flexibility in manufacturing will be a key to success. Low cost, use-and-throw devices will also dominate various application areas in the world market. Faster design optimization/validation of these devices is the key to success toward commercialization. Different 3D printing technologies are already making a difference in these application areas, and many more applications are considering such transition. Many of these ideas are discussed in detail in Chapter 8.

14.4 Innovation in Manufacturing Using AM: Multi-Materials Structures

Apart from building parts without part-specific tools or dies, AM can also help to innovate parts that are difficult, if not impossible, to make using conventional manufacturing. These innovations may come from the design of novel parts of multi-material structures. In conventional manufacturing, multi-material parts need to be joined by welding or brazing or soldering. However, AM processes can be used to directly fabricate parts with multiple significantly different compositions offering different functionality. In one

of our recent work, we have used LENS to design and process parts having bimetallic composition—from Ti_6Al_4V to SS 316. Large thermal residual stresses prevented them to be bonded directly, and therefore, an intermediate layer of Ni-Cr alloy was used to minimize the residual stresses and cracking. Figures 14.3 and 14.4 show images depicting AM of bimetallic structure using LENS.

Figure 14.3 shows SS410 to Ti_6Al_4V bimetallic structures processed via LENS [2]. Figure 14.4 shows cross-sectional microstructures of SS410 to NiCr bond layer to Ti_6Al_4V. Smooth interphase from one composition to another helped to form this bimetallic structure between

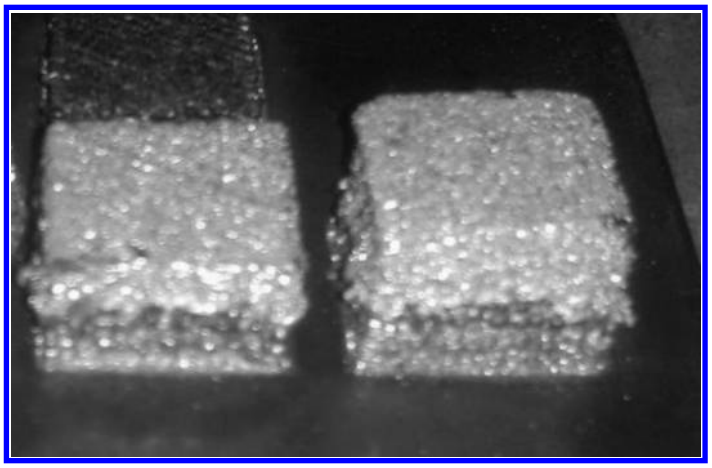

FIGURE 14.3
LENS processed SS410 to Ti6Al4V bimetallic structure with NiCr bond layer.

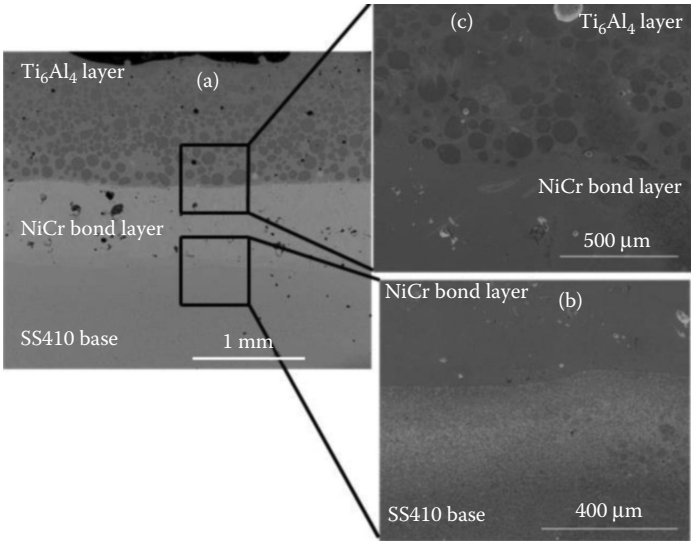

FIGURE 14.4
Cross-sectional microstructures of SS410 to Ti_6Al_4V bimetallic structures with NiCr bond layer in between. (a) Low magnification image showing SS410 to Ti_6Al_4 transition using a NiCr bond layer. (b) High magnification image showing the interphase between Ti_6Al_4 and NiCr layer. (c) High magnification image showing the interphase between SS410 base metal and NiCr bond layer.

otherwise incompatible alloys. Some other groups have also started looking at different combinations of bimetallic/multi-material structures using AM. The main challenge in multi-material AM lies with the design of these structures with built-in properties that is diverse because *.stl* files are still based on one material property only. Multi-material structures, for example, can be used in a variety of applications. For example, structures where one end may experience high temperature can be manufactured in one operation using two different materials in which one is suitable for high temperature application. Similar structures can also be envisioned for materials where corrosion resistance is a key factor.

14.5 Application of AM in Repair

In the coming decade, application of AM toward repair and reconstruction of engineering parts will find significant applications. Many engineering parts need replacements not due to major failure but mainly because of wear or damage in small areas. For large parts, such replacements are quite expensive and sometimes difficult if those are one of kind parts. AM can be used to selectively repair engineering parts based on the CAD design of that specific region. In most cases, a final machining is needed before application. RPM Innovations (RPMI) in South Dakota (USA) specializes in such repair operations using laser-based AM (Wald, N., unpublished data). Due to multi-axial AM operation (up to six axis of freedom), repair in selected region with specific alloy composition can be accomplished easily. Figure 14.5 shows one such example of laser repair of drag line swing shaft. Swing shaft is approximately 5 m long shaft that weighs 25,000 pounds and is used on a drag line of a coal mines. Conventional repairs of swing shaft cause failure problems due to heat input. A novel laser-based repair process was developed at RPMI for bearing surfaces of 4340 swing shaft utilizing 420 SS. Such composition modifications increase wear resistance of surfaces, which extends the shaft life as well. Repair cost using laser-based AM technology is approximately 65% less than a new part. Moreover, due to compositional variations during repair, swing shaft's service is extended compared to new. Such approach can not only save money, but also save a lot of time delay from critical parts. Since AM technologies are not design or material specific, the same machine can be used to repair a variety of parts with different shapes and compositions.

14.6 AM in Tissue Engineering and Drug Delivery

Application of AM has a lot of potential in the areas of tissue engineering and drug delivery. There is always a shortage of organ donors for patients with critical needs. The advent of tissue engineering has offered significant promise to improve human health over the past three decades. However, patient-matched organs are not yet feasible due to many engineering challenges. AM technologies are currently being explored to fabricate different scaffolds that can mimic the size and shape of a particular defect of a patient. The idea behind combining AM technologies and tissue engineering is simple—produce the patient-matched scaffolds using AM with bio-resorbable materials that can dissolve

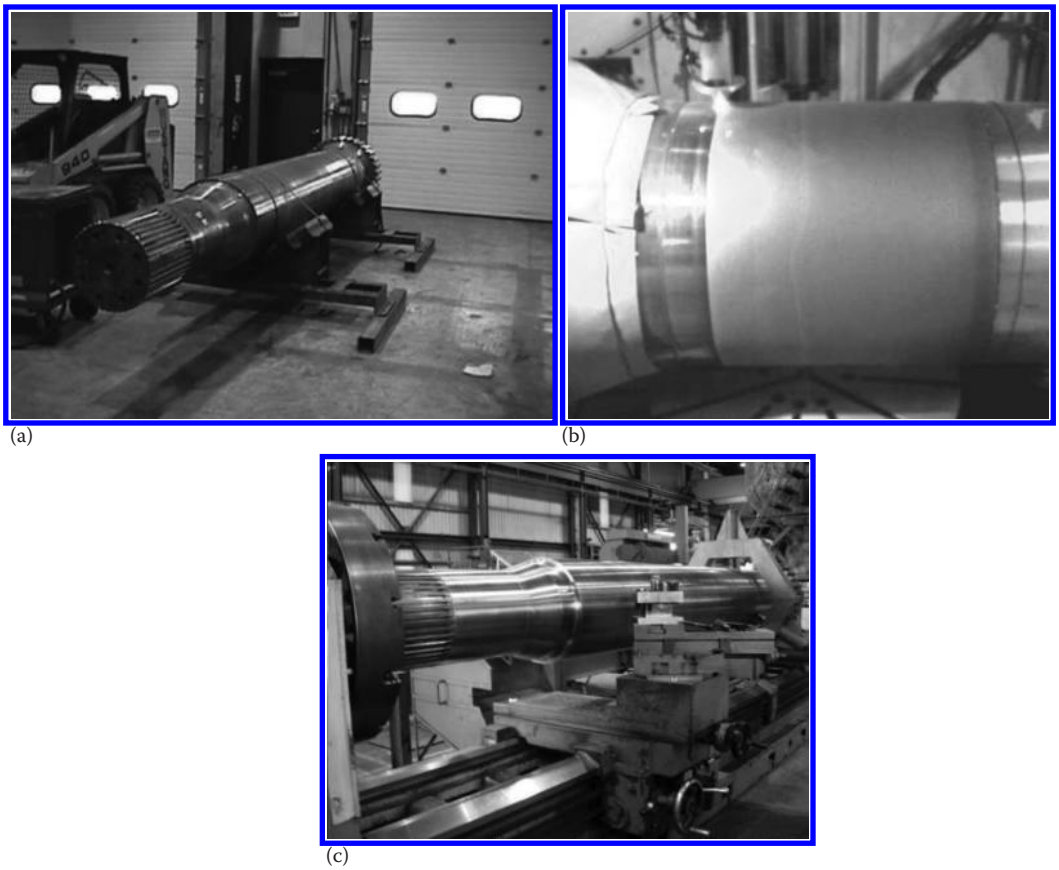

FIGURE 14.5
(See color insert.) (a) Swing shaft worn bearing surface, (b) shaft during deposition, and (c) final machined shaft. (Data from Wald, N., RPM Innovations, Inc., South Dakota, unpublished data.)

within the body after some time. Therefore, when the defect is being healed, the scaffold material will slowly dissolve without any harmful effect to the body. A simple example is bone tissue engineering and AM. Bone defects due to cancer or osteoporosis or ordinary fracture require implants that are mostly made of metals. In most cases, once placed, those metal implants remain in the body. However, instead of metals, if ceramic or polymeric implants can be placed that are bio-resorbable and shaped based on that specific defect size, better healing can be accomplished. To improve healing, implants can be made porous to introduce biological fixation where bone tissue can integrate with the implants better. The pore size and shape can also be tailored based on the patients' anatomy [3–6]. More importantly, specific dopants can be added to the scaffold to further enhance angiogenesis and osteogenesis during healing [7]. All of these ideas are possible now due to AM and pursued by different research groups around the world. This is also a core area of our own research.

Figure 14.6 shows tricalcium phosphate (TCP, $Ca_3(PO_4)_2$)-based bio-resorbable scaffolds with different shapes and porosity produced via a powder bed-based 3D printer (ExOne, PA) in our lab. TCP is a bio-resorbable ceramic, which degrades in the body at a slow rate. The degradation kinetics of TCP ceramics can be tailored by adding different metal ions

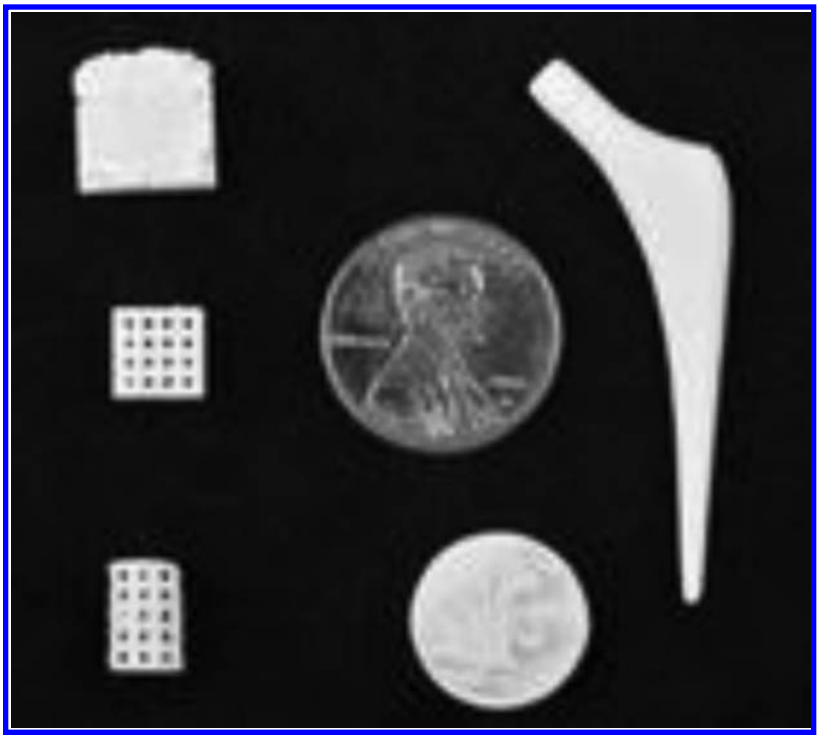

FIGURE 14.6
3D printed TCP scaffolds and different structures with fine features.

such as Mg or Zn or Sr [8–12]. Moreover, the scaffolds degradation kinetics can be further modified through the introduction of porosity of various sizes, shapes, and volume fraction [13,14]. Similar to resorbable ceramics, many resorbable polymers are also currently being used to fabricate scaffolds for various tissue engineering needs. It is expected that such developments will soon result in many products that will positively impact human health.

14.7 On-Site On-Demand Manufacturing versus Mass Production

In 2014, the UPS stores in the United States started an exciting service—3D print your own creation. Just like copiers that can be used to copy materials, customers can come in with their own 3D drawings or create their 3D drawings at the store computer and then 3D print that in a machine next to that. Though the concept is simple, but its implications can be far-fetched. Ordinary citizens now have the access to inexpensive 3D printers to validate their creation—whether it is for fun or for a gift or for a technical project. Such advances have the potential to change the culture of our society in the long run. Companies may start the same approach of distributed on-demand manufacturing houses at different locations as opposed to bulk manufacturing in one location. Certainly,

cost is a big issue that generally drops significantly as a function of production volume. However, for many parts, prediction of future market trends can be tricky and companies may deal with large unsold inventory because of the unpredictable market dynamics. On-demand manufacturing is not suitable for all products, but only for value-added products that are mostly made of one or two materials and smaller in size. These products can be for biomedical industries, space or aerospace industries, or applications in department of defense-related areas just to name a few. More importantly, innovative designs are also possible with the AM approach that can enhance efficiency of many parts and allow incorporation of complex designs that are simply impossible to manufacture using conventional manufacturing approaches. A secondary advantage for the use of AM may come from control over the core designs for a company instead of sharing with many parties at various locations. On-demand manufacturing also offers the possibility of personalization that will be impossible to incorporate in mass manufacturing platform. Special memorable photos such as marriages can no longer need to be in 2D, but can be printed in 3D with color and embedded messages. Patients can see their body parts even before the planned plastic surgery and make changes with the use of AM. Due to lower cost of the AM machines and better understanding from the general population, use of AM does not need to be restricted only in jewelry or dentistry, but can spread in many other ordinary applications. That does not mean that global manufacturing centers will be obsolete in the coming days. However, more and more community centric manufacturing will certainly become a part of our everyday life. Kids can put their input in designing their own toys rather than just buy one. Cars can have owner's name or other information printed on the body instead of just on the license plates. Physicians can order implants for their patients with special needs than tries to retrofit what is commercially available and so on. The future possibilities are endless and the only limiting factor will be our imagination in creativity. And the applications of such technologies will have no geopolitical boundaries. If there is power and Internet access, AM facilities can be installed in a few days even in remote locations on earth to enhance the quality of life for our generation, and the generation to come. The differences between the developing countries and the developed nations or the differences between the manufacturing nations and predominantly consumer nations will decrease because of the use of AM. A flat world has become even more uniform for the generations to come. Even 25 years back, no one could imagine such an impact that could come from the advent of AM. We, the editors of this book, are fortunate to work with this technology for the past 20 years and had a chance to contribute to this technological revolution on our generation.

14.8 Summary

A brief summary of the impact of AM is discussed in this chapter. It is clear that the AM is changing the landscapes of current industrial practices. On-demand manufacturing using AM technologies is a new trend that will significantly influence many industries and product design protocols. It is envisioned that the differences between the developing countries and the developed nations or the differences between the manufacturing nations and predominantly consumer nations will decrease due to the use of AM. In combination with Internet-based technologies and the computer-aided designs, AM will make a flat world even more uniform for the generations to come.

References

1. Balla, V.K., Roberson, L.B., O'Connor, G.W., Trigwell, S., Bose, S., and Bandyopadhyay, A. "First demonstration on direct laser fabrication of lunar regolith parts," *Rapid Prototyping Journal*, 18(6), 451–457 (2012).
2. Sahasrabudhe, H., Harrison, R., Carpenter, C., and Bandyopadhyay, A. "Stainless steel to titanium bimetallic structure using LENS™," *Additive Manufacturing*, 5, 1–8 (2015).
3. Darsell, J., Bose, S., Hosick, H., and Bandyopadhyay, A. "From CT scans to ceramic bone grafts," *Journal of the American Ceramic Society*, 86(7), 1076–1080 (2003).
4. Bose, S., Darsell, J., Kintner, M., Hosick, H., and Bandyopadhyay A. "Pore size and pore volume effects on calcium phosphate based ceramics," *Materials Science and Engineering C*, 23, 479–486 (2003).
5. Bose, S., Roy, M., and Bandyopadhyay, A. "Recent advances in bone tissue engineering scaffolds," *Trends in Biotechnology*, 30(10), 546–554 (2012).
6. Tarafder, S., Balla, V.K., Davies, N., Bandyopadhyay, A., and Bose, S. "Microwave sintered 3D printed tricalcium phosphate scaffolds for bone tissue engineering," *Journal of Tissue Engineering and Regenerative Medicine*, 7(8), 631–641 (2013).
7. Fielding, G. and Bose, S. "SiO_2 and ZnO dopants in 3D printed TCP scaffolds enhances osteogenesis and angiogenesis in vivo," *Acta Biomaterialia*, 9(11), 9137–9148 (2013).
8. Bandyopadhyay, A., Bernard, S., Xue, W., and Bose, S. "Feature article: Calcium phosphate based resorbable ceramics—Influence of MgO, ZnO and SiO_2 dopants," *Journal of the American Ceramic Society*, 89(9), 2675–2688 (2006).
9. Banerjee, S.S., Tarafder, S., Davies, N.M., Bandyopadhyay, A., and Bose, S. "Understanding the influence of MgO and SrO binary doping on the mechanical and biological properties of β-TCP ceramics," *Acta Biomaterialia*, 6, 4167–4174 (2010).
10. Fielding, G., Bandyopadhyay, A., and Bose, S. "Effects of SiO_2 and ZnO doping on mechanical and biological properties of 3D printed TCP scaffolds," *Dental Materials*, 28, 113–122 (2012).
11. Bose, S., Tarafder, S., Banerjee, S.S., and Bandyopadhyay, A. "Understanding in vivo response and mechanical property variation in MgO, SrO and SiO_2 doped β-TCP," *Bone*, 48(6), 1282–1290 (2011).
12. Bandyopadhyay, A., Petersen, J., Fielding, G.. Banerjee, S., and Bose, S. "ZnO, SiO_2 and SrO doping in resorbable tricalcium phosphates: Influence on strength degradation, mechanical properties and in vitro bone cell material interactions," *Journal of Biomedical Materials Research: Part B Applied Biomaterials*, 100(8), 2203–2212 (2012).
13. Tarafder, S., Dernell, W., Bandyopadhyay, A., and Bose, S. "SrO and MgO doped microwave sintered 3D printed tricalcium phosphate scaffolds: Mechanical properties and in vivo osteogenesis in a rabbit model," *Journal of Biomedical Materials Research: Applied Biomaterials*, doi:10.1002/jbm.b.33239 (2014).
14. Ke, D., Bandyopadhyay, A., and Bose, S. "Doped tricalcium phosphate scaffolds by thermal decomposition of naphthalene: Mechanical properties and in vivo osteogenesis in a rabbit femur model," *Journal of Biomedical Materials Research: Part B Applied Biomaterials*, in press. doi: 10.1002/jbm.b.33321 (2014).
15. Wald, N., RPM Innovations, Inc., South Dakota, Unpublished data.

Index

***Note*:** Locators followed by "*f*" and "*t*" denote figures and tables in the text

F

G

L

M

N

O

S

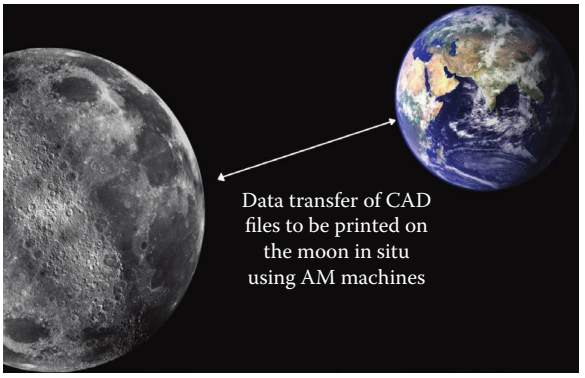

FIGURE 1.4
Data transfer of CAD between Moon and Earth. (Data from iStock. By Getty Images™ Moon and World—Stock Image. Stock Photo: 3928179. 2014.)

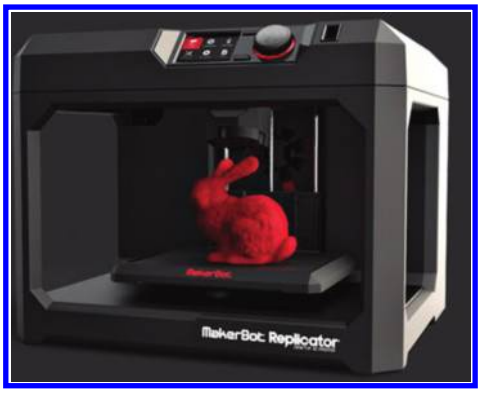

FIGURE 1.7
MakerBot Replicator Desktop 3D Printer. (Data from MakerBot® Replicator Desktop 3D Printer. Makerbot.com. 2009–2014. http://store.makerbot.com/replicator; Courtesy of MakerBot, Brooklyn, NY.)

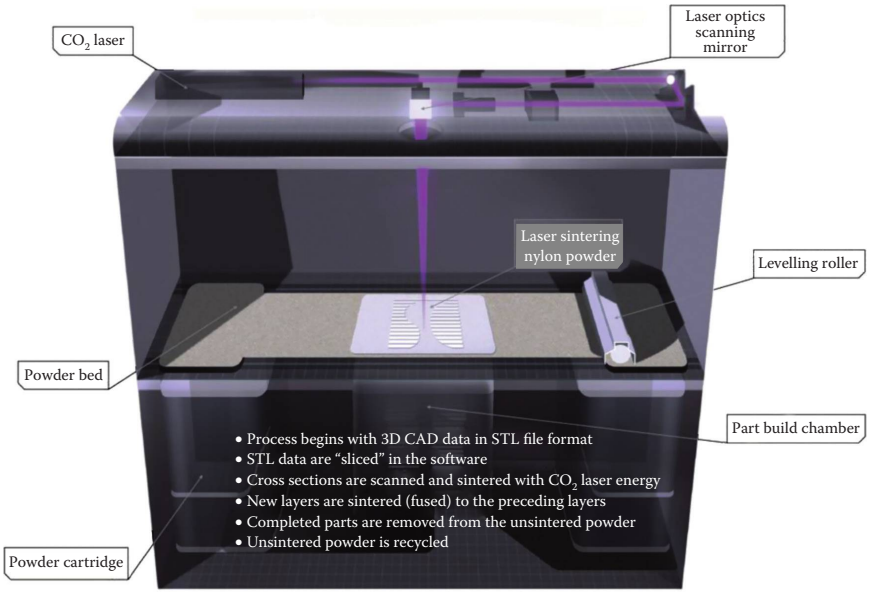

FIGURE 2.3
Schematic of the selective laser sintering AM process. (Courtesy of www.solidconcepts.com.)

FIGURE 2.25
A typical ATP setup used. (Data from Yarlagadda, S., Automated Tow Placement of Composites, 2014.)

FIGURE 2.44
Fabrication of intricate shapes in the FDM process using a water-soluble material as the support material.

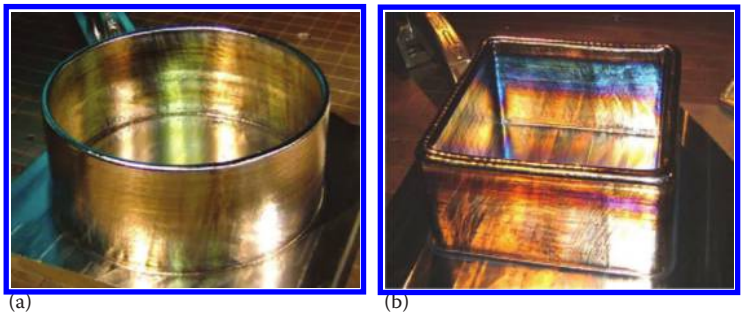

FIGURE 3.12
Tubular parts fabricated using SMD; (a) and (b) thin wall components and (c) thick wall (20 mm) component. (Reprinted with permission from Baufeld, B. et al., *Mater. Design*, 31, S106–S111, 2010.)

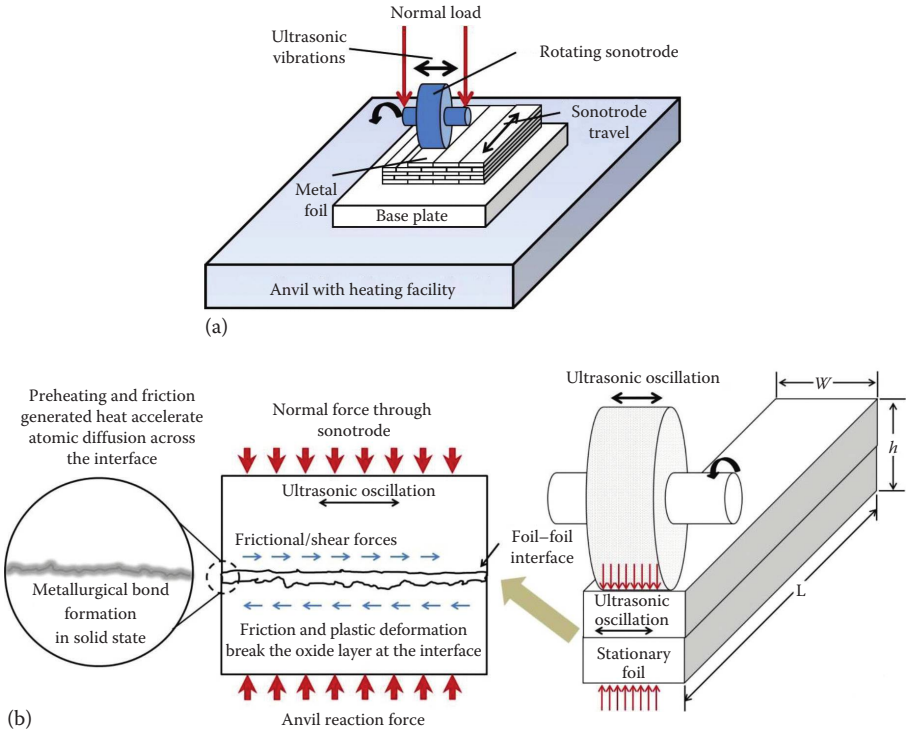

FIGURE 3.13
(a) Ultrasonic consolidation process and its components; (b) illustration of foil geometrical parameter (right) and formation of metallurgical bond between the foils during ultrasonic consolidation (left).

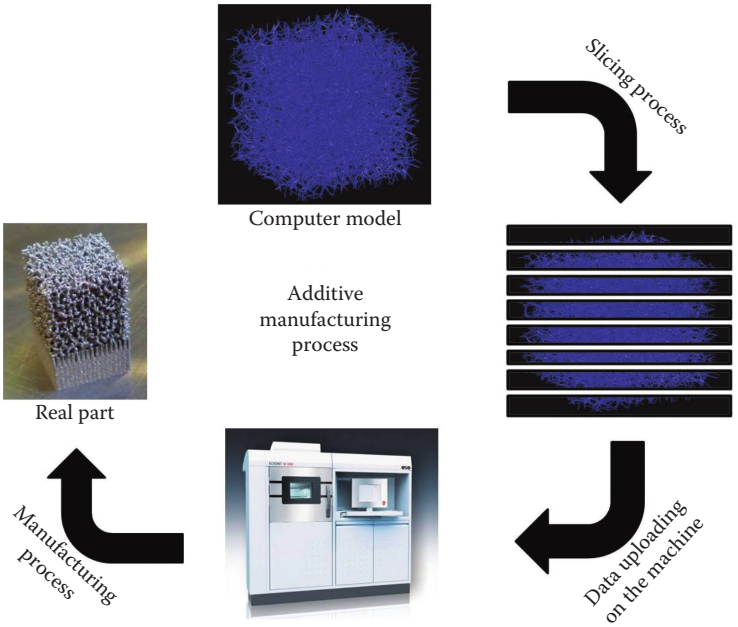

FIGURE 4.5
Functional sequence of additive manufacturing.

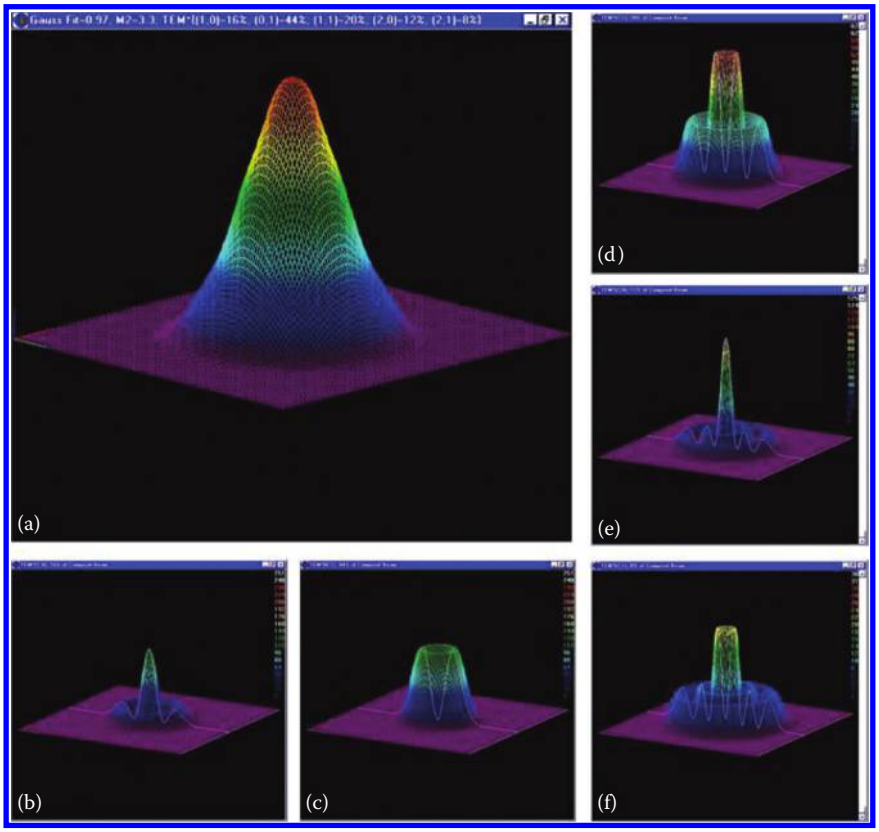

FIGURE 4.13
Beam characterization: (a) Gaussian fit 0.97, (b) TEM_{10}, (c) TEM_{01}, (d) TEM_{11}, (e) TEM_{20}, and (f) TEM_{21}. (Data from http://www.laserfocusworld.com/articles/2008/04/beam-characterization-camera-based-sensors-characterize-laser-beams.html.)

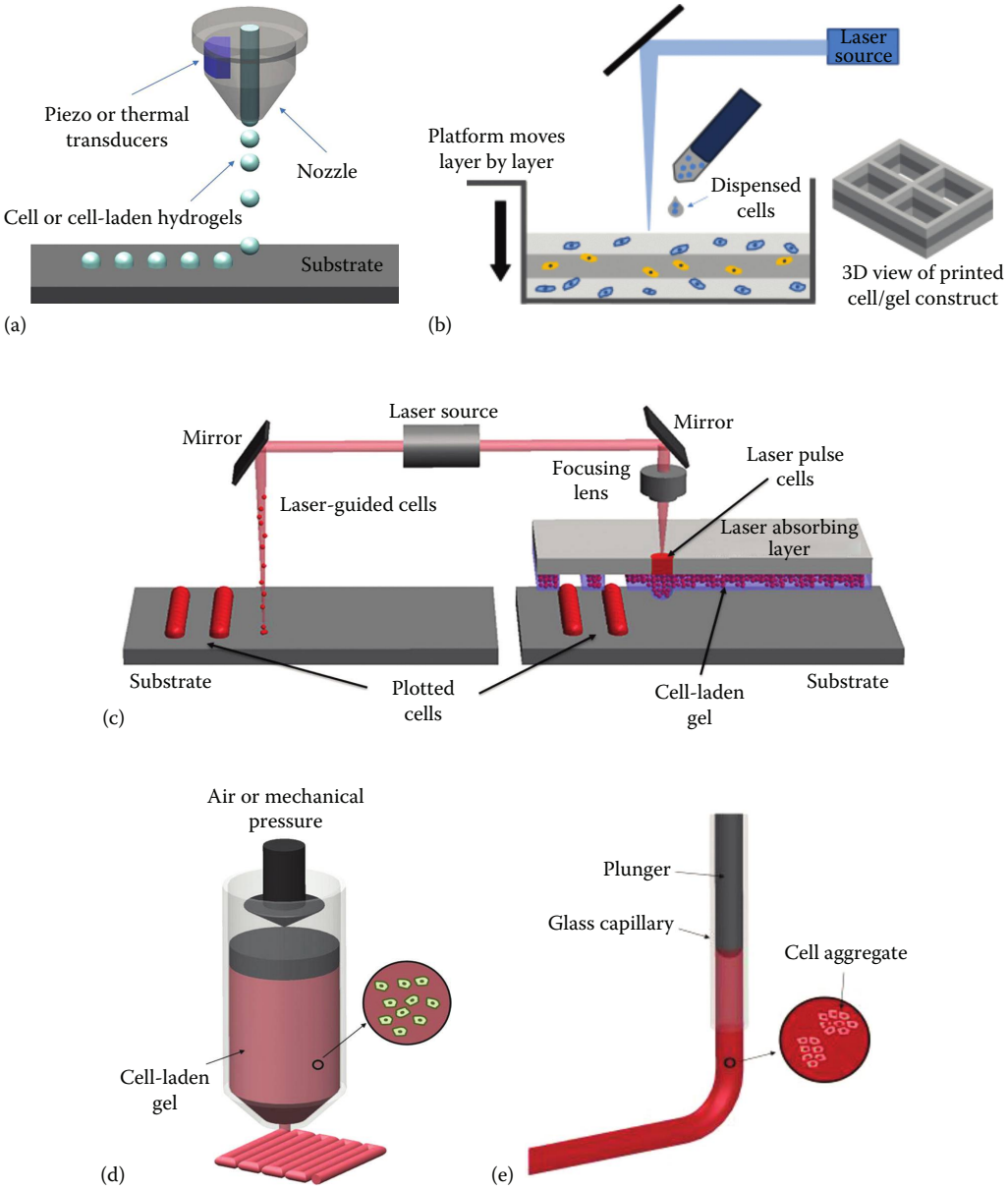

FIGURE 7.2
(a) Thermal and piezoelectric ink-jet bioprinting. (b) Stereolithography-based bioprinting. (c) Laser-based bioprinting setup. Left: Laser-guided direct cell printing. Right: The cell–hydrogel compound is propelled forward as a jet by the pressure of a laser-induced vapor bubble. (d) Extrusion/deposition-based bioprinting. (e) Direct cell-aggregate deposition.

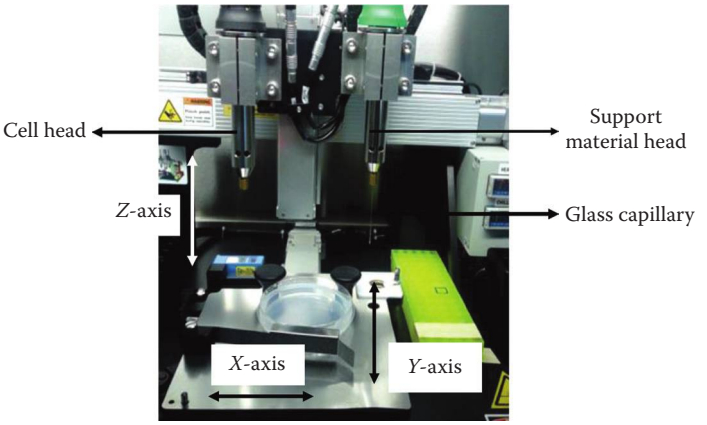

FIGURE 7.6
Organovo Novogen MMX Bioprinter.

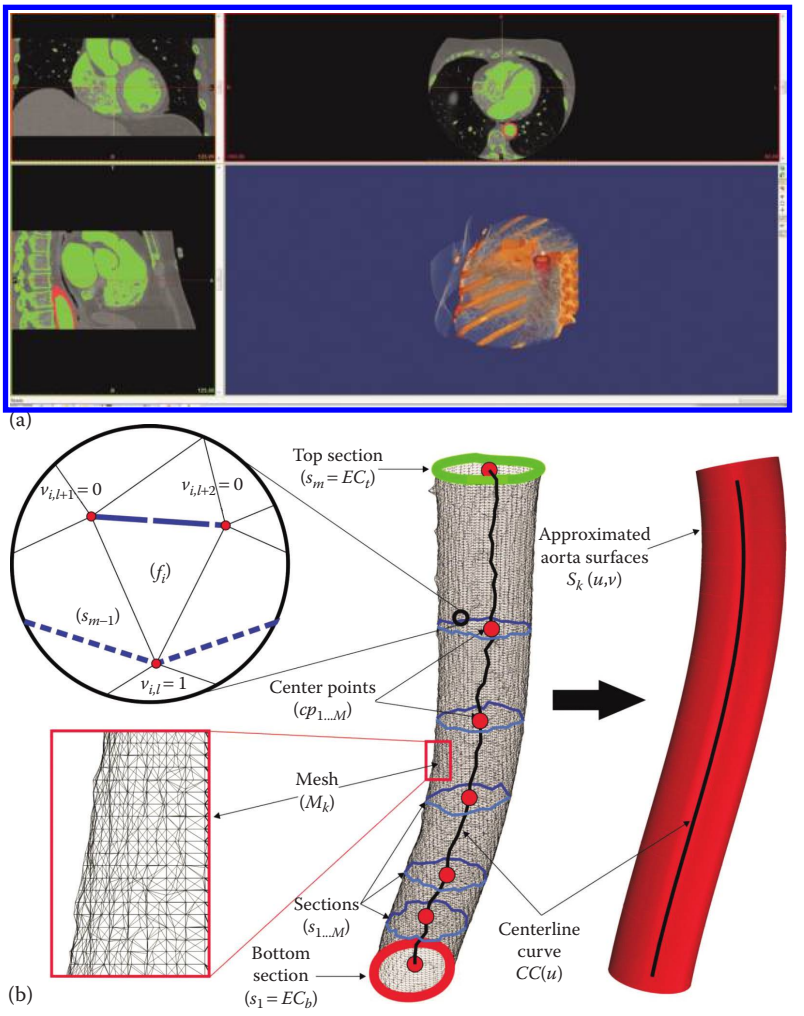

FIGURE 7.7
Proposed methods for 3D bioprinting of macrovascular structures. (a) Capturing accurate geometry of the aorta from a sample magnetic resonance imaging (MRI) data. (b) Segmentation and then transformation of the data into a 3D surface as a stereolithography (STL) model.

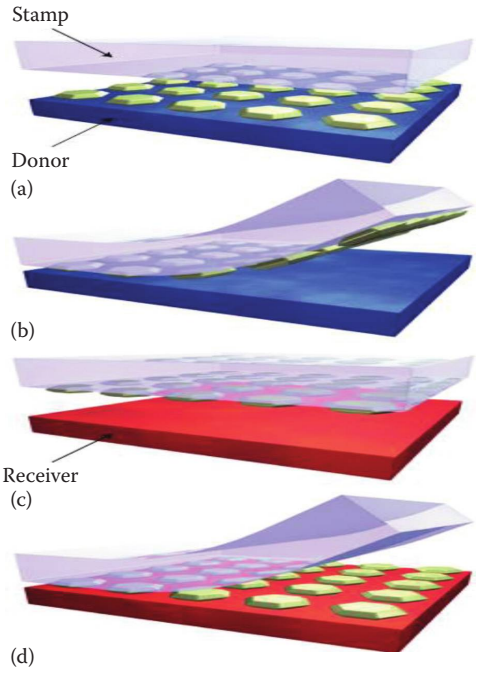

FIGURE 8.6
Schematic illustration of the generic process flow for transfer printing solid objects. (a) Laminating a stamp (TS) against a donor substrate and then quickly peeling it away, (b) pulling the microstructures (PL) from the donor substrate onto the stamp (TS), (c) contacting the stamp (TS) to another substrate (DS), and then (d) slowly peeling it away transfers the microstructures (PL) from the stamp (TS) to the receiver (DS). (Adapted from Meitl, M.A. et al., *Nat. Mater.*, 5, 33–38, 2006.)

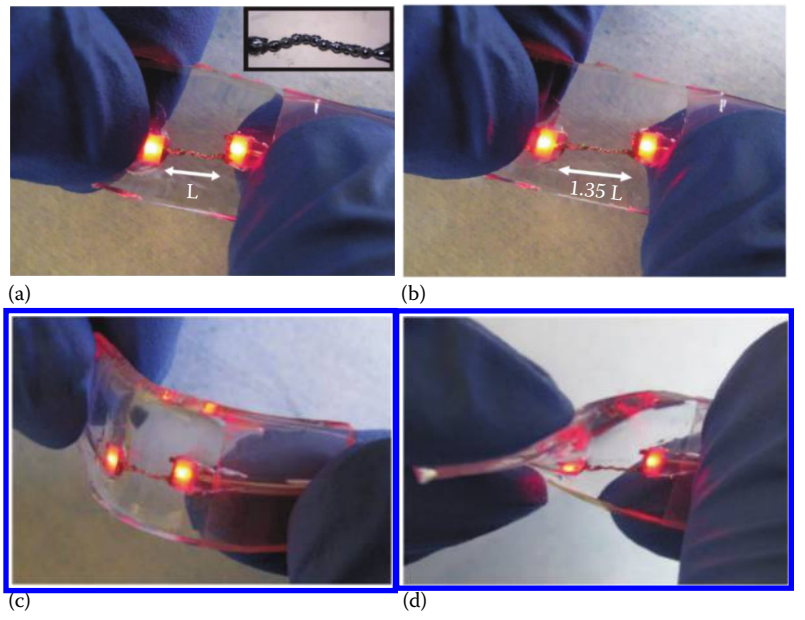

FIGURE 8.20
Stretchable interconnects formed by DW. (a) A prototype device composed of two LEDs connected by a stretchable wire bond and embedded in PDMS (Inset: Microscopy image of the liquid metal wire bonds). (b–d): The fluidic property of the metal wire in the elastomer allows elasticity (b) and flexibility (c, d) of the device and keeps its electrical continuity. (Adapted from Ladd, C. et al., *Adv. Mater.*, 25, 5081–5085, 2013.)

FIGURE 9.4
Three single- to four-port nozzles showing shape-making capability of additive manufacturing. On the left is a part made using standard white ABS, center is Ultem 9085, and on the right is carbon-fiber-filled poly ether imide all manufactured using FDM™. (Copyright Rapid Prototype and Manufacturing, LLC, Avon Lake, Ohio, 2014.)

FIGURE 9.8
Example of a short-run injection molding tool made from ABS using Objet material jetting technology. (Copyright Rapid Prototype and Manufacturing, LLC, Avon Lake, Ohio, 2014.)

FIGURE 9.9
Injection mold core and cavity set for thermoplastic elastomer molding made from Ultem 9085 using Stratasys FDM™. (Copyright Rapid Prototype and Manufacturing, LLC, Avon Lake, Ohio, 2014.)

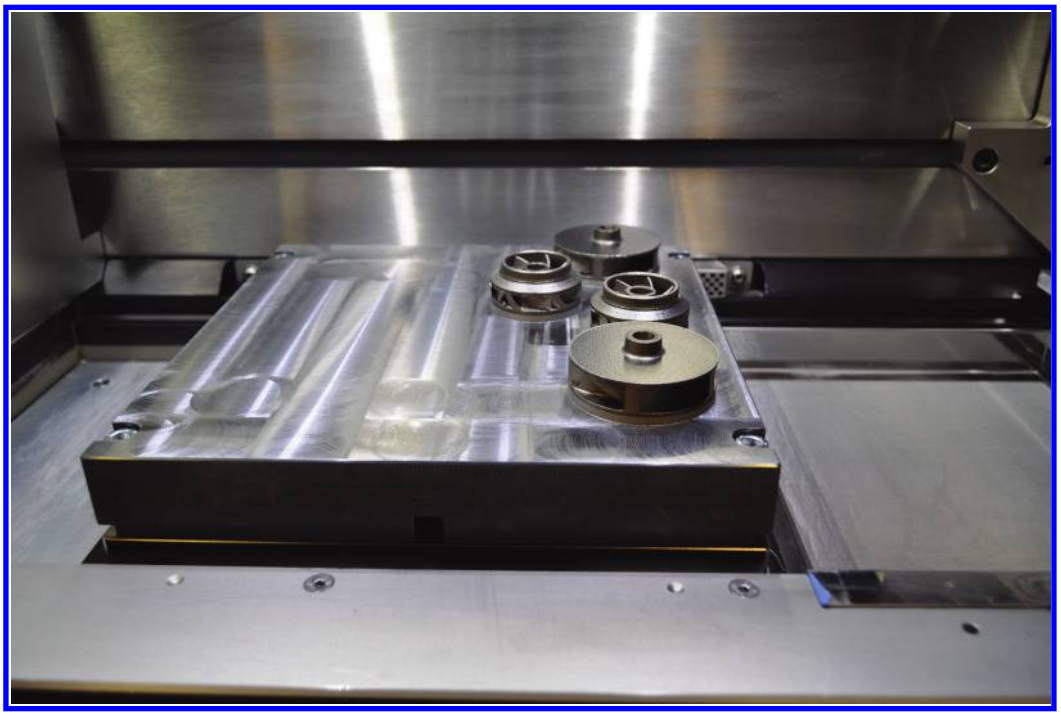

FIGURE 9.13
Stainless steel PH1 (15-5 Cr-Ni) impeller prototypes bonded to the build plate in an EOS DMLS™ M280 build chamber. (Copyright Rapid Prototype and Manufacturing, LLC, Avon Lake, Ohio, 2014.)

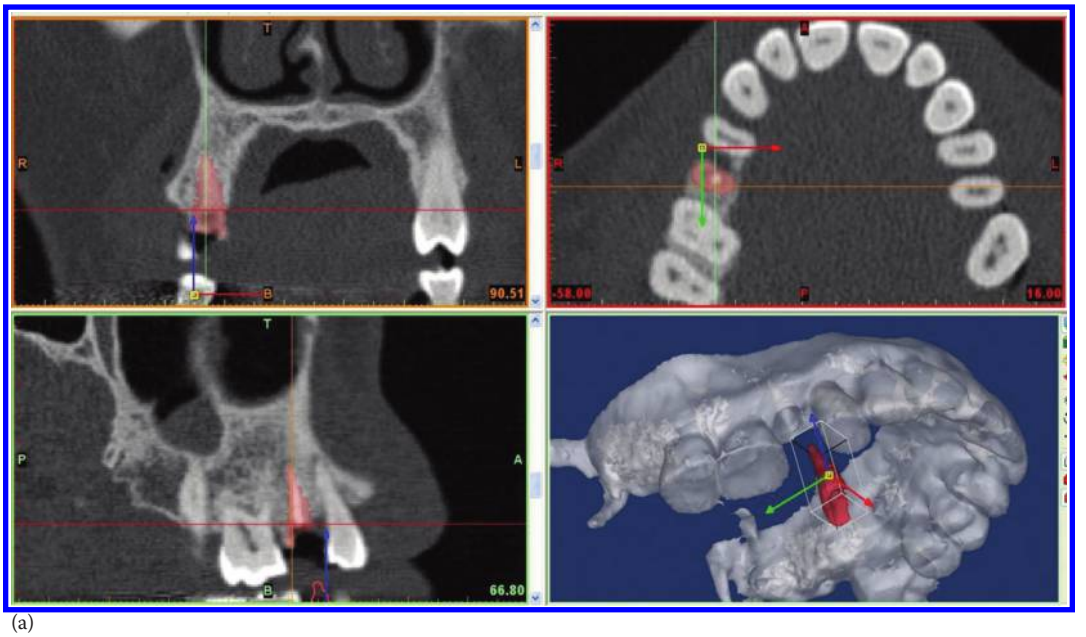

(a)

(b)

(c)

FIGURE 11.22

(a) Designing dental implant using image data of maxilla and the residual root; (b) custom-designed dental root-analogue implant model; and (c) one year post-surgery radiograph of custom dental implant with crown. (Reprinted with permission from Figliuzzi, M. et al., *Int. J. Oral Maxillofac. Surg.*, 41, 858–862, 2012.)

FIGURE 12.9
Sample student rotor-impeller designs.

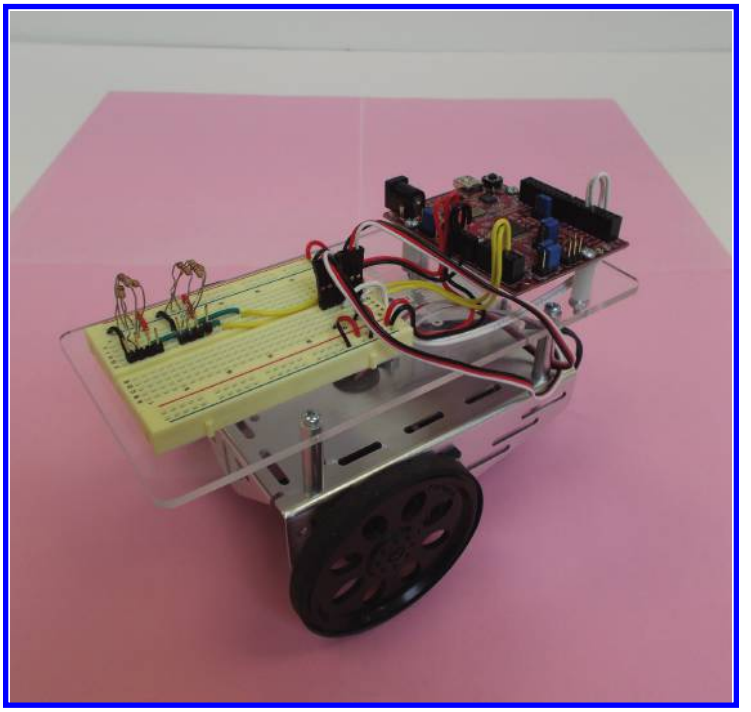

FIGURE 12.12
Original student robot configuration.

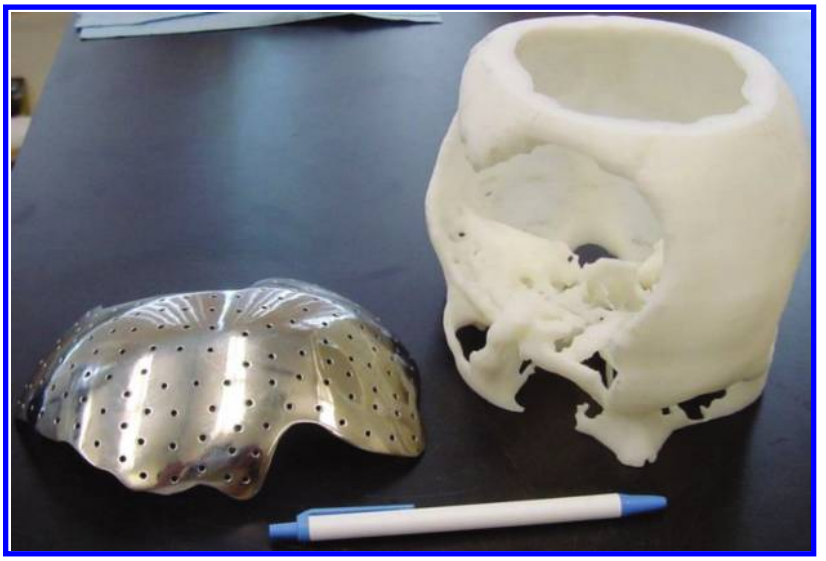

FIGURE 14.2
LENS processed craniofacial Ti implant and FDM processed polymer prototype of the skull with large defect.

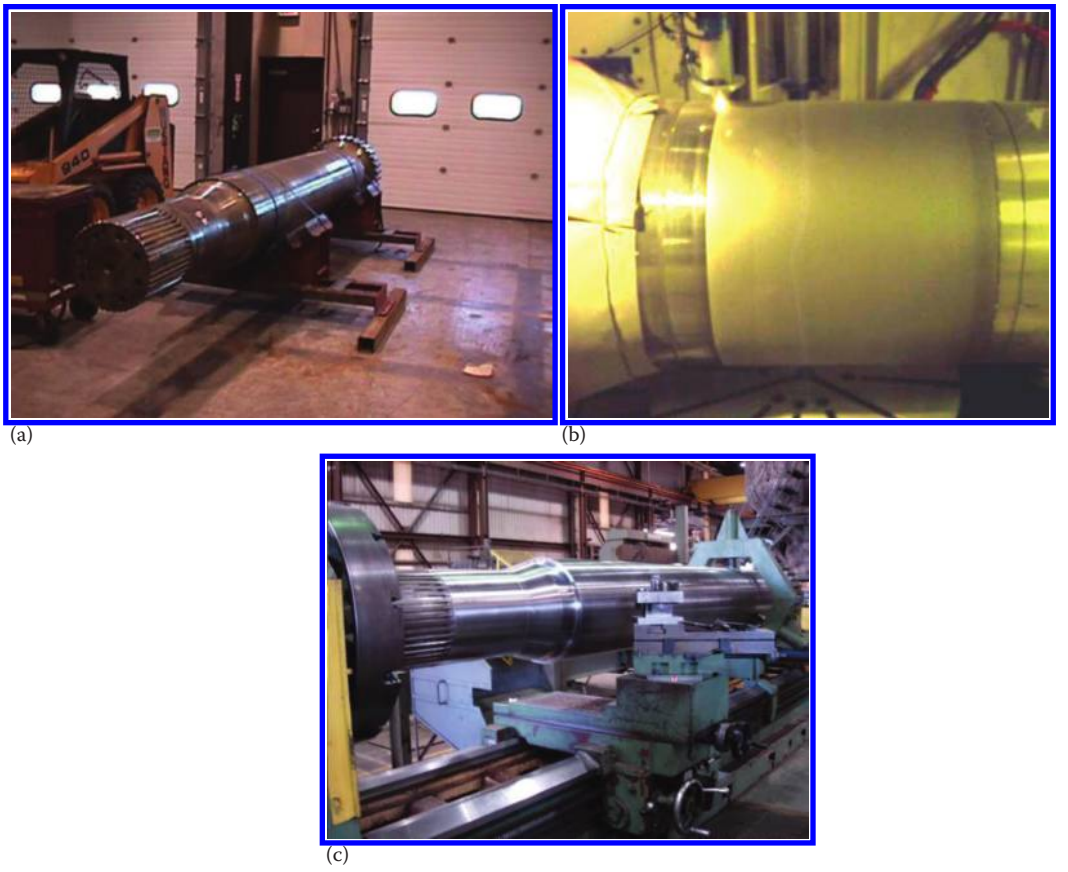

FIGURE 14.5
(a) Swing shaft worn bearing surface, (b) shaft during deposition, and (c) final machined shaft. (Data from Wald, N., RPM Innovations, Inc., South Dakota, unpublished data.)